DOE-ACE-2011AR

2011

annual progress report

Advanced Combustion Engine Research and Development

U.S. DEPARTMENT OF ENERGY | Energy Efficiency & Renewable Energy

U.S. Department of Energy
1000 Independence Avenue, S.W.
Washington, D.C. 20585-0121

FY 2011 PROGRESS REPORT FOR ADVANCED COMBUSTION ENGINE RESEARCH AND DEVELOPMENT

Energy Efficiency and Renewable Energy
Vehicle Technologies Program

Approved by Gurpreet Singh
Team Leader, Advanced Combustion Engine R&D
Vehicle Technologies Program

December 2011
DOE-ACE-2011AR

Acknowledgement

We would like to express our sincere appreciation to Alliance Technical Services, Inc. and Oak Ridge National Laboratory for their technical and artistic contributions in preparing and publishing this report.

In addition, we would like to thank all the participants for their contributions to the programs and all the authors who prepared the project abstracts that comprise this report.

Table of Contents

I. INTRODUCTION

I.1 Subprogram Overview and Status

DEVELOPING ADVANCED COMBUSTION ENGINE TECHNOLOGIES

On behalf of the Department of Energy's Vehicle Technologies Program (VTP), we are pleased to introduce the Fiscal Year (FY) 2011 Annual Progress Report for the Advanced Combustion Engine Research and Development (R&D) subprogram. The mission of the VTP is to develop more energy-efficient and environmentally friendly highway transportation technologies that will meet or exceed performance expectations, enable the United States to use significantly less petroleum, and reduce greenhouse gas and other regulated emissions. The Advanced Combustion Engine R&D subprogram supports this mission by removing the critical technical barriers to commercialization of advanced internal combustion engines (ICEs) for passenger and commercial vehicles that meet future federal emissions regulations. Dramatically improving the efficiency of ICEs and enabling their introduction in conventional as well as hybrid electric vehicles is one of the most promising and cost-effective approaches to increasing vehicle fuel economy over the next 30 years. Improvements in engine efficiency alone have the potential to increase passenger vehicle fuel economy by 25 to 40 percent, and commercial vehicle fuel economy by 30 percent with a concomitant reduction in greenhouse gas emissions, more specifically, carbon dioxide emissions. These improvements are expected to be even greater when coupled with advanced hybrid electric powertrains.

The following are representative goals of the Advanced Combustion Engine R&D subprogram that can contribute to meeting national energy security, environmental, and economic objectives:

- By 2015, increase the efficiency of ICEs for passenger vehicles resulting in fuel economy improvements of 25 percent for gasoline vehicles and 40 percent for diesel vehicles compared to current gasoline vehicles. The emphasis has shifted to improving the vehicle fuel economy over a real-world driving cycle after the peak engine thermal efficiency goal of 45 percent was met in 2010.
- By 2015, increase the efficiency of ICEs for commercial vehicles from 42 percent (2010 baseline) to 50 percent (20 percent improvement) and by 2020, further improve engine efficiency to 55 percent with demonstrations on commercial vehicle platforms.
- By 2015, increase the fuel economy of passenger vehicles by at least 5 percent with thermoelectric generators that convert energy from engine waste heat to electricity.

The passenger and commercial vehicle goals will be met while utilizing advanced fuel formulations that can incorporate a non-petroleum-based blending agent to reduce petroleum dependence and enhance combustion efficiency.

To meet the first two goals, two initiatives were launched in 2010, SuperTruck and the Advanced Technology Powertrains for Light-Duty Vehicles (ATP-LD) to improve the fuel economy of heavy-duty trucks and passenger vehicles, respectively. The funding includes more than $100 million from the American Recovery and Reinvestment Act, and with a private cost share of 50 percent, will support nearly $375 million in total research, development and demonstration projects across the country.

Four SuperTruck projects will focus on cost-effective measures to improve the efficiency of Class 8 long-haul freight trucks by 50 percent, 20 percent of which will come from improvements to engine efficiency. The ATP-LD projects will support efforts to increase the fuel economy of passenger vehicles using an engine/powertrain-only approach.

To meet the third goal, three projects were initiated in 2011 to develop thermoelectric generators with cost-competitive advanced thermoelectric materials that will improve passenger vehicle fuel economy by at least 5 percent by 2015.

This introduction serves to outline the nature, current focus, recent progress, and future directions of the Advanced Combustion Engine R&D subprogram. The research activities of this subprogram are planned in conjunction with U.S.DRIVE (Driving Research and Innovation for Vehicle efficiency and Energy sustainability, formerly the FreedomCAR and Fuel Partnership) and the 21st Century Truck Partnerships and are carried out in collaboration with industry, national laboratories, and universities.

Because of the importance of clean fuels and advanced materials in achieving high efficiency and low emissions, R&D activities are closely coordinated with the relevant activities of the Fuels Technology and Materials Technologies subprograms, also within VTP.

CURRENT TECHNICAL FOCUS AREAS AND OBJECTIVES

The Advanced Combustion Engine R&D subprogram focuses on developing advanced ICE technologies for all highway transportation vehicles. Fuel efficiency improvement is the overarching focus of this activity, but resolving the interdependent emissions challenges is a critical integrated requirement. The reduction of engine-out emissions is key to managing the extra cost of exhaust aftertreatment devices that can be a barrier to market acceptance. (Penetration of even current-technology diesel engines into the light-duty truck market would reduce fuel use by 25-30% per gasoline vehicle replaced.) Accordingly, research has been emphasizing advanced combustion modes including homogeneous charge compression ignition (HCCI), pre-mixed charge compression ignition (PCCI), reactivity controlled compression ignition (RCCI), lean-burn gasoline, and other modes of low-temperature combustion (LTC) which will increase efficiency beyond current state-of-the-art engines and reduce engine-out emissions of nitrogen oxides (NOx) and particulate matter (PM) to near-zero levels. In parallel, research on emission control systems is underway to increase their efficiency and durability for overall emissions compliance at an acceptable cost and with reduced dependence on precious metals. Projects to stretch engine efficiency via innovative combustion methods and thermal energy recovery (such as compound cycles) are in progress as well. In response to the challenges of realizing and implementing higher efficiency engines, the Advanced Combustion Engine R&D subprogram is working toward achieving the following objectives:

- Further the fundamental understanding of advanced combustion processes which simultaneously exhibit low emissions and high efficiency. This will be used in the development of cleaner, more efficient engines which will operate predominately in low-temperature or HCCI combustion modes. These technology advances are expected to reduce the size and complexity of emission control hardware and minimize potential fuel efficiency penalties. A fuel-neutral approach is also being taken, with research addressing gasoline- and diesel-based advanced engines, including renewable fuels. The effects of fuel properties on combustion are addressed in the Fuel & Lubricant Technologies subprogram. Hydrogen engine R&D is underway as well.
- Improve the effectiveness, efficiency, and durability of engine emission control devices as well as reduced dependence on precious metals to enable increased penetration of advanced combustion engines in the light-duty market and maintain and/or expand application to heavy-duty vehicles.
- Extend robust engine operation and efficiency through the development and implementation of high-speed predictive models for improvements in combustion control and thermal management.
- Further the development of approaches to producing useful work from engine waste heat such as through incorporation of bottoming cycles, and application of advanced thermoelectric technologies for direct conversion of energy from engine waste heat to useful energy (electricity), that will significantly increase vehicle fuel economy.
- Advance engine technologies such as turbo-machinery, flexible valve systems, advanced combustion systems, and fuel system components to achieve a reduction in parasitic losses and other losses to the environment to maximize engine efficiency.
- Develop key enabling technologies for advanced engines such as sensors and control systems, diagnostics for engine development, and components for thermal energy recovery.
- Improve the integration of advanced engine/emissions technologies with hybrid-electric systems for improved efficiency with lowest possible emissions.
- In cooperation with the Fuels Technology subprogram, accelerate industry development of a next generation of E85 flexible-fuel engines that exploit ethanol properties for higher efficiency.
- Identify that any potential health hazards associated with the use of new vehicle technologies being developed by VTP will not have adverse impacts on human health through exposure to toxic particles, gases, and other compounds generated by these new technologies.

- Develop thermoelectrics and other solid state systems that provide cooling/heating for vehicle interiors to maintain occupant comfort. This technology is particularly important for hybrid-electric and all-electric vehicles that have insufficient or no engine heat for occupant comfort.

The Advanced Combustion Engine R&D subprogram maintains close communication with industry through a number of working groups and teams, and utilizes these networks for setting goals, adjusting priorities of research, and tracking progress. Examples of the cooperative groups are the Advanced Combustion and Emission Control Tech Team of the U.S.DRIVE Partnership and the Engine Systems Team of the 21st Century Truck. Focused efforts are carried out in the Advanced Combustion Memorandum of Understanding (including auto manufacturers, engine companies, fuel suppliers, national laboratories, and others) and the CLEERS (Cross-Cut Lean Exhaust Emission Reduction Simulation) activity for the Advanced Engine Cross-Cut Team.

TECHNOLOGY STATUS AND KEY BARRIERS

Significant advances in combustion, emission controls, fuel injection, turbo-machinery, and other advanced engine technologies continue to increase the thermal efficiency of ICEs with simultaneous reductions in emissions. With these advances, gasoline and diesel engines continue to be attractive engine options for conventional and hybrid-electric vehicles. These engines offer outstanding drivability, fuel economy, and reliability; they can readily use natural gas and biofuels such as ethanol and biodiesel.

The majority of the U.S. light-duty vehicle fleet is powered by spark-ignition (SI) gasoline engines. Substantial progress in gasoline engine efficiency in recent years has been the result of advances in engine technologies including direct fuel injection, flexible valve systems, improved combustion chamber design, and reduced mechanical friction.

While all gasoline engines sold in the U.S. operate with stoichiometric combustion (needed for emission control by highly cost-effective three-way catalysts), other areas in the world with less stringent emissions regulations are seeing the introduction of higher efficiency lean-burn gasoline engines. Although these engines are characterized by higher efficiencies at part load, they require more costly lean-NOx emission controls that are currently not adequate for U.S. emissions regulations. In addition, the direct injection technology utilized for most advanced gasoline engines produces particulate emissions that although smaller in mass than the diesel engine still represent significant emissions in terms of particulate number counts. Advances in lean-gasoline emission controls are critical for meeting U.S. regulations and ultimately the introduction of this efficiency technology in the U.S. market.

Attaining the high efficiency potential of lean-burn gasoline technology will require better understanding of the dynamics of fuel-air mixture preparation and other enabling technologies. Consistently creating combustible mixtures near the spark plug and away from walls in an overall lean environment is a challenge requiring improved understanding of fuel-air mixture preparation and modeling tools that embody the information. A comprehensive understanding of intake air flows and fuel sprays, as well as their interaction with chamber/piston geometry over a wide operating range is needed. Generating appropriate turbulence for enhancement of flame speed is a further complexity requiring attention. The wide range of potential intake systems, piston geometries, and injector designs makes the optimization of lean-burn systems dependent on the development of improved simulation tools. Furthermore, reliable ignition and combustion of lean (dilute) fuel-air mixtures remains a challenge. Lean and possibly boosted conditions require a more robust, high-energy ignition system that, along with proper mixture control, is needed to reduce combustion variability. Several new ignition systems have been proposed (high-energy plugs, plasma, corona, laser, etc.) and need to be investigated.

Diesel engines are also well-suited for light-duty vehicle applications, delivering fuel economy considerably higher than comparable SI engines. Key developments in combustion and emission controls, plus low-sulfur fuel have enabled manufacturers to achieve the necessary emissions levels and introduce additional diesel-powered models to the U.S. market. DOE research contributed to all of these areas. Primarily due to the cost of the added components and diesel fuel price, diesels in passenger cars have limited market penetration in the U.S. Hence reducing the cost of emission compliance continues to be addressed.

The heavy-duty diesel is the primary engine for commercial vehicles because of its high efficiency and outstanding durability. However, the implementation of increasingly stringent heavy-duty engine emission standards over the last decade held efficiency gains to a modest level. Current heavy-duty diesel engines have efficiencies in the 42-43% range. With stability in NOx and PM regulations in 2010, further gains in efficiency are now seen as achievable. Continued aggressive R&D to improve boosting, thermal management, and the reduction and/or recovery of rejected thermal energy are expected to enable efficiencies to reach 55%. Heavy-duty vehicles using diesel engines have significant potential to employ advanced combustion regimes and a wide range of waste heat recovery technologies that will improve engine efficiency and reduce fuel consumption.

Emissions of NOx (and PM) are a significant challenge for all lean-burn technologies including conventional and advanced diesel combustion strategies, both light-and heavy-duty, as well as lean-burn gasoline. Numerous technologies are being investigated to reduce vehicle NOx emissions while minimizing the fuel penalty associated with operating these devices. These technologies include post-combustion emissions control devices as well as advanced combustion strategies which make use of high levels of dilution to reduce in-cylinder NOx formation.

In early 2007, the U.S. Environmental Protection Agency (EPA) finalized the guidance document for using selective catalytic reduction (SCR) which makes use of urea for regeneration (urea-SCR) technology for NOx control in light-duty and heavy-duty diesel vehicles and engines. This guidance allows for the introduction of SCR technology in Tier 2 light-duty vehicles, heavy-duty engines, and in other future diesel engine applications in the U.S. Strategies to supply the urea-water solution (given the name “diesel exhaust fluid”) for vehicles have been developed and are being implemented. Using urea-SCR, light-duty manufacturers have been able to meet Tier 2, Bin 5 which is the “gold standard” at which diesel vehicle sales do not have to be offset by sales of lower emission vehicles. Most heavy-duty diesel vehicle manufacturers are adopting urea-SCR since it has a broader temperature range of effectiveness than competing means of NOx reduction and allows the engine/emission control system to achieve higher fuel efficiency. Although urea-SCR is a relatively mature catalyst technology, more support research is needed to aid formulation optimization and minimize degradation effects such as hydrocarbon fouling.

Another technology being used to control NOx levels in diesel engines and potentially lean-burn gasoline engines is lean-NOx traps (LNTs), which are also referred to as NOx adsorbers. An example application is that Volkswagen has certified its 2011 diesel Jetta to Tier 2, Bin 5 and California Low Emissions Vehicle (LEV)-II using an LNT in conjunction with EGR, a diesel oxidation catalyst (DOC) and diesel particulate filter (DPF). Although LNTs have been commercialized for light-duty diesels, further advancement of the technology is needed to expand market penetration of light-duty diesels and to enable use of LNTs in lean gasoline engine passenger car vehicles. A primary limitation to further adoption of current light-duty diesels is cost. Complex engine and EGR systems and the larger catalyst volumes associated with LNTs and DPFs result in higher overall costs in comparison to conventional gasoline vehicle systems. Cost is particularly sensitive for LNTs which require substantial quantities of platinum group metals, and the cost of these materials is high and volatile due to limited sources that are primarily mined in foreign countries. Improvements in the temperature range of operation for LNTs are also desired to reduce cost and enable success in the lean gasoline engine application. Both LNTs and DPFs result in extra fuel use, or a “fuel penalty”, as they require fueling changes in the engine for regeneration processes. Aggressive research has substantially decreased the combined fuel penalty for both devices to approximately four percent of total fuel flow; further reduction would be beneficial. While LNTs have a larger impact on fuel consumption than urea-SCR, light-duty vehicle manufacturers appear to prefer LNTs since overall fuel efficiency is less of a concern and urea replenishment is more of a challenge for light-duty customers as compared to heavy-duty vehicle users. Another improvement being pursued for LNT technology is to pair them with SCR catalysts. The advantage is that the SCR catalyst uses the NH_3 produced by the LNT so no urea is needed. Formulation and system geometries are being researched to reduce the overall precious metal content of LNT+SCR systems which reduces cost and makes the systems more feasible for light-duty vehicles.

A highly attractive solution to reducing vehicle emissions is to alter the combustion process such that engine-out emissions are at levels which remove or reduce the requirements for auxiliary devices while maintaining or improving engine efficiency. This is the concept behind advanced combustion processes such as HCCI, PCCI and other modes of LTC, which exhibit high efficiency with significant

reductions in NOx and PM emissions. Note that emissions of hydrocarbons (HCs) and carbon monoxide (CO) are often higher and require additional controls which are often a challenge with the low exhaust temperature characteristic of these combustion modes. Significant progress continues for these advanced combustion systems, and the operational range continues to be expanded to better cover the speed/load combinations consistent with light-duty and heavy-duty drive cycles. In recent years, DOE adopted the term "high-efficiency clean combustion" (HECC) as an all encompassing term which includes a range of combustion modes which are focused on improvements in efficiency with lowest possible emissions. The major R&D challenges include fuel mixing, intake air conditioning, combustion timing control, and expansion of the operational range. To meet these challenges, there has been significant R&D on allowing independent control of the intake/exhaust valves relative to piston motion and on improvements in air-handling and engine controls. Many of these technologies are transitioning to the vehicle market.

High dilution operation through advanced EGR is a key element of HECC and can be a major contributor to meet the 2010 EPA heavy-duty engine emission standards and is also applicable to light-duty diesel and gasoline engines. There are numerous advantages of advanced EGR compared to urea-SCR and LNT packages including lower vehicle weight, less maintenance, and lower operating cost. The disadvantages relative to post-combustion emission controls include increased heat rejection load on the engine and the potential for increased fuel consumption due to more frequent DPF active regeneration. In 2009 the Advanced Engine Cross-Cut Team formed a working group to study the widespread issues of fouling and corrosion in the EGR systems. The DOE Propulsion Materials subprogram is a co-sponsor.

Complex and precise engine and emission controls require sophisticated feedback systems employing new types of sensors. A major advancement in this area for light-duty engines has been the introduction of in-cylinder pressure sensors integrated into the glow plug. Start-of-combustion sensors (other than the aforementioned pressure sensor) have been identified as a need, and several development projects have been completed. Sensors are also beneficial for the emission control system. NOx and PM sensors are under development and require additional advances to be cost-effective, accurate, and reliable. Upcoming regulations with increased requirements for on-board diagnostics will also challenge manufacturers trying to bring advanced fuel efficient solutions to market. The role of sensors and catalyst diagnostic approaches will be a key element of emission control research in the next few years.

Advanced combustion engines must be compatible with, if not optimized, for renewable fuels. The Energy Independence and Security Act of 2007 mandates 36 billion gallons of renewable fuels by 2022, which would be mostly ethanol for SI engines, biodiesel for diesels, and second-generation renewable fuels for both. Research has confirmed the basic compatibility of these fuels with various interpretations of HECC. The impact of these fuels on emission controls is also under study, principally in the Fuels Technology subprogram. Recent tests have shown that biodiesel lowers the regeneration temperature of particulate traps and increases the rate of regeneration with the potential for avoiding or reducing the need for active regeneration and its associated fuel economy penalty.

Waste heat recovery approaches (e.g., bottoming cycles) are being implemented in heavy-duty diesel vehicles and explored for light-duty diesel and gasoline applications. Experiments have shown that waste heat recovery has the potential to improve vehicle fuel economy by as much as 10%.

Another form of waste heat recovery is a thermoelectric generator. Vehicular thermoelectric generators directly convert energy from engine waste heat to electricity and are on a path to commercialization. Several manufacturers intend to introduce thermoelectric generators in their cars later this decade in Europe and North America. Use of thermoelectric devices for vehicle occupant comfort heating or cooling is also being pursued as a more fuel efficient alternative to the conventional mobile air conditioning systems that use refrigerants. It is estimated that thermoelectrics can maintain single occupant comfort conditioning with about one-sixth of the energy used by conventional systems. In addition, conventional systems use the refrigerant gas R-134a, which has a warming potential that is 1,300 times that of carbon dioxide, the primary greenhouse gas. U.S. cars inadvertently release amounts of R-134a that is equivalent to about 41 million metric tons of carbon dioxide from compressor seal leakage and frontal vehicle collisions. Europe is already proscribing use of R-134a for vehicles.

FUTURE DIRECTIONS

Internal combustion engines have a maximum theoretical fuel conversion efficiency that is similar to that of fuel cells and considerably higher than the mid-40% peak values seen today. The primary limiting factors to approaching these theoretical limits of conversion efficiency start with the high irreversibility in traditional premixed or diffusion flames, but more practically the limits are imposed by heat losses during combustion/expansion, structural limits that constrain peak pressures, untapped exhaust energy, and mechanical friction. Emphasis must be placed on enabling the engine to operate near peak efficiency over a real-world driving cycle to improve vehicle fuel economy. For SI engines this means reducing the throttling losses with technologies such as lean-burn, high dilution, and variable geometry. Exhaust losses are being addressed by analysis and development of compound compression and expansion cycles achieved by valve timing, use of turbine expanders, regenerative heat recovery, and application of thermoelectric generators. Employing such cycles and devices has been shown to have the potential to increase heavy-duty engine efficiency to as high as 55%, and light-duty vehicle fuel economy by 35% to 50%.

Analyses of how "advanced combustion regimes" might impact the irreversibility losses have indicated a few directions to moderate reductions of this loss mechanism, but maximizing conversion of availability (or available energy) to work will require compound cycles or similar measures of exhaust energy utilization. The engine hardware changes needed to execute these advanced combustion regimes include variable fuel injection geometries, turbo- and super-charging to produce very high manifold pressures, compound compression and expansion cycles, variable compression ratio, and improved sensors and control methods. Larger reductions in combustion irreversibility will require a substantial departure from today's processes but are being examined as a long-range strategy.

Most of the basic barriers to high engine efficiency hold true for both gasoline- and diesel-based engines. Recognizing the dominance of gasoline-type SI engines in the U.S., VTP intends to increase emphasis on their improvement. Gasoline-based engines, including E85 flexible-fuel, can be made at least 20-25% more efficient through direct injection, boosting/downsizing, and lean-burn. Real-world fuel savings might be even higher by focusing attention on the road-load operating points.

Hydrogen engine efficiencies of roughly 45% have been demonstrated based on single-cylinder engine data. The underlying reasons for these impressive levels suggest a case study for applicability to other fuels.

Meeting anticipated future emission standards will be challenging for high efficiency diesel and lean-burn gasoline engines. To address this issue, research on innovative emission control strategies will be pursued through national laboratory and university projects designed to reduce cost and increase performance and durability of NOx reduction and PM oxidation systems. Project areas include development of low-cost base metal catalysts (to replace expensive platinum group metals), lighter and more compact multifunctional components, new control strategies to lessen impact on fuel consumption, and improved sensors and on-board diagnostics for meeting upcoming regulations. Furthermore, simulations of the catalyst technologies are being developed to enable industry to perform more cost-effective system integration during vehicle development. As advanced combustion approaches evolve and engine-out emissions become cleaner, the requirements of emission controls are expected to change as well.

The majority of lean-NOx emission controls development has been focused on diesel engines. With the potential introduction of high efficiency lean-gasoline engines, these technologies will require further research and development as well as emission controls for managing HC/CO emissions. Engine-out PM emissions from lean-gasoline engines, although lower in mass than the diesel engine, are also a concern and may require new processes due to differences in particle size and morphology.

Enabling technologies being developed by the Combustion and Emission Control R&D activity will address fuel systems, sensors, engine control systems, and other engine technologies. Fuel systems R&D focuses on injector controls and fuel spray development. Engine control systems R&D focuses on developing engine controls and sensors that are precise and flexible for enabling improved efficiency and emission reduction in advanced combustion engines. This also includes a better understanding of stochastic and deterministic in-cylinder processes which limit the speed/load range of many advanced

combustion strategies. Control system technologies will facilitate adjustments to parameters such as intake air temperature, fuel injection timing, injection rate, variable valve timing, and EGR to allow advanced combustion engines to operate over a wider range of engine speed/load conditions. Engine technologies development will be undertaken to achieve the best combination that enables advanced combustion engines to meet maximum fuel economy and performance requirements. These include variable compression ratio, variable valve timing, variable boost, advanced sensors and ignition systems, and exhaust emission control devices (to control hydrocarbon emissions at idle-type conditions) in an integrated system. Upcoming EPA onboard diagnostic requirements will be addressed through research on advanced sensors, improved understanding of emission control aging, and development of models that are integral to the diagnostic method. In FY 2011, VTP announced selection of four new projects for enabling technologies to improve engine efficiency and reduce emissions.

The Combustion and Emission Control R&D activity will continue to perform the critical role of elevating potential health issues related to advanced combustion engine technologies to the attention of industry partners and DOE/VTP management. It will ensure that vehicle technologies being developed will not have adverse impacts on human health through exposure to toxic particles, gases, and other compounds generated by these new engine technologies.

The Solid State Energy Conversion activity will continue on developing advanced thermoelectric generators for converting waste heat from engines directly into useful electrical energy to improve overall vehicle energy efficiency and reduce emissions. Effective use of waste heat from combustion engines would significantly increase vehicle fuel economy. In current gasoline production passenger vehicles, roughly over 70% of the fuel energy is lost as waste heat from an engine operating at full power. About 35 to 40 percent is lost in the exhaust gases and another 30 to 35 percent is lost to the engine coolant. There is an opportunity to recover some of the energy in the engine's waste heat using thermoelectric materials that will convert it directly to electricity for operating vehicle auxiliaries and accessories. Improving the energy conversion efficiency of thermoelectric materials directly supports the overall goals of improving the fuel economy of passenger and commercial vehicles. Achieving the vehicle-based performance goals requires reduction in the cost of thermoelectrics, scaling them up into practical devices, and making them durable enough for vehicle applications. The concept of a zonal, dispersed thermoelectric cooling system will continue to be pursued to provide occupant comfort cooling using about 630 W compared with the 3,500 to 4,000 W used by conventional mobile air conditioning systems. Air conditioning power reductions of greater than 70% are possible. In FY 2011, VTP announced three new awards for the development of advance thermoelectric generators for passenger vehicle application.

The remainder of this report highlights progress achieved during FY 2011 under the Advanced Combustion Engine R&D subprogram. The following 74 abstracts of industry, university, and national laboratory projects provide an overview of the exciting work being conducted to tackle tough technical challenges associated with R&D of higher efficiency, advanced ICEs for light-duty, medium-duty, and heavy-duty vehicles. We are encouraged by the technical progress realized under this dynamic subprogram in FY 2011, but we also remain cognizant of the significant technical hurdles that lay ahead, especially those to further improve efficiency while meeting the EPA Tier 2 emission standards and heavy-duty engine standards for the full useful life of the vehicles.

Gurpreet Singh
Team Leader,
Advanced Combustion Engine R&D
Vehicle Technologies Program

Roland M. Gravel
Vehicle Technologies Program

Kenneth C. Howden
Vehicle Technologies Program

John W. Fairbanks
Vehicle Technologies Program

James Eberhardt
Chief Scientist,
Vehicle Technologies Program

I.2 Project Highlights

The following projects highlight progress made in the Advanced Combustion Engine R&D subprogram during FY 2011.

ADVANCED COMBUSTION AND EMISSION CONTROL RESEARCH FOR HIGH-EFFICIENCY ENGINES

A. Combustion and Related In-Cylinder Processes

The objective of these projects is to identify how to achieve more efficient combustion with reduced emissions from advanced technology engines.

- Argonne National Laboratory (ANL) is studying the mechanisms of spray atomization by making detailed, quantitative measurements in the near-nozzle region of sprays from light-duty diesel injectors. In the past year they completed measurements of six of the 10 Engine Combustion Network (ECN) injectors and discovered significant differences between the nominally identical injectors. They also made the first ever X-ray measurements of the gas jets emerging from a hydrogen/natural gas direct injector. These measurements demonstrated the ability to quantify the jet density with high precision and time resolution. Such measurements will allow the fuel/air mixing in gas-fueled engines to be measured and quantified, and will help to achieve high efficiency with these clean-burning fuels. (Powell, ANL)

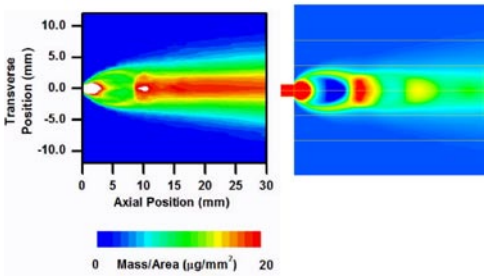

X-ray Measurements (left) and Computational Fluid Dynamics Simulations (right) of Gas Jets from a Hydrogen/Natural Gas Injector (Powell, ANL)

- Sandia National Laboratories (SNL) is developing the physical understanding to guide and the modeling tools to refine the design of optimal, clean, high-efficiency combustion systems. In the past year they demonstrated that the mean flow swirl structure in the General Motors (GM) 1.9-L engine is highly tilted, and that the structure is repeatable on individual cycles, insensitive to swirl ratio, and less variable at high swirl. They also established a quantitative fuel tracer laser-induced fluorescence (LIF) capability, applied the technique to characterize the mixture preparation process, and compared the measurements to model predictions. In addition, they analyzed the factors impacting the modeling of the temperature dependency of the CO LIF signal, enabling quantitative CO measurements for model validation, and developed a phenomenological picture of both early- and late-injection LTC systems describing the mixture formation and subsequent combustion process. (Miles, SNL)
- SNL is developing a fundamental understanding of how in-cylinder controls can improve efficiency and reduce pollutant emissions of advanced LTC technologies. In the past year they found that: (1) a narrow-angle injector shows no significant in-cylinder soot oxidation benefit with post injections, and has a detrimental effect on soot from the main injection, increasing the filter smoke number to 1.5 compared to 0.6 for narrow angle injector; (2) high-speed imaging shows how in-cylinder fuel reactivity gradients affect the in-cylinder progression of combustion, decreasing peak heat release rates by up to 60% with a properly tailored mixture field; (3) the combustion regimes, as defined by propensity for flame growth from artificial spark ignition, ranges from 20% of near the chamber center to almost 80% near the piston bowl wall; and (4) computer models predict that most of RCCI should be dominated by kinetics, but flame propagation can be important locally, especially near the piston bowl wall, similar to experimental observations with artificial spark ignition. (Musculus, SNL)
- SNL is leading a multi-institution, international, research effort on engine spray combustion called the Engine Combustion Network, or ECN, facilitating improvement of engine combustion modeling and accelerating the development of cleaner, more efficient engines. In the past year

they: (1) generated a detailed spray dataset working collaboratively with a dozen institutions from around the world; (2) organized and led the first ECN workshop, where multiple modeling groups submitted results for a side-by-side comparison to this experimental data; (3) demonstrated that the variable-radial-profile model of Musculus and Kattke accurately predicts fuel spray mixture fraction when the model is adjusted (with spreading angle) to match the measured penetration. Comparison with detailed computational fluid dynamics (CFD) modeling shows similar results; and (4) implemented nine different diagnostics at identical spray conditions, combined with rigorous light scattering/extinction analysis, to assess the liquid volume fraction near the liquid length. (Pickett, SNL)

- Oak Ridge National Laboratory (ORNL) is investigating potential near-term technologies for expanding the usable speed-load range and to evaluate the potential benefits and limitations of engine technologies for achieving HECC in a light-duty diesel engine. In the past year they demonstrated significant HECC load expansion across a wide engine speed and load range using RCCI (with a maximum load of 11 bar brake mean effective pressure at 3,000 RPM) and showed diesel-like efficiency or better (up to 5%) with an order of magnitude reduction in NOx across wide engine operating range. They also demonstrated successful RCCI operation with biodiesel and ethanol blends and found ethanol blends were effective for expanding RCCI operation to higher loads. (Curran, ORNL)

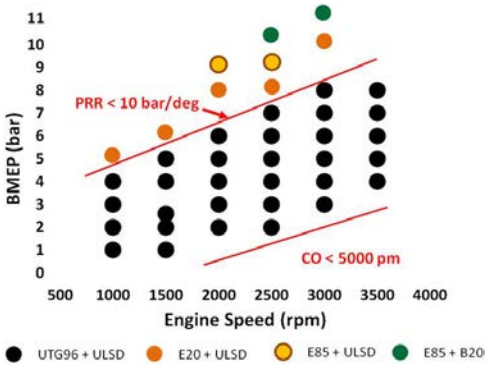

Operational range of RCCI with Self Imposed Limits and Expansion with Biofuels (Curran, ORNL)

- SNL is combining unique state-of-the-art simulation capability based on the large eddy simulation (LES) technique with Advanced Engine Combustion R&D activities to maximize benefits of high-performance massively-parallel computing for advanced engine combustion research. During the past year, SNL addressed critical barriers related to development of predictive models for clean high-efficiency engines using hydrocarbon-based fuels; provided a new LES model base for LTC technologies (i.e., understanding effects of fuel-injection, ignition-timing, heat-transfer and engine-geometry on fuel-air mixing, combustion, soot and emissions over a broad operating range); and established requirements for efficient and routine use of high-performance (exascale) computers with emphasis on development of predictive and affordable models for advanced engine combustion research. (Oefelein, SNL)
- Lawrence Livermore National Laboratory (LLNL) is working on the development and application of computationally efficient and accurate simulation tools for prediction of engine combustion. In the past year they completed implementation of the parallel multi-zone combustion model in two parallel computational fluid dynamics codes (KIVA4-mpi and OpenFOAM), completed a license agreement for the multi-zone combustion model with Convergent Science, Inc., developed a combustion chemistry solver for general purpose graphical processing units that are 11 times faster than conventional central processing unit-based solvers, and developed a new adaptively preconditioned solver for conventional architectures that speeds up combustion chemical kinetics simulation by as much two orders of magnitude compared to traditional approaches and is an order of magnitude faster than the best available commercial solver. (Flowers, LLNL)
- SNL is providing the fundamental understanding (science-base) required to overcome the technical barriers to the development of practical HCCI and HCCI-like engines by industry. In the past year they: (1) showed that the colder gases producing the thermal stratification in the bulk of the charge arise mainly from the cylinder head and piston-top surfaces; (2) discovered that the majority of colder regions in the bulk gas occur in the form of a turbulent structure attached to a wall, indicating that randomly occurring turbulent flows are the primary transport mechanism responsible for the thermal stratification; (3) demonstrated that significant improvements in the thermal efficiency of boosted HCCI could be obtained by using partial fuel stratification; (4) showed that partial fuel stratification also allows a substantial increase in the high-load limit of boosted HCCI over a range of boost pressures, for gasoline fueling; and (5) evaluated the effects of intake temperature on HCCI engine efficiency. (Dec, SNL)

- SNL is conducting acetylene seeding experiments in an automotive HCCI engine to identify ignition-enhancement effects of potential products of negative valve overlap (NVO) reformation. In the past year they improved engine data repeatability through an extensive rework of engine facility components and experimental protocols; quantified the enhancement effect of acetylene on main ignition during HCCI-NVO operation; characterized performance of tunable diode laser (TDL) absorption diagnostic for measuring CO concentration histories in the optical engine and published results in a journal article; and continued the validation of their KIVA engine model using HCCI-NVO experiment data and documented the results in a technical publication. (Steeper, SNL)
- ORNL is supporting DOE and industry partnerships in assessment of state-of-the-art and longer-term advanced engine and combustion technologies for future goal setting. They developed a technique for applying stretch recovery goals to each loss mechanism and evaluating the resulting redistribution of energy within the engine to evaluate the combined benefit of and potential interaction between various strategies for efficiency improvement, and demonstrated that greatest efficiency benefits are provided by strategies that improve work extraction with the piston or increase exhaust energy available to waste-heat recovery systems with other strategies only providing incremental efficiency improvements. (Edwards, ORNL)
- Los Alamos National Laboratory (LANL) is developing code and algorithms for the advancement of speed, accuracy, robustness, and range of applicability of the KIVA combustion modeling software to higher-order spatial accuracy with a minimal computational effort. They developed h-adaptive and hp-adaptive predictor-corrector split (PCS) using Petrov-Galerkin finite element methods for all for flow regimes, from incompressible to high-speed compressible and a two-dimensional overset grid method for moving and immersed actuated parts such as valves for robust grid movement. They also developed and verified the hp-adaptive finite element method framework that uses hierarchical basis for PCS mass, heat and momentum transport solver. (Carrington, LANL)

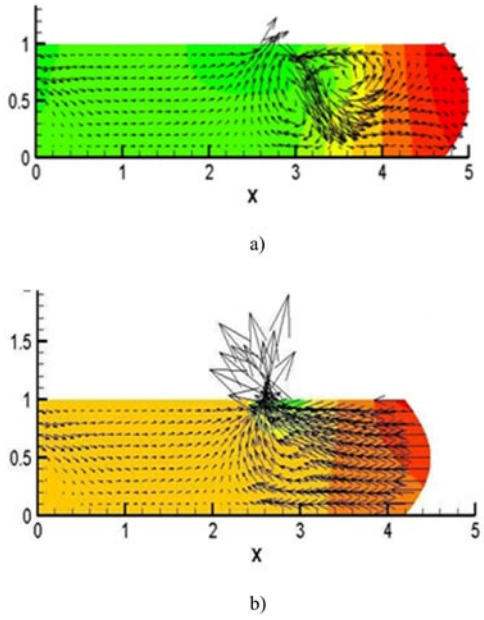

Immersed Moving Piston for PCS FEM System a) and b) Showing Displacement, Velocity Vectors (Carrington, LANL)

- LLNL is developing chemical kinetic models for conventional and next-generation transportation fuels that need to be developed so that engine simulation tools can predict fuel effects. In the past year they: (1) developed a chemical kinetic model for larger aromatics to expand the available components for gasoline surrogate fuels; (2) developed chemical kinetic models for new types of model compounds for iso-alkanes including 3-methyl heptane and 2,5-dimethyl hexane; (3) developed a new approach for formulating gasoline surrogate mixtures for real gasoline fuels and a reduced mechanism for a gasoline surrogate for CFD applications; and (4) developed a functional-group kinetics modeling approach for iso-alkanes that greatly reduces the size of the mechanism for use in multidimensional engine simulations. (Pitz, LLNL)
- SNL is designing a free-piston engine suitable for hybrid vehicle applications. Bounce chamber cylinders, air injection valves, vent manifolds, and pistons were all obtained and assembled in the past year. All mechanical components have now been acquired, and the engine is fully assembled except for the magnets. (Van Blarigan, SNL)
- ANL is assessing the efficiency potential and identifying efficiency/emissions trade-offs of advanced hydrogen internal combustion engine concepts with particular focus on hydrogen direct injection. In the past year they exceeded DOE technical target of 45% peak brake thermal efficiency (BTE) by demonstrating 45.5% BTE at 2,000 revolutions per minute (RPM) and 13.5 bar brake mean effective pressure (BMEP). They also calculated drive-cycle NOx emissions without aftertreatment

of 0.017 g/mile using vehicle simulations based on engine maps which are clearly below the Tier II Bin 5 (0.07 g/mile) target. (Wallner, ANL)

- ORNL is analyzing and defining specific advanced pathways to improve the energy conversion efficiency of internal combustion engines from nominally 40% to as high as 60%, with emphasis on opportunities afforded by new approaches to combustion. In the past year they initiated non-catalytic in-cylinder fuel reforming experiments with a range of fuels in the modified 2-liter GM Ecotec engine with variable valve actuation (VVA); initiated CFD simulations of in-cylinder water injection for exhaust heat recuperation with Reaction Design Fortè engine simulation platform; continued construction for the Regenerative Air Preheating with Thermochemical Recuperation (RAPTR) experiment at a reduced pace to accommodate faster progress on VVA engine experiments; and continued collaboration with the Gas Technology Institute on investigation of catalytic thermochemical recuperation for natural gas engines. (Daw, ORNL)

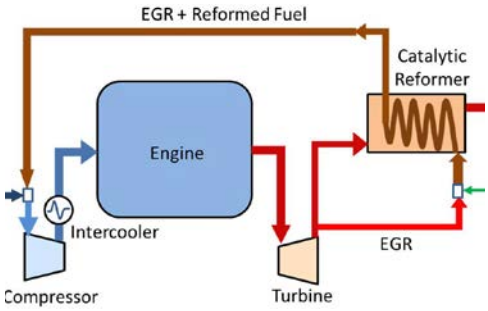

Schematic Representation of the Basic Approach used for EGR-Based Catalytic Thermo-Chemical Recuperation (Daw, ORNL)

- ANL is quantifying the influence of low-cetane fuel ignition properties to achieve clean, high-efficiency combustion, optimize the advanced controls available to create a combustion system that retains diesel-like efficiency while reducing NOx and other criteria pollutants compared to conventional diesel, and demonstrate the use of combustion imaging techniques to aid in determining the operational boundaries of gasoline compression ignition operation. In the past year they demonstrated high power density over a wide range of engine loads using 85 Research octane gasoline, found that control was possible primarily through fuel injection, and found that EGR was very effective in controlling NOx while having minimal fuel efficiency or CO/HC penalty. (Ciatti, ANL)
- ANL is supporting DOE VTP efforts to develop chemical mechanisms of various internal combustion engine fuels so as to gain a predictive capability of in-cylinder combustion and emissions formation. They have redesigned and improved various rapid compression machine (RCM) hardware and were able to achieve an isothermal zone uniform to within 10 K. Such an isothermal zone helps conduct chemical kinetic studies with high accuracy. They also developed a one-dimensional model to analyze RCM pressure data and designed and developed various auxiliary systems that enable testing on a variety of fuels, and helped obtain species concentrations that will serve as valuable metrics for chemical model validation. (Gupta, ANL)
- ORNL is expanding robust HCCI operation with advanced valve and fuel control technologies. In the past year they demonstrated an expansion of the HCCI low-load limit at 2,000 rpm to 160 kPa net indicated mean effective pressure ($IMEP_{net}$) with the combination of multiple fuel injection and valve deactivation; and demonstrated that fuel injection timing and the use of a pilot injection are effective at controlling combustion phasing under HCCI conditions. In many cases the fuel injection parameters offer sufficient control so that only limited variation in valve events is sufficient to change operating load; and showed that HCCI combustion provides a substantial fuel consumption improvement over conventional SI combustion over a load of 200 to 400 kPa $IMEP_{net}$ at 2,000 rpm. (Szybist, ORNL)
- ORNL is quantifying the fuel economy benefit and emissions impact of variable compression ratio (VCR) engine technology to a modern direct-injection gasoline engine. During the past year, the engine block, block bedplate and crankshaft support cradle were designed and casted. Test site preparations for the VCR engine were also completed. (Domingo, ORNL)
- ORNL is improving diesel engine-catalyst system efficiency through better combustion uniformity, engine calibrations and catalyst control. In the past year they applied mid-infra-red light-emitting diode-based CO_2 and fuel-in-oil diagnostics to engine development, improved an EGR-uniformity diagnostic, developed single-entry-point probe for engine measurements where line-of-sight

optical access is not possible, specified laser to enable simultaneous multi-point EGR fluctuation measurements, and applied fuel-in-oil instrument to alternative fuel engine to identify performance variations associated with different fuel-injector spray patterns. (Partridge, ORNL)

- ANL is identifying state-of-the-art engine and vehicle technologies currently in production to quantify the benefits of the state-of-the-art vehicle technologies currently in production, optimize vehicle performance using advanced vehicle level modeling, and accelerate the development of high efficiency internal combustion engines for light-duty vehicle applications, while meeting the future emission standards, using numerical simulations. In the past year they obtained two new vehicles and supplied vehicle data sets for the BMW 530i, Toyota Prius and Toyota Auris to the vehicle systems group for the USDRIVE goal setting exercise. (McConnell, ANL)
- Cummins Inc. is engaged in developing and demonstrating advanced diesel engine technologies to significantly improve the engine thermal efficiency up to 55% and will demonstrate tractor-trailer vehicles with 68% or greater freight efficiency improvement over a 24 hour cycle. In the past year they achieved >48% engine BTE and they completed design and analysis of tractor-trailer baseline aerodynamics and developed new concepts to attain >14% freight efficiency improvement. (Koeberlein, Cummins)
- Daimler Trucks will develop and demonstrate a Class 8, long-haul tractor-trailer which achieves a 50% vehicle freight efficiency improvement (measured in ton-miles per gallon) over a best-in-class 2009 baseline vehicle. In the past year they completed drive cycle tests with the baseline vehicle configuration, developed roadmap of vehicle efficiency metrics needed to achieve 50% vehicle freight efficiency, based on vehicle-level efficiency simulation and analysis, developed roadmap for 50% engine thermal efficiency at road load, conducted air system and turbo-matching simulations at multiple engine-out emission levels, developed model-based engine controller concept with on-board fuel efficiency optimization, and developed a model for the exhaust and EGR-driven Rankine heat engine. (Rotz, Daimler Trucks North America LLC)
- Navistar is demonstrating engine BTE improvements which contribute 20% (of the total 50% required) improvement in the freight efficiency of a combination tractor-trailer. In the past year they built and validated a comprehensive engine simulation model for the Maxxforce 13 diesel engine using GT-POWER that incorporated advanced components such as VVA, turbocompounding, and Rankine cycle; built an engine combustion model using KIVA that helped improve combustion matching with improved fuel efficiency and reduced soot emissions; and built multiple prototype engines to validate the performance of individual subsystems. (Jadin, Navistar)
- Volvo Powertrain North America is identifying concepts and technologies that have potential to achieve 55% BTE on a heavy-duty diesel engine as defined in the SuperTruck project. This project so far has completed a literature review on fuels and chemical mechanisms that are of interest for high-efficiency combustion in compression-ignition engines; completed “version 0” of the combustion model probability density function code; and completed Organic Rankine Cycle testing to expand the maximum efficiency and operating range, and improve low speed and low load operation. (Amar, Volvo Powertrain North America)
- Delphi will develop, implement and demonstrate fuel consumption reduction technologies using a new LTC process; gasoline direct injection compression ignition (GDCI). In the past year they tested a battery-aided start system, researched roller bearings for the crankshaft and camshaft, determined that HCCI had too limited range for this application, and tested various injection strategies as part of GDCI. (Confer, Delphi Automotive Systems LLC)
- Ford will demonstrate 25% fuel economy improvement in a mid-sized sedan using a downsized, advanced gasoline turbocharged direct injection engine with no or limited degradation in vehicle level metrics. In the past year they completed a computer-aided design of a new multi-cylinder engine, initiated component and

Phase 1 Engine with Project Specific Hardware (Confer, Delphi)

systems orders to support multi-cylinder engine builds, and generated data to design and develop the advanced lean-combustion capability. (Wagner, Ford Motor Company)

- General Motors will demonstrate 25% vehicle fuel economy improvement through lean-gasoline combustion while achieving Tier 2 Bin 2 emissions. In the past year they installed and conducted tests on lean-gasoline engine and aftertreatment systems in dynamometers and vehicles, generated initial torque-based engine controls and calibration that enables vehicle operation in lean stratified mode to 55 mph, demonstrated the passive SCR lean-gasoline aftertreatment system capability for NOx conversion efficiency of 68.5% and achieved vehicle highway fuel economy goal of greater than 13% improvement by utilizing single-cylinder fuel consumption data and vehicle simulation. (Smith, General Motors Company)
- Chrysler aims to demonstrate 25% improvement in combined Federal Test Procedure City and Highway fuel economy for the Chrysler minivan. In the past year they completed the Alpha 1 engine design, completed finite element analysis tasks, completed three-dimensional CFD simulation of the designed intake manifold to identify the most efficient air handling system, completed technology review and benchmarking survey, completed design and system layout of the thermal management system, and blocks were designed, procured, assembled and tested. (Reese, Chrysler Group LLC)
- Robert Bosch LLC is improving fuel economy by 30% with minimum performance penalties. In the past year they: completed the design, procurement, and building of the Prototype I engine and its engine management system hardware for multi-mode combustion; defined the engine management system hardware, software and overall control architecture to enable multi-mode combustion; demonstrated fuel economy potential of the supercharger/turbocharger-boosted HCCI combustion strategy over the baseline port fuel injected V-6 engine at selected operating points; and demonstrated the engine management system performance for HCCI controls at the engine dynamometer. (Yilmaz, Robert Bosch)
- Cummins is demonstrating 40% fuel economy improvement over a baseline gasoline V-8 pickup truck and Tier 2 Bin 2 tailpipe emissions compliance. In the past year, they defined technical requirements for the new engine architecture and aftertreatment effectiveness; model validation of low-pressure exhaust gas recirculation fuel consumption and NOx emission benefits required to achieve engine-out emissions and base engine fuel economy targets was completed; and model validation of vehicle drive cycle and fuel economy on baseline diesel was completed. (Ruth, Cummins, Inc.)
- Ford is focusing on complete and optimal system solutions to address boost system challenges, such as efficiency degradation and compressor surge, etc., in diesel combustion/emission control system development, and to enable commercialization of advanced diesel combustion technologies, such as HCCI/LTC. The turbo assembly with active casing treatment was tested on an engine dynamometer during 2011, which demonstrated 3% brake specific fuel consumption improvement at part load and full load, along with 90 horsepower increase in rated power over the base turbocharger. The numerical results indicate an additional 5% improvement in efficiency is possible, with much wider operational range, compared with a scaled-down version of a large compressor. (Sun, Ford)

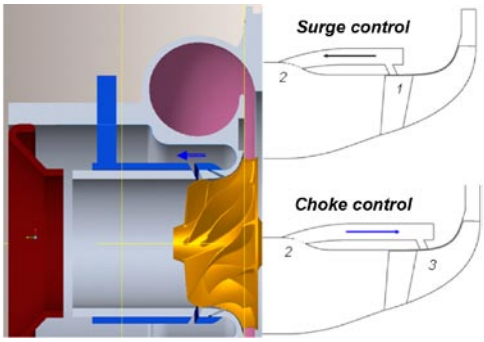

Compressor with Active Casing Treatment that Uses Two Different Slots to Control Surge and Choke Separately (Sun, Ford)

B. Energy-Efficient Emission Controls

The following project highlights summarize the advancements made in emission control technologies to both reduce emissions and reduce the energy needed for emission control system operation.

- PNNL is developing improved modeling capabilities for SCR and DPFs through fundamental experiments. In the past year they: updated PNNL's SCR model for the state-of-the-art commercial

Cu-zeolite SCR catalyst to extract kinetic parameters and to quantitatively describe the effects of hydrothermal aging; examined the effects of hydrothermal aging on the physicochemical properties and SCR reactions using the commercial Cu catalyst in collaboration with ORNL; and investigated the nature of Cu species and obtained kinetic parameters for small-pore zeolite-based Cu SCR catalyst. (Lee, PNNL)

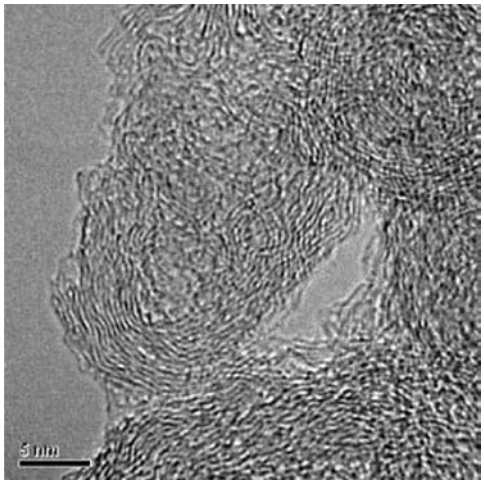

Transmission Electron Spectroscopy of Diesel Soot after Partial Oxidation in Oxygen Showing Pitting on Primary Particle Surfaces (Lee, PNNL)

- PNNL is developing a fundamental understanding of candidate next-generation LNT materials for NOx after-treatment for light-duty lean-burn (including diesel) engines. Results obtained this year demonstrate that direct NO decomposition is not applicable for the real system. When K is used as storage element, the maximum temperature is shifted to 400ºC or higher, depending on the support. PNNL studies demonstrated that a $MgAl_2O_4$ support material provided especially promising NOx uptake performance. Additionally, the characteristics of a fully formulated NOx storage and reduction catalyst supplied from Johnson Matthey were investigated after applying SO_2 and thermal treatments. (Peden, PNNL)
- ORNL is assessing and characterizing catalytic emission control technologies for the reduction of NOx from lean-gasoline engines and identifying strategies for cost reduction of emission controls for lean-gasoline engines. In the past year they distributed a database of exhaust emissions from a modern lean-gasoline engine vehicle including the reductant chemistry for LNT regeneration processes to modeling community via the Cross-Cut Lean Exhaust Emissions Reduction Simulations group, and analyzed the chemical processes occurring in a LNT catalyst specific to high NOx concentration and temperature conditions associated with the lean-gasoline engine application. (Parks, ORNL)
- SNL is identifying a set of microkinetic surface reactions that can account for the observed behavior of a LNT during a complete storage/regeneration cycle. In the past fiscal year, SNL developed a new NOx storage and release mechanism and showed that it could be used to simulate their experimental data set as well as the mechanism proposed previously, modified the overall mechanism to allow for the suppression of ammonia production during short cycles, upgraded their reactor code to account for boundary layer mass transfer and showed that this phenomenon was of minor but not negligible importance, and upgraded their reactor code with a complete energy equation and demonstrated that the simulation of exotherms during a storage/regeneration cycle could be done successfully only if axial heat transfer along and away from the tube wall were included. (Larson, SNL)
- ORNL completed a Cooperative Research and Development Agreement (CRADA) with Navistar, Inc. to develop engine/aftertreatment system configurations and control strategies that meet stringent emissions regulations while improving overall vehicle efficiency. In the last year of the CRADA, they devised an O_2 chemisorption method for measurement of the active surface area of soot loaded on a filter, conducted isothermal pulsed oxidation experiments to measure the rates of soot oxidation over both a catalyzed and an uncatalyzed miniature DPF, and developed rate laws and associated parameters that capture the oxidation kinetics measured in the pulsed oxidation experiments. (Pihl, ORNL)
- ORNL is investigating methods for improving performance and/or durability of LNTs and improving the fundamental understanding of deactivation mechanisms that result during the regeneration of LNTs. In the past year they synthesized and evaluated additional formulations of Ca+Ba LNT catalysts, illustrated ceria addition to alumina in conjunction with Ba leads to a highly active NOx storage and reduction catalyst, and designed and built diffuse reflectance infrared Fourier-transform spectroscopy reactor for spatially resolved analysis of adsorbates on monolithic catalysts, allowing for both gas and surface analysis. (Toops, ORNL)

- ORNL is improving diesel engine-catalyst system efficiency through better combustion uniformity, engine calibrations and catalyst control. In the past year they: (1) characterized distributed performance of model Cu-Beta catalyst under standard SCR conditions and at three temperatures (200, 325 and 400°C); (2) characterized the impact of hydrothermal (HT) ageing on the distributed performance of the same Cu-Beta SCR catalyst; (3) enabled transient analysis determination of distributed catalyst NH_3 capacities via development of analysis methodologies accounting for transient instrument response; and (4) determined that the full NH_3 catalyst capacity is used within the SCR zone for degreened and HT aged samples. (Partridge, ORNL)
- ORNL is assessing the relative merits of meeting emission regulations via catalytic aftertreatment or advanced combustion for diesel engines capable of operating in multiple combustion modes ("multi-mode" engines). In the past year they demonstrated that oxidation catalysts effectively control particulate matter emissions from RCCI combustion for particulate sizes less than 23 nm (oxidation not effective above 23 nm size range); characterized low temperature oxidation performance of Nanostellar diesel oxidation catalysts under PCCI operating conditions; and demonstrated the reversibility of hydrocarbon fouled Cu- and Fe-zeolite SCR catalysts from both conventional and PCCI combustion, and identified the chemical nature of the hydrocarbon species causing the fouling to occur. (Parks, ORNL)

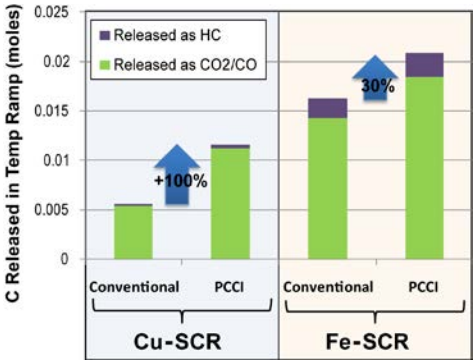

Summary of total C released in $CO+CO_2$ and HC forms from Cu-SCR and Fe-SCR catalysts after exposure to both conventional and PCCI exhaust. (Parks, ORNL)

- ORNL continued to co-lead the Cross-Cut Lean Exhaust Emission Reduction Simulation (CLEERS) Planning Committee and facilitation of the SCR, LNT, and DPF Focus group telecoms with strong domestic and international participation. In the past year they conducted another survey of the Cross-Cut companies and collaborating suppliers to identify updated technical priorities for emissions controls and CLEERS activities; continued to advise and adjust current DOE national lab projects associated with CLEERS to bring them into closer alignment with the updated CLEERS industry partner priority surveys; provided regular update reports to DOE Advanced Combustion Engine Cross-Cut Team; organized the 2011 CLEERS workshop at University of Michigan, Dearborn on April 19–21, 2011; and maintained the CLEERS website (www.cleers.org) including functionalities, security, and data to facilitate web meetings and serve focus group interactions. (Daw, ORNL)
- ORNL is collaborating with SNL and PNNL to produce kinetic information for LNT and urea-SCR aftertreatment devices, both as individual and system integrated components as part of the CLEERS project. In the past year they (1) continued systematic experimental measurements of LNT regeneration chemistry with an emphasis on resolving the effects of different reductants and the spatiotemporal distribution of key reactions; (2) combined experimental lab reactor measurements and modeling results to confirm that reduction of nitrates by intermediate NH_3 is a major source of N_2O in LNTs; (3) continued collaboration with SNL, the Institute of Chemical Technology Prague, and Chalmers University of Technology in LNT modeling and with PNNL in SCR modeling; (4) in collaboration with PNNL revised the CLEERS laboratory transient SCR catalyst characterization protocol to improve its relevance to extraction of key kinetic parameters; and (5) evaluated the impact of hydrothermal aging on a commercial copper zeolite SCR catalyst and identified two distinct types of NH_3 storage sites. (Daw, ORNL)
- ANL is characterizing the oxidation behavior of diesel PM emissions in terms of heat release and oxidation rate. In the past year they measured pore size distributions and pressure drops for three different DPF membranes with different amount of catalytic coating, evaluated kinetic parameters governing the oxidation of surrogate soot, defined the effects of ambient experimental conditions and analytical methodology on kinetic parameters, and characterized the morphology of soot particles from LTC with biofuels. (Lee, ANL)

- PNNL is developing a fundamental understanding of the integration of SCR and DPF technologies for on-road heavy-duty vehicle application. In the past year they identified that the downstream portion of the filter within the wall microstructure is the optimum location for SCR catalyst loading for maximizing NOx reduction efficiency while minimizing pressure drop (with loaded soot), identified that on high-porosity cordierite, it is not advantageous to load additional SCR catalyst past ~90 g/L, and identified an optimum SCR catalyst loading target for facilitating maximum passive soot oxidation in the integrated device while retaining maximum NOx reduction efficiency. (Rappe, PNNL)
- PNNL and their CRADA partner Ford are developing an understanding of the deactivation mechanisms of the urea-SCR catalyst used in diesel aftertreatment systems. In the past year they: completed studies of the differing effects of SO_2 to SO_3, including identification of the mechanism of poisoning by SO_3; characterized the nature and distribution of phosphorus deposits observed on engine-aged urea-SCR catalysts; performed studies aimed at an understanding of unusual hydrothermal aging of zeolite-based urea-SCR catalysts observed at Ford; investigated the physicochemical properties of model zeolite materials with respect to hydrothermal aging; and evaluated the effects of physicochemical properties of model zeolite materials on the adsorption and desorption of ethanol. (Peden, PNNL)
- PNNL is characterizing exhaust particulates from advanced combustion engines such as spark ignition direct injection (SIDI) using readily available fuel blends and using insight gained and prior experience with diesel aftertreatment to jump-start development of optimum aftertreatment technologies. In the past year they characterized soot from a developmental SIDI engine with respect to size distribution, particle morphology, and composition; evaluated the suitability of current exhaust filter technologies for SIDI applications; and developed modeling tools to assist in the development and evaluation of SIDI exhaust filter systems. (Stewart, PNNL}

C. Health Impacts

The Health Impacts activity studies potential health issues related to new powertrain technologies, fuels, and lubricants to ensure that they will not have adverse impacts on human health. The following are highlights of the work conducted in FY 2011.

- ORNL is striving to understand the potential impact of developing fuel, combustion, and aftertreatment technologies on air quality and, thereby, human health. In the past year they completed analysis of PM emissions from both stoichiometric and lean-burn direct-injection SI vehicles operating on gasoline and ethanol blends (E0, E10 and E20), completed measurements of PM emissions from an advanced direct-injection SI engine operating on gasoline-ethanol blends, and completed PM emissions characterization for an engine operating in dual-fueled RCCI. (Storey, ORNL)
- NREL concluded the Collaborative Lubricating Oil Study on Emissions project. The objective of this project was to quantify the relative contributions of fuels and engine lubricating oil on PM) and semi-volatile organic compound emissions from in-use motor vehicles fueled with gasoline, E10, diesel, biodiesel, and natural gas while operating with fresh and used crankcase lubricants. All vehicle emission testing has been completed and final emissions testing results have been published. (Clark, NREL)
- The Health Effects Institute is conducting the Advanced Collaborative Emissions Study to characterize the emissions and assess the safety of advanced heavy-duty diesel engine

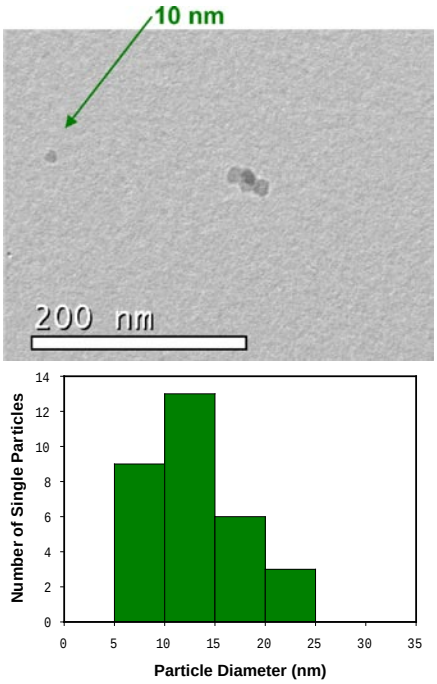

The number and size of single solid particles (non-aggregate soot) analyzed by transmission electron microscopy. The most abundant size was 10-15 nm. Fuel injection was optimized for low particle number emissions. (Storey, ORNL)

and aftertreatment systems and fuels designed to meet the 2007 and 2010 emissions standards for PM and NOx. In the past year they found that there were no exposure-related differences in mortality or clinically-evident morbidity in mice or rats after one or three months of exposure. The primary importance of these early interim results is their demonstration that: 1) the great majority of health tests showed no effect of exposure; 2) several plausibly coherent responses may indicate early, exposure-related, subclinical impacts on lung inflammation, structure, and function of rats; 2) statistically significant effects were observed primarily at the highest exposure level (the lowest level has produced no observable effects to date); and 3) mice are less responsive than rats to three months of exposure. (Greenbaum, Health Effects Institute)

Solid State Energy Conversion

Several projects are being pursued to capture waste heat from advanced combustion engines in both light- and heavy-duty vehicles using thermoelectrics (TEs). Following are highlights of the development of these technologies during FY 2011.

- BSST, LLC is developing a high-efficiency TE waste energy recovery system for passenger vehicle applications. In the past year a fully functional high temperature cylindrical thermoelectric generator (TEG) was built using improved tooling with minor design modifications over the 2010 prototype and tested at Amerigon. TEGs were fitted into BMW and Ford vehicle exhaust systems and operated over extended periods of time including over 3,000 miles of road testing by BMW. The TEG-equipped exhaust systems performed as predicted by the simulation tools developed for the project (a key result) and demonstrated a level of robustness, evidenced by day-over-day repeatable performance that exceeded the expectations of the project partners. (LaGrandeur, BSST)

BMW X6 TEG Installation, Courtesy of the BMW Group (LaGrandeur, BSST)

- General Motors is identifying distributed cooling and heating strategies that can efficiently augment or replace a vehicle's central heating, ventilation and air conditioning (HVAC) system by delivering localized cooling/heating of key human body segments that strongly influence an occupant's perceived thermal comfort. In the past year they: (1) updated the University of California, Berkeley Thermal Comfort model for the localized cooling and heating of vehicle occupants and correlated the model's predictions with the test responses of a thermal mannequin and human subjects; (2) compiled climatic wind tunnel test results and modeling analyses to identify the final set of distributed cooling and heating locations for further development into prototype local cooling/heating components; (3) released and validated a personal computer-based computer-aided engineering tool that uses the updated thermal comfort model and CFD models of vehicle interiors to forecast the performance of future HVAC system configurations that feature energy-saving local cooling/heating components; and (4) completed an initial design concept for a TE device with the potential to heat the passenger compartment of the Chevrolet Volt using less electricity, which would increase the Volt's effective electric-only range during cold weather conditions. (Gundlach, General Motors)
- Ohio State University is developing high-efficiency high figure of merit (zT) thermoelectric materials (PbSe and Mg_2Sn) that contain no rare or precious elements, and are non-toxic. In the past year they: attained a new high zT value for n-type PbSe reaching zT=1.2; used indium as a dopant, but determined indium is not a resonant impurity level; experimental data for galvanomagnetic and thermomagnetic properties gathered/analyzed; and an initial literature study of Mg_2Sn revealed several previously unnoticed properties that theoretically predict may lead to a new approach to obtaining high efficiencies in this material. (Heremans, Ohio State University)
- Purdue University is enabling the broad adoption of TE waste heat recovery systems, or TEGs, at a scale commensurate with the global vehicle manufacturing enterprise. In the past year they: proved that filling in skutterudites can provide new channels for phonon scattering which can significantly

reduce thermal conductivity of skutterudites; identified complex metal oxides as potential candidates for high-temperature TE energy harvesting; developed a strategy for manipulating the electronic properties of ScN semiconductor layers (via Al and Mn alloying) in order to effectively tune the barrier height of metal-semiconductor superlattices for optimized TE performance; and successfully synthesized carbon nanotubes (CNTs) on copper foil, alumina, and graphitic material and increased TE power generation by 40%. (Xu, Purdue University)

- Stanford is performing systems-level modeling and full device-scale characterization, with the ultimate goal of constructing a complete architecture for optimizing a TEG system for recovering waste heat from automobile combustion. In the past year they: developed CNT-based thermal interface material (TIM) tape technology that improves the reliability and performance of TEGs; developed in situ measurement techniques and tools for characterization and reliability testing of TEG devices using high resolution infrared thermometry; measured the thermal transport properties of TE pellets and interfaces; designed and are manufacturing a rig for in situ characterization of TE pellets and TIMs up to 800 K; and completed extensive mechanical and thermal characterization of stand-alone CNT films using nano/picosecond thermoreflectance and atomic force microscopy nanoindentation techniques. (Goodson, Stanford)
- Stony Brook University successfully obtained single-phase higher manganese silicide using melt-spinning and successfully demonstrated thermal spray of silicide materials. They obtained reasonable thermal and electrical property of sprayed Mg_2Si, and identified that the key challenges are to reduce oxides in the deposited material and improve the Seebeck coefficient. They are also developing three-dimensional TEG fabrication techniques using thermal spray and laser cutting. (Zuo, Stony Brook University)
- Texas A&M is synthesizing inorganic nanowires and quantum wires of both $CoSb_3$ and InSb, and organic conducting polymer thin films, and assembling them into inorganic-organic hybrid TE cells with sizes ranging from a few mm^2 to a few cm^2, using conjugated linker molecules to tether the nanowires to each other or to conducting polymer thin films. In the past year they synthesized pristine InSb nanowires, devoid of any oxide, and phase-pure $CoSb_3$ skutterudite nanowires, without any CoSb and $CoSb_2$ phase contaminants. They also determined the effect of nanowire morphology on the thermoelectric performance of an additional material, namely Zn_3P_2. (Vaddiraju, Texas A&M)

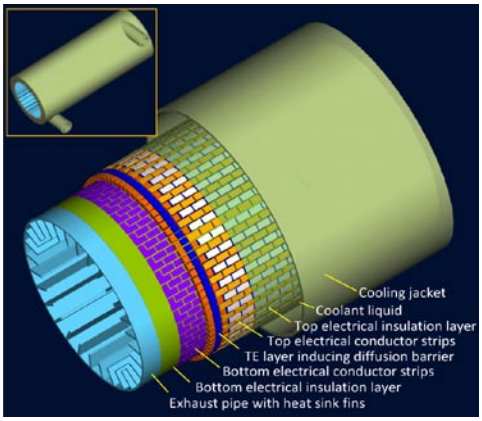

System driven approach to the vehicle TEG: materials are directly deposited onto automotive exhaust component, and integrated heat sink removes exhaust heat and redirects to multilayer conformal thermoelectric device layer. (Zuo, Stony Brook University)

- The University of California, Los Angeles is developing novel materials and interfaces for improved thermomechanical reliability of TE vehicle exhaust waste heat harvesting devices. In the past year they successfully synthesized ZrW_2O_8 powders with isotropic negative thermal expansion coefficients, demonstrated successful production of Ag-based nanocomposites with variable coefficients of thermal expansion from approximately 7 to 15 ppm/°C, and characterized the thermal and electrical transport properties of the composites and achieved values comparable to those of aluminum. (Ju, University of California, Los Angeles)
- The University of California, Santa Cruz, is developing novel TE materials based on abundant and non-toxic Zintl phase magnesium silicide alloys and optimizing the TE power factor and figure of merit by band engineering and electron filtering. In the past year they conducted low temperature synthesis and spark plasma sintering of n-type Mg_2Si with embedded Si nanoparticles and completed characterization and transport modeling. (Shakouri, University of California, Santa Cruz)
- The University of Texas at Austin is increasing the zT of abundant silicide materials to a level competitive with the state of the art found in materials containing much more scarce and expensive elements, and enhancing the thermal management system performance for silicide TE devices

installed in a diesel engine. In the past year they demonstrated the synthesis of manganese silicide (HMS) via solid state reaction, cold press, and annealing; attained bulk-size (20 mm diameter and 5-8 mm thickness) HMS pellets via solid state reaction and spark plasma sintering; achieved thermal conductivity reduction by up to a factor of three in the polycrystalline HMS samples compared to single-crystal HMS; succeeded in Ru substitution to increase the Seebeck coefficient of HMS by 30% at room temperature and below; established a combined heat exchanger and TE device model for optimizing system design; and designed, fabricated, and measured a heat exchanger for verifying the heat transfer computation model. (Shi, University of Texas at Austin)

- Virginia Tech is fabricating and characterizing new TE materials growth with techniques capable of producing large quantities of efficient, yet non-toxic and inexpensive elements capable of long-term operation at high temperatures over thousands of thermal cycles. In the past year they (1) demonstrated feasible isostatic pressing processes capable of making TE elements of various shapes and sizes with minimal wasted material; (2) successfully fabricated N-type Mg silicide TE materials with zT >0.3 from 150-300°C, with performance per raw material cost twice that of state-of-the-art Pb-Te materials; (3) demonstrated that heat exchangers based on swirl jet impingement can reduce cold side TE element temperatures by 6-8°C, leading to efficiency gains of ~0.25%; and (4) synthesized nanostructured ZnO materials, characterized the TE properties, and developed structure-property relationships for Al-modified ZnO. (Huxtable, Virginia Tech)
- The University of Wisconsin-Madison is synthesizing nanostructured abundant HMS in bulk with enhanced TE performance for TE applications. In the past year they attained optimal conditions for the conversion of Si nanoparticles (NPs) to HMS using Mn and $MnCl_2$ vapor, extended the HMS conversion approach using Si NPs to using electrochemically etched Si nanowires (NWs), and minimized the formation of impurity silicide phases by optimizing conditions and using Si NWs. (Jin, University of Wisconsin-Madison)
- The University of California, Davis is developing novel TE materials based on abundant and non-toxic Zintl phase magnesium silicide alloys. In the past year they completed low temperature synthesis and spark plasma sintering of n-type Mg_2Si with embedded Si nanoparticles, and completed characterization and transport modeling. (Kauzlarich, University of California, Davis)
- Virginia Polytechnic Institute and State University is developing an interface bonding metallurgy between TE elements and heat exchangers with an electrical contact resistance smaller than 10-5 Ω cm^2 and a thermal contact resistance smaller than 10^{-3} K W^{-1} cm^2. In the past year they: characterized the surface roughness of deposited Ag/Ti coating on silicon substrate; attained the diffusivity of Ag in Ti at 500°C to be $2\times10^{-15}cm^2/s$; obtained uniform bonding layer of sintered nanosilver paste without large-scale voids and cracks using a low-temperature, low-pressure processing profile; and developed a nanosilver sintering process for bonding on bare copper in nitrogen atmosphere. (Lu, Virginia Polytechnic Institute and State University)
- Northwestern University is doing materials research (led by Ohio State University and Northwestern University) to develop advanced TE materials made from earth-abundant,

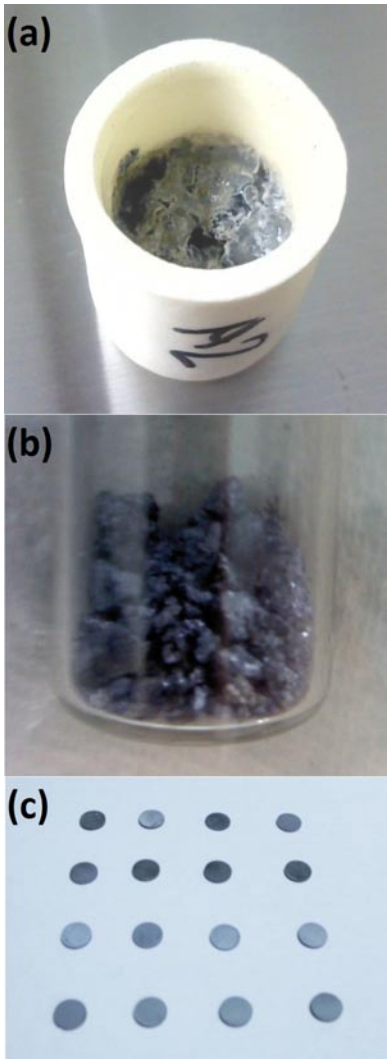

Mg-Silicide Thermoelectric Materials (a) crucible containing doped Mg-silicide elemental materials, (b) granules of the Mg-silicide materials, (c) hot-pressed pucks of N-type Mg-silicide TE elements. (Huxtable, Virginia Tech)

geographically dispersed elements and compounds. In the past year they reduced the lattice thermal conductivity of PbS greatly by adding selected metal sulfide phases. The thermal conductivity at 723 K was reduced by ~50%, 52%, 30% and 42% through introduction up to 5.0 mol% Bi_2S_3, Sb_2S_3, SrS and CaS, respectively. They also achieved lattice thermal conductivity of 0.6 W/m-K at 900 K for a sample of n-type PbS containing Bi_2S_3 nanostructures. (Mercouri, Northwestern University)

University Research

- The University of Michigan (UM) is exploring new high-pressure lean-burn combustion that can enable future gasoline engines with 20-40% improved fuel economy and determining the fuel economy benefits of engines and engine cycles designed to utilize advanced combustion modes. In the past year they: (1) extended the thermodynamic cycle analysis for engines to include effects of turbochargers; (2) autoignition times for gasoline-air mixtures were determined in an RCM for varying equivalence ratio and nitrogen dilution (EGR surrogate); (3) the computational singular perturbation analysis to identify ignition regimes for stratified mixtures has been extended to investigate autoignition of n-heptane/air mixture in the presence of temperature and composition inhomogeneities; (4) in studies of mixing using the Reynolds averaged Navier-Stokes approach it was found that the transport equation for the mixture fraction variable must incorporate the differential diffusion terms that has been commonly neglected for the sake of simplicity; and (5) new image analysis tools have been developed for rapid and automated processing of optical engine imaging data into quantitative metrics on ignition and flame propagation in HCCI and spark-assisted HCCI systems. (Woolridge, UM)

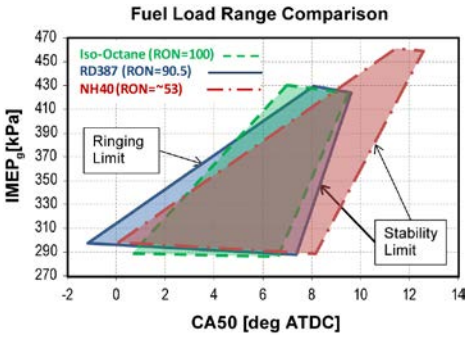

Effect of Octane Number on HCCI Gasoline Maximum Load and Combustion Phasing (Woolridge, UM)

- The University of Wisconsin is developing high efficiency internal combustion engines with goals of improved fuel economy by 20-40% in light-duty and 55% BTE in heavy-duty engines. In the past fiscal year, they improved the thermal efficiency over the stock light-duty engine achieved without the need for NOx and PM after-treatment using dual-fuel RCCI combustion. They also validated combustion and realistic fuel vaporization submodels developed for biofuels and gasoline/diesel surrogates for engine optimization and concept evaluation. (Reitz, University of Wisconsin)
- Michigan State University (MSU) is demonstrating an SI and HCCI dual-mode combustion engine for a blend of gasoline and E85 (85% ethanol and 15% gasoline) for the best fuel economy. In the past year they: (1) completed target fuel injector droplet size study for different blends of fuels from gasoline to E85; (2) the SI combustion optical test was completed and the test results will be used to compare to HCCI and SI-HCCI combustions in the future; (3) the target engine head was redesigned to fit two-step valve and electrical cam phasing systems and the modification of the target head assembly is completed; and (4) hardware-in-the-loop simulation results confirm that smooth mode transition between SI and HCCI can be achieved for an engine equipped with a two-step valve and electrical cam phasing systems. (Zhu, Michigan State University)
- The University of Houston is identifying the NOx reduction mechanisms operative in LNTs and in situ SCR catalysts, and using this knowledge to design optimized LNT-SCR systems in terms of catalyst architecture and operating strategies. In the past year they found that synthesis of double-layer SCR and LNT/SCR catalysts show the potential for novel catalyst compositions and architectures for improved performance. A double-layer Fe/Cu-based SCR catalyst exhibits significant expansion in the temperature window for which high NOx conversion is obtained. Initial findings with double-layer LNT/SCR catalysts reveal potential for further improvements in terms of NOx conversion, N_2 selectivity, and precious metal utilization. (Harold, University of Houston)

- The University of Connecticut is developing three-dimensional composite nanostructures for lean-NOx emission control devices. In the past year they: (1) successful synthesized and characterized three-dimensional metal oxide nanowire/rod arrays (such as ZnO and TiO_2, etc.) on both planar and monolith substrates; (2) successfully fabricated and characterized the Pt-deposited three-dimensional composite nanowire/rod array (such as ZnO/(La,Sr)CoO_3(LSCO) and TiO_2/(La,Sr) MnO_3(LSMO), etc.) on both planar and monolith substrates; (3) investigated the thermal and mechanical stability, CO and NO oxidation performance of the above-mentioned three-dimensional nanostructures; and (4) investigated the oxygen interactions with perovskite (such as [La,Sr] MnO_3[LSMO], etc.) surfaces by the first principle thermodynamics and kinetic Monte Carlo simulations. (Gao, University of Connecticut)
- Michigan Technological University developing experimentally validated DOC, DPF and SCR models with real-time internal state estimation strategies that support future onboard diagnostics, advanced control system, and system optimization objectives for DOC-DPF-SCR aftertreatment systems that minimize the energy penalty of meeting emission regulations. In the past year they: (1) developed a reduced order SCR model for Fe-zeolite SCR and calibrated against Fe-zeolite reactor data from ORNL; (2) completed passive oxidation tests using ultra low sulfur diesel (ULSD), 10 percent biodiesel blended fuel (B10) and 20 percent biodiesel blended fuel (B20); (3) determined activation energy for ULSD, B10, and B20 with the corresponding pre-exponential factors that correlate with the experimental PM active regeneration data; and (4) enhanced a high-fidelity one-dimensional catalyzed particulate filter model for reduced order model/state estimation. (Johnson, Michigan Technological University)

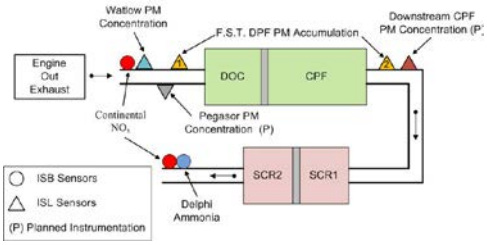

Sensor Utilization on the Cummins 2010 6.7-L ISB and 2007 8.9-L ISL (ISB Aftertreatment Components: DOC, CPF, SCR; ISL Aftertreatment Components: DOC and CPF) (Johnson, Michigan Technological University)

I.3 Honors and Special Recognitions/Patents

HONORS AND SPECIAL RECOGNITIONS

1. Welcoming Address and Executive Panel Discussion Moderator, *2011 Joint JSAE/SAE International Powertrain Fuels and Lubricants Conference, August 30 – Sept. 2, 2011, Kyoto, Japan* (Paul Miles, SNL).

2. Invited Talk: "Quantitative In-Cylinder CO Measurements in Engines," *Gordon Research Conference on Laser Diagnostics in Combustion, August 14–19, 2011, Waterville Valley, NH* (Paul Miles, SNL).

3. Invited Talk: "Laser Diagnostics in IC Engines," *International Energy Agency 33rd Task Leaders Meeting on Energy Conservation and Emissions Reduction in Combustion, August 7–11, 2011, Lund, Sweden* (Paul Miles, SNL).

4. Invited Workshop Presentation: "Spectrally-Resolved, Multi-Photon CO and UHC LIF Diagnostics in Engines," *12th International School of Advanced Optical Technologies Workshop on Engine Diagnostics, March 28–29, 2011, Erlangen, Germany* (Paul Miles, SNL).

5. Invited Workshop Presentation: "Jet and Engine Flow Studies Applying Ruby and Rare Earth Phosphor Particles," *12th International School of Advanced Optical Technologies Workshop on Engine Diagnostics, March 28–29, 2011, Erlangen, Germany* (Ben Petersen, SNL).

6. Chrysler Invention Development Record - Automotive Engine Coolant Heating System with Integrated EGR Cooler (Submitted, Ron Reese, Chrysler).

7. Bill Partridge of ORNL presented an invited Keynote Lecture at EuropaCat X conference in Glasgow Scotland, based on the Cummins CRADA work in partnership with Chalmers University of Technology.

8. On December 9, 2010, Jim Parks and Bill Partridge received 2010 ORNL Key Contributor Awards in recognition for the receipt of the Southeast Regional Federal Laboratory Consortium Award for Excellence in Technology Transfer; the Southeast Regional FLC award was in partnership with Dr. Kent Froelund of Da Vinci Emissions Services.

9. S. Mani Sarathy (LLNL), Postdoc Fellowship, Natural Sciences and Engineering Research Council of Canada, 4/2010 to 4/2012.

10. William J. Pitz (LLNL): 2011 Outstanding Postdoc mentor award from LLNL Physical and Life Sciences Directorate.

11. Charles K. Westbrook (LLNL), President of the Combustion Institute, 2008-2012.

12. SAE Excellence in Oral Presentation Award for paper 2011-01-0897, April 2011 (John Dec, SNL).

13. Invited Speaker, SAE High-Efficiency IC Engines Symposium, April 2011 (John Dec, SNL).

14. Invited Speaker, Workshop on Techniques for High-Pressure Combustion, Argonne National Laboratory, Aug. 29 – Sept. 1, 2011 (John Dec, SNL).

15. J.-S. Choi, "Lean NOx trap regeneration chemistry studies", invited seminar, GM Global R&D Center, Warren, MI, August 17, 2011.

16. Outstanding Innovation Award – 2010 Distinguished Copyright. Awarded to David Carrington (LANL) by Los Alamos National Laboratory Technology Transfer Division, August 5th, 2011.

INVENTION AND PATENT DISCLOSURES

1. Reitz, R.D., Hanson, R., Splitter, D. and Kokjohn, S.L., "Engine Combustion Control at Low Loads via Fuel Reactivity Stratification," WARF Patent application P11092US01, March 2011.

2. US Patent 20110173975A1, Harold Sun, Ford Motor Company.

3. Patent Application 708570m "PENDULUM VIBRATION ABSORBER ON A CRANKSHAFT", Ron Reese, Chrysler.

4. U.S. Patent No. 7,839,492 "Laser-Induced Fluorescence Fiber Optic Probe Measurement of Oil Dilution by Fuel," was issued November 23, 2010 to James E. Parks, II and William P. Partridge Jr.. This technology was developed in the Cummins CRADA and has been licensed and is commercially available for Da Vinci Emissions Services, Ltd.

5. J.A. Pihl, W.P. Partridge, and T.J. Toops, "High-temperature reactor for Diffuse Reflectance Infrared Fourier-Transform Spectroscopy (DRIFTS)", ORNL invention disclosure.

6. Harold, M.P., and P. Metkar, US Provisional Patent Application, "Multi-Component and Layered Formulations for Enhanced Selective Catalytic Reduction Activity," June 6, 2011.

7. Yilmaz, Robert Bosch

- Pending US Patents on "Compounded Dilution Air Charge Device"
- Pending US Patents on "Combustion Mode Switching with a Turbocharger/Supercharged Engine"
- Pending US Patents on "Method for Modeling Cyclic Variability in Lean Controlled-Autoignition Engines"
- Pending US Patents on "Fueling Strategy for Controlled-Autoignition Engines"
- Pending US Patents on "Method for Path Planning during Combustion Mode Switch"

7. New Technology Disclosure, "Cost-Effective and Industrial-Scalable Thermoelectric Material and Device Fabrication for Automotive Applications using Thermal Spray," Stony Brook University, filed 2/3/2011 (Zuo, Stony Brook Laboratory).

I.4 Future Project Directions

ADVANCED COMBUSTION AND EMISSION CONTROL RESEARCH FOR HIGH-EFFICIENCY ENGINES

A. Combustion and Related In-Cylinder Processes

The focus in FY 2012 for combustion and related in-cylinder processes will continue to be on advancing the fundamental understanding of combustion processes in support of achieving efficiency and emissions goals. This will be accomplished through modeling of combustion, in-cylinder observation using optical and other imaging techniques, and parametric studies of engine operating conditions.

- Argonne National Laboratory (ANL) is studying the mechanisms of spray atomization by making detailed, quantitative measurements in the near-nozzle region of sprays from light-duty diesel injectors. In the coming year they plan to measure the remaining Engine Combustion Network injectors to be used to improve spray models. They will also measure the fuel/air mixing from compression ignition and gas-fueled engines and use X-ray data from multi-hole nozzles to test Argonne's KH-ACT model of primary atomization. (Powell, ANL)
- SNL is developing the physical understanding to guide development of modeling tools to refine the design of optimal, clean, high-efficiency combustion systems. In the coming year they will: (1) quantitatively evaluate the influence of swirl ratio and injection pressure on the fuel-air equivalence ratio distributions formed during the mixture preparation process; (2) correlate the impact of the equivalence ratio distributions on engine-out emissions and post-combustion, in-cylinder distributions of unburned hydrocarbons and CO; (3) evaluate the impact of asymmetrical features of the head and piston top on the mixture preparation, combustion, and emissions formation processes, and the appropriateness of sector modeling of the combustion chamber; and (4) extend flow measurements into the squish volume near top-dead center to evaluate the impact of flow structures and asymmetries on the mixture preparation, combustion, and emissions formation processes. (Miles, SNL)
- SNL will continue developing fundamental understanding of how in-cylinder controls can improve efficiency and reduce pollutant emissions of advanced LTC technologies. In the coming year they plan to probe in-cylinder mixing and combustion processes of high-efficiency dual-fuel operation, explore multiple-injection efficiency and emissions, and build understanding of in-cylinder LTC soot and polycyclic aromatic hydrocarbons. (Musculus, SNL)
- SNL is leading a multi-institution, international, research effort on engine spray combustion called the Engine Combustion Network, facilitating improvement of engine combustion modeling and accelerating the development of cleaner, more efficient engines. In the coming year they plan to investigate jet-jet interaction effects on flame lift-off, characterize side-hole sprays compared to axial-hole sprays, and develop spray and combustion datasets for gasoline direct injection-type injectors. (Pickett, SNL)
- ORNL will continue investigating potential near-term technologies for expanding the usable speed-load range and to evaluate the potential benefits and limitations of these technologies for achieving HECC in a light-duty diesel engine. They plan to: characterize efficiency advantages of RCCI as compared to conventional diesel combustion with detailed thermodynamic analysis; evaluate transient RCCI performance including controls and stability concerns; evaluate aftertreatment performance (including effect on PM) over the over light-duty operating range. Data will also be used with a vehicle model to simulate emissions performance over light-duty driving cycles to determine aftertreatment needs for meeting Federal light-duty Tier 2 Bin 5 and Tier 2 Bin 2 emissions standards; and further evaluate the potential of bio-renewable fuels to extend the RCCI operating range in coordination with the DOE VTP Fuel & Lubricant Technologies subprogram. (Curran, ORNL)
- SNL is combining unique state-of-the-art simulation capability based on the large eddy simulation (LES) technique with Advanced Engine Combustion R&D activities to maximize benefits of high-performance massively-parallel computing for advanced engine combustion research. In

the coming year, SNL plans to continue development of multiphase combustion models with emphasis on direct-injection processes in collaboration with Pickett et al. and Engine Combustion Network workshop participants; continue a parallel task focused on HCCI engines in collaboration with Dec et al; coordinate collaborative activities with the LES working group (University of Wisconsin, Penn State, General Motors, University of Michigan); and form a larger industrial consortium focused on the priority research areas defined in the recent PreSICE Workshop report. (Oefelein, SNL)

- LLNL will continue working on the development and application of computationally efficient and accurate simulation tools for prediction of engine combustion. In the coming year they plan to: continue to validate and develop chemistry simulation capabilities that will enable the prediction of performance and emissions in the development of new vehicle powertrain technologies; conduct detailed analysis of HCCI and direct-injection engine experiments and conduct analysis of clean and efficient diesel engines that use stoichiometric and low-temperature combustion modes; implement strategies to deliver new, even-lower computational cost solvers for chemical kinetic systems on conventional central processing units as well as graphical processing units; develop fully-parallelized multi-dimensional CFD-chemistry solvers for analysis of non-homogeneous engine combustion; and distribute advanced combustion solvers to U.S. industrial and academic partners. (Flowers, LLNL)
- SNL will continue providing the fundamental understanding (science-base) required to overcome the technical barriers to the development of practical HCCI and HCCI-like engines by industry. In the coming year, they will: (1) apply side-view thermal imaging to determine how thermal stratification is affected by operating parameters such as engine speed, intake temperature, intake pressure, and swirl; (2) systematically evaluate the potential of adjusting engine operating parameters to improve the thermal efficiency of boosted HCCI engines over a range of loads; (3) explore the potential of increasing the thermal efficiency of boosted HCCI by increasing the engine compression ratio or by increasing the expansion ratio only through the use of a higher compression ratio piston and a Miller-cycle cam; (4) investigate the effects of expected variations in the ethanol content of pump gasoline on the thermal efficiency, high-load limit, and use of partial fuel stratification for boosted HCCI; (5) continue collaborations with General Motors and the University of Michigan on modeling of thermal stratification in HCCI engines and discussions and modeling of boosted HCCI; and (6) continue to collaborate with LLNL on improving chemical-kinetic mechanisms of single components and a gasoline-surrogate mixture. (Dec, SNL)
- SNL is conducting acetylene seeding experiments in the automotive HCCI engine to identify ignition-enhancement effects of potential products of NVO reformation. In the coming year they plan to image NVO fuel injection to quantify piston wetting and identify its effects on NVO and main combustion; apply tunable diode laser absorption and laser-induced fluorescence imaging to further characterize reforming reactions during the NVO period; apply KIVA, CHEMKIN, and GT-POWER models of their optical engine to build a coherent understanding of NVO fueling and its effect on main combustion; and extend their tunable diode laser absorption diagnostic to permit in-cylinder measurement of other species (e.g., H_2O, CO_2, C_2H_2) to clarify the extent of NVO reformation reactions. (Steeper, SNL)
- ORNL is supporting DOE and industry partnerships in assessment of state-of-the-art and longer-term advanced engine and combustion technologies for future goal setting. In the coming year they plan to continue assessment of state-of-the-art engine technologies and advanced combustion processes in coordination with the Advanced Combustion & Emissions Control Tech Team to support goal-setting activities by the VTP, and characterize stochastic and deterministic phenomena for advanced combustion strategies and develop a path toward improved predictive control and avoidance of abnormal combustion events. (Edwards, ORNL)
- LANL is developing code and algorithms for the advancement of speed, accuracy, robustness, and range of applicability of the KIVA combustion modeling software to higher-order spatial accuracy with a minimal computational effort. In the coming year they plan to: (1) develop three-dimensional robust overset grid method for immersed actuated parts such as valves; (2) merge overset grid method into hp-adaptive finite element method framework; (3) develop the parallel solution method for the hp-adaptive PCS algorithm; (4) parallel structure to be supplied by MPICH and/or OpenMP paradigms

for newest computer architectures; and (5) develop even more effort on appropriate turbulence modeling for more predictive modeling. (Carrington, LANL)

- LLNL is developing chemical kinetic models for conventional and next-generation transportation fuels need to be developed so that engine simulation tools can predict fuel effects. During the coming fiscal year, LLNL intends to: (1) develop chemical kinetic models for a higher molecular weight aromatics to represent the aromatics chemical class in diesel fuel; (2) develop more accurate surrogate kinetics models for gasoline; (3) develop a reduced surrogate mechanism for diesel fuel to be used for multidimensional CFD simulations; (4) develop a functional group method for cycloalkanes in diesel fuel so that the chemical kinetic mechanism can be greatly reduced in size for multidimensional engine simulations; and, (5) validate and improve 2- and 3-methyl alkanes and symmetrical di-methyl alkanes mechanisms with new data from shock tubes, jet-stirred reactors, counterflow flames, and premixed flames. (Pitz, LLNL)
- SNL will continue designing a free-piston engine suitable for hybrid vehicle applications. Future planned activities include: (1) install magnets on the piston assembly and pulse pistons to show stabilizing effect of the alternators; (2) initially run the engine under motoring mode only to test capability for continuous piston motion synchronization; and (3) perform combustion experiments and measure indicated thermal efficiency at various compression ratios and equivalence ratios with both conventional and alternative fuels: hydrogen, natural gas, ethanol, biofuels, propane, gasoline, other renewables. (Van Blarigan, SNL)
- ORNL is analyzing and defining specific advanced pathways to improve the energy conversion efficiency of internal combustion engines from nominally 40% to as high as 60%, with emphasis on opportunities afforded by new approaches to combustion. In the coming year they plan to: (1) continue in-cylinder water injection and reforming experiments with the modified GM Ecotec engine with an expanded range of fuels and in-depth analysis of the observed reaction chemistry and potential thermodynamic impact on engine efficiency; (2) continue construction and shakedown of Regenerative Air Preheating with Thermochemical Recuperation bench-top constant volume combustor experiment as budget and experimental priorities permit; (3) continue collaboration with the Gas Technology Institute in analyzing the efficiency potential of the catalytic thermo-chemical recuperation approach used by the Gas Technology Institute and Cummins in their prototype experiments with a natural gas engine; and (4) develop and implement detailed Fortè models for in-cylinder injection and non-catalytic fuel reforming. (Daw, ORNL)
- ANL will continue to quantify the influence of low-cetane fuel ignition properties to achieve clean, high-efficiency combustion. They will evaluate the required EGR level to achieve high efficiency and low emissions, develop the fuel injection approach using double or triple injections to maximize fuel efficiency, and conduct experiments that will allow for transient operation of this combustion system to determine the suitability for application in an automobile. (Ciatti, ANL)
- ANL will continue to support DOE VTP efforts to develop chemical mechanisms of various internal combustion engine fuels so as to gain a predictive capability of in-cylinder combustion and emissions formation. In the coming year, they plan to conduct tests to on gasoline and gasoline surrogates and obtain data relevant to the effort by LLNL to develop a five-component gasoline surrogate. They also plan to conduct tests on various low boiling point temperature alternative fuels and their surrogates to help support chemical mechanism development and conduct tests on various high boiling point temperature fuels, specifically diesels and biodiesels. (Gupta, ANL)
- ORNL is expanding robust HCCI operation with advanced valve and fuel control technologies. They will complete modifications and shakedown to the air handling system of the ORNL single-cylinder hydraulic valve actuation engine, allowing boost, backpressure and external EGR, and conduct an experimental campaign into the HCCI load expansion enabled by boost and external EGR. (Szybist, ORNL)
- ORNL is quantifying the fuel economy benefit and emissions impact of VCR engine technology to a modern direct-injection gasoline engine. In the coming year they plan to complete machining of engine bedplate, engine crankshaft cradle, and fabrication of custom crankshaft and other VCR actuation components, assemble the engine, and conduct experiments to investigate the effect of VCR on engine efficiency at the maximum brake torque spark timing over the engine map with a VCR research engine. (Domingo, ORNL)

- ORNL is improving diesel engine-catalyst system efficiency through better combustion uniformity, engine calibrations and catalyst control. In the coming year they plan to improve EGR uniformity via application of EGR probe to assess performance of candidate intake hardware designs with respect to EGR uniformity, and improve the EGR diagnostic design to allow simultaneous uniformity and fluctuation measurements at multiple engine locations. (Partridge, ORNL)
- ANL is identifying state-of-the-art engine and vehicle technologies currently in production to quantify the benefits of the state-of-the-art vehicle technologies currently in production, optimize vehicle performance using advanced vehicle level modeling, and accelerate the development of high efficiency internal combustion engines for light-duty vehicle applications, while meeting the future emission standards, using numerical simulations. In the coming year they plan to evaluate new technologies such as the Nissan Micra (1.4 liter turbocharged direct-injected engine) and another vehicle to be identified, analyze the new emerging technologies and how they are used, and conduct analysis on the new and emerging technologies to determine their maximum fuel saving potential. (McConnell, ANL)
- Cummins Inc. is engaged in developing and demonstrating advanced diesel engine technologies to significantly improve the engine thermal efficiency up to 55% and will demonstrate tractor-trailer vehicles with 68% or greater freight efficiency improvement. In the coming year they plan to complete demonstration of 50% thermal efficient engine, and complete the build and development testing of the 50% freight efficiency demonstration vehicle. (Koeberlaein, Cummins)
- Daimler Trucks will develop and demonstrate a Class 8, long-haul tractor-trailer which achieves a 50% vehicle freight efficiency improvement (measured in ton-miles per gallon) over a best-in-class 2009 baseline vehicle. In the coming year they plan to build and test prototype vehicle and engine systems for empirical measurement of efficiency improvement, optimize vehicle systems to reach efficiency targets including SuperTruck integration, optimize engine systems and demonstrate 50% BTE, and build and test final SuperTruck vehicle to demonstrate 50% vehicle freight efficiency. (Rotz, Daimler Trucks North America LLC)
- Navistar is demonstrating engine BTE improvements which contribute 20% (of the total 50% required) improvement in the freight efficiency of a combination tractor-trailer. In the coming year they plan to introduce the flexible valve train, friction reduction and Rankine technologies with expectation to attain the 50% BTE target. Modeling will continue on the fuel reactivity and this dedicated engine will undergo its first tests towards the 55% BTE target. (Jadin, Navistar)
- Volvo Powertrain North America is identifying concepts and technologies that have potential to achieve 55% BTE on a heavy-duty diesel engine as defined in the SuperTruck project. In the coming year they plan to install and evaluate the probability density function computer code, install the optical instrumentation for the constant volume combustion chamber, install and test high performance pistons, and calibrate and test the Organic Rankine Cycle system under transient conditions. (Amar, Volvo Powertrain North America)
- Delphi will develop, implement and demonstrate fuel consumption reduction technologies using a new LTC process: gasoline direct injection compression ignition (GDCI). In the coming year they plan to debug Phase 1 hardware and controls, calibrate Phase 1 vehicles, test Phase 1 technologies, build and debug Phase 2 multi-cylinder engine, develop GDCI engine control system, and continue single-cylinder engine tests and detailed FIRE and KIVA simulations to refine the combustion process and component designs. (Confer, Delphi Automotive Systems LLC)
- Ford will demonstrate 25% fuel economy improvement in a mid-sized sedan using a downsized, advanced gasoline turbocharged direct injection engine with no or limited degradation in vehicle level metrics. In the coming year they plan to complete multi-cylinder development and start dynamometer development. They will also build and instrument a demonstration vehicle and components. (Wagner, Ford Motor Company)
- General Motors will demonstrate 25% vehicle fuel economy improvement through lean gasoline combustion while achieving Tier 2 Bin 2 emissions. In the coming year, they plan to optimize lean engine controls and calibration to maximize fuel economy potential to improve transient drivability and minimize engine-out emissions, refine the Gen 2 passive SCR lean aftertreatment system to minimize CO during NH_3 generation, develop an exhaust system thermal management strategy to optimize lean aftertreatment performance under all vehicle operating conditions, develop an

aftertreatment system that combines active and passive SCR systems as a risk mitigation to ensure compliance under all operating conditions, integrate active thermal management and 12 volt stop/start systems to maximize fuel economy potential, and develop second generation lean-gasoline combustion engine with downsizing, boosting and multiple fuel injection capability to extend lean stratified load operation range. (Smith, General Motors Company)

- Chrysler aims to demonstrate 25% improvement in combined Federal Test Procedure City and Highway fuel economy for the Chrysler minivan. In the coming year they plan to perform development tests on Alpha 1 engines in the dynamometer to provide correlation to the simulation results, incorporate base control strategies to run the engine and provide feedback on the fuel economy improvements of the new technologies, demonstrate the combined fuel economy improvement of at least 17% on simulated fuel economy tests for this phase of engine design, optimize simulation and design for the second iteration of engine development, and test the multi-fuel engine at ANL with optical access into the combustion chamber. (Reese, Chrysler Group LLC)
- Robert Bosch LLC is improving fuel economy by 30% with minimum performance penalties. In the coming year they plan to evaluate fuel economy and emissions benefits of boosted HCCI combustion concept on the Prototype I engine platform, complete design, procurement, and building of Prototype II engine, and define combustion and control strategies for combustion mode switch between HCCI and spark ignition combustion. (Yilmaz, Robert Bosch)
- Cummins is demonstrating 40% fuel economy improvement over a baseline gasoline V-8 pickup truck and Tier 2 Bin 2 tailpipe emissions compliance. In the coming year they plan to design and procure a clean-sheet engine to meet technical requirements as outlined via technical requirements from model data; utilize fabricated subsystems on the baseline engine carcass to demonstrate model results for fuel consumption and emission control; and demonstrate fuel economy at target in a mule vehicle with mule engine coincident with greater than 90% NOx reduction aftertreatment. (Ruth, Cummins Inc.)
- Ford is focusing on complete and optimal system solutions to address boost system challenges, such as efficiency degradation and compressor surge, etc., in diesel combustion/emission control system development, and to enable commercialization of advanced diesel combustion technologies, such as HCCI/LTC. In the coming year, Ford plans to fabricate and flow bench test the small turbocharger design/optimization to support light-duty diesel applications. Engine dynamometer test validation will be conducted of the advanced compressor for light-duty diesel vehicle chassis certification applications. (Sun, Ford)

B. Energy-Efficient Emission Controls

In FY 2012, work will continue on LNTs and urea-SCR to reduce NOx emissions. The focus of activities will be on making these devices more efficient, more durable, and less costly. For PM control, the focus will be on more efficient methods of filter regeneration to reduce impact on engine fuel consumption.

- PNNL will: (1) extract the SCR reaction kinetics and examine various reaction pathways over the state-of-the-art Cu SCR catalyst using PNNL's Cu SCR catalyst model; (2) conduct detailed kinetic and mechanistic studies for NO reduction over the state-of-the-art small-pore zeolite-based Cu SCR catalysts; (3) continue fundamental studies of novel high temperature LNT formulations; (4) characterize current production and advanced DPF substrates through advanced image and statistical analysis of high resolution computed tomography data; and (5) investigate the use of micro-scale simulation to improve the commonly used unit collector models for DPF substrates. (Lee, PNNL)
- PNNL is developing a fundamental understanding of candidate next-generation LNT materials for NOx after-treatment for light-duty lean-burn (including diesel) engines. Studies aimed at determining performance limitations, sulfur sensitivity and desulfation behavior of candidate alternative support and NOx storage materials that provide improved high temperature performance will continue. An overall goal of the work will continue to be to develop a deeper understanding of the mechanisms of NOx storage and reduction activity, and performance

degradation of materials that have been reported to show good NOx storage and reduction performance at temperatures considerably higher than BaO/alumina-based materials. These fundamental studies will be carried out in conjunction with baseline performance and stability experiments on fully formulated catalysts provided by Johnson Matthey. (Peden, PNNL)

- ORNL is assessing and characterizing catalytic emission control technologies for the reduction of NOx from lean-gasoline engines and identifying strategies for cost reduction of emission controls for lean-gasoline engines. In the coming year they plan to develop a lean-gasoline engine research platform for catalyst studies and determine catalytic NH_3 production viability under rich engine operation for SCR reactions. (Parks, ORNL)
- ORNL will continue investigating methods for improving performance and/or durability of LNTs and improving the fundamental understanding of deactivation mechanisms that result during the regeneration of LNTs. The plan to combine with engine-based lean-gasoline project that includes automotive manufacturers and catalyst suppliers. The project will set aggressive milestones to drive down fuel penalty and precious metal costs associated with meeting emissions standards in lean-gasoline applications. (Toops, ORNL)
- ORNL will continue improving diesel engine-catalyst system efficiency through better combustion uniformity, engine calibrations and catalyst control. In the coming year they will improve instrument response models for better transient analysis, analyze distributed performance of commercial Cu-chabazite-zeolite SCR catalyst, and apply optical-fiber based NH_3 sensors for intra-catalyst detection, to demonstrate advanced control strategy methodologies. (Partridge, ORNL)
- ORNL will continue to co-lead the CLEERS planning committee, the LNT Focus Group and support the DPF and SCR Focus Groups as needed. They will also provide standard reference LNT materials, data, and kinetic modeling results for focus group evaluation, maintain and expand the CLEERS website, continue providing regular update reports to the DOE Advanced Combustion Engine Cross-Cut team, and will organize and conduct the 2012 CLEERS workshop in the spring of 2012. (Daw, ORNL)
- ORNL is collaborating with SNL and PNNL to produce kinetic information for LNT and urea-SCR aftertreatment devices, both as individual and system integrated components as part of the CLEERS project. In the coming year they plan to: (1) use the CLEERS LNT laboratory protocol to characterize commercial LNT catalyst samples from the BMW 120i spark ignition direct injection vehicle that has been extensively studied in chassis dynamometer experiments at ORNL; (2) develop and publish a set of kinetic and aging parameters for the commercial chabazite Cu-zeolite SCR catalyst under joint investigation by ORNL and PNNL; (3) continue identification of key surface species and associated catalyst sites in SCR zeolite catalysts through diffuse reflectance infrared Fourier-transform spectroscopy measurements; and (4) utilize the above results to improve models for simulating LNT and SCR NOx reduction performance under both laboratory and vehicle drive cycle conditions. (Daw, ORNL)
- ANL is characterizing the oxidation behavior of diesel PM emissions in terms of heat release and oxidation rate. In the coming year they plan to evaluate PM filtration efficiency at different engine conditions, conduct regeneration experiments to evaluate regeneration efficiency and obtain optical images, and perform thermogravimetric experiments of surrogate soot with various flue gases (NOx, CO, CO_2, and O_2) to evaluate kinetic parameters. (Lee, ANL)
- PNNL will continue developing a fundamental understanding of the integration of SCR and DPF technologies for on-road heavy-duty vehicle application. In the coming year they plan to evaluate the value of additional substrates for interrogation, including possibly silicon carbide and onsider quick screening studies for comparison to cordierite wash coating results; continue to interrogate passive soot oxidation feasibility in the integrated device, including continued parametric investigations interrogating the effect of NO_2:NO_X ratio, SCR catalyst loading, NH_3:NO_X ratio; and quickly pursue facilitating on-engine testing, as well as on-truck testing. (Rappe, PNNL)
- PNNL and their CRADA partner Ford will continue developing an understanding of the deactivation mechanisms of the urea-SCR catalyst used in diesel aftertreatment systems. In the coming year they plan to: complete mechanistic studies of phosphorus deactivating effects; conduct detailed studies of hydrothermal dealumination in Cu-SSZ-13; prepare additional Cu-SSZ-13

zeolite for joint Ford/PNNL studies of Cu loading effects; examine the effects of physicochemical properties of zeolite materials with other fuel-component HC species; and investigate the role of metals on HC retention at higher temperatures. (Peden, PNNL)

- PNNL is characterizing exhaust particulates from advanced combustion engines such as spark ignition direct injection (SIDI) using readily available fuel blends and using insight gained and prior experience with diesel aftertreatment to jump-start development of optimum aftertreatment technologies. In the coming year they plan to complete the second round cooperative experiments with a prototype SIDI engine at the University of Wisconsin Engine Research Center using SPLAT II and other advanced analytical tools, publish the second round SIDI soot characterization results, and apply improved unit collector models to likely SIDI applications. (Stewart, PNNL)

C. Health Impacts

The focus of the activities in Health Impacts is to identify and quantify the health hazards associated with exhaust from advanced combustion engines and put them in proper context with other air quality hazards, and to assess the relative hazards of emissions from different fuel, engine, and emission reduction technologies.

- ORNL is striving to understand the potential impact of developing fuel, combustion, and aftertreatment technologies on air quality and, thereby, human health. In 2012, ORNL will assess potential emissions challenges to new combustion regimes. (Storey, ORNL)
- The Health Effects Institute is conducting the Advanced Collaborative Emissions Study to characterize the emissions and assess the safety of advanced heavy-duty diesel engine and aftertreatment systems and fuels designed to meet the 2007 and 2010 emissions standards for PM and NOx. In the coming year they will conduct and complete Phase 2 characterization of 2010-compliant engines, and continue exposure of rats for 24 or 30 months at three selected diesel exhaust exposure concentrations (high, medium, and low) or clean air. (Greenbaum, Health Effects Institute)

SOLID STATE ENERGY CONVERSION

Research will continue in FY 2012 on TEs for converting waste heat from advanced combustion engines directly to electricity. Research will focus on development of practical systems that are suitable for future production.

- Amerigon will build upon their prior work (which provided a proof-of-concept technology-ready platform) and transition the technology from R&D to commercialization. They will continue R&D to: (1) scale up of processes and manufacture of proven Skutterudite materials; (2) scale up of their proof-of-concept TEG based upon their proprietary stack design and integration with gas and liquid heat exchangers in the cylindrical form factor they pioneered in a prior DOE-funded R&D project; (3) integration of the cylindrical TEG into the underfloor exhaust systems of Ford and BMW target vehicles; and (4) confirmatory vehicle testing of the TEG system for performance and fuel economy improvement. (LaGrandeur, Amerigon Inc.)
- General Motors will continue development of a cost-effective TEG that is fully integrated into a GM production light-duty vehicle. To overcome the major obstacles to TEG commercialization they will use electrical and thermal management strategies to reduce electrical accessory load on the alternator using TE-generated power, utilizing the additional power to shift some engine-driven accessories to electrical drive, and use of the excess electrical power for something other than the vehicle electrical load e.g., propulsion (optimal for hybrids). A TEG system will be developed with all vehicle controls and electrical systems for full vehicle integration. They will further optimize compositions and processing parameters for their TE material; develop suitable diffusion barriers, interfaces electrical interconnections, and thermal contacts within TE modules; implement adequate protection of TE materials and modules from degradation during operation, and develop manufacturing and assembly processes for large-scale production of TE materials and components that include scale up plans for the production of 100,000 TEG units per year. (Meisner, General Motors)

- GMZ Energy Inc. will continue development of TEGs using significantly improved nanostructured bulk TE materials that they have developed and an innovative two-stage cascade design. High-temperature compatible nanostructured half-Heusler materials will give both high thermoelectric power generation performance as well as robust, thermally stable and cyclable devices. These devices will form the top layer of a cascade approach using nanostructured bismuth telluride-based materials for the lower temperature stage to create a ~1 kW TEG system, to enable a 5% fuel efficiency improvement in a light-duty vehicle. (Caylor, GMZ Energy Inc.)
- General Motors is identifying distributed cooling and heating strategies that can efficiently augment or replace a vehicle's central heating, ventilation and air conditioning (HVAC) system by delivering localized cooling/heating of key human body segments that strongly influence an occupant's perceived thermal comfort. In the coming year they plan to: complete the development and evaluation of initial prototype local HVAC components that feature TE technology to deliver energy savings; develop final prototype local HVAC components and evaluate the energy savings of the integrated HVAC system in the demonstration vehicle; continue to develop and enhance computer-aided engineering tools that support the inclusion of local cooling/heating HVAC components in future energy-efficient vehicle designs; evaluate and improve the initial design concept for an energy-efficient TE device to replace the passenger compartment resistive heater of the Chevrolet Volt extended-range electric vehicle; and continue to investigate new and improved TE material systems for improved automotive waste heat recovery performance. (Gundlach, General Motors)
- Ohio State University is developing high-efficiency high zT TE materials (PbSe and Mg_2Sn) that contain no rare or precious elements, and are non-toxic. In the coming year they plan to: refine PbSe experimental procedure for optimizing zT varying indium content from 1/8% to 1/4%; confirm previous data with this set of samples and determine optimum doping level for high temperature applications; measure properties of intrinsic material; confirm experimentally the presence of a high anharmonicity; and find resonant acceptor impurity for Mg_2Sn. (Heremans, Ohio State University)
- Purdue University is enabling the broad adoption of TE waste heat recovery systems, or TEGs, at a scale commensurate with the global vehicle manufacturing enterprise. In the coming year they plan to: understand the interaction between the filling metal atoms and the parent skutterudite material; evaluate the impacts of nanostructure size, surface roughness, and composition modulation on TE figure of merit, analyze other material systems and conduct research in the scalable synthesis of nanowire heterostructures to further decouple electron and phonon transport; refine the heat exchanger design with the use of multiple types of TE materials; and explore the possibility of developing other nanostructures for TE application. (Xu, Purdue University)
- Stanford is performing systems-level modeling and full device-scale characterization, with the ultimate goal of constructing a complete architecture for optimizing a TEG system for recovering waste heat from automobile combustion. In the coming year they plan to: develop new processes for fabrication, assembly and integration of carbon nanotube-based thermal interface material tape technology to TE pellets/modules; conduct in situ characterization and reliability tests for TE pellets and Interfaces as well as TE modules; complete and implement the high-temperature (800 K) rig for in situ thermal and mechanical characterization; continue the ab initio computational effort to engineer TE materials (e.g., skutterudites); and develop new TE high-temperature materials such as skutterudites and half-Heusler alloys. (Goodson, Stanford)
- Stony Brook University successfully obtained single-phase higher manganese silicide using melt-spinning and successfully demonstrated thermal spray of silicide materials. In the coming year they plan to: (1) improve the thermal properties of Mg_2Si when thermal spraying, especially the Seebeck coefficient; (2) fine tune the chemical and structural parameters to optimize their TE and mechanical properties in melt spinning, and scale up the non-equilibrium synthesis from melt spinning of higher manganese silicide to thermal spray by taking advantage the similarity between the melt spin and the thermal spray techniques; and (3) demonstrate the fabrication of three-dimensional interconnected TE structures on both flat plate, and then cylindrical pipe substrates using thermal spray and laser micro machining. (Zuo, Stony Brook University)
- Texas A&M is synthesizing of inorganic nanowires and quantum wires of both $CoSb_3$ and InSb, and organic conducting polymer thin films, and assembling them into inorganic-organic hybrid

TE cells with sizes ranging from a few mm^2 to a few cm^2, using conjugated linker molecules to tether the nanowires to each other or to conducting polymer thin films. In the coming year they plan to evaluate the TE performance of $CoSb_3$ and InSb nanowire pellets in the 300-1,100 K temperature range, compare the performance of $CoSb_3$ and InSb nanowire pellets and their hybrids (composed of nanowires bound together with organic conjugated linker molecules) with that of single nanowires, and compare the performance of $CoSb_3$ and InSb nanowire pellets and nanowire-conducting polymer hybrids, with that of individual nanowires. (Vaddiraju, Texas A&M)

- The University of California, Los Angeles is developing novel materials and interfaces for improved thermomechanical reliability of TE vehicle exhaust waste heat harvesting devices. In the coming year they plan to: explore metal-matrix nanocomposites using less expensive metals (such as Cu, Al, or Ni) using similar production methods and having tunable coefficients of thermal expansion; reduce the size of and improve upon the homogeneous dispersion of the oxide inclusions in the metal matrix in order to reduce the scattering of the experimental results and provide even more reliable and reproducible composites; characterize the coefficient of thermal expansion of metal-ceramic nanocomposites up to higher temperature limit of 500°C, for practical use in TE devices; and investigate the feasibility of liquid-based flexible thermal interfaces for high-temperature applications. (Ju, University of California, Los Angeles)
- The University of California, Santa Cruz, is developing novel TE materials based on abundant and non-toxic Zintl phase magnesium silicide alloys and optimizing the TE power factor and figure of merit by band engineering and electron filtering. In the coming year they plan to conduct low temperature synthesis and spark plasma sintering of: n-type $Mg_2Si_{1-x}Sn_x$ with embedded Si and Mg_2Si nanoparticles; n-type $Mg_{2-x}Yb_xSi$ with embedded YbSi nanoparticles; and p-type Mg_2Si with embedded nanoparticles. (Shakouri, University of California, Santa Cruz)
- The University of Texas at Austin is increasing the zT of abundant silicide materials to a level competitive with the state of the art found in materials containing much more scarce and expensive elements, and enhancing the thermal management system performance for silicide TE devices installed in a diesel engine. In the coming year they plan to investigate complex doping of higher manganese silicide to increase the power factor; conduct spark plasma sintering synthesis of n-type Mg_2Si-based pellets; establish a position-dependent doping method to match the peak zT with the local operating temperature of the TE leg; develop a method for spatial mapping of the TE properties; investigate silicide interface materials; and design, fabricate, and model alternative heat exchanger geometries to enhance the heat transfer efficiency. (Shi, University of Texas at Austin)
- Virginia Tech is fabricating and characterizing new TE materials growth with techniques capable of producing large quantities of efficient, yet non-toxic and inexpensive elements capable of long-term operation at high temperatures over thousands of thermal cycles. In the coming year they plan to: (1) develop low cost P-type TE materials to complement the N-type Mg silicide produced this year; (2) create diffusion barriers for the new TE materials and examine those interfaces in series with brazes and thin dielectric layers required for assembly of TE systems (quantify the interfaces in terms of species diffusion, thermal conductance, and electrical resistance); (3) quantify the effects that long-term exposure to high temperatures and thermal cycling has on the TE materials and interfaces; (4) finish assembly of the laboratory-scale exhaust system and TEG test; and (5) fabricate and evaluate modified TE oxides and binary alloys with eutectic decomposition. (Huxtable, Virginia Tech)
- The University of Wisconsin-Madison is synthesizing nanostructured abundant higher manganese silicides (HMS) in bulk with enhanced TE performance for TE applications. In the coming year they plan to acquire phase-pure nanostructured HMS in larger quantity via conversion reactions, prepare nanostructured HMS composites with silicon using phase segregation and precipitation approach, and work with the team members at University of Texas at Austin to evaluate the physical properties of the nanostructured HMS. (Jin, University of Wisconsin-Madison)
- The University of California, Davis is developing novel TE materials based on abundant and non-toxic Zintl phase magnesium silicide alloys. In the coming year they plan to perform low temperature synthesis and spark plasma sintering of n-type $Mg_2Si_{1-x}Sn_x$ with embedded Si, Mg_2Si, and YbSi nanoparticles. They also plan to perform additional characterization and transport modeling. (Kauzlarich, University of California, Davis)

- Virginia Polytechnic Institute and State University is developing an interface bonding metallurgy between TE elements and heat exchangers with an electrical contact resistance smaller than 10-5 Ω cm^2 and a thermal contact resistance smaller than 10^{-3} K W^{-1} cm^2. In the next year they plan to: study other barrier materials, such as titanium-tungsten alloy to evaluate effectiveness for slowing silver diffusion; improve the die-attach process by low-temperature sintering of nanosilver paste; and characterize the thermal and electrical contact resistance, as well as the thermomechanical reliability of nanosilver sintered bonding layer. (Lu, Virginia Polytechnic Institute and State University)
- Northwestern University is doing materials research (led by Ohio State University and Northwestern University) to develop advanced TE materials made from earth-abundant, geographically dispersed elements and compounds. In the coming year they plan to continue to optimize nanostructured n-type PbS and achieve zT~1.3 at 900 K; initiate research on nanostructured p-type PbS; achieve lattice thermal conductivity or 0.6 W/m-K at 900 K on nanostructured p-type PbS and achieve zT~1.1 at 900 K; and initiate research on nanostructured n-type Mg_2Sn and Mg_2Si. (Mercouri, Northwestern University)

UNIVERSITY RESEARCH

In FY 2012, our university partners will continue their fundamental research into combustion and the chemistry of emission control devices.

- UM will continue exploring new high-pressure lean-burn combustion that can enable future gasoline engines with 20-40% improved fuel economy and determining the fuel economy benefits of engines and engine cycles designed to utilize advanced combustion modes. In the coming year, they plan to: (1) expand thermodynamic and system analyses of mixed combustion modes in a representative turbocharged engine system to include realistic combustion constraints, different compression ratios, and if time, hybridization; (2) apply rapid compression machine work on fuel ignition properties to engine experiments with different injection strategies; (3) continue spark-assisted compression ignition imaging studies in the Rapid Compression Facility over wider range of pressures and mixture ratios; and (4) explore opportunities for improved engine efficiency through chemistry and properties of novel fuels. (Woolridge, UM)
- The University of Wisconsin will continue developing high efficiency internal combustion engines with goals of improved fuel economy by 20-40% in light-duty and 55% BTE in heavy-duty engines. Methods to further increase fuel efficiency while maintaining low emissions will continue to be explored. The origins of CO and unburned hydrocarbons in heavy-duty and light-duty LTC engines will be analyzed. They will continue to explore optimized fuel injection strategies, matched with piston geometry and fuel types and demonstrate and test transient control strategies for mixed-mode combustion. (Reitz, University of Wisconsin)
- MSU will continue demonstrating an SI and HCCI dual-mode combustion engine for a blend of gasoline and E85 (85% ethanol and 15% gasoline) for the best fuel economy. They plan to complete the target optical engine integration and tests in HCCI combustion mode, complete HCCI closed-loop combustion control dynamometer tests, along with the determination of the HCCI operational range, develop the final test plan and complete the final performance and emission tests, and complete the test data analysis and final project report. (Zhu, MSU)
- The University of Houston will continue to identify the NOx reduction mechanisms operative in LNTs and in situ SCR catalysts, and to use this knowledge to design optimized LNT-SCR systems in terms of catalyst architecture and operating strategies. They will converge on critical tasks related to experimental and modeling studies of the LNT/SCR technology. The main focus of the third year will be to conduct focused experiments involving the LNT/SCR sequential and double-layer configurations. As they learn more about the catalytic chemistry and kinetics they will incorporate those findings into models. (Harold, University of Houston)
- The University of Connecticut will continue developing three-dimensional composite nanostructures for lean-NOx emission control devices. They plan to further optimize and quantitatively characterize the three-dimensional composite nanowires/nanorods array based on metal oxides (e.g., ZnO, and TiO_2) and perovskite (e.g., LSMO, LSCO); load precious metal nanoparticles (Pt, Au, Pd)

before and after barium oxide and perovskite nanofilm loading on metal oxide three-dimensional composite nanowires/nanorods arrays; further evaluate the catalytic performance of three-dimensional composite nanowires/nanorods arrays on the thermal stability, S-resistance and NOx storage and reduction performance; and calculate the O_2, NO and NO_2 catalytic interactions with various surfaces of LSMO and LSCO, involving dopants like Sr. (Gao, University of Connecticut)

- Michigan Technological University will continue to develop experimentally validated DOC, DPF and SCR models with real-time internal state estimation strategies that support future onboard diagnostics, advanced control system, and system optimization objectives for DOC-DPF-SCR aftertreatment systems that minimize the energy penalty of meeting emission regulations. They plan to test hydrocarbon impact on SCR performance on an ORNL bench reactor, estimation strategies to those for the SCR and DOC will be implemented for CPFs along with evaluation of sensor combinations for on-board diagnostics; complete active regeneration test matrix and additional test points added to further understand the PM oxidation differences between B10, B20, and ULSD; perform engine tests to characterize PM loading maldistribution in the CPF and its dependency on regeneration parameters; transient testing with a Cummins 2010 6.7-L ISB engine SCR system will be done to determine model response as compared to experimental data including NOx and NH_3 sensor data. (Johnson, Michigan Technological University)

II. ADVANCED COMBUSTION AND EMISSION CONTROL RESEARCH FOR HIGH-EFFICIENCY ENGINES

II.A.1 Fuel Injection and Spray Research Using X-Ray Diagnostics

Christopher F. Powell (Primary Contact), Alan Kastengren, Jin Wang
Argonne National Laboratory
9700 S Cass Ave.
Argonne, IL 60439

DOE Technology Development Manager: Gurpreet Singh

Overall Objectives

- Study the mechanisms of spray atomization by making detailed, quantitative measurements in the near-nozzle region of sprays from light-duty diesel injectors.
- Perform these measurements under conditions as close as possible to those of modern engines.
- Utilize the results of our unique measurements in order to advance the state of the art in spray modeling.
- Provide industrial partners in the spray and engine community with access to a unique and powerful spray diagnostic.

Fiscal Year (FY) 2011 Objectives

- Complete the fabrication of a fuel injection system compatible with the hardware and spray conditions defined by the Engine Combustion Network (ECN).
- Measure fuel injection using the hardware and conditions of the ECN's Spray A condition.
- Measure fuel injection under operating conditions that mimic those inside the General Motors 1.9-L engine running using a low-temperature combustion (LTC) strategy.
- Measure the operation of the injector along with the gas jet from a Westport hydrogen/natural gas injector.

Accomplishments

- In collaboration with Sandia's ECN, we completed measurements of six of the 10 ECN injectors. We made precision measurements of the valve operation, and discovered significant differences between the nominally identical injectors. The measurements will be used to improve spray models, simplifying the development of efficient, clean-burning engines.
- We completed measurements of sprays supporting Argonne's LTC engine research. These measurements will be used to validate engine models, and will enable this clean, efficient LTC strategy to be applied to a broader operating range.
- We made the first ever X-ray measurements of the gas jets emerging from a hydrogen/natural gas direct injector. These measurements demonstrated the ability to quantify the jet density with high precision and time resolution. Such measurements will allow the fuel/air mixing in gas-fueled engines to be measured and quantified, and will help to achieve high efficiency with these clean-burning fuels.

Future Directions

- The remaining injectors that are part of the ECN will be studied. As new spray conditions are defined, we will contribute our unique measurements of spray and injector properties.
- Additional measurements will be done in conjunction with Argonne's Engine and Emissions Research group. These will measure the fuel/air mixing from compression ignition and gas-fueled engines, providing these research programs with the data that is needed for high-fidelity modeling.
- X-ray data from multi-hole nozzles will be used to test Argonne's KH-ACT model of primary atomization. This will further validate the model and improve its ability to predict spray breakup.

Introduction

Fuel injection systems are one of the most important components in the design of combustion engines with high efficiency and low emissions. A detailed understanding of the fuel injection process and the mechanisms of spray atomization can lead to better engine design. This has spurred considerable activity in the development of optical techniques (primarily using lasers) for measurements of fuel sprays. Some of these optical techniques have become commercially available and can be readily applied to the testing and development of modern injection systems. Despite significant advances in spray diagnostics over the last 30 years, scattering of light from the large number of droplets surrounding the spray prevents penetration of visible light and limits such measurements to the periphery of the spray. This is especially true in the spray formation region near the injector, which is considered to be the most important region for

developing a comprehensive understanding of spray behavior. Existing models of spray structure have only been compared with data acquired in the region relatively far from the nozzle. It is unknown how well these models apply in the crucial near-nozzle region. The limitations of visible light in the near-nozzle region of the spray have led us to develop X-ray diagnostics for the study of fuel sprays. X-rays are highly penetrative, and measurements are not complicated by the effects of scattering. The technique is non-intrusive, quantitative, highly time-resolved, and allows us to make detailed measurements of the spray, even in the densely-packed region very near the nozzle.

Approach

This project studies the sprays from commercially available fuel injectors. Our approach is to make detailed measurements of the sprays from these injectors using X-ray absorption. This will allow us to map the fuel distribution in these sprays, extending the existing knowledge into the near-nozzle region. The X-ray measurements are performed at the Advanced Photon Source at Argonne National Laboratory. A schematic of the experimental setup is shown in Figure 1; detailed descriptions of the experimental methods are given in [1] and [2]. The technique is straightforward; it is similar to absorption methods commonly used in optical analysis. However, X-ray radiography has a significant advantage over optical techniques in the measurement of sprays: because the measurement is not complicated by the effects of scattering, there is a simple relation between the measured X-ray intensity and the mass of fuel in the path of the X-ray beam. For a monochromatic (narrow wavelength bandwidth) X-ray beam, this relationship is given by

$$I/I_0 = \exp(-\mu_M M)$$

where I and I0 are the transmitted and incident intensities, respectively; μM is the mass absorption constant; and M is the mass/area of fuel. The constant μM is measured in a standard cell, and the incident and transmitted intensities are measured as a function of time by the X-ray detector. This allows direct determination of the mass of fuel at any position in the spray as a function of time. It is the goal of our work to use X-ray radiography to measure sprays from commercial fuel injectors at different injection pressures, different ambient pressures, and using different nozzle geometries. This will enable us to quantify how each of these variables affects the structure of the spray. We will collaborate with industrial partners including engine and fuel injection system manufacturers so that they will have access to these diagnostics for improvement of their products. We will also collaborate with spray modelers to incorporate this previously unknown information about the spray formation region into new models. This will lead to an increased understanding of the mechanisms of spray atomization and will facilitate the development of fuel injection systems designed to improve efficiency and reduce pollutants.

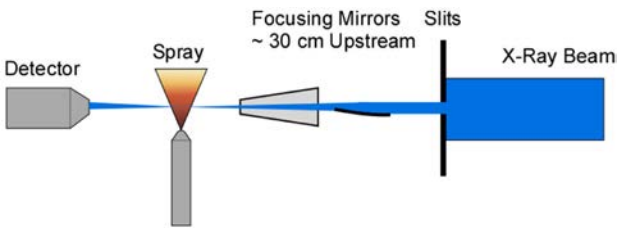

FIGURE 1. Schematic of the experimental setup. The new focusing optics at our dedicated beamline allow us to resolve much finer spray structures.

Results

Much of our experimental work this year focused on measurements performed as part of the ECN. This collaboration is led by Sandia National Laboratories, who has defined a specific set of operating conditions and procured a set of shared identical hardware. We have used Argonne's unique X-ray diagnostics to study the operation and sprays from six of the 10 injectors under the "Spray A" operating conditions.

Our first significant discovery as part of this group was that the injectors, while nominally identical, have significant differences. Figure 2 shows the projected fuel density in a slice through the spray for two of the

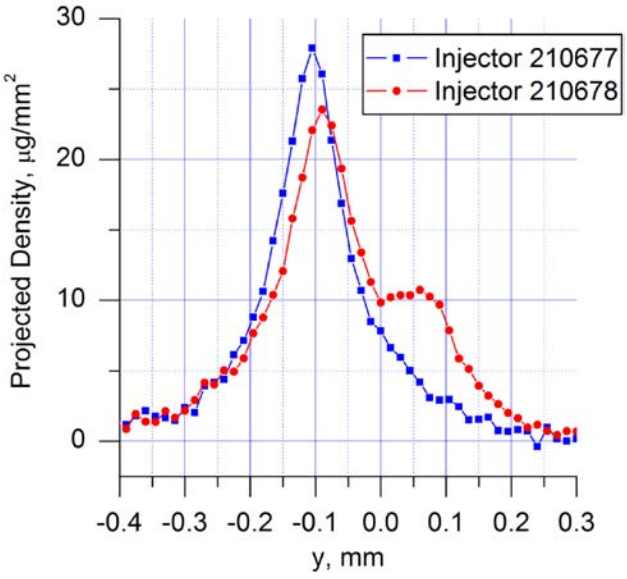

FIGURE 2. Projected fuel density in a slice through the spray for two of the ECN injectors. While they are designed to be the same, the sprays show significantly different fuel distributions.

ECN injectors. While they are designed to be the same, the sprays mix with air very differently and will result in different performance from these two injectors. Differences have also been seen in measurements of the injector valve motion, with some showing large eccentricities during valve operation while others are well-behaved. These differences between nominally identical injectors provide a challenge to the ECN, which must try to understand the differences not only between research institutions but also between injectors. The ECN includes a large group of spray modelers, who will be able to utilize this large data set to improve spray models, simplifying the development of efficient, clean-burning engines.

Over the lifetime of this project, we have strived to increase the relevance of our measurements by studying sprays under conditions even closer to those of modern diesel engines. We have made steady progress over the course of the project, continually increasing the ambient pressure and enabling the use of production nozzles. In FY 2011 we performed measurements on a fuel system copied from the General Motors 1.9-L diesel engine. These measurements matched the hardware, fuel, injection timing, and in-cylinder density that are used in the LTC engine in Argonne's Engine and Emissions Research group. Results from those measurements are shown in Figure 3, which shows the project fuel density in a slice through the spray at two distances from the nozzle for three different injection timings. The measurements quantify the fuel/air mixing at a few specific engine operating conditions. The data will be used to validate spray and engine modeling at those operating points. The validated models can then be used to predict engine performance at other operating points, and will suggest injection strategies for other operating conditions to optimize efficiency and emissions. In this way, our measurements will enable this clean, efficient LTC strategy to be applied to a broader operating range.

In collaboration with Westport Innovations and Argonne's Engine and Emissions Research group, we made the first ever X-ray measurements of a hydrogen/natural gas direct injector. Two different measurements were used. The first imaged the motion of the injector's internal components through the steel body. These measurements are being used by Westport to help understand the operation of the injector in situ, and to evaluate the design for reliability and wear. The second measurements used X-rays to map the density distribution of the gas jet that is emitted from the injector as it mixes with the outside air. These measurements are being used by Argonne's engine group to understand the fuel/air mixing in-cylinder, and to validate their models of engine performance. Figure 4 shows the measured gas jet density (left) along with computational fluid dynamics predictions (right). The X-ray measurements give a very detailed picture of this supersonic jet, including accurate measurements of the shock structures that cannot be obtained in any other way. The measurements will be used to advance the state of the art in gas jet modeling, and will enable the combustion process to be simulated accurately. This will speed the research and development of direct injected natural gas engines, and will help to achieve high efficiency with these clean-burning fuels.

Conclusions

- The X-ray measurements can be used to help understand the mixing of fuel and air in the engine, and its impact on engine emissions and performance. Such measurements are not possible using other imaging techniques, and represent a powerful data set for validating computational models of fuel flow.
- The time-dependent mass measurements provide unique information to spray modelers, and allow

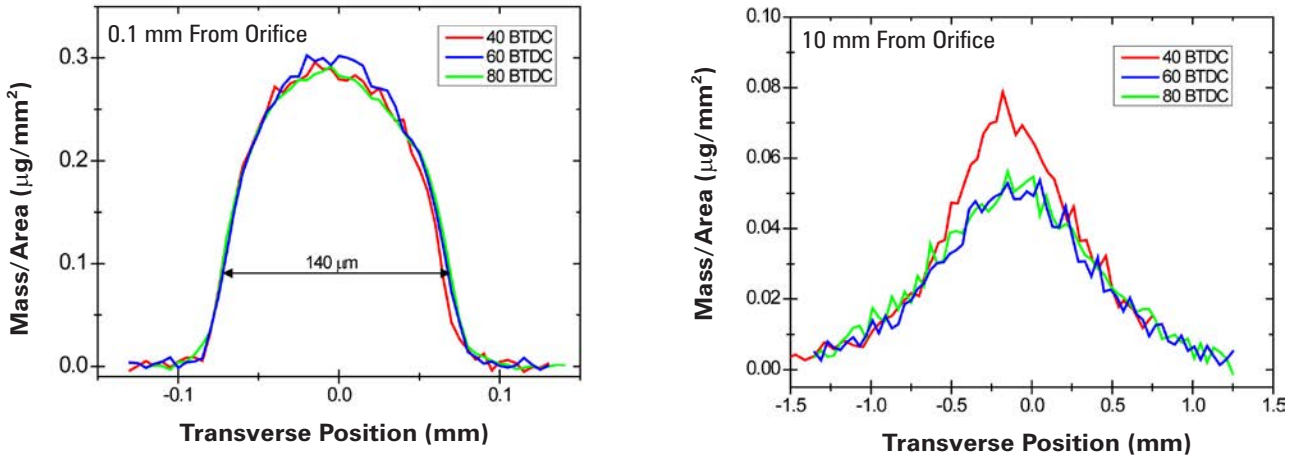

FIGURE 3. Projected fuel density for three different engine operating conditions in slices 0.1 mm (left) and 10 mm (right) from the nozzle. Near the nozzle the distributions are identical, but as the spray develops the in-cylinder density affects the fuel distribution.

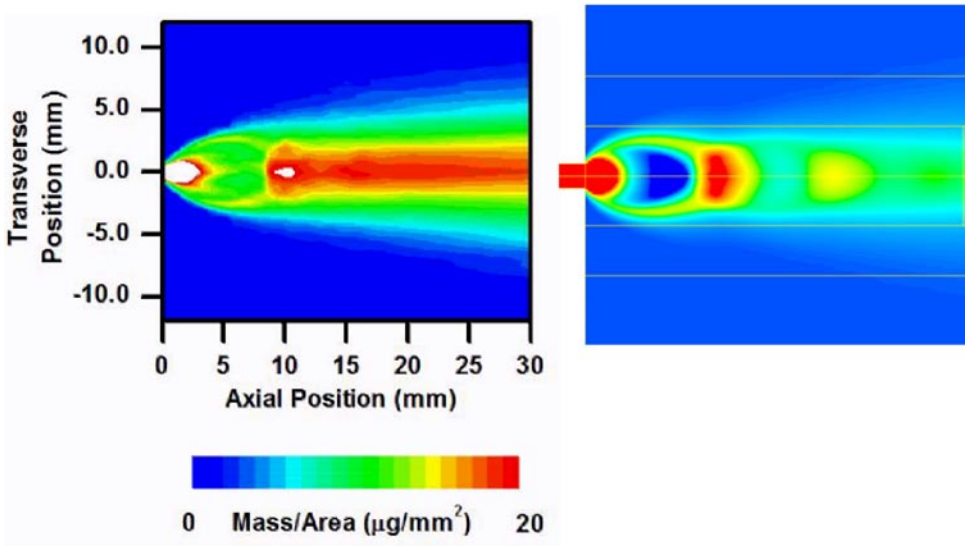

FIGURE 4. Measurements (left) and computational fluid dynamics simulations (right) of gas jets from a hydrogen/natural gas injector.

them to test their models in the spray formation region, something that was impossible previously. This data is crucial for the development of accurate spray models and for the detailed understanding of spray behavior. The quantitative measurements that we have provided may help to elucidate the mechanisms of spray atomization. This could ultimately lead to the design of cleaner, more efficient engines.

- The impact of our work on the engine community is shown by the expanding list of collaborators and by the significant in-kind contributions to our work that are being made by fuel system and engine manufacturers.

References

1. "Time-Resolved Measurements of Supersonic Fuel Sprays using Synchrotron X-rays", C.F. Powell, Y. Yue, R. Poola, and J. Wang, *J. Synchrotron Rad*. 7:356-360 (2000).

2. "Spray Density Measurements Using X-Ray Radiography" A.L. Kastengren, C.F. Powell, *Journal of Automobile Engineering*, Volume 221, Number 6, 2007, pp 653-662.

FY 2011 Publications/Presentations

1. "Application of X-Ray Fluorescence to Turbulent Mixing", A.L. Kastengren, C.F. Powell, E.M. Dufresne, D.A. Walko, Journal of Synchrotron Radiation 18, September 2011, pp. 811-815.

2. "Initial Evaluation of Engine Combustion Network Injectors with X-Ray Diagnostics", A.L. Kastengren, C.F. Powell, S. Moon, J. Gao, X. Zhang, K. Fezzaa. 23rd Annual Conference on Liquid Atomization and Spray Systems, Ventura, CA, May 2011.

3. "Correlation of Split-Injection Needle Lift and Spray Structure", A.L. Kastengren, C.F. Powell, Z Liu, S. Moon, J. Gao, X. Zhang, J. Wang, Society of Automotive Engineers, Paper 2011-01-0383 (2011).

4. "The Effects of Diesel Injector Needle Motion on Spray Structure", C.F. Powell, A.L. Kastengren, Z. Liu, K. Fezzaa. Journal of Engineering for Gas Turbines and Power 133, Issue 1, January 2011.

II.A.2 Low-Temperature Automotive Diesel Combustion

Paul Miles
Sandia National Laboratories
PO Box 969
Livermore, CA 94551-0969

DOE Technology Development Manager:
Gurpreet Singh

Subcontractor:
University of Wisconsin Engine Research Center,
Madison, WI

Overall Objectives

- Provide the physical understanding of the in-cylinder combustion processes needed to minimize the fuel consumption and the carbon footprint of automotive diesel engines while maintaining compliance with emissions standards.
- Develop efficient, accurate computational models that enable numerical optimization and design of fuel-efficient, clean engines.
- Provide accurate data obtained under well-controlled and characterized conditions to validate new models and to guide optimization efforts.

Fiscal Year (FY) 2011 Objectives

- Quantify the in-cylinder swirling flow field in the General Motors (GM) 1.9 L diesel engine to evaluate flow asymmetries and their impact on combustion, and to provide quantitative data for model initialization and evaluation.
- Develop and apply optical diagnostic techniques to characterize quantitatively in-cylinder equivalence ratio and post-combustion CO distributions.
- Formulate a phenomenological model of low-temperature combustion (LTC) processes in light-duty engines to guide combustion system design and calibration engineers.

Accomplishments

The accomplishments below target the barriers of 1) lack of fundamental knowledge, and 2) lack of a predictive modeling capability identified in the DOE Vehicle Technologies Program 2011-2015 multi-year program plan:

- Demonstrated that the mean flow swirl structure in the GM 1.9 L engine is highly tilted, and that the structure is repeatable on individual cycles, insensitive to swirl ratio, and less variable at high swirl. Further developed flow initialization guidelines for closed cycle simulations and assessed the impact of newly developed RNG (Re-normalization Group) turbulence closures for compressible flows on predicted swirl structures.
- Established a quantitative fuel tracer laser-induced fluorescence (LIF) capability, applied the technique to characterize the mixture preparation process, and compared the measurements to model predictions.
- Analyzed the factors impacting and improved the modeling of the temperature dependency of the CO LIF signal, enabling quantitative CO measurements for model validation.
- Developed a phenomenological picture of both early- and late-injection LTC systems describing the mixture formation and subsequent combustion process.

Future Directions

- Quantitatively evaluate the influence of swirl ratio and injection pressure on the fuel-air equivalence ratio distributions formed during the mixture preparation process.
- Correlate the impact of the equivalence ratio distributions on engine-out emissions and post-combustion, in-cylinder distributions of unburned hydrocarbons (UHC) and CO.
- Evaluate the impact of asymmetrical features of the head and piston top on the mixture preparation, combustion, and emissions formation processes, and the appropriateness of sector modeling of the combustion chamber.
- Extend flow measurements into the squish volume near top-dead center (TDC) to evaluate the impact of flow structures and asymmetries on the mixture preparation, combustion, and emissions formation processes.

✧ ✧ ✧ ✧ ✧

Introduction

Direct-injection diesel engines have the highest proven brake fuel efficiency of any reciprocating internal combustion engine technology. However, conventional diesel combustion produces elevated emissions of both soot and oxides of nitrogen (NO_x). To address this shortcoming, LTC techniques that prevent the formation of these pollutants within the engine are being developed. However, these techniques employ high levels of dilution, which creates challenges in mixing

the fuel with sufficient oxidant and which also slows the reaction kinetics. These factors can result in loss of efficiency and in high levels of UHC and CO emissions. A major focus of this work is to understand the main causes of combustion inefficiency, through examination of the in-cylinder mixture preparation process that can lead to slow or delayed combustion and to UHC and CO emissions.

This year, we have particularly concentrated on characterizing the in-cylinder flow, just prior to the start of the mixture formation process, to better understand how it impacts the in-cylinder fuel distributions formed. We have also developed and applied a technique to quantitatively measure the fuel distribution, and we have compared and contrasted both the flow and fuel distribution measurements to the results of numerical simulations—to aid in the development of a truly predictive simulation capability. We have also used these data, in conjunction with UHC and CO distributions measured in FY 2009 and FY 2010, to develop a phenomenological picture of the progress of LTC processes in light-duty engines that can serve as a guide to the engine design or calibration engineer.

Approach

The research approach involves carefully coordinated experimental, modeling, and simulation efforts. Detailed measurements of in-cylinder flows, fuel and pollutant spatial distributions, and other thermo-chemical properties are made in an optical engine facility with geometric and thermodynamic characteristics that allow it to closely match the combustion and engine-out emissions behavior of a traditional, all-metal test engine. These measurements are closely coordinated and compared with the predictions of numerical simulations.

The experimental and numerical efforts are mutually complementary. Detailed measurements of the in-cylinder variables permit the evaluation and refinement of the computer models, while the model results can be used to obtain a more detailed understanding of the in-cylinder flow and combustion physics—a process that is difficult if only limited measurements are employed. Jointly, these efforts address the principal goals of this project: development of the physical understanding to guide and the modeling tools to refine the design of optimal, clean, high-efficiency combustion systems.

Results

Figure 1 depicts the geometry of the optically accessible engine and the experimental set-up used to measure the flow velocity or the equivalence ratio distributions. A horizontal laser sheet is passed through windows in the cylinder liner, and illuminates a plane within the combustion chamber. Elastically scattered light from particles (for velocity measurements) or

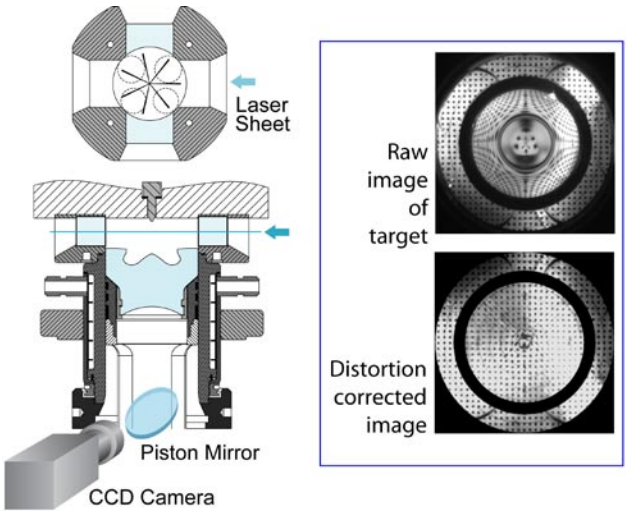

FIGURE 1. Schematic of the optically accessible engine and the experimental configuration employed for both the flow (particle image velocimetry) and scalar (fuel-tracer LIF) measurements.

laser-induced fluorescence (for fuel concentration or equivalence ratio measurements) is collected through the optical piston, and imaged onto a charge coupled device (CCD) camera. The images acquired are distorted by the curved surfaces of the transparent piston; however, a corrective transformation is derived from calibration targets and is employed to obtain distortion-free images.

An example of a mean velocity field, obtained 50° before TDC (bTDC) during the compression stroke, is shown in the upper portion of Figure 2. Notice that the apparent center of the swirling flow is offset considerably from the geometric center of the cylinder. Through analysis of similar images obtained in multiple planes, for several swirl ratios, it is possible to examine the mean swirl structure and how it varies with both swirl ratio and on a cycle-to-cycle basis. The result of this examination is shown in the lower portion of the figure, which depicts the (x,y) coordinates of the swirl center for three different measurement plane heights and for three different swirl ratios. Notice that the tilt of the axis of the swirl structure is severe: the displacement of the swirl center in the y-coordinate direction is generally greater than the axial distance between planes. Thus, the zenith angle between the axis of the swirl structure and the cylinder centerline exceeds 45°.

It is remarkable that as the swirl ratio is varied, the flow structure does not change significantly. Both the zenith angle and the azimuth angle defined by the projection of the swirl axis on a horizontal plane do not vary significantly. This suggests that the tilt of the swirl structure may be determined largely by geometric features of the combustion chamber, rather than the flows created during the induction process. The large circles surrounding the swirl center markers represent

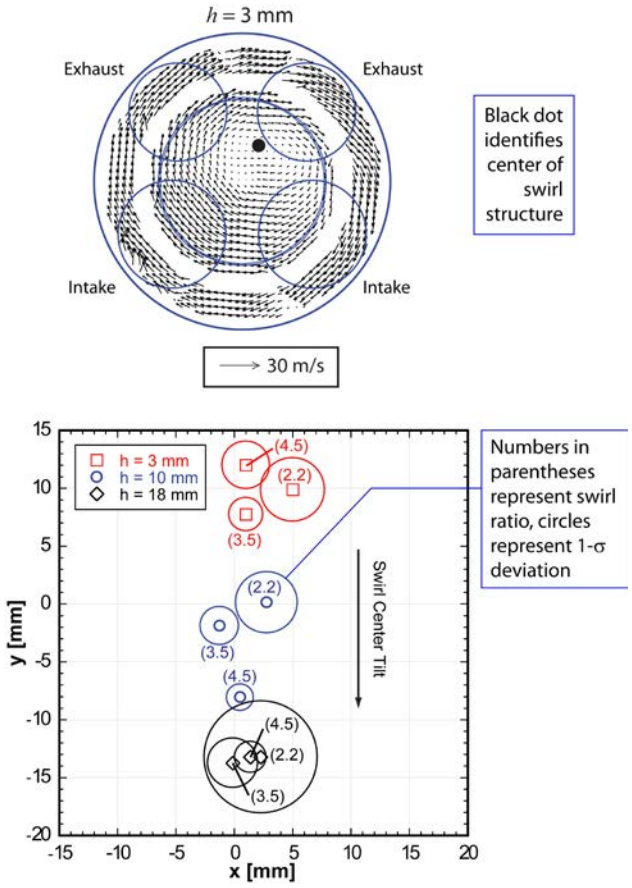

FIGURE 2. Mean velocity field measured at 50° bTDC in the compression stroke (top) and plot of swirl center position as a function of height below the cylinder head and bulk swirl ratio (bottom).

the standard deviation of the swirl center, as determined from 100 single-cycle images. The small standard deviation, relative to the change in the mean swirl center displacement with axial location, indicates that the gross structure of the flow is repeatable from cycle-to-cycle. Furthermore, the repeatability is better at higher swirl ratio—as indicated by the smaller diameter circles associated with the high-swirl measurements. Work is in progress to ascertain if these findings can be predicted via numerical simulation.

In addition to providing test data to validate numerical simulations, these measurements also serve to define appropriate initial conditions for closed cycle simulations—when the full induction stroke is not calculated but is initialized based on swirl ratio R_s, which measures the total in-cylinder angular momentum. The swirl profile is often specified in terms of the Bessel functions J_1 and J_2, the crankshaft rotational speed ω_c, the bore radius r_b, and a non-dimensional parameter α, using the relationship shown in Figure 3. Our measurements, averaged over all measurement locations and swirl ratios, indicate that a close match to the

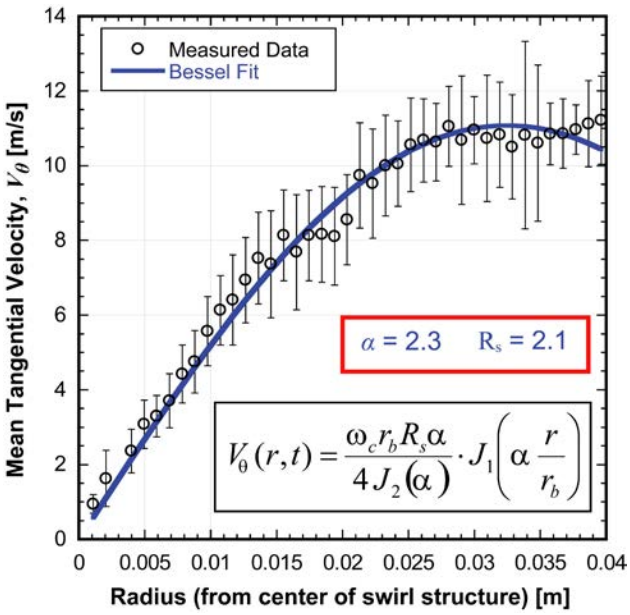

FIGURE 3. An example of the radial profile of the mean tangential velocity, measured 3 mm below the head at a nominal (flow bench) swirl ratio of 2.2.

measured swirl profiles can be obtained by adopting the value 2.2 for α. An example of a measured swirl profile, and the Bessel function based profile, is also shown in Figure 3. Comparison of these measurements with previous measurements [1] made in a different engine show that this value of α has some universality, *i.e.*, it is independent of the particular port geometry or method used to generate the in-cylinder swirl.

The in-cylinder velocity field can also be expected to impact the mixture preparation process, which we have characterized using a toluene tracer to quantitatively measure the in-cylinder equivalence ratio distributions. An example of the results, obtained at a low load, 3 bar indicated mean effective pressure (IMEP) operating condition, just prior to the onset of low-temperature heat release, is shown in Figure 4. Three planes are shown; each one is designated by its distance from the cylinder head. One plane bisects the squish height, one plane lies within the rim of the bowl, and one plane is in the lower, reentrant region of the bowl. Regions which were not visible due to optical distortion or laser sheet obstruction are represented by the white areas in the images. Despite the fact that the ignition dwell is positive (end-of-injection [EOI] ≈ 18° bTDC), there are still significant rich regions present in the cylinder at this early stage of ignition. Note that there are also significant asymmetries, particularly as manifested by the penetration of the individual fuel jets into the squish volume. This asymmetry correlates strongly with the mean flow swirl center offset measured at this crank angle, suggesting a direct link between the flow field and the fuel-air distributions.

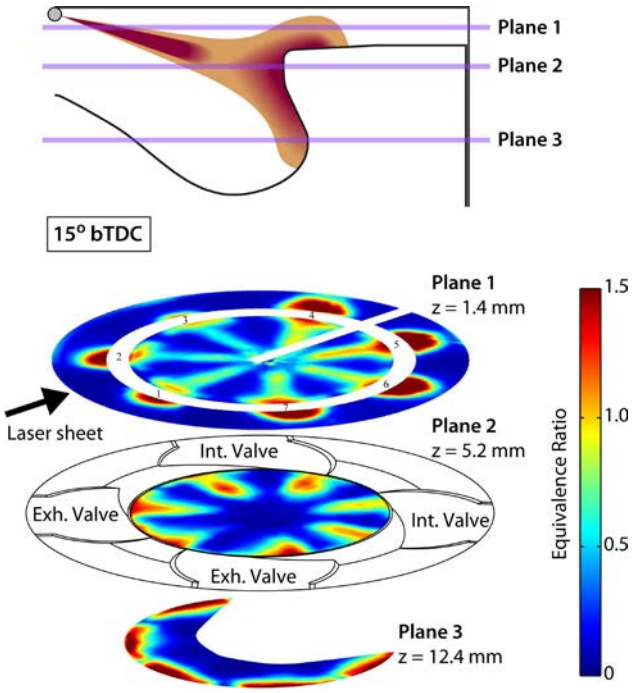

FIGURE 4. Mean fuel-air equivalence ratio distributions measured at a light-load (3 bar IMEP), early-injection LTC operating condition. The distributions were measured approximately 3° after EOI, just prior to the onset of low-temperature heat release.

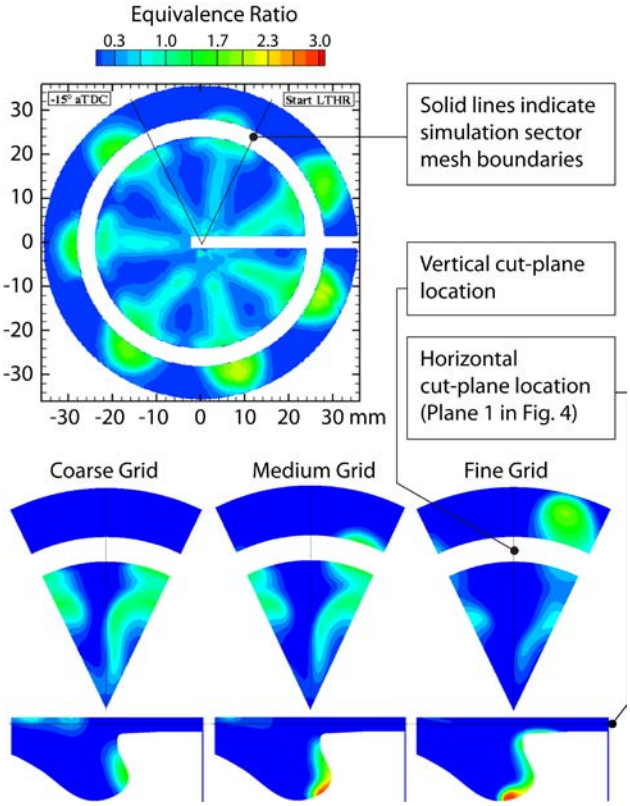

FIGURE 5. Comparison of measured and simulated equivalence ratio distributions in Plane 1 for various computational grid resolutions.

To further examine the impact of the swirling flow on the mixture formation process, the measured equivalence ratio distributions have also been compared with the results of numerical simulations conducted at the University of Wisconsin, and the effect of various computational parameters evaluated to examine the sensitivity of the results to these parameters. An example of such a comparison, targeted at understanding the required computational grid resolution, is shown in Figure 5. This comparison is made for the data shown in Plane 1 in Figure 4; however, a different color scale is used to present the results. Clearly, the results are quite sensitive to the grid resolution, and a very fine grid (158,000 cells at bottom-dead center) is required to capture the penetration accurately. The simulations also predict a significant distortion of the jet structure by swirl, which is not readily apparent in the experimental data. In this regard also, the results obtained with the fine resolution grid—which show the least distortion—better match the experimental data.

A further investigation of the impact of the flow simulation initialization methodology was conducted, which indicated that the impact of flow field inhomogeneity on the fuel-air distributions is expected to be small. This is seemingly in contrast to the large predicted impact of the swirl flow on the jet structure, and on the experimentally observed correlation between flow and mixture asymmetries. Additional measurements, with careful comparison to simulation results, are needed at various swirl ratios to definitively establish if the link between the flow field and the fuel-air distributions at the start of combustion is significant.

Conclusions

Quantitative in-cylinder flow and fuel-air mixture distribution measurements, coupled with numerical simulations, have provided considerable insight into the physics of the mixture formation process. The impact of various modeling parameter choices and modeling practice on the accuracy of the simulation results has also been investigated. Examples of conclusions reached from this work are:

- Significant asymmetries are found in the swirling flow field, which are insensitive to the swirl level and repeatable on a cycle-to-cycle basis.
- Measured radial profiles of the tangential velocity can be well fit with an analytical form based on Bessel functions by specifying the swirl ratio and using a non-dimensional parameter $\alpha = 2.2$. Simulations indicate that initializing the flow field in this manner near intake valve closing provides nearly identical in-cylinder flow fields at start of injection as flow

fields initialized from three-dimensional simulations employing a full-cylinder mesh.

- Asymmetries are also observed in the fuel-air distributions near the start of combustion, which correlate strongly with measured flow asymmetries. On-going work is aimed at identifying the cause of these asymmetries and at understanding their impact on the ensuing combustion process.

References

1. "The Evolution of Flow Structures and Turbulence in a Fired HSDI Diesel Engine," Miles P, Megerle M, Sick V, Richards K, Nagel Z, and Reitz, RD. *SAE Technical Paper 2001-01-3501.*

FY 2011 Publications/Presentations

1. "Equivalence Ratio Distributions in a Light-Duty Diesel Engine Operating under Partially-premixed Conditions," Petersen BR, Miles PC, Sahoo D. *Submitted to the 2012 SAE World Congress, Offer No.: 11PFL-0814.*

2. "Comparison of Quantitative In-Cylinder Equivalence Ratio Measurements with CFD Predictions for a Light Duty Low Temperature Combustion Diesel Engine," Dempsey AB, Wang B-L, Reitz RD, Petersen BR, Sahoo D, Miles PC. *Submitted to the 2012 SAE World Congress, Offer No.: 12PFL-1094.*

3. "Validation of the Generalized RNG Turbulence Model and Its Application to Flow in an HSDI Diesel Engine," Wang B-L, Bergin MJ, Petersen BR, Miles PC, Reitz RD, Han Z. *Submitted to the 2012 SAE World Congress, Offer No.: 12PFL-0782.*

4. "Measurement of Equivalence Ratio in a Light-Duty Low Temperature Combustion Diesel Engine by Planar Laser Induced Fluorescence of a Fuel Tracer," Sahoo D, Petersen BR, Miles PC. *SAE Int. J. Engines August 2011 4:2312-2325; doi:10.4271/2011-24-0064. Presented at ICE2011: 10th International Conference on Engines & Vehicles, September 11–15, 2011, Capri, Napoli, Italy.*

5. "Optical Investigation into Wall Wetting from Late-Cycle Post-Injections used for Diesel Particulate Filter Regeneration," Bozic G, Kook S, Ekoto IW, Petersen BR, Miles PC. *J. Eng. Gas Turbines Power, Vol. 133, No. 9, 092803; September 2011. doi:10.1115/1.400291.*

6. "Advanced Combustion Research for Enabling High-Efficiency, Clean Engines for Future Fuels and "Sources of UHC and CO in Low Temperature Diesel Combustion Systems," Miles PC. *Invited presentations at Korea Institute of Machinery and Materials and Doosan Infracore, Daejeon and Incheon Korea, Sept. 5–6, 2011.*

7. "Measurement of Equivalence Ratio in a Light-Duty Low Temperature Combustion Diesel Engine by Planar Laser-Induced Fluorescence of a Fuel Tracer (Toluene)," Sahoo D, Petersen BR, Miles PC. *US DOE/OVT Advanced Engine Combustion Meeting, August 23–25, 2011.*

8. "PIV Measurements in the Swirl-Plane of a Motored Light-Duty Diesel Engine," Petersen BR, Miles PC. *SAE Int. J. Engines June 2011 4:1623-1641; doi:10.4271/2011-01-1285. Presented at the SAE 2011 World Congress.*

9. "Light-Duty Combustion Experiments and Modeling," Miles PC, Reitz, RD. *DOE EERE-OVT Annual Merit Review, May 10, 2011.*

10. "A Combined Experimental and Numerical Evaluation of RNG Turbulence Closure Dissipation Modeling in Incompressible and Compressible Flows," Wang B-L, Reitz, RD, Han Z, Miles PC, Petersen BR. *SAE Technical Paper 2011-01-0829, Presented at the SAE 2011 World Congress, April 11–14, 2011.*

11. "Effect of Fuel Properties on UHC and CO Emissions from Partially Premixed Combustion," Petersen BR, Ekoto IW, and Miles PC. *Presented and in the Proceedings of the 10th International Congress on Engine Combustion Processes: Current Problems and Modern Techniques, 24–25 March, 2011, Munich, Germany.*

12. "PIV Measurements in the Swirl Plane of a Motored Light-Duty Diesel Engine," Petersen BR, Sahoo D, Miles PC. *US DOE/OVT Advanced Engine Combustion Meeting, Feb. 22, 2011.*

13. "Analysis of EGR Effects on the Soot Distribution in a Heavy Duty Diesel Engine using Time-Resolved Laser Induced Incandescence", Aronsson U, Chartier C, Andersson Ö, Johansson B, Sjöholm J, Wellander R, Richter M, Aldén M, and Miles PC. *SAE Int. J. Engines December 2010 3:137-155; doi: 10.4271/2010-01-2104. Presented at the SAE 2010 International Powertrain, Fuels, and Lubricants Meeting, Oct. 25–27, 2010.*

Special Recognitions

1. Welcoming Address and Executive Panel Discussion Moderator, Miles PC. *2011 Joint JSAE/SAE International Powertrain Fuels and Lubricants Conference, August 30 – Sept. 2, 2011, Kyoto, Japan.*

2. Invited Talk "Quantitative In-Cylinder CO Measurements in Engines," Miles PC. *Gordon Research Conference on Laser Diagnostics in Combustion, August 14–19, 2011, Waterville Valley, NH.*

3. Invited Talk "Laser Diagnostics in IC Engines," Miles PC. *International Energy Agency 33rd Task Leaders Meeting on Energy Conservation and Emissions Reduction in Combustion, August 7–11, 2011, Lund, Sweden.*

4. Invited Workshop Presentation "Spectrally-Resolved, Multi-Photon CO and UHC LIF Diagnostics in Engines," Miles PC. *12th International School of Advanced Optical Technologies Workshop on Engine Diagnostics, March 28–29, 2011, Erlangen, Germany.*

5. Invited Workshop Presentation "Jet and Engine Flow Studies Applying Ruby and Rare Earth Phosphor Particles," Petersen BR. *12th International School of Advanced Optical Technologies Workshop on Engine Diagnostics, March 28–29, 2011, Erlangen, Germany.*

II.A.3 Heavy-Duty Low-Temperature and Diesel Combustion and Heavy-Duty Combustion Modeling

Mark P.B. Musculus
Combustion Research Facility
Sandia National Laboratories
P.O. Box 969, MS9053
Livermore, CA 94551-0969

DOE Technology Development Manager:
Gurpreet Singh

Overall Objectives

This project includes diesel combustion research at Sandia National Laboratories (SNL) and combustion modeling at the University of Wisconsin (UW). The overall objectives are:

- Develop fundamental understanding of how in-cylinder controls can improve efficiency and reduce pollutant emissions of advanced low-temperature combustion (LTC) technologies.
- Quantify the effects of fuel injection, mixing, and combustion processes on thermodynamic losses and pollutant emission formation.
- Improve computer modeling capabilities to accurately simulate these processes.

Fiscal Year (FY) 2011 Objectives

- Quantify oxidation of piston-bowl soot remaining from main injection by narrow included-angle post-injections (SNL).
- Characterize reactivity-controlled compression-ignition (RCCI) combustion using high-speed imaging diagnostics (SNL and UW).
- Define the in-cylinder conditions that govern transitions between flame propagation and distributed autoignition combustion modes (SNL and UW).
- Compare multi-mode combustion model predictions to measurements of combustion propagation (UW).

Accomplishments

- Narrow-angle injector shows no significant in-cylinder soot oxidation benefit with post injections, and has a detrimental effect on soot from the main injection, increasing the filter smoke number to 1.5 compared to 0.6 for narrow angle injector.
- High-speed imaging shows how in-cylinder fuel reactivity gradients affect the in-cylinder progression of combustion, decreasing peak heat release rates by up to 60% with a properly tailored mixture field.
- The combustion regimes, as defined by propensity for flame growth from artificial spark ignition, ranges from 20% of near the chamber center to almost 80% near the piston bowl wall.
- Computer models predict that most of RCCI should be dominated by kinetics, but flame propagation can be important locally, especially near the piston bowl wall, similar to experimental observations with artificial spark ignition.

Future Directions

- Probe in-cylinder mixing and combustion processes of high-efficiency dual-fuel operation:
  - Build a fundamental understanding of in-cylinder processes that contribute to improved efficiency.
  - Incorporate insight and validation data from optical experiments exploring transitions from distributed autoignition to flame propagation to improve model fidelity.
- Explore multiple-injection efficiency and emissions:
  - Quantify emissions and efficiency improvements across wide parameter space to identify critical requirements.
  - Use laser diagnostics (fuel-tracer, formaldehyde, and OH planar laser induced fluorescence) to understand governing in-cylinder mechanisms.
- Build understanding of in-cylinder LTC soot and polycyclic aromatic hydrocarbons (PAH):
  - Use multiple laser wavelengths and high-temporal-resolution imaging/spectroscopy to track PAH growth and conversion to soot.

Introduction

Recently, a dual-fuel strategy with the potential for indicated thermodynamic efficiency above 50% while meeting 2010 particulate matter (PM) and nitrogen oxides (NOx) emissions target at low to moderate loads has been developed at the UW Engine Research Center [1-3]. In this RCCI strategy, two fuels with differing autoignition characteristics (e.g., gasoline and diesel fuel) are blended in the combustion chamber using separate fuel-injection hardware. Unlike many high-

efficiency single-fuel premixed compression-ignition strategies, the in-cylinder mixture of the two fuels creates a variation in reactivity across the combustion chamber, which provides a way to control the overall rate of combustion, and hence the pressure-rise rate. Controlling the pressure-rise rate is important because at higher engine loads, many LTC strategies suffer from excessive pressure-rise rates that can be detrimental for engine durability and noise. Given the novelty of the RCCI operational strategy, the in-cylinder progression of combustion through the dual-fuel charge that yields a controlled energy release is largely unexplored. RCCI combustion needs to be characterized using optical diagnostics to provide a clearer picture of the general in-cylinder development of combustion for RCCI to aid its development and optimization, as well as to support computer modeling of RCCI strategies.

In addition to understanding the influence of fuel reactivity distributions on the progression of combustion, the regime of combustion for RCCI has not been established. With RCCI, the range of fuel-air mixtures and in-cylinder conditions are wide enough that combustion modes ranging from flame propagation to distributed autoignition could conceivably occur, and transitions between modes may also occur. A fundamental understanding of how in-cylinder mixtures and thermodynamic conditions affect RCCI combustion modes and transitions between them is needed to further conceptual understanding and computer model development.

Approach

This project uses an optically accessible, heavy-duty, direct-injection diesel engine (Figure 1). A large window in the piston crown provides primary imaging access to the piston bowl, and other windows at the cylinder wall provide cross-optical access for laser diagnostics. To achieve dual-fueling for RCCI, a new Bosch gasoline direct injector (GDI) capable of injection pressures up to 100 bar was added in place of one of the five cylinder-wall windows (see Figure 1). For diesel-type fuels, the engine retains a centrally located Cummins XPI common rail (CR) injector, which is capable of multiple injections at rail pressures up to 2,200 bar. For other optical diagnostic studies not described here, conventional gasoline and diesel fuels cannot be used because of fluorescence interferences from aromatic components in the fuels. Hence, low-fluorescence surrogate fuels were used in this study, iso-octane for gasoline and n-heptane for diesel fuel.

To image the progression of combustion with RCCI, we use a high-speed Phantom 7.1 complementary metal oxide semiconductor (CMOS) digital camera. The camera is operated at 7,200 frames per second, which corresponds to a resolution of one crank angle degree at the engine crankshaft speed of 1,200 rotations

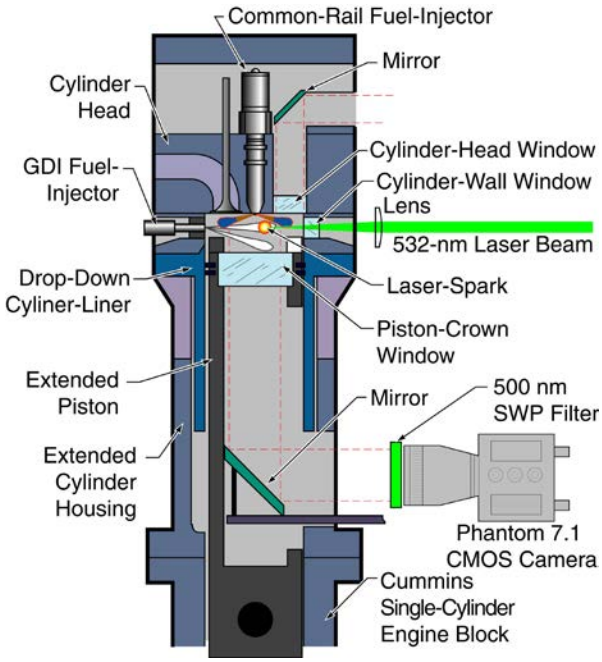

FIGURE 1. Schematic Diagram of the Optically Accessible Direct Injection Diesel Engine and Optical Setup

per minute. The combustion luminosity captured by the camera is filtered with a short wave-pass filter with a cutoff near 500 nm, which helps to reject longer-wavelength soot emission while accepting shorter wavelength chemiluminescence emission from radical species such as CH, C_2, and CH_2O. The camera is sensitive enough to easily capture bright chemiluminescence from second-stage ignition, and under some LTC conditions, it even displays a weak signal from first-stage low-temperature ignition. Additionally, for some conditions, the charge is artificially ignited using a 10-ns long, 100-mJ pulse at 532 nm from a Nd-doped yttrium aluminum garnet laser that is focused to a small (~100 micron) point in the combustion chamber. The focused laser energy exceeds the dielectric strength of the fuel-air mixture so that a plasma (spark) is created, which ignites the fuel if the mixture can support a flame, similar to conventional spark plug ignition. The position of the artificial laser-spark within the chamber may be adjusted by moving the lens shown in Figure 1.

Results

The rate of combustion for RCCI is controlled by the in-cylinder distribution of fuel reactivity, which is dependent on the amount of fuel-air mixing. One way to affect degree of fuel mixing for the diesel-type fuel (n-heptane) is to adjust the start of injection (SOI) – conditions with earlier SOI have more time to mix and are more homogeneous. Figure 2 shows the heat release

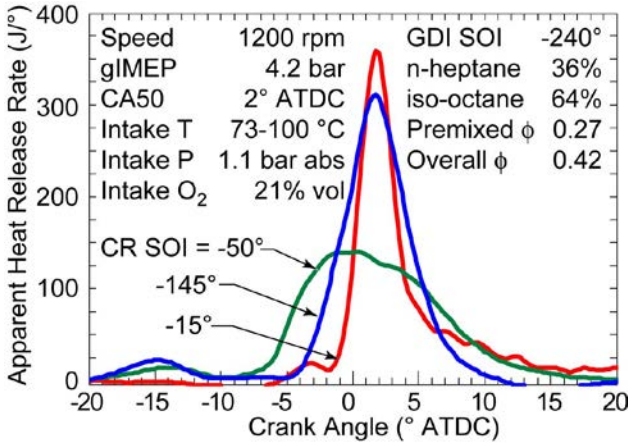

FIGURE 2. Apparent heat release rates for low-load LTC conditions as indicated in the inset table, at three different n-heptane injection timings.

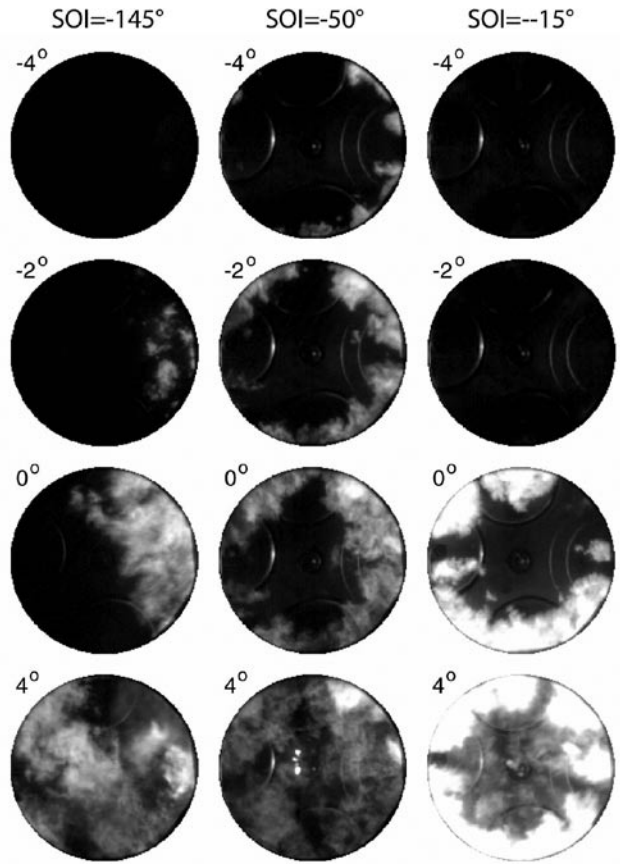

FIGURE 3. Time sequence of combustion luminosity for the three conditions in Figure 2, as viewed through the piston bowl window.

rates for three different CR SOI timings. As indicated in table within Figure 2, all three conditions used the same fueling rate corresponding to a gross indicated mean effective pressure (gIMEP) of 4.2 bar, and with the intake temperature adjusted to keep the 50% heat release timing (CA50) constant at 2° after top-dead center (ATDC). In the full high-resolution timing sweep (not shown), the peak apparent heat release rate (AHRR) is high for more homogeneous conditions with very early CR SOI, such as near -145° ATDC, then decreases by as much as 60% at a typical RCCI condition with an intermediate CR SOI near -50° ATDC, and increases again for later injection timings (such as near -15° ATDC).

Figure 2 clearly shows that the combustion rate with dual fueling of gasoline- and diesel-like fuels is strongly affected by SOI timing. The peak AHRR, and hence the peak pressure rise rate, may be lowered by adjusting the CR SOI. To better understand the in-cylinder mechanisms controlling the peak AHRR, combustion luminosity was recorded using a high-speed CMOS camera as shown in Figure 1. Figure 3 shows time sequences of chemiluminescence images of the in-cylinder ignition and combustion propagation for the three conditions in Figure 2. For the more homogeneous condition with CR SOI at -145° ATDC, combustion progresses rapidly throughout the chamber, with ignition near -2° ATDC, spreading through one side the piston bowl at 0° ATDC, and progressing across the entire bowl by 4° ATDC. By contrast, the typical RCCI condition with some reactivity stratification ignites earlier, near -4° ATDC, and then progresses more slowly through the combustion chamber, generally from the bowl-wall region toward the chamber center. Other measurements of the in-cylinder fuel concentration (not shown here), indicate that the ignition gradually proceeds from regions of higher reactivity (more diesel-like fuel) to regions with lower reactivity (less diesel-like fuel), which helps to spread out the AHRR. Finally, for the late-injection condition (CR SOI = -15° ATDC), ignition occurs very rapidly, starting at 0° ATDC, and progressing throughout the chamber by 4 ATDC. In-cylinder fuel concentration measurements (not shown here) indicate that much of the mixtures for this late-injection condition are near stoichiometric or fuel-rich. Such mixtures ignite at nearly the same time, so that the peak AHRR is high.

Although Figure 3 illustrates how the combustion progression is affected by the CR SOI and hence the in-cylinder fuel reactivity gradients, it does not reveal the regime of combustion, whether flame propagation or distributed autoignition. For RCCI, combustion may progress from one region to another either by flame propagation, where hot combusting regions propagate outward by igniting nearby mixtures, or by sequential autoignition, where different regions ignite on their own as controlled by local conditions, without any influence from nearby hot regions. To help define the ability of local mixtures to support flame propagation, an artificial laser spark was positioned in different regions of the chamber, using the focused laser beam illustrated

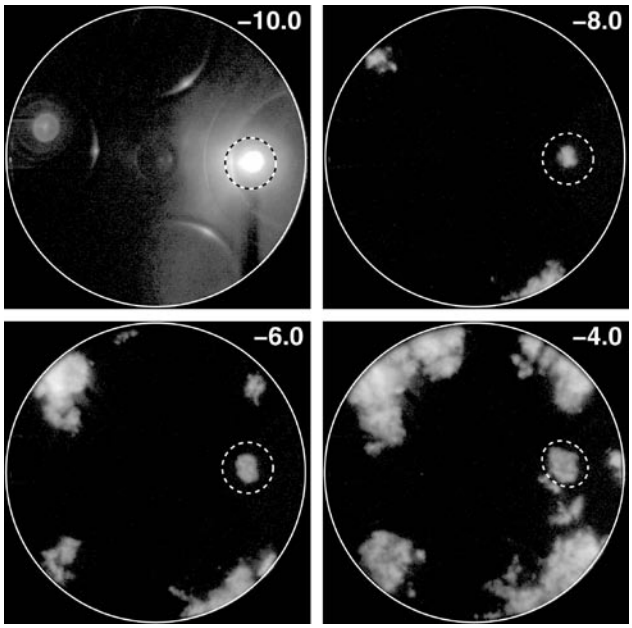

FIGURE 4. Time sequence of artificial laser spark followed by flame kernel growth for RCCI condition similar to the CR SOI = -50° ATDC injection timing in Figure 2.

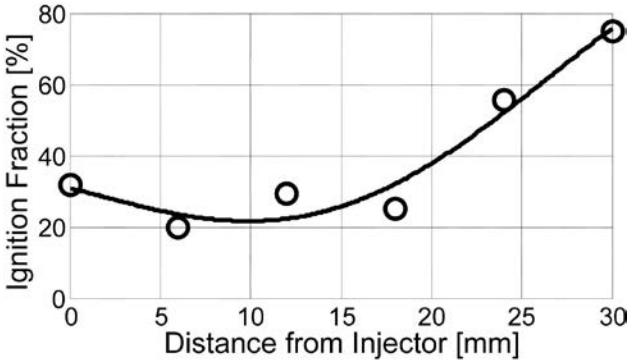

FIGURE 5. Probability of flame kernel growth following artificial spark at various locations for RCCI condition similar to the CR SOI = -50° ATDC injection timing in Figure 2.

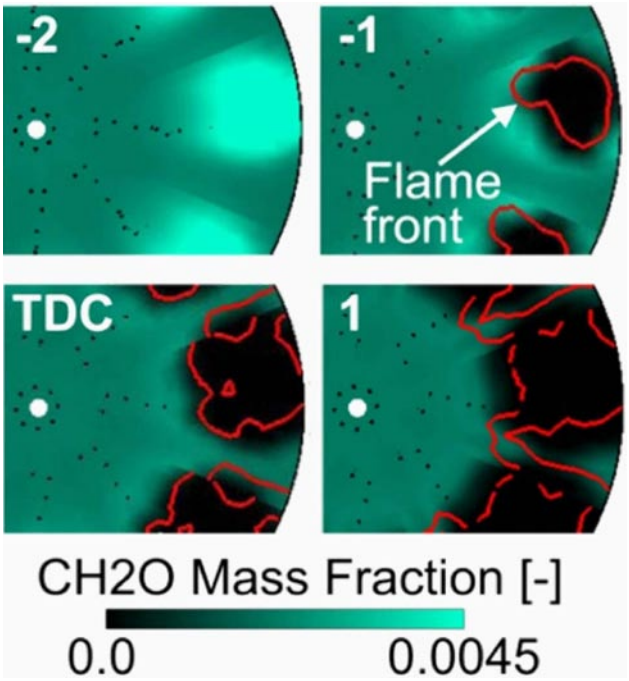

FIGURE 6. Model predictions of formaldehyde (CH_2O) mass fraction (color map) and flame front growth (red curves) for RCCI condition similar to the CR SOI = -50° ATDC injection timing in Figure 2. The images show a partial view of the piston bowl, with the CR injector indicated by the white dot on the left and the curved bowl wall on the right.

in Figure 1. Figure 4 shows an example time-series of images following an artificial laser spark focused at 30 mm from the injector for an RCCI condition similar to the CR SOI = -50° ATDC injection timing in Figure 2. The spark, which is inside the dash-line circle in the -10° ATDC image, is introduced just before the mixture would ignite on its own. This spark timing was intentionally selected to probe the flammability of mixtures under conditions most similar to where ignition occurs naturally. After the artificial spark, the kernel grows over the next several images, until other nearby regions ignite and start to merge with the sparked kernel. Not all artificial sparks lead to flame kernel growth, and the probability of growth depends on the spark location within the chamber. Figure 5 shows that sparks near the center of the chamber have a lower probability of growth, near 20%, while sparks near the piston bowl-wall lead to kernel growth nearly 80% of the time.

Although the artificial sparks show that certain mixtures can support flame propagation, sequential autoignition may still be important during combustion. To further explore the importance of flame propagation, computer modeling can provide some insight, and the experiments can further validate the model predictions. Figure 6 shows model predictions of formaldehyde (CH_2O) distributions near ignition, along with flame zones (red curves), for an RCCI condition similar to the CR SOI = -50° ATDC injection timing in Figure 2. Formaldehyde is a combustion intermediate, and its consumption is indicative of second-stage ignition. The model switches between kinetics calculations (sequential autoignition) and a G-equation model (flame propagation) depending on the local Damkohler number. Figure 6 shows that when ignition occurs, about 40% of local regions transition to flame propagation, and most are located near the bowl wall. The model predictions of more flame propagation near the bowl wall agree with the experimental observations of greater probability of flame propagation near the bowl wall.

Conclusions

The recent research efforts described in this report provide improved understanding of in-cylinder LTC mixing and combustion processes required by industry to build cleaner, more efficient, heavy-duty engines. Specific conclusions include:

- High-speed imaging shows how in-cylinder fuel reactivity gradients affect the in-cylinder progression of combustion from regions of higher reactivity to regions of lower reactivity, which can decrease peak heat release rates by up to 60% compared to more homogeneous mixtures.
- Artificial spark ignition shows that the probability of local fuel-air mixtures to support flame propagation ranges 20% of near the chamber center to almost 80% near the piston bowl wall.
- Computer models predict that most of RCCI should be dominated by kinetics, but flame propagation can be important in up to 40% of the chamber, especially near the piston bowl wall, similar to experimental observations with artificial spark ignition.

References

1. Kokjohn, S.L., Splitter, D.A., Hanson, R.M., and Reitz, R.D. "Experiments and modeling of dual fuel HCCI and PCCI combustion using in-cylinder fuel blending," SAE International Journal of Engines 2(2), 24-39 (2010).

2. Hanson, R.M, Kokjohn, S.L., Splitter, D.A., and Reitz, R.D. "An experimental investigation of fuel reactivity controlled PCCI combustion in a heavy-duty engine," SAE International Journal of Engines 3(1), 700-716 (2010).

3. Kokjohn, S.L., Hanson, R.M, Splitter, D.A., and Reitz, R.D. "Fuel reactivity controlled compression ignition (RCCI) combustion in light- and heavy-duty engines," SAE Technical Paper 2011-01-0357 (2011).

FY 2011 Publications/Presentations

1. "Planar Laser-Diagnostics of Soot and OH with Post-Injections in a Heavy-Duty LTC Diesel Engine," M. Bobba, M. Musculus, C. Chartier, THIESEL 2010 Conference, September 2010.

2. "Effects of Post-Injection Strategies on Near-Injector Over-Lean Mixtures and Unburned Hydrocarbon Emission in a Heavy-Duty Optical Diesel Engine," C. Chartier, O. Andersson, B. Johansson, M.P.B. Musculus, M.K. Bobba, Sandia National Laboratories , SAE Paper 2011-01-1383, April 2011.

3. "Relationship Between Diesel Fuel Spray Vapor Penetration/Dispersion and Local Fuel Mixture Fraction," L.M. Pickett, J. Manin, C.L. Genzale, D.L. Siebers, M.P.B. Musculus, C.A. Idicheria, SAE Paper 2011-01-0686, April 2011.

4. "Laser Diagnostics of Soot Precursors in a Heavy-Duty Diesel Engine at Low-Temperature Combustion Conditions," M.K. Bobba and M.P.B. Musculus, Submitted to Combustion and Flame, Jan. 2011.

5. "Diesel Engine Emissions and Combustion Predictions using Advanced Mixing Models Applicable to Fuel Sprays," N. Abani and R.D. Reitz, Combustion Theory and Modeling (14): 715-746, 2010.

6. "High Efficiency, Low Emissions Reactivity Controlled Combustion through use of a Fuel Additive," D.A. Splitter, R. Hanson, and R.D. Reitz, SAE paper 2010-01-2167, 2010.

7. "Fuel Reactivity Controlled Compression Ignition (RCCI): A Pathway to Controlled High-Efficiency Clean Combustion," S.L. Kokjohn, R.M. Hanson, D.A. Splitter, R.D. Reitz, Accepted for publication, International Journal of Engine Research, Special Issue on Fuel Efficiency, 2011.

8. "Investigation of the Roles of Flame Propagation, Turbulent Mixing, and Volumetric Heat Release in Conventional and Low Temperature Diesel Combustion," S.L. Kokjohn and R.D. Reitz, Accepted for publication, ASME J. Eng. Gas Turbines Power, 2011.

9. "Fuel Reactivity Controlled Compression Ignition (RCCI) Combustion in Light-and Heavy-duty Engines," S.L. Kokjohn, R.M. Hanson, D.A. Splitter, J. Kaddatz, R.D. Reitz, SAE Paper 2011-01-0357, 2011.

10. "Fuel Effects on Reactivity Controlled Compression Ignition (RCCI) Combustion at Low Load," R.M. Hanson, S.L. Kokjohn, D.A. Splitter, R.D. and Reitz, SAE Paper 2011-01-0361, 2011.

11. "Reactivity Controlled Compression Ignition (RCCI) Heavy-Duty Engine Operation at Mid-and High-Loads with Conventional and Alternative Fuels," D.A. Splitter, R.M. Hanson, S.L. Kokjohn, and R.D. Reitz, SAE Paper 2011-01-0363, 2011.

II.A.4 Spray Combustion Cross-Cut Engine Research

Lyle M. Pickett
Sandia National Laboratories
P.O. Box 969, MS 9053
Livermore, CA 94551-9053

DOE Technology Development Manager:
Gurpreet Singh

Overall Objectives

Facilitate improvement of engine spray combustion modeling, accelerating the development of cleaner, more efficient engines.

Fiscal Year (FY) 2011 Objectives

- Lead a multi-institution, international, research effort on engine spray combustion called the Engine Combustion Network (ECN).
- Use quantitative engine fuel spray mixing measurements to evaluate the predictive capability of computational fluid dynamics (CFD) and other fuel spray models.
- Quantify the liquid volume fraction distribution near the maximum liquid-phase penetration position in evaporating sprays.

Accomplishments

- Generated a detailed spray dataset working collaboratively with a dozen institutions from around the world. Organized and led the first ECN workshop, where multiple modeling groups submitted results for a side-by-side comparison to this experimental data.
- Demonstrated that the variable-radial-profile model of Musculus and Kattke accurately predicts fuel spray mixture fraction when the model is adjusted (with spreading angle) to match the measured penetration. Comparison with detailed CFD modeling shows similar results.
- Implemented nine different diagnostics at identical spray conditions, combined with rigorous light scattering/extinction analysis, to assess the liquid volume fraction near the liquid length.

Future Directions

- Investigate jet-jet interaction effects on flame lift-off.
- Characterize side-hole sprays compared to axial-hole sprays.
- Develop spray and combustion datasets for gasoline direct injection (GDI)-type injectors.

Introduction

All future high-efficiency engines will have fuel directly sprayed into the engine cylinder. Engine developers agree that a major barrier to the rapid development and design of these high-efficiency, clean engines is the lack of accurate fuel spray CFD models. The spray injection process largely determines the fuel-air mixture processes in the engine, which subsequently drives combustion and emissions. More predictive spray combustion models will enable rapid design and optimization of future high-efficiency engines, providing more affordable vehicles and also saving fuel.

Approach

To address this barrier, we have established a multi-institution, international collaboration, called the ECN, to both improve spray understanding and develop predictive spray models. By providing highly leveraged, quantitative datasets (made available online [1]) CFD models may be evaluated more critically. Multiple CFD groups have already performed simulations at well-defined conditions, comparing results side-by-side at the first major ECN workshop held this year.

Experimentally, we have focused on providing quantitative fuel-ambient mixing measurements over a range of diesel spray conditions [2], including a select target condition known as Spray A [1]. This set of data is extremely pertinent for CFD evaluation, because prior to our efforts, no mixing data had been used to explore the validity of mixing models, either with detailed CFD or with more simplistic analytical models for fuel jet mixing [2]. Mixing measurements are performed using Rayleigh scattering in a constant-volume vessel that mimics the conditions in a diesel engine as shown in Figure 1. A common-rail diesel injector (single-hole) generates a spray that penetrates into the chamber. The jet is illuminated from the side using a laser sheet. By avoiding the liquid-phase portion of the spray, and after correction for laser intensity variation, the technique provides the mixture fraction, or fuel mass fraction, in the vapor region of the jet as shown in Figure 2.

In addition to mixing measurements, spray quantities such as the vapor-phase penetration, liquid-phase penetration, spreading angle, and nozzle flow coefficients are measured using techniques that are described in [2]. The mixture fraction data are used

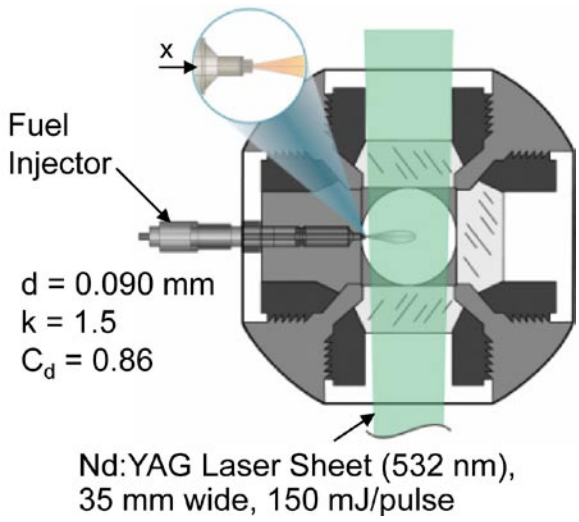

FIGURE 1. Combustion Vessel and Optical Setup for Rayleigh Scattering Measurements

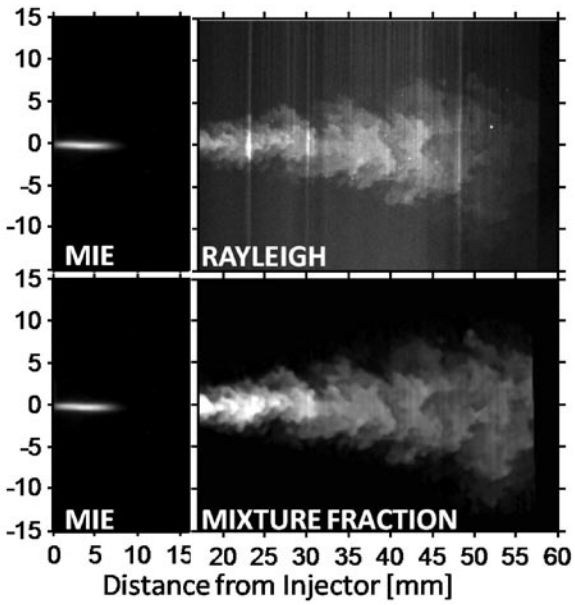

FIGURE 2. Composite Image of Mie Scattering (left) and Rayleigh Scattering (right) (Top is raw Rayleigh image with laser sheet propagating from the bottom. Bottom is corrected image for mixture fraction.)

to more rigorously assess so-called "global" quantity measurements like spreading angle or spray penetration. Together, these data are then used to evaluate the performance of a simple analytical jet model, as a first step towards more detailed CFD evaluation. The analytical jet model is that of Musculus and Kattke [3], which is shown in Figure 3. The model includes assumptions for the radial distribution of fuel mass and velocity, which are indicated as a near-Gaussian shape

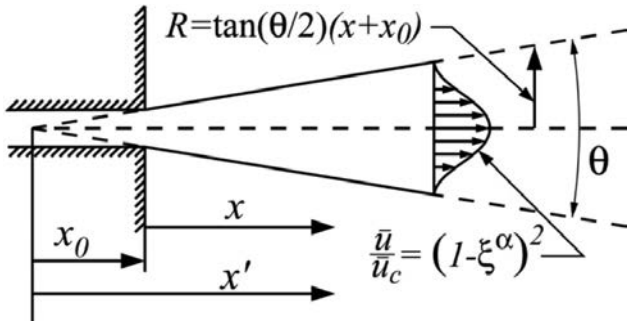

FIGURE 3. Variable-Profile Jet Model of Musculus and Kattke [3]

in Figure 3. Such analytical jet models are convenient for rapid assessment of mixing and penetration trends, but as mentioned above, there had been no evaluation to determine the suitability of the model mixing predictions.

Results

Experimental measurements by Schlieren imaging provide the spray penetration rate, as well as the spreading angle. Examples of penetration results are shown in Figure 4 for a range of fuel injection pressures. To evaluate the utility of model predictions for penetration, some background information is needed. Most fuel spray modeling involves adjustment of model parameters to account for spray spreading angle or dispersion, which is currently not predicted well. The analytical jet model of Musculus and Kattke is no different, and it requires spreading angle as one of the fundamental inputs. Model predictions for penetration are shown in Figure 4 where the full spreading angle is held constant at 21.5° for all conditions. This model spreading angle is in agreement with the experimental measurements using high-sensitivity Schlieren imaging. Therefore, spreading angle and penetration results are consistent, and point to a single jet-mixing model input for spray dispersion to match both spreading angle and penetration. Intuitively, this self-consistency should be expected because the penetration is dependent upon the total entrainment and mixing, with the spreading angle being proportional to the rate of ambient entrainment.

Because spreading angle measurements are more difficult to quantify experimentally [2], we recommend that the model input spreading angle be adjusted to give a best fit to the penetration data rather than relying upon the measured spreading angle. Figure 4 shows that the same spreading angle (21.5°) matches the penetration rate for a wide range of fuel injection pressures, indicating that spreading angle does not change with fuel injection pressure. An implication from this result is that local fuel-ambient mixture also does not change with fuel injection pressure.

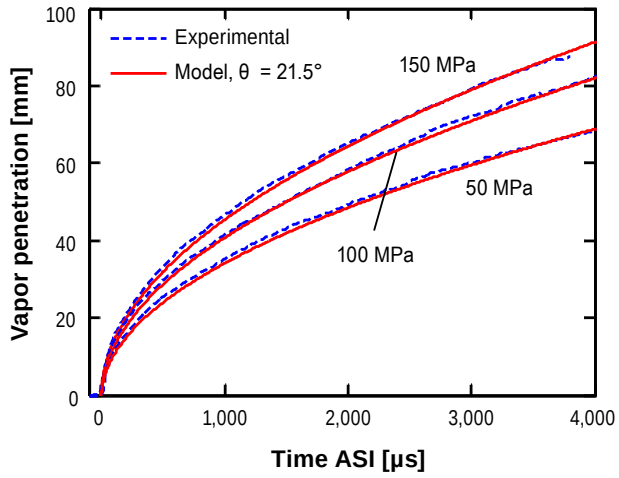

FIGURE 4. Measured Spray Vapor Penetration as a Function of Injection Pressure, and Modeled Spray Penetration with 21.5° Full Spreading Angle (Ambient conditions: 900 K, 22.8 kg/m^3, 6.0 MPa. Injector conditions: 0.090-mm orifice, n-dodecane, 363 K.)

Adjusting the ambient entrainment into the model based on measured spray penetration was shown to work well over a large range of ambient and injector conditions, yielding close agreement with the spreading angle and penetration extracted from high-sensitivity Schlieren measurements. However, the important point is whether or not this methodology produces accurate mixing predictions.

Rayleigh-scatter mixing results are compared to mixing predictions using the variable-profile model in Figure 5. To illustrate how well the model compares to the experimental results in a meaningful, quantitative manner, we show the axial decay of centerline mixture fraction at the top and several radial profiles of mixture fraction at a particular axial position at the bottom. The ensemble-averaged experimental results are shown as blue lines, the model predictions as red lines, and measurement uncertainty 95% confidence intervals are shown as gray fill. If model predictions pass within the gray fill region, they are accurate within the uncertainty of the experimental measurements.

While the model appears to give accurate predictions of mixing at the particular set of conditions of Figure 5, model predictions of mixture fraction are also achieved for a range of ambient densities, fuel injector nozzle shapes, injection pressures, and types of fuels [2]. Since the spreading angle that matched jet penetration is also used for the model predictions, this shows that adjustment of ambient entrainment based on penetration is a good practice. The experimental/model comparison also shows that the radial distribution used in the Musculus and Kattke model, which resembles a Gaussian error function, is an appropriate representation of mixture fraction in a fully developed, vaporized diesel spray.

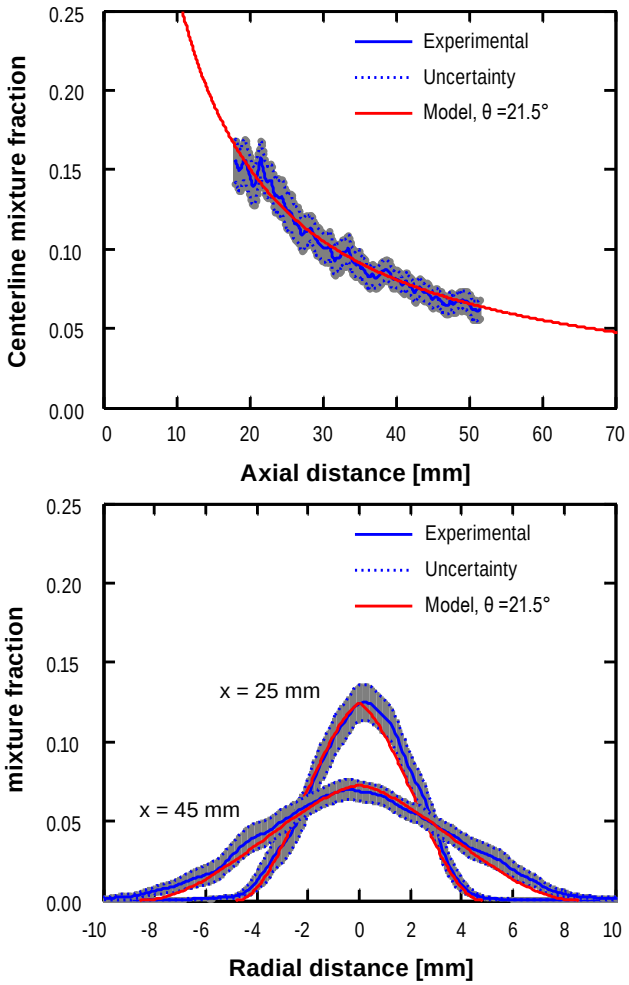

FIGURE 5. Measured Mixture Fraction and Model Predictions at Centerline (top) and Radial Positions (bottom) (Ambient conditions: 900 K, 22.8 kg/m^3, 6.0 MPa. Injector conditions: 0.090-mm orifice, 150 MPa, n-dodecane, 363 K.)

Conclusions

The fuel-ambient mixture produced by sprays is fundamental to the performance and operation of engines. However, evaluation of models that predict mixing is limited without quantitative mixing measurements. Results show that spreading angles based on measurement of the most sensitive outer boundary of the jet are needed as inputs to the Musculus and Kattke analytical jet model to obtain a match between modeled and measured fuel jet penetration rates. By adjusting the model (with spreading angle) to match the measured penetration, the model predictions also produce local mixture fractions that are within the Rayleigh scattering experimental uncertainty.

Further comparison with detailed CFD measurements from multiple groups at the first ECN workshop also shows accurate mixing predictions when model parameters are adjusted to match penetration.

Evaluation of fuel-ambient mixing is a major step forward towards more comprehensive modeling that includes ignition, combustion, and pollutant formation. Collectively, this project provides unique information needed for the development of high-fidelity CFD models that will be used to optimize future engine designs.

References

1. Engine Combustion Network, http://www.sandia.gov/ECN.

2. Pickett, L.M., Manin, J., Genzale, C.L., Siebers, D.L., Musculus, M.P.B., and Idicheria, C.A., "Relationship between Diesel Fuel Spray Vapor Penetration/Dispersion and Local Fuel Mixture Fraction," SAE Paper 2011-01-0686, 2011.

3. Musculus, M.P.B. and Kattke, K., "Entrainment Waves in Diesel Jets," SAE Int. J. Engines 2:1170-1193, 2009, Paper 2009-01-1355.

FY 2011 Publications/Presentations

1. Bajaj, C., Abraham, J., and Pickett, L.M., "The Role of Vaporization in Determining Transient Diesel Spray Structure," ILASS 2011-116, 2011.

2. Dahms, R., Pickett, L.M., and Oefelein, J.C., "A Dense Fluid Approximation for the Simulation of Diesel Engine Fuel Injection Processes," ILASS 2011-161, 2011.

3. Genzale, C.L. and Pickett, L.M., "Laser Ignition of Multi-Injection Gasoline Sprays," SAE 2011-01-0659, 2011.

4. Idicheria, C.A. and Pickett, L.M., "Ignition, soot formation, and end-of-combustion transients in diesel combustion under high-EGR conditions," Int. J. Engine Research 12:376-392, 2011.

5. Kook, S. and Pickett, L.M., "Liquid Length and Vapor Penetration of Conventional, Fischer-Tropsch, Coal-Derived, and Surrogate Fuel Sprays at High-Temperature and High-Pressure Ambient Conditions," Fuel, http://dx.doi.org/10.1016/j.fuel.2011.10.004, 2011.

6. Nerva, J.-G., Yamaguchi, T., Iguma, H., Nishigai, H., Kondo, K., Takano, S., Aizawa, T., Genzale, C.L., and Pickett, L.M., "Transmission Electron Microscopy of Soot Particles Sampled Directly from a Biodiesel Spray Flame," SAE Paper 2011-01-2046, 2011.

7. Nesbitt, J.E., Johnson, S.E., Pickett, L.M., Siebers, D.L., Lee, S.-Y., and Naber, J.D., "Minor Species Production from Lean Premixed Combustion and Their Impact on Autoignition of Diesel Surrogates," Energy & Fuels 25:926-936, 2011.

8. Pickett, L.M., Manin, J., Genzale, C.L., Siebers, D.L., Musculus, M.P.B., and Idicheria, C.A., "Relationship between Diesel Fuel Spray Vapor Penetration/Dispersion and Local Fuel Mixture Fraction," SAE Paper 2011-01-0686, 2011.

9. Pickett, L.M., Genzale, C.L., Manin, J., Malbec, L.-M., and Hermant, L., "Measurement Uncertainty of Liquid Penetration in Evaporating Diesel Sprays," ILASS 2011-111, 2011.

II.A.5 High-Efficiency Clean Combustion in Light-Duty Multi-Cylinder Diesel Engines

Scott J. Curran (Primary Contact),
Robert M. Wagner, and Kukwon Cho
Oak Ridge National Laboratory
2360 Cherahala Boulevard
Knoxville, TN 37932

DOE Technology Development Manager:
Gurpreet Singh

Overall Objectives

- Develop and evaluate the potential of high efficiency clean combustion (HECC) strategies with production viable hardware and aftertreatment on a multi-cylinder engine. This includes expanding the operational range for conditions consistent with the Urban Dynamometer Driving Schedule as well as other operational modes consistent with down-sizing and hybrid electric vehicle/plug-in hybrid electric vehicle operation.
- Improve the fundamental thermodynamic understanding of efficiency opportunities and challenges of HECC.
- Characterize the fundamental instability mechanisms which may limit the operational range of potential of HECC. This includes the development of low-order models for prediction and avoidance of abnormal combustion events.
- Support demonstration of DOE FreedomCAR emissions milestones for light-duty diesel engines.

Fiscal Year (FY) 2011 Objectives

- Demonstrate the potential of reactivity controlled compression ignition (RCCI) on a multi-cylinder light-duty diesel engine for improved efficiency and emissions.
- Quantify the effects of piston geometry and compression ratio on RCCI operation.
- Demonstrate load-expansion and performance potential of biofuels with RCCI.
- Evaluate the fuel economy and emissions performance potential of RCCI over light-duty drive cycles using experimental data (ad-hoc modal point weighting factor estimates).
- Investigate RCCI particulate matter (PM) characteristics and detailed hydrocarbon (HC) speciation for conventional and biofuels.

Accomplishments

- Demonstrated significant HECC load expansion across a wide engine speed and load range using RCCI (with a maximum load of 11 bar brake mean effective pressure at 3,000 RPM) and showed diesel like of efficiency or better (up to 5%) with an order of magnitude reduction in oxides of nitrogen (NO_X) across wide engine operating range.
- Installed and evaluated re-designed pistons for RCCI operation based on University of Wisconsin modeling.
- Demonstrated successful RCCI operation with biodiesel and ethanol blends and found ethanol blends were effective for expanding RCCI operation to higher loads.
- Characterized RCCI PM and HC emissions across a range of operating points and fuels.

Future Directions

- Characterize efficiency advantages of RCCI as compared to conventional diesel combustion (CDC) with detailed thermodynamic analysis.
- Evaluate transient RCCI performance including controls and stability concerns.
- Evaluate aftertreatment performance (including effect on PM) over the over light-duty operating range. Data will also be used with vehicle model to simulate emissions performance over light-duty drive cycle to determine aftertreatment needs for meeting Federal light-duty Tier 2 Bin 5 and Tier 2 Bin 2 emissions standards.
- Further evaluate the potential of bio-renewable fuels to extend the RCCI operating range in coordination with the DOE Vehicle Technologies Program Fuel Technologies subprogram.
- Motoring dynamometer installation will allow investigation into partially premixed combustion (PPC) on light-duty multi-cylinder engine.
- 2012 DOE Vehicle Technologies Program milestones:
  - Develop RCCI combustion map with maximized efficiency with lowest possible emissions suitable for drive cycle simulations.
  - Demonstrate 15% increase in fuel economy over 2009 port fuel injection gasoline vehicle in vehicle simulation solely from improved powertrain efficiency.

Introduction

Advanced combustion regimes have shown promise in meeting high efficiencies with ultra-low NO_x and PM emissions but have traditionally been limited in operating range by the compression ratio of the engine and the reactivity of the fuel used. RCCI combustion makes use of in-cylinder blending of two fuels with differing reactivity for improved control of the combustion process. This approach has been shown in simulations and single-cylinder engine experiments at the University of Wisconsin to have the potential for very high efficiency with very low NO_x and PM emissions. Previous multi-cylinder experiments (MCE) at Oak Ridge National Laboratory (ORNL) had demonstrated successful RCCI combustion at a single engine operating point.

For advanced combustion regimes to allow for real-world improvements on fuel economy and reduced NOx and PM, they have to be able to be implemented in a real-world vehicle using production-viable hardware. RCCI provides the additional control necessary for real-world applicability while using all production viable hardware. These experiments at ORNL aim to transition the modeling and single-cylinder efforts to a light-duty MCE with production viable hardware in order to identify technical barriers and to further understand the potential of this approach under more real-world conditions.

Approach

A 4-cylinder General Motors 1.9-L diesel engine installed at ORNL was modified to include a port fuel injection system using conventional gasoline injectors. A flexible microprocessor-based control system allowed for control over both fueling systems and complete authority over engine operating parameters. MCE experiments were performed without the direct use of modeling for obtaining stable RCCI operation at a given engine speed and load, but instead through the use of a systematic approach based on the previous MCE experimental results and modeling. Initial experiments were carried out using the original equipment reentrant bowl pistons, but because this led to low combustion efficiency accompanied by high CO and HC emissions, follow-on experiments were conducted with a re-designed piston by the University of Wisconsin, using computational fluid dynamics modeling, made specifically for RCCI. The redesigned piston had an open bowl shape similar to a heavy-duty diesel piston which minimizes surface area and the squish region in order to minimize the area for heat transfer and the area for unburned fuel to be trapped during the combustion event respectively. Pictures of the stock piston and the RCCI piston are shown in Figure 1.

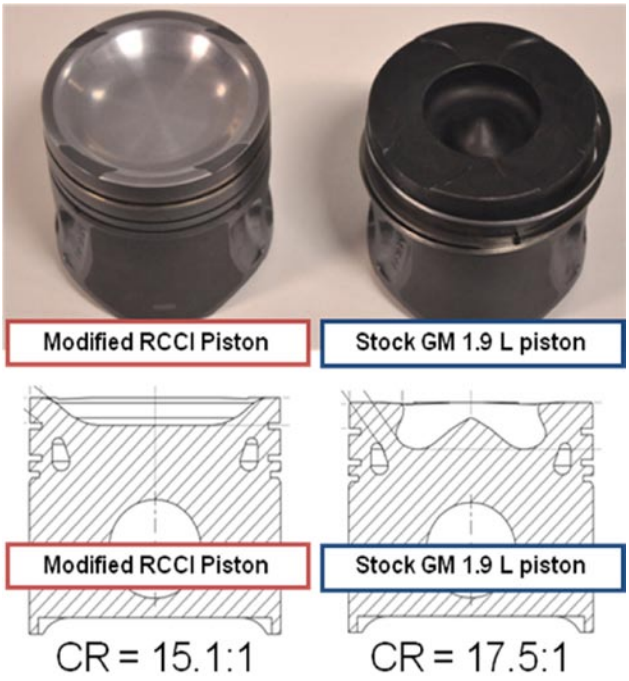

CR - compression ratio

FIGURE 1. Re-Designed RCCI Piston (left) and Stock Piston (right)

Results

The MCE experiments at ORNL demonstrated the potential of RCCI to produce very low NO_x and PM emissions while achieving diesel-like or higher efficiency (4-5% higher at higher loads) across a wide range of steady-state operating points consistent with the light-duty Federal drive cycle. Figure 2 shows the brake thermal efficiency of RCCI compared to CDC for a range of engine speeds and how RCCI efficiency improves over diesel at higher engine speeds. HC and CO emissions were observed to be much higher than CDC, and more similar to levels seen in PFI gasoline engines. Similar emissions and efficiency performance were observed for both pistons showing a remarkable robustness in RCCI performance over significant changes in combustion chamber geometry. Similar HC and CO emissions results between the two pistons indicate the ring pack and near liner regions are most likely responsible for trapping unburned fuel. Challenges for the MCE implementation included matching turbo-machinery with exhaust gas recirculation (EGR) and providing sufficient EGR cooling with production viable hardware. EGR is important to controlling in-cylinder pressure rise rates and combustion noise. The low intake temperatures needed for RCCI operation meant that EGR had to be cooled to a point risking HC and water condensation in the EGR cooler. Lower exhaust temperatures observed with RCCI operation provided lower quality exhaust to drive turbomachinery limiting performance at the lowest and highest loads. The

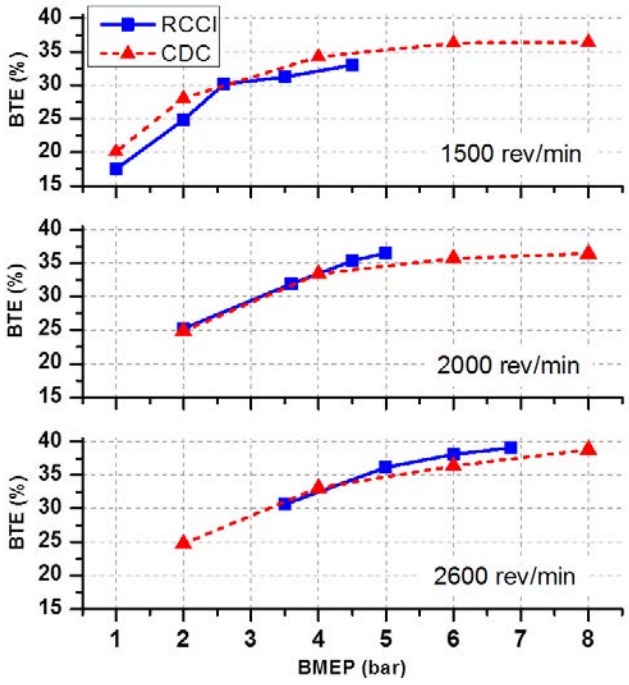

FIGURE 2. Brake Thermal Efficiency (BTE) vs. Brake Mean Effective Pressure (BMEP) for RCCI and CDC for 1,500, 2,000 and 2,600 Rev/Min

combination of high CO and HC emissions with low exhaust temperatures will be a significant challenge due to the limited effectiveness of current oxidation catalysts at low temperatures.

Ethanol blends were found to extend the high-load operating range of RCCI without the use of EGR due to the higher octane and increased charge cooling effect of ethanol. The use of biodiesel blends along with E85 allowed this load to be extended even further as shown in Figure 3 along with self-imposed constraints on CO and pressure rise rates (PRRs) limiting low- and high-load operation, respectively.

To address the potential for RCCI to increase engine efficiency and reduce NO_x and PM emissions, drive-cycle emissions estimates were conducted using the ad-hoc modal points. Weighting factors applied to the emissions results were used to estimate the drive-cycle emissions performance of RCCI which showed a 50-66% reduction in engine-out NO_x compared to CDC and that some level of NO_x aftertreatment would most likely still be needed. Initial RCCI mapping was carried out to explore RCCI operation across a wide range of the light-duty drive cycle range with the re-designed pistons. This initial mapping allows trends such as the ratio of gasoline to diesel fuel as a function of engine speed and load as shown in Figure 4. The initial results will guide further mapping which will be used with a vehicle model in simulations to allow for a more complete estimate of drive-cycle emissions and fuel economy performance.

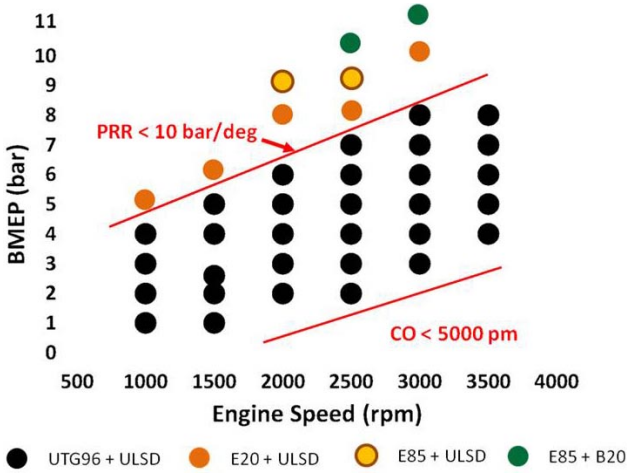

ULSD - ultra-low sulfur diesel; UTG96 - unleaded test gasoline

FIGURE 3. Operational range of RCCI with Self Imposed Limits and Expansion with Biofuels (PRR limit shown for UTG96/ULSD)

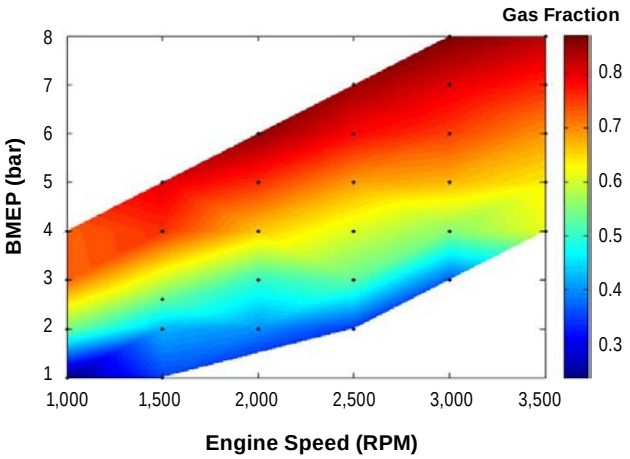

FIGURE 4. Mass of PM Emissions Upstream (Engine Out) and Downstream (Post Diesel Oxidation Catalyst [DOC]) of the DOC for Conventional, premixed charge compression ignition (PCCI), and RCCI Combustion

A detailed PM and HC speciation investigation was completed and found RCCI operation results in lower PM mass emissions than CDC and that RCCI PM is almost entirely organic carbon. A diesel oxidation catalyst was shown to be effective at further reducing RCCI PM mass up to ~50% due to high organic carbon composition as shown in Figure 5.

Conclusions

- RCCI has been shown to achieve diesel like efficiency or better (~5%) over a wide speed and load range with ultra-low NO_x emissions (~order of magnitude reduction).

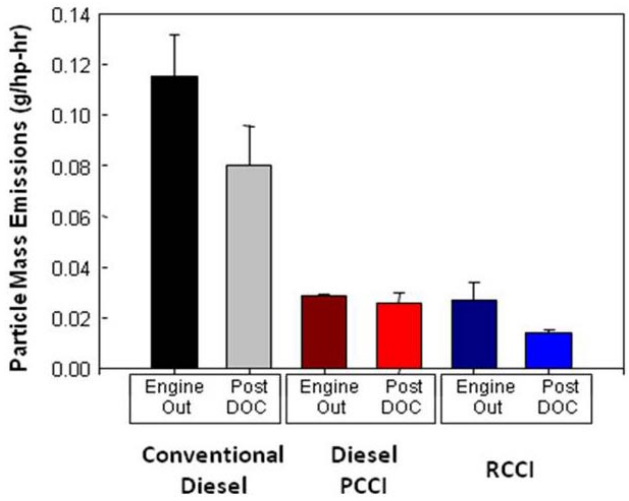

FIGURE 5. Gasoline Fraction of Fuel as a Function of Engine Speed and Load Showing ~20% Gasoline at Low Load and ~85% Gasoline used at High Load (RCCI with Gasoline and Diesel Fuel)

- HC and CO emissions similar level to modern gasoline engine but with added challenge of very low exhaust temperatures (i.e., CO/HC oxidation more difficult).
- Ethanol-gasoline blends enable higher load operation reliving constraints on stock EGR system (also in collaboration with the DOE Vehicle Technologies Program Fuel Technologies subprogram).
- PM mass emissions are much lower than CDC and consist mainly of organic carbon allowing a DOC to be effective at further reducing PM mass emissions.
- Hardware challenges still exist including limits on cooling EGR and better turbocharger matching which are needed for maximizing both low- and high-load performance.

FY 2011 Publications/Presentations

1. Cho, K., Curran, S.J, Prikhodko, V.Y, Sluder, C.S., Parks, J.E., Wagner, R.M., "Experimental Investigation of Fuel-Reactivity Controlled Compression Ignition (RCCI) Combustion Mode in a Multi-Cylinder, Light-Duty Diesel Engine", Proceedings of the 7th U.S. National Combustion Meeting, (Atlanta, GA; March 2011).

2. Briggs, T.E, Cho, K., Curran, S.J., Kim, J, Nafziger, E., R.M. Wagner "High Efficiency Clean Combustion in Multi-Cylinder Light-Duty Engines", Presentation, 2011 DOE Hydrogen Program and Vehicle Technologies Merit Review (Washington, D.C.; May 2011).

3. S.J. Curran, R.M. Hanson, K. Cho, T.L. Barone, R.M. Wagner, S. Kokjohn, R.D. Reitz, "Range Extension and Multi-Cylinder Performance of RCCI", Presentation, Advanced Engine Combustion Working Group Meeting (Detroit, MI; August 2010).

4. R.M. Wagner, S.J. Curran, R.M. Hanson, T.L. Barone, S. Kokjohn, R.D. Reitz, "Addressing the Challenges of RCCI Operation on a Light-Duty Multi-Cylinder Engine", Presentation, Directions in Engine-Efficiency and Emissions Research (DEER) Conference (Detroit, MI; September 2011).

5. S.J. Curran, K. Cho, T.E. Briggs, R.M. Wagner, "Drive Cycle Efficiency and Emissions Estimates for Reactivity Controlled Compression Ignition in a Multi-Cylinder Light-Duty Diesel Engine", ICEF2011-60227, Proceedings of the 2011 Internal Combustion Engine Division Fall Technical Conference ICEF2011, 2011.

6. S.J. Curran, R.M. Hanson, T.L. Barone, J.M. Storey, R.M Wagner, "RCCI Operation on a Light-Duty Multi-Cylinder Engine Using SME B20 with Gasoline and Ethanol Blends", Presentation, National Biodiesel Board Biodiesel Technical Workshop (Kansas City, MO; November 2011).

7. R.M. Wagner, S.J. Curran, R.M. Hanson, T.L. Barone, S. Kokjohn, R.D. Reitz, "Addressing the Challenges of RCCI Operation on a Light-Duty Multi-Cylinder Engine", Presentation, Global Powertrain Congress (Troy, MI; November 2011).

II.A.6 Large Eddy Simulation (LES) Applied to Advanced Engine Combustion Research

Joseph C. Oefelein
Sandia National Laboratories
7011 East Avenue, Mail Stop 9051
Livermore, CA 94551-0969

DOE Technology Development Manager:
Gurpreet Singh

Overall Objectives

- Combine unique state-of-the-art simulation capability based on the large eddy simulation (LES) technique with Advanced Engine Combustion R&D activities.
- Perform companion simulations that directly complement optical engine and supporting experiments being conducted at the Combustion Research Facility and elsewhere.
- Maximize benefits of high-performance massively-parallel computing for advanced engine combustion research using DOE leadership computer platforms.

Fiscal Year (FY) 2011 Objectives

- LES of direct-injection processes for high-pressure low-temperature combustion (LTC) and diesel engine applications with emphasis on hydrocarbon fuels.
  - Work in FY 2010 focused on transient jet dynamics and entrainment processes typically associated with diesel injection processes.
  - Extended the model in FY 2011 to include complex injector geometries using the Engine Combustion Network (ECN) for validation (see www.sandia.gov/ECN).

Accomplishments

- Addressed critical barriers related to development of predictive models for clean high-efficiency engines using hydrocarbon-based fuels.
- Provided new LES model base for LTC technologies (i.e., understanding effects of fuel-injection, ignition-timing, heat-transfer and engine-geometry on fuel-air mixing, combustion, soot and emissions over a broad operating range).
- Established requirements for efficient and routine use of high-performance (exascale) computers with emphasis on development of predictive and affordable models for advanced engine combustion research.

Future Directions

- Continue development of multiphase combustion models with emphasis on direct-injection processes in collaboration with Pickett et al. and ECN workshop participants.
- Continue a parallel task focused on homogeneous charge compression ignition (HCCI) engines in collaboration with Dec et al.
- Coordinate collaborative activities with the LES working group (University of Wisconsin, Penn State, General Motors, University of Michigan).
- Form a larger industrial consortium focused on the priority research areas defined in the recent PreSICE Workshop report (see http://science.energy.gov/bes/news-and-resources/reports/abstracts/#Presice).

Introduction

A key focal point of our research this year is detailed modeling and analysis of high-pressure phenomena to understand its potential effects on the fundamental physics of fuel injection in diesel engines. In particular, we focus on conditions when cylinder pressures exceed the thermodynamic critical pressure of the injected fuel and analyze the major differences that occur compared to classical spray theory. To facilitate the analysis, we present a detailed model framework based on LES that is designed to account for key high-pressure phenomena. This framework is then used to perform a thermodynamic analysis of the flow. We focus on the experiments being conducted in the high-pressure combustion vessel at Sandia National Laboratories using n-heptane as a reference fuel. The calculations are performed by rigorously treating the experimental geometry and operating conditions, with detailed treatment of relevant thermophysical mixture properties. Results demonstrate that n-heptane enters the chamber as a compressed liquid, not a spray, and is heated at supercritical pressure. Further analysis suggests that the classical view of spray atomization as an appropriate model at these particular conditions is questionable. Instead, non-ideal real fluid (gas/liquid) multiphase behavior must be taken into account using

a multicomponent formulation that applies to arbitrary hydrocarbon mixtures at high-pressure supercritical conditions.

Approach

The analysis is performed using a single unified code framework called RAPTOR [1]. Unlike conventional solvers, RAPTOR is a direct numerical simulation solver that has been optimized to meet the strict algorithmic requirements imposed by the LES formalism. The numerical formulation treats the compressible form of the conservation equations, but can be evaluated efficiently in the incompressible limit. A noteworthy aspect of RAPTOR is that it is designed specifically for LES using non-dissipative, discretely conservative, staggered, finite-volume differencing. This eliminates numerical contamination of the subgrid-scale models due to artificial dissipation and provides discrete conservation of mass, momentum, energy and species, which is an imperative requirement for LES. The baseline subgrid-scale closure is obtained using the "mixed" dynamic Smagorinsky model [2-7]. Thus, there are no tuned constants employed anywhere in the closure.

The RAPTOR code framework includes a detailed property evaluation scheme that is designed to account for thermodynamic nonidealities and transport anomalies over a wide range of pressures and temperatures. The scheme is comprehensive and intricate, thus only a skeletal description can be given here (see [8] for details). The extended corresponding states model is employed with the Benedict-Webb-Rubin (BWR) equation of state to evaluate the pressure-volume-temperature (PVT) behavior of dense multicomponent multiphase mixtures. Use of modified BWR equations of state in conjunction with the extended corresponding states principle has been shown to provide consistently accurate results over the widest range of pressures, temperatures and mixture states, especially at near-critical conditions. Using the BWR equation, we establish an analytical representation for real mixture PVT behavior, and then evaluate the thermodynamic properties in two steps. First, respective component properties are combined at a fixed temperature to obtain the mixture state at a given reference pressure. A pressure correction is then applied using thermodynamic departure functions. These functions are exact relations derived using the Maxwell relations and use of the real mixture PVT path dependencies dictated by the equation of state. Molecular transport properties are evaluated in an analogous way.

Results

Using RAPTOR and the real-fluid model described above, we have performed a series of studies focused on the treatment of transcritical injection dynamics. To facilitate the analysis, we considered the operating conditions associated with the baseline n-heptane experiment being studied in the high-pressure combustion vessel at Sandia National Laboratories by Pickett et al. [9]. These experiments provide a relevant set of operating conditions for diesel engines. The LES calculations were performed by identically matching the experimental operating conditions, injector geometry, and combustion chamber.

The experimental apparatus, corresponding computational domain, and key operating conditions used in the calculations are shown in Figures 1 and 2, respectively. The experiment involves a liquid n-heptane jet injected into a hot quiescent mixture of gaseous products. For the case considered here, all the oxygen has been consumed to prevent the onset of combustion so we can focus on the thermophysical processes associated with injection. Fuel is injected with an electronically controlled common rail injector at a pressure of 154.33 MPa and 373 K. The ambient gas composition in the vessel is conditioned to provide an inert composition of N_2, CO_2, and H_2O. The actual mole fractions of these components are summarized in Figure 2. The thermodynamic characteristics of

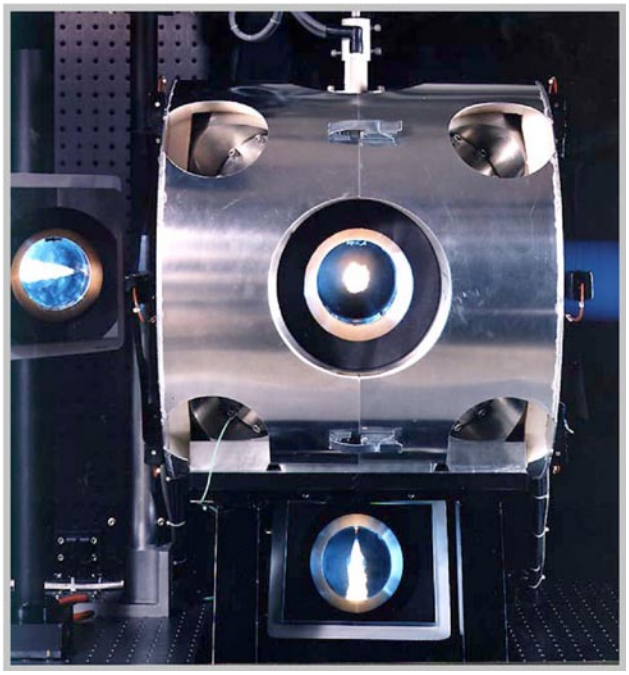

FIGURE 1. Photograph of the Sandia high-pressure combustion vessel.

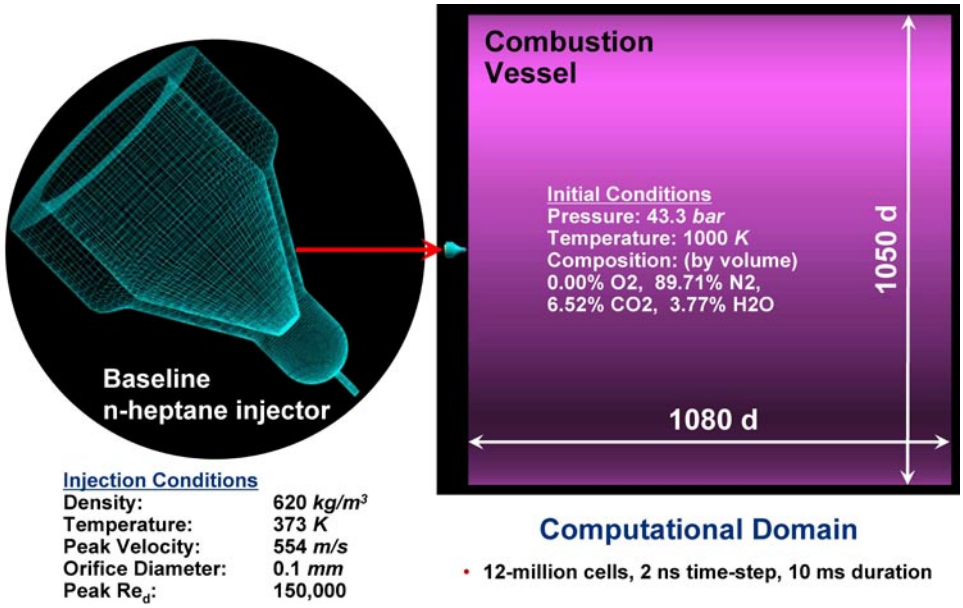

FIGURE 2. Computational domain used for LES of the baseline n-heptane injector configuration. The injector is mounted at the head-end of the vessel, as indicated by the red arrow. The grid and operating conditions identically match the experiment.

n-heptane are shown in Figure 3. Its critical point is 540 K, and 27.4 bar. Thus, n-heptane is injected into the chamber as a compressed liquid (i.e., supercritical with respect to pressure, subcritical with respect to temperature). The current calculations were performed using a grid that contained approximately 12-million cells in total. The transient jet pulse was simulated to closely approximate the actual experimental conditions. This produces a peak bulk velocity of 554 m/s and corresponding jet Reynolds number of 150, 000 inside the injector nozzle. The quasi-steady portion of the pulse lasted for 6.66 ms. At 6.69 ms, the jet was ramped down to zero velocity, with the end of injection occurring at 6.93 ms. The total integration time was 10 ms using a time-step of 2 ns.

Figure 4 shows a representative comparison of the mixture fraction distribution predicted using LES with the corresponding experimentally measured Rayleigh images. Note that the color maps and contour spacing used is identical for both the LES and measured data. In general, predictions agree well with the available experimental data. To perform a comprehensive analysis of the fuel mixing states, we use the time evolving fields given by LES to map the relationship between mixture fraction and temperature. A mixture fraction of 1 represents the fuel stream (C_7H_{16}), and 0 represents the "oxidizer" stream (N_2-CO_2-H_2O). Using these data, a scatter plot of mixture temperature conditioned on mixture fraction was produced, which reveals that there is only a slight variation in mixture temperature as a function of mixture fraction.

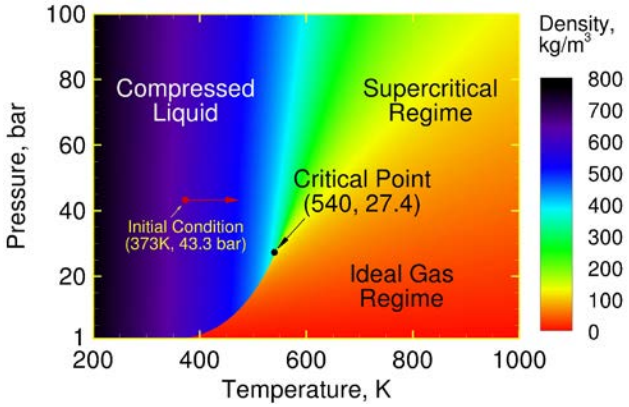

FIGURE 3. Thermodynamic characteristics of n-heptane showing key regimes and its initial state when injected into the combustion vessel. The jet enters as a compressed liquid and is heated at supercritical pressure.

Analysis of the critical mixture properties reveals two important features associated with the local state of the field. First, the local mixture temperature is greater than the critical mixture temperature for all values of mixture fraction less than 0.86. Second, the ambient mixture pressure is greater than the critical mixture pressure for all values of mixture fraction greater than 0.05. Using these data, we can plot the entire envelope of mixture states on a thermodynamic regime diagram, as shown in Figure 5. The results of this analysis demonstrate that the mixing path associated with all states throughout the duration of the calculation never

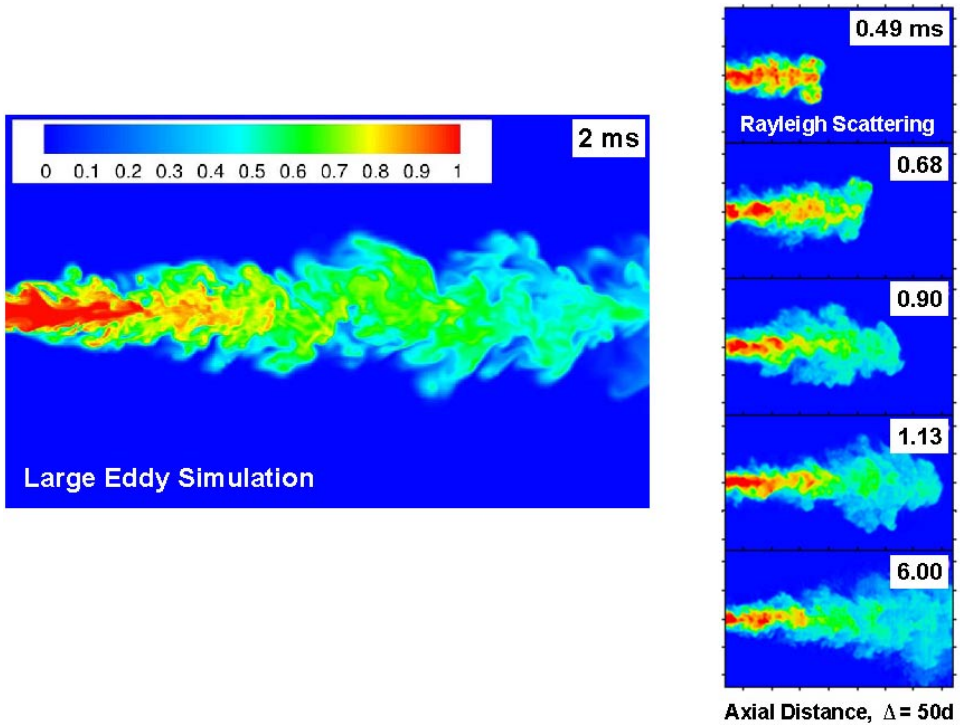

FIGURE 4. Comparison of the mixture fraction distribution from LES (left) with measured Rayleigh images (right).

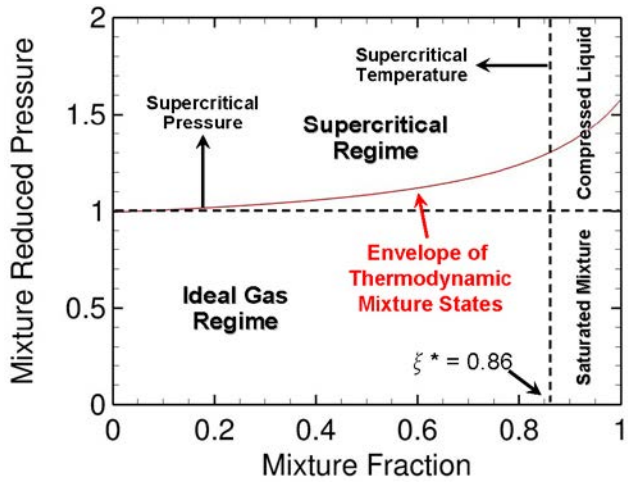

FIGURE 5. Envelope of mixture states predicted as a function of mixture fraction.

crosses the liquid/vapor regime (i.e., the mixture is never saturated). Instead, the n-heptane is injected as a compressed liquid, and the resultant interfacial mixing layer dynamics occur in the transcritical regime where surface tension effects are negligible. Further details are given by Oefelein et al. [10,11].

Using the findings above, we can now perform further analysis to understand details related to the actual time evolving mixture. As an example, Figure 6 shows a typical instantaneous LES field with iso-lines that mark the thermodynamic transition of the mixture from a compressed liquid to a supercritical state (black) and the separation between nonideal and ideal fluid behavior (white). These results demonstrate for the first time that the injected n-heptane enters the combustion chamber as a compressed liquid (not a spray) and is heated at supercritical pressure. Results indicate 1) that applying the ideal gas assumption just prior to autoignition in these types of flows is not valid, and 2) the classical view of spray atomization and secondary breakup processes as an appropriate model (as is widely assumed currently) is questionable. Instead, nonideal real-fluid behavior associated with the dense liquid jet must be taken into account.

Conclusions

LES coupled with the baseline n-heptane experiment being conducted in the high-pressure combustion vessel at Sandia National Laboratories has been used to provide new insights into the instantaneous mixing characteristics of direct-injection processes at high pressures. Results reveal that, under the conditions here, the envelope of thermodynamic mixture conditions range from a compressed liquid state as the fuel enters the combustion chamber, to supercritical mixture conditions as the fuel mixes with the ambient chamber gases. Under these conditions, the classical view of spray atomization as an appropriate model comes into

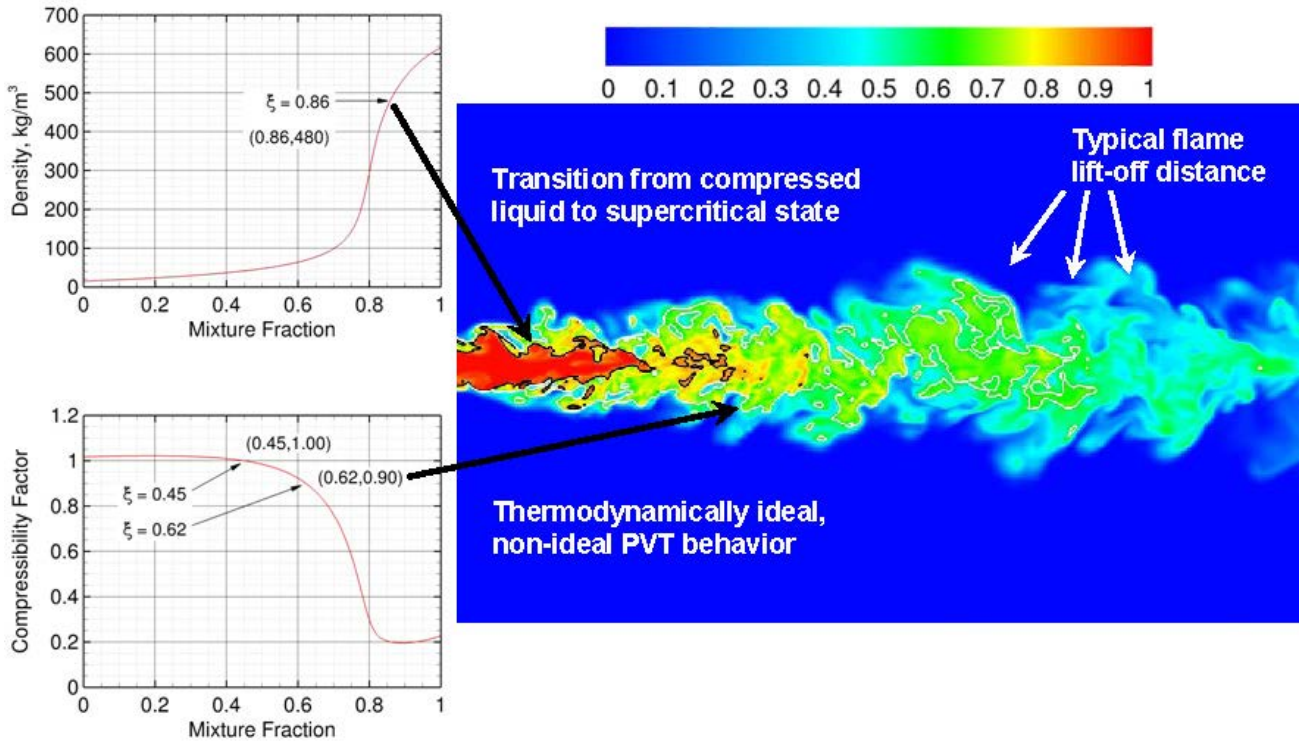

FIGURE 6. LES field with iso-lines that mark the transition of the mixture from a compressed liquid to supercritical state (black) and separation between regions of nonideal and ideal fluid behavior (white).

question. Iso-lines mark the transition from compressed liquid to supercritical mixture states and the separation between regions of nonideal and ideal fluid behavior. The envelope of mixture states observed as a function of mixture fraction were also mapped to show that (for the particular set of conditions selected here) the assumptions related to the dense fluid approximation were valid. A key issue highlighted in applying the real fluid approximation revolves around treatment of the steep but continuous gradients that develop as the jet boundary transitions from a compressed liquid to supercritical mixture states. The combination of steep density gradients and strong differential diffusion can induce significant numerical instabilities, mass conservation errors, and flame structure anomalies. Treating these issues is the subject of ongoing research as we continue to refine our model and analysis of the key processes.

References

1. J.C. Oefelein. Large eddy simulation of turbulent combustion processes in propulsion and power systems. Progress in Aerospace Sciences, 42(1):2–37, 2006.

2. J. Smagorinsky. General circulation experiments with the primitive equations. I. The basic experiment. Monthly Weather Review, 91:99–164, 1963.

3. M. Germano, U. Piomelli, P. Moin, and W.H. Cabot. A dynamic subgrid-scale eddy viscosity model. Physics of Fluids, 3(7):1760–1765, 1991.

4. P. Moin, K. Squires, W. Cabot, and S. Lee. A dynamic subgrid-scale model for compressible turbulence and scalar transport. Physics of Fluids, 3(11):2746–2757, 1991.

5. D.K. Lilly. A proposed modification of the germano subgrid-scale closure method. Physics of Fluids, 3(11):633–635, 1992.

6. Y. Zang, R.L. Street, and J.R. Koseff. A dynamic mixed subgrid-scale model and its application to turbulent recirculating flows. Physics of Fluids, 5(12):3186–3195, 1993.

7. B. Vreman, B. Geurts, and H. Kuerten. On the formulation of the dynamic mixed subgrid-scale model. Physics of Fluids, 6(12): 4057–4059, 1994.

8. J.C. Oefelein. Simulation and Analysis of Turbulent Multiphase Combustion Processes at High Pressures. PhD thesis, The Pennsylvania State University, University Park, Pennsylvania, May 1997.

9. L.M. Pickett. Engine combustion network. www.ca.sandia.gov/ECN, 2005-2011. Combustion Research Facility, Sandia National Laboratories.

10. J.C. Oefelein and G. Lacaze. Low-temperature injection dynamics and turbulent flame structure in high-pressure supercritical flows. Proceedings of the 23rd International

Colloquium on the Dynamics of Explosions and Reactive Systems, July 24–29, 2011. Irvine, California.

R.N. Dahms, L.M. Pickett, and J.C. Oefelein. A dense fluid approximation for the simulation of Diesel engine fuel injection processes. Proceedings of the 23rd Annual Conference on Liquid Atomization and Spray Systems, May 15–18, 2011. Ventura, California.

FY 2011 Publications/Presentations

1. B. Hu, M.P. Musculus, and J. C. Oefelein. The influence of large-scale structures on scalar mixing and entrainment in a decelerating transient turbulent jet revealed by large eddy simulation. Physics of Fluids, 2011. Submitted.

2. G. Lacaze and J.C. Oefelein. A nonpremixed combustion model based on flame structure analysis at supercritical pressures. Combustion and Flame, 2011. Accepted.

3. J.C. Oefelein and R. Sankaran. High-fidelity large eddy simulation of combustion for propulsion and power. Journal of Physics, 2011. In Press.

4. A.M. Kempf, B.J. Geurts, and J.C. Oefelein. Error analysis of large eddy simulation of the turbulent non-premixed Sydney bluff-body flame. Combustion and Flame, 158:2408-2419, 2011.

5. R.N. Dahms, L.M. Pickett, and J.C. Oefelein. Understanding diesel engine fuel injection phenomena using a real-fluid thermodynamic mixture property model. Proceedings of the 2011 Fall Meeting of the Western States Section of the Combustion Institute, October 16–18 2011. Riverside, California.

6. G. Lacaze and J.C. Oefelein. A tabulated chemistry model for nonpremixed combustion at high-pressure supercritical conditions. Proceedings of the Seventh Mediterranean Combustion Symposium, September 11–15, 2011. Sardinia, Italy.

7. V. Sick, P. Abraham, O. Almagri, D. Reuss, X. Yang, V. Gopalakrishnan, T.-W. Kuo, Y. Zhang, C. Rutland, K. Liu, D. Haworth, and J. Oefelein. Validation of internal-combustion engine large eddy simulations. Gordon Research Conference on Laser Diagnostics in Combustion, August 14–19 2011. Waterville Valley, New Hampshire.

8. J.C. Oefelein and G. Lacaze. Low-temperature injection dynamics and turbulent flame structure in high-pressure supercritical flows. Proceedings of the 23rd International Colloquium on the Dynamics of Explosions and Reactive Systems, July 24–29, 2011. Irvine, California.

9. R.N. Dahms, L.M. Pickett, and J.C. Oefelein. A dense fluid approximation for the simulation of Diesel engine fuel injection processes. Proceedings of the 23rd Annual Conference on Liquid Atomization and Spray Systems, May 15–18, 2011. Ventura, California.

10. R. Sankaran and J.C. Oefelein. Efficient data management and analysis for high-fidelity combustion simulations on petascale supercomputers. Proceedings of the 13th International Conference on Numerical Combustion, April 27–29, 2011. Corfu, Greece.

11. J.H. Frank, S.A. Kaiser, and J.C. Oefelein. Analysis of scalar mixing dynamics in LES using high-resolution imaging of laser Rayleigh scattering in turbulent non-reacting jets and non-premixed jet flames. Proceedings of the Combustion Institute, 33:1373–1381, 2011.

12. V. Sick, D. Reuss, C. Rutland, D. Haworth, J. Oefelein, J. Janicka, T.-W. Kuo, X. Yang, and M. Freitag. A common engine platform for LES development and validation. IFP Workshop on Large Eddy Simulation for Internal Combustion Flows, November 18–19, 2010. Ruell-Malmaison, France.

13. C.R. Shaddix, J. Zhang, R.W. Schefer, J.J. Doom, J.C. Oefelein, S. Kook, L.M. Pickett, and H. Wang. Understanding and predicting soot generation in turbulent nonpremixed jet flames. Technical Report SAND2010-7178, Sandia National Laboratories, 2010.

II.A.7 Computationally Efficient Modeling of High Efficiency Clean Combustion Engines

Daniel L. Flowers (Primary Contact), Salvador Aceves, Jonas Edman, Mark Havstad, Nick Killingsworth, Matt McNenly, Tom Piggott, Russell Whitesides, Randy Hessel (University of Wisconsin), Robert Dibble (University of California, Berkeley), J.Y. Chen (University of California, Berkeley)
Lawrence Livermore National Laboratory (LLNL)
P.O. Box 808, L-792
Livermore, CA 94551

DOE Technology Development Manager:
Gurpreet Singh

Subcontractors:
- University of Wisconsin, Madison, WI
- University of California, Berkeley, CA

Overall Objectives

- Enhance understanding of clean and efficient engine operation through detailed numerical modeling.
- Gain fundamental and practical insight into high efficiency clean combustion (HECC) regimes through numerical simulations and experiments.
- Develop and apply numerical tools to simulate HECC by combining multidimensional fluid mechanics with chemical kinetics.
- Reduce computational expense for HECC simulations.
- Democratize high fidelity engine simulation by bringing computational tools to the desktop computer for use by engine designers and researchers.

Fiscal Year (FY) 2011 Objectives

- Implement the multi-zone combustion chemistry model into parallel fluid mechanics solvers.
- Complete license agreement for multi-zone model with U.S. engine simulation software vendor.
- Develop high-efficiency numerical solvers for combustion chemical kinetics simulation on conventional computational architectures.
- Develop high-efficiency numerical solvers for combustion chemical kinetics simulation on new computational architectures (general purpose graphical processing units [GPUs]).

Accomplishments

- Completed implementation of the parallel multi-zone combustion model in two parallel computational fluid dynamics codes (KIVA4-mpi and OpenFOAM).
- Completed license agreement for the multi-zone combustion model with Convergent Science, Inc.
- Developed combustion chemistry solver for general purpose GPUs that is 11 times faster than conventional central processing unit (CPU)-based solvers.
- Developed a new adaptively preconditioned solver for conventional architectures that speeds up combustion chemical kinetics simulation by as much two orders of magnitude compared to traditional approaches and is an order of magnitude faster than the best available commercial solver.

Future Directions

- Continue to validate and develop chemistry simulation capabilities that will enable the prediction of performance and emissions in the development of new vehicle powertrain technologies.
- Conduct detailed analysis of homogeneous charge compression ignition (HCCI) and direct-injection engine experiments and conduct analysis of clean and efficient diesel engines that use stoichiometric and low-temperature combustion modes.
- Implement strategies to deliver new, even-lower computational cost solvers for chemical kinetic systems on conventional CPUs as well as GPUs.
- Develop fully-parallelized multi-dimensional computational fluid dynamics (CFD)-chemistry solvers for analysis of non-homogeneous engine combustion.
- Distribute advanced combustion solvers to U.S. industrial and academic partners.

Introduction

This research and development project focuses on the development and application of computationally efficient and accurate simulation tools for prediction of engine combustion. Simulation of combustion aids in development of new high-efficiency and low-emissions engines by allowing detailed characterization

of in-cylinder engine processes that are difficult to measure directly. Simulation also allows suppositional investigation of new concepts, such as new combustion chamber geometry, allowing valuable and limited experimental resources to be focused on the most promising strategies.

Combustion simulation is computationally demanding because it combines three-dimensional turbulent fluid flow with highly exothermic chemical reactions proceeding at rates that span several orders of magnitude. As such, simulation of an internal combustion engine cycle with chemistry and fluid flow typically requires access to large-scale computing resources. One major motivation of this research is to use physical and mathematical methods to reduce computational expense of combustion simulation with minimal loss of accuracy. These computationally efficient tools are applied to understanding the fundamental physical processes occurring in engines utilizing high efficiency clean combustion strategies.

Approach

We use high-fidelity simulations to predict internal combustion engine operation, looking to maximize computational performance by taking advantage of physical discretization strategies, numerical methods, and new computer architectures. Thermo-kinetic chemistry and fluid mechanics that occurs in engine combustion (diesel, spark ignition, HCCI, etc.) is challenging to simulate because of the large gradients present and the wide range of time-scales over which processes occur, from picoseconds to milliseconds. We developed a multi-zone solver that significantly reduces the computational burden of chemistry simulation combined with computational fluid mechanics with little loss in accuracy. The multi-zone model solves chemistry in a non-geometric thermo-chemical phase-space, significantly reducing the number of chemistry calculations needed to calculate an engine cycle relative to the standard geometric discretization.

Multi-zone chemistry modeling allows for higher fidelity of combustion simulation that effectively utilizes available computational resources. Combining multi-zone modeling with parallel CFD gives increased fidelity to the fluid mechanics part of combustion simulation along with the chemistry. However, chemistry simulation for complex fuels still can be computationally expensive. Through applied mathematics and computational science methods we have been able to significantly reduce the computational cost of combustion chemistry simulation. LLNL results from 2010 [1] show that using a block pre-conditioner for a one-way coupled KIVA-Multi-zone simulation yielded more than 100 times speedup. Building on this fundamental result, the preconditioning techniques have been extended further to reduce the cost by another two orders of magnitude for calculating the chemistry in each individual reactor, fluid cell, or block in the multi-zone pre-conditioner. This development of high efficiency solvers for parallel CFD and multi-zone chemistry provides a higher degree of physical resolution of engine processes using computational resources available to engine designers.

Results

This year has been focused on further development of computational tools to most effectively simulate advanced high-efficiency engine combustion strategies. The multi-zone combustion model has been demonstrated to be accurate and effective for predicting HCCI and premixed charge compression ignition (PCCI) combustion using reasonable resolution fluid mechanics with detailed chemical kinetic mechanisms [2-4]. The multi-zone model involves solving fluid mechanics using a geometric discretization, and solving combustion chemical kinetics with a chemical coordinate and temperature discretization. While the multi-zone model part of the simulation has been implemented on parallel computing platforms for several years, engine fluid mechanics simulations has relied on the serial KIVA3V computational fluid mechanics code. However, CFD codes such as KIVA4-mpi [5], openFOAM [6], and Converge [7] are now available that effectively handle engine fluid flow processes on parallel computers. Solving parallel CFD and multi-zone chemistry simultaneously is challenging because the CFD and multi-zone models need different levels of information sharing between the parallel processors.

For parallel CFD, the domain can be geometrically divided and regions of the CFD domain only need to interact at the boundaries of the different regions. Multi-zone chemistry is most effective when chemical composition information is shared throughout the entire computational domain. Parallel CFD performs best with local information sharing. However, parallel multi-zone performs best with global information sharing. Figure 1 illustrates strategies that can be implemented for parallel CFD multi-zone calculations, showing schematically the distribution of information from processors where CFD calculations are conducted (red squares) to processors where multi-zone chemistry is calculated (green circles). In Figure 1(a), all fluid mechanics and multi-zone chemistry information is kept local to a physical region of the overall flow domain. This strategy is relatively straightforward to implement and requires less data transfer between regions of the domain, but can result in redundant multi-zone chemistry calculations or imbalanced workloads that may increase the overall time of the calculation. Figure 1(b) illustrates a strategy where information about thermochemical state is shared between processors and the multi-zone chemistry is calculated on a global basis. In this strategy,

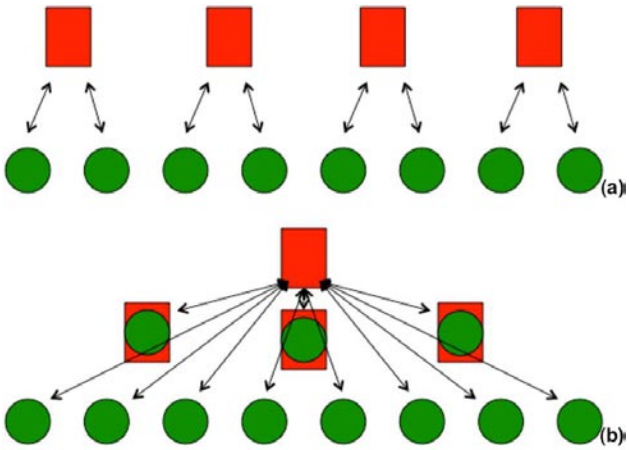

FIGURE 1. [Efficient implementation of parallel CFD and the parallel multi-zone model requires judicious management of processors. Red squares represent processors used for CFD and green circles represent processors used for multi-zone chemistry. (a) shows a local strategy where no chemistry information is shared between CFD processors, and (b) shows a strategy where fluid mechanics (local sharing) and chemistry (global sharing) can occupy the same processor to best balance the load and eliminate redundancies in the fluid mechanics and multi-zone chemistry calculations.

some processors can calculate either fluid mechanics or chemistry depending on the current need in the simulation. The strategy in 1(a) may be computationally fast for relatively simple problems, but for complex geometries with complex fuels strategy 1(b) is more computationally efficient.

This year we have fully implemented the multi-zone solver in the parallel computational fluid mechanics codes KIVA4-mpi and openFOAM. In addition, Convergent Sciences, Inc., a Madison, Wisconsin based engine CFD software maker, has licensed the multi-zone combustion model for implementation in their Converge software package that is licensed by many industrial partners.

Many advanced engine combustion strategies rely on direct injection of liquid fuel into the combustion chamber, resulting in multi-phase and non-homogeneous fuel and air distributions within the cylinder. Even though LLNL's combustion models are very accurate, they rely on other sub-models, such as the spray model, to provide an accurate representation of the spatial distribution of fuel and air and associated thermodynamics conditions. One key limit to the spray models in CFD codes such as KIVA3V and KIVA4-mpi is the droplet collision model. Actual direct injected sprays in engines have billions of droplets that evolve during injection, but tracking billions of droplets is not practical in a simulation, as it would push the limits of today's fastest computers. Instead, in engine CFD codes like the KIVA family, groups of droplets (called "parcels") are tracked to capture the equivalent behavior in a statistical sense. In KIVA3V, engine simulations with sprays are often limited to 10,000 to 20,000 parcels because greater numbers of parcels result in excessive computational time, and the largest part of this computational cost is in the collision model. The collision model determines if two parcels are statistically likely to collide in the spray, and then if the colliding parcels will subsequently bounce off each other, coalesce, or breakup further. A significant portion of the collision model computational cost in KIVA3V is in the algorithm for determining the proximity of parcels. We developed a much more efficient strategy for determining collision pairs that requires significantly less computational time, without affecting the model accuracy. Figure 2 shows the speedup of this improved parcel sorting routine. The new method reduces the time for a one million-parcel simulation from over 100 hours to about seven hours. We also find that a larger number of parcels (>250,000) is necessary to achieve statistical similarity of spray solutions, which significantly improves the consistency of spray simulation.

Practical fuels for advanced engine involve large hydrocarbon molecules, and the kinetics of these large combustion mechanisms can involve thousands of chemical species and tens-of-thousands of elementary reactions. Using elementary mechanisms for these large hydrocarbon fuels is very computationally intensive because of the range of time scales over which reactions occur. Some important reactions occur on picosecond timescales, while others occur on microsecond or millisecond timescales. We continue to develop solvers that dramatically reduce the computational cost of chemical kinetics simulations. Our approach involves using applied mathematics and computational science practices to develop well-conditioned systems of equations that can be quickly solved by available

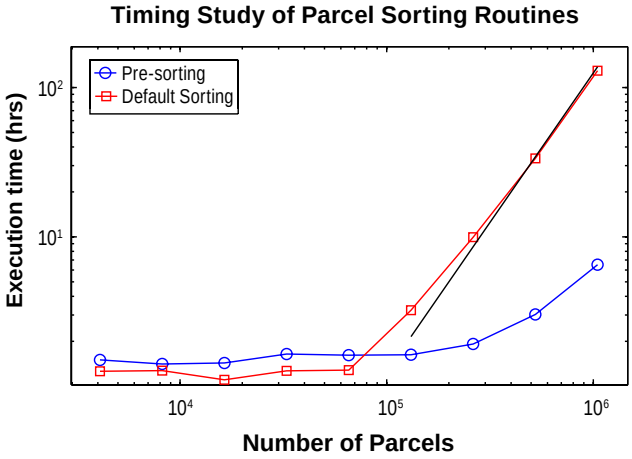

FIGURE 2. Significant reduction of computational cost for the KIVA collision model is achieved by applying a more effective algorithm for determining collision pairs. The black line shows growth in computational cost proportional to the square of the number of parcels.

iterative solvers. This year, we have developed an "adaptive preconditioner" that demonstrates up to two orders of magnitude speedup for chemical kinetic ignition delay calculations. Figure 3 shows the simulation time for constant volume ignition delay calculations with three large hydrocarbon chemical kinetics mechanisms: iso-octane (857 species), n-hexadecane (cetane, 2,115 species), and methyl-decanoate (2,887 species). These fuels are representative of compounds that make up a significant portion of diesel and gasoline. The constant volume ignition delay calculation involves taking a homogenous mixture of fuel and air at a specified temperature and determining the time it takes for that mixture to ignite. For each fuel and each solver strategy on Figure 3, 17 different fuel/air composition and temperature conditions are studies. The individual time for each simulation is shown with solid circles and the lines show the average value for each solution methodology. It is important to note that these constant volume calculation are essentially the fundamental calculation unit in our multi-zone and multidimensional CFD. Therefore, the speedup achieved here benefits all engine models.

The standard approach to solving chemical kinetics until recently is to use a "dense" solver such as LAPACK [8] on a CPU; the simulation times for that solver are shown with the red curve in Figure 3. We investigated using a sparse solver, SuperLU [9], on the CPU for simulating the chemical kinetic system (green curve) and achieved up to five times faster simulations compared to the dense solver. By combining our new adaptive preconditioning strategy with the sparse solver on the CPU we demonstrated 20-fold speed up for ignition delay calculations relative to the dense solve (purple curve). Figure 3 also shows a comparison with the leading commercial solver (black curve), and we have demonstrated that the adaptive preconditioner is up to five to eight times faster. We have also implemented solvers on an alternative architecture, the GPU. Originally designed solely for graphics acceleration, GPUs have been generalized to deliver high-performance at a lower energy and financial cost per floating point operation than traditional CPUs. The yellow curve in Figure 3 shows that by using the GPU for doing part of the dense solve calculations (CULA [10] solver package) speedup by a factor of two can be achieved. The blue curve on Figure 3 shows using the GPU for the dense solver solution of ignition delay, but with a strategy that uses a novel direct inverse approach to matrix solution. This direct inverse approach results in up to 11 times speedup of ignition delay relative to the dense solver. The sparse solver and adaptive preconditioning strategies have not yet been applied on the GPU, but we expect that they will provide dramatic simulation time reductions as observed on the CPU.

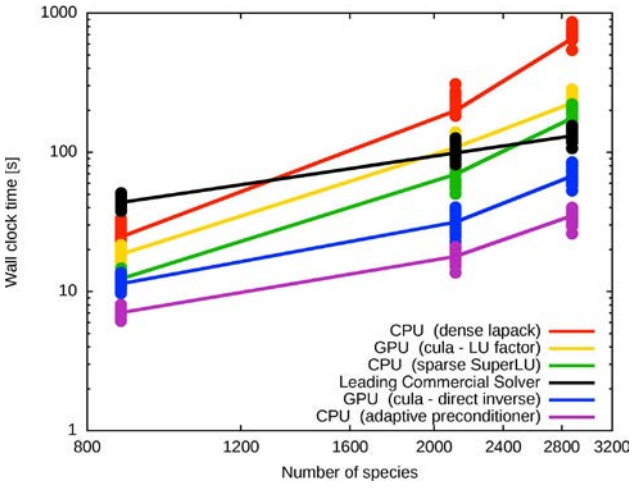

CPU — central processing unit; GPU — graphical processing unit

FIGURE 3. Adaptive preconditioning delivers up to two orders of magnitude speedup for combustion chemical kinetics calculations.

Conclusions

We have achieved significant advances developing high performance computing tools for simulation of advanced engine combustion:

1. Implemented LLNL's parallel multi-zone combustion model in parallel engine CFD solvers.
2. Licensed the multi-zone combustion model to Convergent Science, Inc. for use in their software that is widely used for engine combustion simulation by U.S. engine and automobile manufacturers.
3. Developed an improved collision sorting algorithm that reduces computational time for direct injection in a CFD simulation by as much as an order of magnitude.
4. Developed adaptive preconditioning for chemical kinetic combustion simulations that is at least 5 times faster than any other solver available.
5. Implemented chemical kinetic solvers on GPUs that demonstrate the potential for even greater speedup of chemical kinetics calculations.

In the next year we will apply these high performance simulation tools to investigating fundamental characteristics of advanced engine combustion regimes. We also plan to distribute our models and solvers to support the simulation efforts of our U.S. industry partners.

References

1. McNenly, M.J., Havstad, M.A., Aceves, S.M. and Pitz, W.J., "Integration strategies for efficient multizone chemical kinetics models," SAE International Journal for Fuels and Lubricants, Volume 3, No. 1, pages 241–255, 2010.

2. Babajimopoulos, A., Assanis, D.N., Flowers, D.L., Aceves, S.M. and Hessel, R.P., "A fully coupled computational fluid dynamics and multi-zone model with detailed chemical kinetics for the simulation of premixed charge compression ignition engines," International Journal Engine Research, Volume 6, Issue 5, pages 497-512, 2005.

3. Hessel, R., Babajimopoulos, A., Foster, D., Aceves, S., Davisson, M, Espinosa-Loza, F.J., Flowers, D.L., Pitz, W., Dec, J., Sjoberg, M., " Modeling Iso-octane HCCI using CFD with Multi-Zone Detailed Chemistry; Comparison to Detailed Speciation Data over a Range of Lean Equivalence Ratios, 2008-01-0047.

4. Flowers, D.L., Aceves, S.M., Babajimopoulos, A., "Effect of Charge Non-uniformity on Heat Release and Emissions in PCCI Engine Combustion," SAE Paper 2006-01-1363.

5. Torres, D.J., Trujillo, M.F., "Kiva-4: An unstructured ALE code for compressible gas flow with sprays," Journal of Computational Physics, Volume 219, Issue 2, 10 December 2006, pages 943-975.

6. http://www.openfoam.org/

7. http://convergecfd.com/products/converge/

8. Anderson, E. et al., LAPACK Users Guide, 3rd Edition, Philadelphia, PA: Society for Industrial and Applied Mathematics, 1999.

9. Demmel, J.W. et al., "A Supernodal Approach to Sparse Partial Pivoting," SIAM Journal of Matrix Analysis and Applications, Volume 20, No. 3, 1999, pages 720-755.

10. J.R. Humphrey, D.K. Price, K.E. Spagnoli, A.L. Paolini, E.J. Kelmelis, "CULA: Hybrid GPU Accelerated Linear Algebra Routines," SPIE Defense and Security Symposium (DSS), April, 2010.

FY 2011 Publications/Presentations

1. McNenly, M.J. "Advanced Numerics for Large Scale Kinetic Mechanisms in Combustion Modeling," AEC/HCCI Working Group Meeting, Aug 2011.

2. Edman, J. "Improving Physical Accuracy and Computational Efficiency of Fuel Injection and Multizone Modeling" AEC/HCCI Working Group Meeting, Aug 2011.

3. Whitesides, R.A., Piggott, W.T., Flowers, D.L., Hessel, R.P., "Improved Sub-models for Parallel Computation of Advanced Engine," International Multi-dimensional Engine Modeling Meeting, April 2011, Detroit MI.

4. Whitesides, R.A., Hessel, R.P., Flowers, D.L., Aceves, S.M., "Application of gaseous sphere injection method for modeling under-expanded H2 injection," Combustion Theory and Modelling, Volume 15, Issue 3, 2011.

5. McNenly, M.J. "Advanced Numerics For Combustion Modeling," AEC/HCCI Working Group Meeting, Feb 2011.

6. Hessel, R.P., Steeper, R., Fitzgerald, R., Aceves, S.M., Flowers, D.L. "Full Cycle CFD Simulations to Study Thermal and Chemical Effects of Fuel Injection during Negative Valve Overlap in an Automotive Research Engine," SAE Paper, 2010-01-2236, Oct 2010.

7. Flowers, D.L. "Chemical Kinetics Research on HCCI & Diesel Fuels and Computationally Efficient Simulation Modeling of High-Efficiency Clean Combustion Engines," DEER 2010, Sept 27, 2010.

II.A.8 HCCI and Stratified-Charge CI Engine Combustion Research

John E. Dec
Sandia National Laboratories
MS 9053, P.O. Box 969
Livermore, CA 94551-0969

DOE Technology Development Manager:
Gurpreet Singh

Overall Objectives

Provide the fundamental understanding (science-base) required to overcome the technical barriers to the development of practical homogeneous charge compression ignition (HCCI) and HCCI-like engines by industry.

Fiscal Year (FY) 2011 Objectives

- Determine the main sources of colder near-wall gases that becomes dispersed though the bulk gases to produce the required thermal stratification in an HCCI engine.
- Develop an understanding of the primary mechanisms for transport and dispersion of these colder gases into the hotter bulk gas, at a base operation condition.
- Improve the planar laser induced fluorescence (PLIF)-based thermal imaging technique used to study thermal stratification to obtain higher resolution temperature images with a better signal to noise ratio.
- Examine various operating techniques to determine their potential for increasing the thermal efficiency of intake-boosted HCCI engines.
- Support chemical-kinetic, computational fluid dynamics, and other modeling of HCCI at Lawrence Livermore National Laboratory, the University of Michigan, and General Motors.

Accomplishments

- Showed that the colder gases producing the thermal stratification in the bulk of charge arise mainly from the cylinder-head and piston-top surfaces.
- Discovered that the majority of colder regions in the bulk gas occur in the form of turbulent structures attached to a wall, indicating that randomly occurring turbulent flows are the primary transport mechanism responsible for the thermal stratification:
  - Also showed that there is no evidence of consistent flows from cycle to cycle transporting colder gas from the near-wall regions into the central bulk gas.
- Demonstrated that significant improvements in thermal efficiency of intake-boosted HCCI could be obtained by using partial fuel stratification.
- Showed that partial fuel stratification also allows a substantial increase in the high-load limit of boosted HCCI over a range of boost pressures, for gasoline fueling.
- Evaluated the effects of intake temperature on HCCI engine efficiency.
- Investigated the benefits of partial fuel stratification with ethanol, in collaboration with M. Sjöberg of the Advanced Spark-Ignition Fuels Laboratory.
- Provided data and analysis to support chemical-kinetic, computational fluid dynamics, and other modeling of HCCI at Lawrence Livermore National Laboratory, the University of Michigan, and General Motors.

Future Directions

- Apply side-view thermal imaging to determine how thermal stratification is affected by operating parameters such as engine speed, intake temperature, intake pressure, and swirl.
- Systematically evaluate the potential of adjusting engine operating parameters to improve the thermal efficiency of boosted HCCI engines over a range of loads.
- Explore the potential of increasing the thermal efficiency of boosted HCCI by increasing the engine compression ratio or by increasing only the expansion ratio through the use of a higher compression-ratio piston and a Miller-cycle cam.
- Investigate the effects of expected variations in the ethanol content of pump gasoline on the thermal efficiency, high-load limit, and use of partial fuel stratification for boosted HCCI.
- Continue collaborations with General Motors and the University of Michigan on modeling of thermal stratification in HCCI engines, and discussions and modeling of boosted HCCI.
- Continue to collaborate with Lawrence Livermore National Laboratory on improving chemical-kinetic mechanisms of single components and a gasoline-surrogate mixture.

Introduction

Improving the efficiency of internal combustion engines is critical for meeting global needs to reduce petroleum consumption and CO_2 emissions. HCCI engines have a strong potential for contributing to these goals since they have high thermal efficiencies and ultra-low oxides of nitrogen (NO_X) and particulate emissions. However, several technical barriers must be addressed before it is practical to implement HCCI combustion in production engines. One of the most important barriers is extending HCCI operation to higher loads. Also, further improvements in the efficiency of HCCI engines will increase the incentive for introducing them into the marketplace. Toward these goals, two main areas of research were pursued in FY 2011. First, thermal imaging studies were conducted in our optical engine to better understand the development of the naturally occurring thermal stratification (TS) during the latter part of the compression stroke and to investigate the mechanisms producing it. Understanding TS is important because it is critical for slowing HCCI combustion to allow high loads without knock and/or to minimize the combustion-phasing retard required to control knock, for improved thermal efficiency. Second, well-controlled experiments were conducted in our all-metal engine to determine the potential of using partial fuel stratification to further slow the combustion heat-release of gasoline-fueled HCCI for both naturally aspirated and intake-pressure boosted conditions. Additional studies evaluated the effects of intake temperature on HCCI engine efficiency, and the potential of using partial fuel stratification with ethanol to reduce the HCCI combustion heat-release rate.

Approach

Studies were conducted in our dual-engine HCCI laboratory using a combination of experiments in both the optically accessible and all-metal HCCI single-cylinder research engines (displacement = 0.98 liters). This facility allows operation over a wide range of conditions, and it can provide precise control of operating parameters such as combustion phasing, injection timing, intake temperature and pressure, and mass flow rates of supplied fuel and air. The facility also allows the use of cooled exhaust gas recirculation (EGR). For the current studies, both engines were fitted with compression ratio = 14 pistons, and all data presented are at 1,200 rpm. Additionally, the laboratory is equipped with a full emissions bench (HC, CO, CO_2, O_2, NO_X, and smoke).

Laser-sheet imaging studies of the thermal stratification were conducted in the optically accessible engine using a special optical configuration that allows simultaneous viewing of both the near-wall and bulk-gas portions of the charge. For these experiments, the laser sheet was oriented vertically as it passed through windows in the upper part of the cylinder wall. Images were acquired from the side through a third cylinder-wall window, which also acts a diverging lens to allow viewing out to the cylinder walls. Thus, images can be obtained showing a representative cross-section of the bulk gas as well as the near-wall regions along the firedeck, piston top, and cylinder walls. Temperature images were derived from PLIF images acquired using toluene as a fluorescent tracer in the fuel. Toluene was selected as the tracer because it allows noise from visible-light background fluorescence (present with this optical configuration) to be removed with spectral filtering.

Investigations of the potential of partial fuel stratification (PFS) were conducted in the all-metal engine in two steps. First, the sensitivity of gasoline autoignition-chemistry to variations in fuel/air equivalence ratio (ϕ-sensitivity), which is required for PFS to be effective, was evaluated. This was accomplished using a unique firing scheme (fire 19/1) that isolates the critical fuel-chemistry effects, which occur at only some conditions, from the thermal effects, which are always present [1,2]. Second, for the intake-boosted conditions at which gasoline was found to be ϕ-sensitive, well-controlled PFS was applied using a combination of premixed and direct-injection (DI) fueling. An electrically heated vaporizer assisted the premixing of the majority of the fuel, while a centrally mounted gasoline-type direct injector allowed the remaining fuel to be supplied in the latter part of the compression stroke to produce the desired stratification. Cooled EGR was used to help control the combustion phasing. In addition to these investigations of PFS, separate studies of the effects of intake temperature and ethanol fueling were also conducted in the all-metal engine.

Results

Naturally occurring thermal stratification reduces the HCCI heat-release rate (HRR) because it causes the charge to autoignite sequentially, producing a staged combustion event. This reduction in HRR allows higher loads and/or more advanced combustion phasing without engine knock than would otherwise be possible. Thus, increasing the TS has a strong potential for increasing the high-load limit of HCCI and/or improving the thermal efficiency by allowing operation with less combustion-timing retard to control knock. Previous studies, have shown that for our engine configuration (conventional valve timing), TS arises mainly from wall heat transfer and convection [3,4]. They have also shown that it is the thermal non-uniformities within the bulk gas that are most critical for controlling the HRR [4,5]. Working toward the goal of finding a method of increasing the TS, a study has been conducted to determine the nature of the in-cylinder flows that produce the temperature variations within the bulk gas.

Figure 1 presents temporal sequences of temperature-distribution images (T-maps) during the latter part of the compression stroke. These images were acquired using the optical setup described in the Approach section and shown schematically at the top of Figure 1. As indicated by the black line around each image showing the outline of the combustion chamber, this setup provides a full view of the combustion chamber except for recesses in the firedeck (at the top of the images) for two valves and the centrally mounted injector blank. Since the TS develops prior to combustion, and previous data have shown that thermal distributions during this time period are similar for motored and fired operation [3], these images were acquired for motored operation. The sequence on the left shows the temperature distribution ensemble-averaged over 100 engine cycles, while representative single-cycle images are shown at the right.

The average image sequence shows thermal-distribution patterns that are consistent from cycle to cycle. As can be seen, colder boundary-layer regions develop at the cylinder walls (on the right and left sides of the images), and at the firedeck along small regions on either side of the centrally mounted fuel injector where the laser sheet skims along the cooled firedeck surface, i.e. the regions between the injector-blank location and the recessed valve pockets. Other than these boundary-layer regions, the temperature distribution of the averaged images is fairly uniform. Of particular significance, there is no evidence of consistent in-cylinder flows convecting colder gases from the near-wall regions into the central bulk-gas.

In contrast, the single-cycle images show a progressively increasing amount of TS in the central bulk gases, and by top-dead center (TDC, 360° crank angle, CA) substantial thermal non-uniformities exist throughout the charge. Thus, the critical bulk-gas TS near TDC is dominated by a randomly fluctuating pattern of cold pockets, indicating that they result from in-cylinder turbulence. Closer examination of the images (and similar images from many engine cycles) shows that most of the cold pockets in the central charge are part of turbulent structures extending from the wall regions into the bulk gas. Good examples of this may be seen in the 360° CA image in Figure 1. About halfway between the center and the left side of this image, large turbulent structures of cold gas are seen extending into the central region, one from the top (firedeck near-wall region) and one from the bottom (piston-top near-wall region).

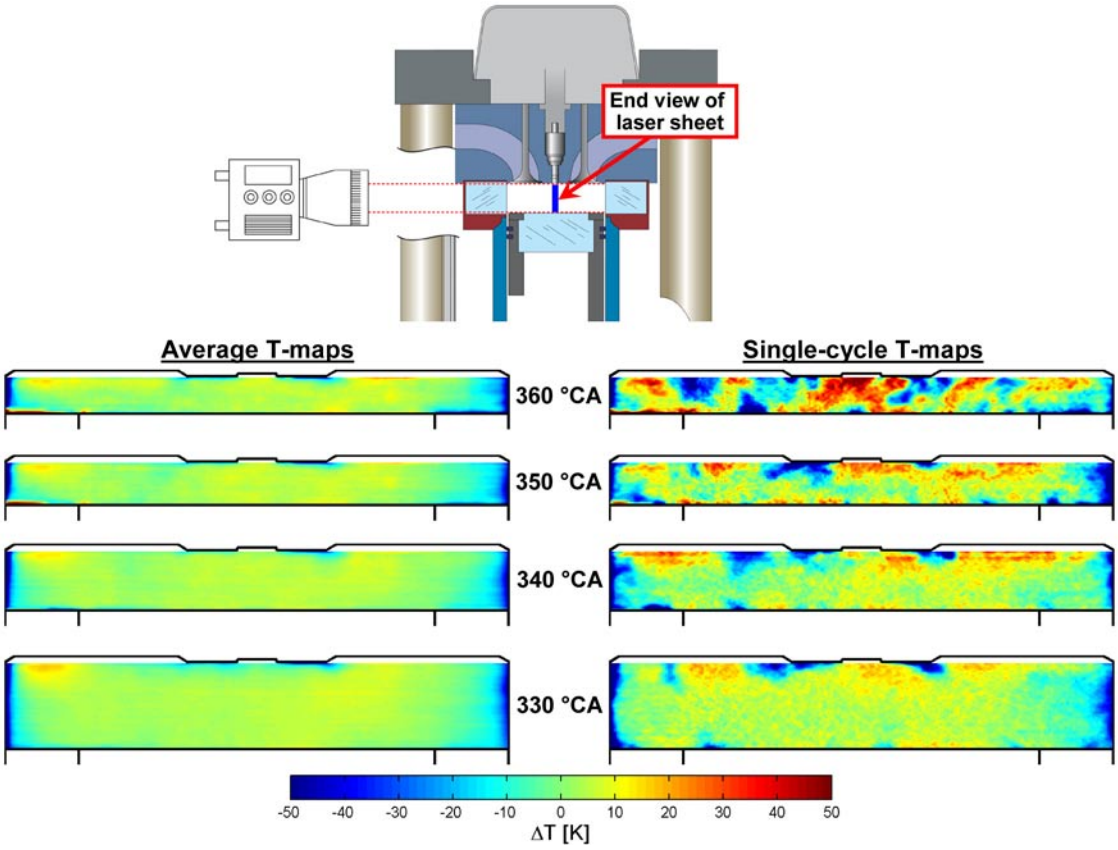

FIGURE 1. Temporal sequences of average (left) and single-cycle (right) T-maps showing the temperature variation about the mean, ΔT. The optical setup for side-view imaging is shown at the top.

A statistical analysis of images from all 100 cycles acquired at each crank angle confirms that this characteristic of the cold pockets being connected to the wall occurs consistently. As can be seen in Figure 2, the average percentage of the image area covered by cold pockets increases progressively up to TDC, with most cold pockets being part of turbulent structures extending from the firedeck or the piston-top walls. Only a very few cold regions occur as isolated pockets, and these could be connected to the wall out of the plane of the laser sheet. Summing the cold-pocket area percentages in Figure 2 over all three locations shows that the total percentage of the image area consisting of cold pockets peaks at TDC, and falls slightly by 370° CA. This finding is consistent with trends in the standard deviation of the turbulent temperature fluctuations, which also peaks at TDC (not shown).

Another method of reducing the HRR in HCCI engines is through partial fuel stratification. For PFS to be effective, autoignition must occur at different times for regions with different local equivalence ratios to produce a staged combustion event (i.e. the fuel must be ϕ-sensitive). Our previous works [1,6] have shown that not all fuels have the necessary ϕ-sensitivity. Since it is desirable to operate with conventional gasoline, particularly with intake boost, the ϕ-sensitivity of gasoline was tested for intake pressures (P_{in}) of 1.0, 1.6 and 2.0 bar using the fire 19/1 technique discussed in the Approach section. As shown in Figure 3, gasoline is not ϕ-sensitive for naturally aspirated operation (P_{in} = 1.0 bar) since all equivalence ratios tested have nearly the same 10% burn point (CA10). However, when P_{in} is increased to 2.0 bar, gasoline becomes highly ϕ-sensitive, with richer regions autoigniting much earlier than leaner regions. For P_{in} = 1.6 bar, gasoline is moderately ϕ-sensitive.

Based on the results in Figure 3, the effectiveness of PFS for reducing the HRR was tested experimentally. As expected, PFS has no benefit for P_{in} = 1.0 bar (not shown), but with the intake-pressure boosted to P_{in} = 2.0 bar, PFS can greatly reduce the HRR and the associated pressure-rise rate (PRR). As shown in Figure 4, both the peak pressure and the PRR are reduced substantially as the amount of PFS is increased by increasing the percentage of fuel directly injected at 300° CA (60° before TDC). With this reduction in PRR, fueling can be increased for a given combustion phasing without inducing engine knock, or combustion phasing can be advanced for the same fueling to provide higher efficiency. A combination of the two can also be applied.

Figure 5 shows that PFS, with its ability to reduce the PRR, can extend the high-load limit of HCCI for intake-boost pressures ranging from P_{in} = 1.6-2.4 bar. For P_{in} = 1.6 and 1.8 bar, the increase is modest, but as the fuel becomes more ϕ-sensitive for $P_{in} \geq 2$ bar, greater gains in the maximum load can be achieved. The

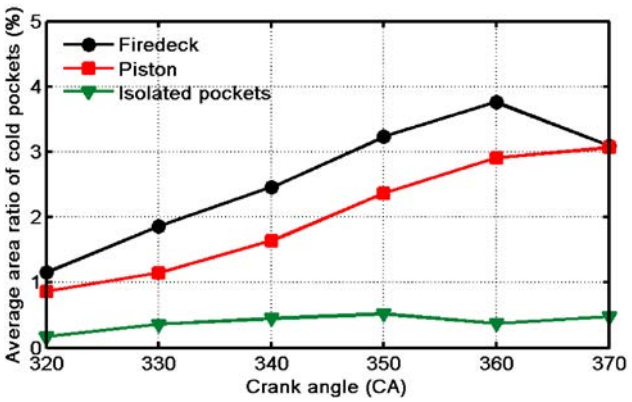

FIGURE 2. Average percentage of the image area covered by cold pockets attached to the firedeck, piston-top, or occurring as isolated cold pockets.

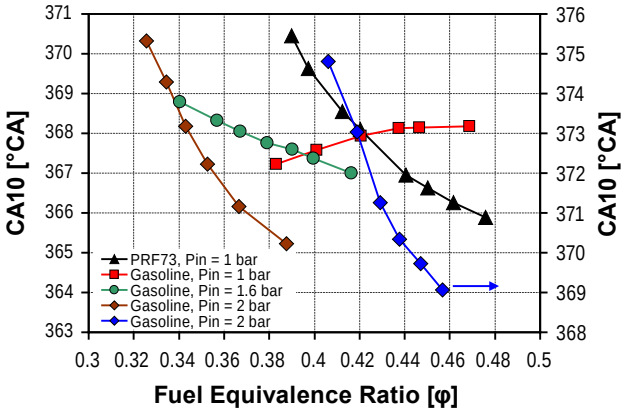

FIGURE 3. ϕ-sensitivity of gasoline for P_{in} = 1, 1.6 and 2 bar, compared to PRF73 (73% iso-octane and 27% n-heptane by volume) at P_{in} = 1 bar. Data were acquired using the fire 19/1 technique [1].

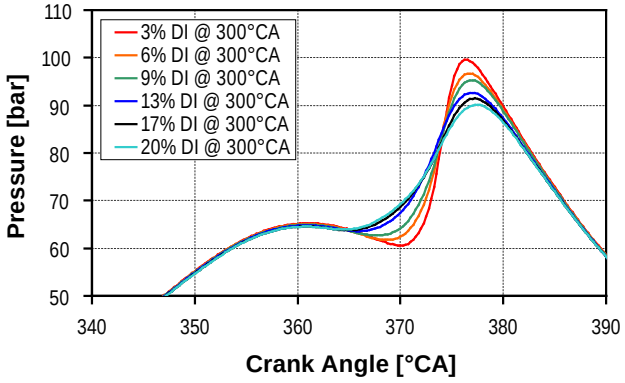

FIGURE 4. Changes in cylinder pressure produced by varying the amount of PFS by varying the DI fraction at a constant DI timing = 300° CA, for P_{in} = 2 bar. The 50% burn point was held constant by varying EGR.

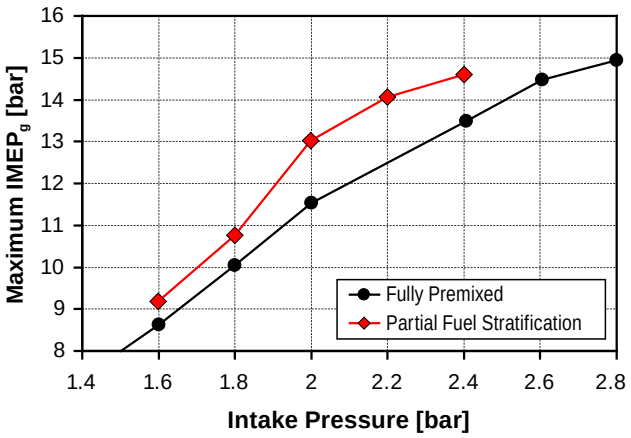

FIGURE 5. High-load limit (IMEP$_g$) as a function of intake boost for fully premixed and PFS fueling. All data have ultra-low NO_x and soot emissions and no engine knock.

largest improvement is for $P_{in} = 2$ bar, where the load is increased from 11.7 to 13.0 bar gross indicated mean effective pressure (IMEP$_g$). For P_{in} above 2 bar, the load increase is less because of the limited oxygen availability due to EGR requirements.

Alternatively, when PFS is applied for the same fueling rate, combustion phasing can be advanced to provide higher thermal efficiencies for the same maximum PRR. Figure 6 presents examples of the efficiency improvements that were obtained for loads from IMEP$_g$ = 8.9-14.4 bar over range of boost pressures.

As can be seen, efficiency increases ranged from 0.3 to 1.6 thermal-efficiency percentage units for fuel economy gains of 0.7-3.6%. A complete discussion of the benefits of PFS for gasoline-fueled HCCI may be found in Ref. [2]

Conclusions

The studies described in this article produced significant results toward three DOE, Office of Vehicle Technologies technical goals: 1) developing an improved understanding of in-cylinder processes, 2) extending the high-load capability of low-temperature HCCI combustion while maintaining NO_x and particulate emissions well below U.S. 2010 standards, and 3) increased thermal efficiency.

- An improved side-view imaging technique provided higher-quality T-map images showing the central bulk gas and near-wall regions simultaneously. Analysis of these images gives an improved understanding of the mechanisms producing TS in HCCI engines.
- Multi-cycle average T-maps show no evidence of consistent flows from cycle to cycle transporting colder gas from the near-wall regions into the central bulk gas.
- Single-cycle T-maps show that the TS of the bulk gas, which is primarily responsible for controlling the HRR, varies randomly from cycle to cycle, indicating that it arises from turbulent flows:

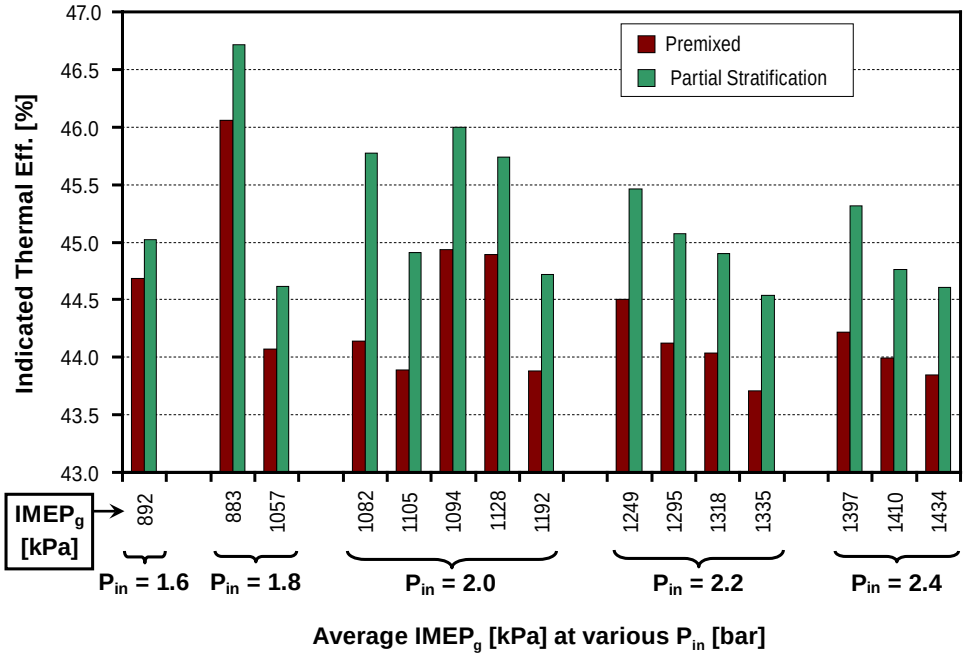

FIGURE 6. Comparison of indicated thermal efficiency for PFS and premixed operation for a range of loads and intake pressures. All data have ultra-low NO_x and soot emissions and no engine knock.

  - The large majority of colder regions in the bulk gas occur in the form of turbulent structures extending into the bulk gas from the near-wall regions along the cylinder-head and piston-top, and only to a much lesser extent from cylinder-wall regions. Only a small fraction of the TS occurs as isolated cold pockets.

- Gasoline autoignition becomes very sensitive to variations in the fuel/air mixture for intake-boosted operation (P_{in} ≥ about 1.6 bar), enabling large reductions in the HRR and PRR with PFS. For naturally aspirated operation, gasoline autoignition chemistry is not sensitive to mixture stratification.
- PFS significantly increases the high-load limit of gasoline-fueled HCCI for intake pressures in the range of 1.6-2.4 bar.
- PFS is also effective for increasing the thermal efficiency of gasoline-fueled, intake-boosted HCCI, giving typical fuel economy improvements of 2-2.5%.
- Reducing the intake temperature increases the thermal efficiency by reducing the amount of EGR required, reducing the heat capacity of the charge gas, and reducing heat transfer losses.
- Ethanol's autoignition chemistry is not sensitive to variations in the fuel/air mixture, but with its high heat of vaporization, PFS can be used with ethanol to increase the thermal stratification, which reduces the HRR. However, this reduction in HRR is much less than the reduction obtained with PFS for boosted gasoline operation.

References

1. Dec, J.E. and Sjöberg, M., "Isolating the Effects of Fuel Chemistry on Combustion Phasing in an HCCI Engine and the Potential of Fuel Stratification for Ignition Control," *SAE Transactions*, 113(4): 239-257, SAE paper 2004-01-0557, 2004.

2. Dec, J.E., Yang, Y., and Dronniou, N., "Boosted HCCI – Controlling Pressure-Rise Rates for Performance Improvements using Partial Fuel Stratification with Conventional Gasoline," *SAE Int. J. Engines*, 4(1): 1169-1189, SAE paper 2011-01-0897, 2011.

3. Snyder, J.A., Dronniou, N., Dec, J.E., and Hanson, R.K., "PLIF Measurements of Thermal Stratification in an HCCI Engine under Fired Operation," *SAE Int. J. Engines*, 4(1): 1669-1688, SAE paper 2011-01-1291, 2011.

4. Dec, J.E. and Hwang, W., "Characterizing the Development of Thermal Stratification in an HCCI Engine Using Planar-Imaging Thermometry," *SAE Int. J. Engines*, 2(1): 421-438, paper 2009-01-0650, 2009.

5. Dec, J.E., Hwang, W., and Sjöberg, M., "An Investigation of Thermal Stratification in HCCI Engines using Chemiluminescence Imaging," *SAE Transactions*, 115(3): 759-776, SAE paper 2006-01-1518, 2006.

6. Yang, Y., Dec, J.E., Dronniou, N., and Sjöberg, M. "Tailoring HCCI Heat Release Rates with Partial Fuel Stratification: Comparison of Two-Stage and Single-Stage Ignition Fuels", *Proc. Combustion Institute,* 33: 3047-3055, 2011.

FY 2011 Publications/Presentations

1. Dec, J.E., Yang, Y., and Sjöberg, M., "The Importance of Intermediate-Temperature Reactions in HCCI and HCCI-like Engines," Workshop on Techniques for High-Pressure Combustion, Argonne National Lab, Aug. 29 – Sept. 1, 2011.

2. Dec, J.E., Yang, Y., and Dronniou, N., "Improving Efficiency and using E10 for Higher Loads in Boosted HCCI Engines," DOE Advanced Engine Combustion Working Group Meeting, Aug. 2011.

3. Yang, Y. and Dec, J.E., "Strategies to Control Heat Release Rate of High-Load HCCI Engine Combustion," 4th Int'l. Symposium on Clean and High-Efficiency Combustion in Engines, Tianjin, China, Aug. 2011.

4. Dec, J.E., Yang, Y., and Dronniou, N., "Boosted HCCI – Controlling Pressure-Rise Rates for Performance Improvements using Partial Fuel Stratification with Conventional Gasoline," SAE paper 2011-01-0897, SAE International Congress, April 2011.

5. Yang, Y., Dec, J.E., Dronniou, N., Sjöberg, M., and Cannella, W. J., "Partial Fuel Stratification to Control HCCI Heat Release Rates: Fuel Composition and Other Factors Affecting Pre-Ignition Reactions of Two-Stage Ignition Fuels," SAE paper 2011-01-1359, SAE International Congress, April 2011.

6. Snyder, J.A., Dronniou, N., Dec, J.E., and Hanson, R.K., "PLIF Measurements of Thermal Stratification in an HCCI Engine under Fired Operation," SAE paper 2011-01-1291, SAE International Congress, April 2011.

7. Dec, J.E., Yang, Y., Sjöberg, M., and Dronniou, N., "Improving Performance of High-Efficiency HCCI Engines with Partial Fuel Stratification," SAE High-Efficiency IC Engines Symposium, April 2011.

8. Sjöberg, M. and Dec, J.E., "Smoothing HCCI Heat Release with Vaporization-Cooling-Induced Thermal Stratification using Ethanol," SAE paper 2011-01-1760, SAE Powertrain, Fuels, and Lubricants Meeting, Kyoto, Japan, Aug. 30 – Sept. 2, 2011.

9. Tsujimura, T., Pitz, W. J., Yang, Y., and Dec, J.E., "Detailed Kinetic Modeling of HCCI Combustion with Isopentanol," SAE paper 2011-24-0023, SAE/NA ICE2011, 10th International Conference on Engines and Vehicles, Capri/Naples, Italy, Sept. 2011.

10. Yang, Y., Dronniou, N., Sjöberg, M., and Dec, J.E., "Tailoring HCCI Heat Release Rates with Partial Fuel Stratification: Comparison of Two-Stage and Single-Stage Ignition Fuels," *Proc. Combustion Institute*, 33: 3047-3055, 2011.

11. Sjöberg, M., Dec, J.E., "Effects of EGR and Its Constituents on HCCI Autoignition of Ethanol," *Proc. Combustion Institute*, 33: 3031-3038, 2011.

12. Dec, J., Yang, Y., and Dronniou, N., "Controlling Pressure-Rise Rates of Boosted HCCI using Partial Fuel Stratification with Conventional Gasoline," DOE Advanced Engine Combustion Working Group Meeting, Feb. 2011.

13. Dronniou, N. and Dec, J.E., "Investigating the Development of Thermal Stratification from the Near-wall Regions to the Bulk-gas in an HCCI Engine with Planar Imaging Thermometry," DOE Advanced Engine Combustion Working Group Meeting, Feb. 2011.

14. Yang, Y., Dec, J.E., Dronniou, N., and Simmons, B., "Characteristics of Isopentanol as a Fuel for HCCI Engines," *SAE Int. J. Fuels Lubricants*, 3(2): 725-741, SAE paper 2010-01-2164, 2010.

15. Dec, J.E. and Yang, Y., "Boosted HCCI for High Power without Engine knock and with Ultra-Low NO_X Emissions – using Conventional Gasoline," *SAE Int. J. Engines*, 3(1): 750-767, SAE paper 2010-01-1086, 2010.

16. Sjöberg, M. and Dec, J.E. "Ethanol Autoignition Characteristics and HCCI Performance for Wide Ranges of Engine Speed, Load and Boost," *SAE Int. J. Engines*, 3(1): 84-106, SAE paper 2010-01-0338, 2010.

Special Recognitions & Awards/Patents Issued

1. SAE Excellence in Oral Presentation Award for paper 2011-01-0897, April 2011.

2. Invited Speaker, SAE High-Efficiency IC Engines Symposium, April 2011.

3. Invited Speaker, Workshop on Techniques for High-Pressure Combustion, Argonne National Laboratory, Aug. 29 – Sept. 1, 2011.

II.A.9 Automotive HCCI Combustion Research

Richard Steeper
Sandia National Laboratories, MS 9053
P.O. Box 969
Livermore, CA 94551-0969

DOE Technology Development Manager:
Gurpreet Singh

Overall Objectives

- Perform fundamental engine research addressing technical barriers to the achievement of DOE efficiency and emissions goals for automotive gasoline engines.
- Develop and apply advanced diagnostics in an optically accessible homogeneous charge compression ignition (HCCI) engine to enhance our knowledge of fundamental in-cylinder processes.
- Advance the capabilities of engine simulation and analysis tools by validating with research-engine data.
- Disseminate knowledge gained from experiments through collaborative interaction with industry, academic, and national lab partners.

Fiscal Year (FY) 2011 Objectives

- Conduct acetylene seeding experiments in the automotive HCCI engine to identify ignition-enhancement effects of potential products of negative valve overlap (NVO) reformation.
- Complete the characterization of our tunable diode laser (TDL) absorption diagnostic developed to measure CO production during HCCI-NVO operation.
- Continue validation/application of the collaborative KIVA model of our research engine.

Accomplishments

- Improved engine data repeatability through an extensive rework of engine facility components and experimental protocols.
- Quantified the enhancement effect of acetylene on main ignition during HCCI-NVO operation.
- Characterized performance of TDL absorption diagnostic for measuring CO concentration histories in the optical engine and published results in a journal article.
- Continued the validation of our KIVA engine model using HCCI-NVO experiment data and documented the results in a technical publication.

Future Directions

- Image NVO fuel injection to quantify piston wetting and identify its effects on NVO and main combustion. Apply TDL absorption and laser-induced fluorescence (LIF) imaging to further characterize reforming reactions during the NVO period.
- Apply KIVA, CHEMKIN, and GT-POWER models of our optical engine to build a coherent understanding of NVO fueling and its effect on main combustion.
- Extend our TDL absorption diagnostic to permit in-cylinder measurement of other species (e.g., H_2O, CO_2, C_2H_2) to clarify the extent of NVO reformation reactions.

Introduction

Challenges to the implementation of gasoline HCCI combustion, include phasing control, operating-range extension, and emissions control, all can benefit from advanced charge-preparation strategies. Alternative strategies such as retarded injection and variable valve timing can be used to modify local charge composition and temperatures, thereby controlling ignition phasing, rate of heat release, combustion efficiency, and engine-out emissions. A current focus of our research is understanding the NVO strategy for HCCI combustion. Partial fueling during the NVO period can affect main combustion both thermally (NVO reactions elevate residual gas temperature) and chemically (NVO reformation reactions produce species that are carried over to main combustion), and understanding these effects is necessary in order to take full advantage of the strategy. Knowledge gained in this project supports DOE's goal of developing advanced energy-efficient, low-emission engine technologies.

Approach

Multiple optical diagnostics are applied in our gasoline HCCI engine to quantify in-cylinder processes. Direct imaging allows assessment of fuel injection; LIF imaging quantifies composition and temperature distributions; laser-absorption produces time-resolved species concentration histories; and chemiluminescence imaging characterizes ignition and combustion

processes. Development of new diagnostics as well as computational fluid dynamics (CFD)/combustion models is facilitated through continuing collaborations with university and national lab partners. Regularly scheduled technical exchanges with manufacturers, national labs, and academia leverage the knowledge gained in the research project.

Results

NVO seeding experiments were begun last year as a means of testing the effect of potential products of reformation in an HCCI engine operating with NVO. NVO operation enables injection and reformation of fuel during recompression as a means of controlling main combustion phasing. In our seeding experiments, we isolate chemical effects of specific reformed species by mixing them with the intake air stream. To avoid influence of other hydrocarbons, we eliminate fuel injection during NVO and compensate for its thermal energy by increasing intake air temperature.

Acetylene (C_2H_2) has been identified as a species of interest by an industrial partner due to its potential enhancement of engine ignition. Since acetylene is a product of rich combustion associated with wall wetting in direct-injection engines, it could be produced during NVO fueling, depending on injection timing. Based on this reasoning, acetylene was selected as a candidate species for our seeding experiments.

Our first challenge was optimizing the C_2H_2 seeding process. As a hazardous combustible gas, C_2H_2 is typically stored dissolved in acetone and delivered at pressures below 15 psi gauge. Since higher delivery pressures are needed in order to make use of accurate mass-flow orifices, we initially tried a high-pressure mix of dilute C_2H_2 in N_2, but the extra N_2 delivered during seeding skewed combustion performance unacceptably. Switching then to a low-pressure source of undiluted C_2H_2 (welding tank), we employed a flame ionization detector (FID) hydrocarbon analyzer to determine C_2H_2 seeding concentration. Since the triple bonds of C_2H_2 could respond atypically in an FID instrument, we used gas-chromatograph analysis to establish accurate C_2H_2 concentrations, and then compared them to the FID measurements. Figure 1 characterizes the important finding that FID response to C_2H_2 is consistently 28% higher than its response to a single-bonded hydrocarbon with the same number of carbon atoms (i.e., ethane).

Figure 2 illustrates typical experiment results from low-load HCCI experiments at several seed concentrations of C_2H_2. For the reference case (*no seed*), 9 mg of an 87-octane research gasoline are direct-injected during intake (no other fuel or seed added). The remaining cases represent increasing addition of C_2H_2 seed, with reference fuel reduced in each case to hold constant the total chemical energy added.

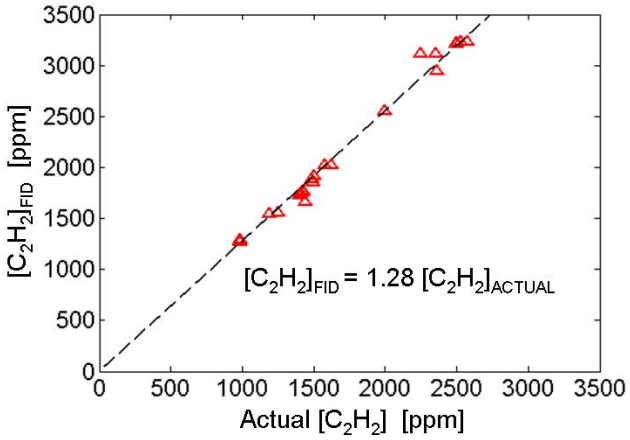

FIGURE 1. Flame ionization detector response to acetylene. Values of $[C_2H_2]_{ACTUAL}$ are determined by gas chromatograph. The linear trend line on the graph indicates an anomalous but consistent C_2H_2 response factor of 1.28.

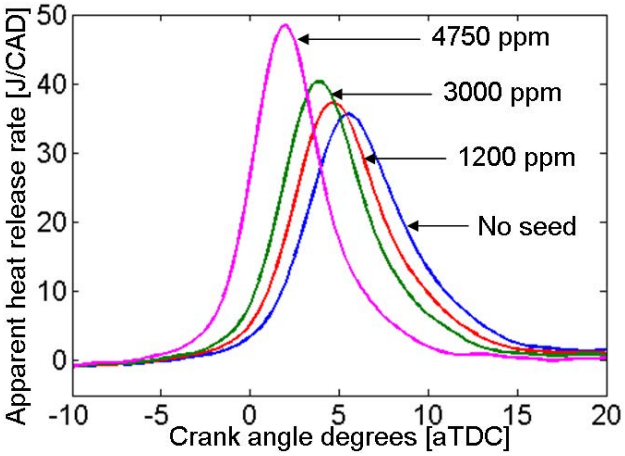

FIGURE 2. Apparent heat-release rates for gasoline with and without acetylene seeding (acelylene concentrations in ppm). Engine operation at 1,200 rpm with 9 mg of gasoline, or with an equivalent amount of gasoline plus acetylene.

Conceptually, this approximates NVO-fueled operation in which a varying fraction of total fuel is converted to C_2H_2 and is carried over from NVO to main ignition.

The effect of C_2H_2 on main combustion is clear in Figure 2: it advances combustion phasing by several degrees and increases peak combustion heat-release rate by up to 40% for the seeding levels selected. Future tests will attempt to quantify the production of C_2H_2 during NVO-fueled operation, but the current work establishes that relatively small concentrations of C_2H_2 produced in this way could chemically affect main combustion phasing. In fact, manufacturer interest in the topic arises from the potential for using the technique to gain cycle-by-cycle authority over ignition phasing.

The acetylene-seeding results in last year's annual report included an analysis of cumulative apparent heat release prior to main ignition that suggested possible early heat release (occurring between -60 crank angle degrees [CAD] and the time of ignition). An inability to consistently reproduce these results led this year to extensive modification of engine components and experimental protocols to decrease data uncertainty. As a result of these improvements, operating conditions are now more stable and repeatability is improved, allowing us to re-examine the early heat-release issue. The four traces in Figure 3 represent the same experiments as in Figure 2, but data are plotted as *cumulative* apparent heat release to focus on the relatively flat apparent heat release trends of the compression stroke. All the curves show nearly identical heat-transfer losses from intake valve closing to -10 CAD, with no evidence of early chemical reactions. The curves begin to diverge only at the so-called hot ignition point between 10 and 5 CAD before top-dead center. We are forced to conclude that our prior observations of early C_2H_2 heat release were likely caused by variations in engine wall temperatures from run to run. Note that the results in Figures 2 and 3 still show a significant chemical effect of C_2H_2 on combustion phasing, but it is an effect that apparently does not turn on until hot ignition.

To assist our studies of HCCI-NVO operation, we have developed a TDL absorption diagnostic for spatially averaged, temporally resolved measurements of in-cylinder CO concentration. CO is an important marker of reaction progress, so the diagnostic will provide an estimate of the extent of reformation reactions occurring during the NVO period. Performance tests of the instrument were conducted in the engine last year; this year we completed analysis of the data and published the results in a journal article.

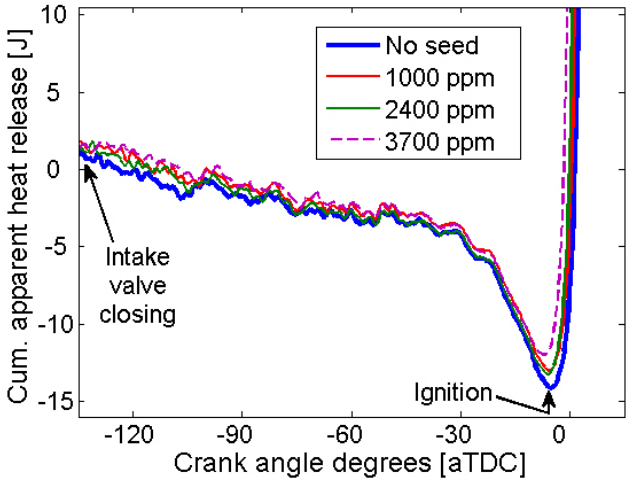

FIGURE 3. Cumulative apparent heat release during the compression stroke for the same experiments as Figure 2.

In collaboration with the University of Wisconsin and Lawrence Livermore National Laboratory, we continue to develop, validate, and apply a CFD model of our optical engine. The KIVA/multi-zone combustion model accurately simulates HCCI-NVO operation and provides a tool for interpreting and guiding experiments. The design, application, and performance of the model this year were documented in a technical publication.

Conclusions

- Seeding experiments quantified the ignition-enhancement effect of acetylene in a gasoline HCCI engine. The work highlights the potential role of NVO-produced acetylene as a mediator of main combustion phasing in gasoline HCCI engines.
- The development of a CO absorption diagnostic for our optical engine provides data to estimate the extent of NVO combustion reactions. Performance of the instrument has been summarized in a journal article.
- The collaborative CFD/combustion model of our research engine provides accurate simulations of HCCI-NVO operation. Recent progress in validation and application of the model has been documented in a technical publication.

FY 2011 Publications/Presentations

1. Fitzgerald, R.P., "Application of a Tunable-Diode-Laser Absorption Diagnostic for CO Measurements in an Automotive HCCI Engine," presented at 2010 SAE PF&L Meeting, San Diego, Oct. 27, 2010.

2. Hessel, R.P., Steeper, R., Fitzgerald, R., Aceves, S., and Flowers, D., "Full Cycle CFD Simulations to Study Thermal and Chemical Effects of Fuel Injection during Negative Valve Overlap in an Automotive Research Engine," SAE Technical Paper 2010-01-2236, 2010, doi:10.4271/2010-01-2236.

3. Fitzgerald, R.P. and Steeper, R.R., "Application of a Tunable-Diode-Laser Absorption Diagnostic for CO Measurements in an Automotive HCCI Engine," *SAE Int. J. Engines* **3**(2):396-407, 2010, doi:10.4271/2010-01-2254.

4. Steeper, R.R., "Automotive HCCI Combustion Research," DOE/OFCVT Advanced Combustion Technologies Annual Report, 2010.

5. Steeper, R.R., "Optical Measurements in an Automotive HCCI Engine," presented at UC-Davis Graduate Seminar, Davis, CA, Jan. 13, 2011.

6. Steeper, R.R., "Automotive HCCI Engine Research," presented at DOE Vehicle Technologies Annual Merit Review, Washington, D.C., May 10, 2011.

7. Puranam, Sri, "Acetylene Seeding Experiments in a Gasoline HCCI-NVO Engine," presented at DOE Advanced Engine Combustion Working Group Meeting, USCAR, Aug. 24, 2011.

II.A.10 Engine-Systems Technology Assessment in Support of Vehicle Technologies Engine Efficiency Goals

K. Dean Edwards (Primary Contact),
Robert M. Wagner
Oak Ridge National Laboratory (ORNL)
2360 Cherahala Boulevard
Knoxville, TN 37932

DOE Technology Development Manager:
Gurpreet Singh

Overall Objectives

Support DOE and industry partnerships in assessment of state-of-the-art and longer-term advanced engine and combustion technologies for future goal setting.

Fiscal Year (FY) 2011 Objectives

Perform thermodynamic assessment of state-of-the-art engine technologies in coordination with the USCAR Advanced Combustion & Emissions Control (ACEC) Tech Team to identify efficiency opportunities and aid establishment of efficiency goals for the Vehicle Technologies Program.

Accomplishments

- Developed a technique for applying stretch recovery goals to each loss mechanism and evaluating the resulting redistribution of energy within the engine to evaluate the combined benefit of and potential interaction between various strategies for efficiency improvement.
- Demonstrated that greatest efficiency benefits are provided by strategies that improve work extraction with the piston or increase exhaust energy available to waste-heat recovery (WHR) systems with other strategies only providing incremental efficiency improvements.

Future Directions

- Continue assessment of state-of-the-art engine technologies and advanced combustion processes in coordination with the ACEC Tech Team to support goal-setting activities by the Vehicle Technologies Program.
- Characterize stochastic and deterministic phenomena for advanced combustion strategies and develop a path toward improved predictive control and avoidance of abnormal combustion events.

Introduction

This project supports DOE and industry partnerships in assessment of state-of-the-art and longer-term advanced engine and combustion technologies as well as goal setting and demonstration of efficiency and emissions milestones for the Vehicle Technologies Program. Technologies of particular interest to this activity include advanced combustion, thermal energy recovery, aftertreatment, thermal management, adaptive controls, and advanced materials. An important aspect of this activity is thermodynamic assessment of state-of-the-art engine technologies in coordination with the ACEC Tech Team for identifying efficiency opportunities.

Approach

The overall goal of this work is to evaluate the practical and thermodynamic efficiency limits of internal combustion engines, define the barriers to approaching these limits, and develop and evaluate technologies and strategies to overcome those barriers. Our approach begins with a complete 1st and 2nd Law thermodynamic analysis of engine data and/or simulation results from advanced engine models. Such an analysis provides important insight to how fuel energy supplied to the engine is used to produce work or consumed by inefficient processes within the engine such as friction, heat loss, and combustion irreversibility. Simply reducing these losses is seldom sufficient as the recovered energy is often lost by another mechanism. For example, reducing heat loss from the engine cylinder tends to increase exhaust energy leaving through the tailpipe rather than producing additional work from the piston. Understanding how these various processes interact is crucial to developing strategies which not only reduce energy loss, but also redirect the recovered energy to where it can provide the largest efficiency benefit.

Results

In this report, we focus on the assessment of potential efficiency improvements for light-duty transportation engines. A complete thermodynamic analysis was performed on engine data from a modern 1.9-L diesel engine installed at ORNL and data supplied by the ACEC Tech Team for a modern light-

duty gasoline engine. As an example, the results and following discussion focus only on analysis of the diesel engine at two steady-state operating points: a typical road-load case (2,000 RPM, 2-bar brake mean effective pressure, BMEP) and the peak brake thermal efficiency point (2,250 RPM, 18.8-bar BMEP).

Table 1 provides an overview of the exergy distribution of the light-duty diesel engine at both operating points with tabulated values representing the percentage of the fuel's work potential (or exergy) used or consumed by each mechanism. The largest losses are due to combustion irreversibility and heat loss to the coolant, oil, and ambient environment.

Combustion irreversibility losses are mainly due to the combustion reaction occurring away from thermal and chemical equilibrium. Significant reduction of these losses will require radical strategies such as staged combustion or thermochemical recuperation which may be difficult to implement in a transportation engine and could radically change engine architecture.

Reducing radiant and convective heat loss from the engine increases in-cylinder temperature and pressure and thus the amount available work that could be extracted with the piston. However, the increase in temperature also decreases the specific heat ratio (gamma) of the exhaust gases which lowers the work-extraction efficiency of the piston. As a result, this strategy typically produces much less additional work than might be expected with the recovered energy simply producing hotter exhaust gases. However, this is not necessarily an undesirable result as hotter exhaust gases provide better opportunities for WHR systems such as bottoming cycles or thermoelectric systems. Higher thermal and physical stresses in the engine will require advances in durable, high-temperature materials. Alternatively, use of advanced, low-temperature combustion strategies may provide lower heat loss without increasing in-cylinder temperatures and pressures, but with lower combustion efficiency and higher combustion irreversibility due to high dilution rates.

While friction and parasitic losses tend to consume more power at higher engine speeds and loads, as shown in Table 1, they have a larger impact on engine efficiency at low loads. Reducing friction and electrification and intelligent control of parasitic loads will directly benefit brake work output.

This engine uses a high exhaust gas recirculation (EGR) advanced combustion strategy for in-cylinder reduction of oxides of nitrogen (NOx) and particulate matter (PM) at low load that impacts efficiency by increasing pumping work and combustion irreversibility and decreasing combustion efficiency. However, high dilution also increases the gamma of the exhaust gases improving work-extraction efficiency with the piston. Additional energy is lost in the EGR cooler in a trade-off to maintain high charge density and better work extraction with the piston. Some of this heat loss may be recovered with a bottoming cycle.

TABLE 1. Exergy Distribution for 1.9-L Diesel Engine At Two Operating Conditions (Values are percentage of fuel exergy)

	Road Load	Peak BTE
Brake Work	24.7%	40.6%
Friction and Parasitic Loads	10.7%	2.0%
Pumping Work	5.7%	0.4%
Exhaust	4.7%	9.9%
Incomplete Combustion	1.5%	0.5%
EGR Cooler	3.4%	0%
Turbocharger	3.0%	3.8%
Other Heat Losses	22.7%	23.3%
Combustion Irreversibility	23.6%	19.5%

BTE - brake thermal efficency

A combination of strategies will likely be needed to dramatically increase engine efficiency. To evaluate how various strategies might interact and their potential combined benefit, we developed a technique for applying stretch recovery goals to each loss mechanism and evaluating the resulting redistribution of energy. Figures 1 and 2 present the potential efficiency impact of one such scenario for our light-duty diesel engine. In this example, reduction factors shown in Table 2 are applied to the road-load and peak-efficiency energy distributions shown in Table 1, and redistribution factors determine where that recovered energy shows

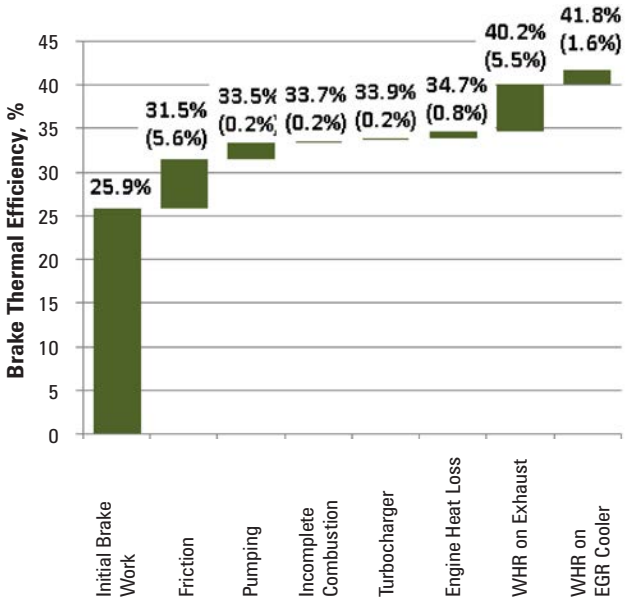

FIGURE 1. Contribution to Engine Efficiency at Road Load (2,000 RPM, 2-bar BMEP) by the Different Approaches in the Example Scenario

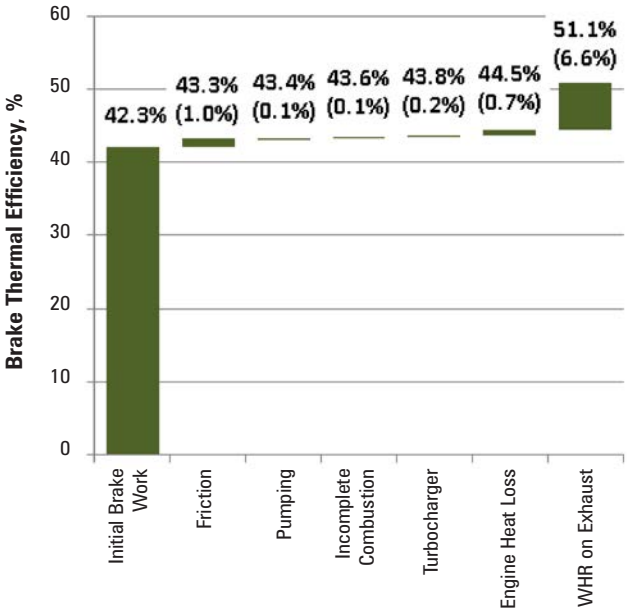

FIGURE 2. Contribution to Engine Efficiency at Peak Brake Thermal Efficienty (2250 RPM, 18.8-bar BMEP) by the Different Approaches in the Example Scenario

TABLE 2. Reduction and Redistribution Factors Applied to the 1.9-L Diesel Engine in the Example Scenario

Loss Category	Reduction Factor	Redistribution Factors			
		Brake Work	Heat Loss	Exhaust	Comb. Irrev.
Friction & Parasitics	0.5	1	-	-	-
Pumping Work	0.3	1	-	-	-
Exhaust & EGR Cooler	0.2	1	-	-	-
Incomp. Comb.	0.5	Based on original energy distribution			
Turbo.	0.5	0.2	-	0.8	-
Heat Loss	0.3	0.1	-	0.9	-

up. Applying recovery factors equally at both conditions allows evaluation of where a particular strategy may be most effective. Note that final efficiency values shown in this example are less important than the relative impact of each approach.

As shown in Table 2, aggressive targets of 50% reduction in friction and parasitic loads and 30% reduction in pumping losses were chosen – even higher pumping-loss reductions should be possible for spark-ignition applications, particularly at low load. This strategy has a significant impact on engine efficiency, especially at low loads as shown in Figure 1.

Improved combustion controls are assumed to provide a 50% reduction in unburned fuel losses with recovered energy redistributed according to the original energy distribution. A 50% reduction in turbocharger losses through improved design or multi-turbine strategies is assumed to significantly increase exhaust energy while providing some additional work due to improved boost (particularly at low loads). As previously discussed, reductions in heat loss primarily produce hotter exhaust with little increase in brake work. Despite aggressive, stretch goals, the direct impact of these strategies on overall engine efficiency is only incremental (see Figures 1 and 2). However, combining these strategies roughly doubles exhaust energy, and the addition of a Rankine bottoming cycle with a target efficiency of 20% to recover waste heat from the exhaust and EGR cooler provides a dramatic efficiency benefit.

Conclusions

Achieving significant improvements in engine efficiency will require balancing multiple strategies to improve work extraction with the piston, reduce friction and heat loss, and concentrate as much remaining energy as possible in the exhaust where some may be recovered with a WHR system. Significant advances will be required in a number of areas including advanced materials and lubricants with high thermal tolerance and durability, advanced low-temperature combustion techniques, electrification and intelligent control of accessory loads, and turbo-machinery.

FY 2011 Publications/Presentations

1. K.D. Edwards, R.M. Wagner, T.E. Briggs, T.J. Theiss (2011), "Defining engine efficiency limits". 2011 Directions in Engine-efficiency and Emissions Research (DEER) Conference.

2. K.D. Edwards, R.M. Wagner, T.J. Theiss (2011), "Exploring practical efficiency limits for goal setting". AEC/HCCI Working Group Meeting. 23–25 August 2011; Southfield MI, USA.

3. K.D. Edwards, T.E. Briggs, R.M. Wagner (2011), "Assessment of engine-efficiency opportunities for future goal setting (diesel)". ACEC Tech Team Meeting. 21 July 2011; Southfield MI, USA.

4. K.D. Edwards, R.M. Wagner (2011), "Assessment of engine-efficiency opportunities for future goal setting (gasoline)". ACEC Tech Team Meeting. 8 September 2011; Southfield MI, USA.

II.A.11 KIVA Development

David B. Carrington
Los Alamos National Laboratory
P.O. Box 1663
Los Alamos, NM 87545

DOE Technology Development Manager:
Gurpreet Singh

Subcontractors:
- Dr. Juan Heinrich, University of New Mexico, Albuquerque, NM
- Dr. Darrell W. Pepper, University of Nevada, Las Vegas. Las Vegas, NV
- Dr. Xiuling Wang, Purdue University, Calumet, Hammond, IN
- Dr. Song-Charng Kong, Iowa State University, Ames, IA

Objectives

- Develop algorithms and software for the advancement of speed, accuracy, robustness, and range of applicability of the KIVA internal engine combustion modeling – to be more predictive. This is to be accomplished by employing higher-order spatially accurate methods for reactive turbulent flow, and spray injection, combined with robust and accurate actuated parts simulation and more appropriate turbulence modeling.
- To provide a KIVA software that is easier to maintain and is easier to add models to than the current KIVA. To reduce code development costs into the future via more modern code architecture.

Fiscal Year (FY) 2011 Objectives

- Continue developing code and algorithms for the advancement of speed, accuracy, robustness, and range of applicability of the KIVA combustion modeling software to higher-order spatial accuracy with a minimal computational effort. Continue research and developing the foundational discretization for engine modeling to utilize an *hp*-adaptive predictor-corrector split (PCS).
- Develop two-dimensional (2-D) overset grid method for moving and immersed actuated parts such as valves for a robust method.
- Develop a grid generation capability using mostly hexahedral elements for engines.
- Extend KIVA-4 capability to predict heat transfer to and from the combustion chamber via conjugate heat transfer modeling. This is for more accurate prediction in wall film and its effects on combustion and emissions under.
- Develop a web-based electronic manual for KIVA-4 and KIVA4-mpi.

Accomplishments

- Developed *h*-adaptive and *hp*-adaptive PCS using Petrov-Galerkin (P-G) finite element methods for all for flow regimes, from incompressible to high-speed compressible.
- Develop 2-D overset grid method for moving and immersed actuated parts such as valves for robust grid movement.
- Developed and verified the *hp*-adaptive finite element method (FEM) framework that uses hierarchical basis for PCS mass, heat and momentum transport solver.
- Continue to provide more appropriate turbulence modeling in PCS system.
- KIVA-4mpi capability has been extended to predict heat conduction and heat flux.
- Developed nearly automatic grid generation using only hexahedral elements with Cubit grid generator.
- Started an email list to report changes and code bugs.
- Starting a web-based forum/blog venue for KIVA on http://www.cfd-online.com/.
- Developed a web-based electronic manual for KIVA-4 and KIVA4-mpi, http://www.lanl.gov/orgs/t/t3/codes/KIVA-4-WebManual/kiva4_users_manual.htm.

Future Directions

- Continue developing the *hp*-adaptive FEM for multispecies flows in all flow regimes. Begin implementing this method to perform modeling of internal combustion engines, other engines, and general combustion.
- Continue developing comprehensive comparative results to benchmark problems and to commercial software as part of the verification and validation of the algorithms.
- Develop three-dimensional (3-D) robust overset grid method for immersed actuated parts such as valves.
- Merge overset grid method into *hp*-adaptive FEM framework.
- Develop the parallel solution method for the *hp*-adaptive PCS algorithm. Parallel structure to be supplied by MPICH and/or OpenMP paradigms for newest computer architectures.

- Develop even more effort on appropriate turbulence modeling for more predictive modeling.
- Incorporate KIVA multi-component particle/spray injection algorithm into the PCS solver.
- Incorporate KIVA chemistry package in the PCS solver.
- Investigate other spray modeling methods for more predictive modeling capability.

Introduction

Los Alamos National Laboratory and its collaborators are facilitating engine modeling by improving accuracy of the modeling, and improving the robustness of software. We also continue to improve the physical modeling methods. We are developing and implementing new mathematical algorithms, those which represent the physics within an engine. We provide software that others may use directly or that they may alter with various models e.g., sophisticated chemical kinetics, different turbulent closure methods or other fuel injection systems.

Approach

Development of computational fluid dynamics (CFD) models and algorithms relies on basic conservation laws and various mathematical and thermodynamic concepts and statements including calculus of variations. The process encompasses a great many requirements including:

1. Knowledge of turbulent modeling for multiphase/multispecies fluid dynamics.
2. Knowledge of combustion dynamics and models.
3. Skill at implementing and solving numerical methods for multi-physics CFD on complex domains.
4. Careful validation and verification of the developed code and algorithms.

Results

We proceed with the idea in mind that it is better to have algorithms which are more accurate at a given resolution and provide for higher resolution and accuracy only where and when it is required.

We recently began researching use of FEM, similar to that developed by Zienkiewicz and Codina, the characteristic-based split or CBS method [1]. This construction is a Galerkin type FEM that utilizes conservative momentum and energy transport. We have determined the precise P-G stabilization [2] is more appropriate than CBS method of discretized equation stabilization.

Both algorithms are known as projection methods; methods now having great popularity in the finite element community. These methods, combined with higher order polynomial approximation for model dependent physical variables (p-adaptive) along with grid enrichment (locally higher grid resolution – h-adaptive) and overset grids for actuated and immersed moving parts will provide for highly accurate and robust solutions in the next generation of KIVA, particularly on complex domains. We have been developing this PCS algorithm for KIVA from our h-adaptive and hp-adaptive FEM research to create a new KIVA combustion code [2-6].

As shown in Figure 1, the PCS conservative formulated projection scheme using P-G stabilization

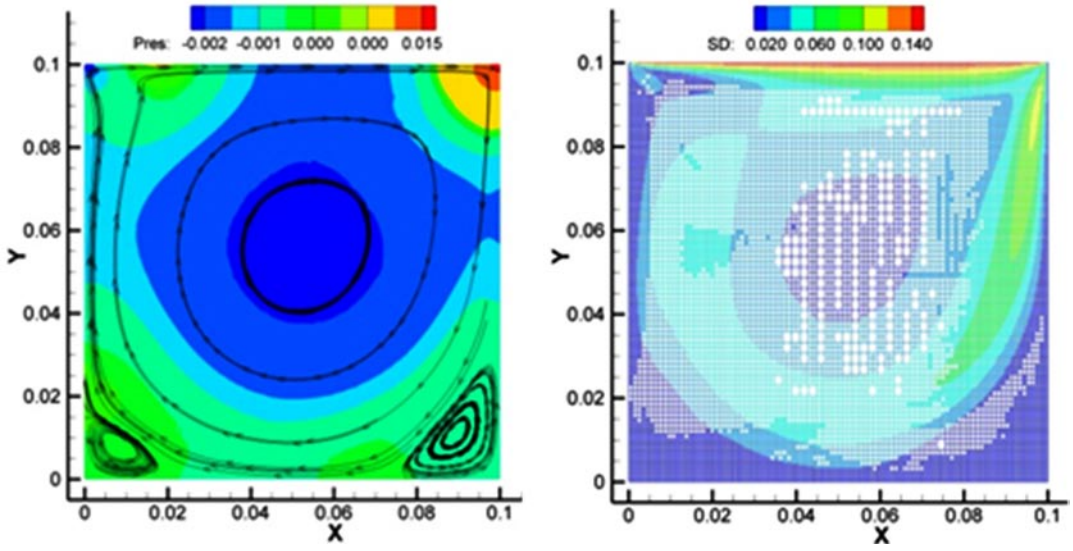

FIGURE 1. 2-D Driven Cavity at Re = 1,000 using an Initial 40x50 Mesh (2,000 cells) a) Isobars and Streamlines, b) Adapted Grid and Isotachs

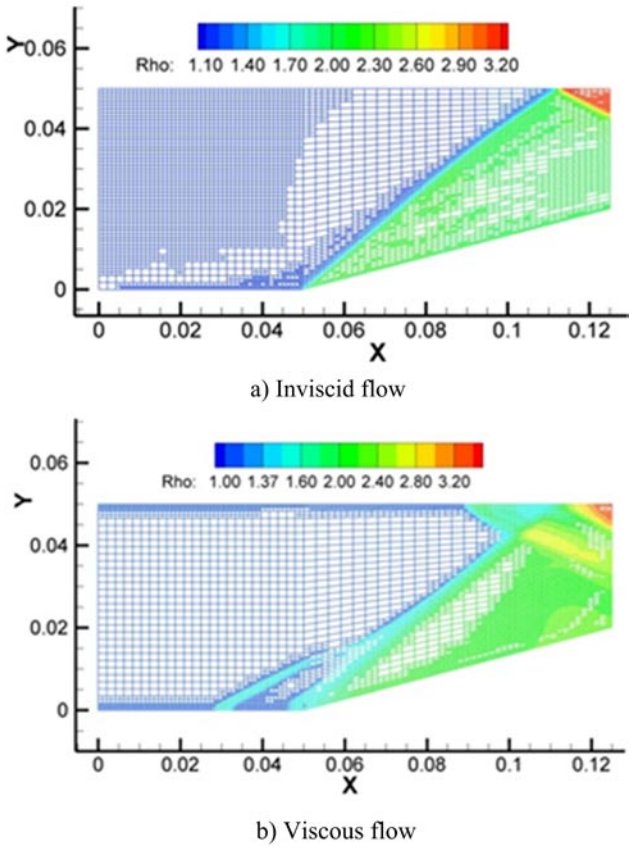

FIGURE 2. Density Contours for 2-D Supersonic Flow through a 15° Compression Ramp a) Inviscid Flow, b) Viscous Flow

works well, matching available data extremely well, particularly when using the adaptive grid technique.

Figure 2 shows the *h*-adaptive solution for both inviscid and viscous Mach 2.2 supersonic flow through a 2-D compressor. The solutions are in excellent agreement with known solutions.

Verification results shown in Figure 3 are using PCS fractional-step algorithm [4,5], natural convection in partially divided enclosure. The left and right walls are maintained at hot and cold temperatures, respectively. Figure 3 (a) shows the final *hp*-adaptive mesh where the initial coarse mesh consisted of 388 quadirlateral elements with 435 nodes, the final mesh consists of 1,261 elements and 4,714 degrees of freedom.

A new method is being developed for immersed actuated parts in the engine. By using an overset grid system and local adjustments to the grid only when the actuated parts cross the boundary of a fluid element the method maintains 2nd order spatial accuracy. Once the part leaves the element, or when the part is outside the element, the element returns to its original shape. The development strategy is for 2-D constructions first that are extensible to 3-D. In Figure 4, a 2-D piston is shown at two different times during the cycle. The solution

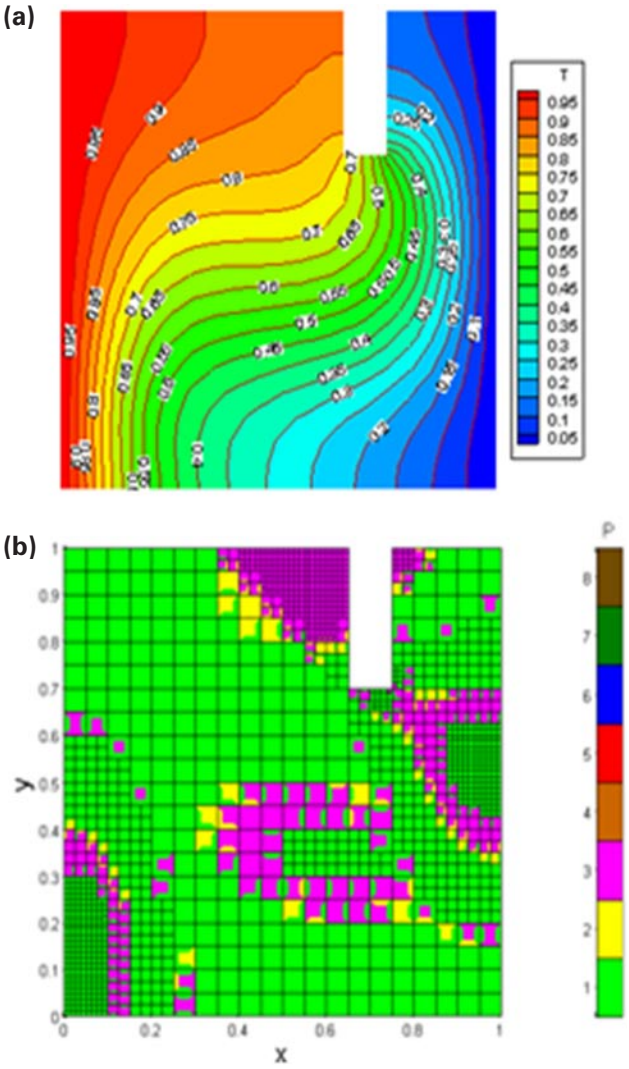

FIGURE 3. Partial Diveded Differentially Heated Enclosure a) Isotherms, b) Final *hp*-Adaptive Mesh

is performed for incompressible flow to facilitate development and validation.

Error for this formulation against a known solution, a benchmark, is a fraction of a percent. The error is bounded, and the method shows 2nd order spatial convergence.

A conjugate formulation to predict heat conduction or conjugate heat transfer in the solid domain and spray combustion on the fluid domain was developed for multi-dimensional engine simulation using KIVA-4mpi. Heat transfer through the wall affects the combustion process in the cylinder and the thermal loading on the combustion chamber surface. Detailed understanding of the wall heat flux is important in improving engine efficiency and durability. To account for the temporal and spatial variations of temperature on the combustion chamber surface, a fully coupled numerical procedure

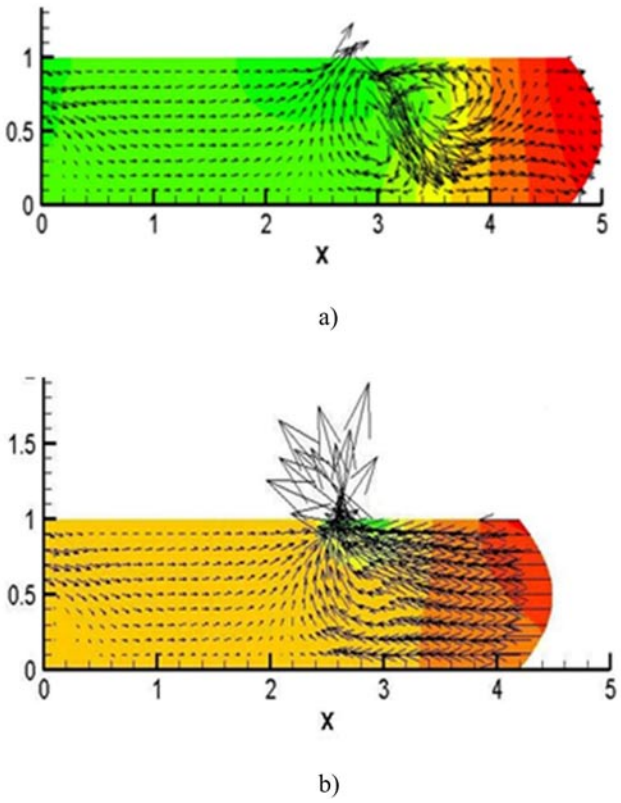

FIGURE 4. Immersed Moving Piston for PCS FEM System
a) and b) Showing Displacement, Velocity Vectors (Color Represents Isobars Variation)

was developed and applied to calculate in-cylinder flow and solid component heat conduction simultaneously.

In the present engine, spray is injected from the center of the cylinder head. Both spray atomization and combustion models are based on the original KIVA models. The temperature distribution at certain timing is shown in Figure 5. Inside the engine cylinder, gas temperature along fuel spray decreases due to vaporization of liquid drops. In the solid domain, it can be seen that the model is able to predict the temperature gradient due to heat transfer between in-cylinder gas and the solid.

Using Cubit [http://cubit.sandia.gov/] for engine grid generation is being investigated (Figure 6). Once the commands (technology) are implemented in script, the grid generation process is automatic. The command scripts (technology) are easily altered for various engine domains and grid refinements. This work supports our effort to produce hexahedral grid generation that is essentially automatic. The converter for both KIVA-4mpi and the FEM formulation for KIVA has already been developed. Because the FEM grid is designed for use with the overset grid scheme discussed previously, it is much easier to produce a grid nearly automatically than it is for the current KIVA-4 unstructured grid code that utilizes a grid snapping system.

Conclusions

The following conclusions are drawn from the work described.

1. Development of an *hp*-adaptive PCS FEM for all for regimes has been achieved. Compressible flow verification and validation has been performed and continues. This projection method is a new solution algorithm for advancing the accuracy, robustness, and range of applicability of the KIVA combustion code. The system if one of higher-order spatial and temporal accuracy while providing a minimal amount of computational effort.
2. Development of new algorithm for immersed moving parts, or actuated parts, has be accomplished. The work in 2-D is extensible to 3-D and provides 2nd order spatial accuracy.

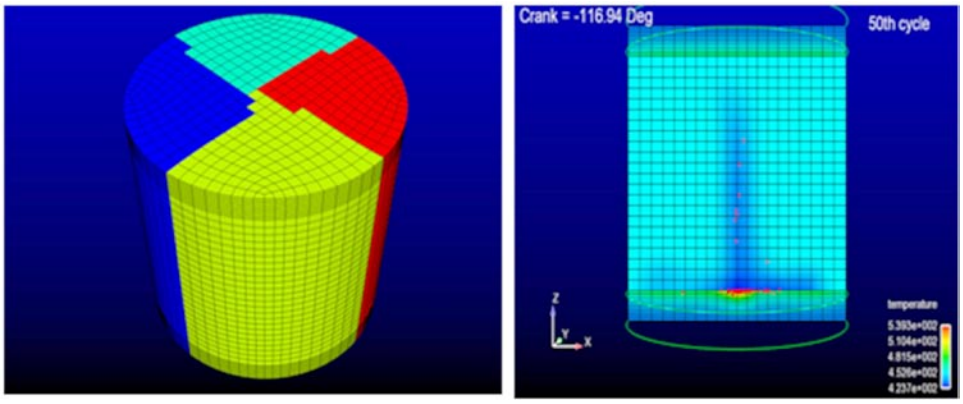

FIGURE 5. Solution of Conjugate Heat Transfer in Internal Combustion Engine, with Injection
a) Parallel Domain Decomposition, b) Temperature in both the Fluid and Solid Regions

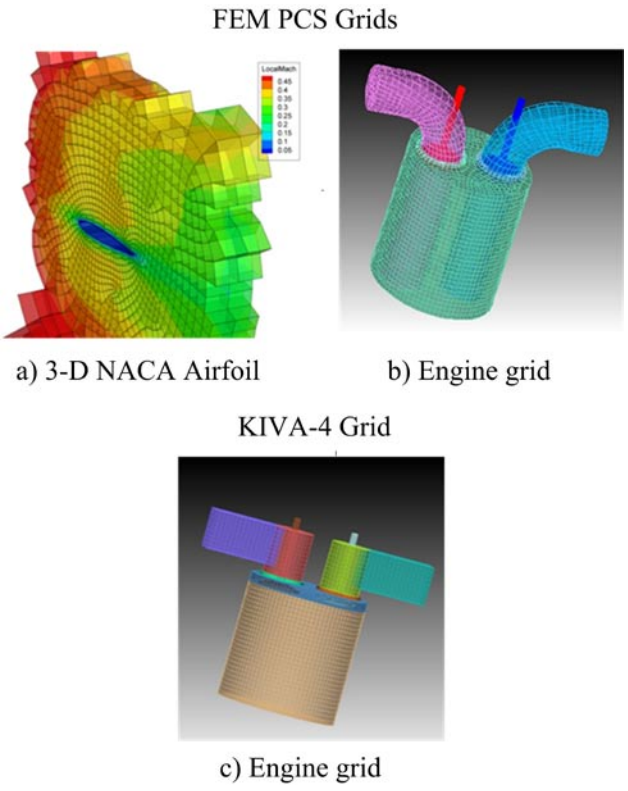

FIGURE 6. Cubit Grid Generation for New KIVA and for KIVA-4 using all Hexahedral Elements a) NACA-0012 Local Mach Values from PCS algorithm, b) Grid for PCS Algorithm, c) Grid for KIVA-4

3. The use of Cubit for generation of unstructured grids has been achieved for the PCS FEM algorithm. Cubit for use with KIVA-4mpi is progressing. Cubit supplies nearly automatic grid generation once the technology or journal file of commands has been constructed. These commands are generally easily adjusted for variations in the domain.
4. Extending KIVA-4mpi capability to predict heat conduction in solids, that is, in the combustion chamber, has been achieved. This to provide more accurate prediction of wall film wetting and subsequent evaporation. For example, to provide more accurate wall heat flux effects on combustion and emissions under PCCI engine conditions injected with fuel having wall impingement.

References

1. Zienkiewicz O.C. and Codina, R., (1995) "A general algorithm for compressible and incompressible flow, Part I, The split characteristic based scheme," International Journal of Numerical Methods in Fluids, Vol. 20, pp. 869– 885.

2. Carrington, D.B., Wang, X., Pepper, D.W., (2010) "An h-Adaptive Finite Element Method for Turbulent Heat Transfer," Computer Modeling in Engineering & Sciences, Tech Science Press, vol. 61, no 1, pp. 23-44.

3. Wang, X, Carrington, D.B., Pepper, D.W., (2009) "An Adaptive FEM Model for Unsteady Turbulent Convective Flow Over a Backward-Facing Step," Journal of Computational Thermal Sciences, Begell House Inc., vol. 1, no. 2, pp. 121-135.

4. Carrington, D.B., (2009) "A characteristic-based split hp-adaptive finite element method for combustion modeling in KIVA-hpFE," Los Alamos National Laboratory, report. LA-UR-09- 06527, Los Alamos, NM.

5. Wang, X. and Pepper, D.W. (2007) "Application of an *hp*-adaptive FEM for Solving Thermal Flow Problems," *AIAA Journal of Thermophysics and Heat Transfer,* vol. 21, No.1, pp. 190 – 198.C.

6. Carrington, D.B., (2011) "A Fractional step *hp*-adaptive finite element method for turbulent reactive flow," Los Alamos National Laboratory Report, LA-UR-11-00466.

7. This report has been assigned LA-UR-11-11973 for public release.

FY 2011 Publications/Presentations

1. Carrington, D.B., "A Fractional step hp-adaptive finite element method for turbulent reactive flow," Los Alamos National Laboratory Report, LA-UR-11-00466, 2011.

2. Carrington, D.B., Wang, X., Pepper, D.W., "An h-Adaptive Finite Element Method for Turbulent Heat Transfer," Computer Modeling in Engineering & Sciences, Tech Science Press, vol. 61, no 1, pp. 23-44, 2010.

3. Carrington, D.B.,(2011) "2011 DOE Vehicle Technologies KIVA-4 Development," 2011 DOE/EERE Advanced Combustion Merit Review, Washington, D.C., May, LA-UR-11-01879,2011.

4. Carrington, D.B., "KIVA Update," AEC/HCCI Working Group Meeting- USCAR,, Detroit, MI; Sept. 1, 2011, Washington, D.C., LA-UR 11-11130, 2011.

5. Carrington, D.B., "KIVA Update," AEC/HCCI Working Group Meeting- AEC/HCCI Working Group Meeting - Sandia National Laboratory, Livermore, CA; Feb., LA-UR 11-01159, 2011.

6. Carrington, D.B., "KIVA-4 Development," 2010 DOE/EERE Advanced Combustion Merit Review, Washington, D.C., June , LA-UR-10-01879, 2010.

7. Torres, D.J., Li, Y. H., Kong, S.-C., "Partitioning Strategies for Parallel KIVA-4 Engine Simulations," Computers and Fluids, Vol. 39, no. 2, p.301-309, 2010.

8. Carrington, D.B., Wang, X. Pepper, D.W., "An h-Adaptive Finite Element Method for Turbulent Heat Transfer," International Conference on Computational and Experimental Engineering and Sciences, Las Vegas, NV, March 23, LA-UR 10-01692, 2010.

9. Carrington, D.B., "T-3 Combustion Modeling KIVA-4mpi and KIVA-hpFE Development," Invited Talk at UNM Mechanical Engineering Seminar, University of New Mexico, Albuquerque, NM, March 21, (LA-UR-10-00727), 2010.

10. Carrington, D.B, "Adaptive Finite Element Methods for Turbulent Reactive Flow," Los Alamos ADTSC Science Highlights, 2010.

11. Carrington, D.B., "T-3 Combustion Modeling KIVA Combustion Model Development," DOE/CFR meeting, Los Alamos, NM, April 21st, 2010. LA-UR 10-01878.

Special Recognitions & Awards/Patents Issued

1. Outstanding Innovation Award – Distinguished Copyright. Awarded by Los Alamos National Laboratory Technology Transfer Division, August 5th, 2011.

II.A.12 Chemical Kinetic Models for HCCI and Diesel Combustion

William J. Pitz (Primary Contact),
Charles K. Westbrook, Marco Mehl,
S. Mani Sarathy
Lawrence Livermore National Laboratory (LLNL)
P.O. Box 808, L-372
Livermore, CA 94551

DOE Technology Development Manager:
Gurpreet Singh

Overall Objectives

- Develop detailed chemical kinetic models for fuel components used in surrogate fuels for diesel and homogeneous charge compression ignition (HCCI) engines.
- Develop surrogate fuel models to represent real fuels and model low-temperature combustion strategies in HCCI and diesel engines that lead to low emissions and high efficiency.
- Characterize the role of fuel composition on low-temperature combustion modes of advanced combustion engines.

Fiscal Year (FY) 2011 Objectives

- Develop a chemical kinetic model for a high molecular-weight aromatic.
- Develop a chemical kinetic mechanism for a new series of iso-alkanes to help represent the iso-alkane chemical class in diesel fuel.
- Provide validation of the chemical kinetic mechanisms of the 2-methyl alkane series.
- Develop improved gasoline surrogate fuels for HCCI engines.
- Develop a functional group method to represent iso-alkanes in diesel fuel.

Accomplishments

- Developed chemical kinetic model for larger aromatics to expand the available components for gasoline surrogate fuels.
- Development of chemical kinetic models for new types of model compounds for iso-alkanes including 3-methyl heptane and 2,5-dimethyl hexane.
- Developed new approach for formulating gasoline surrogate mixtures for real gasoline fuels and a reduced mechanism for a gasoline surrogate for computational fluid dynamic (CFD) applications.
- Developed a functional-group kinetics modeling approach for iso-alkanes that greatly reduces the size of the mechanism for use in multidimensional engine simulations.

Future Directions

- Develop chemical kinetic models for a higher molecular weight aromatics to represent the aromatics chemical class in diesel fuel.
- Develop more accurate surrogate kinetics models for gasoline.
- Develop a reduced surrogate mechanism for diesel fuel to be used for multidimensional CFD simulations.
- Develop a functional group method for cycloalkanes in diesel fuel so that the chemical kinetic mechanism can be greatly reduced in size for multidimensional engine simulations.
- Validate and improve 2- and 3-methyl alkanes and symmetrical di-methyl alkanes mechanisms with new data from shock tubes, jet-stirred reactors, counterflow flames, and premixed flames.

Introduction

Predictive engine simulation models are needed to make rapid progress towards DOE's goals of increasing combustion engine efficiency and reducing pollutant emissions. These engine simulation models require chemical kinetic submodels to allow the prediction of the effect of fuel composition on engine performance and emissions. Chemical kinetic models for conventional and next-generation transportation fuels need to be developed.

Approach

Gasoline and diesel fuels consist of complex mixtures of hundreds of different components. These components can be grouped into chemical classes including n-alkanes, iso-alkanes, cycloalkanes, alkenes, oxygenates, and aromatics. Since chemical kinetic models cannot be developed for hundreds of components, specific components need to be identified to represent each of these chemical classes. Then detailed chemical kinetic models for these selected components can be developed. These component models are subsequently merged to produce a "surrogate" fuel model for gasoline, diesel, and next-generation transportation fuels. This approach can create realistic surrogates for gasoline or diesel fuels

that reproduce experimental behavior of the practical real fuels. Detailed kinetic models for surrogate fuels can then be simplified as needed for inclusion in multidimensional CFD models or used in full detail for purely kinetic modeling.

Results

Iso-alkanes are present in diesel fuel in large concentrations [1] and are a chemical class that needs to be represented in a diesel surrogate model to correctly predict ignition properties. During FY 2011, we continued our work on expanding the available fuel components in this chemical class for chemical kinetic modeling. We further validated our component models for this chemical class by making comparisons of simulated results with experimental measurements in high-pressure stirred reactors and shock tubes. Specifically, we have developed chemical kinetic models for 3-methyl heptane and 2,5-dimethyl hexane as new model fuel components in the iso-alkane chemical class. We have validated the models for the aforementioned fuels against atmospheric pressure premixed laminar flame speeds from University of Southern California (Figure 1) and counter-flow diffusion flame species profiles obtained at the University of Toronto (Figure 2). The present comparisons between model predictions and experiments show a satisfactory level of agreement; however, we are awaiting additional experimental data covering a wider range of pressures and temperatures to further validate these models.

We have also made further validations of our 2-methyl heptane chemical kinetic model that we developed last year by comparing the computed results of the model with experiments in a high-pressure shock tube at Rensselaer Polytechnic Institute, a high-pressure stirred reactor at Orleans, a high pressure flow reactor at Princeton University and counterflow ignition and extinction experiments at University of California, San Diego. Figure 3 shows the agreement with the model and the high pressure jet stirred reactor experiments that cover the entire low and high temperature combustion regimes. The model correctly predicts the behavior in the negative temperature coefficient (NTC) region that is essential for simulating low-temperature combustion in diesel engines. Also, the model shows good qualitative agreement with high-pressure ignition experiments

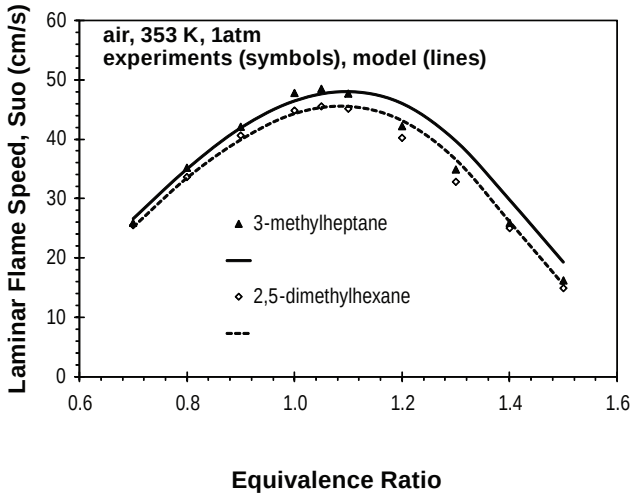

FIGURE 1. Comparison of flame speeds predicted by the 3-methylheptane and 2,5-dimethyl hexane models with experimental measurements from the University of Southern California [5].

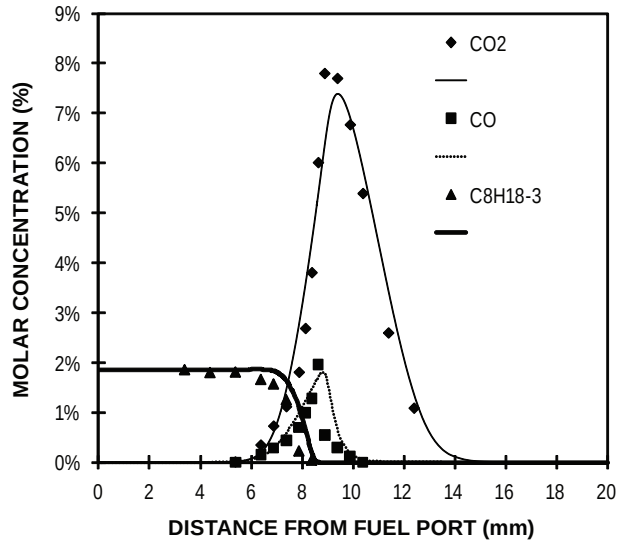

FIGURE 2. Comparison of species profiles predicted by the 3-methyl heptane model (C_8H_{18}-3) and measured experimentally in an atmospheric pressure counterflow diffusion flame [6].

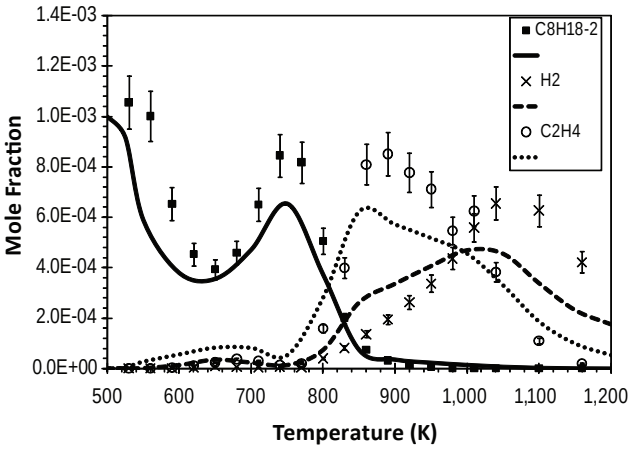

FIGURE 3. 2-Methylheptane oxidation in a jet stirred reactor at 10 atm, residence time = 0.7 s and equivalence ratio = 1.0. The initial fuel (C_8H_{18}-2) mole fraction was 0.1%. Experimental data (symbols) [7] are compared to calculations (lines).

in a shock tube when the equivalence ratio is varied (Figure 4). Further work needs to be done to improve the quantitative agreement for these ignition delay times.

Gasoline and diesel fuels are composed of hundreds of components and it is not possible to represent all these in a detailed chemical kinetic model. Surrogates containing a limited number of components are used to represent gasoline and other real fuels. We have developed a new approach for formulating surrogates for gasoline fuels. This approach matches the reactivity of the gasoline fuel in NTC regime which is essential for predicting the low and intermediate temperature heat release for gasoline fuels in HCCI engines. The octane number and octane sensitivity of the real gasoline fuel was used for matching the fuel reactivity [2]. Secondly, we match the C/H ratio which also helps to match the adiabatic flame temperature, flame speed, and heat of combustion of the target gasoline. Thirdly, we match the relative amounts of alkanes, alkenes, and aromatics which further helps to match the reactivity of the fuel, particularly in the NTC region. We demonstrated the efficacy of this procedure in a recent publication [2]. In this work, we also developed a 312 species reduced mechanism that reproduces well the ignition behavior of an 87 octane gasoline over a wide range of pressure and temperature and simulates well the reported flame speeds of gasoline. This mechanism is of the size they can now be readily handled by recently developed CFD engine codes [3].

Chemical kinetic models for real fuels need to be reduced to allow their use in CFD engine simulation codes. In FY 2010, we developed a new approach called the functional group approach that greatly reduces the size of a chemical kinetic fuel mechanism and its accompanying computational requirements. Each fuel molecule is divided up into function groups based on the molecular structure of fuel. In FY 2011, we have applied this method to the case of iso-alkanes which allowed the reduction of a mechanism for C8 to C20 iso-alkanes from 7,900 species to 280 species. This is a tremendous reduction in size of almost a factor of 30 in number species. The resources required for CFD models are mostly sensitive to the number species. The results of using this functional group model to simulate the oxidation of 2-methyl heptane in a jet stirred reactor is shown in Figure 5 and compared to the detailed model and experimental measurements. The approach works nearly as well as the detailed model.

In FY 2011, we expanded our capability to model larger allyl aromatics including ortho-, para- and meta-xylene and ethylbenzene. These alkyl aromatics are of the carbon size range important for gasoline fuels. Their inclusion in gasoline surrogate models helps to simulate the octane sensitivity and C/H ratio of gasoline. A detailed chemical kinetic model that included all these alkylated benzenes was developed and extended our FY 2010 efforts on toluene and benzene to higher molecular weight aromatics. The results using the model under typical engine conditions are shown in Figure 6 and compared to ignition delay times measured in a shock tube at high pressure [4]. The agreement with the experimental data is quite good, especially considering the challenges to modeling the chemistry of aromatics.

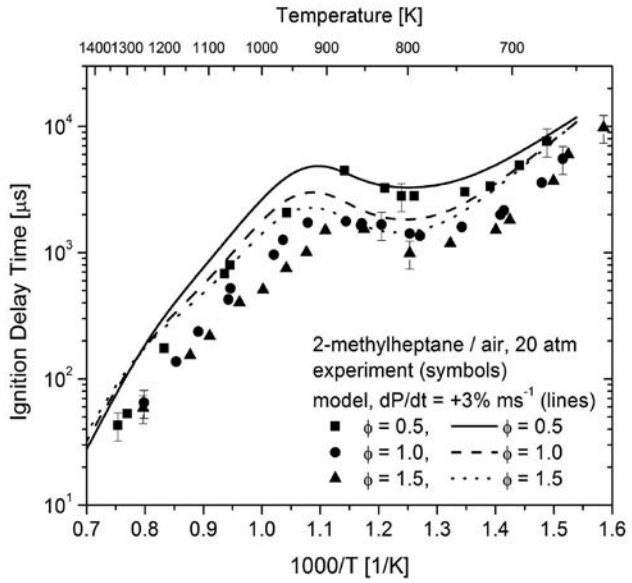

FIGURE 4. Measured shock tube ignition delay times at 20 atm with comparison to kinetic modeling predictions for 2-methylheptane. ϕ is fuel/air equivalence ratio, where ϕ=1 is stoichiometric. Measurements are from [7].

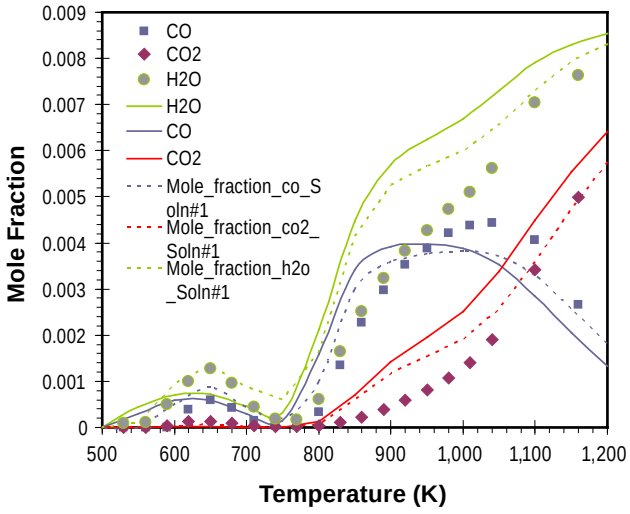

FIGURE 5. Intermediates and final products in the oxidation of 2-methylheptane in a jet stirred reactor at 10 atm, ϕ=1, 0.5 s residence time, 0.1% initial fuel concentration: solid lines are functional group model, dotted lines are detailed model, symbols are experiments [7].

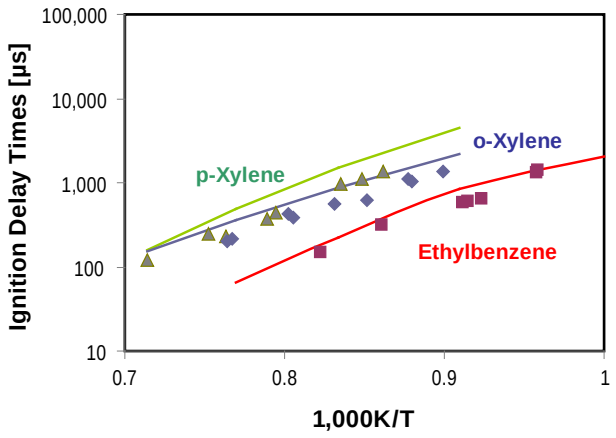

FIGURE 6. Ignition delay times for stoichiometric, alkyl-benzene/air mixtures at conditions relevant to internal combustion engines (initial conditions: 10 atm and 1,000-1,400 K). The symbols are experiments [4] and the curves are from the detailed chemical kinetic model.

Our goal for FY 2012 is to increase our capabilities further into the diesel range of aromatic compounds.

Conclusions

- Our detailed kinetic modeling capabilities have been extended to higher molecular weight alkylated aromatics which are important compounds for gasoline fuel.
- We have developed detailed kinetic models for new types of iso-alkanes including 3-methyl heptane and 2,5-dimethyl hexane. Both are important model components for iso-alkanes in transportation fuels.
- We have used the LLNL functional group approach to develop a mechanism for a whole series of iso-alkanes that is highly reduced by a factor of 30 in number of species from its conventional detailed mechanism.

References

1. W.J. Pitz and C.J. Mueller, "Recent progress in the development of diesel surrogate fuels," *Progress in Energy and Combustion Science* 37 (3) (2011) 330-350.

2. M. Mehl, J.Y. Chen, W.J. Pitz, M.S. Sarathy, and C.K. Westbrook, "An approach for formulating surrogates for gasoline with application towards a reduced surrogate mechanism for CFD engine modeling", Energy and Fuels: 25 (11) 5215-5223, 2011.

3. C.V. Naik, K.V. Puduppakkam, C. Wang, J. Kottalam, L. Liang, D. Hodgson and E. Meeks, "Applying Detailed Kinetics to Realistic Engine Simulation: the Surrogate Blend Optimizer and Mechanism Reduction Strategies," SAE Paper No. 2010-01-0541 (2010).

4. H.-P.S. Shen and M.A. Oehlschlaeger, "The autoignition of C8H10 aromatics at moderate temperatures and elevated pressures," *Combust. Flame* 156 (5) (2009) 1053-1062.

5. C. Ji, S.M. Sarathy, P.S. Veloo, C.K. Westbrook, F.N. Egolfopoulos, "An experimental and computational study of the propagation of octane isomers flames", Combustion and Flame, (2011). http://dx.doi.org/10.1016/j.combustflame.2011.12.004

6. S.M. Sarathy, C.K. Westbrook, C. Yeung, U. Niemann, M. Plomer, Z. Luo, M. Mehl, W.J. Pitz, K. Seshadri, M.J. Thomson and T. Lu, "A counterflow diffusion flame study of lightly methylated alkanes," *Fall Technical Meeting of the Western States Section of the Combustion Institute*, 2011.

7. S.M. Sarathy, C.K. Westbrook, M. Mehl, W.J. Pitz, C. Togbe, P. Dagaut, H. Wang, M.A. Oehlschlaeger, U. Niemann, K. Seshadri, P.S. Veloo, C. Ji, F. Egolfopoulos and T. Lu, "Comprehensive chemical kinetic modeling of the oxidation of 2-methylalkanes from C7 to C20," Combust. Flame 158 (12) (2011) 2338-2357

FY 2011 Publications/Presentation

1. Sarathy, S.M., C. Yeung, C.K. Westbrook, W.J. Pitz, M. Mehl and M.J. Thomson. "An experimental and kinetic modeling study of n-octane and 2-methylheptane in an opposed flow diffusion flame." Combustion and Flame: 158 (7): 1277-1287, 2011.

2. S.M. Sarathy, C.K. Westbrook, M. Mehl, W.J. Pitz, C. Togbe, P. Dagaut, H. Wang, M.A. Oehlschlaeger, U. Niemann, K. Seshadri, P. S. Veloo, C. Ji, F. Egolfopoulos and T. Lu, "Comprehensive chemical kinetic modeling of the oxidation of 2-methylalkanes from C7 to C20," Combust. Flame 158 (12) (2011) 2338-2357

3. M. Mehl, W.J. Pitz, J.E. Dec, Y. Yang, "Detailed kinetic modeling of conventional gasoline at highly boosted conditions", 2012 SAE World Congress, submitted.

4. M. Mehl, J.Y. Chen, W.J. Pitz, M.S. Sarathy, and C.K. Westbrook, "An approach for formulating surrogates for gasoline with application towards a reduced surrogate mechanism for CFD engine modeling", Energy and Fuels: 25 (11) 5215-5223, 2011.

5. M. Mehl, G. Kukkadapu, K. Kumar, S.M. Sarathy, W.J. Pitz, and C.J. Sung, "Gasoline surrogate modeling of gasoline ignition in a rapid compression machine and comparison to experiments", Western States Section of the Combustion Institute, Riverside, CA, Paper #11F-32, 2011.

6. M. Mehl, W.J. Pitz, S.M. Sarathy, C.K. Westbrook, H.J. Curran, "Modeling the combustion of high molecular weight fuels by a functional group approach", International Journal of Chemical Kinetics, In Press, 2011.

7. M.A. Carr, P.A. Caton, L.J. Hamilton, J.S. Cowart, M. Mehl and W.J. Pitz, "An Experimental and Modeling-Based Study into the Ignition Delay Characteristics of Diesel Surrogate Binary Blend Fuels," American Society of Mechanical Engineers, ICEF2011-60027 (2011).

8. Zhaoyu Luo, Max Plomer, Tianfeng Lu, Sibendu Som, Douglas E. Longman, S.M. Sarathy, William J. Pitz, "A Reduced Mechanism for Biodiesel Surrogates for Compression Ignition Engine Applications", Fuel, submitted, 2011.

9. C. Ji, S.M. Sarathy, P.S. Veloo, C.K. Westbrook, F.N. Egolfopoulos, "An experimental and computational study of the propagation of octane isomers flames", Combustion and Flame, (2011). http://dx.doi.org/10.1016/j.combustflame.2011.12.004

Special Recognitions & Awards/Patents Issued

1. S. Mani Sarathy, Postdoc Fellowship, Natural Sciences and Engineering Research Council of Canada, 4/2010 to 4/2012.

2. William J. Pitz: 2011 Outstanding Postdoc mentor award from LLNL Physical and Life Sciences Directorate.

3. Charles K. Westbrook, President of the Combustion Institute, 2008-2012.

II.A.13 Free-Piston Electric Generator

Peter Van Blarigan
Sandia National Laboratories
PO Box 969, MS 9661
Livermore, CA 94551-0969

DOE Technology Development Manager:
Gurpreet Singh

Overall Objectives

- Study the effects of continuous operation (i.e. gas exchange) on indicated thermal efficiency and emissions of an opposed free-piston linear alternator engine utilizing homogeneous charge compression ignition (HCCI) combustion at high compression ratios (~20-40:1).
- Concept validation of passively synchronizing the opposed free pistons via the linear alternators, providing a low cost and durable design.
- Proof of principle of electronic variable compression ratio control, allowing optimized combustion timing and fuel flexibility, by means of mechanical control of bounce chamber air pressure.
- Provide a research tool to explore the free-piston engine operating envelope across multiple inputs: boost level, equivalence ratio, alternative fuels.

Fiscal Year (FY) 2011 Objectives

- Demonstrate functionality of compressed helium starting system.
- Quantify piston friction by executing piston movement tests prior to magnet installation.
- Develop and validate a thermodynamic model of research prototype.

Accomplishments

- Bounce chamber cylinders, injection valves, vent manifolds, and pistons obtained and assembled.
- A compressed helium gas injection starting system was designed, simulated and tested to show capability to bring pistons to desired operating compression ratio in one stroke with good piston synchronization.
- Piston movement testing following helium injection starting pulse has allowed piston friction model to be developed.
- Modeling and experiments with piston pulsing showed deficiency in bounce chamber venting ports; bounce chamber ports enlarged.

Future Directions

- Install magnets on piston assembly and pulse pistons to show stabilizing effect of alternators.
- Initially run the engine under motoring mode only to test capability for continuous piston motion synchronization.
- Perform combustion experiments and measure indicated thermal efficiency at various compression ratios and equivalence ratios with both conventional and alternative fuels: hydrogen, natural gas, ethanol, biofuels, propane, gasoline, other renewables.

Introduction

As fuel efficiency of the typical American automobile becomes more important due to hydrocarbon fuel cost and availability issues, powertrain improvements will require smaller output engines combined with hybrid technologies to improve efficiency. In particular, the plug-in hybrid concept will require an electrical generator of approximately 30 kW output. Unfortunately, current crankshaft spark-ignition internal combustion engines with optimized power outputs of 30 kW have thermal efficiencies of less than 32%.

The free-piston generator of this project has a projected fuel-to-electricity conversion efficiency of 50% at 30 kW output. The project has progressed by conducting idealized combustion experiments, designing and procuring the linear alternators required for control and power conversion, and conducting computational fluid dynamics design of the inlet/exhaust processes.

Approach

By investigating the parameters unique to free-piston generators (linear alternator, opposed piston coupling, uniflow port scavenging) as separate entities, each piece can be used at its optimum design point. More importantly, upon assembly of a research prototype for performance demonstration (the goal of this project), understanding of the pieces in the device will allow the proper contribution of each component to the combined performance of the assembly. Collaboration with General Motors and the University of Michigan continues on a detailed model of the Sandia free-piston electric generator (FPEG) research prototype.

Results

Figure 1 shows the Sandia FPEG research prototype. Bounce chamber cylinders, air injection valves, vent manifolds, and pistons were all obtained and assembled in the past year. All mechanical components have now been acquired, and the engine is fully assembled except for the magnets. These components were left out during assembly to allow piston movement tests and assessment of friction, which is discussed in the following. Instrumentation and data acquisition systems have also been set up. Piston position measurements are made using Fastar FS5K variable inductor displacement transducers. Dynamic pressure measurements in the combustion chamber and in the bounce chambers are made using quartz piezoelectric transducers with overall output calibrated against reference transducers in the Sandia calibration records. Two water-cooled Kistler 7061B transducers are utilized in the combustion chamber where thermodynamic calculations will be performed, while a Kistler 6123 transducer is utilized in each of the bounce cylinders. Several diagnostic pressure measurements are made using Teledyne Taber strain gage transducers. Accelerometers mounted on the bounce chamber head along the piston axis measure movement of the overall experiment, which would be indicative of poorly synchronized pistons. Electrical current measurements are made on the helium injection solenoid valves, fuel injectors, and linear alternator output. Data for piston movement tests was acquired using three synchronized IOtech 6230 24-bit voltage input modules.

Following engine assembly, tests were performed using the compressed helium starting system to drive the pistons to compression ratios in the intended operating range. These tests demonstrated proper operation of the compressed helium starting system and allowed indirect measurement of piston friction at realistic pressure and speed. Results were also used to validate a thermodynamic model including dynamics of piston motion. In addition, a deficiency in bounce chamber venting was discovered and resolved. Figure 2 shows a computer-aided design (CAD) model of the bounce chamber. For piston movement tests, it was desired to drive the pistons to operating compression ratio on the first stroke using the compressed helium starting system and allow friction to damp out their motion. In order to seal the bounce chambers, it was necessary to put pressure behind the air injection valve. To prevent addition of air when the pistons bounced back, the pins to actuate the valve were not installed. In this way, no additional energy was introduced after injection and expansion of the compressed helium. Pistons were positioned prior to each test such that the distance between the bounce cylinder head and piston top was approximately 1 inch, corresponding to the position at which the air injection valve would be actuated if the pins were installed.

To estimate piston friction, a dynamic force balance was performed using measured pressure forces, acceleration calculated from piston position data, and measured piston mass. Digital signal processing was used to apply low-pass filtering to the position record in order to remove noise which would be amplified upon calculation of derivatives. Friction was also modeled for use with a thermodynamic model of the engine. For simplicity, only a constant and a velocity dependent term were used, though a pressure dependence may be present as well. The friction model was adjusted to obtain agreement between thermodynamic model results and measured pressure and position records. The resulting friction model agreed well with results from the dynamic force balance, as seen in Figure 3.

Figures 4 and 5 show results from piston movement testing with a starting helium pressure of 78 bar in each 80 cc reservoir. Without the alternator load (no magnets installed), these starting conditions were found to provide sufficient energy to achieve a geometric compression ratio of around 23:1 on the first stroke,

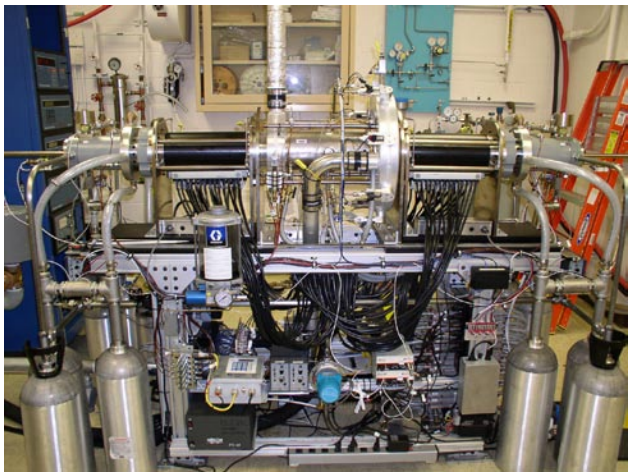

FIGURE 1. Sandia FPEG Research Prototype

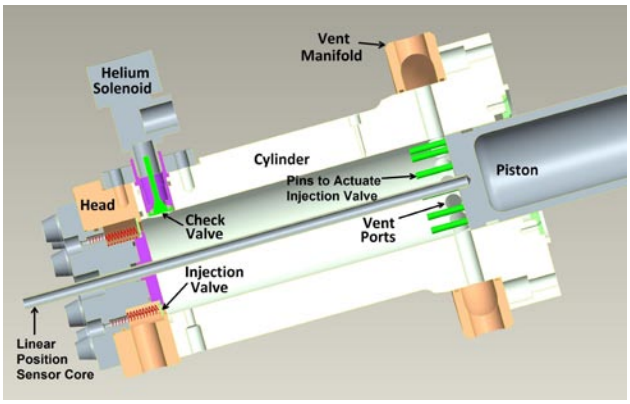

FIGURE 2. CAD Model of Bounce Chamber with Compressed Helium Starting and Air Motoring Systems

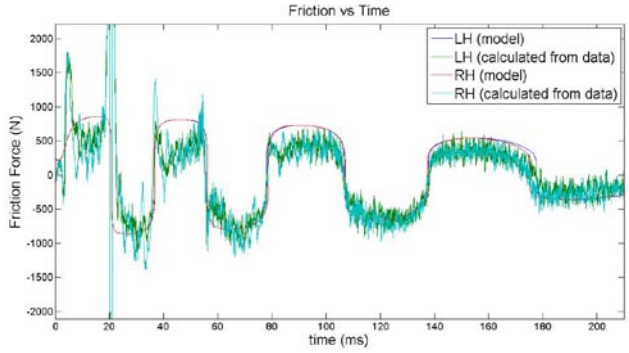

FIGURE 3. Friction Calculation and Model Based on Piston Movement Tests

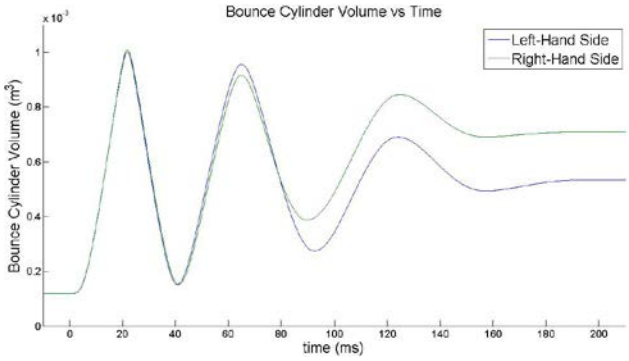

FIGURE 4. Bounce Cylinder Volume vs. Time from Test Data with Original Vent Configuration

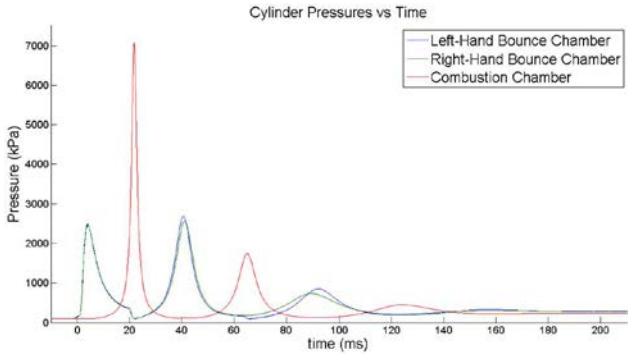

FIGURE 5. Cylinder Pressures vs. Time from Test Data with Original Vent Configuration

on the lower end of the intended operating regime. Bounce cylinder pressure is seen to rise sharply and simultaneously on each side of the engine as helium is injected through the starting system. As the pistons accelerate toward the combustion chamber, the injected helium expands until vent ports in the bounce chamber are uncovered, at which point it blows down to the manifold pressure. Meanwhile, the combustion chamber air is being compressed by the energy of the moving pistons. The pistons bounce back and forth in this

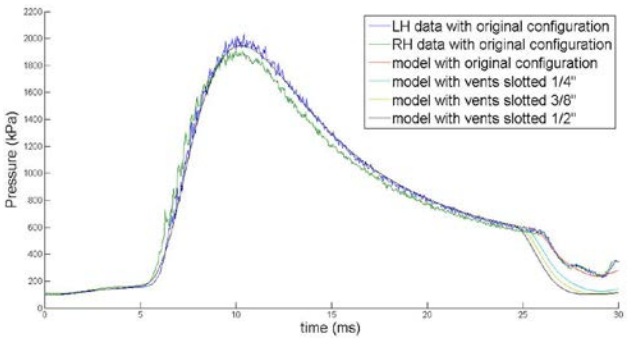

FIGURE 6. Modeling to Determine Resizing of Bounce Chamber Vent Ports

manner with decreasing amplitude and frequency as energy is lost to friction and gas venting. As seen in the volume plot, the pistons fail to bounce back as far as the starting position on the first stroke, which would be problematic for the air injection scheme, and addition of the alternator load would make the problem worse. In this test, the bounce chamber pressures reach near atmospheric following blowdown. Given that venting of helium was barely sufficient, tests were run injecting compressed air through the helium starting system to determine how much excess air would be retained. Bounce chamber pressure results are shown in Figure 6, along with model results used to determine resizing of vent ports. With the original port configuration, the bounce cylinder pressure vented air to approximately 2.5 atmosphere absolute, indicating that larger flow area or additional open time was required. For modification of the vent ports, it was determined that slotting the existing ½" holes toward the bounce chamber head would meet the requirements. For the first stroke of helium, the reduction in trapped volume at port closure would reduce the work required to bounce back to the starting position and begin air injection. For motoring the engine with compressed air, the additional open time and larger flow area would assist in fully venting the air and ensuring similar trapped mass in each bounce chamber for compression, a key component of synchronized piston motion. Modeling indicated that slotting the existing holes by ½" would provide sufficient venting of air to reach atmospheric pressure following blowdown. With the vent ports enlarged, piston motion tests were run again with helium.

Bounce chamber volume results from the test with modified vent ports are shown in Figure 7. These results also correspond to a geometric compression ratio of around 23:1. A significant improvement in piston synchronization is seen toward the end of the test compared with the results in Figure 4, a result of better consistency in trapped mass between the two bounce cylinders. The pistons also bounce back beyond the starting position on the first stroke as needed for actuating the air injection system.

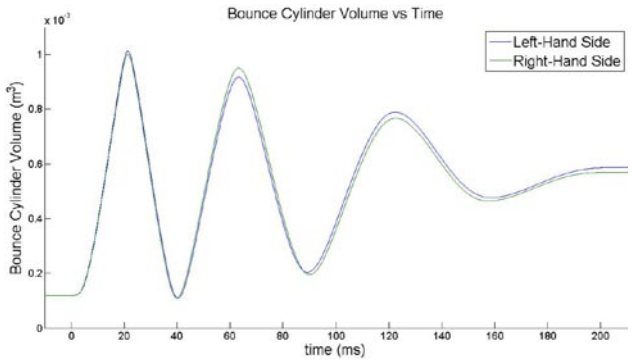

FIGURE 7. Bounce Cylinder Volume vs. Time from Test Data with Modified Vent Configuration

Conclusions

- Designed, simulated, and tested a compressed helium gas injection starting system with adequate performance.
- Procured final parts needed for FPEG research prototype.
- Implemented a computer control and data acquisition system.
- Conducted piston movement tests, resulting in validation of thermodynamic model of engine, development of friction model, enlargement of bounce chamber vent ports.
- Collaboration with General Motors and University of Michigan on modeling of Sandia prototype engine and various alternator designs is ongoing.

II.A.14 Optimization of Direct Injection Hydrogen Combustion Engine Performance, Efficiency and Emissions

Thomas Wallner (Primary Contact),
Riccardo Scarcelli, Nicholas S. Matthias
Argonne National Laboratory
9700 S. Cass Avenue
Argonne, IL 60439

DOE Technology Development Manager:
Gurpreet Singh

Overall Objectives

- Assess efficiency potential and identify efficiency/emissions trade-offs of advanced hydrogen internal combustion engine concepts with particular focus on hydrogen direct injection.
- Quantify the potential of advanced engine technologies, such as exhaust gas recirculation, water injection and turbocharging, in combination with hydrogen direct injection.
- Develop and apply advanced diagnostic and development tools tailored for hydrogen engine applications as needed for efficient combustion system development.

Fiscal Year (FY) 2011 Objectives

- Assess optimized injection strategies and injector nozzle designs through integration of experimental work with predictive three-dimensional computational fluid dynamics (3D-CFD) simulation.
- Demonstrate 45% peak brake thermal efficiency (BTE) while meeting Tier II Bin 5 oxides of nitrogen (NOx) emissions.
- Evaluate drive-cycle NOx emissions based on steady-state single-cylinder engine test results and determine requirements for in-cylinder emissions reduction.

Accomplishments

- Exceeded DOE technical target of 45% peak BTE by demonstrating 45.5% BTE at 2,000 revolutions per minute (RPM) and 13.5 bar brake mean effective pressure (BMEP).
- Exceeded DOE technical target of 31% part-load efficiency by demonstrating 33.3% BTE at the part-load point (2 bar BMEP @ 1,500 RPM).
- Expanded test regime and generated maps from 1,000 to 3,000 RPM and 1.7 to 14.2 bar BMEP demonstrating power densities higher than conventional gasoline engines.
- Calculated drive-cycle NOx emissions without aftertreatment of 0.017 g/mile using vehicle simulations based on engine maps which are clearly below the Tier II Bin 5 (0.07 g/mile) target.

Future Directions

- FY 2011 was the final year for this project and all DOE targets have been exceeded through experimental work on a single-cylinder engine combined with multi-cylinder and drive-cycle predictions.
- The actual demonstration of efficiency and emissions levels on a multi-cylinder hydrogen direct-injection (DI) engine remains as an open issue.
- The DI hydrogen injector turned out to be the most critical component which currently is at a prototype stage requiring further development to meet production level durability.

Introduction

Hydrogen has been identified as a promising alternative fuel with the internal combustion (IC) engine as a transition technology to enable the introduction of a large-scale hydrogen infrastructure. Research is being conducted worldwide to assess the potential of hydrogen IC engines and hydrogen DI engines have been found to have particularly high potential [1]. The DOE has set challenging targets for the performance and emissions behavior of hydrogen IC engine vehicles including a peak BTE of 45%, NOx emissions as low as 0.07 g/mile and a power density comparable to gasoline engines [2,3].

This report summarizes the efficiency improvements gained through optimization of the base engine combined with a novel injection strategy, shows how the optimized engine performs over a broader range of operating conditions, and provides vehicle simulation results based on engine maps to evaluate vehicle level efficiency and NOx emissions.

Approach

Collaboration has proven to be the key to success for meeting DOE's challenging goals for hydrogen IC engines. Argonne National Laboratory operates a single-cylinder research engine that has been optimized to achieve high engine efficiency. Optimization of the injection strategy including injector nozzle design is crucial for achieving the efficiency goals. At Argonne 3D-CFD simulation has been introduced as a diagnostic and cost-effective development tool. The 3D-CFD simulation tool has been carefully tested and validated against optical results from a hydrogen engine operated at Sandia National Laboratories. These close-coupled activities receive valuable guidance from experts at Ford Motor Company and also integrate hydrogen injector development at Westport Innovations Inc. In collaboration with Argonne's Vehicle Simulation Group steady-state engine efficiency and emissions maps are fed into Argonne's Autonomie software package to estimate drive-cycle fuel economy and emissions.

Results

Optimization of Injection Strategy

To enable optimization of injection strategy, the fuel delivery system was equipped with a piezo-actuated injector. The piezo-injector allows greater flexibility in terms of injection strategy because it is faster acting with higher mass flow rate than the previously used solenoid injector. Thus, the engine can be operated at higher speeds and loads and the injection can start later in the compression stroke. The evident benefit of a later start of injection (SOI) is a reduction in compression work. The potential for efficiency improvement in terms of compression work is 0.5 to 2% depending on engine operating condition [1,4].

A less evident benefit of later SOI is its effect on mixture formation. Delaying the start of injection increases mixture stratification because there is less time for fuel-air mixing. Mixture stratification means that part of the charge may be stoichiometric or even rich while the global equivalence ratio remains lean. Proper mixture stratification around the spark plug at time of ignition increases combustion efficiency (rich mixture close to the spark plug) while maintaining low losses due to wall heat transfer (ultra-lean mixture close to the cylinder walls). This research focuses on controlling the mixture stratification using different injector nozzle designs.

Knowledge from previous studies and findings from the CFD modeling work resulted in the design of a 4-hole nozzle which was selected for the final test sequence. This nozzle was derived from the original 5-hole design used in previous studies. In particular, the 4-hole nozzle lacks the center hole which is known to cause jet-to-jet interaction. Due to its geometry the 4-hole nozzle allows delaying SOI and achieving higher engine efficiency than the previously used nozzles. A BTE of 45.5% was achieved with the 4-hole nozzle (2,000 RPM, 13.5 bar BMEP, and an SOI of 80° crank angle before top dead center) at a hydrogen injection pressure of 100 bar.

Engine Maps

With successful peak efficiency results, a series of engine maps were run to provide a more complete picture of the engine performance. Intake and exhaust pressures were controlled to simulate turbocharging and to achieve a lean ($\lambda = 3.3$, $\phi = 0.3$) control strategy. Based on previous SOI sweeps, optimal SOI was found to be a function of engine speed so this information was used to define SOI throughout the engine map. BTE values are calculated using friction values from a friction-optimized multi-cylinder engine.

The operating range for the maps is 1,000 to 3,000 RPM and 1.7 to 14.2 bar BMEP. Figure 1 shows the resulting efficiency map with an island of 45% BTE with the peak value being 45.5% as mentioned in the previous section. This gradually decreases to 33.3% at 1,500 RPM and 2 bar BMEP, thus meeting the DOE target of 31% BTE for this part-load point [3].

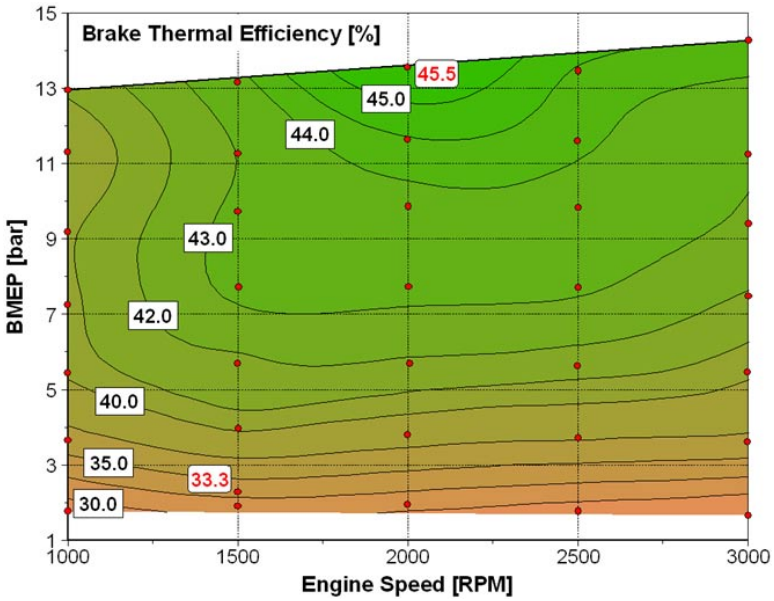

FIGURE 1. BTE Map of the Hydrogen DI Engine

On the NOx map shown in Figure 2, emissions at the peak efficiency point are 0.87 g/kWh and increase from there to form a 1.50 g/kWh island around 3,000 RPM and 14.2 bar BMEP. Apart from this small island, the NOx emissions decline sharply and the majority of the map exhibits very low NOx emissions, less than 0.10 g/kWh. Efficiency and NOx maps for the engine with the 4-hole nozzle were used in subsequent evaluation of vehicle performance.

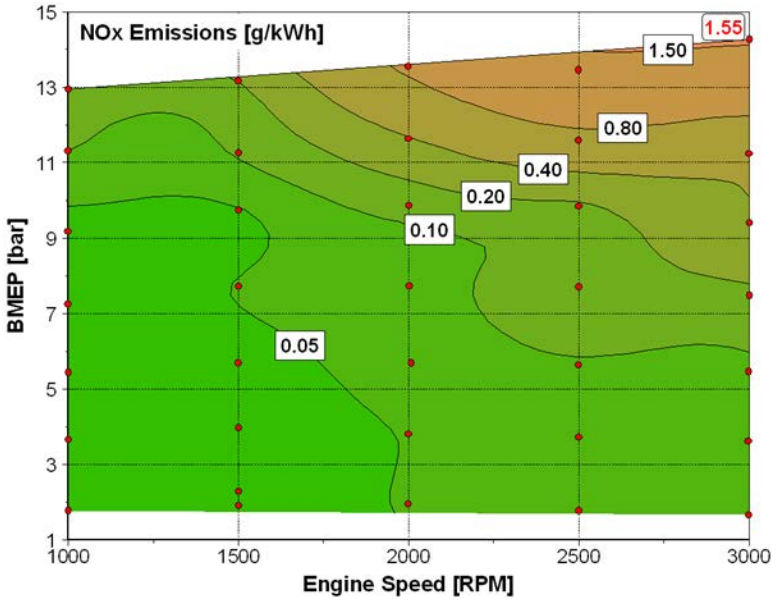

FIGURE 2. NOx Emissions Map of the Hydrogen DI Engine

Vehicle Level Efficiency and NOx Emissions

In order to evaluate drive-cycle NOx emissions it was necessary to integrate the single-cylinder engine performance and emissions data into a vehicle model. The engine geometry is intended for light-duty applications so the vehicle model is a midsize sedan weighing 1,553 kg with a conventional (non-hybrid) powertrain and a 5-speed automatic transmission. The engine displacement was scaled up to 3.0 L and the rate of NOx emissions was scaled up proportionally to match the larger engine. Assumptions imbedded in scaling NOx emissions are that the larger engine has the same volumetric efficiency and combustion characteristics as the single-cylinder research engine.

The hydrogen-powered vehicle was then run through a series of standardized driving cycles. The Urban Dynamometer Driving Schedule (UDDS) driving cycle was used for NOx emissions and the UDDS along with the Highway Fuel Economy Test (HWFET) cycle were used for quantifying fuel economy. This series of simulations was run using Autonomie which provides time resolved fuel consumption and emissions, which are plotted together with vehicle speed for the UDDS driving cycle shown in Figure 3.

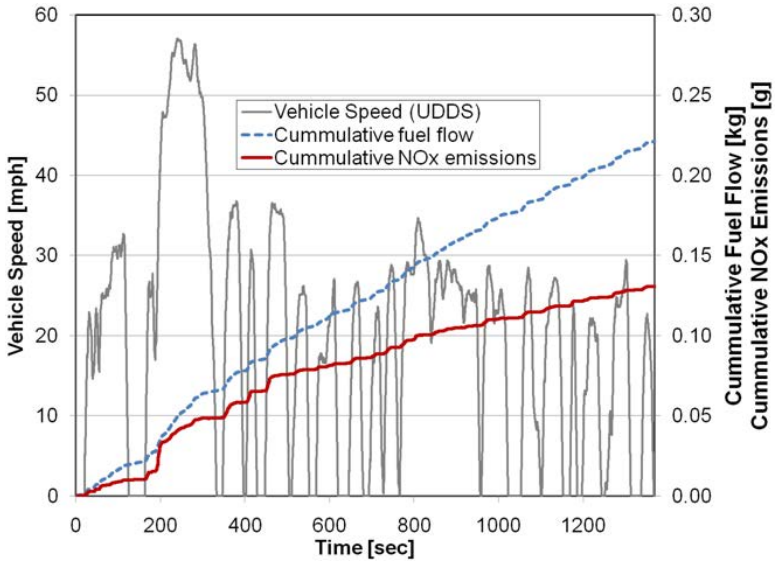

FIGURE 3. UDDS Drive Cycle Fuel Consumption and NOx Emissions

Cumulative NOx emissions show that certain parts of the cycle are most critical. For example, one acceleration event from 17 to 57 mph around 200 seconds into the cycle demands particularly high engine power. This acceleration corresponds to 0.026 grams of NOx, nearly 20% of the total drive cycle emissions. With the exception of a few hard accelerations the rate of NOx emissions remains relatively low as anticipated by analyzing the NOx map. The cumulative effect of the engine emissions performance throughout the UDDS cycle is 0.017 g/mile of NOx. The DOE goal that this project set out to achieve was Tier II Bin 5 NOx emissions of 0.07 g/mile. At 0.017 g/mile the hydrogen engine meets the DOE emissions target and furthermore is within the Super Ultra-Low Emissions Vehicle (SULEV) II range of 0.02 g/mile.

As seen in Figure 3, the cumulative fuel flow is quantified along with NOx emissions in order to evaluate vehicle fuel economy. Fuel flow is calculated in Autonomie based on the engine speed/load and corresponding efficiency on the BTE map. Hydrogen

consumption is then converted into gasoline equivalent based on energy content to yield fuel economy in miles per gallon (mpg). Load points for both driving cycles are overlaid on the BTE map in Figure 4 to show where the 3.0 L hydrogen DI engine operates in the simulated vehicle. The density of load points in Figure 4 shows that the engine is operating far from its peak efficiency point in a relatively narrow window at the bottom of the map.

The potential of engine downsizing to improve drive-cycle performance was assessed by estimating fuel economy and emissions for a 2.5 and 2.0 L hydrogen engine using the same methodology as for the 3.0 L engine. Downsizing is expected to push the engine load points into more efficient operating regimes. Figure 5 shows the effect of downsizing the engine to 2.5 L and 2.0 L on the time the engine is operated in different efficiency brackets. The most interesting difference is in the 40% to 45% range where downsizing the engine significantly increases the amount of time spent in this high efficiency range.

Unadjusted Environmental Protection Agency fuel economy values are presented to provide meaningful values for comparison to Corporate Average Fuel Economy (CAFE) standards. Likewise, CAFE credits for alternative fuels are not considered in calculating fuel economy numbers. Results from both the UDDS and HWFET driving cycles allowed a calculation for city, highway, and combined fuel economy (weighted 55/45, respectively).

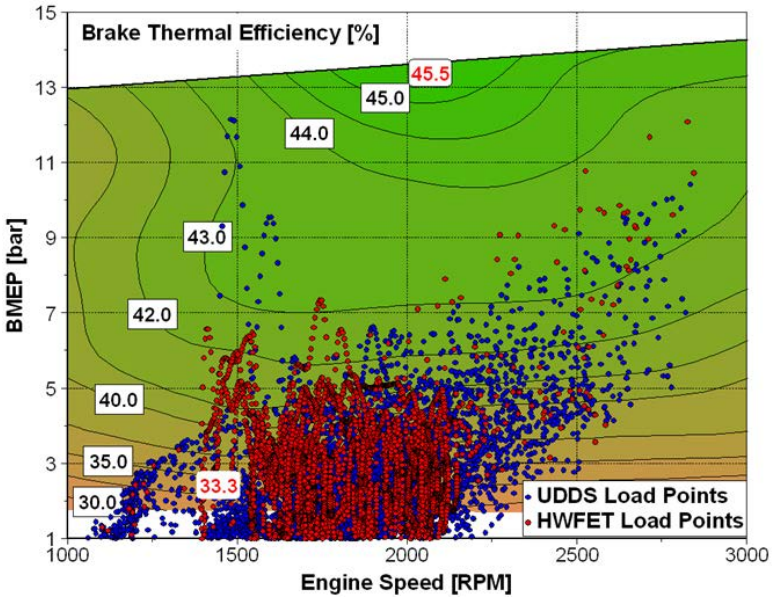

FIGURE 4. UDDS and HWFET Load Points Superimposed on the Efficiency Map

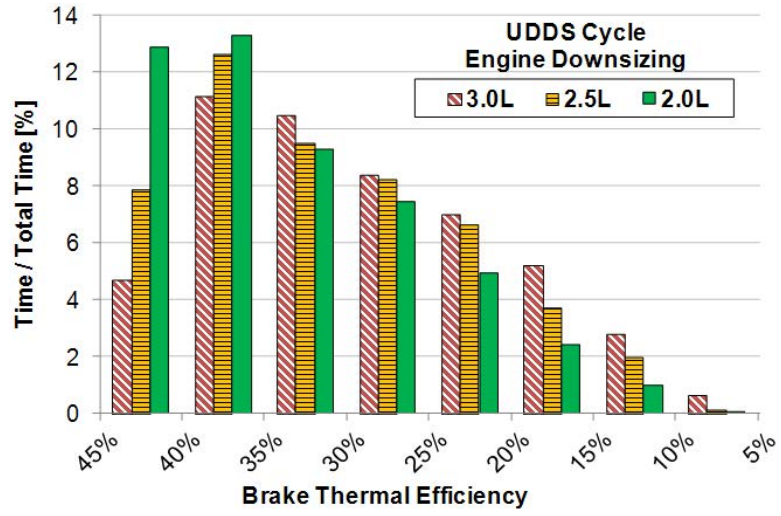

FIGURE 5. Time-Weighted Breakdown Showing the Effect of Engine Downsizing

The resulting fuel economy for this midsize sedan is 32.4 mpg in the city and 51.5 mpg on the highway for a combined city/highway fuel economy of 38.9 mpg as shown in Figure 6. To frame this result in terms of vehicle standards, CAFE numbers were calculated for the simulated vehicle. A vehicle footprint of 47.6 ft^2 was used for the calculation resulting in a 2016 CAFE standard of 35.9 mpg combined. Thus, the hydrogen-powered vehicle with a 3.0 L DI engine exceeds future fuel economy standards while maintaining SULEV II emissions levels without the need for exhaust aftertreatment.

Figure 6 also summarizes the vehicle simulation results in the context of Tier II NOx regulations and CAFE standards with engine downsizing. Pushing the engine to operate in its higher efficiency range directly increases vehicle fuel economy. City fuel economy which was 32.4 mpg with the 3.0 L engine is 38.3 mpg with the 2.0 L based on UDDS data. HWFET data follows a similar trend and the combined fuel economy increases to 45.4 mpg with the 2.0 L engine. The midsize sedan powered by a 2.5 L hydrogen DI engine achieves 41.9 mpg combined. There is clearly a tradeoff between fuel economy and NOx emissions that comes with engine downsizing. NOx emissions with the 2.0 L engine amount to 0.028 g/mile which falls outside the SULEV II range but is still well within the DOE target of Tier II Bin 5.

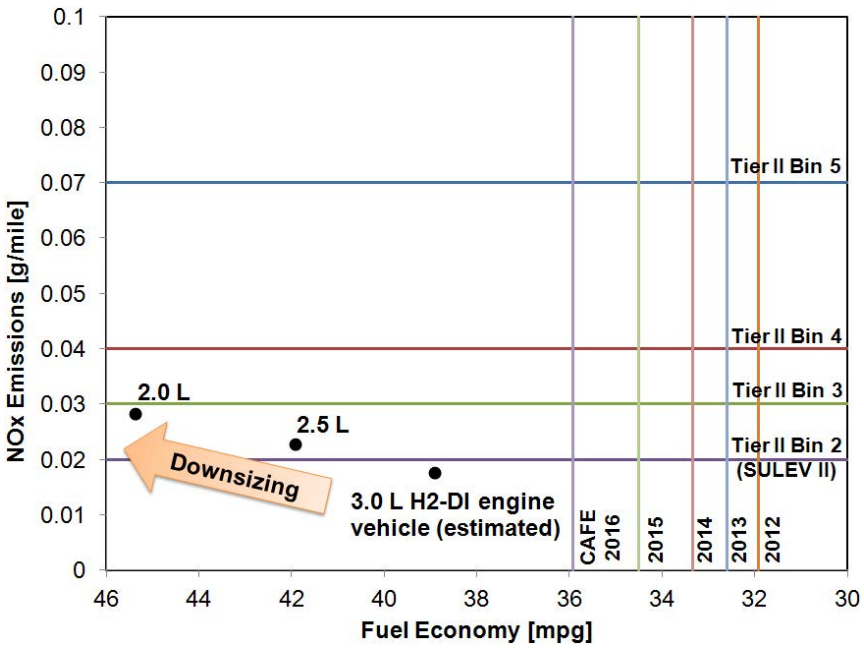

FIGURE 6. Effect of Engine Downsizing in terms of Tier II NOx Regulations and CAFE Standards

Conclusions

- Nozzle development combining CFD modeling and experimental activities yielded a 4-hole nozzle with which the hydrogen direct injection engine met both DOE efficiency targets. Engine mapping revealed a peak BTE of 45.5% (target: 45%) and 33.3% (target: 31%) at the part-load point (2 bar BMEP @ 1,500 rpm). The corresponding NOx map had a small 1.50 g/kWh island around 3,000 rpm and 14.2 bar BMEP but the emissions sharply declined resulting in a map dominated by less than 0.10 g/kWh of NOx.
- Autonomie vehicle simulation showed that a midsize sedan powered by a 3.0 L hydrogen engine exceeds CAFE 2016 fuel economy standards while emitting only 0.017 g/mile of NOx without exhaust aftertreatment. This emissions level is within the SULEV II range which is well below the Tier II Bin 5 DOE target.
- There is a tradeoff between fuel economy and NOx emissions that comes with engine downsizing. Simulating the same midsize sedan with a 2.0 L hydrogen DI engine showed a combined city/highway fuel economy improvement from 38.9 to 45.4 mpg as the engine was pushed into a more efficient operating range. The corresponding NOx increased to 0.028 g/mile which falls outside the SULEV II range but is still well within the Tier II Bin 5 DOE target.

References

1. Verhelst, S. Wallner, T. *Hydrogen-fueled internal combustion engines*, Progress in Energy and Combustion Science, Volume 35, Issue 6, December 2009, Pages 490-527, 2009.

2. U.S. Department of Energy, *FreedomCAR and Fuel Technical Partnership Technical Goals*, Washington, D.C., 2002.

3. US DOE office of Energy Efficiency & Renewable Energy, Vehicle Technologies Program. *Multi-Year Program Plan 2011-2015*. December 2010. http://www1.eere.energy.gov/vehiclesandfuels/pdfs/program/vt_mypp_2011-2015.pdf

4. T. Wallner, "*Development of combustion concepts for a hydrogen powered internal combustion engine*", PhD thesis, Graz University of Technology, 2004.

FY 2011 Publications/Presentations

1. Obermair, H.; Scarcelli, R.; Wallner, T.: *'Efficiency improved combustion system for hydrogen direct injection operation.'* SAE Paper No 2010-01-2170. Powertrains, Fuels & Lubricants Meeting . San Diego / CA. 2010.

2. Wallner, T.: *'Efficiency and emissions potential of hydrogen internal combustion engine vehicles.'* SAE Paper No 2011-26-0003. Symposium on International Automotive Technology. Pune/India. 2011.

3. Scarcelli, R.; Wallner, T.; Matthias, N.S.; Kaiser, S.; Salazar, V.: *'Numerical and Optical Evolution of Gaseous Jets in Direct Injection Hydrogen Engines.'* SAE Paper No 2011-01-0675. SAE World Congress. Detroit / MI. 2011.

4. Wallner, T.; Matthias, N.S.; Scarcelli, R.: *'Influence of injection strategy in a high-efficiency hydrogen direct injection engine.'* 2011 JSAE/SAE International Powertrains, Fuels and Lubricants Meeting. Kyoto / Japan. 2011.

5. Scarcelli, R.; Wallner, T.; Matthias, N.S.; Kaiser, S.; Salazar, V.: *'Mixture Formation in Direct Injection Hydrogen Engines: CFD and Optical Analysis of Single- and Multi-Hole Nozzles.'* ICE2011 - 10th International Conference on Engines & Vehicles. Capri/Italy. 2011.

6. Matthias, N.S.; Wallner, T.; Scarcelli, R.: *'A Hydrogen Direct Injection Engine Concept that Exceeds U.S. DOE Light-Duty Efficiency Targets.'* SAE World Congress. Detroit / MI. 2012.

7. Wallner, T.; Scarcelli, R.; Matthias, N.S.; Kwon, J.: *'Evaluation of Efficiency and Drive Cycle Emissions for a Hydrogen Direct Injection Engine.'* Proceedings of the Institution of Mechanical Engineers, Part D, Journal of Automobile Engineering. 2012.

8. Verhelst, S.; Demuynck, J.; Sierens, R.; Scarcelli, R.; Matthias, N.; Wallner, T.: *'Update on the progress of hydrogen-fueled internal combustion engines.'* Renewable Hydrogen Technologies: Production, Purification, Storage, Applications and Safety. Elsevier. 2012.

Special Recognitions & Awards/Patents Issued

1. The results of this project will be included in the accomplishment report to the National Academy of Science as a 2011 U.S. DRIVE Highlight.

2. The presentation *''Influence of injection strategy in a high-efficiency hydrogen direct injection engine'* at the 2011 JSAE/SAE International Powertrains, Fuels and Lubricants Conference received the 'Presentation Award for Young Researchers and Engineers'.

II.A.15 Stretch Efficiency – Exploiting New Combustion Regimes

C. Stuart Daw (Primary Contact), Josh A. Pihl, James P. Szybist, Bruce G. Bunting
Oak Ridge National Laboratory
NTRC Site
2360 Cherahala Blvd.
Knoxville, TN 37932

DOE Technology Development Manager:
Gurpreet Singh

Objectives

- Analyze and define specific advanced pathways to improve the energy conversion efficiency of internal combustion engines from nominally 40% to as high as 60%, with emphasis on opportunities afforded by new approaches to combustion.
- Implement proof of principle experiments for the identified pathways to stretch efficiency.

Accomplishments

- Published the final report on the Transportation Combustion Engine Efficiency Colloquium held at USCAR, March 3–4, 2010 as an ORNL Technical Memorandum.
- Published peer-reviewed article in Energy and Fuels on possible alternative approaches for achieving the thermodynamic benefits of chemical looping combustion (CLC).
- Prepared journal manuscript summarizing in-depth thermodynamic analyses of the impact of fuel type on ideal theoretical engine efficiency.
- Initiated non-catalytic in-cylinder fuel reforming experiments with a range of fuels in the modified 2-liter General Motors (GM) Ecotec engine with variable valve actuation (VVA).
- Initiated computational fluid dynamics (CFD) simulations of in-cylinder water injection for exhaust heat recuperation with Reaction Design Fortè engine simulation platform.
- Continued construction for the Regenerative Air Preheating with Thermochemical Recuperation (RAPTR) experiment at a reduced pace to accommodate faster progress on VVA engine experiments above.
- Continued collaboration with the Gas Technology Institute (GTI) on investigation of catalytic thermochemical recuperation for natural gas engines.

Future Directions

- Continue in-cylinder water injection and reforming experiments with the modified GM Ecotec engine with an expanded range of fuels and in-depth analysis of the observed reaction chemistry and potential thermodynamic impact on engine efficiency.
- Continue construction and shakedown of RAPTR bench-top constant volume combustor experiment as budget and experimental priorities permit.
- Continue collaboration with GTI in analyzing the efficiency potential of the catalytic thermo-chemical recuperation (TCR) approach used by GTI and Cummins in their prototype experiments with a natural gas engine.
- Develop and implement detailed Fortè models for in-cylinder injection and non-catalytic fuel reforming.

Introduction

In conventional single-stage internal combustion engines, most of the unutilized fuel energy ends up in the form of exhaust heat. The exergy in the exhaust heat cannot be utilized directly by the piston, but it can be converted into other forms which can be recycled and used to boost piston output. The goal of this project is to identify and demonstrate strategies that enable exhaust heat recuperation and transformation into forms that can be utilized to boost the thermodynamic efficiency of single-stage engines. Two potential forms of exhaust heat recycling, steam generation and TCR, are of particular interest in this study. In the former, exhaust heat is used to convert liquid water into pressurized steam that generates additional piston work. In the latter, exhaust heat is used to chemically transform fuel into a higher exergy state. Under the proper conditions, the resulting higher exergy fuel can be converted more efficiently to work by the piston.

Approach

Our approach to improving internal combustion engine efficiency is based on developing a better understanding of the exergy losses in current engines and then developing ways to mitigate them. Previous studies of internal combustion engine thermodynamics conducted in collaboration with Professors Jerald Caton (Texas A&M University) and David Foster (University of Wisconsin) identified combustion irreversibility as the largest single contributor to fuel exergy loss. In addition, these studies revealed that the thermal exergy

remaining in engine exhaust is not directly usable by the piston, unless it is first transformed into a more suitable state. Our current efforts are focused on development, analysis, and experimental evaluation of novel concepts that can transform and recuperate thermal exhaust exergy to boost engine output. We are guided by combined input from industry, academia, and national labs, such as that summarized in the recently published report from the Colloquium on Transportation Engine Efficiency held in March 2010 at USCAR [1].

In previous years we identified three promising approaches for improving single-stage engine efficiency: counterflow preheating of inlet fuel and air with exhaust heat [2]; TCR [3]; CLC [4, 5]. This year we began more detailed numerical and experimental investigations of how these approaches, along with in-cylinder liquid water injection, might be implemented in an advanced engine with VVA [6]. We also continued a basic thermodynamic analysis of how variations in fuel molecular properties can affect the theoretical efficiency of current internal combustion engines [7]. In parallel with the studies aimed at current engine architectures, we are also developing an experimental platform (RAPTR) designed to experimentally evaluate concepts that would involve highly modified engine architectures. The primary purpose of the RAPTR platform is to provide basic measurements of the time scales for heat transfer and chemical reaction steps (both catalytic and non-catalytic) that control the rates and efficiency of the different exhaust heat transformation approaches.

Results

Results from our fundamental thermodynamic analyses of CLC have been published in an article in Energy & Fuels [5]. CLC uses an oxygen storage material to separate the fuel oxidation and air reduction processes into two separate chemical reactors. The potential efficiency benefits of CLC are derived from several critical operating strategies that exploit this separation: internal heat rejection during work generation, isothermal chemical reactions, and low-temperature-gradient heat exchange between the reactant streams. The success of these strategies requires a balance between rates of reaction and heat transfer, as well as reaction enthalpies, and we have concerns about the feasibility of finding materials and designs that meet these requirements. Further, the complexity of any system that could exploit these strategies severely limits the potential value of CLC for transportation applications. Since CLC has questionable practical value, we have concluded that it should not have a high priority for near-term studies. However, some of the thermodynamic benefits of CLC might be realized without the need for impractical oxygen storage materials. For example, TCR could provide an internal heat sink for work generation like the CLC reduction reactor. Combining TCR heat rejection with isothermal reaction can theoretically achieve Second Law efficiencies 10-15% higher than are currently possible for ideal heat engines.

This year we investigated two different experimental TCR approaches, in-cylinder TCR and exhaust gas recirculation (EGR)-based TCR. To investigate the former approach, we are studying the degree of non-catalytic reforming that can be achieved in the ORNL modified Ecotec engine if fuel is injected into recompressed exhaust gases in the 6-stroke cycle illustrated in Figure 1.

Preliminary experiments have been conducted on the Ecotec engine with isooctane, ethanol, and methanol. In-cylinder reforming was observed for all of the fuels. The extent of reforming was dependent on the fuel type, injection timing, and cylinder temperature and pressure. The products of reforming are shown in Figure 2, and at the best conditions in-cylinder reforming produced a mixture that was over 2% hydrogen and 3%

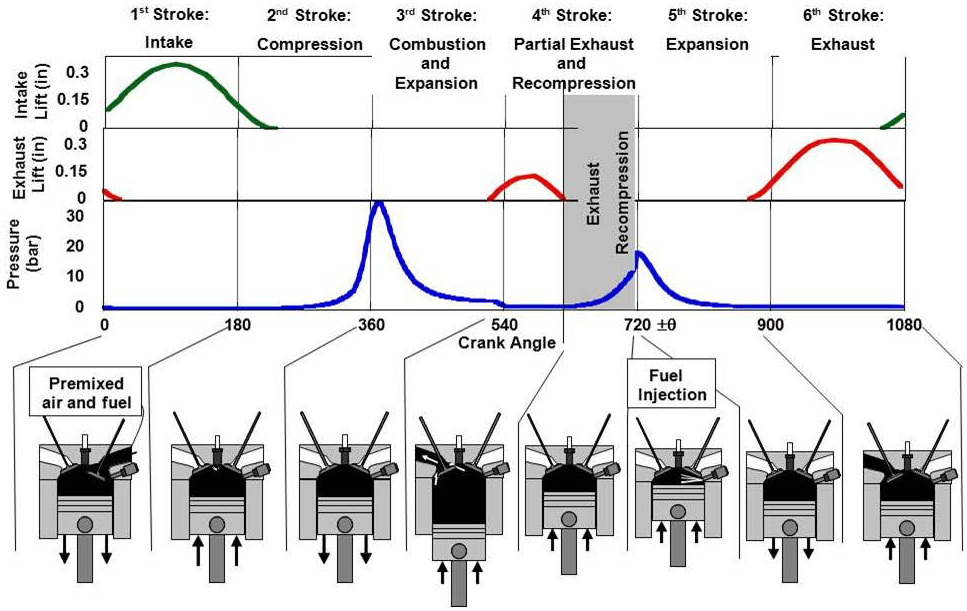

FIGURE 1. Profile for the 6-stroke cycle experimentally implemented on the ORNL modified Ecotec engine with variable valve actuation. Injection of a range of fuels is being studied to understand the chemistry and kinetics of in-cylinder, non-catalytic reforming.

carbon monoxide. Reforming of iso-octane and ethanol was limited by smoke production, but no detectable levels of smoke were observed when reforming methanol. Analysis of the experimental results is continuing in Fiscal Year (FY) 2012.

Preliminary in-cylinder CFD simulations of in-cylinder exhaust heat recuperation with water and fuel reforming were also initiated using the Reaction Design Fortè computational simulation platform. Effort this year has focused on implementing and validating water injection, with a plan to shift to fuel injection and reforming in FY 2012.

To investigate the potential of EGR-based TCR, we continued technical discussions with GTI concerning their pilot-scale experiments with a Cummins natural gas engine (see schematic in Figure 3). The GTI team reported that rapid deactivation of the reforming catalyst was the key technical barrier to successfully achieving TCR in their experiments. GTI supplied ORNL with catalyst samples (Figure 4) for detailed microscopic and laboratory bench reactor evaluations. As funding permits, we plan to analyze these samples in FY 2012 to determine the deactivation mechanisms and possible approaches for regenerating and/or improving the catalyst.

Progress on the RAPTR experiment for measuring fundamental transport and reaction rates involving heat recuperation and catalyst materials has continued to be delayed in order to accommodate the experimental in-

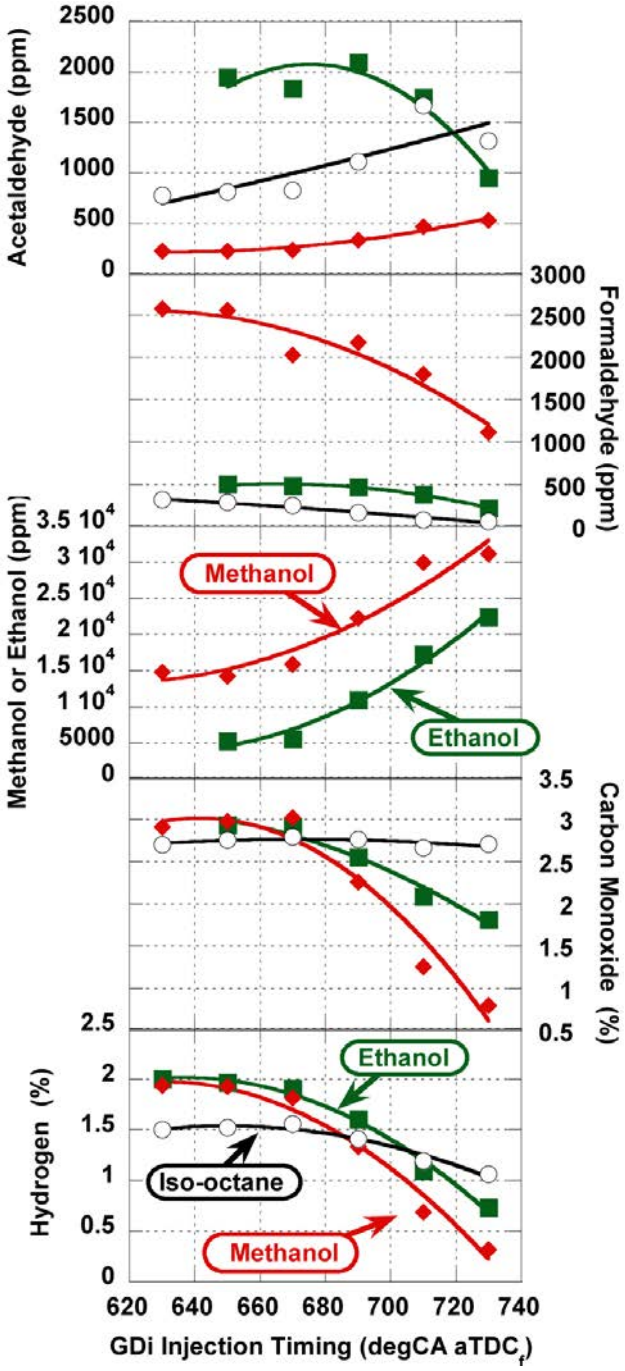

FIGURE 2. Concentrations of Species as a Function of Injection Timing for Ethanol, Methanol and Iso-Octane

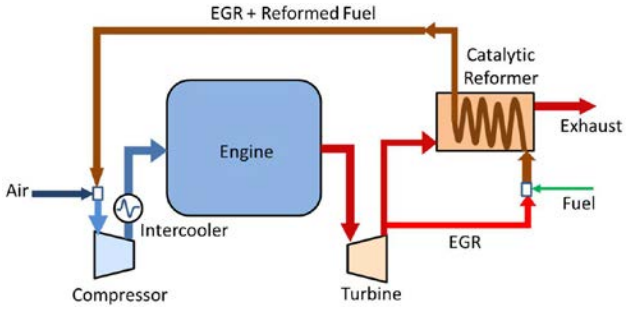

FIGURE 3. Schematic Representation of the Basic Approach used for EGR-Based Catalytic TCR

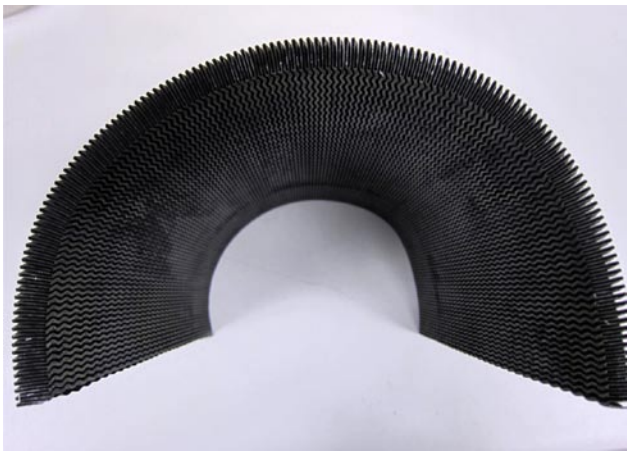

FIGURE 4. Photograph of the metal-supported reforming catalyst used in GTI's experiments with EGR-based TCR. The active catalyst is washcoated on a waffle-like metal substrate, which provides a good heat transfer path between the hot exhaust and endothermic fuel reforming reactions.

cylinder TCR and EGR catalyst studies described above. Most of the system assembly is complete; the remaining hurdles include control software development and safety approvals. We anticipate that both of these tasks will be completed in the coming FY.

Theoretical thermodynamic analyses this year have focused on the potential effects of varying fuel molecular properties on the ultimate efficiency limits of an ideal engine. We found that the First Law efficiency can deviate by as much as nine percentage points between fuels while Second Law efficiency exhibits a much smaller degree of variability. We also found that First and Second Law efficiency can be nearly the same for some fuels (methane and ethane) but differ substantially for other fuels (hydrogen and ethanol). The differences in First and Second Law efficiency are due to differences in the lower heating value (LHV) and exergy for different fuels. The molar expansion ratio (MER), defined as the ratio of product moles to reactant moles for complete stoichiometric combustion, helps in accounting for fuel-specific efficiency differences as well as differences between First and Second Law efficiency (Figure 5). We will be submitting a journal article on these findings early in FY 2012.

Conclusions

Recent experimental data for both in-cylinder non-catalytic TCR and EGR-based catalytic TCR are helping to refine our understanding of the technical barriers and potential feasibility of these approaches for increasing engine efficiency. ORNL is now actively engaged in carrying out additional engine experiments, laboratory measurements, and theoretical analyses to resolve the remaining technical questions. Future modeling studies will require using more sophisticated models for multi-phase reforming under in-cylinder and EGR heat exchanger conditions. Variations in fuel properties are likely to have a large impact on the potential efficiency benefits.

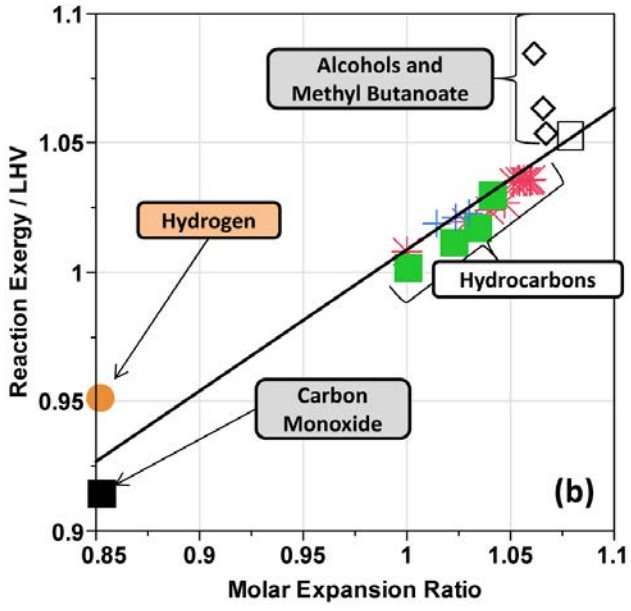

FIGURE 5. Relationship among MER, fuel LHV, and fuel exergy revealed from a thermodynamic analysis of an ideal engine operated with a range of fuels.

References

1. C.S. Daw, R.L. Graves, R.M. Wagner, and J.A. Caton, "Report on the Transportation Combustion Engine Efficiency Colloquium Held at USCAR, March 3–4, 2010," ORNL/TM-2010/265, October 2010.

2. C.S. Daw, K. Chakravarthy, J.C. Conklin and R.L. Graves, "Minimizing destruction of thermodynamic availability in hydrogen combustion," International Journal of Hydrogen Energy, 31, (2006), pp 728-736.

3. V.K. Chakravarthy, C. S. Daw, J.A. Pihl, J.C. Conklin, "A Study of the Theoretical Potential of Thermochemical Exhaust Heat Recuperation in Internal Combustion Engines," Energy & Fuels, 2010, 24 (3), pp 1529-1537.

4. N.R. McGlashan, Proceedings of the Institution of Mechanical Engineers, Part C: Journal of Mechanical Engineering Science 2008, 222, 1005–1019.

5. V.K. Chakravarthy, C.S. Daw, and J.A. Pihl, "A thermodynamic analysis of alternative approaches to chemical looping combustion," Energy & Fuels, 25 (2011), pp 656–669.

6. J.C. Conklin and J.P. Szybist, "A highly efficient six-stroke internal combustion engine cycle with water injection for in-cylinder exhaust heat recovery," Energy, 35 (2010), pp 1658–1664.

7. J.P. Szybist, V. K. Chakravathy and C. S. Daw, "Molar Expansion Ratio, Enthalpy and Exergy: Modeling Fuel-Specific Efficiency Differences of an Almost-Ideal Otto Cycle," Presentation at the Spring 2011 AEC/HCCI Working Group Meeting at Sandia National Laboratory (Sandia, CA USA, February 2011).

FY 2011 Publications/Presentations

1. V.K. Chakravarthy, C.S. Daw, and J.A. Pihl, "A thermodynamic analysis of alternative approaches to chemical looping combustion," Energy & Fuels, 25 (2011), pp 656–669.

2. J.P. Szybist, V.K. Chakravathy and C.S. Daw, "Molar Expansion Ratio, Enthalpy and Exergy: Modeling Fuel-Specific Efficiency Differences of an Almost-Ideal Otto Cycle," Presentation at the Spring 2011 AEC/HCCI Working Group Meeting at Sandia National Laboratory (Sandia, CA USA, February 2011).

3. C.S. Daw, J.A. Pihl, V. K. Chakravarthy, J.P. Szybist, J.C. Conklin, and R.L. Graves, "Stretch Efficiency for Combustion Engines: Exploiting New Combustion Regimes," 2011 DOE OVT Peer Review, May 9–13, 2011, Project ace_15_daw.

4. C.S. Daw, V.K. Chakravarthy, J.A. Pihl, and J.C. Conklin, "The Theoretical Potential of Thermochemical Exhaust Heat Recuperation for Improving the Fuel Efficiency of Internal Combustion Engines," Invited presentation to the local Chicago section of the American Institute of Chemical Engineers, May 17, 2011.

II.A.16 Visualization of In-Cylinder Combustion R&D

Stephen Ciatti
Argonne National Laboratory
9700 S. Cass Ave.
Bldg 362
Argonne, IL 60439

DOE Technology Development Manager:
Gurpreet Singh

Subcontractor:
University of Wisconsin–Madison, Engine Research Center, Madison, WI

Objectives

- Quantify the influence of low-cetane fuel ignition properties to achieve clean, high-efficiency combustion.
- Optimize the advanced controls available to create a combustion system that retains diesel-like efficiency while reducing oxides of nitrogen (NO_x) and other criteria pollutants compared to conventional diesel.

Fiscal Year (FY) 2011 Objectives

Demonstrate the use of combustion imaging techniques to aid in determining the operational boundaries of gasoline compression ignition operation.

Accomplishments

- The General Motors 1.9-L turbodiesel engine, operating on 85 Research Octane Number gasoline, was successful in producing high power density (3,000 RPM - 20 bar brake mean effective pressure, BMEP), high efficiency (40% brake thermal efficiency [BTE] at 2,500 RPM - 18 bar BMEP) and low NO_x (less than 1 g/kW-hr at 2,750 RPM - 12 bar BMEP).
- Use of the injection system, combined with long ignition delay, to control the engine at a variety of speeds and loads with little difficulty (1,500 RPM – 2 bar, 2,000 RPM – 2, 5, 6, 8, 10, 12, 14, 16, 18 bar BMEP, 2,500 RPM – 6, 8, 10, 12, 14, 16, 18, 20 bar BMEP and 2,750 RPM – 12 bar).
- Exhaust gas recirculation (EGR) was found to significantly reduce NO_x while having minimal fuel efficiency or CO/hydrocarbon (HC) penalty.

Future Directions

- Evaluate the required EGR level to achieve high efficiency and low emissions.
- Develop the fuel injection approach using double or triple injections to maximize fuel efficiency.
- Conduct experiments that will allow for transient operation of this combustion system to determine the suitability for application in an automobile.
- Begin measuring soot through the use of a filter paper smokemeter.

Introduction

Current diesel engines already take advantage of the most important factors for efficiency – no throttling, high compression ratio and low heat rejection. However, diesel combustion creates a significant emissions problem. Mixing or diffusion combustion creates very steep gradients in the combustion chamber because the ignition delay of diesel fuel is extremely short. Particulate matter (PM) and NO_x are the result of this type of combustion, requiring expensive after-treatment solutions to meet Environmental Protection Agency emissions regulations.

The current work seeks to overcome the mixing controlled combustion dilemma by taking advantage of the long ignition delay of gasoline to provide much more premixing of fuel and air before ignition occurs. This premixing allows for the gradients of fuel and air to be much less steep, significantly reducing the PM-NO_x tradeoff of mixing controlled combustion.

Approach

The intent of this project is to utilize the long ignition delays of low-cetane fuels to create an advanced combustion system that generates premixed (but not homogeneous!) mixtures of fuel and air in the combustion chamber. As reported in several articles, if the local equivalence ratio is below 2 (meaning at most, twice as much fuel as oxidizer) and the peak combustion temperature is below 2,000 K (usually using EGR to drop the O_2 concentration below ambient 21%, thereby slowing the peak reaction rates and dropping the peak combustion temperature), a combustion regime that is very clean and yet retains reasonably high power density is achieved. Figure 1 shows this contour plot, generated by Kitamura et al. [1].

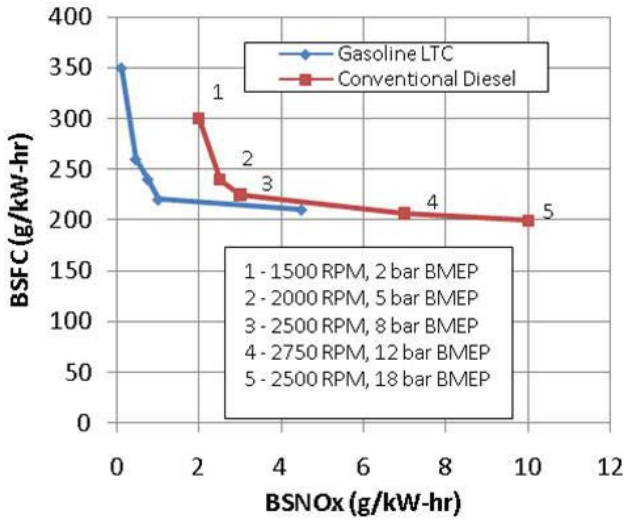

FIGURE 1. Brake Specific Fuel Consumption vs. Brake Specific NO_x for Gasoline Low-Temperature Combustion and Conventional Diesel Combustion

The challenge to this type of combustion system is the metering of fuel into the combustion chamber needs to be precise, both in timing and amount. If too much fuel is added too early, a "knocking" type of combustion occurs, which creates unacceptably high combustion noise or worse. If not enough fuel is added, ignition may not occur at all and raw HC exits the exhaust. Control over the relevant operating parameters is very important.

Results

Successful operation of several different points, provided by General Motors, was achieved using gasoline fuel. The long ignition delay allows for significant premixing, leading to low NO_x formation. The NO_x emissions decrease by a factor of 3-5, while HC and CO emissions only slightly increase under the same conditions.

The primary control method for this type of combustion regime is injection timing, which is very desirable because injection timing can be adjusted very rapidly as engine conditions may change. Further work will be done to test the sensitivity of parameters like intake temperature, EGR level and boost to make this combustion system even more robust.

Conclusions

- Partially premixed charge compression ignition, using gasoline fuel, can be a very effective way to maintain power density and high efficiency while reducing NO_x by up to 300-500%.
- The opportunity to utilize this combustion system is excellent, because of the high responsiveness of injection systems to changing engine conditions.
- The efficiency of this combustion system is significantly higher than that of conventional spark-ignition gasoline, especially at mid range speeds and loads.

References

1. Kitamura et al, SAE paper 2003-01-1789.

FY 2011 Publications/Presentations

1. Ciatti, S.A., Subramanian, S., "An Experimental Investigation of Low Octane Gasoline in Diesel Engines", GTP – 10 – 1362, ASME Journal of Engineering for Gas Turbines and Power Systems.

2. Subramanian, S., Ciatti, S.A., "Low Cetane Fuels in Compression Ignition Engine to Achieve LTC", ASME ICED Fall Technical Conference 2011-60014.

3. Ciatti, S.A., "Use of Low Cetane Fuel to Enable LTC", Presentation at Columbia University, Sept. 2011, New York, NY.

II.A.17 Collaborative Combustion Research with Basic Energy Sciences

Sreenath B. Gupta (Primary Contact),
Michael Johnson, Bipin Bihari, Raj Sekar
Argonne National Laboratory
9700 South Cass Ave.
Argonne, IL 60565

DOE Technology Development Manager:
Gurpreet Singh

Overall Objectives

- To support DOE Vehicle Technologies Program efforts to develop chemical mechanisms of various internal combustion (IC) engine fuels so as to gain a predictive capability of in-cylinder combustion and emissions formation.
- Provide complementary experimental data to support DOE Basic Energy Science efforts to develop improved chemical kinetic mechanisms of various fuels.
- Conduct highly accurate tests under high-pressure and low-temperature conditions that are typical of IC engines by using Argonne's rapid compression machine (RCM).

Fiscal Year (FY) 2011 Objectives

- Improve hardware associated with Argonne's RCM so as to be able to conduct highly accurate chemical kinetic studies.
- Develop a 1-dimensional code to analyze data gathered using Argonne's RCM. Validate the model through tests on a standard fuel.
- Develop auxiliary systems that enable tests on various alternative fuels. Also, develop advanced diagnostics to provide metrics relevant to chemical combustion model validation.

Accomplishments

- Redesigned and improved various RCM hardware and were able to achieve an isothermal zone uniform to within 10 K. Such an isothermal zone helps conduct chemical kinetic studies with high accuracy.
- Developed a 1-dimensional model to analyze RCM pressure data.
- Designed and developed various auxiliary systems that enable testing on a variety of fuels, and helped obtain species concentrations that will serve as valuable metrics for chemical model validation.

Future Directions

- Conduct tests to on gasoline and gasoline surrogates. Thereby obtain data relevant to the effort by Lawrence Livermore National Laboratory to develop a five-component gasoline surrogate.
- Conduct tests on various low boiling point temperature (BPT) alternative fuels and their surrogates to help support chemical mechanism development.
- Conduct tests on various high-BPT fuels, specifically diesels and biodiesels.

Introduction

In spite of the notable achievements over the last 40 years in developing chemical mechanisms, a predictive capability over the wide range of combustion conditions that exist in a typical IC engine has remained elusive. Further still, the formation of pollutant emissions, such as oxides of nitrogen (NO_x) cannot be predicted with a high degree of certainty. This deficiency is more pronounced with the extension of the fuel matrix to include various alternative fuels – mostly bioderived alocohols and esters. To address this issue, DOE Basic Energy Science currently supports a number of efforts, both experimental and analytical, to help develop relevant chemical mechanisms. The current effort is a part of Vehicle Technologies Program activities to supplement such efforts in developing chemical mechanisms under engine specific combustion conditions. The end product is an engineering level model that can be used by manufacturers.

Approach

Of most relevance to IC engines are combustion studies conducted in an RCM. Such a machine helps establish a quiescent premixed fuel-air mixture under temperature and pressure conditions typical of in-cylinder conditions. The mixtures can be established with a high degree of accuracy in equivalence ratios, temperature and pressure conditions. The RCM has come to be the standard method of measurement for chemical kinetic studies under low-temperature combustion (LTC) conditions that are highly favorable to achieving high efficiencies and low polluting emissions. Quite often, it is used to obtain data under high-pressure and low-temperature conditions, i.e., data complementary to that obtained in a shock tube.

In this effort Argonne will improve an existing RCM for features that are amenable to chemical kinetic studies (see Figure 1). Also, it was decided to develop capabilities beyond pressure trace analysis, for more accurate validation of chemical mechanisms. With such a capability, combustion tests on various hydrocarbon fuels will be conducted. Initial tests will be performed on gasoline and gasoline surrogates. These will be followed by tests on relatively nonvolatile fuels like diesels and its surrogates.

Results

Early in the process of rebuilding the RCM, computational fluid dynamics modeling of the compression process was performed. Through such simulations, the combustion chamber was modified to result in vortex-free conditions that ensure temperature uniformity within 10 K at the end of compression process. This entailed incorporating creviced pistons to trap cold gases from the boundary layers, as well as removing a step from the combustion chamber. Also, a new sealing arrangement was used to reduce the amount of gas leak past the piston seals.

In parallel, with help from the University of Akron, a model was developed to incorporate heat transfer to be able to analyze the measured pressure data. Such a model was validated under non-combusting conditions using inert gases (see Figure 2). However, validation under combustion conditions could not be performed as the gas temperature at the end of compression was not sufficient to initiate auto ignition. As a result, efforts were spent in designing a mixture preparation system that enables substituting nitrogen in combustion air with argon. Design of such a system has been completed and it will be commissioned shortly.

In the meantime, attention was focused in developing various auxiliary systems, and unique diagnostics that enhance the capabilities of Argonne's RCM.

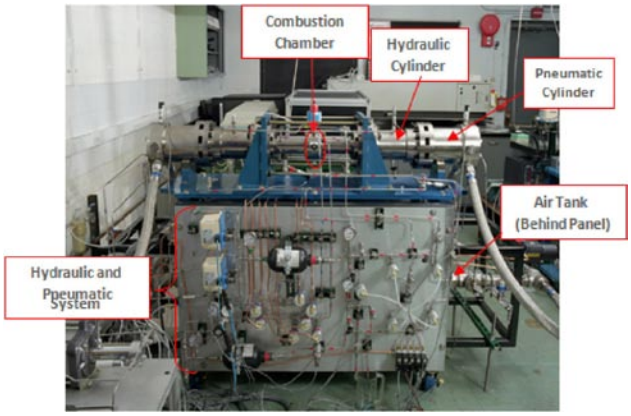

FIGURE 1. A Photograph of Argonne's Rapid Compression Machine

Liquid Fueling System: A cursory review of the fuels of interest showed that they can be classified in to two main categories based on their boiling temperatures: low-BPT fuels and high-BPT fuels. Based on a methodology developed by Massachusetts Institute of Technology, a system was developed to facilitate testing on low-BPT fuels. However, testing fuels like diesels and its surrogates that have boiling temperatures ~350°C is challenging. To facilitate testing of such fuels, modeling and bench-scale testing was performed to evaluate introduction of the fuel in the form of an aerosol. While such a scheme has been successfully used in a shock tube [1], this is the first attempt towards its adaptation for a RCM. Modeling and subsequent lab testing has shown that introduction of the fuel with Sauter mean diameters <2 microns is necessary to avoid pooling and subsequent separation.

Rapid Sampling Valve: A survey conducted among the prominent researchers that use RCMs [3] has shown that species concentrations at various stages of combustion in a RCM are more valuable as metrics for model validation as compared to pressure and radical chemiluminescence/fluorescence that are used currently. Towards this end, the design of a rapid sampling valve was obtained from the Toyota R&D Center and it was subsequently manufactured (see Figure 3). This valve provides a capability to sample the combustion gases with a 55 microsecond precision. Such a fast valve used in tandem with gas chromatograph/mass spectrometer analysis is likely to provide a unique capability that is not available in other RCMs.

Imaging/Flame Speed: As laminar flame speed is an important metric for model validation, it was attempted to develop a methodology of obtaining this

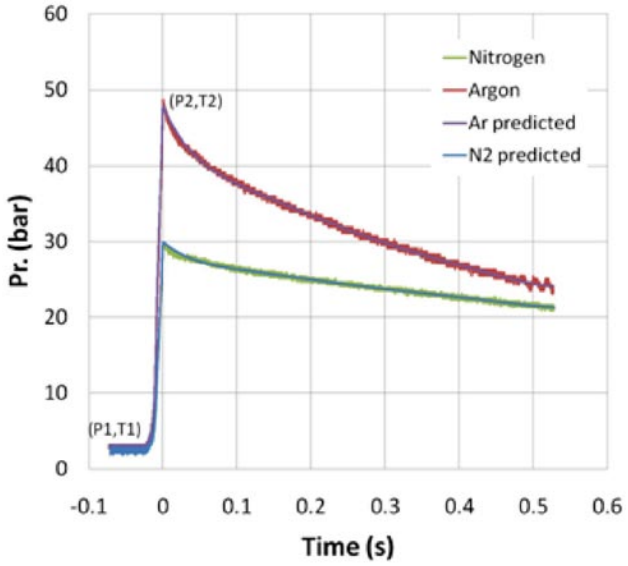

FIGURE 2. Heat Transfer Model Validation using Inert Gases

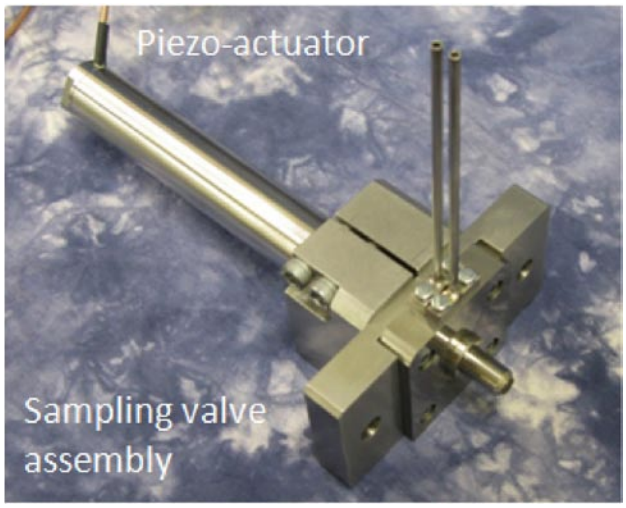

FIGURE 3. Rapid Sampling Valve

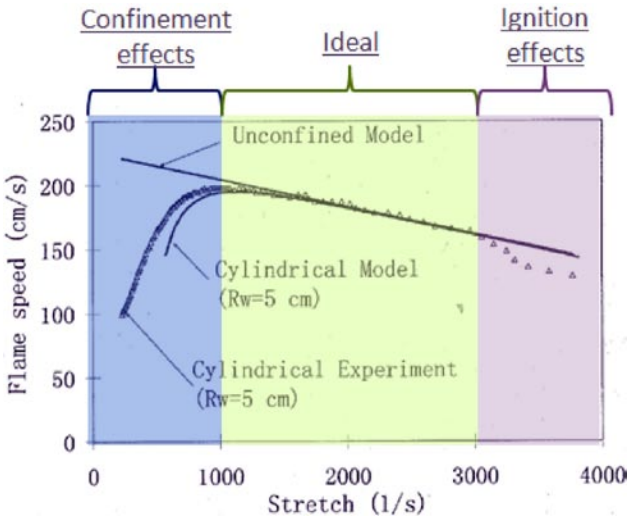

FIGURE 4. Flame Stretch Effect on Flame Speed [2]

metric using the current RCM. Special optics were developed to accommodate the limited optical access of the opposed piston RCM, and high-speed imaging was performed on various fuels for typical in-cylinder conditions. As previously analyzed by Burke et al. [2], after an initial stage dominated by ignition plasma kernel, the flame speed increases linearly as the flame front develops. In later stages the confinement effects of the combustion chamber walls have a dominating effect (see Figure 4). Due to the small aspect ratio of the current RCM combustion chamber, confinement effects were found to be very dominating. As a result, a higher degree of analysis will be necessary in order to measure flame speeds using the current RCM, which is beyond the scope of the current effort.

Conclusions

Argonne's RCM, a remnant of a previous research effort, was rebuilt. Various hardware associated with this machine were improved to reduce leak past piston seals and further to improve temperature uniformity within the combustion chamber. Also, various auxiliary systems were designed and developed to enable testing a variety of fuels. Also, the design of a rapid sampling valve was obtained from Toyota R&D, to enable species concentration measurements which will serve as important metrics for model validation. Early in the project, in September 2010, a meeting was organized in Washington, D.C., where several university researchers having experience with various vintage RCMs participated [3]. With the current design changes, Argonne's RCM is the one best suited for the intended experiments.

In FY 2012, tests will be conducted on various low-BPT fuels like gasoline/gasoline surrogates and various alcohols. These will be followed by tests on high-BPT fuels like diesels and diesel surrogates.

References

1. Haylett, D.R., Davidson, D.F., Hanson, R.K., "Ignition delay times of low-vapor pressure fuels measured using an aerosol shock tube," Combustion and Flame, 2011.

2. M.P. Burke et al., Combustion and Flame, 2009.

3. Proceedings of 1st RCM meeting, Washington, D.C., Aug. 2010.

FY 2011 Publications/Presentations

1. Mittal, G. and Gupta, S.B., "Computational Assessment of an approach for Crevice Containment in Rapid Compression Machines", submitted to Fuel, 2011.

2. "Flame speed measurements at in-cylinder conditions using an opposed-piston RCM," submitted to Central States Section of Combustion Institute, 2012.

3. Proceedings of 1st RCM meeting, Washington, D.C., Aug. 2010.

II.A.18 Expanding Robust HCCI Operation with Advanced Valve and Fuel Control Technologies

James P. Szybist (Primary Contact), Adam Weall and K. Dean Edwards
Oak Ridge National Laboratory (ORNL)
2360 Cherahala Boulevard
Knoxville, TN 37932

Matt Foster (Primary Contact), Wayne Moore and Keith Confer
Delphi - Advanced Powertrain
3000 University Drive
Auburn Hills, MI 48326

DOE Technology Development Manager:
Gurpreet Singh

Overall Objectives

- Determine limits of conditions conducive to robust homogeneous charge compression ignition (HCCI) operation and the engine controls most effective at controlling HCCI.
- Develop robust model of negative valve overlap (NVO) HCCI combustion with GT-POWER.
- Operate multi-cylinder engine with cam-based valve train under HCCI conditions, demonstrating the widest-possible HCCI operating regime.

Fiscal Year (FY) 2011 Objectives

- Evaluate the effect of valve strategies on HCCI operation, including valve deactivation.
- Demonstrate the effectiveness of a split-injection fueling strategy to expand the operating load range.
- Develop GT-POWER model to simulate NVO HCCI combustion.

Accomplishments

- Demonstrated an expansion of the HCCI low load limit at 2,000 rpm to 160 kPa net indicated mean effective pressure ($IMEP_{net}$) with the combination of multiple fuel injection and valve deactivation,
- Demonstrated that fuel injection timing and the use of a pilot injection are effective at controlling combustion phasing under HCCI conditions. In many cases the fuel injection parameters offer sufficient control so that only limited variation in valve events is sufficient to change operating load.
- Showed that HCCI combustion provides a substantial fuel consumption improvement over conventional spark ignited (SI) combustion over a load of 200 to 400 kPa $IMEP_{net}$ at 2,000 rpm.

Future Directions

- Complete modifications and shakedown to the air handling system of the ORNL single-cylinder hydraulic valve actuation (HVA) engine, allowing boost, backpressure and external exhaust gas recirculation (EGR).
- Conduct an experimental campaign into the HCCI load expansion enabled by boost and external EGR.

Introduction

HCCI combustion has a great deal of promise for improved efficiency and reduced emissions, but faces implementation barriers. This study aims to better understand the engine conditions that are conducive to HCCI combustion, and the engine operating sensitivities to engine controls. Specifically, we aim to develop an understanding of engine parameters that can provide robust control and are applicable to a production-intent engine with a versatile cam-based valve train.

Approach

In order to guide development of a production-intent multi-cylinder HCCI engine with a cam-based valve train, this project utilizes single-cylinder engine experiments and engine system modeling at ORNL in combination with multi-cylinder engine experiments at Delphi.

The ORNL single-cylinder engine shown in Figure 1 is equipped with HVA which allows full control over valve timing, duration and lift. This versatile research tool can be used to readily identify and characterize engine operating conditions that are conducive to HCCI combustion, and because of its versatility it can perform parametric studies with valve train parameters that are not possible with a cam-based system. The valve strategies used on the HVA engine as part of this project were limited to approximate the capabilities of Delphi's cam-based variable valve actuation valve train. An example of the comparison of valve profiles can be seen in Figure 2. Results from the single-cylinder HVA engine

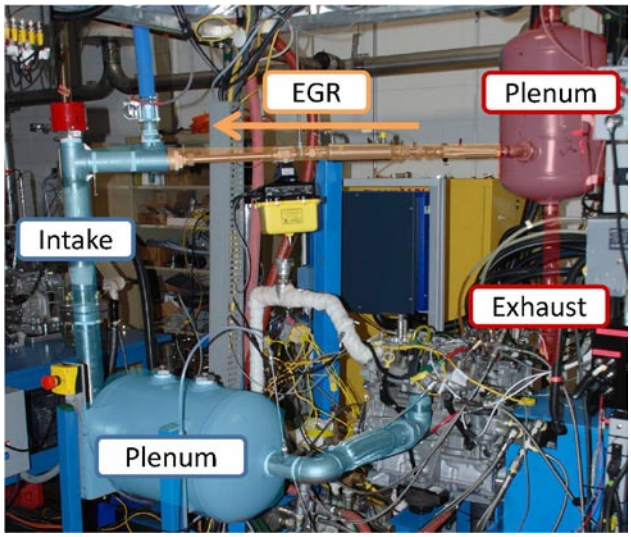

FIGURE 1. ORNL's Single-Cylinder Engine with HVA, Boost, and Cooled External EGR

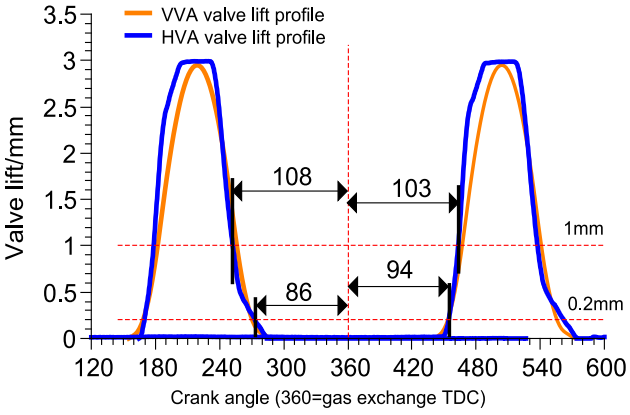

FIGURE 2. Comparison of HVA Valve Profile and Cam-Based HCCI Valve Profile

were modeled with GT-POWER for translation onto a multi-cylinder engine platform.

Results

Single-Cylinder Experiments

The effect of fuel injection timing was assessed at an engine load of 300 kPa $IMEP_{net}$ while using the single fuel injection strategy. Figure 3 shows that advancing fuel injection timing has only a minor impact on $ISFC_{net}$ but that combustion phasing (crank angle at which 50% of the combustion heat release has occurred, CA50) is advanced. The advanced CA50 was accompanied by increasing combustion stability and combustion noise increases (not shown). Also shown in Figure 3 is the effect of a change in valve opening duration from

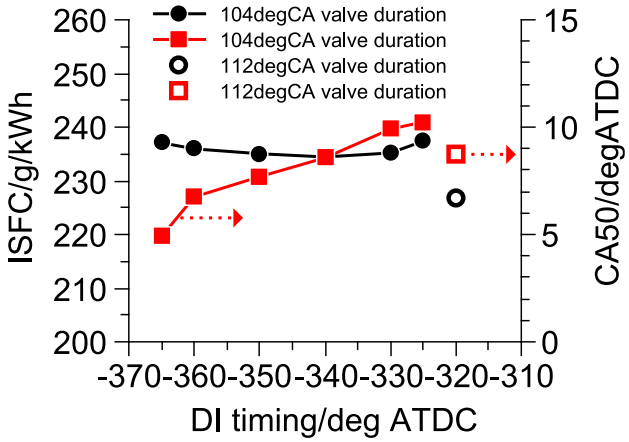

ATDC - after top dead center

FIGURE 3. Effect of Fuel Injection Timing and NVO Duration on $ISFC_{net}$ and Combustion Phasing for the Single Fuel Injection Strategy at 300 kPa $IMEP_{net}$

104 deg crank angle (CA) to 112 deg CA, which also reduced the NVO. The same combustion phasing could be produced with the longer valve opening by retarding injection timing. The longer valve opening duration also decreased fuel consumption.

The effect of fuel injection strategy with a pilot injection followed by a main injection was also investigated and is shown in Figure 4 at a load of 300 kPa $IMEP_{net}$. Results show that pilot injection mass and timing affect CA50, and that the pilot injection strategies also show a small improvement in $ISFC_{net}$ compared to the single injection strategy (Figure 3). Nearly identical engine performance can be achieved with pilot injections mass fractions of 5 and 15%, but the former required more advanced pilot injection timing. Thus, as with the single injection strategy, the fuel injection timing can control combustion over a wide range of conditions.

Engine load could successfully be reduced to 160 kPa $IMEP_{net}$ by using a pilot injection strategy combined with intake valve deactivation. At the lowest attainable engine load, the pilot injection accounted for 50% of the total fuel injected. Deactivation of one of the intake valves had the effect of reducing the air flow into the engine, thereby increasing the equivalence ratio of the air/fuel mixture to make it more ignitable. This point was successfully modeled using GT-POWER software, as is shown in Figure 5 and the residual exhaust fraction is calculated to 35% while maintaining stable combustion, with a coefficient of variance of $IMEP_{net}$ of 5.4%.

At the lowest attainable engine loads, pilot injection was necessary for combustion stability and performance because of the interaction of the fuel with the hot gases during NVO. Figures 3 and 4 show that at a load

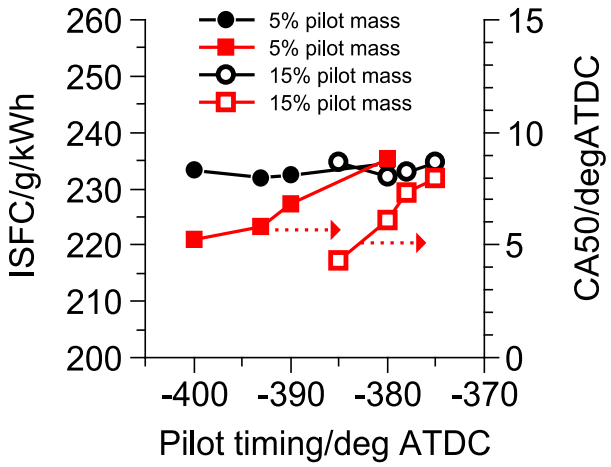

FIGURE 4. Effect of Pilot Fuel Injection Timing and Pilot Injection Percent Mass on $ISFC_{net}$ and Combustion Phasing for the Multi-Injection Strategy at 300 kPa $IMEP_{net}$

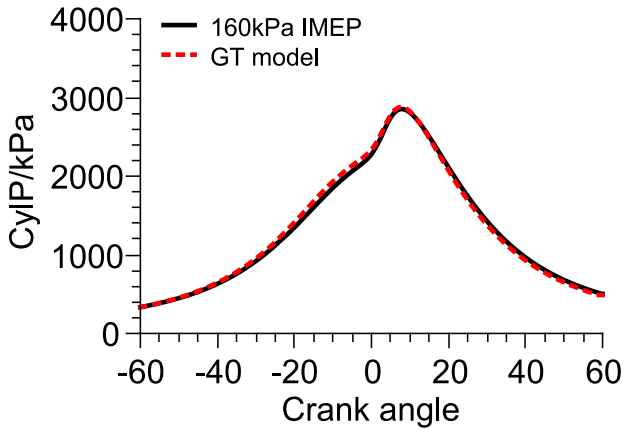

FIGURE 5. Modeled and Experimental Cylinder Pressure at an Engine Load of 160 kPa $IMEP_{net}$ with a Deactivated Intake Valve Strategy

of 300 kPa $IMEP_{net}$ the performance is very similar with and without a pilot injection. As engine load is increased further, a pilot injection becomes detrimental to the combustion process, leading to overly advanced combustion phasing, loud combustion and an increase in fuel consumption and NO_x. The high-load limit of HCCI combustion under naturally aspirated was encountered at 390 kPa $IMEP_{net}$, where limits to both ringing intensity (5 MW/m^2 max) and NO_x emissions (50 ppm max) were simultaneously encountered. Thus, pilot injection is a valuable tool to use for NVO HCCI, but it is most valuable at the lowest engine loads.

A comparison of $ISFC_{net}$ under HCCI and conventional SI combustion is shown in Figure 6 as a function of $IMEP_{net}$. As expected, $ISFC_{net}$ for HCCI is substantially better than conventional SI combustion, with a decrease of nearly 100 g/kWh at a load of 200

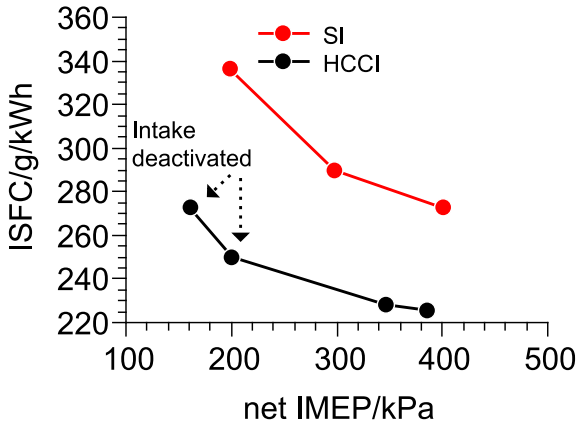

FIGURE 6. $ISFC_{net}$ as a Function of Engine Load for Conventional SI Combustion and HCCI Combustion

kPa $IMEP_{net}$, and a decrease of more than 40 g/kWh at a load of 400 kPa $IMEP_{net}$. The improvement in $ISFC_{net}$ can be attributed to a reduction in pumping work, fuel lean operation, and a shorter combustion duration.

GT-POWER Modeling and Multi-Cylinder Experiments

Two GT-POWER models were developed as part of this project. The first was used to simulate performance of the single-cylinder HVA engine and the second was used to simulate performance of the multi-cylinder engine operated at Delphi. The objective of these models was to develop a simple, rapid procedure for matching conditions between the two engines.

The first GT-POWER model was able to simulate the performance of the single-cylinder HVA engine reasonably well, as is show in Figure 5. However, the experimental data from the multi-cylinder engine could not be reproduced through GT-POWER simulations or experimentally on the single-cylinder HVA engine despite substantial effort. It appeared that the multi-cylinder engine breathed substantially differently than the HVA engine and what was predicted by the GT-POWER simulation. The root cause of the breathing differences between the engines was not able to be determined definitively.

Conclusions

- The load range for naturally aspirated HCCI does not require the full authority of the HVA valve train. Fuel injection strategy is an effective tool to control combustion, including both single and pilot injection strategies, pilot injection mass, and injection timing. Intake valve deactivation also enables the lowest load point to be achieved.

- Pilot injection is advantageous at the lowest engine loads, but becomes detrimental at loads above 300 kPa $IMEP_{net}$. The effect of fuel injection parameters in terms of pilot timing and quantity was to advance or retard the combustion phasing and allow some control of combustion phasing.
- Nearly identical HCCI performance can be achieved with different pilot injection quantities by changing the timing of the pilot fuel injection.
- The maximum load achieved for naturally aspirated HCCI was 390 kPa $IMEP_{net}$, which is in agreement with previous researchers. Limits to both NO_X emissions and ringing intensity were encountered nearly simultaneously.

FY 2011 Publications/Presentations

1. Szybist, J.P., K. Confer, A. Weall, M. Foster, K.D. Edwards, and Wayne Moore. "*Expanding Robust HCCI Operation: A CRADA Project with Delphi Automotive systems.*" 2011 DOE Vehicle Technologies Annual Merit Review, Project ID ACE053, presented May 11, 2010.

2. Weall, A., J.P. Szybist, M. Foster, K.D. Edwards, K. Confer and W. Moore. *"HCCI Load Expansion Opporunities using a Fully Variable HVA Research Engine to Guide Development of a Production Intent Cam-based VVA Engine: The Low Load Limit."* To be presented at the 2012 SAE World Congress, Detroit, MI.

II.A.19 Variable Compression Ratio to Enable Higher Efficiency in Gasoline Engines

Norberto Domingo
Oak Ridge National Laboratory (ORNL)
2360 Cherahala Boulevard
Knoxville, TN 37932

DOE Technology Development Manager:
Roland Gravel

Subcontractor:
ENVERA, Los Angeles, CA

Overall Objectives

- Under subcontract with Envera LLC, design, prototype, and deliver to ORNL one variable compression ratio (VCR) gasoline direct injection (GDI) engine with combined direct fuel injection and port fuel injection capabilities. Conduct high-load dynamometer testing prior to delivery ORNL to validate functionality of all mechanical systems.
- Set up VCR engine at ORNL and quantify the fuel economy benefit of VCR engine technology to a modern direct-injection gasoline engine, and the impact on emissions.
- Map VCR engine performance and emissions over multiple control variables, including compression ratio, spark timing, and cam phasing.
- Utilize experimental engine maps as inputs to drive cycle simulation software to estimate the real-world fuel economy and emissions impact.

Fiscal Year (FY) 2011 Objectives

- Release ORNL VCR engine design.
- Complete crankcase castings.
- Complete crankcase machining.
- Procure 90 percent of engine hardware.
- Complete buildup of ORNL engine test facility for VCR engine evaluation.

Accomplishments

- A custom, four-cylinder crankcase block, designed by Envera LLC, was casted and machined. This custom block was designed to allow installation of a mass production GDI cylinder head cylinder head and permit the integration of the VCR mechanism to be fully contained within the crankcase. Figure 1 shows picture of completed crankcase block.
- Engine block bedplate and crankshaft support cradle were designed and casted. Figures 2 and 3 shows picture of casted block and crankshaft cradle, respectively.
- Completed purchase of 90% of engine hardware.
- ORNL test site preparations for the VCR engine were completed. The test facility incorporates state-of-the-art common fueling system, cooling system, air handling system, emissions bench, and data acquisition system that are fully functional.

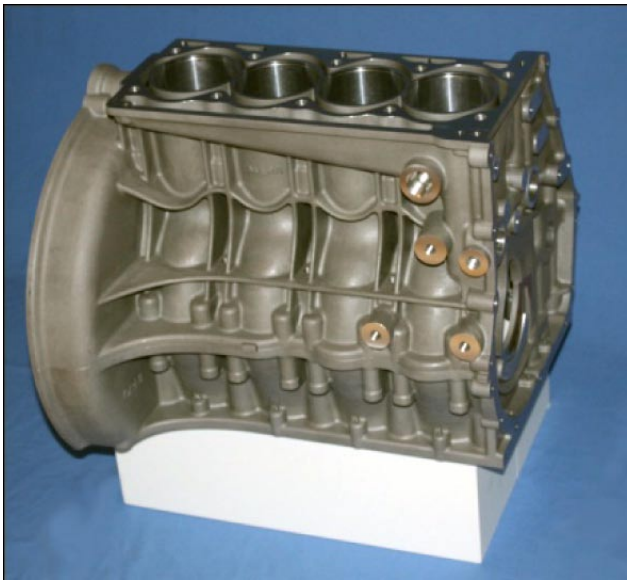

FIGURE 1. Finished Crankcase Block

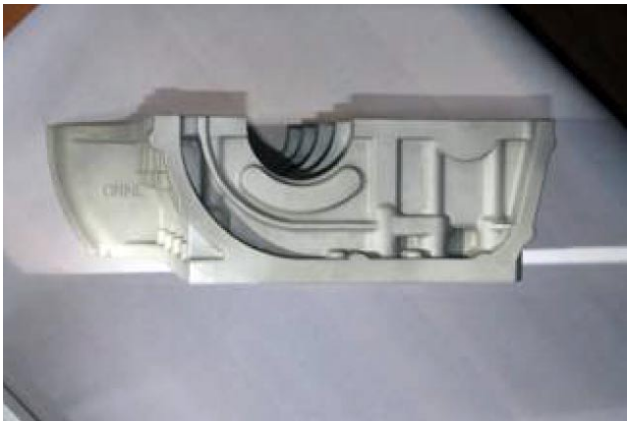

FIGURE 2. Engine Block Bedplate Casting

FIGURE 3. Crankshaft Cradle Housing Casting

Future Directions

- Envera LLC to continue work on fabrication of prototype VCR research engine. This includes machining of engine bedplate, engine crankshaft cradle, and fabrication of custom crankshaft and other VCR actuation components.
- Deliver all engine components to Automotive Specialist in Concord, NC., for engine build and demonstration testing. Measurements of the engine performance, including the VCR actuator mechanism response time and fuel consumption, will be made at Automotive Specialist.
- Conduct a post-test inspection of key engine components by Automotive Specialist and reassemble engine for delivery to ORNL.
- Install engine at ORNL dynamometer test facility and conduct experiments to investigate the effect of VCR on engine efficiency at the maximum brake torque (MBT) spark timing over the engine map with a VCR research engine. Engine experiments will combine parametric sweeps of spark timing, compression ratio (CR), and cam phasing to determine the optimal efficiency at each engine speed/load operating condition. Emissions from the engine will also be measured before and after a 3-way catalyst.

Introduction

Basic thermodynamics dictate that the efficiency of internal combustion engines is proportional to the CR. However, the CR of modern gasoline engines is relatively low from a thermodynamic standpoint, in the range of about 8.5 to 12.5, because of practical constraints at higher CR such as engine knock, increased friction work, and increased heat transfer. It is only the knock-prone conditions (low speed, high load) that constrain the engine CR. The efficiency of most part-load engine conditions can be increased by raising the CR, and it is these part-load conditions that have the most direct impact the real-world fuel economy.

Figure 4 illustrates the potential impact of increased part-load efficiency on fuel economy. Figure 4 (a) shows a contour map of engine efficiency as functions of engine speed and load for a Saab Biopower vehicle, and is qualitatively representative of modern engines. Peak engine efficiency is approximately 32%. Figure 4 (b) shows the vehicle speed as a function of time for a Federal Test Procedure (FTP) driving cycle, used in determining Environmental Protection Agency (EPA) “City” fuel economy, which contains numerous decelerations, stops, and accelerations. In Figure 4 (c), data points from the FTP cycle are superimposed on the map of engine efficiency. Nearly all of the driving cycle takes place under low efficiency part-load engine conditions, conditions where higher compression could increase engine efficiency.

There are currently several ongoing investigations aimed at increasing efficiency, at least in part, by utilizing high mechanical CR and reducing the effective CR with late intake valve closing [1,2]; a technique that is particularly attractive for optimizing E85 engines. However, reducing the effective CR in this manner actually decreases the maximum torque at all engine speeds because of reduced volumetric efficiency, which is a direct result of late intake valve closing. An earlier investigation to increase part-load efficiency was made with a predecessor of the research engine proposed here [3]. The earlier investigation demonstrated proof of principle and showed promise, but did not include a comprehensive study on the effects of VCR engine emissions and is no longer representative of modern engine technology.

Engine downsizing is viewed by U.S .and foreign automobile manufacturers as one of the best options for improving fuel economy. While this strategy has already demonstrated a degree of success, downsizing and fuel economy gains are currently limited. With new VCR technology however, the degree of engine downsizing and fuel economy improvement can be greatly increased. A small VCR engine has the potential to return significantly higher vehicle fuel economy while also providing high power.

To meet torque and power requirements, a smaller engine needs to do more work per stroke. This is typically accomplished by boosting the incoming charge with either a turbocharger or supercharger so that more energy is present in the cylinder per stroke to do the work. With current production engines the degree of engine boosting (which correlates to downsizing) is limited by engine knock at high boost levels. Engine

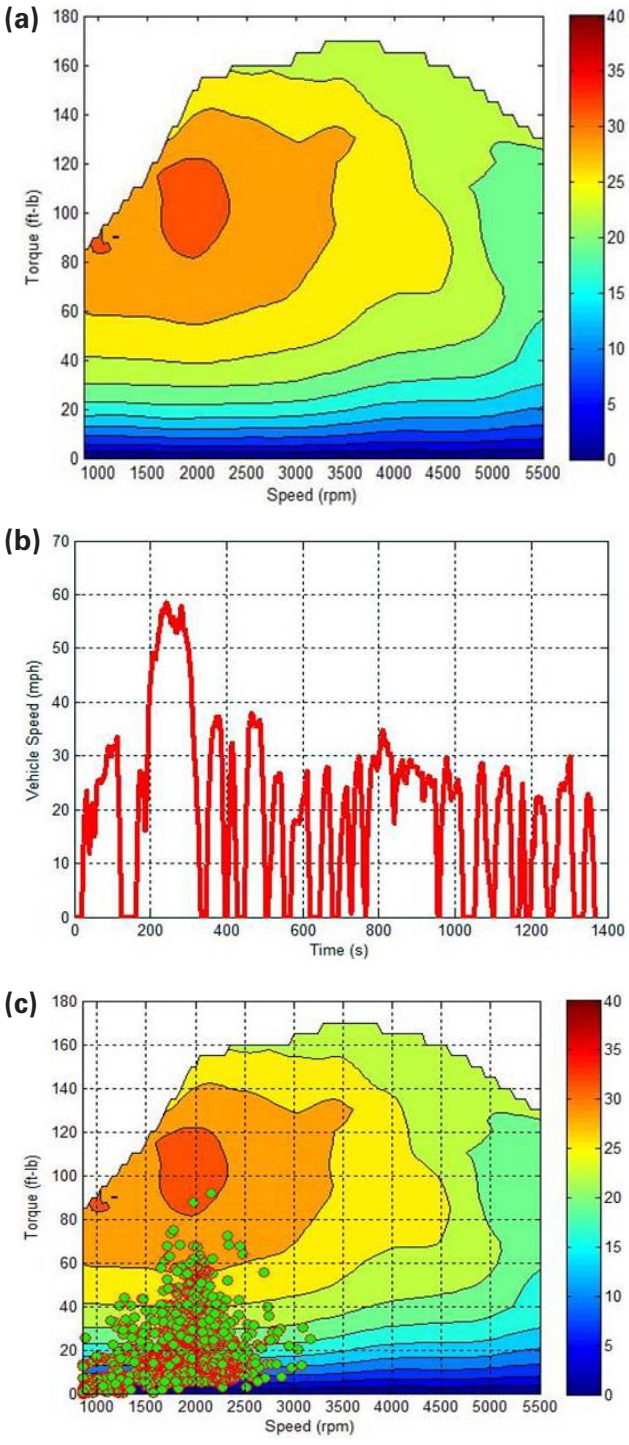

FIGURE 4. (a) Engine efficiency contour plot for the Saab Biopower, (b) Vehicle speed trace for the FTP driving cycle, and (c) Operating points from the FTP driving cycle superimposed on the engine efficiency contour plot. Data collected at the ORNL chassis dynamometer laboratory in 2007.

knock or detonation can be prevented by lowering the CR and using premium octane fuel, but as stated earlier, lowering CR reduces engine efficiency and using premium fuel increases customer cost.

VCR technology eliminates the limitation of engine knock at high load levels by reducing CR to ~8.5:1 (or whatever level is appropriate) when high boost pressures are needed and regular grade fuel is used. By reducing the CR during high load demand periods there is increased volume in the cylinder at top-dead center which allows more charge (or energy) to enter the cylinder without increasing the peak pressure. Cylinder pressure is thus kept below the level at which the engine would begin to knock. When loads on the engine are low the CR can be raised (to as much as 18:1) providing high engine efficiency. It is important to recognize that for a well-designed VCR engine cylinder pressure does not need to be higher than found in current production turbocharged engines. As such, there is no need for a stronger crankcase, bearings and other load bearing parts within the VCR engine.

Under the current project, Envera is delivering a prototype GDI VCR engine to ORNL. In the proposed study, ORNL will provide an update of the potential benefit of variable mechanical CR on efficiency and emissions using Envera's state-of-the-art VCR engine technology.

Fuel Efficiency Comparison

The fuel efficiency benefit of downsizing from a naturally aspirated V8 engine to a turbocharged V6 engine was assessed by the EPA (A Study of Potential Effectiveness of Carbon Dioxide Reducing Vehicle Technologies, Revised Final Report, June 2008, US EPA) [4] and Ricardo (SAE Paper No. 2007-01-1410) [5]. In Figure 5, engine efficiency projections for an in-line 4-cylinder Envera VCR engine are added to the earlier EPA/Ricardo comparison. Figure 5 includes brake specific fuel consumption (BSFC) curves for a GDI turbocharged 3.6 L V6 engine (DI Boost) and a naturally aspirated engine 5.7 L V8 engine as reported by EPA. Efficiency projections for the Envera VCR engine (dashed black line) have been added to the graph. All three engine BSFC curves correspond to an engine speed of 2,000 rpm. The Envera VCR engine will operate according to the Atkinson Cycle at light load, with engine calibration settings similar to (or better than) that of the 2010 Toyota Prius. The solid portion of the "--- VCR BOOST" curve is drawn from engine efficiency data presented by Toyota in SAE paper 2009-01-1061 [6]. The data has been scaled from an engine having a displacement of 1.8 L (the stock 2010 Toyota Prius) to 2.2 L so that the peak torque of the Envera VCR engine matches the peak torque of the V8 engine at 2,000 rpm, which is 445 Nm (328 ft-lb). In this comparison the Envera VCR engine employs turbocharging in order to provide V8-like power and torque. VCR and variable valve actuation enable the Envera engine to operate according to the high-efficiency Atkinson cycle at light loads and according to the Otto cycle with aggressive

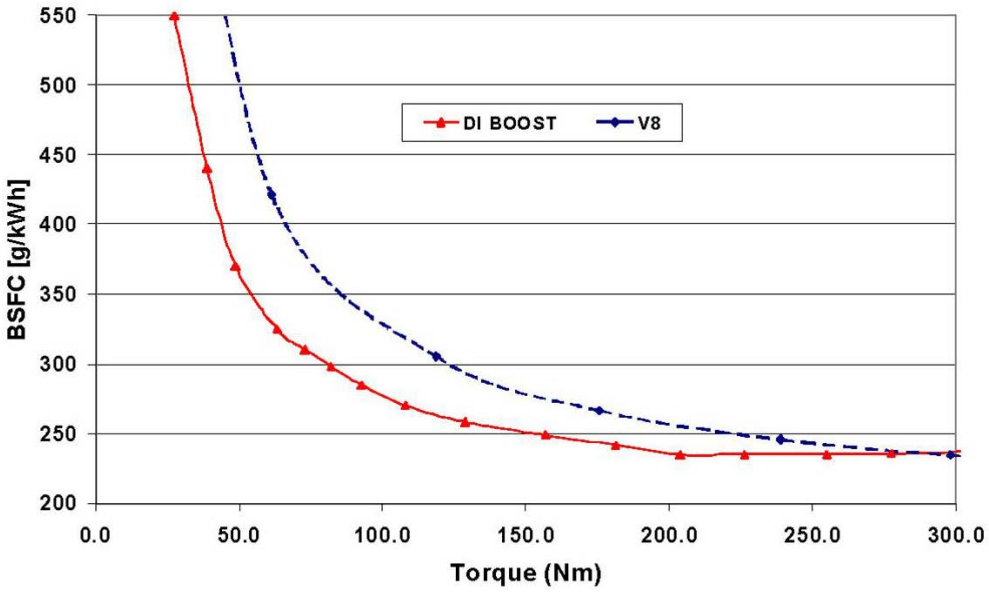

FIGURE 5. Fuel Efficiency Comparison of a 5.7 L V8, a 3.6 L Turbo DI V6, and a 2.2 L Turbo VCR 4-Cylinder Engine (Projected Data)

turbocharging at high loads. Data for the three engines is shown in Table 1. At 100 Nm and 2,000 rpm, all three engines produce about 28 horsepower. The V6 Turbo DI engine is expected to consume 19.6 percent more fuel than the I4 turbocharged VCR engine at 100 Nm. The V8 engine is expected to consume 43 percent more fuel than the I4 turbocharged engine at 100 Nm. At 50 Nm (14 hp) the V8 engine is expected to consume 67 percent more fuel than the I4 turbocharged engine. The VCR engine in this comparison has port fuel injection. Even larger gains in fuel efficiency may be attainable for GDI VCR engines. In general, VCR technology enables significantly larger fuel economy gains to be achieved than can be accomplished with fixed CR engines.

TABLE 1. Engine Comparison Data

Type	V8	V6 Turbo DI	I4 Turbocharged VCR
Displacement	5.7L	3.56L	2.2L
Power	298 kW	283 kW	271 kW
At 2,000 RPM			
Peak Torque	445 Nm	560 Nm	445 Nm
Peak BMEP	9.8 bar	19.7 bar	25.4 bar
Fuel efficiency			
@ 100 Nm	328 g/kWh	276 g/kWh	230 g/kWh
@ 50 Nm	500 g/kWh	362 g/kWh	300 g/kWh

BMEP – brake mean effective pressure

Approach

We propose to investigate the effect of VCR on engine efficiency at the MBT spark timing over the engine map with a VCR research engine designed and built by Envera LLC. This state-of-the-art engine will combine a production cylinder head utilizing direct fuel injection, cam phasers, and a custom engine block containing the VCR mechanism. Specifications for the engine are shown in Table 2.

TABLE 2. ORNL Envera GDI VCR Engine Specifications

Cylinders	Inline 4-cylinder
Displacement	1.886 L
Bore / Stroke	81.0/91.5 mm
Compression ratio	Variable
Maximum	18:1
Minimum	8.5:1
Crankcase material	A356 aluminum
Cooling	Electric water pump
Valve train	16-valve DOHC
Phase shifters	Intake and exhaust camshafts
Fuel delivery	GDI
Aspiration	Naturally aspirated as delivered (turbocharge upgrade capable)

DOHC - dual overhead cam

Engine experiments will combine parametric sweeps of spark timing, CR, and cam phasing to determine the

optimal efficiency at each engine speed/load operating condition. Emissions from the engine will also be measured before and after a 3-way catalyst.

The experimental data of engine performance and emissions will be used to generate composite engine maps of engine efficiency and emissions (i.e. at best efficiency, constant CR, lowest emissions, etc). The engine maps will be used as inputs for computer simulations of vehicle drive cycles using the PSAT software to determine the real-world impact of variable CR on fuel economy and emissions.

Results

All castings surpassed quality requirements. Crankcase machining was completed to specification. Purchased parts currently in hand are to specifications.

Conclusions

VCR technology enables significantly larger fuel economy gains to be achieved than can be accomplished with fixed CR engines. Under the current project, Envera is delivering a prototype GDI VCR engine to ORNL. ORNL will then conduct dynamometer tests to independently assess engine efficiency values, and use the engine for efficiency research and benchmarking.

References

1. Confer, K., "E85 Optimized Engine through Boosting, Spray Optimized DIG, VCR, and Variable Valvetrain." Presented at 2008 DOE Vehicle Technology Merit Review, http://www1.eere.energy.gov/vehiclesandfuels/resources/proceedings/2008_merit_review.html#fuels.

2. Yilmaz, H., "DOE Merit Review – Flex Fuel Vehicle Systems." Presented at 2008 DOE Vehicle Technology Merit Review, http://www1.eere.energy.gov/vehiclesandfuels/resources/proceedings/2008_merit_review.html#fuels.

3. Mendler, C. and R. Gravel, "Variable Compression Ratio Engine." Society of Automotive Engineers, 2002, Technical Paper 2002-01-1940.

4. A study of Potential Effectiveness of Carbon Dioxide Reducing Vehicle Technologies, Revised Final Report, June 2008, US EPA.

5. Christie, M. et. al Ricardo Ltd.: DI Boost: Application of a High Performance Gasoline Direct Injection Concept, SAE Paper no. 2007-01-1410, Pub. SAE 2007.

6. Kawamoto, N. et al. Toyota Motor Corporation: Development of New 1.8-Liter Engine for Hybrid Vehicles, SAE Paper 2009-01-1061, Pub SAE 2009.

II.A.20 Cummins-ORNL Combustion CRADA: Characterization and Reduction of Combustion Variations

Bill Partridge[1] (Primary Contact), Sam Geckler[2], Maggie Connatser[1], Jon Yoo[1], Jim Parks[1], Craig Hetisimer[2], Patrick Helman[2]
[1]Oak Ridge National Laboratory (ORNL),
[2]Cummins Inc.
2360 Cherahala Blvd.
Knoxville, TN 37932

DOE Technology Development Manager:
Ken Howden

Overall Objectives

- Improve diesel engine-catalyst system efficiency through better combustion uniformity, engine calibrations and catalyst control.
- Work with industrial partner to develop full-scale engine-catalyst systems to meet efficiency and emissions goals.

Fiscal Year (FY) 2011 Objectives

- Demonstrate mid-infra-red (MIR)-light-emitting diode (LED)-based CO_2 diagnostic at the Cummins Technical Center (CTC), in Columbus, Indiana, for monitoring fast exhaust gas recirculation (EGR) fluctuations in the intake.
- Develop diagnostic for resolving 1% EGR fluctuations in the intake at nominal 25% EGR level (corresponds to detecting ca. 0.1% CO_2 changes with 12% CO_2 exhaust concentrations).
- Develop a single-entry-point measurement probe to allow EGR-variation measurements in applications where line-of-sight access is not possible.
- Adapt Fuel-in-Oil (FiO) diagnostic to assess impact of fuel-injector design on oil dilution with alternative fuels.
- Apply FiO at CTC to assess performance of different fuel-injector designs.

Accomplishments

- Applied MIR-LED-based CO_2 and FiO diagnostics to engine-development applications at CTC:
  - Resolved fast 20-ms EGR fluctuations.
  - Adapted FiO diagnostic to alternative fuel applications.
- Improved EGR-uniformity diagnostic:
  - Reduced uncertainty by 3x.
  - Improved sensitivity by 10x.
- Developed single-entry-point probe for engine measurements where line-of-sight optical access is not possible.
- Specified laser to enable simultaneous multi-point EGR fluctuation measurements.
- Applied FiO instrument to alternative fuel engine to identify performance variations associated with different fuel-injector spray patterns.

Future Directions

- Improve EGR uniformity via application of EGR probe to assess performance of candidate intake hardware designs with respect to EGR uniformity.
- Improve the EGR diagnostic design to allow simultaneous uniformity and fluctuation measurements at multiple engine locations.

Introduction

A combination of improved technologies for engine and aftertreatment control of oxides of nitrogen (NO_x) and particulate emissions are required to efficiently meet increasingly stringent emission regulations. This Cooperative Research and Development Agreement (CRADA) section focuses on engine and combustion-uniformity technologies, while a parallel section (NO_x Control and Measurement Technology for Heavy-Duty Diesel Engines) focuses on emissions and catalyst technologies. Improved efficiency, durability and cost can be realized via combustion-uniformity improvements which enable reduction of engineering margins required by nonuniformities; specifically, these margins limit efficiency. Specific needs exist in terms of reducing cylinder-to-cylinder and cycle-to-cycle combustion variations, and continuous catalyst-state monitoring. For instance, combustion variations mandate system-calibration tradeoffs which move operation away from optimum efficiency points. Combustion variations are amplified at high EGR conditions which are expected in advanced engine systems. Advanced efficiency engine systems require understanding and reducing combustion variations. This requires development and application of enhanced diagnostic tools to realize these technology improvements, which is a major focus of this CRADA.

Approach

Development and application of minimally invasive advanced diagnostic tools to resolve spatial and temporal variations within operating engines and catalysts has been central to the historical successes of this CRADA partnership, and continues to be a key element of the project approach. These include small capillary and optical-fiber-based technologies which are able to resolve spatiotemporal variations without changing the measurement environment or requiring significant hardware modifications for applications. Integral to this work are coating technologies to create localized fiber and capillary transducers to detect variations; e.g., species, temperature, pH, etc. The approach relies heavily on optical and mass-spectrometry, but also includes other techniques such as electrical impedance spectroscopy. Diagnostics are developed and demonstrated on bench reactors and engine systems (as appropriate) at ORNL prior to field application at Cummins. In some cases discrete-sensor technology is a stepping stone and may be further developed and integrated in system components; e.g., to create self-diagnosing smart catalyst systems.

Diagnostics are applied at ORNL and Cummins to study the nature and origins of performance variations. For example, this may be manifested in cylinder-to-cylinder CO_2 variations due to nonuniform fueling, air and/or EGR charge, fuel spray, component tolerance stacking, or other variations. Detailed measurements can be used to identify and evaluate corrective measures; e.g., hardware and control changes.

Results

A diagnostic for quantifying intake EGR fluctuations via CO_2 measurements was developed based on MIR LED sources; these are more compact, less expensive, and do not entail laser-safety issues. Compared to our past approach using a near-infra-red (NIR) fiber ring laser for the previous fast exhaust H_2O measurements, moving to the MIR provides orders-of-magnitude greater sensitivity (absorption crossection) and a significant reduction in H_2O interferences for CO_2 measurements. Moreover, whereas our previous exhaust H_2O measurements were a responsive indication of combustion nonuniformities, the current intake EGR fluctuation measurements are a direct contributor to combustion nonuniformities. Figure 1 shows a schematic of the diagnostic and how it is applied to engine measurements of EGR uniformity. The initial instrument is intended for line-of-sight optical access; on the pitch optics side (i.e., getting light into the intake evaluation zone), light from two LEDs is combined and launched into a hollow waveguide (HWG). The Probe LED centered at 4.2 µm overlaps the CO_2 absorption features near 4.3 µm, while the reference LED centered at 3.8 µm served as the reference signal that does not coincide with CO_2 absorption features or known interference species. Water is the major potential interference species, but its absorption features are several orders of magnitude smaller than those of CO_2, in this region of the MIR spectrum, and H_2O interference can therefore be neglected. The LEDs are driven at different modulation frequencies (50 and 77 kHz), and the two corresponding signal components are separated at the single detector using Fourier transform. A collimator at the HWG's measurement end pitches the light beam across the intake or exhaust manifold. The beam is collected and focused on the detector via the catch-side optics. The experimental setup was evaluated in an engine cell at ORNL prior to the CTC campaign. A calibration curve, 0–2% CO_2, collected from the ORNL engine experiment showed good CO_2 sensitivity in that region. Exhaust measurements were also made with the windows purged with dry air to prevent fouling.

Figure 2 is from work at the CTC and shows the EGR-fluctuation instrument positioned in the intake of a development engine just downstream of the low-pressure EGR injection point. Notably, in this manifestation the instrument windows were positioned directly on the sides of the intake plenum (i.e., without off-setting purge tubes to mitigate window fouling), and no significant fouling was observed over a full day of operation. To induce CO_2 fluctuations, the EGR valve was cyclically dithered with equivalent on and off dwell times. A range of CO_2 transient widths were investigated by making measurements at different EGR-valve dwell times (10, 2, 0.5, 0.1, 0.05 and 0.02 s) as shown in

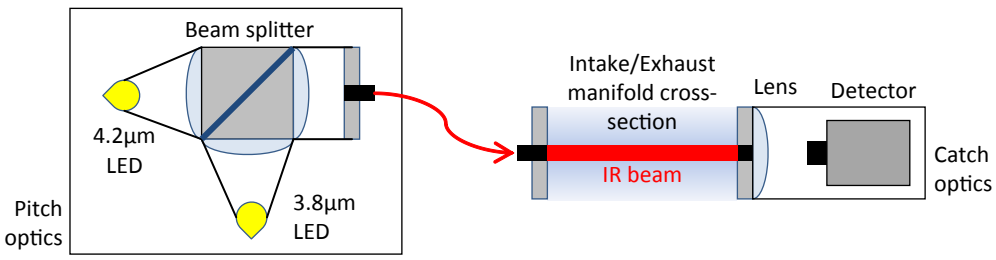

FIGURE 1. Schematic of the MIR LED Experimental Setup for Transient Intake EGR (CO_2) Measurements

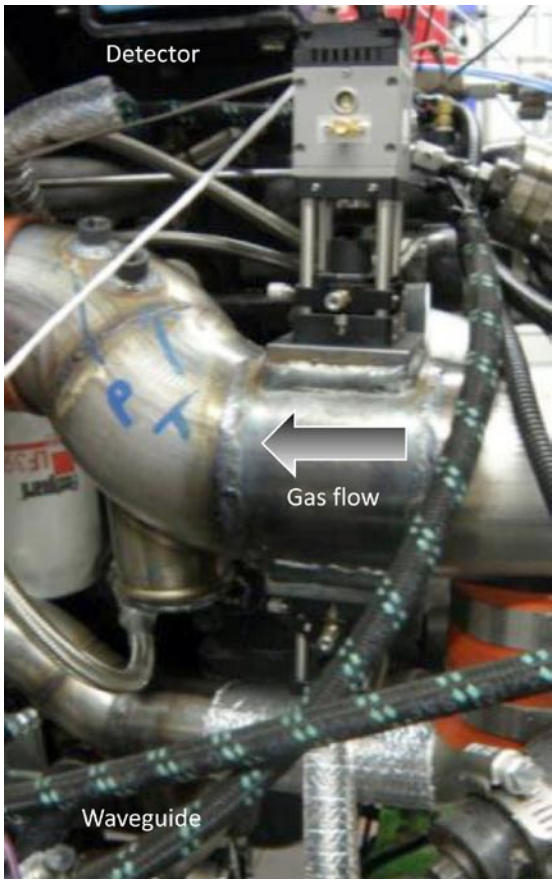

FIGURE 2. EGR-fluctuation instrument positioned on the intake manifold, proximal to low-pressure EGR injection point. The fresh air and exhaust gas mixes just beyond the right side of the image. The turbocharger is located to the left of the image.

Figure 3. The Sub-1s measurements in Figure 3 were smoothed using a moving average. At slower dithering speeds (10 s, 2 s, 0.5 s, 0.1 s), the measured CO_2 concentration dynamics match the commanded EGR valve dithering speed. However, the EGR valve begins to lag behind the commanded modulation and starts behaving erratically at higher speeds resulting in inconsistent signal periodicity at 0.05 and 0.02 s dwell times; this is not unusual as these dwell times are beyond the specifications for the injector valve, and may result in needle bounce and other nonproduction behavior. Nevertheless, the EGR valve functioned for some short time in this extreme command regime and allowed assessment of the diagnostic for monitoring fast EGR fluctuations. Figure 3 shows that the MIR-LED-based diagnostic was able to accurately follow fast EGR fluctuations on timescales as fast as 20 ms.

Significant improvements were made to the EGR-fluctuation instrument following the CTC measurement campaign, resulting in 3x greater LED power and ca. 10x greater sensitivity; and correspondingly lower uncertainty and detection limit, respectively. The resulting sensor is capable of detecting smaller EGR fluctuations on shorter time scale than what was demonstrated at CTC. And, specifically is capable of measuring 1% EGR fraction fluctuations. Higher output power for both the CO_2 and reference LEDs centered at 4.2 µm and 3.8 µm, respectively, was achieved by reconfiguring LED-driving electronics. Long-term durability tests were conducted to determine stable operating conditions for both LEDs. The study showed 300% improvements in stable LED output power are possible without irreversible damage. Measurement sensitivity was improved by selectively filtering out unnecessary portions of the LED emission spectra. Both LEDs have spectrally broad emission characteristics. The CO_2 absorption band near 4.3 µm only accounts for a small portion of the overall CO_2 LED emission profile; the non-resonant emission effectively reduces the sensor sensitivity, since a majority of the CO_2 LED emission is unaffected by the presence of CO_2. Sensor sensitivity is further reduced due to the overlap of the CO_2 absorption band and the reference LED spectrum. Two band-pass filters, CO_2 and reference filters, were employed to restrict the spectral emission of the LEDs. The CO_2 filter, centered at 4.26 µm, only transmits the spectral regions most sensitive to CO_2 absorption. The reference filter, centered at 3.48 µm, transmits spectral regions not sensitive to CO_2 or other interfering signal. The (ca. 10x) increased sensitivity resulting from incorporation of the two LED optical filters is shown in Figure 4. Over the 0 to 2% CO_2 concentration range, the calibration curves indicate about an order of magnitude sensitive enhancement attributable to incorporation of the LED filters. Above 2% CO_2, the measurement sensitivity decreases slightly compared to the lower concentration range, but the sensitivity remains relatively constant up to 5% CO_2 which corresponds to roughly 40% EGR.

Development was started on an EGR probe which will be applicable to a significantly broader range of engine development application due to requiring only single-point access versus the line-of-sight access used in the initial CTC measurement campaign. Specifically, the existing CO_2 sensor requires two-point optical access, pitch and catch, along the beam path. In the April CTC measurement campaign, bulky pitch and catch optics were attached on either side of the intake manifold. This practically limits applications to sampling points external to the engine (e.g., external EGR and intake piping) and to not tightly packaged components. There are many applications such as internal EGR and intake systems, and further developed and highly packaged systems where two-point optical access would be practically impossible. Similar limitations apply to in-cylinder measurements, where clearance and optical access is limited. Figure 5 shows bread-board evaluation and a schematic of the optical EGR probe being developed. Bread-board evaluation has indicated design is capable of measuring the specified 1% EGR

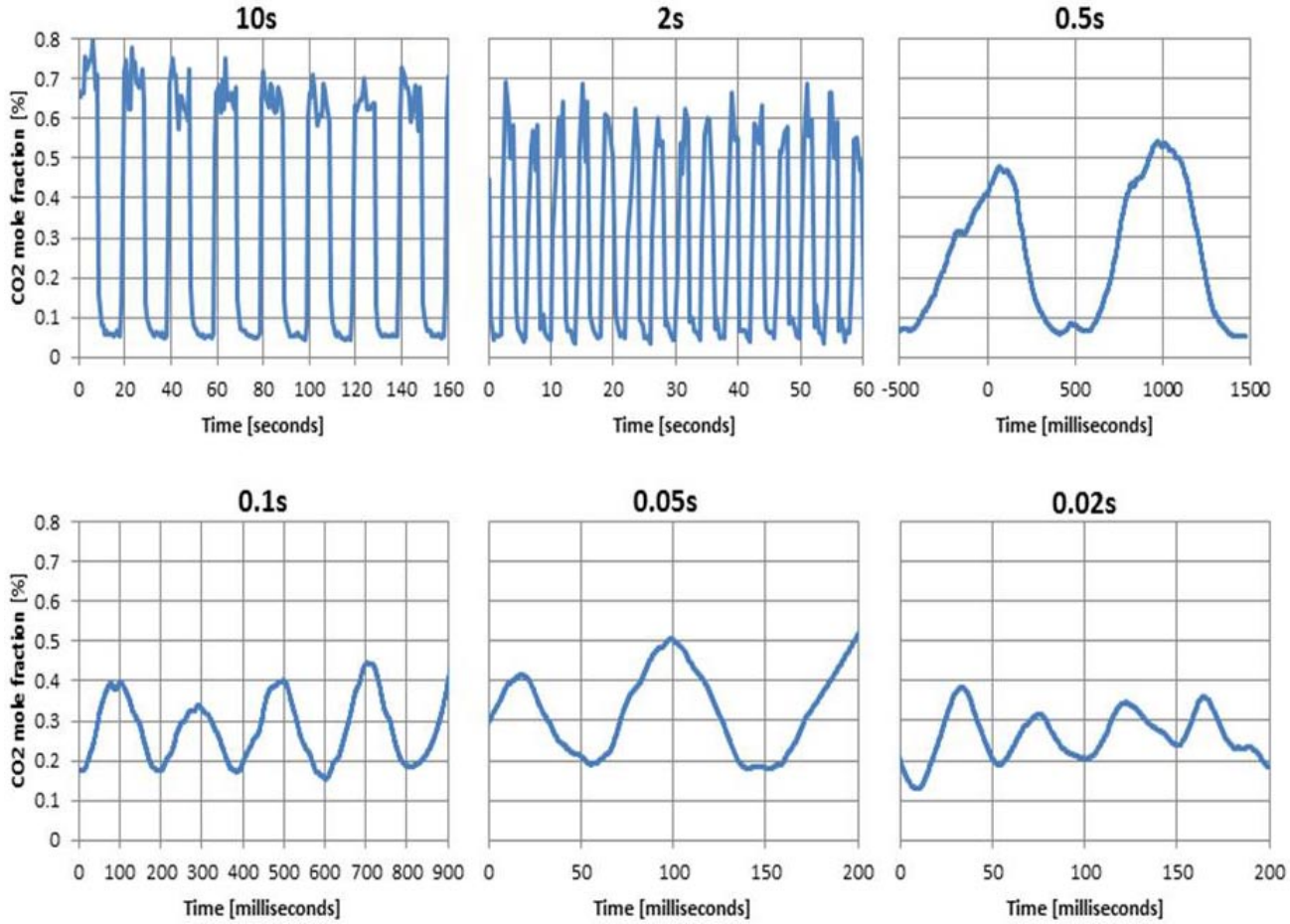

FIGURE 3. Measured CO_2 transients while dithering the EGR valve at various dwell times. For example, 2s indicates EGR valve dithering with 2 s on and 2 s off times.

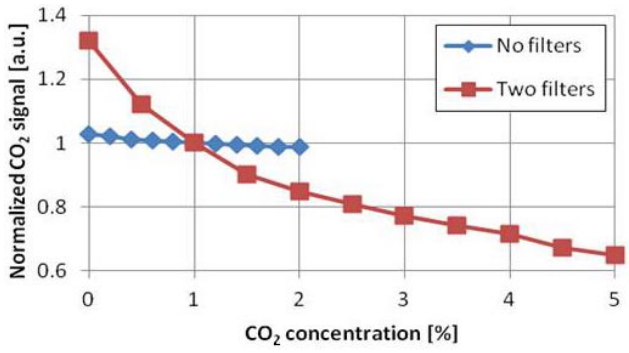

FIGURE 4. Calibration curves showing ca. 10x improvement in EGR-fluctuation sensitivity resulting from incorporating LED emission filters into the diagnostic.

fluctuations, and the actual probe will be evaluated in early FY 2012. In addition to significantly expanding the engine applications, the EGR probe will also allow for simultaneous multi-point measurements in an engine system, and provides an optical access platform applicable to other CRADA diagnostics (e.g., air-to-fuel ratio, O_2, etc.).

Conclusions

- Improved performance of alternative fuel engine system via FiO assessment of various fuel-injector spray patterns.
- Enabled better engine efficiency via tool to quantify EGR uniformity and assess mitigation strategies; specifically, EGR probe capable of resolving 1% EGR fluctuations and millisecond-order response time.

Special Recognitions & Awards/Patents Issued

Awards

The CRADA-developed FiO technology was selected as a winner of the 2011 Federal Laboratory Consortium (FLC) National Award for Excellence in Technology Transfer. The award recognizes outstanding work in the process of transferring a technology developed by a federal

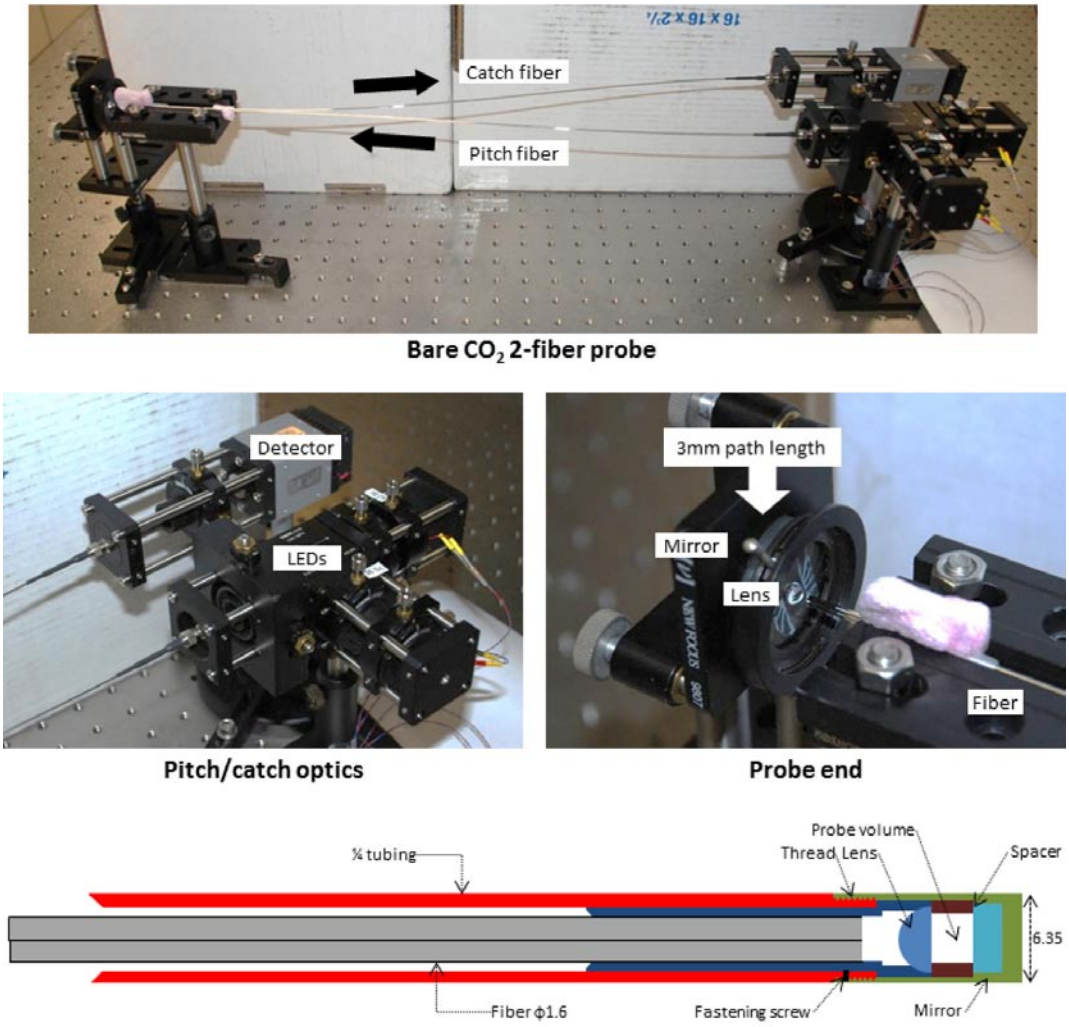

FIGURE 5. Bread-board evaluation and schematic of an optical EGR probe design to allow single-port (vs. line-of-sight) access for broader engine applications.

laboratory to the commercial marketplace. The technology was licensed to and is being commercially developed by Da Vinci Emissions Services.

Patents

U.S. Patent No. 7,839,492 "Laser-Induced Fluorescence Fiber Optic Probe Measurement of Oil Dilution by Fuel," was issued November 23, 2010 to James E. Parks, II and William P. Partridge Jr.. This technology was developed in the Cummins CRADA and has been licensed and is commercially available for Da Vinci Emissions Services, Ltd. (as described in previous reports).

II.A.21 Engine Benchmarking CRADA

Steve McConnell (Argonne National Laboratory),
David Lancaster (General Motors),
Tom Leon (Ford), John Opra (Chrysler)

Argonne National Laboratory
9700 South Cass Avenue
Argonne, Il 60439

United States Council for Automotive Research (USCAR)
1000 Town Center Drive
Suite 300
Southfield, MI 48075

DOE Technology Development Manager:
Gurpreet Singh

Subcontractor:
David Gian (FEV), Auburn Hills, MI

Overall Objectives

- Identify state-of-the-art engine and vehicle technologies currently in production, such as 2-stage lift exhaust valves, advanced turbochargers, spray on engine liners and advanced engine controls.
- Quantify the benefits of the state-of-the-art vehicle technologies currently in production.
- Optimize vehicle performance using advanced vehicle level modeling such as Autonomie® and the performance maps of advanced technologies evaluated in the Cooperative Research and Development Agreement (CRADA).
- Accelerate the development of high efficiency internal combustion engines for light-duty vehicle applications, while meeting the future emission standards, using numerical simulations.
- Support DOE programs with data and analysis of advanced vehicle technologies.

Fiscal Year (FY) 2011 Objectives

- Identified and procured two vehicles with multiple advanced technologies for testing.
- Supplied five data sets from the engine benchmarking data base for USDRIVE goal setting.
- Currently testing two vehicles and evaluating the advanced technologies within each vehicle.

Accomplishments

- Obtained a 2012 Audi A4 with twin variable geometry turbochargers, direct injection and variable valve lift 2.0 liter engine for testing:
  - The vehicle level testing is complete and the vehicle is being torn down for engine level and component testing.
- Obtained a 2012 Mini Cooper with a 1.6 liter turbocharged direct-injected variable valve timing engine:
  - The vehicle level testing is complete and the vehicle will be torn down for engine level and component testing when the engine dynamometer becomes available.
- Supplied vehicle data sets for BMW 530i, Toyota Prius and Toyota Auris to the vehicle systems group for the USDRIVE goal setting exercise.

Future Directions

- Evaluate new technologies such as the Nissan Micra (1.4 liter turbocharged direct-injected engine) and another vehicle to be identified.
- Analyze the new emerging technologies and how they are used.
- Conduct analysis on the new and emerging technologies to determine their maximum fuel saving potential.

Introduction

The goal of the engine benchmarking CRADA is to accelerate the development of high efficiency internal combustion engines for light-duty vehicle applications, while meeting future emission standards, using numerical simulations. The CRADA will support this goal by gathering engine and engine component data for use in DOE's programmatic efforts.

Approach

The CRADA partners continuously research current and future model engines and vehicles with new features to assist the USCAR and laboratory members in selecting vehicles for investigation; a brief one-page summary of published specifications and features for each vehicle under consideration will be provided.

Once procured, the vehicle baseline testing will then be conducted followed by instrumentation and the vehicle level investigation. The vehicle investigation may include electronic control unit mapping to determine calibration settings. The testing will document the engine controller features, inputs and outputs with an electronic control unit analysis report. The powertrain will then be removed from the vehicle and prepared for engine dynamometer testing. The engine, in the as-installed vehicle configuration, would be installed in an engine test cell for full load performance and a full engine map to investigate emission characteristics, fuel consumption, performance and implementation of engine control hardware. As an option, additional motored strip-down engine tests could be conducted to analyze friction losses following the thermodynamic investigations. The final step in the engine investigation will be a detailed design analysis and documentation of all of the engine components. The entire engine will be disassembled and the parts will be documented and described in detail with regard to their function and geometry.

Results

The CRADA partnership was finalized late in the fiscal year. No results have been reported yet. Testing is underway and results will be reported shortly.

Conclusions

The engine and vehicle performance data provided from the engine benchmarking database has already been useful in the USCAR Advanced Combustion and Emission Controls Technical Team goal setting exercises and is currently in use for the USDRIVE programs goal-setting exercises.

II.A.22 Recovery Act: Technology and System Level Demonstration of Highly Efficient and Clean, Diesel-Powered Class 8 Trucks

David Koeberlein
Cummins Inc.
PO Box 3005
Columbus, IN 47201-3005

DOE Technology Development Manager:
Roland Gravel

NETL Project Manager: Ralph Nine

Subcontractors:
- Peterbilt Motors Company, Denton, TX
- Eaton Corporation, Southfield, MI
- Delphi Powertrain Systems, West Henrietta, NY
- Oak Ridge National Laboratory, Oak Ridge, TN
- VanDyne SuperTurbo, Fort Collins, CO
- Modine Manufacturing Company, Racine, WI
- Purdue University, West Lafayette, IN

Objectives

- Objective 1: Engine system demonstration of 50% or greater brake thermal efficiency in a test cell at an operating condition indicative of a vehicle traveling on a level road at 65 mph.
- Objective 2:
  - Tractor-trailer vehicle demonstration of 50% or greater freight efficiency improvement (freight-ton-miles per gallon) over a defined drive cycle utilizing the engine developed in Objective 1.
  - Tractor-trailer vehicle demonstration of 68% or greater freight efficiency improvement (freight-ton-miles per gallon) over a defined 24-hour duty cycle (above drive cycle plus extended idle) representative of real world, line haul applications.
- Objective 3: Technology scoping and demonstration of a 55% brake thermal efficiency engine system. Engine tests, component technologies, and model/analysis will be developed to a sufficient level to validate 55% brake thermal efficiency.

Fiscal Year (FY) 2011 Objectives

- Investigate contributing component designs and technologies to achieving brake thermal efficiency and freight efficiency targets.
- Design and build a vehicle inclusive of waste heat recovery and road load management for early system development.
- Complete design and analysis of advanced transmission and engine; begin procurement.
- Complete design and analysis of vehicle aerodynamic and weight reductions; begin procurement.

Accomplishments

- Achieved engine efficiency, which when waste heat recovery benefits are added in, results in >48% brake thermal efficiency.
- Demonstrated waste heat recovery system improvements, including system simplification with removal of magnetic coupling and a closed oil management system.
- Completed design and analysis for a higher cylinder pressure capability, low pump parasitic engine.
- Baseline vehicle freight efficiency testing completed over defined, repeatable drive cycle route.
- Completed design and analysis of tractor-trailer baseline aerodynamics and developed new concepts to attain >14% freight efficiency improvement. Began hardware fabrication.
- Completed design study of tractor-trailer weight reduction opportunities resulting in >3% freight efficiency improvement.
- Completed design for advanced heavy-duty transmission.
- A solid oxide fuel cell idle management system was designed into the truck chassis and electrical systems. The driver communication interface has been interlaced within the vehicle network and truck display systems.

Future Directions

- Complete demonstration of 50% thermal efficient engine.
- Complete the build and development testing of the 50% freight efficiency demonstration vehicle.

✧ ✧ ✧ ✧ ✧

Introduction

Cummins Inc. is engaged in developing and demonstrating advanced diesel engine technologies to significantly improve the engine thermal efficiency while meeting U.S. Environmental Protection Agency 2010 emissions. Peterbilt Motors is engaged in the design and manufacturing of heavy-duty class 8 trucks.

Together, Cummins and Peterbilt provide a comprehensive approach to achievement of a 68% or greater increase in vehicle freight efficiency over a 24-hour operating cycle. The integrated vehicle demonstration includes a highly efficient and clean diesel engine with 50% or greater brake thermal efficiency including advanced waste heat recovery, aerodynamic Peterbilt tractor-trailer combination, reduced rolling resistance tire technology, advanced transmission, and an efficient solid oxide fuel cell auxiliary power unit for idle management. In order to maximize fuel efficiency, each aspect associated with the energy consumption of a Class 8 tractor/trailer vehicle will be addressed through the development and integration of advanced technologies.

In addition, Cummins will scope and demonstrate evolutionary and innovative technologies for a 55% brake thermal efficient engine system.

Approach

Cummins and Peterbilt's approach to these project objectives emphasizes an analysis-led design process in nearly all aspects of the research. Emphasis is placed on modeling and simulation results to lead to attractive feasible solutions. Vehicle simulation modeling is used to evaluate freight efficiency improvement technologies. Technologies are evaluated individually along with combination effects resulting in our path to target measure of project status and for setting project direction.

Data, experience, and information gained throughout the research exercise will be applied wherever possible to the final commercial products. We continue to follow this cost-effective, analysis-led approach both in research agreements with the Department of Energy as well as in commercial product development. We believe this common approach to research effectively shares risks and results.

Results

A vehicle powertrain system analysis was used to outline a path to target for the freight efficiency improvement. The path to target study involved an analysis of the various powertrain component changes, including both hardware and control algorithms, and their freight efficiency impact. This analysis was conducted using the Powertrain System Analysis Toolkit with the application of map-based models for the various sub-components. Figure 1 shows the path to target roadmap for both the drive cycle 50% improvement and 68% improvement on the 24-hour cycle. Path to target analysis is an on-going effort that seeks to increase accuracy and fidelity of expected vehicle performance as new component data is verified.

The baseline truck fuel economy and freight efficiency testing was completed. The drive cycle route is 311 miles in length, with approximately 550 feet of elevation change over the route course and eight controlled stop/starts are included. The round trip route

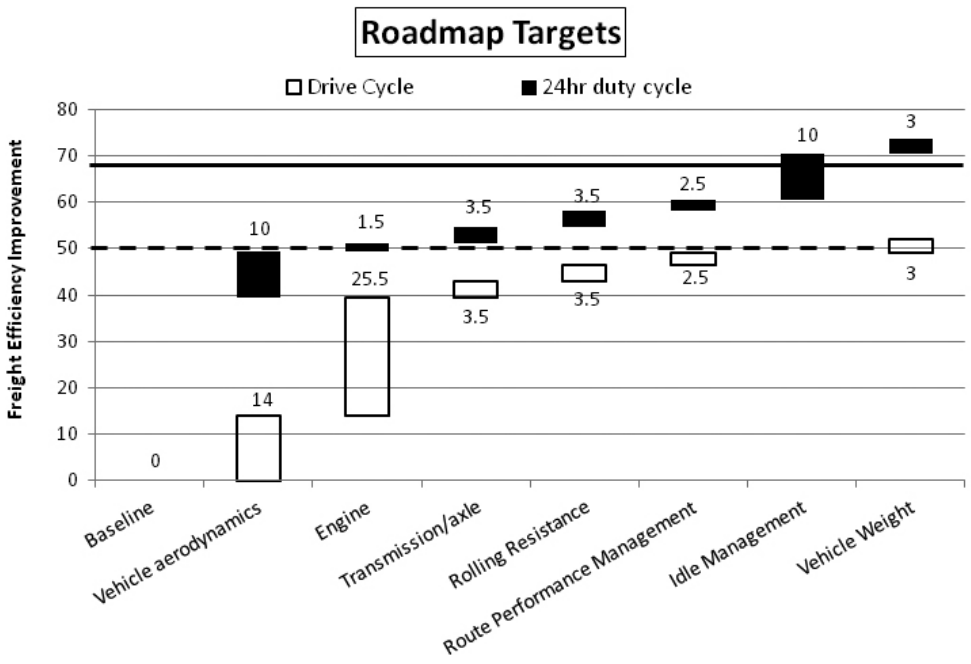

FIGURE 1. Freight Efficiency Roadmap Targets

starts northwest of Fort Worth, Texas, on a northwest route toward Vernon, Texas.

A comparison study of the baseline vehicle fuel economy test results over the SuperTruck test route was found to be within 2.5% of the simulated value. This 2.5% difference between measurement and simulation is considered very good, given the various sources of uncertainty associated with driver behavior modeling, aftertreatment thermal management and route simulation accuracy.

An exhaust gas recirculation engine architecture combined with high efficiency selective catalytic reactor aftertreatment and waste heat recovery has been selected for our 50% brake thermal efficiency engine and vehicle demonstrations. Maturation of the specific engine components and their specifications is on-going work.

A fully functional waste heat recovery vehicle has been built. This vehicle has a uniquely designed vehicle cooling system module with sized components for drive cycle efficiency gains. The functional vehicle allows for system model verification and development toward maximization of recovery capacity. Component and engine system integration development continues in parallel with vehicle level activities.

An aerodynamic drag improvement over the baseline tractor/trailer combination of 40% has been shown with a full tractor/trailer aerodynamic computational fluid dynamics analysis. Procurement of these first generation aerodynamic devices is underway. Decision analysis considers aerodynamic device mass, performance and complexity, as the project transitions from concept to demonstration design and hardware.

Conclusions

The SuperTruck Engine and Vehicle System Level Demonstration of Highly Efficient and Clean, Diesel-Powered Class 8 Truck project has successfully completed the first year of the four-year duration. The following conclusions have come from the first year:

- Vehicle powertrain system analysis shows the path to achievement of project freight efficiency goals.
- Baseline truck freight efficiency test results are within 2.5% of analytical predictions.
- Exhaust gas recirculation engine architecture with high efficiency selective catalytic reactor aftertreatment and waste heat recovery has been selected.
- A fully functional waste heat recovery equipped vehicle with specific cooling module has been built.
- Analysis results show a 40% aerodynamic drag improvement over the baseline tractor/trailer combination.

FY 2011 Publications/Presentations

Journal Publications

1. Lyle Kocher, Ed Koeberlein, Dan Van Alstine, Karla Stricker, and Gregory M. Shaver, *Physically-Based Volumetric Efficiency Model for Diesel Engines Utilizing Variable Intake Valve Actuation*, Accepted (August 2011), to appear in: International Journal of Engine Research.

Conference Papers and Presentations

1. Lyle Kocher, Ed Koeberlein, Karla Stricker, Daniel Van Alstine, and Gregory M. Shaver, *Control-Oriented Modeling of Diesel Engine Gas Exchange*, 2011 American Control Conference.

2. Ed Koeberlein, Lyle Kocher, Daniel Van Alstine, Karla Stricker, and Gregory M. Shaver, *Physics-based Control-Oriented Modeling of Exhaust Gas Enthalpy for Engines Utilizing Variable Valve Actuation*, 2011 Dynamic Systems and Control Conference.

3. Karla Stricker, Lyle Kocher, Ed Koeberlein, Daniel Van Alstine, and Gregory M. Shaver, *Turbocharger Map Reduction for Control-Oriented Modeling*, 2011 Dynamics Systems and Control Conference.

4. Lyle Kocher, Ed Koeberlein, Daniel Van Alstine, Karla Stricker, and Gregory M. Shaver, *Physically-Based Volumetric Efficiency Model for Diesel Engines Utilizing Variable Intake Valve Actuation*, 2011 Dynamics Systems and Control Conference.

5. David Koeberlein, *Cummins SuperTruck Program, Technology Demonstration of Highly Efficient Clean, Diesel Powered Class 8 Trucks,* 2011 DEER conference.

II.A.23 Recovery Act: Systems Level Technology Development and Integration for Efficient Class 8 Trucks

Derek Rotz
Daimler Trucks North America
4747 North Channel Avenue
MailCode: POC-AE
Portland, OR 97217

Kevin Sisken
Detroit Diesel Corporation
HPC A-08
13400 Outer Drive West
Detroit, MI 48239-4001

DOE Technology Development Manager:
Roland Gravel

NETL Project Manager: Carl Maronde

Overall Objectives

- Demonstration of a 50% total increase in vehicle freight efficiency measured in ton-miles per gallon (at least 20% improvement through the development of a heavy-duty diesel engine).
- Development of a heavy-duty diesel engine capable of achieving 50% brake thermal efficiency on a dynamometer under a load representative of road load.
- Identify key pathways through modeling and analysis to achieving a 55% brake thermal efficient heavy-duty diesel engine.

Fiscal Year (FY) 2011 Objectives

- Phase 2: Comprehensively analyze efficiency potential across all vehicle systems to define major system specification and down-select technologies.
- Screen engine technologies through detailed cycle simulation at boundary conditions representative of SuperTruck operation. Optimize turbocharging and aftertreatment for efficiency gains while maintaining emissions. Evaluate and develop waste heat recovery technologies of turbo-compounding and Rankine heat engine. Investigate reductions in parasitics. Finalize engine power rating and displacement.

Accomplishments

- Phase 1:
  - Completed drive cycle tests with the baseline vehicle configuration.
  - Developed roadmap of vehicle efficiency metrics needed to achieve 50% vehicle freight efficiency, based on vehicle-level efficiency simulation and analysis.
  - Developed roadmap for 50% engine thermal efficiency at road load.
  - Conducted air system and turbo-matching simulations at multiple engine-out emission levels.
  - Developed model-based engine controller concept with on-board fuel efficiency optimization.
  - Developed a model for the exhaust and exhaust gas recirculation (EGR)-driven Rankine heat engine.
- Phase 2:
  - Specified major vehicle components based on theoretical analysis to be included in SuperTruck, including engine displacement/rating, transmission, hybrid architecture, drivetrain components, vehicle auxiliary systems and lightweight chassis.
  - Completed analytical work leading to a finalized engine torque curve.
  - Evaluated fuel efficiency potential of optimized engine controller.
  - Initiated dynamometer testing of targeted SuperTruck engine.
  - Investigated fuel economy potential of clutched air compressor and low friction piston kit.
  - Initiated test stand build for a Rankine cycle-based waste heat recovery system.
  - Simulated benefits of turbo-compounding with targeted SuperTruck engine.
  - Design of a high efficiency aftertreatment device.

Future Directions

- Phase 3:
  - Build and test prototype vehicle and engine systems for empirical measurement of efficiency improvement.
- Phase 4:
  - Optimize vehicle systems to reach efficiency targets including SuperTruck integration.
  - Optimize engine systems and demonstrate 50% brake thermal efficiency.

- Phase 5:
  - Build and test final SuperTruck vehicle to demonstrate 50% vehicle freight efficiency.

Introduction

SuperTruck is a five-year research and development project with a focus on improving diesel engine and vehicle efficiencies. The objective is to develop and demonstrate a Class 8, long-haul tractor-trailer which achieves a 50% vehicle freight efficiency improvement (measured in ton-miles per gallon) over a best-in-class 2009 baseline vehicle. The engine for the SuperTruck program will deliver 50% brake thermal efficiency.

Approach

In FY 2011, SuperTruck entered the second phase of the project. The approach used in Phase 2 of the project has primarily centered on system analysis through the use of modeling and simulation, bench testing and on-road vehicle tests (Table 1). Vehicle efficiency simulation software, Autonomie, was used for determining the optimal engine, powertrain and drivetrain specification, including engine rating, transmission/axle gear ratio sets, driveline efficiencies and rolling resistance. External aerodynamics and vehicle cooling systems have been analyzed through the use of one-dimensional thermodynamics and three-dimensional fluid dynamic modeling in addition to the use of scale model wind tunnel testing. Finite element analysis software has been used in the design of load optimized chassis design with lightweight materials with subsequent testing both in bench tests and on-vehicle.

The approach for the engine development in Phase 2 consisted of both testing and engine simulations to evaluate various technology pathways. Separate models for waste heat recovery and aftertreatment systems were used to size and optimize components for procurement. Some of the parasitic reduction measures were tested on component dynamometer.

TABLE 1. Specification Status of Vehicle Systems, Phase 2 Status

SuperTruck Vehicle Systems	Specification Status
Engine Displacement and Rating	complete
Transmission	complete
Hybrid Architecture	complete
Axles	complete
Wheels/Tires	complete
External Aerodynamics	on-going
Vehicle Cooling	on-going
Idle Reduction	on-going
Lightweight Chassis	complete
Lightweight Cab	on-going
A/C, Cab Thermal	on-going
Vehicle Parasitic Loads	complete
Intelligent Controls	on-going
Driver Coaching/Efficient Operations	on-going

Results

To date, the SuperTruck project is on track towards reaching the 50% freight efficiency target. A roadmap of vehicle systems and their performance targets exists which cascade to the system level. Progress on each vehicle system has been gauged and numerous systems have been specified based on the analysis conducted to date (see Figure 1). Work continues toward the specification of the remaining systems, followed by the buildup and testing of system prototypes.

Engine, powertrain and drivetrain analysis was conducted to determine the optimal specification to meet the efficiency targets while maintaining comparable driving performance. Various hybrid configurations were qualitatively evaluated to determine the preferred architecture which balances the desired functionality, performance and weight. Load optimized chassis designs were investigated to minimize the material and weight requirements and to determine the applicability of lighter weight materials. Basic shape analysis continues, using scale model wind tunnels and computational fluid dynamics simulation to determine an optimal aerodynamic shape that minimizes the drag force, while accommodating adequate cooling systems and providing an adequate envelope for vehicle packaging. Two idle reduction solutions are also under consideration that provides adequate climate control in

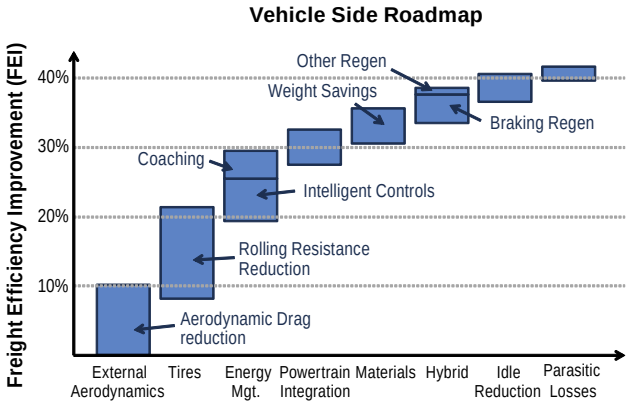

FIGURE 1. Vehicle Technologies Roadmap

summer and winter modes. The vehicle parasitic loads were analyzed and modeled to determine the baseline power consumption and to develop system models for power reduction.

Engine cycle simulation focused on turbocharger matching for optimum boost and EGR levels yielding a higher engine-out oxides of nitrogen (NOx) calibration that will be coupled with a high efficiency aftertreatment, resulting in a significant gain in engine thermal efficiency. Engine cycle simulations with an electric turbo-compounder also demonstrated fuel economy benefits. Next steps include matching of the overall engine system. In parallel, engine testing was conducted with varying combustion parameters. Engine sizing and rating studies were conducted using route fuel economy analysis software.

Model-based engine control logic was tested under transient operating conditions representative of SuperTruck routes. The evaluation showed measurable fuel efficiency improvement potential over the baseline controller. With regards to waste heat recovery, Rankine heat engine components were sized and optimized so that they can be procured for the test stand. The test stand build is in process and is expected to be completed soon. A high efficiency, reduced backpressure aftertreatment device was designed to match with higher engine-out NOx emissions while maintaining Environmental Protection Agency 2010 level tailpipe emissions and this system will be tested shortly. In the area of parasitics reduction, benefits of a clutched air compressor and a low friction piston kit were evaluated on component dynamometer.

Conclusions

The analysis provides a technology path that when implemented and tested will demonstrate the overall 50% freight efficiency target and 50% engine brake thermal efficiency. The SuperTruck project is on track towards reaching that goal and the vehicle specification is scheduled to be defined at the end of Phase 2 in the first quarter of 2012. Similarly, engine sub-system specifications are being defined and components procured to be tested at system level prior to the overall integration of technologies for meeting the overall goal of 50% brake thermal efficiency.

FY 2011 Publications/Presentations

1. Sisken, Kevin: “Super Truck Program: Engine Project Review Recovery Act –Class 8 Truck Freight Efficiency Improvement Project”, Project ID:ACE058, DOE Annual Merit Review, May 12, 2011.

2. Rotz, Derek: “Super Truck Program: Vehicle Project Review Recovery Act –Class 8 Truck Freight Efficiency Improvement Project”, Project ID ARRAVT080, DOE Annual Merit Review, May 12, 2011.

3. Singh, Sandeep: “Exhaust Heat Driven Rankine Cycle for a Heavy Duty Diesel Engine”, Project ID:ACE058, DOE DEER Conference, October 5th, 2011.

4. Sisken, Kevin: “Super Truck -- 50% Improvement In Class 8 Freight Efficiency”, Project ID:ACE058, DOE DEER Conference, October 5th, 2011.

II.A.24 Development and Demonstration of a Fuel-Efficient Class 8 Tractor and Trailer

Dennis Jadin (Primary Contact),
Willy De Ojeda
Director, Advanced Vehicle Technologies
Navistar, Inc.
2601 Navistar Drive
Lisle, IL 60532

DOE Technology Development Manager:
Roland Gravel

NETL Project Manager: Ralph Nine

Subcontractors:
- Bosch, Farmington Hills, MI
- Behr America, Troy, MI
- Federal-Mogul, Ann Arbor, MI
- Argonne National Laboratory, Argonne, IL
- Wisconsin Engine Research Center, Madison, WI

Overall Objectives

- Demonstrate engine brake thermal efficiency (BTE) improvements which contribute 20% (of the total 50% required) improvement in the freight efficiency of a combination tractor-trailer as a part of the DOE SuperTruck Program.
- Demonstrate a BTE target of 50% at an engine operational point which corresponds to an on-road driving condition of 65 mph.
- Demonstrate a path towards achieving a peak BTE target of 55%.

Fiscal Year (FY) 2011 (Phase 1) Objectives

- Build and calibrate a comprehensive engine simulation model for the evaluation of overall engine performance with detail engine subs-systems (combustion, turbocharger, exhaust gas recirculation [EGR], fuel and aftertreatment).
- Build and exercise an engine combustion model to help guide the selection of the engine compression ratio, combustion chamber profile, EGR rate, boost, and fuel injection rate.
- Extend the combustion simulation to investigate the use of reactivity controlled combustion as a building block to meet the 55% BTE stretch target.
- Explore waste heat recovery configurations (varying sources of heat, working fluids, choice of system components etc.).
- Assemble prototype engines using the results of the simulations and modeling exercises to evaluate and develop performance of the various subsystems.

Accomplishments

- Built and validated a comprehensive engine simulation model for the Maxxforce 13 diesel engine using GT-POWER that incorporated advanced components such as variable valve actuation (VVA), turbocompounding (TUCO), and Rankine cycle.
- Built an engine combustion model using KIVA that helped improve combustion matching with improved fuel efficiency and reduced soot emissions.
- Built multiple prototype engines to validate the performance of individual subsystems:
  - A dedicated engine at Bosch houses a fuel injection system with higher injection pressures (2,900 bar). Tests have mapped out the effect of the increased injection pressure in combination with other combustion parameters.
  - A dedicated engine at Navistar has mapped out combustion and emissions impact across a range of engine-out oxides of nitrogen (NOx). Tests have been performed with high-injection pressure (up to 2,900 bar), optimized combustion system, and increased peak cylinder pressure (up to 220 bar).
  - A second engine at Navistar was dedicated to evaluate the first generation electric TUCO system consisting of high efficiency turbochargers, electric turbo generator and power electronics.
  - An engine has been sent to Federal-Mogul for systematic friction testing and evaluation of friction reduction technologies and improved engine accessories.
- Navistar, Bosch and Argonne have closely collaborated to adapt the Maxxforce 13 engine to run with multiple fuels to demonstrate the path towards 55% BTE. The engine is currently installed at the Argonne facility.

Future Directions

The criterion for proceeding to Phase II is that the combination of subsystem improvements demonstrate a path to meet 50% BTE. The modeling shows this target to be within reach. The early deployment of combustion and TUCO has tracked the forecasted 47% BTE. The

next phase will introduce the flexible valve train, friction reduction and Rankine technologies with expectation to attain the 50% BTE target. Modeling will continue on the fuel reactivity and this dedicated engine will undergo its first tests towards the 55% BTE target.

Introduction

The overall goal of the DOE-supported SuperTruck Program is to demonstrate a 50% improvement in freight efficiency (measured in ton-miles/gallon) of a combination tractor-trailer. Truck efficiency improvements will come from improvement to both the engine and the vehicle, the project objectives state that 20% of the overall 50% improvement is to be gained through engine improvements.

A target has been established for the BTE of the engine in isolation. This target is 50% which is an 8 percentage point improvement from the current benchmark of 42% attained at an engine operating point equivalent to a 65 mph truck speed. An additional goal of the project is to demonstrate a path towards 55% BTE.

Approach

In order to optimize the tradeoffs in technologies to be examined Navistar will use analytical tools to guide the process of technology selection and their combination. The success of the project will require the combination of cost containment, robustness, and reduced weight with improved engine thermal efficiency. The approach aims at low engine-out NOx emissions. Particulate matter will be controlled by use of a diesel particulate filter.

Technologies to be examined include:

- Increased fuel injection pressure.
- Optimized combustion strategies.
- Improved aftertreatment systems.
- Control strategies.
- Low-friction components and accessories.
- Advanced air handling.
- Improved thermal management including waste heat recovery.

Results

Engine Modeling and Simulation

The engine team completed a comprehensive engine model that encompasses the engine and engine technologies investigated in the project. The study yielded the roadmap illustrated in Figure 1 towards 50% BTE. This includes combustion and aftertreatment, TUCO, VVA with improved turbocharger system, friction reduction and the Rankine cycle. The simulation is helpful in understanding the interactions and optimum combination of the proposed technologies. Figure 1 also shows the engine testing progress to date, which includes combustion and TUCO, attaining 47% BTE at the road-load condition. Engines with 50% BTE are expected to be installed on the vehicle demonstrator at the end of 2013, with a final dynamometer steady-state and transient emissions certification at the end of 2014.

Combustion Simulation

A design-of-experiments model using KIVA-3v coupled to a GT-POWER cycle simulation was used to provide combustion chamber and fuel injection nozzle geometries and injection strategies to maximize BTE across a broad range of compression ratios. Figure 2

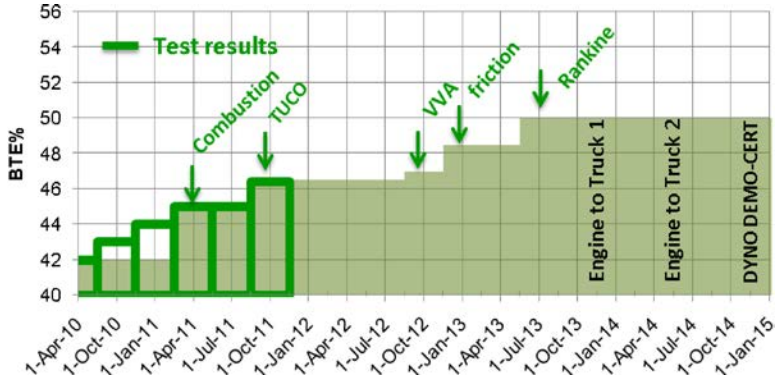

FIGURE 1. BTE Roadmap and Progress to Date at the Road Load Condition

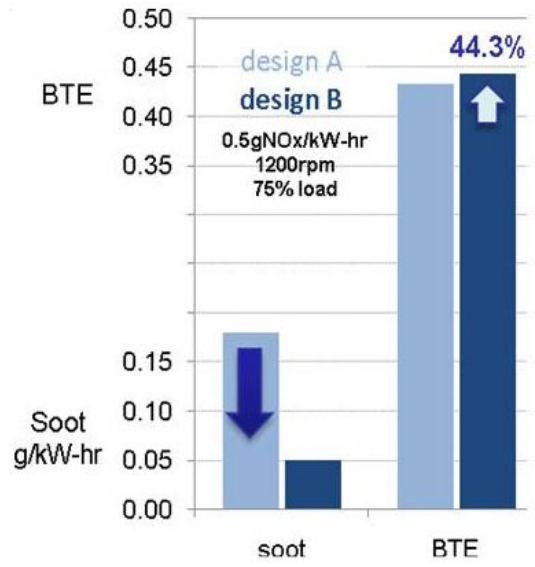

FIGURE 2. Engine Test Results of New Combustion System

shows the impact of the simulation proposal (design B) in engine tests over the baseline (design A). Tests showed the new design reduced soot over 70% while attaining better BTE.

Injection Pressure

Figure 3 illustrates the impact of raising injection pressure from the current 2,200 bar max level to 2,900 bar hardware provided by Bosch. The results show a consistent improvement in BTE and soot as pressure is raised across the engine map as illustrated by points A75 (1,200 rpm – 75% load), B50 (1,500 rpm – 50% load), and C100 (1,800 rpm – 100% load).

VVA

Modeling of the thermodynamic effects alone show that VVA is effective across a wide range of engine-out NOx to raise the BTE as it improves the turbo-matching across engine speeds. The impact on BTE and air-to-fuel ratio (and lambda) is exemplified in Figure 4 at same points as above as the intake valve closing (IVC) is advanced. Current efforts are focused in extending the gains of B and C speeds to the lower A speed.

Friction

It is expected that 1.5% BTE points will be attained by combination of power cylinder, power transfer and accessory improvements.

Waste Heat Management

The first generation TUCO was validated in engine testing (shown earlier in Figure 1), and the current results are being used to configure the second generation

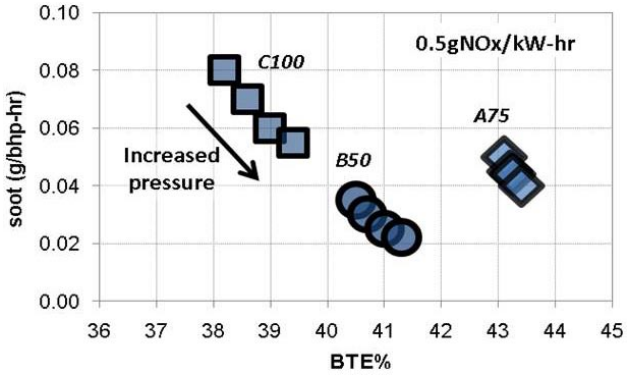

FIGURE 3. BTE and Soot Improvements with High Injection Pressure

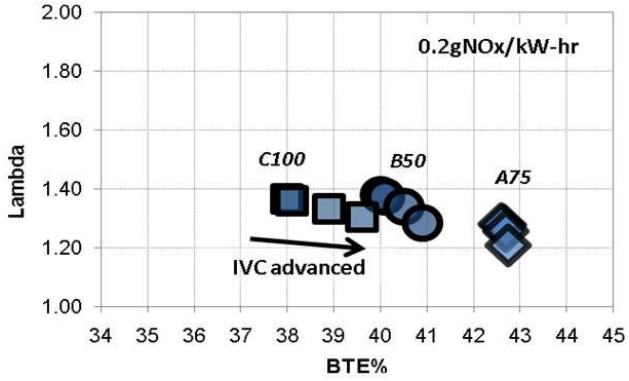

FIGURE 4. BTE Improvements and Impact on Air System with VVA

hardware. The first project phase was also used to consider multiple Rankine cycle configurations. Future activities will be focused on the final concept selection and kick-off of design and procurement.

Dual Fuel Simulation

With collaboration of the Wisconsin Engine Research Center, the combustion modeling has been extended to fuel reactivity controlled combustion to evaluate thermal efficiency/emission improvements. Simulation has shown that 55% BTE target is feasible by leveraging fuel reactivity to run lean and homogenous at a higher compression ratio.

Conclusions

The Phase 1 activities have demonstrated an improvement in the efficiency of the base engine from 42% to 47% by combustion system improvements and the implementation of electrical TUCO. The work will continue into Phase 2 with the expectation to integrate a flexible valve train and friction reduction components. The work will be followed by implementation of a Rankine cycle to extract heat from the EGR circuit. Work to date indicates that the 50% BTE target is achievable.

FY 2011 Publications/Presentations

1. Directions in Engine-Efficiency and Emissions Research (DEER), October 3, 2011, Detroit, MI.

2. Annual Merit Review, USDOE, May 12, 2011, Washington, D.C.

3. Commercial Vehicle Innovation Summit (CVIS), September 27, 2011, Washington, D.C.

4. High Efficiency Heavy Duty Vehicles Symposium, November 30, 2011, Troy, MI.

II.A.25 Gasoline Ultra-Efficient Fuel Vehicle with Advanced Low-Temperature Combustion

Keith Confer (Primary Contact), Harry Husted, Mark Sellnau
Delphi
3000 University Drive
Auburn Hills, MI 48326

DOE Technology Development Manager:
Ken Howden

NETL Project Manager: Ralph Nine

Subcontractors:
- John Juriga, Hyundai America Technical Center, Inc., Superior Township, MI
- Dr. Rolf Reitz, Wisconsin Engine Research Consultants, LLC, Madison, WI
- Dr. Ming-Chia Lai, Wayne State University, Detroit, MI

Objectives

- Develop, implement and demonstrate fuel consumption reduction technologies using a new low-temperature combustion process; gasoline direct injection compression ignition (GDCI).
- Refine and demonstrate several near-term fuel consumption reduction technologies including advanced valvetrain and parasitic loss reduction.
- Design and build engine hardware required.
- Develop engine controls strategies.
- Demonstrate benefits of new hardware and refined engine operation.

Fiscal Year (FY) 2011 Objectives

- Design and build Phase 1 hardware (start cart, dyno engine, three vehicles).
- Bench test Phase 1 hardware and algorithms.
- Complete testing of homogeneous charge compression ignition (HCCI).
- Initial mapping of GDCI operation using single cylinder engine.
- Design Phase 2 multi-cylinder engine hardware.

Accomplishments

- Completion of Phase 1 content controls algorithm and software development on the hardware-in-the-loop bench and on the start cart development engine.
- Integration and demonstration of fuel economy improvement with exhaust heat recovery system which shortens oil warm-up time leading to reduced friction and better fuel economy during the Federal Test Procedure (FTP)75 drive cycle.
- Test and performance validation of camshaft roller bearing application. Maximum friction improvement was recorded below 2,500 engine rpm range which will reflect in improved fuel economy in the FTP75 drive cycle.
- Design and build completed for the following project specific hardware (see Figure 1):
  - Gasoline direct injection fuel injectors, fuel pump and fuel rail,
  - Advanced valvetrain cylinder head with 2-step valve lift and electric cam phasing.
  - Cooled external exhaust gas recirculation system.
  - Belt alternator starter system for start stop operation.
  - Engine controller, engine management system and engine harness.
  - Exhaust heat recovery system (oil warm up).
  - Rollerized cranktrain and camtrain systems.
- Completion of Phase 1 calibration dyno engine and Phase 1 vehicle integration of project specific hardware (see Figure 2 and Figure 3).
- Completed testing of HCCI multi-cylinder dyno engine.

FIGURE 1. Phase 1 Start Cart Engine

FIGURE 2. One of the Three Phase 1 Vehicles

FIGURE 3. Phase 1 Engine with Project Specific Hardware

- Detailed FIRE and KIVA simulations were performed to develop the fuel injection, mixing, and combustion processes for GDCI.
- Advanced fuel injector development is underway with needed spray characteristics to produce in-cylinder stratification for low oxides of nitrogen (NOx), low particulate matter (PM), and low combustion noise using Research Octane Number (RON)-91 gasoline with low injection pressures. Initial results showed indicated efficiency was 9.5% lower than the same engine operating with diesel fuel. Indicated specific CO_2 emissions were 14 percent lower.
- Advanced valvetrain systems are under development to provide the lift profiles and fast response necessary for full-time GDCI over a wide operating range.
- A new GDCI multi-cylinder engine was designed with a peak cylinder pressure rating of 200 bar. The cylinder heads were designed to include a unique GDCI combustion chamber, central injection and high compression ratio, and continuously-variable rollerized valvetrain. GDCI pistons with unique bowl characteristics were also designed. The block design includes new crankshaft, bedplate, bearings, connecting rods, and liners. Detailed thermo-structural analyses were performed on all components. Fabrication is underway for these engine components.
- The GDCI engine system mechanization was established and engine controls activity launched.

Future Directions

- Debug Phase 1 hardware and controls.
- Calibrate Phase 1 vehicles.
- Test Phase 1 technologies.
- Build and debug Phase 2 multi-cylinder engine.
- Develop GDCI engine control system.
- Continue single-cylinder engine tests and detailed FIRE and KIVA simulations to refine the combustion process and component designs.

Introduction

This project will develop, implement and demonstrate fuel consumption reduction technologies which are focused on improvement of thermal efficiency from in-cylinder combustion complemented by a reduction of friction and parasitic losses.

The investigation includes extensive simulation efforts combined with bench, engine and vehicle testing in a comprehensive four-year project conducted in two phases. The conclusion of each phase is marked by an on-vehicle technology demonstration.

The single largest gain in fuel economy will come from development and demonstration of a breakthrough low-temperature combustion scheme called GDCI to be developed in Phase II of the project. Limited initial steady-state dynamometer testing of this new combustion scheme showed that thermal efficiencies can be greater for GDCI combustion than for diesel combustion. During the project substantial development work will be done in the areas of combustion control, base engine design, fuel system design and valve train design to fully validate and reduce to practice a combustion scheme implementing GDCI in a gasoline engine which is suitable for mass production. Phase 2 development work will span the full four years of this project.

Phase 1 concentrates on nearer term technologies to reduce friction and parasitic losses. The on-vehicle implementation of these technologies will be performed using a systems engineering approach to optimize the

collective value of the technologies. The duration of Phase I will be two years.

Approach

Phase 1 technologies have been divided into two demonstration vehicles and one development vehicle. The development vehicle as well as several bench test rigs and three dyno engines were used to develop the Phase 1 technologies which will be tested and demonstrated on two vehicles. These two vehicles will be equipped with different Phase 1 technologies and hardware.

For Phase 2 a wide range of analytical and experimental tools were assembled within small expert teams. Detailed FIRE and KIVA simulations were used with spray chamber tests of real injectors. Single-cylinder engine tests using the design of experiment method were combined with response surface modeling using Mathworks model-based control software. Custom combustion analysis macros were developed to quickly process large amounts test data. GT-POWER was used to develop efficient boost systems. Multiple analysis tools were used for base engine and component development including coolant flow computational fluid dynamics, thermo-structural analysis, and fatigue analysis. Controls-oriented models of the total engine system were developed to begin co-simulation of transient engine characteristics.

Results

Phase 1

Integration and implementation of the Phase 1 controls systems content has been completed with tryout and debugging activities in process. Initial testing of the 14-V battery-aided start micro hybrid system has demonstrated the ability of the system to restart the engine when driven on the FTP75 test schedule using the production valvetrain system. Further testing with the new valvetrain configuration has presented additional restart difficulties with the higher compression efforts due to earlier valve closing timing. Expectations remain positive on the ability of the battery-aided start system to meet the projected fuel economy improvement targets for Phase 1.

Rollerization of the crankshaft development involved replacing hydrodynamic bearings with needle roller bearings. The crankshaft main and connecting rod big-end bearings are now needle roller bearings. This helped reduced engine friction <2,500 rpm leading to ~4% fuel economy improvement on the Hyundai America Technical Center, Inc. 5-point specific fuel consumption map. However, due to the nature of the cranktrain kinematics, non-uniform velocity leads to higher friction and poor high-speed performance of the rollerized crank. Additionally, high speed durability runs performed at 5,000 rpm wide-open throttle caused high loading on the needle roller bearing cages leading to premature failures.

Additional rollerization efforts are focused on the camshaft support bearings. All development work to measure friction improvement has been successfully completed with results showing improvement in friction <2,500 rpm compared to plain hydrodynamic bearings with no subsequent degradation of friction at higher speeds.

Phase 2

HCCI

Tests of the HCCI combustion process has verified very limited usable speed load range. The results for the GDCI combustion process has on the other hand shown that GDCI will operate over a wide speed load range. Based on these results, the HCCI development work has been wrapped up as the final plan for the Phase 2 vehicle is to use GDCI over the entire speed load range of operation.

Injection Strategies

Extensive simulations and start cart engine tests were performed for various late injection strategies involving single injection, double injection, and triple injection strategies (among other premixed-direct injection strategies). It was demonstrated that triple injection could be used to stratify the mixture both regionally in the combustion chamber and locally near the spray plume. Triple injection produced the lowest fuel consumption at the lowest injection pressure, while meeting targets for NOx, smoke, and noise (see Figure 4).

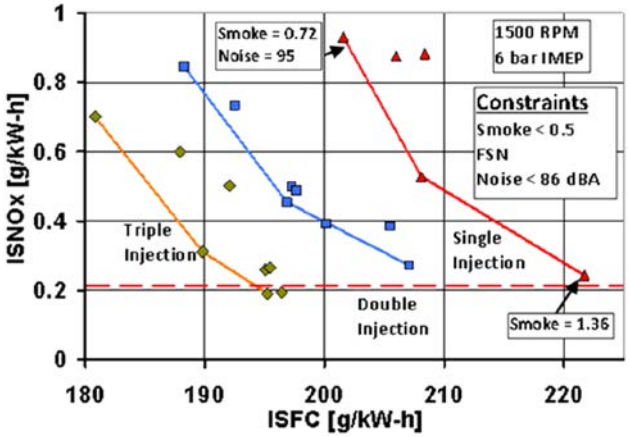

FIGURE 4. Indicated Specific NOx as a function of Indicated Specific Fuel Consumption for GDCI Three Injection Strategies

Injector Development

Four injector designs were fabricated and tested on a single-cylinder Hydra engine. Improved spray characteristics and injection rate helped reduce indicated specific fuel consumption while also lowering injection pressure requirements. Burn duration (10-90 crank angle degrees) could be increased to effectively control heat release rate and noise levels. The latest injector builds exhibited very low smoke while meeting emissions and noise constraints.

GDCI Operation

From the single-cylinder GDCI engine work, fuel consumption and noise levels show trends similar to diesel, however injection pressures are reasonably low. NOx and smoke emissions are very low. Depending on transient and cold-start emissions, aftertreatment for NOx and smoke may not be needed. Hydrocarbon and CO emissions are above targets, and while lower levels are expected, an oxidation catalyst will likely be needed.

Conclusions

Phase 1

- The application range of 14-V battery-aided start micro hybrid system shows promise to be extended to 2.4-L 4-cylinder engines whereas it was previously limited to 1.6-L 4-cylinder.
- Roller bearings exhibit significant improvement in friction at low speeds but do have application limitations.
- Roller bearings require significantly lower quantity and pressure of lubricating oil to maintain adequate lubrication which helps reduce parasitic losses at the oil pump.
- HCCI is not a practical combustion mode for this project. GDCI functions over a large speed load range while HCCI functions over a very small range which is eclipsed by the GDCI range.

Phase 2

- GDCI fuel consumption and noise levels show trends similar to diesel, however injection pressures are reasonably low. For GDCI operation at 1,500 rpm and 6 bar indicated mean effective pressure, indicated efficiency was about 9% higher and indicated specific CO_2 was about 14% lower than the same engine operating with diesel fuel and a modern diesel fuel system (see Figure 5).

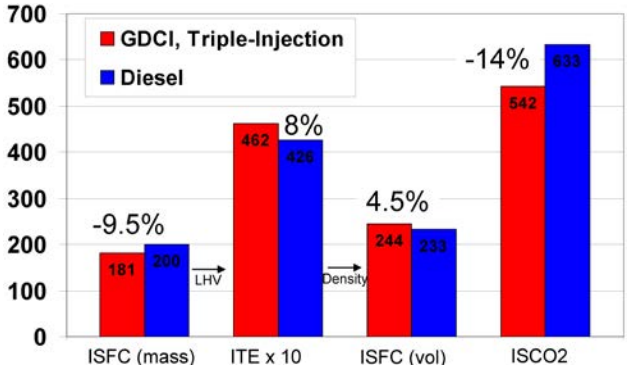

FIGURE 5. GDCI Combustion compared to Diesel Combustion on the same Start Cart Engine

- Low-temperature combustion was demonstrated from 2 to 15 bar indicated mean effective pressure with NOx less than 0.2 g/kWh, and PM emissions less than 0.1 filter smoke number. Results suggest that aftertreatment for NOx and PM might be reduced or possibly eliminated. The concept of "full-time GDCI" was proven.

FY 2011 Publications/Presentations

1. *"Development of Full-time Gasoline Direct-Injection Compression-Ignition (GDCI) for High Efficiency and Low CO2, NOx and PM"*, M. Sellnau et al., Aachen Colloquium Automobile and Engine Technology.

2. UFEV Project Merit Review presentation, K. Confer, Merit Review, Washington, D.C., May 2011.

3. SAE 2011-01-1386 Gasoline Direct Injection Compression *Ignition (GDCI) – Diesel-like Efficiency with Low CO2 Enmissions,* M. Sellnau et al., SAE World Congress 2011.

4. '*Gasoline Direct-Injection Compression-Ignition (GDCI): Diesel-Like Efficiency with Low CO2 Emissions*', M. Sellnau DOE DEER conference 2010.

II.A.26 Advanced Gasoline Turbocharged Direct Injection (GTDI) Engine Development

Terry Wagner
Ford Motor Company
2101 Village Road
Dearborn, MI 48121

DOE Technology Development Manager:
Ken Howden

NETL Project Manager: Ralph Nine

Subcontractor:
Michigan Technological University, Houghton, MI

Overall Objectives

Ford Motor Company Objectives:

- Demonstrate 25% fuel economy improvement in a mid-sized sedan using a downsized, advanced GTDI engine with no or limited degradation in vehicle level metrics.
- Demonstrate vehicle is capable of meeting Tier 2 Bin 2 emissions on the Federal Test Procedure (FTP)-75 cycle.

Michigan Technological University Objectives:

- Support Ford Motor Company in the research and development of advanced ignition concepts and systems to expand the dilute/lean engine operating limits.

Fiscal Year (FY) 2011 Objectives

- Engine architecture agreed.
- Analytical results support ability to meet fuel economy.
- Multi-cylinder development engines designed and parts purchased.
- Single cylinder development shows capability to meet intermediate combustion metrics supporting fuel economy and emissions objectives.

Accomplishments

Concept Evaluation:

- On October 1, 2010, a 1.8-L inline-4 (I4) cylinder conventional engine architecture was selected to initiate the project.
- Initiated development of top level engine attribute assumptions, architecture assumptions, and systems assumptions to support project targets.
- Initiated development of detailed fuel economy, emissions, performance, and noise, vibration and harshness (NVH) targets to support top-level assumptions.
- Initiated development of individual component assumptions to support detailed targets, as well as to guide combustion system, single-cylinder engine, and multi-cylinder engine design and development.
- Initiated detailed, cycle-based computer-aided engineering (CAE) analysis of fuel economy contribution of critical technologies to ensure vehicle demonstrates greater than 25% weighted city/highway fuel economy improvement.
- On May 2, 2011, a 2.3-L I4 high expansion ratio engine architecture was selected in order to “right-size” the engine with future North American, high volume, mid-size vehicle applications.
- Following the above architecture revision, completed development of top level engine attribute assumptions, architecture assumptions, and systems assumptions to support program targets.
- Completed development of detailed fuel economy, emissions, performance, and NVH targets to support top-level assumptions.
- Completed development of individual component assumptions to support detailed targets, as well as to guide combustion system, single-cylinder engine, and multi-cylinder engine design and development.
- Completed detailed, cycle-based CAE analysis of fuel economy contribution of critical technologies to ensure vehicle demonstrates 25% weighted city/highway fuel economy improvement; analysis predicts >2% margin to 25% target.

Combustion System Development:

- Completed detailed multi-dimensional engine simulation analyses to design and develop an advanced lean combustion system, inclusive of intake and exhaust ports, combustion chamber, piston top surface, and injector specifications.

Single Cylinder Build and Test:

- Generated surrogate single-cylinder engine data to design and develop the advanced lean combustion capability, with primary emphasis on maximizing fuel economy while minimizing oxides of nitrogen

(NOx) and particulate matter (PM) emissions. Testing included air-fuel ratio sweeps, multiple injection split and timing sweeps, cooled exhaust gas recirculation sweeps, and cam timing sweeps.
- Completed design, build, and installation of new single-cylinder engine based on the 1.8-L I4 conventional engine architecture. Engine to provide data for correlation to detailed multi-dimensional engine simulation analyses, thus providing high confidence in the planned subsequent single-cylinder engine based on the 2.3-L I4 high expansion ratio engine architecture.

Engine Design/Procure/Build:

- Initiated computer-aided design (CAD) design of new multi-cylinder engine, inclusive of all base engine components, advanced engine systems, and advanced integrated powertrain systems.
- Initiated required CAE analyses (acoustic, structural, thermo-mechanical, etc.), in support of CAD design of critical components and systems.
- Following the above architecture revision, completed CAD design of new multi-cylinder engine, inclusive of all base engine components, advanced engine systems, and advanced integrated powertrain systems.
- Completed required CAE analyses (acoustic, structural, thermo-mechanical, etc.), in support of CAD design of critical components and systems.
- Initiated component and systems orders to support multi-cylinder engine builds.

Vehicle Cooling Design and Optimization:

- Completed detailed CAE analysis of total engine and vehicle cooling system, with primary emphasis on internal engine cooling flow to optimize the split, parallel, cross-flow cooling configuration.

Aftertreatment Development:

- Designed and assessed a three-way catalyst plus lean-NOx trap/selective catalytic reactor (TWC plus LNT/SCR) system to satisfy the hydrocarbon (HC) and NOx slip targets during lean/rich cycling, in order to meet Tier 2 Bin 2 emissions on the FTP-75 cycle. Determined the required TWC plus LNT/SCR volumes and temperatures, lean/rich durations, and lean NOx concentrations to satisfy the NOx slip target.
- Demonstrated that the rich purge times required to satisfy the NOx slip target can be significantly reduced by decreasing the oxygen storage capacity of the TWC and the LNT.
- Designed and assessed a TWC plus SCR/LNT/SCR system with increased volume of SCR but decreased volume of LNT to improve the cost-effectiveness of the system. Determined the lean/rich durations and lean/rich NOx concentrations to satisfy the NOx slip target.
- Designed and assessed a TWC plus passive SCR system (i.e. no LNT but also without NH_3 or urea injection) to further improve the cost-effectiveness of the system, as well as to improve the tolerance to sulfur poisoning (relative to LNT systems). Determined the required TWC plus passive SCR volumes, lean/rich durations and lean/rich NOx concentrations to satisfy the NOx slip target.

Combustion Research:

- Progressed all facets of research and development of advanced ignition concepts. Continued development of the high feature combustion pressure vessel, including multiple optical access ports, multiple camera systems, multiple gaseous fuels, dual fans for wide range charge motion, and adapters for production spark plugs; laser-based characterization of vessel revealed need for continued development to represent engine-like conditions. Completed installation of 3.5-L EcoBoost engine and initiated advanced ignition hardware investigations, including ignition energy and phasing, spark plug geometry, and charge motion control. Completed additional hardware installation and initiated testing on advanced ignition control concepts, including combustion sensing and knock detection. Received and prepared second 3.5-L EcoBoost engine for combustion surface temperature measurements.

Future Direction

- Multi-cylinder development engines completed and dynamometer development started.
- Demonstration vehicle and components available to start build and instrument.

Introduction

Ford Motor Company has invested significantly in GTDI engine technology in the near term as a cost effective, high volume, fuel economy solution, marketed globally as EcoBoost technology. Ford envisions further fuel economy improvements in the mid- and long-term by further advancing the EcoBoost technology. This project is directed toward advancing these mid- and long-term EcoBoost technologies, as well as related additional technologies, in order to achieve the project objectives:

- Demonstrate 25% fuel economy improvement in a mid-sized sedan using a downsized, advanced GTDI engine with no or limited degradation in vehicle level metrics.
- Demonstrate vehicle is capable of meeting Tier 2 Bin 2 emissions on the FTP-75 cycle.

Approach

Engineer a comprehensive suite of gasoline engine systems technologies to achieve the project objectives, utilizing:

- Aggressive engine downsizing in a mid-sized sedan from a large V6 to a small I4.
- Mid- and long-term EcoBoost technologies:
  - Advanced dilute combustion with cooled exhaust gas recycling and advanced ignition.
  - Advanced lean combustion with direct fuel injection and advanced ignition.
  - Advanced boosting systems with active and compounding components.
  - Advanced cooling and aftertreatment systems.
- Additional technologies, including advanced friction reduction technologies, engine control strategies, and NVH countermeasures.
- Progressively demonstrate the project objectives via concept analysis/modeling, single-cylinder engine, multi-cylinder engine, and vehicle-level demonstration on chassis rolls.

Results

A 2.3-L I4 high expansion ratio engine architecture was selected in order to "right-size" the engine with future North American, high volume, mid-size vehicle applications. Subsequently, the project team completed development of top level engine attribute assumptions, architecture assumptions, and systems assumptions, then completed development of individual component assumptions, and lastly completed detailed, cycle-based CAE analysis of fuel economy contribution of critical technologies to ensure the vehicle demonstrates 25% weighted city/highway fuel economy improvement. As shown in Table 1, the CAE analysis predicts >2% margin to 25% target.

Following the development of assumptions, the project team then completed CAD design of a new multi-cylinder engine, inclusive of all base engine components, advanced engine systems, and advanced integrated powertrain systems, then completed the required CAE analyses (acoustic, structural, thermo-mechanical, etc.), and lastly initiated component and systems orders to support multi-cylinder engine builds. As shown in Figure 1, the multi-cylinder engine design is complete, representing a comprehensive suite of gasoline engine systems technologies to achieve the project objectives.

Using the surrogate single-cylinder engine, the project team generated data to design and develop the advanced lean combustion capability. The advanced lean combustion capability appears promising, approaching the ideal function, specifically: good fuel economy, low NOx, low PM, practicable controls, and acceptable NVH. As shown in Figure 2, the advanced lean combustion capability extends the combustion stability/misfire limits (relative to homogeneous lean), thereby decreasing NOx to a level favoring NOx aftertreatment efficiency via the LNT/SCR aftertreatment system.

TABLE 1. CAE Analysis of Fuel Economy - 2.3-L I4 High Expansion Ratio Engine Architecture vs. 3.5-L V6

Technology		% FE Improvement
3.5 ⇨ 2.3L	+	15.6% - Engine Architecture Downsized Miller w High CR
10.3 ⇨ 11.5 CR	+	
583 ⇨ 565 CC / Cyl	~	
1.07 ⇨ 0.93 Bore / Stroke	~	
iVCT ⇨ tiVCT	+	
PFI ⇨ DI (fuel pump losses)	-	
DAMB ⇨ RFF	+	7.8% - Component Actions
Variable Displacm't Oil Pump & Cam Roller Bearings	+	
IEM / Fast Warm-Up	+	
Assisted Direct Start (ADS)	+	
Electric Power Assisted Steering (EPAS)	+	
V6 ⇨ I4 Idle & Lug	-	
Active Mount & Pendulum Damper	+	
Optimize Torque Converter & Final Drive Ratio	+	0.2% - Power Conversion
Cooled EGR	+	4.4% - Combustion / Air Path
Advanced Lean Combustion (incl. 0.6% purge penalty)	+	
Active Wastegate	+	
Total based on 2.3L Miller GTDI Engine	**28.0**	

CR - compression ratio; iVCT - ?; tiVCT - ?; PFI - port fuel injection; DAMB - ?; RFF - ?; IEM - ?

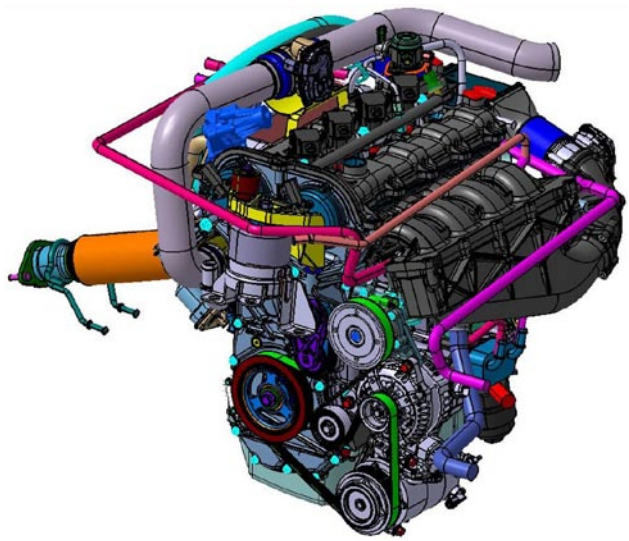

FIGURE 1. Multi-Cylinder Engine Design

Conclusions

- The project will demonstrate a 25% fuel economy improvement in a mid-sized sedan using a downsized, advanced GTDI engine with no or limited degradation in vehicle level metrics, while meeting Tier 2 Bin 2 emissions on FTP-75 cycle.
- Ford Motor Company has engineered a comprehensive suite of gasoline engine systems technologies to achieve the project objectives and progressed the project through the concept evaluation and design tasks with material accomplishments to date.
- Ford Motor Company is in collaboration with Michigan Technological University on a critical facet of the project, specifically advanced ignition concepts.

FY 2011 Publications/Presentations

1. Completed Ford/DOE Kick-Off Meeting, Ford Advanced GTDI Engine Development, held November 30, 2010.

2. Completed presentation at the 2011 U.S. Department of Energy Hydrogen and Fuel Cells Program and Vehicle Technologies Program Annual Merit Review and Peer Evaluation Meeting (AMR), held May 9–13, 2011, Crystal City Marriott, Arlington, Virginia.

3. Completed project status presentation for Ralph Nine and Gupreet Singh at Ford Motor Company on July 20, 2011; reviewed status of all primary tasks and received concurrence on selection of 2.3L I4 high expansion ratio engine architecture.

4. Completed project status summary for Ralph Nine in support of DEER Conference Newsletter on August 22, 2011.

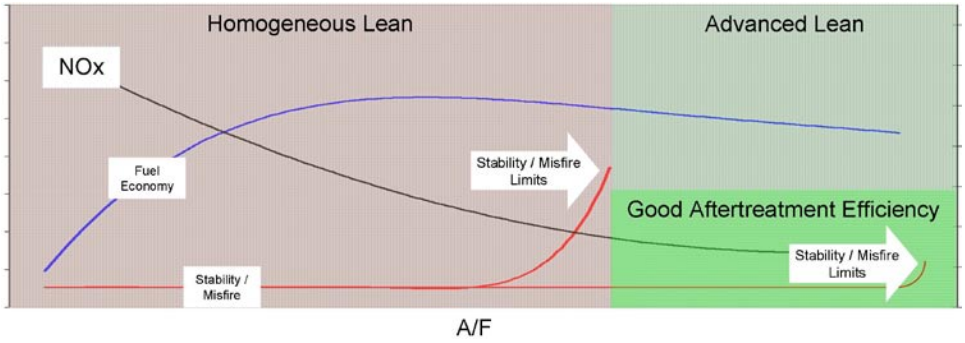

FIGURE 2. Advanced Lean Combustion

II.A.27 Recovery Act: Lean Gasoline System Development for Fuel Efficient Small Cars

Stuart R. Smith
Powertrain Division
General Motors, LLC
895 Joslyn Avenue
Pontiac, MI 48340-2920

DOE Technology Development Manager:
Ken Howden

NETL Project Manager: Ralph Nine

Overall Objectives

- Demonstrate 25% vehicle fuel economy improvement while achieving Tier 2 Bin 2 emissions.
- Develop a novel passive selective catalytic reactor (SCR) aftertreatment system for lean gasoline combustion with robust controls for oxides of nitrogen (NOx) reduction.
- Comprehend system level integration for an optimal combination of advanced technologies to provide the highest fuel economy for potential production implementation.

Fiscal Year (FY) 2011 Objectives

- Design, procure, build and install the first generation SG5 lean combustion engines and passive SCR aftertreatment systems in to three advance development vehicles.
- Develop initial torque-based engine controls architecture to support lean combustion.
- Quantify lean gasoline aftertreatment hardware provides NOx efficiency >60%.
- Demonstrate lean gasoline vehicle highway fuel economy improvement >13%.

Accomplishments

- Installed and conducting tests on lean gasoline engine and aftertreatment systems in dynamometers and vehicles.
- Generated initial torque-based engine controls and calibration that enables vehicle operation in lean stratified mode to 55 mph.
- Demonstrated the passive SCR lean gasoline aftertreatment system capability for NOx conversion efficiency of 68.5%.
- Achieved vehicle highway fuel economy goal of greater than 13% improvement by utilizing single-cylinder fuel consumption data and vehicle simulation.

Future Directions

- Optimize lean engine controls and calibration to maximize fuel economy potential to improve transient drivability and minimize engine-out emissions.
- Refine the Gen 2 passive SCR lean aftertreatment system to minimize CO during NH_3 generation.
- Develop an exhaust system thermal management strategy to optimize lean aftertreatment performance under all vehicle operating conditions.
- Develop an aftertreatment system that combines active and passive SCR systems as a risk mitigation to ensure compliance under all operating conditions.
- Integrate active thermal management and 12 volt stop/start systems to maximize fuel economy potential.
- Develop second generation lean gasoline combustion engine with downsizing, boosting and multiple fuel injection capability to extend lean stratified load operation range.

Introduction

The project accelerates development and synergistic integration of four cost-competitive technologies to improve fuel economy of a light-duty vehicle by 25% while meeting Tier 2 Bin 2 emissions standards. These technologies are targeted to be broadly implemented across the U.S. light-duty vehicle product line between 2015 and 2025 and are compatible with future and renewable biofuels. The technologies in this project are: lean gasoline combustion, innovative passive SCR lean aftertreatment, 12 volt stop/start and active thermal management. The technologies are initially developed on engine dynamometers, further refined on development vehicles, fully integrated and then calibrated in a mid-size sedan for final demonstration.

Approach

The development approach is structured to garner fundamental understanding of technology areas, innovate novel solutions to challenges, optimize

solutions and implement mitigation to address limitations. Initial phases of the project center on fundamental modeling, analysis and experimental investigation for lean gasoline combustion and aftertreatment. Comprehensions of the fundamentals are then distilled to hardware designs and control strategies. The hardware and controls are then utilized on engine dynamometers and development vehicles to refine the technology areas and ascertain barriers. The barriers, that expectedly occur during research innovation projects, are assessed to enact investigative mitigation technologies.

Results

Engine and Aftertreatment Hardware

The fundamental analysis and experimental investigations drove the design of the first generation naturally aspirated SG5 lean stratified gasoline combustion engine (Figure 1). The design of the lean combustion system comprises of: central direct fuel injection, intake port deactivation for swirl-based stratified mixture preparation, optimized piston with lean combustion bowl and high flow exhaust gas recirculation (EGR) system. Engines with this combustion system are built and are currently being tested on dynamometers and in vehicles.

Fundamental modeling, analysis and experimental investigations guided the design of the passive SCR aftertreatment system. The aftertreatment system incorporates conventional close-coupled three-way catalyst along with precious group metals formulation optimized for NH_3 generation. The Gen 1 passive SCR lean gasoline aftertreatment systems are assembled and currently undergoing evaluation on dynamometers and in vehicles.

Torque-Based Engine Controls

Controls are a fundamental challenge for enabling a path to production for lean stratified gasoline combustion systems. A key deliverable is to develop combustion and aftertreatment controls within General Motors torque-based controls structure. This allows internal controls expertise to be leveraged and supports potential production implementation. New combustion and aftertreatment algorithms are developed in a model-based, rapid prototype environment. These algorithms are currently being used in development dynamometer and vehicle testing.

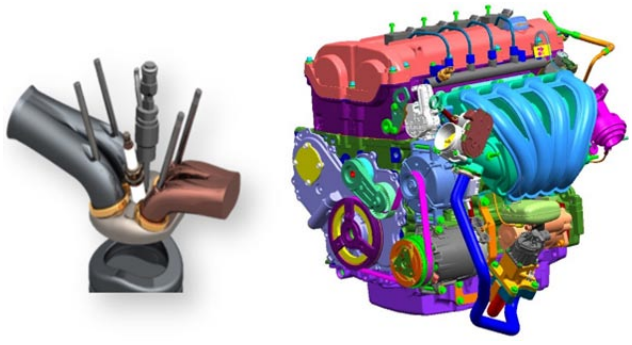

FIGURE 1. SG5 Lean Stratified Combustion Engine

Combustion controls development has focused on a regression-based torque model algorithm. Stoichiometric homogenous and lean stratified data has been generated to support algorithm and calibration development. An accurate torque model will be critical to combustion mode transitions as passive SCR aftertreatment will require transitions to homogenous mode for NH_3 generation. Algorithms are also being modified and developed for precise EGR control. Lean stratified combustion requires significantly more external EGR than homogenous applications. This has driven development of new transient EGR algorithms, including the addition of intake oxygen sensors to support mode transition algorithms.

Vehicle Aftertreatment Emissions

Vehicle dynamometer test results indicate that the Gen 1 passive lean aftertreatment system achieves the interim milestone goal or achieving NOx reduction efficiency of greater than 60%. Vehicle emissions test data additionally indicates CO levels greater than desired. The excess CO is generated during homogenous rich operation in the NH_3 generation events.

Initial vehicle test results indicate that initial locations for the SCRs are not optimal for NOx emissions reduction performance. The Gen 1 lean aftertreatment system design targeted the under-floor SCR catalyst to be in the optimum temperature range during low to mid-speed operation and the rear SCR catalysts being in the optimum temperature range during high-speed operation. Exhaust gas temperatures measured during the Federal Test Procedure (FTP) City and Highway tests indicate the front SCR temperature is generally above 350 degrees C and the rear SCR temperatures are generally in the recommended SCR temperature range (Figure 2). The excessive temperatures are primarily due to running homogeneous mode during acceleration maneuvers; this is targeted to be addressed by combustion system development improvement.

Vehicle Engine Fuel Economy

Calibration enhancements have improved vehicle drivability which results in increased lean stratified operation during FTP City and Highway fuel economy tests. Lean stratified operation is enabled at part throttle when vehicle speed is above 28 kph and driver requested

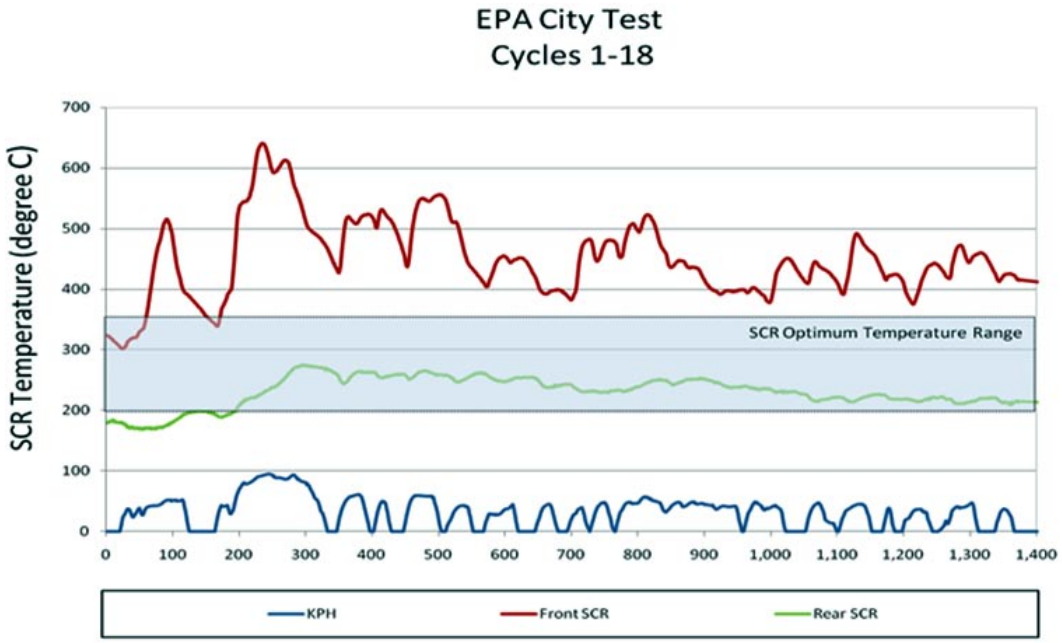

FIGURE 2. Vehicle Gen 1 SCR Temperatures

torque is below the brake mean effective pressure (BMEP) threshold. For this initial testing the idle and low rpm deceleration maneuvers are in homogeneous mode as the lean idle control algorithm is currently under development. FTP City testing (Figure 3) demonstrates when lean stratified operation is enabled during cycles 1-18 of the test. Although steady-state fuel economy is promising (Figure 4), the data also indicates that current lean stratified operation BMEP level is limited during the accelerations on the FTP and subsequently does not project to achieve the fuel economy goal of 25% improvement.

In attempt to address the load operation limitation, the project initiated a risk mitigation strategy to investigate the impact of boosted lean stratified combustion systems. Initial computational fluid dynamics modeling and single-cylinder testing are promising, with significant improvement in lean stratified load capability. Testing focused on a load hook at an engine speed of 2,000 RPM with intake temperature held constant at 30 degrees C to ensure limited negative knock and NOx effects. Boost levels up to an intake manifold pressure of 170 kPa and EGR mass fraction levels up to 45% were tested. Combustion stability results as a function of engine load are favorable (Figure 5). The initial data indicates that the target coefficient of variation of indicated mean effective pressure of 3% can be achieved for engine loads in the range 350 to 750 kPa net mean effective pressure.

Vehicle simulations have been utilized to evaluate lean downsize boost potential. Net mean effective pressure requirements for a downsized and turbocharged engine in a Malibu test weight class under both FTP and Highway tests have been assessed (Figure 6). In order to get the maximum vehicle fuel economy benefit of the lean stratified combustion system, a 90% target for residence time in lean stratified mode has been selected. This requirement is being used for the combustion system development of the second generation lean stratified engine.

Conclusions

- Torque-based lean stratified gasoline engine controls are possible and support transition operation between lean stratified and stoiciometric homogeneous modes. Refinement is required to meet internal targets for mode transition disturbance.
- Passive SCR aftertreatment is generating greater than desired CO during NH_3 generation.
- Gen 2 passive SCR development will focus on; three-way catalyst formulation optimization, potential CO oxidation solutions, improving SCR thermal environment through hardware and controls, and may require a combined active dosing system to achieve effective lean NOx reduction during all expected operation conditions.
- The current lean stratified combustion system will not support the fuel economy targets due to load limitations. To further extend the vehicle lean load operating range to achieve the fuel economy goals, a second generation engine is required that

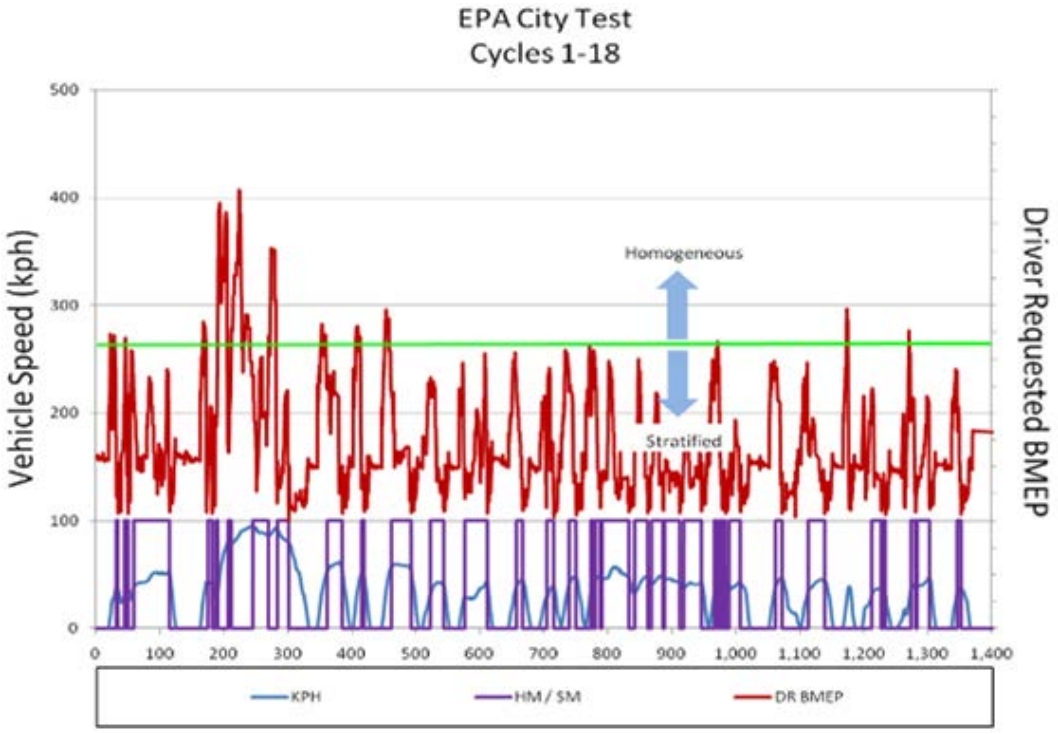

FIGURE 3. Vehicle Operation Modes

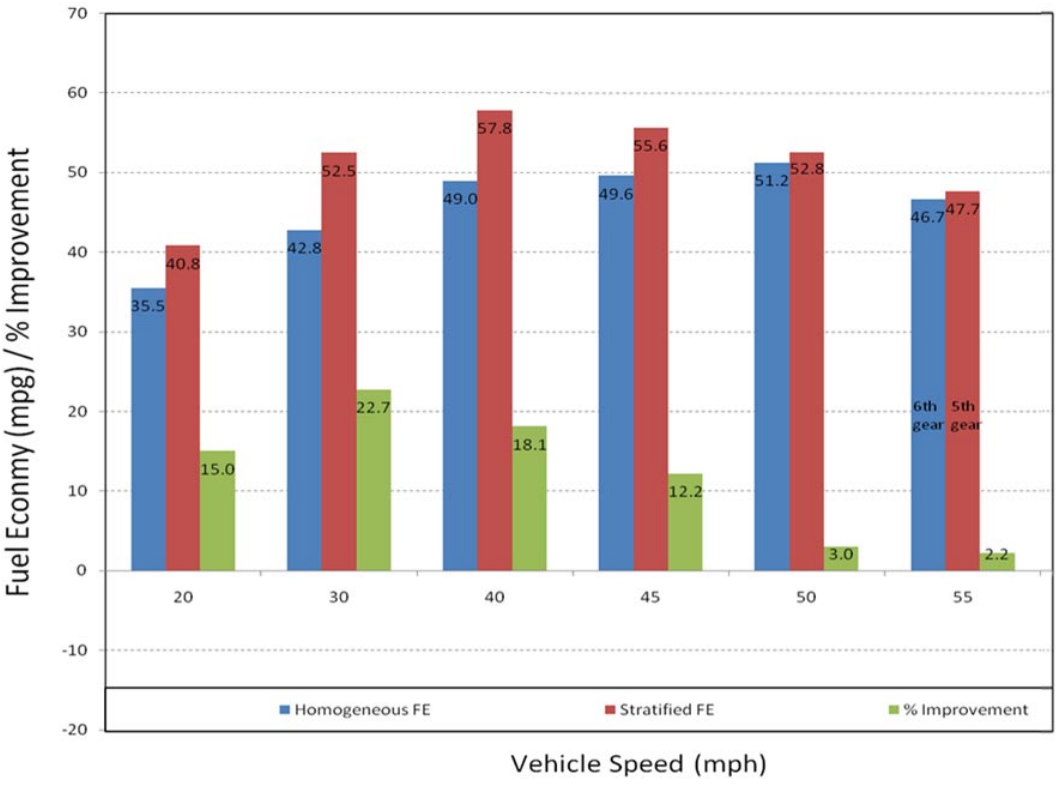

FIGURE 4. Lean Stratified Fuel Economy

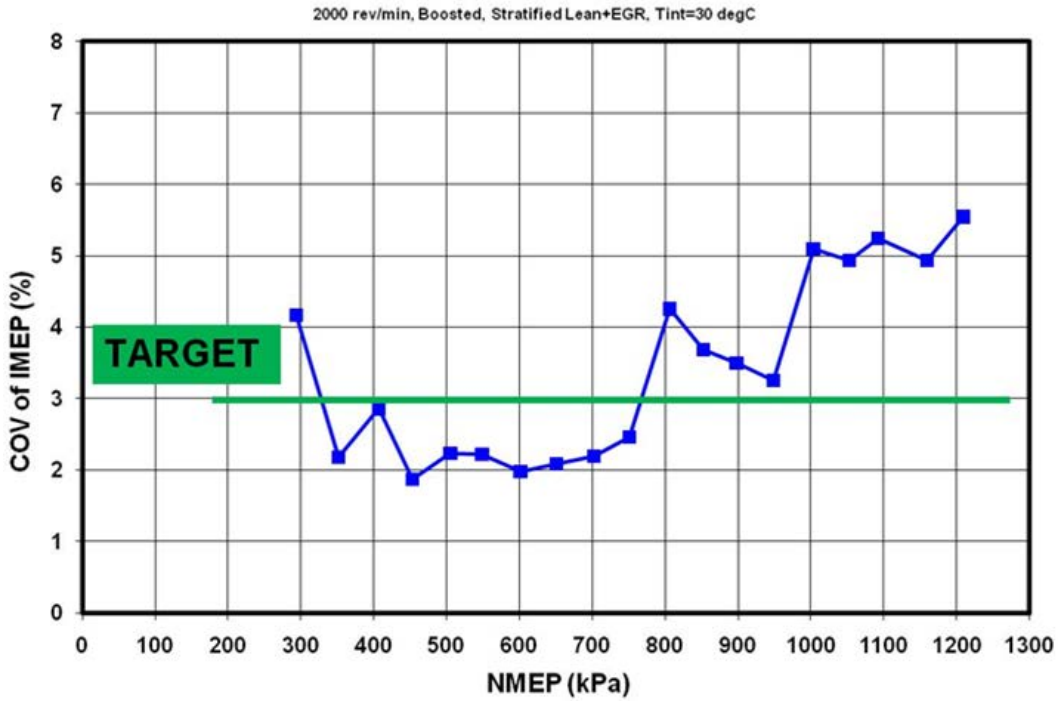

FIGURE 5. Boosted Lean Stratified Combustion Stability

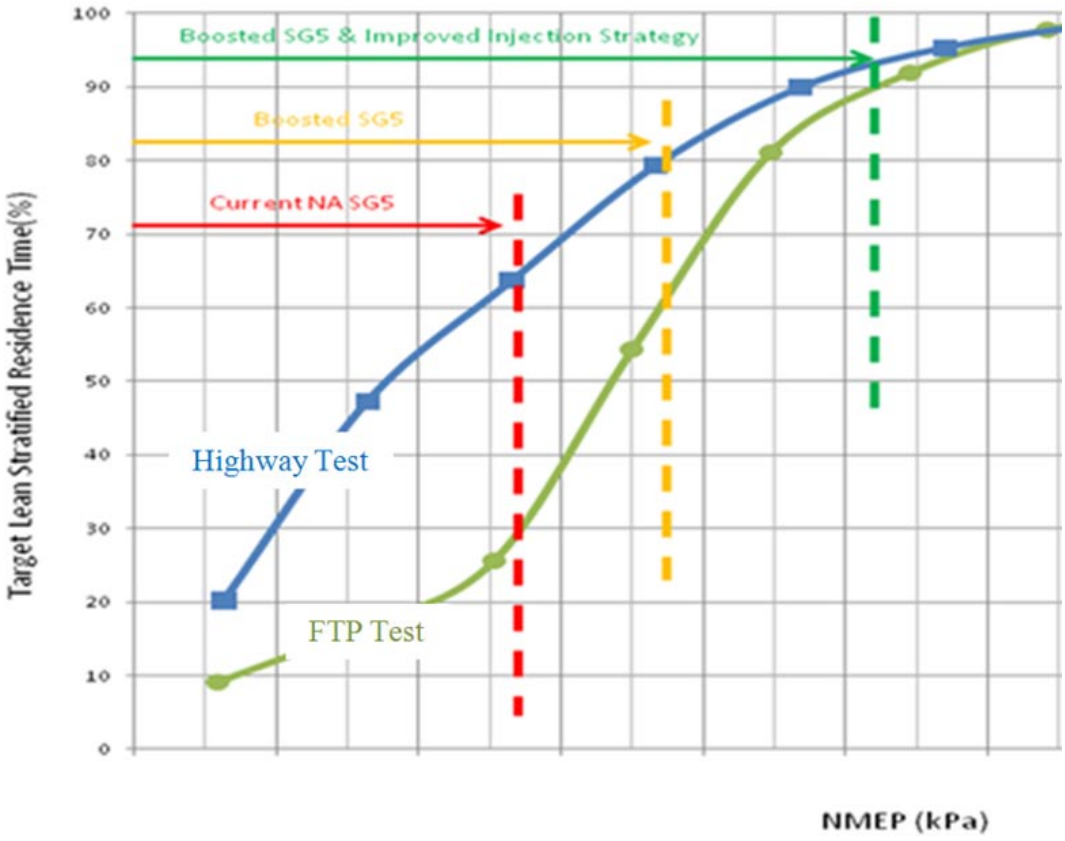

FIGURE 6. Lean Stratified Residence Time

incorporates displacement downsizing, boosting and multiple fuel injection capability.

- Continued focus by the 27 full-time-equivalent development staff on optimization and innovation of solutions provides the greatest opportunity that the optimal combination of advanced technologies will emerge to achieve the highest fuel economy potential.

FY 2011 Publications/Presentations

1. Viola, Mike, "Catalyst Design for Urea-less Passive Ammonia SCR Lean-Burn SIDI Aftertreatment System", 2010 U.S. DOE DEER Conference, Detroit, MI, September 28, 2010.

2. Smith, Stuart R., "Lean Gasoline System Development for Fuel Efficient Small Car", 2011 U.S. DOE Vehicle Technologies Program Annual Merit Review and Peer Evaluation Meeting, Arlington, VA, May 13, 2011.

II.A.28 Recovery Act – A MultiAir/MultiFuel Approach to Enhancing Engine System Efficiency

Ron Reese
Chrysler Group, LLC
800 Chrysler Drive
Auburn Hills, MI 48326

DOE Technology Development Manager:
Ken Howden

NETL Project Manager: Ralph Nine

Subcontractors:
- The Ohio State University, Columbus, OH
- Bosch, Farmington, MI
- Delphi, Troy, MI
- FEV, Auburn Hills, MI
- Argonne National Laboratory, Argonne, IL

Overall Objectives

- Chrysler aims to demonstrate 25% improvement in combined Federal Test Procedure (FTP) City and Highway fuel economy for the Chrysler minivan.
- Accelerate the development of highly efficient engine and powertrain systems for light-duty vehicles, while meeting future emissions standards.
- Create and retain jobs in support of the American Recovery and Reinvestment Act of 2009.

Fiscal Year (FY) 2011 Objectives

- Demonstrate the possible ability of meeting a 25% fuel economy improvement using vehicle simulation.
- Develop detailed designs for all engine components and complete analysis to assure no high failure risk areas.
- Procure all parts and build prototype engines.

Accomplishments

- The design for the Alpha 1 engine has been completed. As of September 2011, 95% of all engine components have been procured (see Figures 1 and 2).
- Extensive one-dimensional (1D) performance modeling, vehicle simulations and three-dimensional (3D) combustion simulations have been completed. Completed 3D computational fluid dynamics (CFD) simulation of the designed intake manifold to identify the most efficient air handling system.
- Preliminary vehicle simulation results indicate there is sufficient project content to achieve the 25% fuel economy improvement goal.
- Finite element analysis modeling tasks have been completed. Analysis shows that all components evaluated have sufficient structure/safety factor to withstand all development and durability loading without concern of failure.
- Design, packaging and performance projections for 2nd order torsional mitigation approach have been completed.
- Controller architecture to support engine design and selected technology is completed.

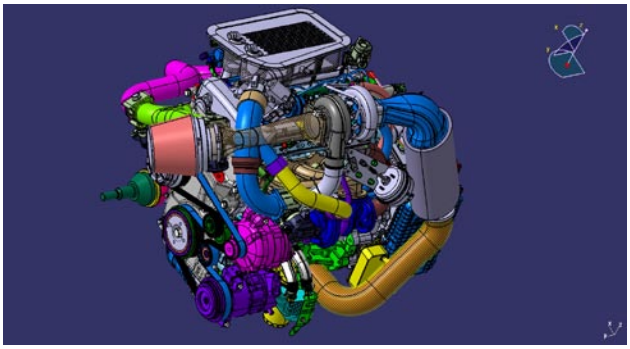

FIGURE 1. Alpha 1 Engine

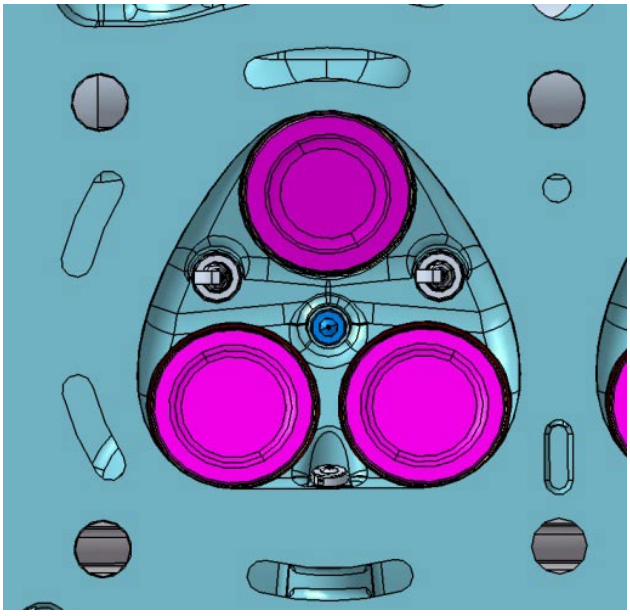

FIGURE 2. Alpha 1 Combustion Chamber Design

- Completed technology review and benchmarking survey of literature, Web and industrial know-how in ancillary loads reduction technologies and thermal management system, including mapping of existing hardware and simulation tools.
- Performed preliminary engine dynamometer tests using diesel micro pilot (DMP) ignition system on proof-of-concept engine.
- Completed design and system layout of the thermal management system.
- Blocks were designed, procured, assembled and tested which were made with a spray-on bore liner process, eliminating the typical cast iron liner. Parts procured for Phase 2 testing.

Future Directions

- Perform development tests on Alpha 1 engines in the dynamometer to provide correlation to the simulation results.
- Incorporate base control strategies to run the engine and provide feedback on the fuel economy improvements of the new technologies.
- Demonstrate the combined fuel economy improvement of at least 17% on simulated fuel economy tests for this phase of engine design.
- Based on learning gained from Alpha 1 testing, optimize simulation and design for the second iteration of engine development.
- Test the multi-fuel engine at Argonne National Laboratory with optical access into the combustion chamber.

Introduction

The aim of this project is to demonstrate a 25% improvement in fuel economy while maintaining comparable vehicle performance to the baseline engine, a state-of-the-art 4.0-L V6. Tier 2, Bin 2 tailpipe emissions are also intended to be demonstrated. Chrysler will downsize and down speed the engine through fundamental combustion improvements implemented via combination of engine technologies with the concurrent development of other system enhancements.

Main technologies that are being explored as part of this development project include in-cylinder combustion improvements, waste heat recovery and thermal management strategies, friction reduction, ancillary load management and emissions controls.

Approach

Chrysler's approach for this project utilizes a five phase development that incorporates two distinct design and test cycles. The five phases are:

Phase 1 – Design, Simulation and Analysis of MultiAir, Boosted, Cooled Exhaust Gas Recirculation (CEGR), Direct Injected, Single and MultiFuel Solutions (Alpha 1 engine)

Phase 2 – Hardware Procurement, Build and Development of MultiAir, Boosted, CEGR, Direct Injected, Single and MultiFuel Solutions (Alpha 1 engine)

Phase 3 – Design Optimization of MulitAir, Boosted, CEGR, Direct Injected, Single fuel and MultiFuel Solutions (Alpha 2 engine)

Phase 4 – Hardware Procurement, Build and Refinement of an Optimized Single Fuel Engine and a MultiFuel Engine (Alpha 2 engine)

Phase 5 – Vehicle Build, Calibration and Fuel Economy Demonstration (Alpha 2 engine)

The basic approach for this advanced combustion system development is to complete two design/development iterations. Each iteration encompassing two development phases – one phase for design and simulation efforts, the second phase for procurement, engine build and test. The combination of Phase 1 and Phase 2 will result in development of the Alpha 1 engine. Phases 3 and 4 will incorporate the learning that occurred in the early phases of development to produce the Alpha 2 engine. This engine will be used in Phase 5 Fuel Economy Demonstration.

Results

The original approach included investigation and possible inclusion of MultiAir technology. MultiAir was dropped from the project in early 2011 due to difficulty packaging the technology, unrealistic production design and insufficient supplier support. Also factoring into the decision was the identification of an improved transmission option that could be considered as part of this project. Modeling indicates that the improved transmission can contribute up to a 7% improvement in fuel economy.

Extensive finite element analysis, 1D and 3D engine simulation and vehicle modeling have been completed. Results indicate that the design is capable of meeting or exceeding the efficiency and performance targets for this project. Verification and test activities in Phase 2 will confirm the completed analysis.

Two-stage boosting devices were analyzed using GT-POWER, comparing two turbochargers to a supercharger-turbocharger. The supercharged-

turbocharged engine is less efficient under boost, but slightly more efficient at light load compared to two turbochargers. 1D engine simulation and vehicle modeling results show that the twin turbo is 2.1% better on FTP City and 1.0% better on FTP Highway fuel economy than the supercharger-turbocharger.

DMP ignition has been demonstrated in the surrogate proof-of-concept engine. This technology provides the ability to achieve a compression ignition event with the DMP system and very high levels of EGR, resulting in highly efficient engine operation (see Figure 3).

The 1D simulation of the thermal system was completed, proving capability to cool all new powertrain components and facilitate rapid warm-up of the engine and transmission. This proves that the thermal management system is a sufficient enabler for the combustion side fuel economy improvement strategies. This simulation work shows that the strategies for rapid warm-up of the engine and transmission are sufficient to achieve the 4% thermal system fuel economy improvement target.

The design, fabrication, installation and testing of a new prototype crankshaft was completed. This crankshaft design controls second order torsional vibrations. Torsional measurements taken before and after the crankshaft installation confirmed a clear 2nd order benefit. Test data demonstrated that key vibrational metrics – such as steering wheel, seat track, second-order noise and direct ring gear torsional measurements – are significantly improved. For low to moderate torsional vibrations, testing has yielded a 40-50% reduction in the torsional peak-to-peak amplitude. This is in line with original predictions (see Figure 4).

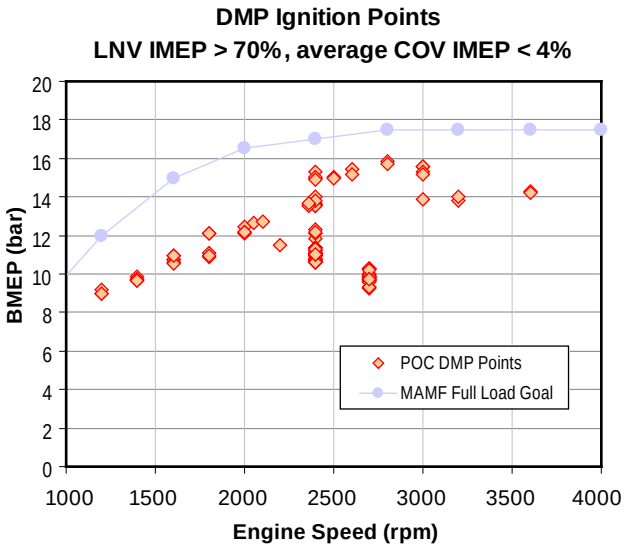

FIGURE 3. Speed/Load Cases Tested with DMP Ignition

Testing of the spray-on bore liner showed a significant friction reduction and combustion phasing improvement as compared to a standard cast-in-place cast iron liner)see Figures 5 and 6).

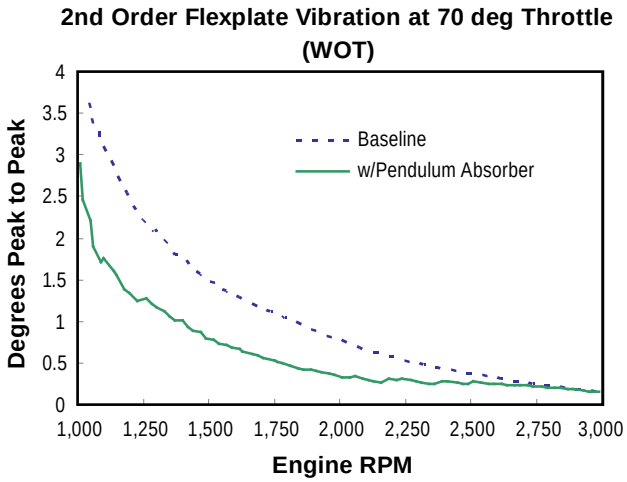

FIGURE 4. 2nd Order Pendulum Correction

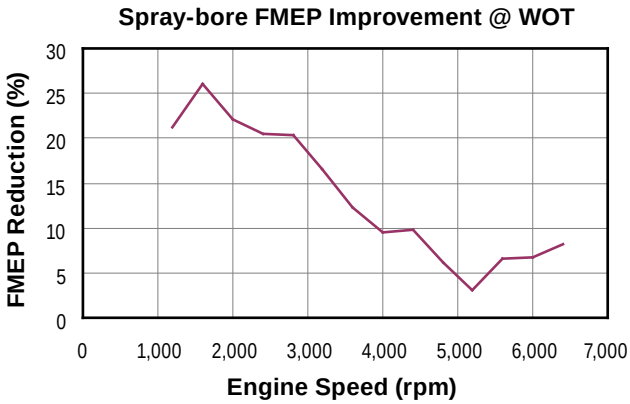

FIGURE 5. Spray-Bore FMEP Reduction @ WOT

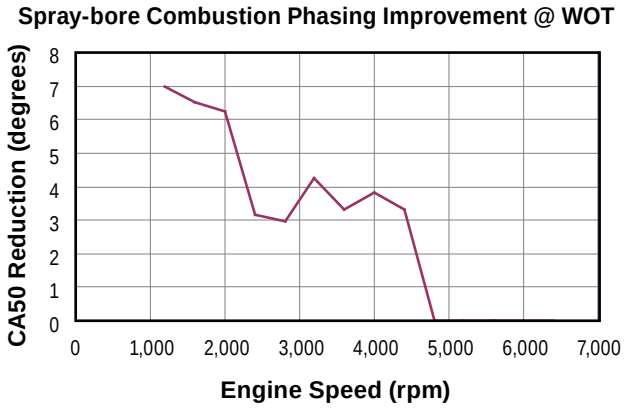

FIGURE 6. Spray-Bore Combustion Phasing Improvement @ WOT

Conclusions

- There is sufficient data from Phase 1 modeling and simulation activities to support the further development of engine technologies to support the project goals of 25% improvement in combined FTP City and Highway fuel economy for the Chrysler minivan.
- Engine efficiency at high load is improved with a diesel fuel ignition system on a gasoline engine. However, controlling the combustion process will be challenging in an automatic control system.

FY 2011 Publications/Presentations

1. Department of Energy Project Review – DOE MAMF Project Team, September, 2010.

2. 2011 DOE Vehicle Technologies Program Annual Merit Review, May 2011.

3. Department of Energy Project Review – DOE MAMF Project Team, July 2011.

Special Recognitions & Awards/Patents Issued

1. Chrysler Invention Development Record - Automotive Engine Coolant Heating System with Integrated EGR Cooler (Submitted).

2. Patent Application 708570m " PENDULUM VIBRATION ABSORBER ON A CRANKSHAFT".

II.A.29 Advanced Combustion Controls – Enabling Systems and Solutions (ACCESS)

Hakan Yilmaz (Primary Contact), Alan Mond, Li Jiang
Robert Bosch LLC
38000 Hills Tech Drive
Farmington Hills, MI 48331

DOE Technology Development Manager: Ken Howden

NETL Project Manager: Ralph Nine

Subcontractors:
- AVL Powertrain, Plymouth, MI
- Emitec, Auburn Hills, MI
- University of Michigan, Ann Arbor, MI
- Stanford University, Palo Alto, CA

Overall Objectives

- Improve fuel economy by 25% with minimum performance penalties.
- Achieve Super Ultra-Low Emission Vehicle level emissions with gasoline.
- Demonstrate multi-mode combustion engine management system (EMS).

Fiscal Year (FY) 2011 Objectives

- Quantify the fuel economy and emissions benefits of the boosted homogenous charge compression ignition (HCCI) combustion concept.
- Define EMS hardware and software architecture.

Accomplishments

- Completed the design, procurement, and building of the Prototype I engine and its EMS hardware for multi-mode combustion.
- Defined the EMS hardware, software and overall control architecture to enable multi-mode combustion.
- Demonstrated fuel economy potential of the supercharger/turbocharger boosted HCCI combustion strategy over the baseline port fuel injected (PFI) V-6 engine at selected operating points.
- Demonstrated the EMS performance for HCCI controls at the engine dynamometer.

Future Directions

- Evaluate fuel economy and emissions benefits of boosted HCCI combustion concept on the Prototype I engine platform.
- Complete design, procurement, and building of Prototype II engine.
- Define combustion and control strategies for combustion mode switch between HCCI and spark ignition (SI) combustion.

Introduction

Due to availability and security of energy resources, environmental concerns, and cost factors, the automotive industry is facing the challenge of improving fuel economy and reducing the emissions without sacrificing performance. Although there are promising developments in electrification of powertrain with hybrid systems, battery electric vehicles and fuel cell electric vehicles; internal combustion engines are expected to be the mainstream power source of future high-efficiency vehicles for the next decade. The feasible future advanced engine and powertrain configuration must address the topics such as emission and fuel economy requirements for worldwide applications, transition to bio fuels, and synergies with future powertrain trends.

The ACCESS project has the primary objective of developing highly capable and flexible advanced control concepts with enabling system, sub-system and component level solutions for the management of multi-mode combustion events in order to achieve up to 30% fuel economy improvement in a gasoline fueled light-duty vehicle without compromising its performance while meeting future emission standards as outlined in DOE solicitation targets.

Approach

This project, through a three-phase approach, addresses the development, testing, and demonstration of the proposed advanced technologies and the associated emission and fuel economy improvement at an engine dynamometer and on a full-scale vehicle. The project investigates the synergistic mainstream advanced combustion and system concepts such as:

- SI combustion with high compression ratio and high boost assisted with cooled external exhaust gas recirculation (EGR).

- HCCI assisted with controlled boost, external EGR and fueling strategies for operation range extension.
- Port direction injection (PDI) – dual injection system for combining the benefits of PFI and direct injection.
- Multi-hole direct injection with individual nozzle geometry design for improved mixture preparation and combustion efficiency.
- Start-stop and thermal management systems to eliminate fuel consumption at idling conditions and enhanced engine warm-up behavior.

As a result, a substantial improvement in thermal efficiency by exploiting the advantages of SI/HCCI combustion on a turbocharged downsized engine with high compression ratio is proposed. The target engine, equipped with the capabilities of dual-stage turbo-charging, external EGR system, electric dual cam phasing, dual cam profile switching and in-cylinder pressure sensing, enables the investigation and development of combustion and control strategies to maximize engine thermal efficiency.

Results

The first prototype engine already built and shown in Figure 1 has been fired and initial results have been generated. Prototype 1 has been equipped with state-of-the-art components to allow all combustion modes to be operated flawlessly. This engine comprises central mounted direct injection (1), 120 mJ Bosch ignition coils and 10 mm spark plugs (2), a stock BorgWarner K03 turbocharger (3), Denso electric variable cam phasers (4), a new generation Eaton R410 supercharger with magnetic clutch (5), Delphi control valves for hydraulic cam profile switching (6), a PFI injection system (7) and finally a high pressure EGR valve (8).

Initial fuel consumption results of boosted HCCI operation can be observed in Figure 2. These preliminary results were collected early in the project during a rigorous assessment of the optimal boosting configuration for this application. The black rings represent the engine operating points during a Federal Test Procedure (FTP)75 cycle simulation and their diameters correspond to the frequency of visits during the test cycle. The baseline vehicle chosen for the FTP75 cycle simulation was a 2009 Cadillac CTS. These early results offer a glimpse into the potential BSFC numbers achievable with turbocharged HCCI operation.

In addition to experimental results, a simulation study was performed [1] comparing two radically different boosting systems for HCCI operation: two-stage turbocharged HCCI versus two-stage supercharged-turbocharged HCCI. The results of the study are shown in Figure 3 where friction, pumping, and supercharger losses are normalized with mean effective pressure for ease of comparison. A turbocharger small enough for HCCI operation generates high exhaust backpressure, leading to a fuel economy penalty. As shown in Figure 3, the supercharger shows lower cumulative losses when operated at low speeds, sufficient to match the air mass flow of a turbocharger and provide adequate air charge dilution. Based on the study, the supercharger-turbocharger configuration has been selected as the preferred boosting configuration for HCCI operation.

For ease integration of future control functionalities, the control architecture in Figure 4 is established based on the existing Bosch MED17 system structure. The four main components of the controller are the Engine Torque Structure (ETS), Air System (AS), Fuel System

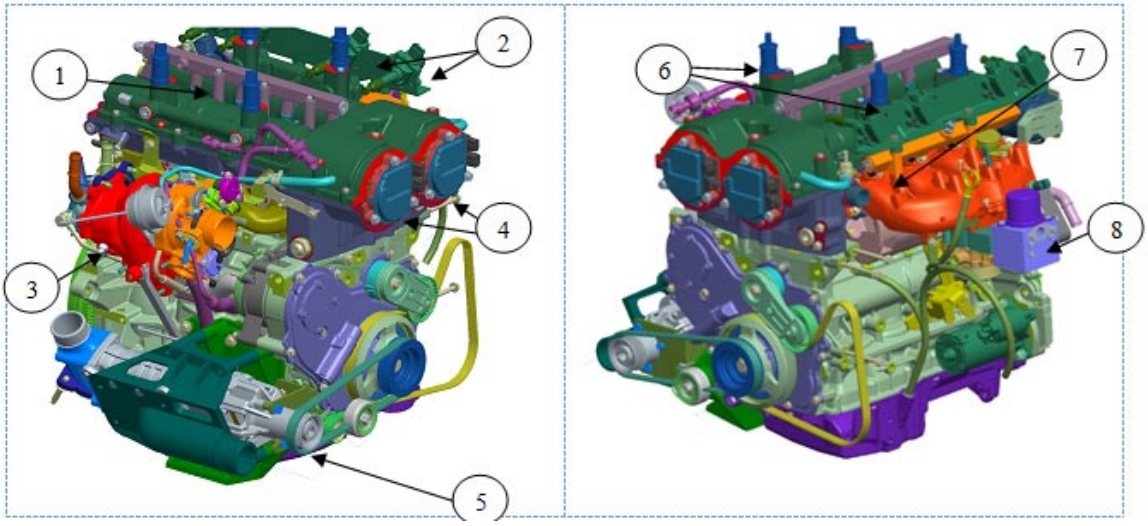

FIGURE 1. Prototype I Engine Configuration

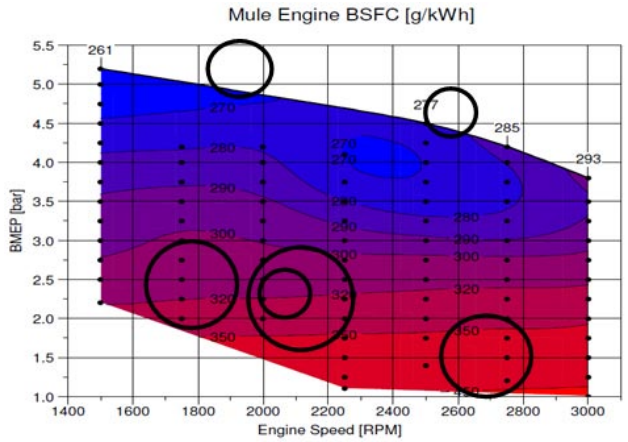

FIGURE 2. Brake Specific Fuel Consumption (BSFC) Comparison V-6 PFI vs. Boosted HCCI

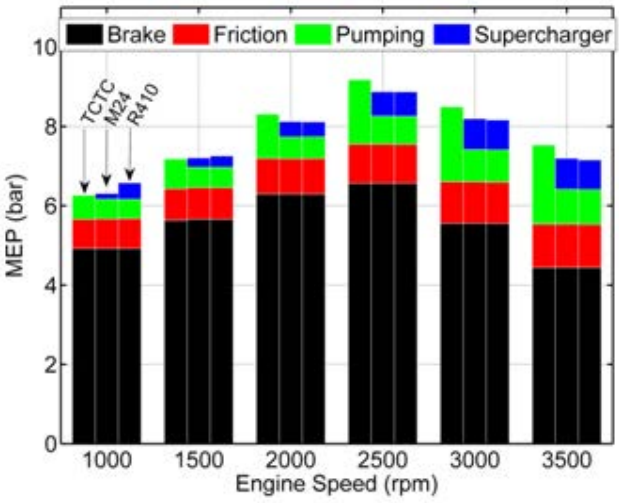

FIGURE 3. Simulation Results from Shingne et al. [1]

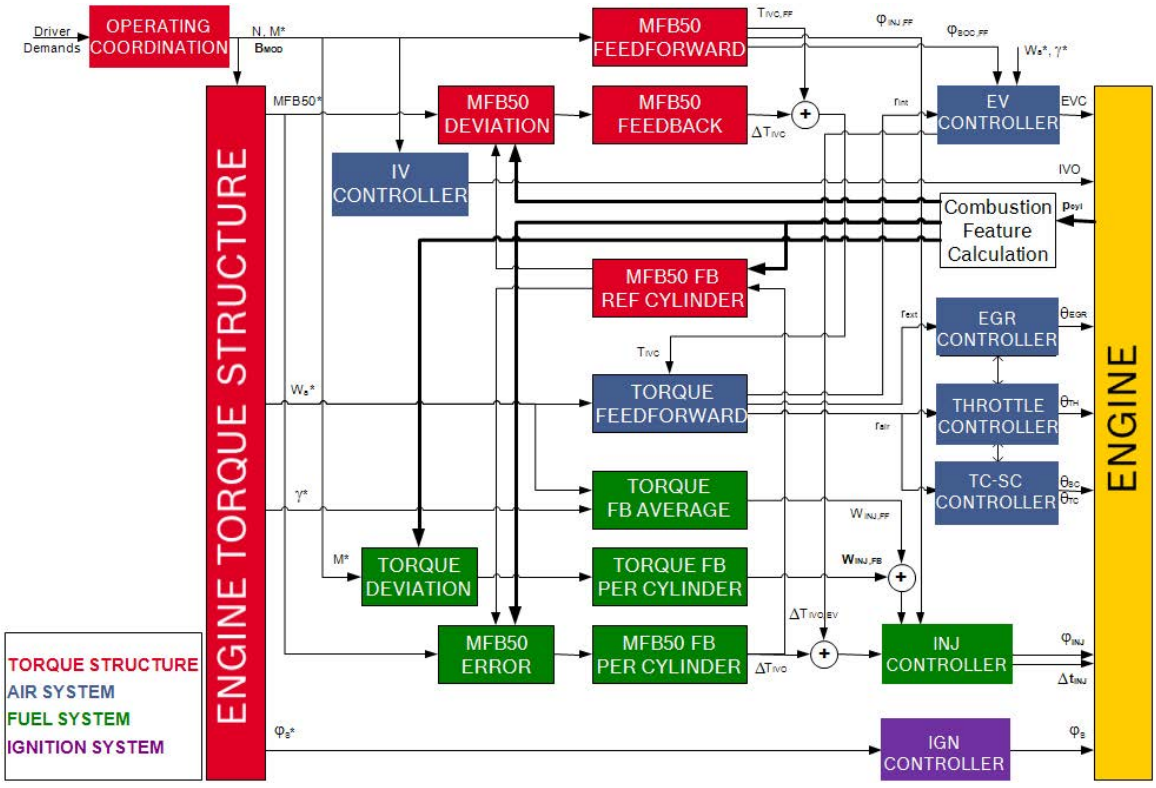

FIGURE 4. Overall Controller Architecture for HCCI Combustion Control

(FS), and Ignition System (IS). Based on the driver demands, the Operating Coordinator first determines the engine operation conditions, speed and torque, as well as the desired combustion mode considering the possibility of combustion mode switch. Then, ETS decides the key engine control set-points, such as the desired fresh charge and air-to-fuel ratio, for the target combustion mode. Next, the AS, FS and IS take these control set-points and determine the commands for the actuators, such as throttle angle and ignition angle.

During the HCCI combustion, combustion phasing and torque are the two main control variables. It has been identified in literature and observed during experiments that exhaust valve closing (EVC) and

start of injection (SOI) are the two main actuators for the control of combustion phasing. In this work, the combustion phasing control strategy employs the information derived from the cylinder-individual combustion pressure sensor for feedback control of the crank angle at 50% mass fraction burn (CA50), and adopts the reference cylinder approach to coordinate between the EVC and SOI actuation. To enable fast and reliable transient operation during HCCI combustion, a dynamic model-based feedforward controller is currently being developed to compensate the effects of an EVC step change on combustion phasing via SOI. In addition, a cylinder-individual combustion pressure feedback controller is also used to balance the torque among the cylinders via injected fuel quantity.

To enable the model-based feedforward control, a reduced-order model is developed to capture the influence of actuator EVC and SOI on the cylinder charge composition and temperature that determines the HCCI combustion performance. As illustrated in Figure 5, a model with a few key states describing the charge composition, such as oxygen and fuel concentration, and temperature is capable of capturing the effects of EVC on combustion phasing as well as air charge dynamics.

Conclusions

- Control architecture is designed based on the existing Bosch MED17 software to enable multi-mode combustion.
- Supercharger-turbocharger configuration as boosting device for HCCI has been selected.
- Prototype I engine is operational and all actuators are performing as expected with Bosch MED17 controller.

References

1. P. Shingne, D. Assanis, A. Babajimopoulos, A. Mond, and H. Yilmaz, "Application of a supercharger in a two-stage boosting system for a gasoline HCCI engine: a simulation study", In Proceedings of *ASME-ICEF Conference*, Morgantown, WV, Oct 2011.

FY 2011 Publications/Presentations

1. H. Yilmaz, "Advanced Combustion Concepts – Enabling Systems and Solutions (ACCESS) for High-Efficiency Light Duty Vehicles", 2011 DEER Conference, Detroit, MI, Oct 2011.

2. H. Yilmaz, "Advanced Combustion Controls – Enabling Systems and Solutions", 2011 Annual Merit Review, Washington, D.C., May 2011.

3. P. Shingne, D. Assanis, A. Babajimopoulos, A. Mond, and H. Yilmaz, "Application of a supercharger in a two-stage boosting system for a gasoline HCCI engine: a simulation study", In Proceedings of *ASME-ICEF Conference*, Morgantown, WV, Oct 2011.

4. S. Jade, E. Hellström, L. Jiang, and A. Stefanopoulou, "On the influence of composition on the thermally-dominant recompression HCCI dynamics", In Proceedings of *ASME Dynamic System and Control Conference*, Arlington, VA, Oct 2011.

5. E. Hellström and A. Stefanopoulou, "Modeling cyclic dispersion in autoigntion combustion", In Proceedings of *IEEE Control and Decision* Conference, Orlando, FL, Dec 2011.

Special Recognitions & Awards/Patents Issued

1. Pending US Patents on "Compounded Dilution Air Charge Device."

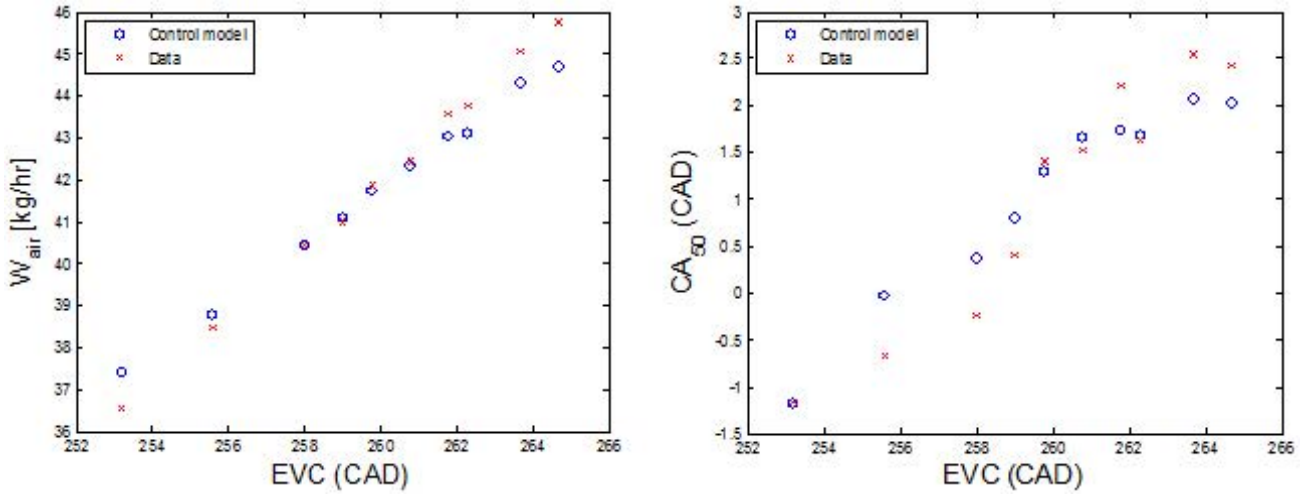

FIGURE 5. Comparison between a Reduced-Order Combustion Model ad Experimental Data during an EVC Sweep at 2,500 RPM, 2.5 bar Brake Mean Effective Pressure (BMEP)

2. Pending US Patents on "Combustion Mode Switching with a Turbocharger/Supercharged Engine."

3. Pending US Patents on "Method for Modeling Cyclic Variability in Lean Controlled-Autoignition Engines."

4. Pending US Patents on "Fueling Strategy for Controlled-Autoignition Engines."

5. Pending US Patents on "Method for Path Planning during Combustion Mode Switch."

II.A.30 Cummins Next Generation Tier 2 Bin 2 Diesel

Michael J. Ruth
Cummins, Inc.
PO Box 3005
Columbus, IN 47201-3005

DOE Technology Development Manager:
Roland Gravel

NETL Project Manager: Carl Maronde

Subcontractor:
Johnson-Matthey Inc., Wayne, PA

Overall Objectives

- Demonstrate 40% fuel economy improvement over baseline gasoline V-8 pickup truck.
- Demonstrate Tier 2 Bin 2 tailpipe emissions compliance.

Fiscal Year (FY) 2011 Objectives

- Determine baseline values for fuel economy/ emissions on the target gasoline-powered vehicle.
- Create a baseline reference map of fuel consumption and emissions for the Cummins 2.8 L engine.
- Create models for vehicle, engine and aftertreatment, and control system.
- Enable engine testing of advanced fuel and air handling systems.
- Complete mule vehicle build.

Accomplishments

- Technical requirements defined for new engine architecture.
- Technical requirements defined for new aftertreatment effectiveness.
- Model validation completed of low-pressure exhaust gas recirculation (LP-EGR) fuel consumption and oxides of nitrogen (NOx) emission benefits required to achieve engine-out emissions and base engine fuel economy targets.
- Model validation completed of vehicle drive cycle and fuel economy on baseline diesel.

Future Directions

- Design and procure clean-sheet engine to meet technical requirements as outlined via technical requirement from model data.
- Utilize fabricated subsystems on baseline engine carcass to demonstrate model results for fuel consumption and emission control.
- Demonstrate fuel economy at target in mule vehicle with mule engine coincident with greater than 90% NOx reduction aftertreatment.

Introduction

The overall objective of this project, Cummins Next Generation Tier 2 Bin 2 Diesel, is to design, develop, and demonstrate in a light-duty (1/2 ton pickup truck) a state-of-the-art light-duty diesel engine that meets Environmental Protection Agency Light-Duty Tier 2 Bin 2 emission standards and increases fuel efficiency by at least 40% compared with a state-of-the-art port fuel injected gasoline engine.

The U.S. new, personal use vehicle fleet has changed slightly over the past two years, with car purchases increasing, but by and large, pickup trucks and sport utility vehicles (SUVs) account for nearly half of sales in this segment. An improvement in fuel economy by 40% in the light truck and SUV segment would reduce the U.S. oil consumption by 1.5 million bbl/day and reduce greenhouse gas emissions by 0.5 million metric tons/day.

Approach

The project is a four phase plan. The first phase included the baseline establishment for the target vehicle (2010 Nissan Titan) as well as the fuel consumption and emission rate of the Cummins 2.8 L ISF Euro III engine. Model development in phase one will direct technology test and development to create technical profile for new engine design. This phase of work will determine viable technologies to carry forward. The technologies will be considered with regard to performance on fuel economy and emissions as well as cost and weight. The technologies are primarily focused on reducing emissions without negatively affecting fuel economy. High priority has been given to weight reduction and cost control technologies for the base engine, and air handling and aftertreatment for emissions reduction.

In phase two, the base engine and vehicle will be modified for tests to validate the models. Additionally,

phase two will include engine design and procurement based on technical profiles.

Phase three will entail the development work required to bring the new engine to achieve Tier 2 Bin 5 with the majority of all systems working properly. Phase four will be the optimization of all subsystems, including vehicle systems such as charging and vacuum system as well as fueling and transmission shift logic. The fourth and final phase will be the ultimate goal of Tier 2 Bin 2 emissions with 40% fuel economy improvement over the baseline gasoline power train.

Results

NxtGen on-board synthesis gas generation systems were being considered with the intention of reducing the time required for aftertreatment warm-up during cold-start conditions. This particular system promised reduced time delay for effective aftertreatment reduction of hydrocarbons and NOx. In contrast to these valuable benefits, there exist certain characteristics which negatively impact the consideration of such a system. Specifically, the increased system cost ~$500 per engine represents a substantial increase in the overall cost of the engine package and added weight. Eventually it was decided to no longer pursue this technology for two reasons; the emissions of unregulated emissions (methane) and created an inapt situation for integration of other systems. The NxtGen system would have pushed all the aftertreatment approximately 24 inches rearward, effectively eliminating any opportunity to utilize a LP-EGR system.

Simulation work has shown LP-EGR to be very effective at lowering engine-out NOx (to the same extent as standard, high-pressure [HP]-EGR) while not negatively affecting fuel consumption. Analysis of the several options for air handling conditions (i.e. HP-EGR, LP-EGR and various temperatures for cooling – standard coolant temperature, a low temperature coolant loop, or ambient air-to-air medium) at light load has led to an understanding of how the LP loop might be used. A series of cases were considered by holding speed, fueling and fresh air/fuel ratio constant and allowing charge flow (fresh air plus EGR) to vary via the EGR rate only. Each case considered a different cooling scenario. Figure 1 shows the potential for optimizing pumping work as EGR is increased. The simulation results show that an un-cooled EGR route with air-to-air charge air cooling would yield a low pumping work penalty for low-flow EGR conditions. For high EGR flow conditions, the maximum cooling on a LP loop is preferred. There needs to be additional analysis of the cooling schemes to understand the condensation of the EGR portion of the charge flow. Condensation needs to be avoided in order to eliminate issues like freezing and corrosion. Work in the design phase will include scheme of a cooling system to avoid condensation while

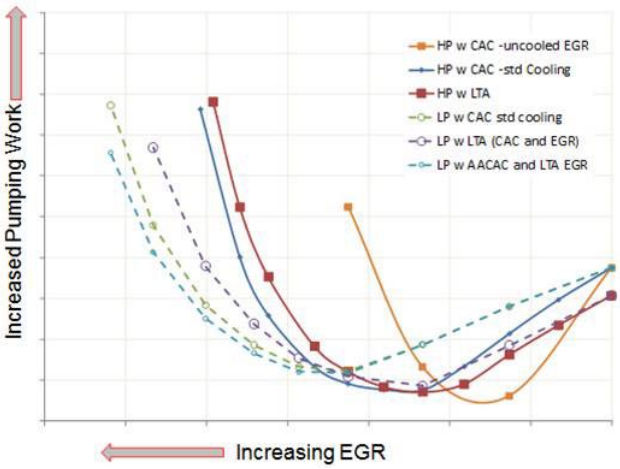

CAC – charge air cooling; AACAC – air-to-air CAC, LTA – low temperature coolant loop; std coolant – normal coolant loop

FIGURE 1. Results for Steady Speed and Fueling with Fixed Air/Fuel Ratio and Varying EGR Paths and Cooling Conditions

providing the lowest possible intake charge temperature for power density.

The baseline engine was built with a fabricated system to study the actual performance of a HP and LP EGR system. The engine with HP and LP EGR options created a platform in which to quickly explore schemes for warm-up strategy and other "off nominal" operating conditions. A short study of combined dual loop (HP and LP EGR) was conducted. The data was collected in the open-loop operation control system format (i.e. commanding valve position as opposed to mass or charge flow type parameters). The data proved that dual loop can be advantageous under light loads in comparison to either an exclusive HP or LP loop. The dual loop allows for very high EGR rates (in excess of 50%) without the typical penalty of high pumping work. Figure 2 is a summary of NOx, smoke and fuel consumption from the test. Zero HP valve position would indicate all EGR flow through the LP loop (LP is the primary loop for this condition).

Investigation of the benefit of oil viscosity was also conducted using the baseline engine. This investigation went beyond the normal suite of oils to test, which consists of all U.S. available CJ-4 American Petroleum Institute (API) specified oil grades. Additional testing used oil which is lighter than the minimum specification for an API CJ-4. U.S. specification CJ-4 oils have a "limiting specification" parameter for viscosity at 100 deg C. In the case of 15W40, 10W30, and 5W30, the high-temperature, high-shear (HTHS) viscosity specification for CJ-4 (also known as diesel specification) is limited to be not less than 3.4 centipoise (cP). Therefore, the 10W30 and 5W30 viscosity is reduced under the cold operation, but as the temperature increases, the viscosity

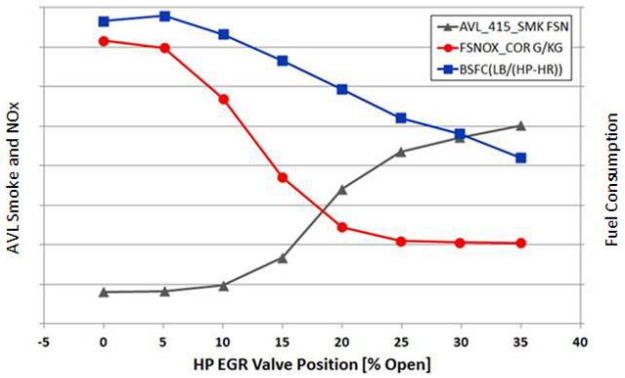

FSN – filter smoke number; FSNOX – filter smoke NOx; BSFC – brake specific fuel consumption

FIGURE 2. Dual-Loop Operation at 1,000 RPM 2 bar Brake Mean Effective Pressure

of all CJ-4 oils come together and look nearly identical at normal operating temperature.

In addition to the CJ-4 oils, a European sourced 5W30 with an HTHS rating of 2.9 cP was included. Results of testing are included in Table 1.

The data clearly show the reduction of oil viscosity will improve the fuel economy over the drive cycles. Unfortunately, the cold portion of the FTP test was unable to be completed with the "Low V" oil. It can be surmised the FTP could be significantly improved from the baseline 15W40 oil. The properties of the "Low V" oil will be used in the design of the new engine, ensuring compatibility for bearing and wear surfaces.

A course aftertreatment model including passive NOx adsorber (PNA) technology was employed to consider the tailpipe emissions under cold-start conditions. This analysis divided the cold bag (bag 1) into two phases, bag 0 and bag 1. Bag 0 includes the time from 0 to 180 seconds. Employing the PNA technology as a 2.8 L catalyst to the baseline engine data in bag 0, the model shows no NOx emission getting past the PNA until 100 seconds into the cycle. In order to control the tailpipe emissions, the selective catalytic reactor would need to be functioning by the 100 second mark, or the PNA would need to be increased in capacity for this baseline case. For the target conditions, using a ratio of engine-out emission targets, the baseline engine-out emissions were modified to meet the target values and a 0.9 L PNA was used. The plan moving forward will include the 0.9 L PNA and close coupling of the selective catalytic reduction system.

TABLE 1. Test Results of Oil Viscosity Testing (The "Low V" has 2.9 cP HTHS value, all other oils meet the standard CJ-4 specification for diesel oil.)

CFR (Y)	Baseline	10W30	5W30	5W30	Units
	15w40			Low V	
Fuel Economy FTP75	23.8	24.0	24.1	N/A	MPG
Fuel Economy Bag1	23.1	23.6	23.7	N/A	MPG
Fuel Economy LA4	24.6	24.6	25.0	25.9	MPG
Fuel Economy HWFET	29.6	30.0	30.0	30.4	MPG

Conclusions

The Cummins next generation Tier 2 Bin 2 light-duty diesel engine project has successfully completed the first year of the four year project. The follow conclusions have come from the first year of modeling and testing;

- Fuel reforming technology is currently not capable of meeting cost, fit and performance (low fuel consumption and low emissions) requirements for high volume automotive applications.
- LP-EGR system model and test data indicate NOx and fuel consumption can be reduced simultaneously.
- Low viscosity oil formulations have shown significant fuel economy improvement over the light-duty drive cycle on the order of 5%.
- The PNA is a promising technology for cold-start emission mitigation over the U.S. light-duty drive cycle.

FY 2011 Publications/Presentations

1. PRESENTATION: Program progress update, DEER conference 2011 (Ruth – High Efficiency Engine Technologies, Part 2).

2. PRESENTATION: Detailed update on cold start emission mitigation, DEER conference 2011 (Henry – Emission Control Technologies, Part 1).

3. PRESENTATION: Engineering the diesel for US LDT market, SAE Light Duty Diesel Emission Control Symposium (Ruth).

II.A.31 SuperTruck Initiative for Maximum Utilized Loading in the United States

Pascal Amar (Primary Contact),
Arne Andersson, Sam McLaughlin,
John Gibble, Jian Li
Volvo
13302 Pennsylvania Avenue
Hagerstown, MD 21742

DOE Technology Development Manager:
Roland Gravel

NETL Project Manager: Ralph Nine

Subcontractor:
Penn State University, State College, PA

Overall Objectives

- Identify concepts and technologies that have potential to achieve 55% brake thermal efficiency (BTE) on a heavy-duty diesel engine as defined in the SuperTruck project. A thorough analysis of the limiting factors and potential areas for improving the engine's efficiency using analytical simulations will be performed. This will include research into alternative thermodynamic cycles, advanced component design, fuel formulation and new engine designs.
- Demonstrate a partially premixed combustion (PPC) combustion concept operating on a specially formulated fuel that can operate in the fuel, load, and speed range of a normal diesel engine but with significantly improved thermal efficiency. The aim is to demonstrate 50% brake efficiency in at least some operating points.

Fiscal Year (FY) 2011 Objectives

- Develop simulation tools and models for PPC and evaluation of new concept.
- Identify new concepts for further analysis.
- Simulate, test and evaluate PPC combustion.
- Organic Rankine Cycle (ORC) testing: expand the maximum efficiency and operating range of the waste heat recovery (WHR) system, improve low speed and low load.

Accomplishments

- Within combustion computational fluid dynamics (CFD) two deliverables were met for September 2011: a literature review on fuels and chemical mechanisms that are of interest for high-efficiency combustion in compression-ignition engines; and a "version 0" of the combustion model probability density function (PDF) code.
- Within the ORC system several tasks were completed: established concept to achieve targets, development of transient simulation and control strategy, design (procure and build ORC system in test bed), steady-state manual operation of ORC system across speed/load range.

Future Directions

Combustion CFD

The transported PDF code will be installed and evaluated in the Volvo computer cluster. We will evaluate predictive capability and computer power requirements. This work will be supported at Penn State by a spray and combustion CFD specialist from Volvo. A key deliverable will be a version of the PDF code that is compatible with moving meshes in STAR-CD.

Combustion CFD Validation

The optical instrumentation for the constant volume combustion chamber will be received and installed in the chamber of the CID 510 instrument.

Test and Modeling of High Performance Pistons

In the upcoming months, the pistons will be installed in a multi-cylinder engine and tested.

ORC System

Activities underway: controls development underway in test bed, calibration of system under transient conditions, and comparison of test data to simulation results.

Introduction

The combustion chamber design is critical to the overall performance of the heavy-duty diesel engine. Changes to this portion of the system can dramatically affect the efficiency and emissions of the engine. This project proposes to improve engine efficiency and

validate the design through this approach. Three-dimensional CFD combustion simulations were carried out to evaluate new piston prototypes for efficiency and emissions improvement.

A variety of different concepts of PPC combustion are currently proposed. They differ in the way of achieving partial inhomogeneity in local equivalence ratio but also reactivity of the fuel. One main concept is the use of a single fuel with rather high octane numbers in the range of 70-85 making use of multiple injections to reach a certain degree of premixing of the charge. One of the main challenges with this approach is to ensure operability in the complete engine range, in particular at low loads and cold temperatures (see Figure 1).

Approach

Combustion Concept Development

- Identify concepts and technologies that have potential to achieve 55% BTE on a heavy-duty diesel engine as defined in the SuperTruck project. A thorough analysis of the limiting factors and potential areas for improving the engine's efficiency using analytical simulations will be performed. This will include research into alternative thermodynamic cycles, advanced component design, fuel formulation and new engine designs. The final assessment of the 55% efficiency goal will include the additional gains that are expected from the use of a Rankine WHR system, optimized auxiliaries and reduced friction losses.
- One interesting new concept is PPC. The goal of this activity is to demonstrate a PPC combustion concept operating on a specially formulated fuel that can operate in the fuel, load, and speed range of a normal diesel engine but with significantly improved thermal efficiency. The aim is to demonstrate 50% brake efficiency in at least some operating points.
- Enhanced versions of the more traditional diesel engine are also investigated. The improvement potential of all engine systems will be analyzed, including ultra-high PCP, flexible variable valve actuation cam timing, advanced piston bowl geometries, high peak injection pressures and advanced fuel injection systems and strategies as well as highly efficient turbocharging systems and insulation. A very efficient and highly integrated oxides of nitrogen (NOx) and particulate aftertreatment system will be assumed.

Simulating the new combustion regimes require updated tools. This is implemented via user coding in a commercial CFD code (STAR-CD) and also in GT-Power for system simulation. It is anticipated that the CFD approach will be able to capture the multiple regimes of compression-ignition combustion that are of interest for this project, including conventional diesel combustion, low-temperature combustion, PPC, and dual-fuel combustion.

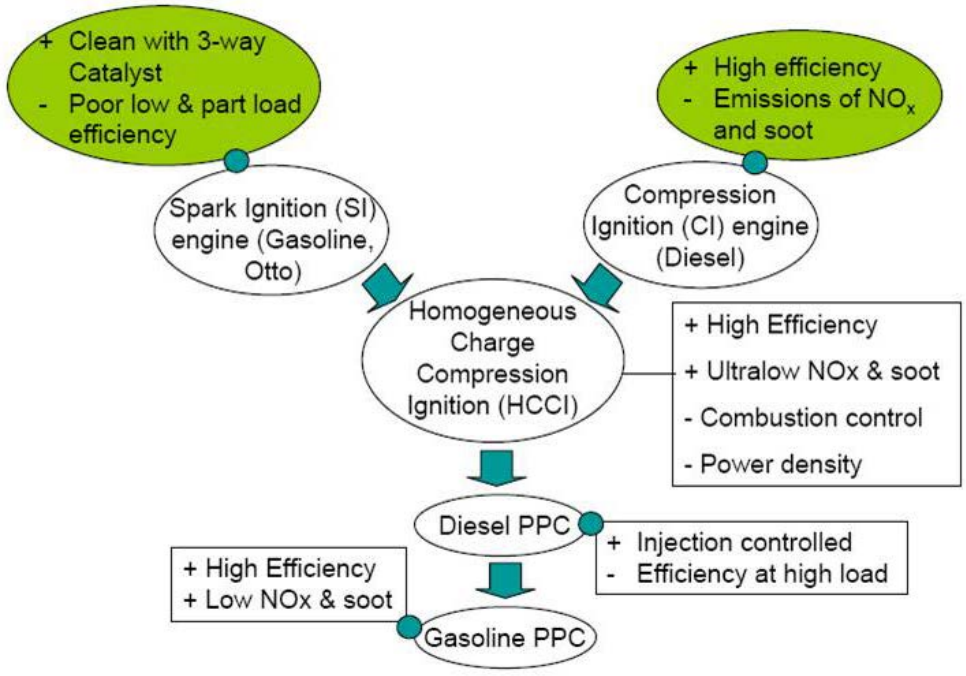

FIGURE 1. The Roadmap to Gasoline PPC

Results

Combustion CFD

- The focus of the modeling activity to date has been high-pressure, constant-volume turbulent spray combustion. Detailed quantitative comparisons are being made between model results and experimental measurements available through the Engine Combustion Network (ECN - http://www.sandia.gov/ecn/).
- Work to date has focused on identification and selection of chemical mechanisms, and on establishing the degree to which turbulent fluctuations in composition and temperature influence the computed ignition event and turbulent flame structure.

Combustion CFD Validation

- Regarding the constant volume combustion chamber experiments, optical instrumentation was selected and ordered for the chamber for visualization of spray (digital photography using a borescope) and detection of the onset of chemiluminescence in the chamber (photomultiplier tube with supporting optics).
- Also, an ignition quality test apparatus (PAC LLC, "CID 510" derived cetane number analyzer) has been received for this project.
- Volvo Powertrain has been working with Penn State University on the engine reference parameters correlation for combustion data and engine test, so Volvo engine results can be correlated with Penn State's engine results, and vice versa.

Test and Modeling of High Performance Pistons

- Simulations concluded the optimal injector spray angles but showed no clear advantage in terms of fuel economy and emissions, between 6-hole and 7-hole injectors.

ORC Design and Simulation Transient Drive Cycle Results

- Net fuel economy benefit is strongly dependent on drive cycle, e.g. topography (>4% to <2.5%). Limiting factors for higher fuel economy benefit are:
  - Low heat input operation: expander is bypassed resulting in drag torque.
  - High heat input operation: bypass boiler/expander.
  - Pressure limitation of heat exchangers: limits power at high load points (expander sized for cruise).

ORC Testing and Controls Development Changes in Speed and Load Test Results

- Control of system is challenging due to:
  - Thermal inertia
  - Flow restriction changes
  - Pump delivery with speed
  - Expander flow with speed, pressure and temperature (see Figures 2 and 3)
- Steady state for system is difficult to achieve:
  - Variation in working fluid flow due to changing restriction
  - Thermal inertia of system

Conclusions

The work on implementing the new tools capable of new combustion regimes proceed according to plan. Our experience so far indicates a substantial increase in computational power requirement.

High Performance Pistons

As of mid-2010, it has been determined that the high performance piston design gives improved fuel economy over the current production design with all

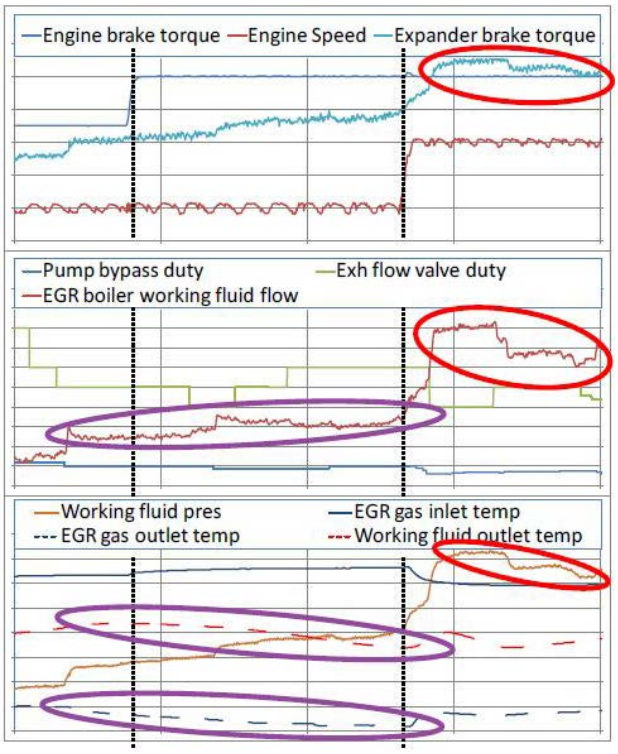

FIGURE 2. Speed and Load Test Results

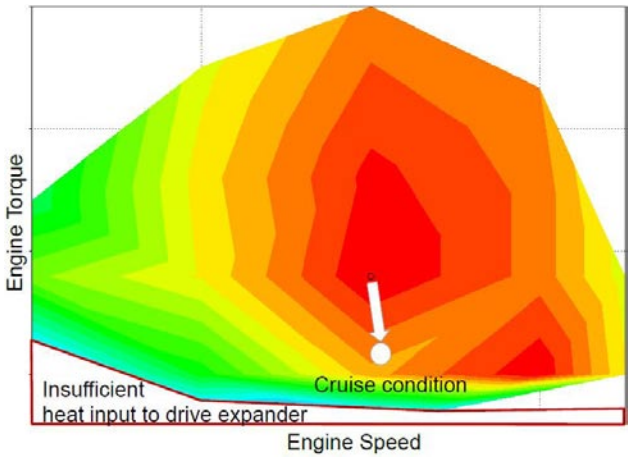

FIGURE 3. Speed v. Torque to Expand Max Efficiency and Operation of ORC System

other hardware and control parameters held the same. Currently controlled gaseous emissions remained the same while the soot emitted was reduced slightly.

ORC System

- **Simulation:** REFPROP® access and calculation too slow to enable transient simulation–utilize map-based fluid properties.
- **Controls:** Long system time period (thermal inertia) creates challenging transient control, and gas outlet temperature is leading indicator of working fluid temperature.
- **Operation:** Get out of the saturation dome as quickly as possible, and heat input management of exhaust stream is very effective control.

II.A.32 Advanced Boost System Development For Diesel HCCI Application

Harold Sun
Ford Motor Company
2101 Village Road
Dearborn, MI 48121

DOE Technology Development Manager:
Ken Howden

NETL Project Manager: Ralph Nine

Subcontractors:
- Wayne State University, Detroit, MI
- ConceptsNREC, White River Junction, VT

Objectives

The overall objective is to support industry efforts of clean and efficient diesel engine development for passenger and commercial applications. More specifically:

- ConceptsNREC objectives: leads boost system design, optimization, computer-aided engineering stress analysis and fabrication of prototypes as well as flow bench test; provides turbocharger maps for various turbo technologies to support system level simulation/integration.
- Wayne State University objectives: leads computational fluid dynamics analysis and analytical validation of various turbocharger concepts designed by ConceptsNREC.
- Ford Motor Company objectives: leads system integration, cascade system requirement, boost system development design target, validation and demonstration of fuel economy improvement of light-duty diesel engine performances on engine test bench.

Fiscal Year (FY) 2011 Objectives

- Design and hot flow bench test validation of advanced compressor with active casing treatment.
- Actuation system development of compressor active casing treatment.
- Redesign of small turbocharger for light-duty diesel applications.
- Fabrication of actuation system and small turbocharger.

Accomplishments

- The advanced compressor design with active casing treatment is truly a technical breakthrough (US Patent 20110173975A1) and has demonstrated 12% flow capacity enhancement at the supplier's flow bench.
- The actuation system for active casing treatment is fabricated.
- The turbo assembly with active casing treatment was tested on an engine dynamometer during 2011, which demonstrated 3% brake specific fuel consumption (BSFC) improvement at part load and full load, along with 90 horsepower increase in rated power over the base turbocharger that was used as donor turbocharger.
- Compressor design and analyses are complete. The redesign is not a scale-down from a large turbocharger previously developed for heavy-duty diesel engine applications. It is an attempt to trying a "large wheel" concept to have low cost but more efficient compressor and mixed flow turbine wheel. Of course, the active casing treatment will be a core technology and utilized in small turbocharger compressor design. The numerical results indicated an additional 5% improvement in efficiency is possible, with much wider operational range, compared with a scaled-down version of a large compressor.

Future Directions

- Fabricate and flow bench test the small turbocharger design/optimization to support light-duty diesel applications.
- Engine dynamometer test validation of the advanced compressor for light-duty diesel vehicle chassis certification applications.

✧ ✧ ✧ ✧ ✧

Introduction

Diesel homogeneous charge compression ignition (HCCI) and low-temperature combustion (LTC) have been recognized as effective approaches to dramatically reduce diesel emissions. However, high levels of exhaust gas recirculation (EGR) is needed to achieve homogeneous or partially homogeneous modes, which often drives the compressor and turbine into less efficient or even unstable operational areas.

To support industry efforts of clean and efficient internal combustion engine development for passenger and commercial applications, this project focuses on complete and optimal system solutions to address boost system challenges, such as efficiency degradation and compressor surge, etc., in diesel combustion/emission control system development, and to enable commercialization of advanced diesel combustion technologies, such as HCCI/LTC.

Approach

There are several boosting concepts that have been published and will potentially be helpful to extend operation range with decent efficiency. They are primarily single-stage turbochargers so that they are cost effective, have small package space, and small thermal inertia while providing enough EGR that is required by advanced combustion concepts such as HCCI/LTC.

This project has now particularly focused on the following:

- Optimal compressor impeller design that is focused on efficiency and surge margin improvement.
- The innovative active casing treatment that separates the function of surge and low-end performance from the flow capacity enhancement at full load, which is a major departure from conventional design concept.
- The mixed-flow turbine is an attractive option to improve efficiency on the turbine side. Base production turbine efficiency at light load and low speed is substantially lower than its peak efficiency. This project focuses on high turbine efficiency at lower speed ratios to improve EGR pumping capacity and vehicle fuel economy on customer driving cycles as well as enhancement of flow capacity.

The above technologies have been fully investigated and validated through numerical simulations. Some of them have been investigated via flow bench testing, followed by engine dynamometer testing. The advanced compressor impeller, active casing treatment for high compressor efficiency over wide operation range, together with the mixed flow turbine (matched to production variable nozzle geometry turbine and center housing) has demonstrated superior performance at part load and full load.

Results

- Figure 1 is the fabricated parts of two compressor wheels and the mixed flow turbine wheel.
- Figure 2 is schematic of the advanced compressor with active casing treatment to address the surge and choke design requirement for optimal performance over a wide operational range.
- Figure 3 shows that the advanced compressor efficiency has been improved over a wider operational range, compared with a base production centrifugal compressor.
- Figure 4 shows that the turbine efficiencies at partial-open positions and full-open have been substantially improved at low turbine speed ratio areas, i.e. the turbine performs more efficiently at near choke and high EGR conditions.
- The engine dynamometer test (Figure 5) also demonstrated BSFC improvement at part load and low speed due to improvement of turbocharger efficiency.
- The engine BSFC improvement (Figure 6) extended to full load; the full-load torque and power are increased dramatically, at even lower turbine inlet temperature, due to superior performance of the turbocharger at near-choke conditions.

FIGURE 1. Mixed Flow Turbine Wheel was Fabricated as Well as Compressor Wheels with Arbitrary Surface

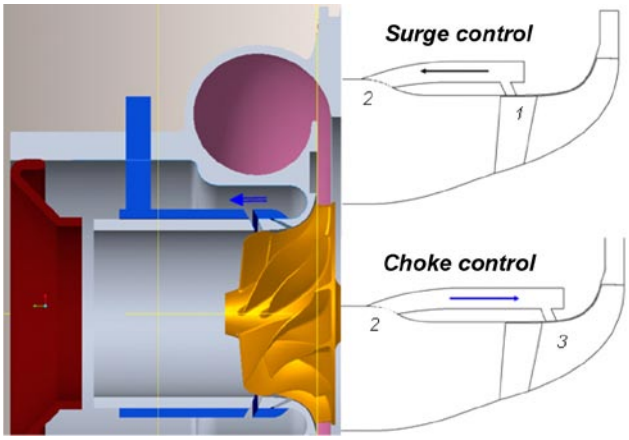

FIGURE 2. Compressor with Active Casing Treatment that Uses Two Different Slots to Control Surge and Choke Separately

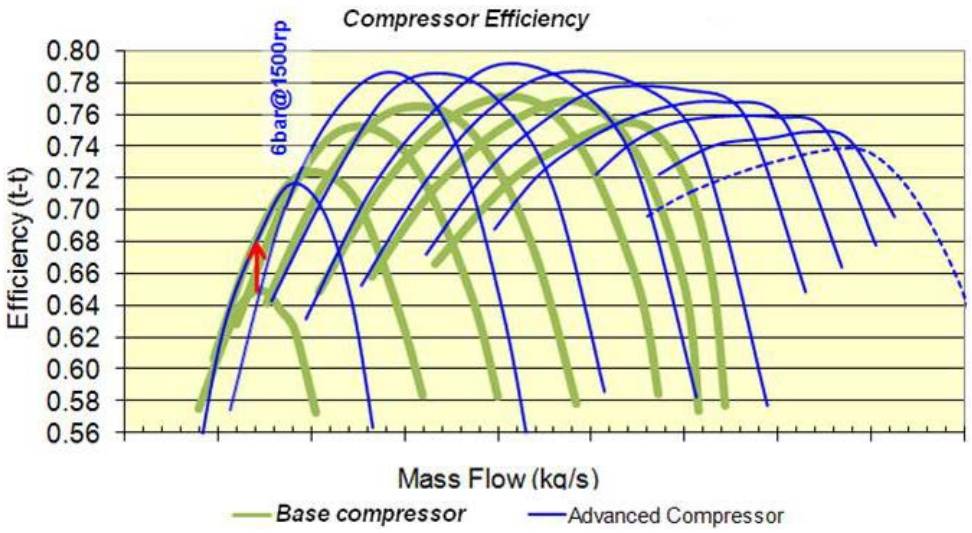

FIGURE 3. Compressor Efficiency Comparison, Advanced Compressor with Active Casting Treatment vs. Base Production Compressor

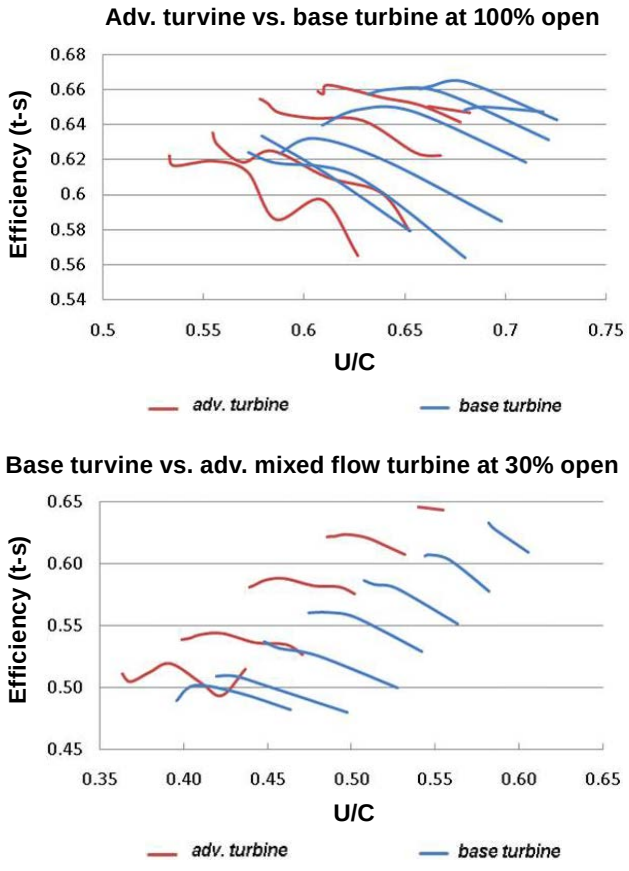

FIGURE 4. Hot flow bench tests indicated that the mixed flow turbine has better efficiency at low turbine speed ratios (U/C) at full open position as well as small open positions.

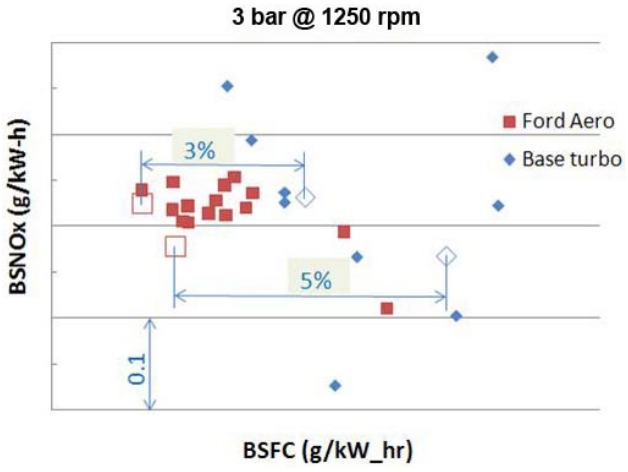

FIGURE 5. Engine dynamometer tests indicated improved BSFC at part-load conditions (key for city cycle fuel economy improvement) at the same level of feed gas brake specific oxides of nitrogen (BSNOx) emissions.

Conclusions

The large turbocharger development for heavy-duty diesel application is complete. The flow bench tests have demonstrated efficiency improvement on both the compressor and turbine, especially at low compressor mass flow and low turbine speed ratio area where most customer driving takes place. The back-to-back engine dynamometer test between the advanced turbo and the base production turbo demonstrated ~3% BSFC improvement at low load and low speed, as well as 90 horsepower increase in rated power (with reduced turbine inlet temperature), indicating

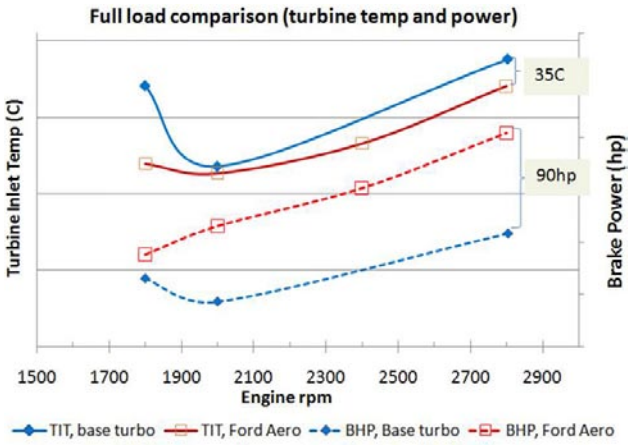

FIGURE 6. Engine Full-Load Performance

that the advanced turbocharger has better efficiency over a wider operational range. A major technical innovation, advanced compressor design with active casing treatment, has been patented. The next steps will include: fabrication and flow bench test of the redesigned small compressor and turbine wheels for light-duty diesel application, followed by test validation on an engine dynamometer.

FY 2011 Publications/Presentations

1. "Optimization of a Turbocharger for High EGR Applications", DEER 2011, October 5, 2011.

Patents Issued

1. US 20110173975(A1).

II.B.1 CLEERS Aftertreatment Modeling and Analysis

Maruthi Devarakonda, Darrell Herling, Do Heui Kim, Ja Hun Kwak, Chuck Peden, Mark Stewart, Andrea Strzelec, Janos Szanyi, Diana Tran, Jong Lee (Primary Contact)
Institute for Integrated Catalysis
Pacific Northwest National Laboratory (PNNL)
902 Battelle Boulevard
Richland, WA 99352

DOE Technology Development Manager:
Ken Howden

Objectives

- Lead and contribute to the Cross-Cut Lean Exhaust Emissions Reduction Simulations (CLEERS) activities:
  - Provide project updates to the industry sub-team, solicit feedback, and adjust work scope accordingly.
  - Lead technical discussions, invite distinguished speakers, and maintain an open dialogue on selective catalytic reduction (SCR), lean-NOx trap (LNT), and diesel particulate filter (DPF) modeling issues.

Fiscal Year (FY) 2011 Objectives

- Develop improved modeling capabilities for SCR and DPFs through fundamental experiments.
- Develop a fundamental understanding of SCR and LNT catalysts with primary focus on reaction mechanisms and material characterization.

Accomplishments

- Participated in monthly CLEERS teleconferences and coordinated the calls focused on SCR, LNT and DPF technologies.
- Updated PNNL's SCR model for the state-of-the-art commercial Cu-zeolite SCR catalyst to extract kinetic parameters and to quantitatively describe the effects of hydrothermal aging.
- Examined the effects of hydrothermal aging on the physicochemical properties and SCR reactions using the commercial Cu catalyst in collaboration with Oak Ridge National Laboratory (ORNL).
- Investigated the nature of Cu species and obtained kinetic parameters for small-pore zeolite-based Cu SCR catalyst.
- Examined the effects of support materials for Ba-based LNT catalysts, and found magnesium aluminate may improve the oxides of nitrogen (NO_x) reduction performance at high temperatures.
- Investigated soot oxidation mechanisms for relevant oxidants (O_2, NO_2) through reactor experiments and transmission electron spectroscopy (TEM) analysis.
- Seven publications and 21 public presentations (eight invited) during the past FY.
- Co-organized sessions on emission control and modeling for the SAE World Congress and the American Society of Mechanical Engineers Internal Combustion Engine Conference.

Future Directions

- Extract the SCR reaction kinetics and examine various reaction pathways over the state-of-the-art Cu SCR catalyst using PNNL's Cu SCR catalyst model.
- Conduct detailed kinetic and mechanistic studies for NO reduction over the state-of-the-art small-pore zeolite-based Cu SCR catalysts.
- Continue fundamental studies of novel high temperature LNT formulations.
- Characterize current production and advanced DPF substrates through advanced image and statistical analysis of high resolution computed tomography data.
- Investigate the use of micro-scale simulation to improve the commonly used unit collector models for DPF substrates.

Introduction

CLEERS is a research and development focus project of the Diesel Cross-Cut Team. The overall objective is to promote the development of improved computational tools for simulating realistic full-system performance of lean-burn engines and the associated emissions control systems. Three fundamental research projects are sponsored at PNNL through CLEERS: DPF, SCR, and LNT. Resources are shared between the three efforts in order to actively respond to current industrial needs. In FY 2011, more emphasis was placed on the SCR and LNT activities because of urgent application issues associated with these technologies.

Approach

Among the catalysts for SCR technology, base metal exchanged zeolite catalysts are being considered for vehicle applications because of their high NO_x reduction efficiency over a wide temperature range [1]. In particular, the state-of-the-art small-pore zeolite-based Cu catalysts have been proven very effective and are currently used for diesel NO_x emission controls in Europe and North America. Thus, we have investigated the physicochemical properties of the latest commercial Cu-zeolite catalyst with respect to hydrothermal aging in great details. We also updated PNNL's SCR model to examine the effects of hydrothermal aging on kinetic parameters to quantitatively describe the changes induced by the aging process.

As the industry began using the latest Cu SCR technology, we continued to explore the small-pore zeolite-based Cu catalysts for their activities and physicochemical properties. Since commercial Cu SCR catalysts are fully formulated, Cu-SSZ-13 (Cu ion-exchanged Chabazite zeolite) catalysts were prepared in-house using the method published [2] and examined in comparison with previously known Cu-zeolite catalysts to investigate the nature of Cu species. We also initiated the first open literature studies on the NO_x reduction mechanism and kinetics over Cu-SSZ-13.

The LNT technology is based on the ability of certain oxides, such as alkaline and alkaline earth oxide materials, to store NO_x under lean conditions and reduce it during rich engine operation cycles. Among the catalysts developed to date, the most extensively studied catalyst system continues to be based on BaO (barium oxide) supported on a high surface area alumina (Al_2O_3) material [3]. Our project is aimed at developing a fundamental understanding of the operation of the LNT technology especially with respect to the development of new LNT materials able to operate at significantly higher temperatures than the current generation of LNT materials.

We continued to utilize the state-of-the-art techniques, such as solid-state nuclear magnetic resonance (NMR) [4], X-ray diffraction (XRD), TEM/energy-dispersive spectroscopy, Fourier transform infrared, Brunauer-Emmett-Teller (BET), and temperature-programmed desorption (TPD)/temperature-programmed reaction (TPR) available at PNNL and ORNL, and synchrotron X-ray absorption spectroscopy available at Brookhaven National Laboratory, to probe the changes in physicochemical properties of the catalyst samples. The model LNT catalysts were prepared by the incipient wetness method, using an aqueous alkaline earth nitrate solution and γ-alumina or magnesium aluminate support materials, and NO_x reduction performance was examined in a fixed bed reactor under lean-rich cycling conditions.

Soot oxidation rates are an important consideration for efficient regeneration of DPFs. Rates encountered in real devices have a complex relationship to a number of operational parameters. Micro-reactor studies were carried out to explore fundamental aspects of soot oxidation and to investigate differences arising from engine, fuel type, and oxidant (O_2 or NO_2). Experiments were carried out with soot from light-duty (Mercedes-Benz 1.7 L) and medium-duty (Cummins ISL) diesel engines. Soot produced from ultra-low sulfur diesel as well as a number of biodiesel blends was examined. Volatile components were removed and examined by TPD. Temperature programmed oxidation (TPO) was used to compare non-isothermal rates across a wide range of temperatures, while isothermal partial oxidation was used to develop rate parameters by differential oxidation steps at a number of discrete temperatures. Surface area evolution during oxidation was examined by in situ BET. TEM was used to examine the morphology of partially oxidized soot particles.

While current U.S. particulate emissions standards are evaluated on a mass basis, regulations around the world may move toward a number basis, which heavily weights smaller particles. This shift could require modification of current filter systems. Unit collector models have commonly been used to estimate mass capture efficiency and pressure drop in DPFs [5]. The ability of standard unit collector models to predict number efficiency over a range of particle sizes is currently being evaluated. Micro-scale models have been used to investigate fundamental filtration mechanisms and the impact of filter substrate microstructure on performance. Micro-scale modeling tools continue to evolve to allow more accurate prediction of capture efficiency as a function of substrate morphology and particulate size. It may be possible to use the results of micro-scale simulations to enhance the simpler unit-collector models.

Results

Catalyst Model Development

SCR modeling activities focused on updating PNNL's one-dimensional (1D) global kinetic model, which had been developed for the Fe-zeolite catalyst, for the latest commercial Cu SCR catalyst. All the sub-models previously developed for competitive adsorption by H_2O and hydrocarbons were also included. The total NH_3 adsorption capacity was considered as the number of active sites. Steady-state surface isotherms were collected to generate the Langmuir isotherms, from which the rate parameters for NH_3 adsorption-desorption were determined. The rate parameters were then used in the 1D Cu SCR catalyst model, which simulates the gas phase and surface phase concentrations of NH_3 along the axial direction. Kinetic

parameters for various SCR reaction steps, such as NH_3 oxidation and NO oxidation, are included.

CLEERS SCR transient reactor protocol, previously developed by ORNL, was used to generate data needed for model calibration and performance evaluation. The protocol consists of various steady-state and transient points, evaluating various SCR reaction steps and the effects of NH_3/NO_x and NO/NO_2 ratios on the NO_x reduction efficiency. Model parameters were tuned using the steady-state reactor test results, and the model was then validated against the transient reactor test results (shown in Figure 1). This model is currently being used to extract kinetic parameters for various SCR reaction steps, and to study the effects of hydrothermal aging on the kinetic parameters over the latest commercial Cu-zeolite SCR catalyst.

Catalyst Fundamental Research

The latest commercial Cu-zeolite catalysts have been reported to exhibit excellent NO_x reduction efficiency and durability. As they have been reportedly prepared on small-pore Chabazite zeolite, we initiated studies to understand the structure-activity relationship, and have recently published the first open literature paper on the performance of Cu-SSZ-13, which has the Chabazite structure [6]. Compared to extensively studied Cu-beta and Cu-ZSM-5 catalysts, it was found Cu-SSZ-13 is not only more active in the NO_x reduction performance, but also more selective toward nitrogen formation, resulting in significantly lower N_2O formation.

During FY 2011, we examined the effects of hydrothermal aging on various Cu-zeolite catalysts to better understand the nature of Cu species. After hydrothermal treatment at 800°C for 16 h, Cu-SSZ-13 was found to maintain high initial activity (shown in Figure 2). On the other hand, Cu-Y was found to lose its NO_x reduction activity completely, and both Cu-beta and Cu-ZSM-5 were found to lose NO_x reduction activity primarily at low temperatures (<350°C). In the presence of equimolar amounts of NO and NO_2, NO_x reduction activities of Cu-beta and Cu-ZSM-5 were recovered, but significant amounts of N_2O were produced [7].

The effects of hydrothermal aging on the physicochemical properties of Cu-zeolites were examined to probe the nature of Cu species. XRD measurement indicated that the zeolite structure was largely intact for all Cu-zeolites, except Cu-Y. However, when the extent of dealumination of zeolite structure was probed by solid state ^{27}Al NMR, some dealumination was observed for Cu-beta and Cu-ZSM-5, while little change was seen for Cu-SSZ-13. As no octahedral Al signal was observed despite the loss of tetrahedral Al signal, it was suggested that alumina moieties must be in very strong contact with Cu ions in Cu-beta and Cu-ZSM-5. When the redox properties of Cu species were examined by H_2-TPR, it was found that CuO and Cu-aluminate-like species were formed in Cu-beta and Cu-ZSM-5, while Cu ions

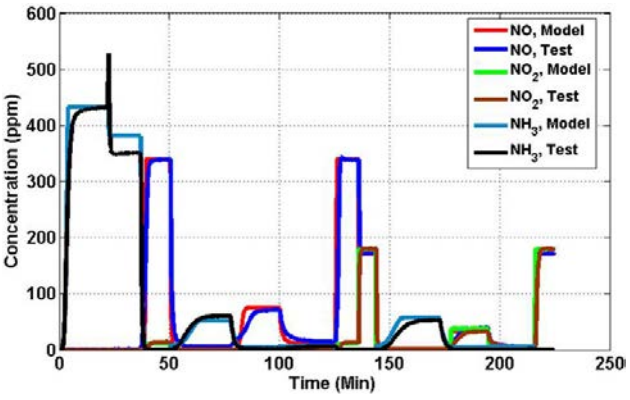

FIGURE 1. Comparison between the Model Prediction and Experimental Measurement of CLEERS SCR Transient Reactor Protocol

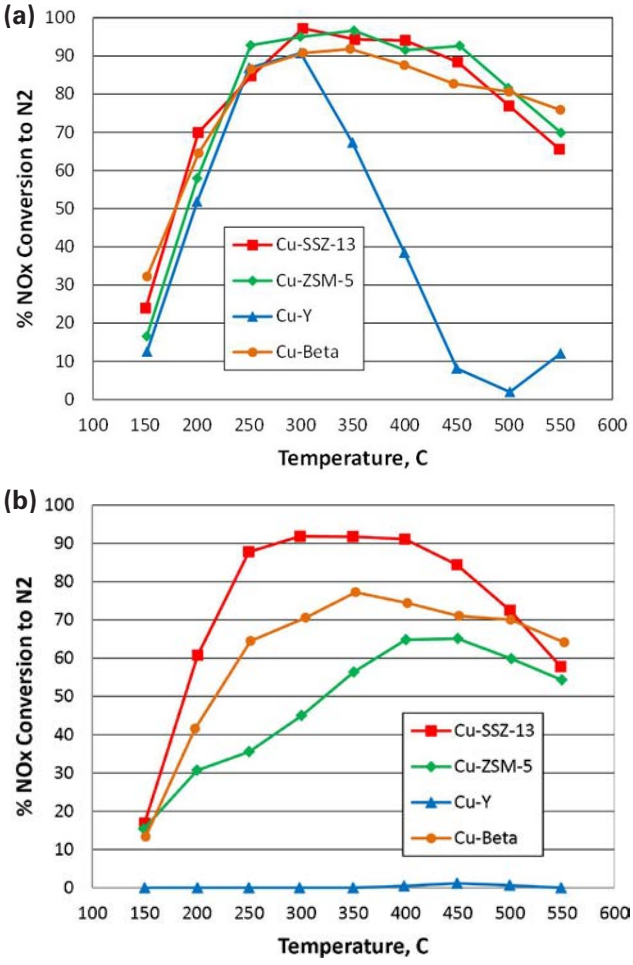

FIGURE 2. Percent NO Conversion to N_2 over Cu-Zeolites (a) Fresh and (b) Hydrothermally-Aged (Feed: 350 ppm NO, 350 ppm NH_3, 14% O_2, 10% H_2O in balance N_2)

could remain as isolated ions in Cu-SSZ-13 after the hydrothermal aging [7].

Our fundamental studies of possible new LNT formulations able to function at higher temperatures than the current generation of Ba-based materials have focused on changes in the composition of both the NO_x storage and support materials. In particular, substituting K for Ba as the NO_x storage material is known to provide higher temperature performance. During FY 2011, we examined the effects of LNT catalyst support on the NO_x reduction performance of Ba-based catalysts, and found that $MgAl_2O_4$ support material help improve the high-temperature NO_x reduction performance of Ba-based LNT catalyst [8].

We have recently compared the structural and chemical characteristics of the Pt/BaO LNT catalyst supported on γ-Al_2O_3 and $MgAl_2O_4$. The Pt-BaO/$MgAl_2O_4$ sample shows relatively low NO_x uptake at temperatures below 300°C, and the temperature of maximum NO_x uptake (T_{max}) is shifted to 350°C in comparison to that of Pt-BaO/Al_2O_3 (T_{max} ~250°C). More importantly, the NO_x uptake over the $MgAl_2O_4$-supported catalyst at 350°C is twice that of the alumina-based one as shown in Figure 3. The shift toward the higher temperature NO_x uptake is explained by the larger interfacial area between Pt and BaO, due to smaller Pt clusters as evidenced by TEM and Pt L3 Extended X-ray absorption fine structure. In situ time resolved X-ray diffraction results demonstrated that the formation of a $BaAl_2O_4$ phase in the BaO/$MgAl_2O_4$ LNT catalyst occurs at a temperature about 100°C higher than on BaO/Al_2O_3, which may also represent a beneficial attribute of the BaO/$MgAl_2O_4$ LNT with respect to catalyst stability.

Regarding soot oxidation over a DPF, while previous oxygen TPO studies had shown significant variation in oxidation rates depending upon the proportion of biodiesel in the fuel blend, we found that this was not the case for TPO with NO_2. The evolution of surface area during oxidation was also much different between the two oxidants. During NO_2 oxidation, the surface area followed a path similar to a shrinking core model, while very different behavior was observed for oxidation with O_2. Figure 4 shows a TEM image of soot partially oxidized by O_2. In the case of oxygen oxidation of both light-duty and medium-duty engine soot, pits can be seen forming in the exterior surface of primary particles. These features were not observed in samples oxidized by NO_2. "Fringes" observed in the two-dimensional TEM images indicate the position of graphene sheets in the three dimensional soot particle. Aspects of these features have been quantified by image analysis [9]. Sites at the edges of graphene layers tend to be more reactive, as do regions of high curvature, due to the effects of bond strain. Images of soot oxidized by NO_2 exhibited a higher proportion of short and curved lamella compared to soot oxidized by O_2. Taken together, these results suggest fundamentally different oxidation modes for the two oxidants. While the less reactive oxygen preferentially attacks edge sites and curved regions, resulting in surface pitting and a reduction in the proportion of curved lamella, NO_2 indiscriminately attacks carbon sites near the primary particle surfaces, breaking up long lamella into shorter sections.

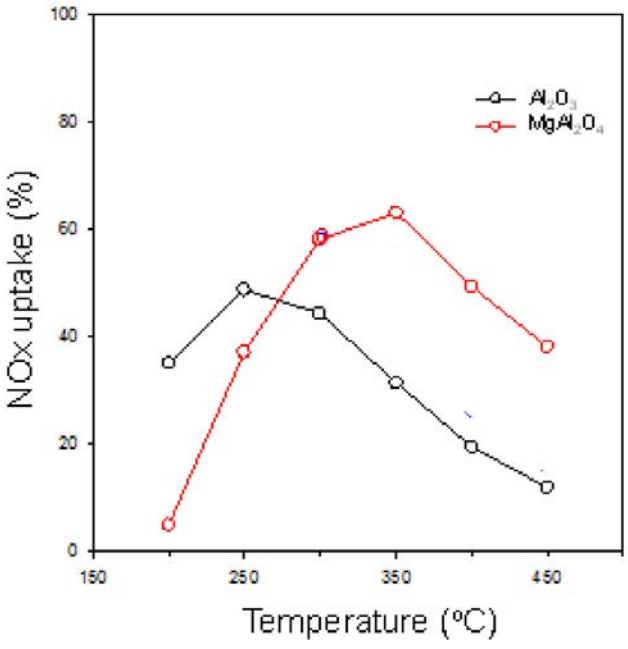

FIGURE 3. Percent NO_x Uptake over Pt-BaO/Al_2O_3 and Pt-BaO/$MgAl_2O_4$

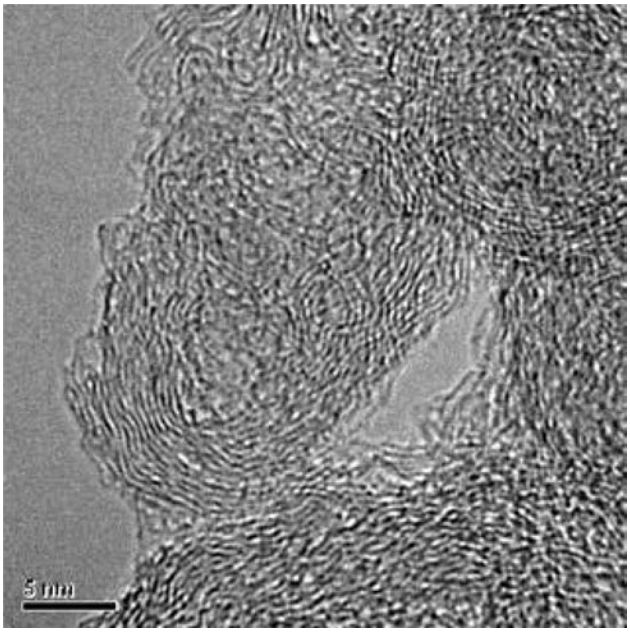

FIGURE 4. TEM of Diesel Soot after Partial Oxidation in Oxygen Showing Pitting on Primary Particle Surfaces

Conclusions

- Updated PNNL's SCR model for the state-of-the-art commercial Cu-zeolite SCR catalyst to extract kinetic parameters and to quantitatively describe the effects of hydrothermal aging.
- Examined the effects of hydrothermal aging on the physicochemical properties and SCR reactions using the model Cu-zeolite catalysts, and found that Cu species in small pore zeolite and commercial Cu catalysts are isolated Cu ions even after hydrothermal treatment at 800°C for 16 h.
- Examined the effects of support materials on Ba-based LNT catalysts for improved high-temperature performance, and found that the NO_x uptake over the $MgAl_2O_4$-support catalyst is twice higher than that of alumina-based one at 350°C.
- While significantly different reaction rates were observed for O_2 oxidation of particulates from fuel blends having different proportions of biodiesel, reaction rates for NO_2 oxidation seem to be much more similar.
- Fundamentally different oxidation modes appear to be involved in oxidation of diesel soot by NO_2 and O_2. Experiments suggest that O_2 attacks locations of higher reactivity within the solid particle matrix, while NO_2 indiscriminately attacks sites near the surfaces of primary particles.

References

1. G. Cavataio, J. Girard, J. Patterson, C. Montreuil, Y. Cheng and C. Lambert, DOE Cross-cut Lean Exhaust Emissions Reduction Simulations (*CLEERS*) Workshop, www.cleers.org, May 2007.

2. D.W. Fickel, R.F. Lobo, J. Phys. Chem. C 2010, 114, 1633.

3. W.S. Epling, L.E. Campbell, A. Yezerets, N.W. Currier, J.E. Parks, Catal. Rev.–Sci. Eng. 2004, 46, 163.

4. J.H. Kwak, J.Z. Hu, D.H. Kim, J. Szanyi, C.H.F. Peden, J. Catal. 2007, 251, 189.

5. A. Konstandopoulos, J.H. Johnson, *SAE* 890405.

6. J.H. Kwak, R.G. Tonkyn, Y. Wang, J. Szanyi, C.H.F. Peden, J. Catal. 2010, 275, 187.

7. J.H. Kwak, D. Tran, S.D. Burton, J. Szanyi, J.H. Lee, C.H.F. Peden, J. Catal. (submitted).

8. J.H. Kwak, D.H. Kim, J. Szanyi, S.J. Cho, C.H.F. Peden, Topics Catal. (submitted).

9. Vander Wal, R. and A. Tomasek, Comb. Flame, 2003, 134, 1.

FY 2011 Presentations

Invited

1. C.H.F. Peden, "Fundamental studies of catalytic NOx vehicle emission control," BASF Company Research Labs, Iselin, NJ, October 2010.

2. C.H.F. Peden, J.H. Kwak, D. Mei, R.J. Rousseau, J. Szanyi, Y. Wang, "Adsorption and reaction of alcohols on poorly crystalline γ–Al_2O_3 surfaces."

- 57th International Symposium of the American Vacuum Society, Albuquerque, NM, October 2010.
- 241st National Meeting of the American Chemical Society, Anaheim, CA, April 2011.

3. D.H. Kim, "Understanding the NO_x storage process in NO_x storage-reduction catalysts: similarities and differences between Ba and K," 241st National Meeting of the ACS, Anaheim, CA, April 2011.

4. C.H.F. Peden, "CLEERS Aftertreatment Modeling and Analysis," DOE Annual Merit Review, May 2011.

5. C.H.F. Peden, "Monomers and small clusters of metals and metal oxides on solid oxide supports: preparation, characterization, and catalytic reactivity," Gordon Research Conference on Clusters, Nanocrystals and Nanostructures, South Hadley, MA, July 2011.

6. J.H. Kwak, "NH_3-SCR activity and hydrothermal stability of Cu-SSZ-13," 242nd National Meeting of ACS, Denver, CO, August 2011.

7. C.H.F. Peden, "Excellent activity and selectivity of Cu-SSZ-13 in the selective catalytic reduction of NO_x with NH_3," EuropaCat-X Meeting, Glasgow, Scotland, UK, August 2011.

Contributed

1. C.H.F. Peden, D.H. Kim, K. Mudiyanselage, J. Szanyi, J.H. Kwak, H. Zhu, "NOx storage reduction catalysts: similarities and differences between Ba and K," DOE CLEERS Workshop, Dearborn, MI, April 2011.

2. D.H. Kim, K. Mudiyanselage, J.H. Kwak, J. Szanyi, H. Zhu, C.H.F. Peden, "Characteristics of Pt-K/$MgAl_2O_4$ lean NO_x trap catalysts," 22nd North American Catalysis Society Meeting, Detroit, MI, June 2011.

3. D.H. Kim, K. Mudiyanselage, J. Szanyi, J.H. Kwak, H. Zhu, C.H. F. Peden, "Nitrate formation/decomposition on Ba- and K-based model LNT catalysts: similarities and differences," 22nd North American Catalysis Society Meeting, Detroit, MI, June 2011.

4. C.H.F. Peden, J.H. Kwak, R.G. Tonkyn, D.H. Kim, J. Szanyi, D. Tran, J.H. Lee, "Excellent activity and selectivity of Cu-SSZ-13 in the selective catalytic reduction of NO_x with NH_3," 22nd North American Catalysis Society Meeting, Detroit, MI, June 2011.

5. J.H. Kwak, D. Mei, C.H.F. Peden, L.F. Allard, J. Szanyi, "The role of uncoordinated surface Al^{3+} ions in the anchoring and stabilization of catalytically active phases on

γ–Al_2O_3," 22nd North American Catalysis Society Meeting, Detroit, MI, June 2011.

6. L. Kovarik, R.A. Dagle, H. Wan, J.H. Kwak, B.C. Kabius, C.M. Wang, S. Thevuthasan, C.H.F. Peden, "Atomic level characterization of transition metal catalytic clusters and nanoparticles on $MgAl_2O_4$ substrate," Microscopy & Microanalysis 2011 Meeting, Nashville, TN, August 2011.

7. M.N. Devarakonda, R.G. Tonkyn, D.N. Tran, J.H. Lee, D.R. Herling, "Modeling competitive adsorption in urea-SCR catalysts for effective low temperature NOx control," ASME International Congress, Vancouver, BC, Canada, November 2010.

8. M.N. Devarakonda, J.H. Lee, J.A. Pihl, S. Daw, "Development of Cu SCR model using CLEERS SCR transient reactor protocol," DOE CLEERS Workshop, Dearborn, MI, April 2011.

9. M.N. Devarakonda, R.G. Tonkyn, J.H. Lee, "Modeling hydrocarbon inhibition of SCR reactions in Fe-zeolite catalyst using a competitive adsorption model," ASME Internal Combustion Engine Fall Conference, Morgantown, WV, October 2011.

10. M.N. Devarakonda, J.H. Kwak, J.A. Pihl, S. Daw, J.H. Lee, "Effects of hydrothermal aging on commercial Cu SCR catalyst," Directions in Engine-Efficiency and Emissions Research Conference, Detroit, MI, October 2011.

11. A Strzelec, TJ Toops, CS Daw, R Vander Wal, "Investigation of NO_2 Oxidation Kinetics and Burning Mode for Medium Duty Diesel Particulate: Contrasting $O_2$and NO_2 Oyxidation," Directions in Engine-Efficiency and Emissions Research Conference, Detroit, MI, October 2011.

12. A Strzelec, TJ Toops, CS Daw, R Vander Wal, "Trends in Particulate Nanostructure," Directions in Engine-Efficiency and Emissions Research Conference, Detroit, MI, October 2011.

13. A Strzelec, TJ Toops, CS Daw, R Vander Wal, "Impact of Biodiesel on Particulate Emissions Control," American Filtration and Separations Society Annual Meeting, Louisville, KY, May 2011.

FY 2011 Publications

1. K. Zhu, J. Sun, J. Liu, L.Q. Wang, H. Wan, J.Z. Hu, Y. Wang, C.H.F. Peden, Z. Nie, "Solvent evaporation assisted preparation of oriented nanocrystalline mesoporous MFI zeolites, "ACS Catalysis 2011, **1**, 682.

2. J.H. Kwak, R.G. Tonkyn, Y. Wang, J. Szanyi, C.H.F. Peden, "Using a surface-sensitive chemical probe and a bulk structure technique to monitor the γ- to θ-Al_2O_3 phase transformation," J. Phys. Chem. C. 2011, 115, 12575.

3. M. Devarakonda, D.R. Herling, D.H. Kim, J.H. Kwak, C.H.F. Peden, M.L. Stewart, J. Szanyi, R.G. Tonkyn, D. Tran, J.H. Lee, "CLEERS Aftertreatment Modeling and Analysis," FY2010 Progress Report for Advanced Combustion Engine Research and Development, pp. 130-135.

4. M.N. Devarakonda, R. Tonkyn, D.N. Tran, J.H. Lee, D.R. Herling, " Modeling species inhibition of NO oxidation in urea-SCR catalyst for diesel engine NOx control." ASME J. Eng. Gas Turbines Power 2011, **133**, 67102.

5. J.H. Kwak, D.N. Tran, S.D. Burton, J. Szanyi, J.H. Lee, C.H.F. Peden, "Effects of Hydrothermal Aging on NH_3-SCR reaction over Cu/zeolites." *Journal of Catalysis* (2012) submitted for publication.

6. J.H. Kwak, R. Tonkyn, D. Mei, S.J. Cho, L. Kovarik, J.H. Lee, C.H.F. Peden, J. Szanyi, "Size-Dependent Catalytic Performance of CuO on γ-Al_2O_3: NO Reduction Versus NH_3 Oxidation," *Journal of Physical Chemistry C* (2012) submitted for publication.

7. J.H. Kwak, D.H. Kim, J. Szanyi, S.J. Cho, C.H.F. Peden, "Enhanced High Temperature Performance of $MgAl_2O_4$-Supported Pt-BaO Lean NOx Trap Catalysts," *Topics in Catalysis* (2012) submitted for publication.

II.B.2 Enhanced High Temperature Performance of NOx Storage/Reduction (NSR) Materials

Do Heui Kim, George Muntean,
Chuck Peden (Primary Contact)
Institute for Interfacial Catalysis
Pacific Northwest National Laboratory (PNNL)
P.O. Box 999, MS K8-93
Richland, WA 99354

DOE Technology Development Manager:
Ken Howden

Cooperative Research and Development Agreement (CRADA) Partners:
- Neal Currier, Junhui Li, Randy Stafford, Alex Yezerets, - Cummins Inc., Columbus, IN
- Hai-Ying Chen, Howard Hess - Johnson Matthey, London, Great Britain

Objectives

Identify approaches to significantly improve the high temperature performance and stability of the oxides of nitrogen (NOx) storage and reduction (NSR) technology via a pursuit of a more fundamental understanding of:

- The various roles for the precious metals.
- The mechanisms for these various roles.
- The effects of high temperatures on the precious metal performance in their various roles.
- Mechanisms for higher temperature NOx storage performance for modified and/or alternative storage materials.
- The interactions between the precious metals and the storage materials in both optimum NOx storage performance and long-term stability.
- The sulfur adsorption and regeneration mechanisms for modified and/or alternative storage materials.

Fiscal Year (FY) 2011 Objectives

- Initial activity measurements of several candidate high-temperature NSR catalysts as suggested by prior publications in the open scientific literature. These will be followed by experiments probing the thermal stability and sensitivity to sulfur of the NSR catalysts.
- Initiate catalyst characterization of these model high-temperature NSR catalysts with a variety of state-of-the-art methods.
- Continue baseline performance measurements of fully formulated development NSR catalyst provided by Johnson Matthey (JM). These studies are limited to only performance measurements as a function of thermal treatments and sulfur exposure. No catalyst characterization will be performed on these materials.

Accomplishments

Two major research thrusts continued this year:

- Fundamental studies of high-temperature NSR catalysts prepared by PNNL:
  - Model catalysts were prepared at PNNL based on materials described in the open literature.
  - Initial studies of the sulfur tolerance, desulfation, and sensitivity to high temperatures (required for desulfation) of these model catalysts were performed this year.
- Fully formulated high-temperature NSR catalysts supplied from JM:
  - JM-supplied materials are being used solely to provide baseline performance and stability data of a potential commercial high-temperature NSR catalyst. Materials characterization (e.g., composition, morphology, etc.) of these catalysts are not being performed because these properties represent proprietary information.
  - Following up prior baseline performance and sulfation/desulfation experiments on these developmental catalysts, we carried out measurements of the thermal stability of these materials this past year.
  - Sensitivity of the gas-phase environment and sulfur removal efficiencies of these catalysts were also determined.

Future Directions

Studies aimed at determining performance limitations, sulfur sensitivity and desulfation behavior of candidate alternative support and NOx storage materials that provide improved high temperature performance will continue. An overall goal of the work will continue to be to develop a deeper understanding of the mechanisms of NOx storage and reduction activity, and performance degradation of materials that have been reported to show good NSR performance at temperatures considerably higher than BaO/alumina-based materials. As have the initial studies to be described here, these fundamental studies will be

carried out in conjunction with baseline performance and stability experiments on fully formulated catalysts provided by JM.

Introduction

The NOx adsorber (also known as the lean-NOx trap, LNT, or NOx storage reduction, NSR) technology is based upon the concept of storing NOx as nitrates over storage components, typically barium species, during a lean-burn operation cycle, and then desorbing and subsequently reducing the stored nitrates to N_2 during fuel-rich conditions over a precious metal catalyst [1]. This technology has been recognized as one of the most promising approaches for meeting stringent NOx emission standards for diesel vehicles within the Environmental Protection Agency's 2007/2010 mandated limits and, in fact is being commercialized for this application. However, in looking forward to 2012 and beyond with expected more stringent regulations, the continued viability of the NSR technology for controlling NOx emissions from lean-burn engines such as diesels will require at least two specific, significant and inter-related improvements. First, it is important to reduce system costs by, for example, ***minimizing the precious metal content*** while maintaining, even improving, performance and long-term stability. A second critical need for future NSR systems will be significantly ***improved higher temperature performance*** and stability. Furthermore, these critically needed improvements will contribute significantly to minimizing the impacts to fuel economy of incorporating the NSR technology on lean-burn vehicles. To meet both of these objectives, NSR formulation changes will almost certainly be necessary. Importantly, such material changes will require, at a minimum an improved scientific understanding of the following things:

- The various roles for the precious metals.
- The mechanisms for these various roles.
- The effects of high temperatures on the precious metal performance in their various roles.
- Mechanisms for higher temperature NOx storage performance for modified and/or alternative storage materials.
- The interactions between the precious metals and the storage materials in both optimum NOx storage performance and long-term stability.
- The sulfur adsorption and regeneration mechanisms for modified and/or alternative storage materials.

The objective of this CRADA project is to develop a fundamental understanding of candidate next-generation NSR materials for NOx after-treatment for light-duty lean-burn (including diesel) engines. The project will focus on characterizing and understanding the six issues described just above. Model catalysts that are based on literature formulations are the focus of the work being carried out at PNNL. In addition, the performance and stability of a realistic high temperature NSR catalyst, supplied by JM, is being studied in order to provide baseline data for the model catalysts that are, again, based on formulations described in the open literature.

Approach

In a microcatalytic reactor system, NSR performance is evaluated in a fixed bed reactor operated under continuous lean-rich cycling. Rapid lean-rich switching is enabled just prior to the elevated temperature zone (furnace) where the NSR materials are contained in quartz tubing. After removing water, the effluent of the reactor can be analyzed by mass spectrometry and by a chemiluminescent NOx analyzer. For a typical baseline performance testing, the sample is heated to a reaction temperature in flowing He, the feed switched to a 'lean-NOx' mixture containing oxygen and NO, as well as CO_2 and/or H_2O. After an extended period (15 minutes or more), multiple rich/lean cycles of 1 and 4 minute duration, respectively, are run and NOx removal performance is assessed after at least three of these are completed. In the NSR technology, the state of the system is constantly changing so that performance depends on when it is measured. Therefore in studies at PNNL, we obtain NOx removal efficiencies as "lean conversion (30 minutes)", which measures NOx removal efficiencies for the first 30 minutes of the lean-period. We have established a reaction protocol, which evaluates the performance of samples after various thermal aging and sulfation condition. In this way, we could identify optimum de-sulfation treatments to rejuvenate catalyst activities.

Based on formulations described in the literature, PNNL prepared several candidate samples for NSR performance measurements. Activity and performance stability measurements were performed. In addition, we investigated a more fully formulated catalyst for high temperature activity supplied from Johnson Matthey to provide baseline performance measurements. State-of-the-art catalyst characterization techniques were utilized to probe the changes in physicochemical properties of the PNNL-prepared model catalyst samples under deactivating conditions; *e.g.*, thermal aging and SO_2 treatment.

Results

As noted above, work on this CRADA this past year has focused on two areas:

- High temperature NSR catalysts prepared by PNNL; and

- Fully formulated high-temperature NSR catalysts supplied from JM.

High-Temperature NSR Catalysts prepared by PNNL

As described in last year's annual report [2], PNNL has prepared several NSR catalysts to assess their high temperature performance. The storage element was potassium, known to operate effectively at higher temperatures than Ba-based NSR catalysts. However, very little has been published in the open scientific literature on the chemical/physical properties of K-based NSR catalysts. As such, PNNL has initiated studies of these fundamental materials properties in order to provide scientific insight into their performance and stability. In particular, PNNL initiated investigations of the effect of alternative support materials and K loading on the NOx storage activity. PNNL has also recently shown that use of a $MgAl_2O_4$ support to prepare a Ba-based NSR catalyst gives rise to the shift in the temperature at which maximum performance is observed from 300ºC to 400ºC [3]. As such, PNNL prepared new K-based NSR materials using $MgAl_2O_4$ as the support material. For the case of this new Pt-K/$MgAl_2O_4$ sample, the maximum NOx uptake performance temperature (not shown here) shifted to 400ºC and 450ºC, in addition to providing larger total NOx uptake compared with the Al_2O_3-supported sample. In the last year, we have performed studies of the sensitivity of these catalysts to sulfur poisoning and to the high temperatures encountered under typical desulfation conditions.

One of the critical challenges NSR catalysts face is their rather poor sulfur resistance. Prior to this work, we have extensively investigated the sulfation/desulfation properties of BaO-based NSR catalysts using a number spectroscopy and microscopy tools [4]. In order to be able to compare the sulfur resistance of these new K_2O-based systems to the BaO-based ones we examined the durability of the Pt-K(10)/$MgAl_2O_4$ sample with respect to SO_2 poisoning. As demonstrated in Figure 1(a), when this sample was exposed to even a small amount SO_2, its NOx uptake capacity decreased gradually. Figure 1(b) plots the NOx uptake against the sulfur exposure time, showing that the NOx uptake decreases with increasing SO_2 exposures. Furthermore, note that the exposure of this catalyst to even a small amount of SO_2 results in a significant decrease in NOx uptake. Thus, this catalytic system (Pt-K/$MgAl_2O_4$) suffers from serious SO_2 poisoning, due to has strong affinity of K_2O for SO_2, and will require frequent regeneration (desulfation) at high temperatures.

In order to investigate the desulfation behavior of pre-sulfated Pt-K/$MgAl_2O_4$ sample, a mixture of rich gases (H_2, H_2O and CO_2) was introduced while raising the temperature linearly, designated as an H_2 temperature-programmed reaction (TPRX) experiment. Through the reaction between sulfate in the sample and H_2, sulfur is removed from the sample as H_2S (note that SO_2 is not observed during H_2 TPRX). The amount and the temperature where H_2S evolves allow us to estimate how difficult removal of sulfate from the sample will be. Figure 2 shows the evolution of H_2S obtained during H_2 TPRX spectra on a pre-sulfated Pt-K(10)/$MgAl_2O_4$ catalyst, where it can be seen that H_2S begins to desorb above 500ºC followed by the gradual increase in desorption rate with temperature. Finally, the evolution of H_2S has a maximum peak at 800ºC. The full range of desulfation behavior for this Pt-K/$MgAl_2O_4$ sample cannot be inferred from a single experiment. In particular, desulfation can strongly depend on the amount of sulfur loading as shown for the case of

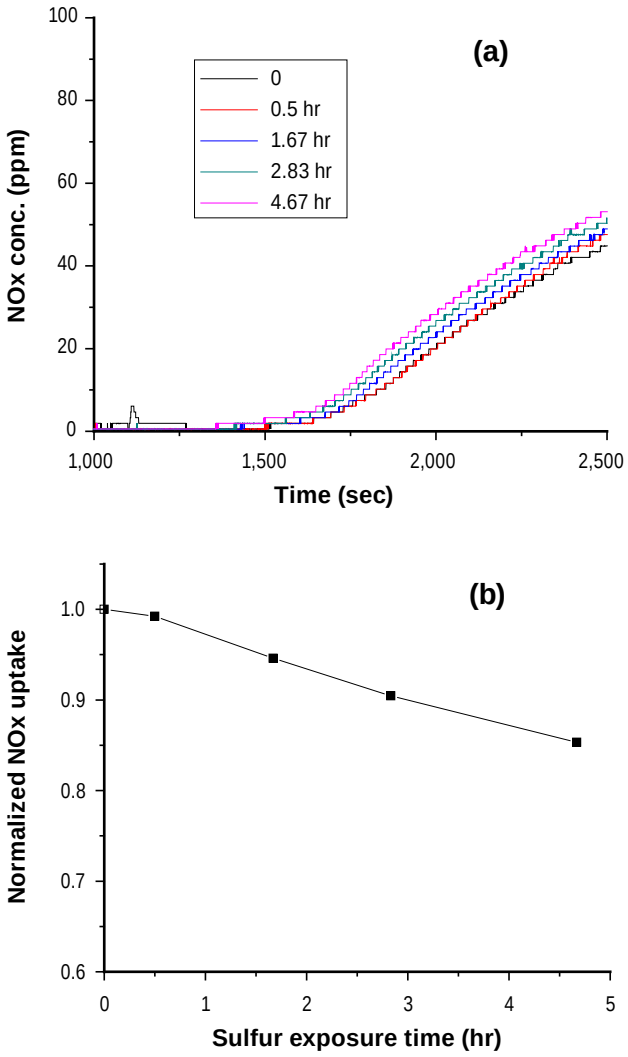

FIGURE 1. Change in the NOx uptake curves (a) and uptake amounts (b) for a PtK_2O(10)/$MgAl_2O_4$ catalyst as a function of SO_2 exposure time. SO_2 concentrations in these experiments were 25 ppm in a total gas flow of 400 standard cubic centimeters per minute.

Pt-Ba/Al_2O_3 NSR catalysts. Therefore, more extensive studies of the desulfation behavior of Pt-K/$MgAl_2O_4$ catalysts are ongoing.

Another important thing to note from the data shown in Figure 2 is that the temperature where most of the H_2S is removed is rather high. Increases in the desulfation temperature are expected to give rise to a corresponding decrease in NOx uptake due to the more dominance of thermal deactivation effect such as Pt sintering [2,5]. To more directly assess the thermal stability of these catalysts, we first treated them at various temperatures in an oxidizing environment and then remeasured their NOx uptake performance, with the results shown in Figure 3. For this freshly degreened (500ºC calcined) catalyst, even a first reaction run results in a small decrease in performance. As shown in the figure, thermal treatment at still higher temperatures resulted in a monotonic decrease in activity with temperature.

The studies described in this subsection are being pursued at PNNL in order to provide a more fundamental understanding of issues in NSR catalysts that have been shown in the open scientific literature to display improved high temperature NOx storage/reduction performance relative to BaO/alumina-based materials. To provide a baseline for the overall performance as well as the stability of the materials being studied at PNNL, JM provided a fully formulated developmental catalyst. PNNL studies of this JM catalyst are limited to performance testing and performance stability measurements as described next.

Fully Formulated High-Temperature NSR Catalysts Supplied from JM

For a fully formulated sample supplied from JM, maximum NOx uptake is demonstrated around 400 and 450ºC as presented in Figure 4. (Note that quantitative comparison of performance with the model catalyst described above is not straightforward because the studies were performed on powders and monolith supported catalysts for the model and developmental catalysts, respectively. Still, qualitative behavior is usefully compared.) Even at 500ºC, the NOx uptake performance is more than 60% of the maximum values. After calcination at various temperatures, NOx uptakes were remeasured as also shown in Figure 4, indicating that full uptake decreases with increasing treatment temperature. Because desulfations are often performed

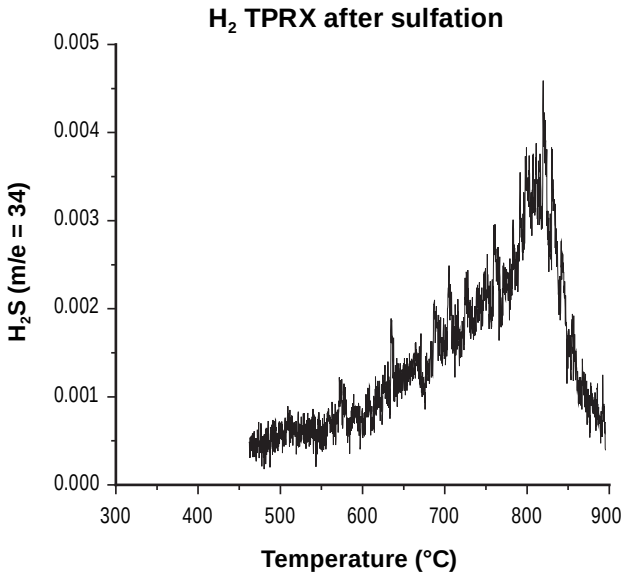

FIGURE 2. H_2 TPRX Data Obtained from a Pre-Sulfated Pt-K_2O(10)/$MgAl_2O_4$

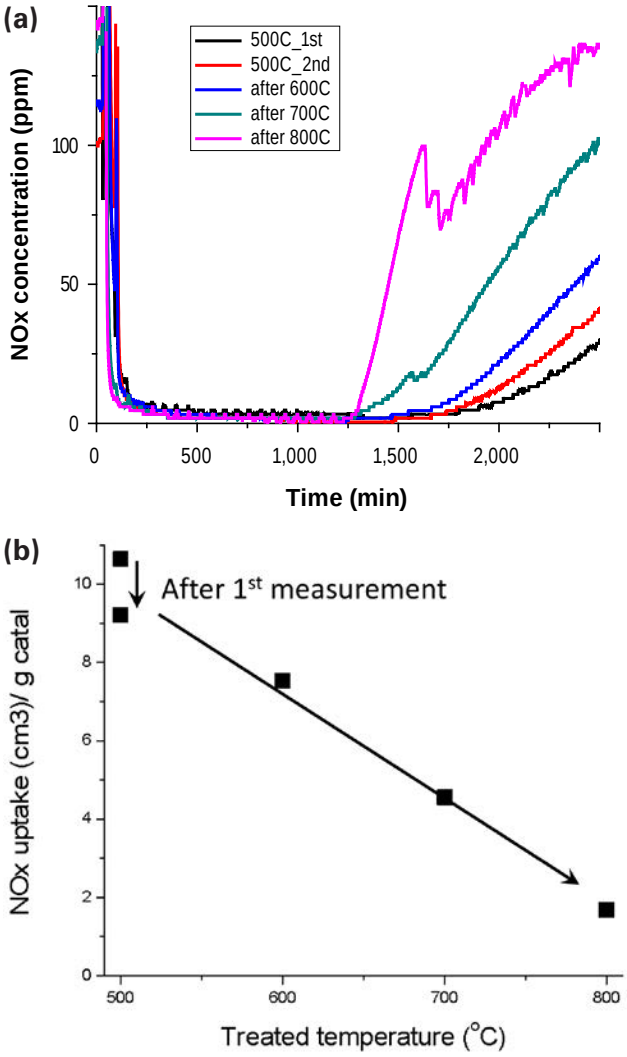

FIGURE 3. Thermal stability of a model PtK_2O(10)/$MgAl_2O_4$ NSR catalyst: (a) NOx uptake curves; and (b) NOx uptake amounts. Activity was measured at 500ºC after thermal treatment at each temperature for 1 hour (lean conditions).

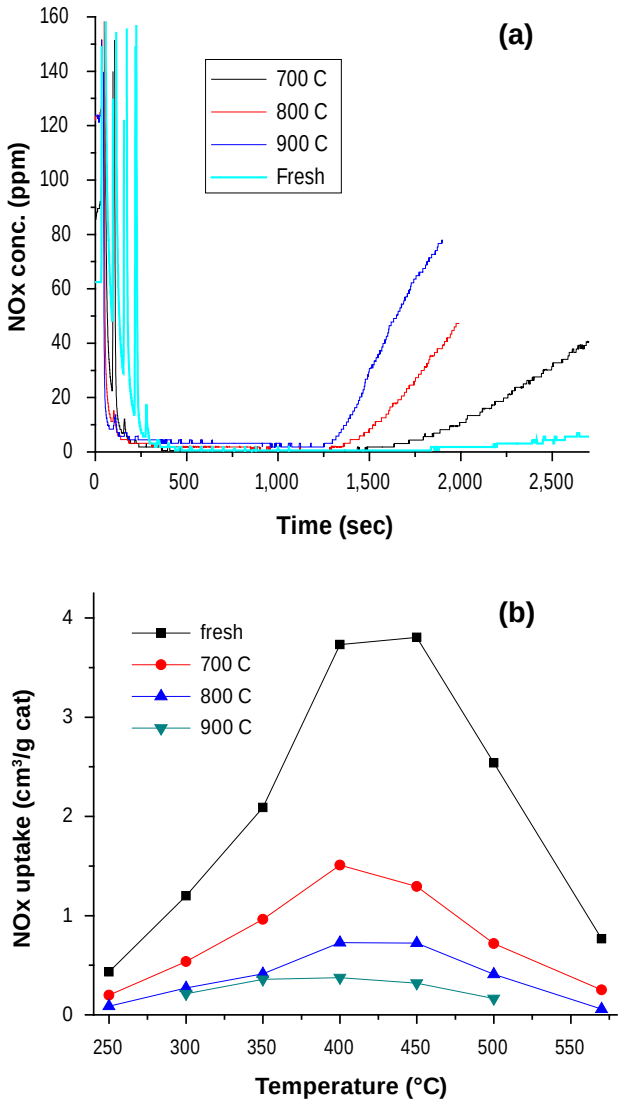

FIGURE 4. Thermal stability of a fully formulated NSR catalyst: (a) NOx uptake curves at 450ºC; and (b) NOx uptake amounts at various temperatures. Activity was measured after thermal treatment at each temperature for 1 hour (lean conditions).

under lean/rich cycling conditions, the comparative effects of oxidizing and reducing conditions were assessed. As shown in Figure 5, oxidizing treatments at 700ºC are responsible for more severe deactivation than reducing treatments. We note that these are initial measurements and the "loss in activity" reported are relative to a fresh (not degreened) catalyst. In this respect, the large drops in activities are not surprising although the data do suggest that the treatment conditions play a role in determining the extent of activity loss.

Finally, Figure 6 shows the results of a specific desulfation treatment for the fully formulated sample supplied from JM. Figure 6(a) is the H_2S mass

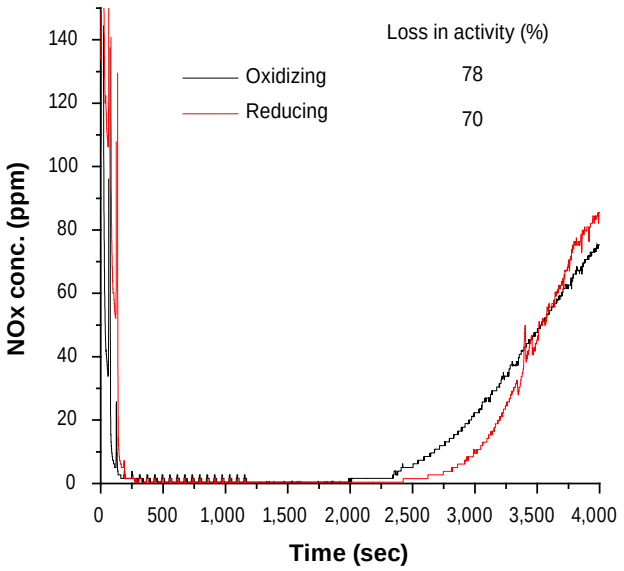

FIGURE 5. Comparison of NOx uptake performance at 450ºC of a fully formulated NSR catalyst after thermal treatment at 700ºC under either oxidizing or reducing conditions. "Loss in activity" reported in the figure is relative to the performance of a fresh catalyst (data not shown).

spectrometry signal obtained during consecutive desulfations at various temperatures after a single sulfation. These results show that a desulfation temperature of even 800ºC is insufficient to remove all of the sulfur as was also the case for the model catalyst described above (see Figure 2). However, as clearly demonstrated in the data shown in Figure 5, complete sulfur removal at the highest temperatures will result in significant and permanent deactivation. Again, this was also the case for the model catalyst as shown in Figure 3. Further investigations are aimed at determining optimum regeneration conditions.

Conclusions

PNNL and its CRADA partners from Cummins Inc. and JM have initiated a new CRADA project aimed at improving the higher temperature performance and stability of the NSR technology. Results obtained this year demonstrate that direct NO decomposition is not applicable for the real system. When K is used as storage element, the maximum temperature is shifted to 400ºC or higher, depending on the support. PNNL studies demonstrated that a $MgAl_2O_4$ support material provided especially promising NOx uptake performance. Additionally, the characteristics of a fully formulated NSR catalyst supplied from JM were investigated after applying SO_2 and thermal treatments. Overall, these studies are expected to provide valuable information for the development of durable NSR catalysts for high temperature applications.

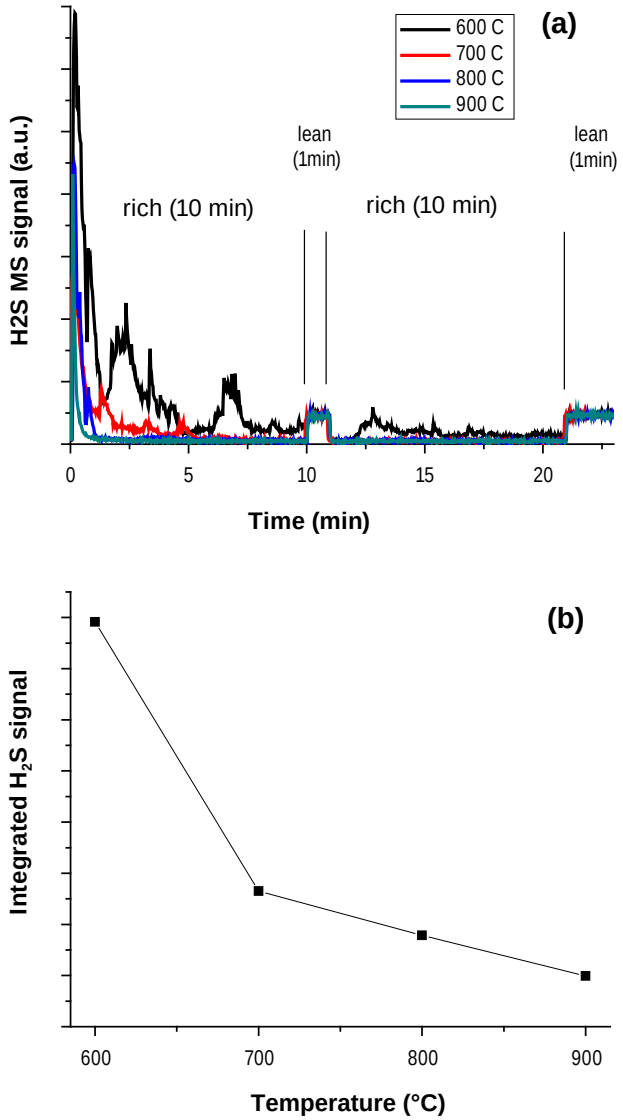

FIGURE 6. (a) Mass spectrometry signal for H_2S obtained during desulfation (10 minutes rich, 1 minute lean) treatment (repeated two times) at various temperatures. Experiments were run back-to-back at increasing temperatures without resulfating the sample. (b) The integrated H_2S signal as a function of temperature.

References

1. W.S. Epling, L.E. Campbell, A. Yezerets, A., N.W. Currier, J.E. Parks, *Catalysis. Review.–Science and Engingeering* 46 (2004) 163.

2. D.H. Kim, X.Q. Wang, G.G. Muntean, C.H.F. Peden, K. Howden, N. Currier, J. Li, R.J. Stafford, A. Yezerets, H.-Y. Chen, H. Hess, "Enhanced High Temperature Performance of NOx Storage/Reduction (NSR) Materials" in *Advanced Combustion Engine Research and Development: FY2010 Annual Progress Report*, 136-141.

3. M. Devarakonda, D.R. Herling, D.H. Kim, J.H. Kwak, C.H.F. Peden, M.L. Stewart, A. Strzelec, J. Szanyi, D.N. Tran, J.H. Lee, "CLEERS Aftertreatment Modeling and Analysis," in *Advanced Combustion Engine Research and Development: FY2011 Progress Report*, in press.

4. D.H. Kim, J. Szanyi, J.H. Kwak, X.Q. Wang, J. Hanson, M. Engelhard, C.H.F. Peden, *Journal of Physical Chemistry C* **113** (2009) 7336, and references therein.

5. D.H. Kim, Y.H. Chin, G.G. Muntean, A. Yezeretz, N.W. Currier, W.S. Epling, H.Y. Chen, H. Hess, C.H.F. Peden, *Industrial & Engineering Chemistry Research* **45** (2006) 8815.

FY 2011 Publications/Presentations

1. X. Wang, D.H. Kim, J.H. Kwak, C. Wang, J. Szanyi, C.H.F. Peden, "Effect of Reductive Treatments on Pt Behavior and NOx Storage in Lean NOx Trap Catalysts." *Catalysis Today* **175** (2011) 78-82.

2. D.H. Kim, X.Q. Wang, G.G. Muntean, C.H.F. Peden, K. Howden, N. Currier, J. Li, R.J. Stafford, A. Yezerets, H.-Y. Chen and H. Hess, "Enhanced High Temperature Performance of NOx Storage/Reduction (NSR) Materials" in *Advanced Combustion Engine Research and Development: FY2010 Annual Progress Report*, 136-141.

3. D.H. Kim, J.H. Kwak, J. Szanyi, C.H.F. Peden, "Isothermal desulfation of pre-sulfated Pt-BaO/γ-Al_2O_3 lean NO_x trap catalysts with H_2: the effect of H_2 concentration and the roles of CO_2 and H_2O." *Applied Catalysis B* (2012) in press.

4. D.H. Kim, K. Mudiyanselage, J. Szanyi, H. Zhu, J.H. Kwak, C.H.F. Peden, "Characteristics of Pt-$MgAl_2O_4$ Lean NO_x Trap Catalysts." *Catalysis Today* (2012) in press.

5. D.H. Kim, A. Yezerets, N. Currier, J. Li, H.-Y. Chen, H. Hess, M.H. Engelhard, G.G. Muntean, C.H.F. Peden, "Effect of sulfur loading on the desulfation chemistry over a commercial lean NOx trap catalyst." *Industrial Engineering Chemical Research*, submitted for publication.

6. D.H. Kim, K. Mudiyanselage, J.H. Kwak, J. Szanyi, H. Zhu, C.H.F. Peden, "Characteristics of Pt-K/$MgAl_2O_4$ lean NO_x trap catalysts," 22nd North American Catalysis Society Meeting, Detroit, MI, June 2011.

7. D.H. Kim, G.G. Muntean, C.H.F. Peden, N. Currier, J. Li, R. Stafford, A. Yezerets, H.Y. Chen, H. Hess, "Enhanced High Temperature Performance of NOx Storage/Reduction (NSR) Materials", presentation at the DOE Combustion and Emission Control Review, Washington DC, May 2011.

8. D.H. Kim, J.H. Kwak, J. Szanyi, X.Q. Wang, G. Li, C.H.F. Peden, "Various effects of CO_2 in Pt-BaO/Al_2O_3 lean NOx trap catalysts", presentation at the 2010 AIChE annual meeting, Salt Lake City, UT, November 2010.

9. X.Q. Wang, D.H. Kim, J.H. Kwak, J. Szanyi, C.M. Wang, C.H.F. Peden, "Effect of reductive treatments on Pt dispersion and NOx storage in lean NOx trap catalysts", presentation at the 6th International Conference on Environmental Catalysis, Beijing, China, September 2010.

II.B.3 Emissions Control for Lean-Gasoline Engines

James Parks (Primary Contact), Josh Pihl, Todd Toops
Oak Ridge National Laboratory (ORNL)
2360 Cherahala Boulevard
Knoxville, TN 37932

DOE Technology Development Manager:
Ken Howden

Objectives

- Assess and characterize catalytic emission control technologies for the reduction of oxides of nitrogen (NOx) from lean-gasoline engines.
- Identify strategies for cost reduction of emission controls for lean-gasoline engines.
- Characterize exhaust composition and the resulting evolution of chemistry in catalysts for lean-gasoline engines.

Fiscal Year (FY) 2011 Objectives

Determine effect of NOx concentration on the storage capacity of lean-NOx traps (LNTs) at high temperature conditions associated with lean-gasoline engines.

Accomplishments

- Distributed database of exhaust emissions from a modern lean-gasoline engine vehicle including the reductant chemistry for LNT regeneration processes to modeling community via the Cross-Cut Lean Exhaust Emissions Reduction Simulations consortium.[1]
- Analyzed the chemical processes occurring in an LNT catalyst specific to high NOx concentration and temperature conditions associated with the lean-gasoline engine application.

Future Directions

- Develop a lean-gasoline engine research platform for catalyst studies.
- Determine catalytic NH_3 production viability under rich engine operation for selective catalytic reduction reactions.

[1] A consortium of industry, national laboratory, and university researchers that promotes development of performance models for emissions control components (for more information, visit www.cleers.org).

Introduction

Currently, the U.S. passenger car market is dominated by gasoline engine powertrains that operate at stoichiometric air-to-fuel ratios (sufficient fuel is mixed in air such that all of the oxygen in the air is consumed during combustion). Stoichiometric combustion leads to exhaust conditions suitable for three-way catalyst technology to reduce NOx, CO, and hydrocarbon (HC) emissions to extremely low levels. Operating gasoline engines at lean air-to-fuel ratios (excess air) leads to less fuel consumption; however, the resulting oxygen in the exhaust prevents the three-way catalyst technology from performing. It is relatively straightforward to operate an engine lean over a good portion of the load and speed operating range; so, the largest challenge preventing fuel-saving lean combustion in gasoline applications is the control of emissions, primarily NOx. This project addresses the challenge of reducing emissions from fuel-saving lean gasoline engines to enable their market introduction in the U.S.

Approach

This project will utilize a lean-gasoline engine on an engine dynamometer to investigate catalytic emission control technologies to enable lean-gasoline engines to meet NOx emission standards; the engine platform is currently being pursued as this project is in its beginning stages. While efforts to develop this experimental platform are ongoing, research was conducted on a bench flow reactor with gas mixtures simulating lean gasoline engine exhaust.

The LNT technology operates by adsorbing NOx during lean (excess oxygen) operation, and then releasing and reducing the NOx to N_2 during rich (oxygen-depleted) operation. The lean phase is typically 30-120 sec and the rich "regeneration" phase is typically 1-5 sec in duration. Extra fuel is required to create the rich conditions, so there is a "fuel penalty" associated with LNT operation. It is critical to balance the NOx released with the reductants (CO, H_2, HCs) produced during the short regeneration event to obtain effective NOx reduction and LNT regeneration while minimizing any release or "slip" of excess reductants.

LNTs have already been commercialized for light-duty diesel applications in the U.S., and are currently available on a limited number of lean-gasoline vehicles in Europe. However, to date, LNTs have not been successfully deployed on lean-gasoline vehicles under the more stringent emissions regulations in the U.S.

There are two primary characteristics of lean-gasoline engine exhaust that make it more challenging for LNTs than diesel exhaust: high temperatures, and high NOx concentrations (in excess of 1,000 ppm). High temperatures reduce the NOx storage capacity, and high NOx concentrations should saturate the storage capacity more quickly. The combination of lower storage capacity and higher inlet NOx requires more frequent LNT regeneration events, increasing the fuel penalty associated with LNT operation. However, since there is a thermodynamic equilibrium between NOx in the gas phase and NOx on the catalyst surface, storage capacity is expected to increase with higher inlet NOx concentrations.

Our bench reactor experiments for FY 2011 focused on understanding LNT behavior with high NOx concentrations and at high temperatures. In particular, we sought to determine if the higher effective storage capacity could offset the need to store more NOx at higher NOx concentrations, thereby minimizing the impacts on the overall fuel penalty. The experiments were also designed to determine what other aspects of LNT chemistry might limit performance under lean-gasoline conditions.

Results

Data from operation of the LNT on the bench flow reactor is shown in Figure 1. NOx emissions occur early in the rich regeneration phase (often called the NOx "puff"). Then, toward the end of the rich phase reductants begin to slip from the LNT, and the regeneration is stopped (based on sensing the reductant slip with a universal exhaust gas oxygen sensor).

NOx conversion of the LNT as a function of temperature for varying inlet NOx concentrations is shown in Figure 2. NOx conversion drops off at high temperatures, and the effect is more pronounced at high inlet NOx concentrations. This was unexpected since NOx storage capacity (Figure 3) does, in fact, increase at higher NOx concentrations. The problem is not with uptake; it is with regeneration. Figure 4 shows the percentage of NOx released but not reduced from the LNT after being adsorbed. The higher quantity

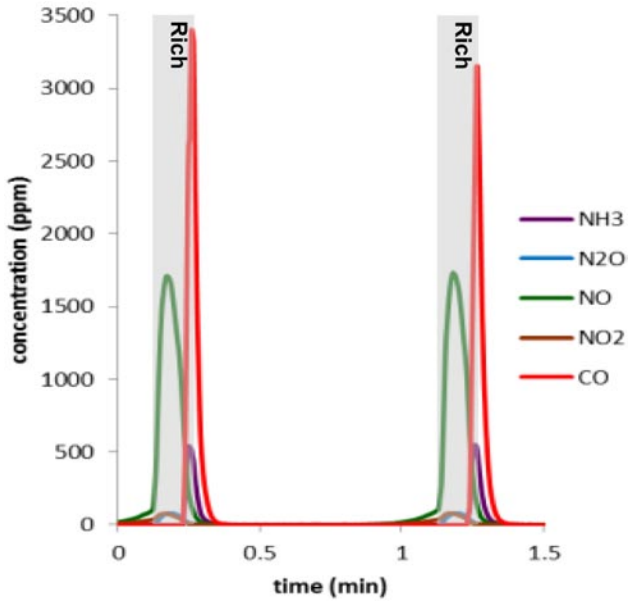

FIGURE 1. Profile of Exhaust Species Downstream of the LNT during Regeneration Showing Reductant Slip Occurring Toward the End of the Regeneration Event

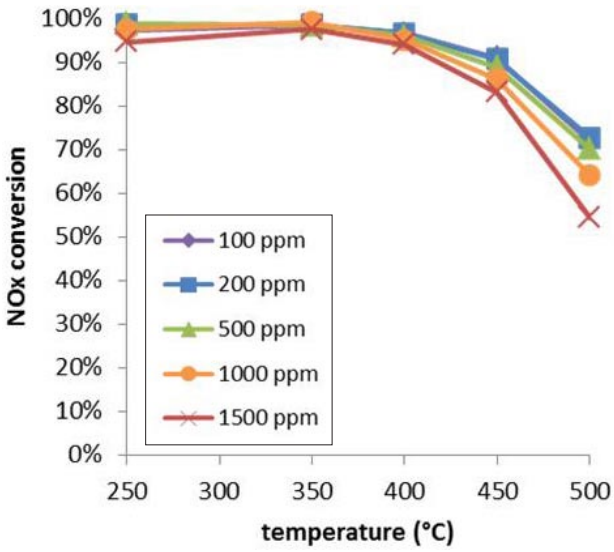

FIGURE 2. NOx Conversion as a Function of Temperature for Varying Inlet NOx Concentrations to the LNT

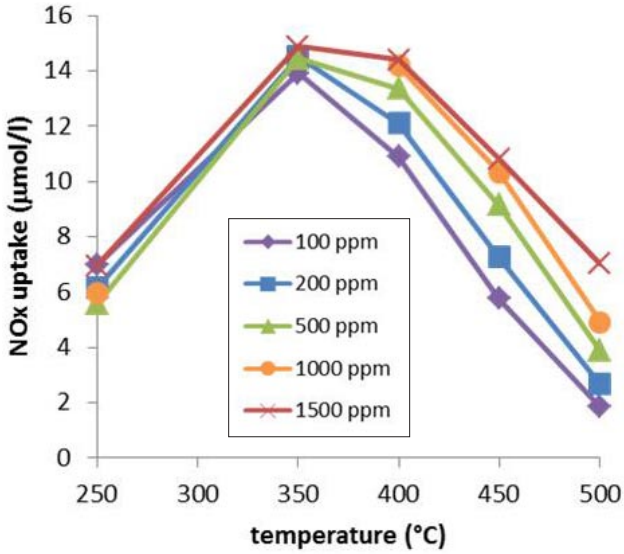

FIGURE 3. Adsorbed NOx Uptake per LNT Volume for the Data Shown in Figure 2

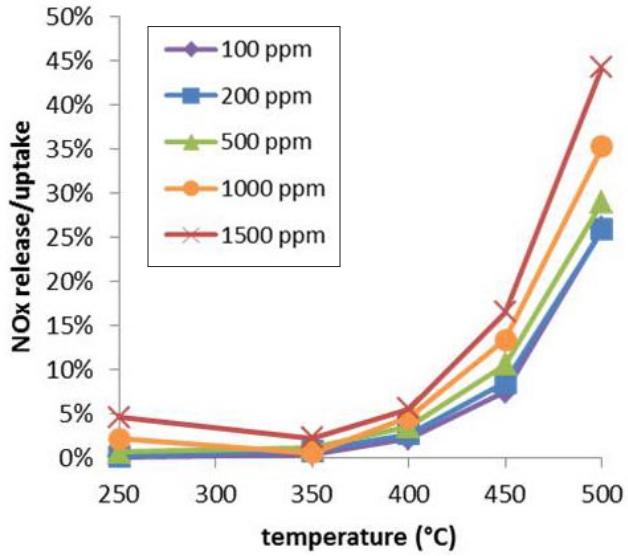

FIGURE 4. Percentage of NOx Released from the LNT vs. Adsorbed Showing that Higher NOx Release is Associated with Higher Temperatures and NOx Inlet Concentration

of NOx stored on the surface results in faster release during regeneration, and there is insufficient reductant to reduce all of the released NOx. While increased NOx adsorption capacity was observed at higher inlet NOx concentrations, the gains in capacity coupled with less efficient reduction during regeneration are not sufficient to enable the LNT to achieve high (>90%) NOx conversion at the challenging lean-gasoline conditions.

Conclusions

Lean-gasoline engines challenge LNT technology with high NOx concentrations in the exhaust. Furthermore, a wide temperature range of operation is required to address the transient drive cycle operation. Studies on a bench flow reactor found a modest increase in NOx adsorption capacity associated with higher inlet NOx concentration. Furthermore, the regeneration process of the LNT was less efficient for NOx reduction to N_2 (vs. unreduced release) at high temperatures and high NOx concentration with temperature being the most dominant effect. Further research and advancement of the LNT technology will be required to enable performance over all of the conditions associated with the lean-gasoline engine application.

FY 2011 Publications/Presentations

1. Jim Parks, Vitaly Prikhodko, Bill Partridge, Jae-Soon Choi, Kevin Norman, Paul Chambon, Shean Huff, "Lean Gasoline Engine Reductant Chemistry During Lean NOx Trap Regeneration", *SAE Technical Paper Series* 2010-01-2267 (2010).

2. Jim Parks, Vitaly Prikhodko, Bill Partridge, and Jae-Soon Choi, "Reductant Chemistry during LNT Regeneration for a Lean Gasoline Engine", *2010 Directions in Engine-Efficiency and Emissions Research Conference (DEER)*, September 27-30, 2010 (2010).

3. Website Publication of Data: Jim Parks (with Shean Huff, Vitaly Prikhodko, Dean Edwards, Paul Chambon, Jae-Soon Choi, Bill Partridge, and John Thomas), "Lean Gasoline Engine Vehicle", *Cross-Cut Lean Exhaust Emissions Reduction Simulations (CLEERS) Website Database*, March 31, 2011. [Website address: http://www.cleers.org/databases/filepage.php?fileid=12].

II.B.4 Development of Chemical Kinetics Models for Lean-NO_x Traps

Richard S. Larson
Sandia National Laboratories
MS 9052, P.O. Box 969
Livermore, CA 94551-0969

DOE Technology Development Manager:
Kenneth Howden

Collaborators:
V. Kalyana Chakravarthy, Josh A. Pihl, Jae-Soon Choi, and C. Stuart Daw
Oak Ridge National Laboratory, Knoxville, TN

Overall Objectives

- Identify a set of microkinetic surface reactions that can account for the observed behavior of a lean-NO_x trap (LNT) during a complete storage/regeneration cycle.
- Optimize the kinetic parameters associated with these reactions by matching model predictions with laboratory reactor data.
- Extend the mechanism to include reactions involving sulfur-containing species, with the aim of describing both catalyst degradation during normal operation and catalyst restoration during high-temperature desulfation.
- Use the validated reaction mechanism to suggest improvements in the usage of existing LNT materials and to help in the development of a new generation of catalysts.

Fiscal Year (FY) 2011 Objectives

- Reconstruct the previously developed NO_x storage and release mechanism in order to bring it more into accord with existing proposals in the literature.
- Account for and assess the role of boundary layer mass transfer during operation of an LNT under various conditions.
- Demonstrate the ability to simulate exotherms in an LNT channel with an upgraded reactor code and computed thermodynamic properties for the surface species.

Accomplishments

- Developed a new NO_x storage and release mechanism and showed that it could be used to simulate our experimental data set as well as the mechanism proposed previously.
- Modified the overall mechanism to allow for the suppression of ammonia production during short cycles.
- Upgraded our reactor code to account for boundary layer mass transfer and showed that this phenomenon was of minor but not negligible importance.
- Upgraded our reactor code with a complete energy equation and demonstrated that the simulation of exotherms during a storage/regeneration cycle could be done successfully only if axial heat transfer along and away from the tube wall were included.

Future Directions

- No additional work on this project is planned by the current investigator.
- Future work in this area should be focused on the new LNT catalyst whose performance is now being evaluated at Oak Ridge National Laboratory.

Introduction

The increasingly strict constraints being placed on emissions from diesel and other lean-burn engines require the development of a new generation of aftertreatment technologies. LNTs represent one option for achieving the stated targets with regard to NO_x emissions. In an LNT, NO_x produced during normal lean engine operation is trapped and stored as nitrites and nitrates on alkaline oxide sites, and periodically this stored NO_x is released and reduced to harmless N_2 on precious metal sites by imposing rich conditions for a short time. While this qualitative description is widely accepted, a detailed quantitative understanding of the underlying chemistry is not yet available. Such knowledge is needed in order to use the LNT concept to best advantage, so it is the principal goal of this project to develop a microkinetic reaction mechanism that describes both phases of LNT operation. A secondary focus arises from the fact that sulfur-containing contaminants in the fuel can lead to degradation in the LNT catalyst performance over time, so that periodic desulfation episodes are needed in addition to the ordinary regeneration (deNO_x) excursions. Simulation of these phenomena requires that reactions of sulfur-containing species be included alongside those describing the storage, release, and reduction of NO_x.

Clearly, a kinetics model with the ability to simulate all phases of LNT operation must account for the chemistry occurring on several kinds of catalytic sites:

the metal oxide sites used to store NO_x, additional oxide sites used (sometimes) for oxygen storage, and the precious metal sites involved primarily in the reduction of released NO_x. While it is tempting to associate each of these kinds of sites with a particular part of the LNT cycle, it must be remembered that the desorption of NO_x from the storage sites is an integral part of the regeneration process, while oxidation of NO on the precious metal sites is thought to be a key part of the storage phase. Nevertheless, it is possible to design experiments that isolate (to a large extent) a particular subset of the chemistry, and this has been used to facilitate model development in this project. Thus, work in early years led first to a tentative mechanism for the precious metal sites alone, and the basic mechanism was then completed by appending reactions for the storage sites. However, from time to time it has been necessary to revisit and refine this mechanism in order to overcome newly discovered deficiencies, as tends to occur when the mechanism is used under new circumstances. Ideally, work on the supplementary sulfation/desulfation chemistry proceeds via the addition of suitable reactions to a finalized NO_x storage and reduction (NSR) mechanism, taking advantage of the fact that the roles of nitrogen- and sulfur-containing species are largely analogous. In reality, the sulfation/desulfation submechanism has undergone continuous refinement not only due to perceived flaws of its own, but also to account for changes in the underlying NO_x chemistry.

Approach

Our basic approach to mechanism development is to assemble a candidate set of microkinetic reactions, generally with poorly known rate parameters, and then to optimize the parameters by fitting the results of reactor simulations to bench-scale experimental data provided by our collaborators at Oak Ridge National Laboratory. This process requires two principal pieces of supporting software: a reactor code to simulate flow through a single monolith channel using the proposed reaction mechanism (expressed in CHEMKIN format), and an optimization code to carry out the fitting process on a massively parallel computer. For the simulation of both cyclical and steady flow experiments, we have used primarily a specially developed transient plug flow code (although a steady-state code was used in some early work), and for the optimization we have adopted the Sandia APPSPACK code [1], which is ideally suited to this application.

As mentioned above, a tentative mechanism for the chemistry occurring on the precious metal sites was constructed and validated in previous years [2]. Our original intention was to incorporate this essentially without modification into the complete mechanism, thus minimizing the number of parameters to be determined on the basis of time-consuming transient simulations. However, it eventually became clear that this approach would lead to noticeable and avoidable errors, so the decision was made to treat the precious metal parameters once again as adjustable. A comprehensive LNT mechanism was then constructed by adding a set of candidate reactions for the storage sites, and the entire set of kinetic parameters was estimated by fitting simultaneously the experimental data (specifically, the exit gas concentrations) for not only a set of three long storage/regeneration cycles [3], but also the complete set of steady flow temperature sweeps used previously [2]. This same approach has continued to be used throughout numerous attempts to improve not only the details of the chemical mechanism, but also the fidelity of the reactor simulations. With regard to the sulfation/desulfation mechanism, the chosen experimental protocol is more complex, the simulations are more time-consuming, and the objective function is more intuitively-based, but the basic approach is unchanged.

Results

During the year we devoted a large amount of effort to a complete reconstruction of our NO_x storage and release mechanism in order to bring it more into accord with the consensus of the catalysis community. In particular, the set of nitrite and nitrate species representing NO_x stored on the BaO surface was chosen to be the same as that appearing in conventional treatments in the literature. The reactions describing the storage (and thus also the thermal release) process were likewise based on those proposed by others, but some reconfiguration was done in order to achieve the best possible fit to the data. While allowance was still made for the presence of carbonates, these were now treated simply as competitors for the storage sites, and hydroxides were discarded completely. As in our previous work, we supplemented the basic storage/release mechanism with a modest set of spillover reactions describing the oxidation or reduction of species on the BaO phase by entities residing on adjacent precious metal sites. Of course, it was necessary to reformulate these reactions in terms of the newly adopted list of species.

In carrying out the optimization process to evaluate the kinetic parameters in the new mechanism, a new form of constraint was employed, namely that all molecular adsorptions on the precious metal sites were required to have negative enthalpy changes. In spite of this and the major alterations to the mechanism itself, the overall fit to the long cycle and temperature ramp data was not significantly different from what it had been previously. This simply suggests that there are equivalent ways to describe the basic chemistry and that distinguishing between them can be difficult. However, this does not diminish the usefulness of the microkinetic

approach, because only in this case can one be reasonably confident in assuming mass-action kinetics.

Apart from this fundamental alteration to the mechanism, two changes to the simulation procedure were adopted in order to address questions about the fidelity of the computations. First, the transient plug flow code was used exclusively, whereas our previous work had employed a steady-state code for the upper parts of most of the temperature ramps. The new approach was found to be far more time-consuming and to have little effect on the results, but it was retained nonetheless in order to eliminate any questions of validity. More significantly, the transient code was upgraded to account for boundary layer mass transfer in the gas phase. This had a noticeable (but still modest) effect on the results and did not drastically increase the computation time, so it was deemed a worthwhile enhancement.

Finally, a considerable effort was made to address two undesirable and stubborn features of the simulation results. Most important was the observation that very large amounts of NH_3 were produced when the otherwise optimized mechanism was applied to a short (60 s/5 s) storage/regeneration cycle with a large excess of reductant. This was seemingly dictated by the temperature ramp and long cycle data but was in sharp conflict with reality for the short cycle. This problem was solved by introducing a step in which adsorbed NH_3 is converted to N_2 via reaction with both adsorbed NO and stored oxygen. Remarkably, this was successful in bringing about the desired NH_3 curtailment without seriously affecting the primary data fits. While this could certainly be regarded as fortunate, it does appear to confirm that the temperature ramp and long cycle experiments are by themselves not quite sufficient to solidify all facets of the mechanism.

Another persistent feature of the simulation results was a small amount of NO slip through the catalyst during the regeneration phase of the long cycle at 200°C, most noticeably coinciding with the peak in NH_3 production. We had partial success in addressing this problem by reformulating one of the spillover reactions to produce adsorbed nitrogen atoms rather than NO; however, this slightly degraded other aspects of the simulations, so the unwanted NO could not be eliminated completely in the optimized results.

Figures 1 and 2 compare the simulated and experimental outlet compositions, respectively, for the long cycle at 300°C, using the final (optimized) version of the mechanism for the former. While there are some differences in the details, the overall agreement is excellent, especially considering that the mechanism is optimized over far more than just this data set. An analogous comparison for the temperature ramp experiment using 500 ppm NO_2 and 5,000 ppm CO in the feed is shown in Figures 3 and 4. There are again

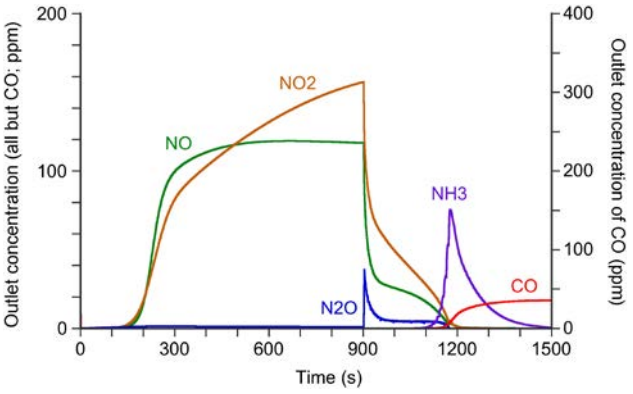

FIGURE 1. Simulated Outlet Concentrations for the Benchmark Long Storage/Regeneration Cycle at 300°C

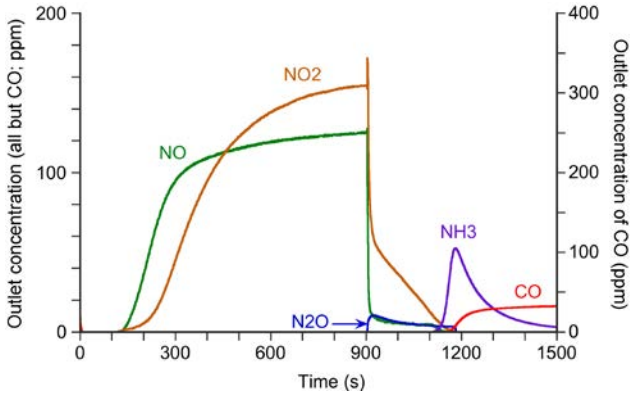

FIGURE 2. Experimental Outlet Concentrations for the Benchmark Long Storage/Regeneration Cycle at 300°C [3]

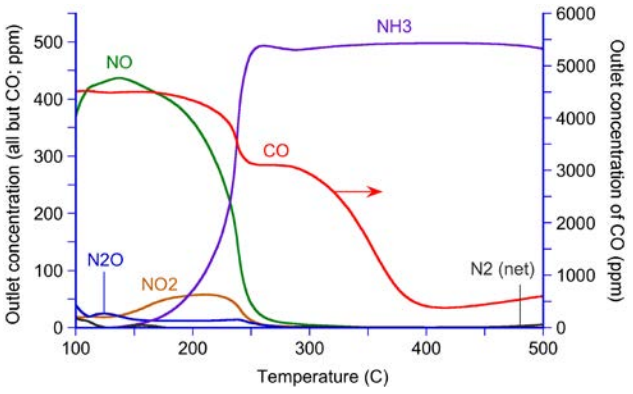

FIGURE 3. Simulated Outlet Concentrations for Steady Flow Temperature Sweep with 1:10 NO_2/CO

some discrepancies for the minor species, but the partial reduction of NO_2 to NO is reproduced extremely well, as is the striking two-step drop in the CO concentration.

The reconstruction of the NO_x storage/release mechanism, and in particular the adoption of a new set

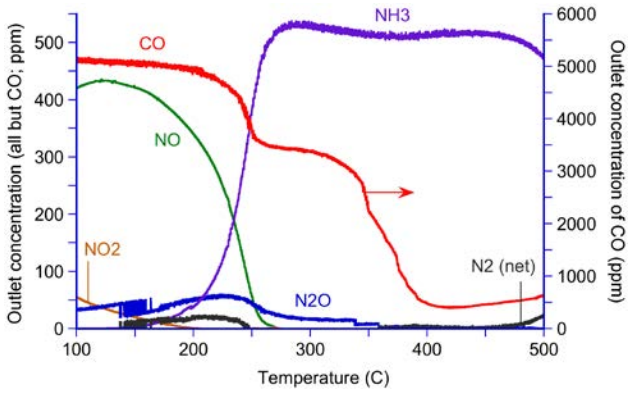

FIGURE 4. Experimental Outlet Concentrations for Steady Flow Temperature Sweep with 1:10 NO_2/CO [3]

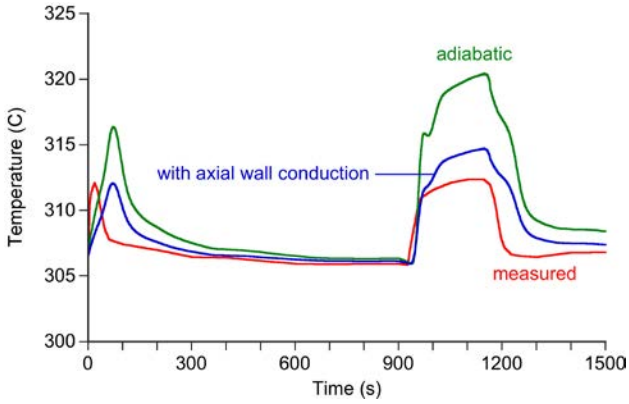

FIGURE 5. Simulated and Experimental Exit Temperatures for the Benchmark Long Storage/Regeneration Cycle at 300°C

of surface species, required that the sulfation/desulfation mechanism be reformulated as well. In keeping with the new philosophy, carbonates were now assumed to have only a bystander role here as well. In addition, both singly and doubly sulfated species were now assumed to exist on the oxygen storage sites. Nevertheless, optimization of the kinetic parameters led to an overall fit that was not significantly better or worse than that achieved before. The results did reinforce the conclusion that sulfur trapping on the oxygen storage sites plays a crucial role in preventing the NO_x storage capacity from being severely degraded.

Finally, we made major progress in our attempts to simulate the exotherms that occur at various points during an NSR cycle. Thermodynamic properties for all of the surface species had already been extracted from the equilibrium constants obtained via the standard data fitting procedure. The transient plug flow code was then upgraded with a complete energy balance, allowing temperature changes in the reactor to be predicted rather than simply specified from experimental measurements. While symmetry considerations allow a monolith channel to be treated as adiabatic in the radial direction, axial heat conduction along the tube wall and convective heat transfer from the annular end surface are potentially important, so these were included in the upgrade. Figure 5 shows simulated and experimental results for the exit temperature during the long cycle of Figures 1 and 2. Clearly, the code is able to reproduce the qualitative features of the experimental temperature trace fairly well, but quantitative agreement is not possible if the channel is taken to be completely adiabatic. The inclusion of axial heat transfer along and away from the tube wall gives reasonable results for this one-dimensional model.

Conclusions

- Boundary layer mass transfer effects in a monolith channel appear to be of minor importance but are not completely negligible.
- Ammonia production during short NO_x storage/regeneration cycles is suppressed by a process that involves stored oxygen and plays only a minor role during long cycles.
- Axial heat transfer along and away from the tube wall is effective in dampening the exotherms that occur at various points during an NSR cycle.

References

1. J.D. Griffin, T.G. Kolda, and R.M. Lewis, Sandia National Laboratories Report SAND2006-4621, 2006.

2. R.S. Larson, J.A. Pihl, V. K. Chakravarthy, T.J. Toops, and C.S. Daw, *Catal. Today* **136**, 104 (2008).

3. J.A. Pihl, M.S. Thesis, University of Wisconsin–Madison, 2005.

FY 2011 Publications/Presentations

1. R.S. Larson, V.K. Chakravarthy, J.-S. Choi, J.A. Pihl, and C.S. Daw, "Comprehensive Microkinetic Modeling of LNT Chemistry," Fourteenth CLEERS Workshop, Dearborn, Michigan, April 21, 2011.

2. R.S. Larson, "Development of Chemical Kinetic Models for Lean NO_x Traps," DOE Vehicle Technologies Program Annual Merit Review, Arlington, VA, May 12, 2011.

3. R.S. Larson, V.K. Chakravarthy, J.A. Pihl, and C.S. Daw, "Microkinetic Modeling of Lean NO_x Trap Storage and Regeneration," *Chemical Engineering Science* (under review).

II.B.5 Advanced Engine/Aftertreatment System R&D CRADA with Navistar, Inc.

Josh A. Pihl (Primary Contact), Todd J. Toops
Oak Ridge National Laboratory
2360 Cherahala Blvd.
Knoxville, TN 37932

Cooperative Research and Development Agreement (CRADA) Partner
Brad Adelman, Ed Derybowski
Navistar, Inc.

DOE Technology Development Manager:
Ken Howden

Objectives

- Develop engine/aftertreatment system configurations and control strategies that meet stringent emissions regulations while improving overall vehicle efficiency.
- Enhance fundamental understanding of diesel particulate filter (DPF) operating principles to facilitate fuel-optimal control strategy formulation.
- Develop experimental methods that probe the underlying chemical kinetics and changes in soot reactivity under carefully controlled DPF regeneration conditions.
- Exercise experimental methods to measure the reaction kinetics and operating parameters of DPFs needed in development of accurate simulation tools and detailed control strategies.

Accomplishments

- Devised an O_2 chemisorption method for measurement of the active surface area of soot loaded on a filter.
- Conducted isothermal pulsed oxidation experiments to measure the rates of soot oxidation over both a catalyzed and an uncatalyzed miniature DPF.
- Developed rate laws and associated parameters that capture the oxidation kinetics measured in the pulsed oxidation experiments.

Future Directions

The CRADA ended in Fiscal Year (FY) 2011.

Introduction

High efficiency lean-burn combustion engines offer a promising strategy for reducing petroleum consumption. However, meeting increasingly stringent emissions standards with lean-burn engines has proven to be a challenge. The engine modifications and aftertreatment systems used to reduce exhaust emissions typically increase fuel consumption, eroding the efficiency advantages of lean-burn operation. These complex systems also increase costs, creating a barrier to penetration of lean-burn engines into new market segments.

Development of lean-burn engine systems that meet stringent emissions standards while improving overall vehicle efficiency requires simultaneous optimization of both engine and aftertreatment operating strategies. This optimization often relies heavily on simulation tools. Formulation of simulation tools and operating strategies is complicated by the presence of storage functions in aftertreatment devices (soot in DPFs, NOx in lean-NOx traps, and NH_3 in selective catalytic reduction catalysts), which precludes the use of the steady-state operating maps typically used for engine control. The focus of this CRADA is to assist Navistar in the development and calibration of detailed simulation tools that will be used in control strategy formulation. These efforts will help Navistar bring to market high efficiency engine systems that reduce fuel consumption while complying with emissions regulations. The protocols and findings from this project will also provide useful insights to the engine aftertreatment research and development community as a whole.

Approach

During FY 2010 we shifted the focus of the CRADA from catalytic NOx aftertreatment systems to DPFs. This shift was a logical consequence of Navistar's strategic decision to utilize in-cylinder NOx control, precluding a current need for NOx aftertreatment. While in-cylinder NOx control reduces or eliminates the need for NOx aftertreatment, it places more of a demand on the DPF due to increased particulate production and/or reduced passive filter regeneration by NOx. If not managed carefully, the resulting higher soot loading rates could require more frequent active regeneration events to avoid excessive filter backpressure or runaway regeneration events. Since active regeneration requires increasing the exhaust temperature (typically achieved through injection of excess fuel), more frequent regenerations could incur a larger fuel penalty

and possibly impact filter durability. The goal of the current phase of the project is to measure relevant soot oxidation kinetics that will be integrated into Navistar's DPF regeneration control models.

Due to the complexity and cost of engine experiments, we decided to conduct our kinetic measurements on a bench-scale flow reactor system at ORNL. Navistar identified several DPF formulations of interest and obtained miniature (2.5 cm outer diameter by 7.6 cm long) particulate filter samples from suppliers. Half of the filters were washcoated with an oxidation catalyst; the other half were left uncoated. The filters were loaded with soot in an engine exhaust slip stream at a Navistar engine testing partner facility. The filters were subsequently sent to ORNL for detailed characterization of the regeneration process in an automated flow reactor. Flow reactor experiments conducted in FY 2010 focused on temperature programmed oxidations. These controlled burnout experiments enabled characterization of soot oxidation rates and pressure drop evolution over the course of a complete regeneration.

Our goal for FY 2011 was to measure the detailed kinetic parameters required to simulate soot oxidation in DPF control models. We decided to use pulsed oxidation experiments to maintain the filter under isothermal and differential conditions, thereby facilitating kinetic parameter estimation. Two soot-loaded (7 g/l) aluminum titanate miniature DPFs (one washcoated, the other bare) were run through a series of pulsed oxidation experiments over a wide range of temperatures, gas compositions, and burnout levels. In addition to pulsed oxidation steps, we included periodic O_2 chemisorption measurements to probe the evolution of active soot surface area over the course of burnout. These measurements were motivated by previous work in our laboratory that showed soot oxidation rate correlates with soot surface area [1].

Results

Figure 1 shows a sample data set from one of the pulsed oxidation experiments. The complete data set for each sample included dozens of runs similar to this one. An average of the last three pulses from each experiment was used to calculate a reaction rate for each set of experiment conditions. These measured rates were than analyzed to extract the kinetic parameters for a rate law such as the following:

$$r = Ae^{-Ea/RT}C^{\alpha}P_{O2}^{\beta}$$

(see nomenclature section for variable definitions). Taking logarithms of both sides of this equation allows estimation of the parameters A, E_a, α, and β from linear fits of the rate data. For example, a plot of $\ln(r)$ versus $\ln(C)$, shown in Figure 2, should give lines with a slope

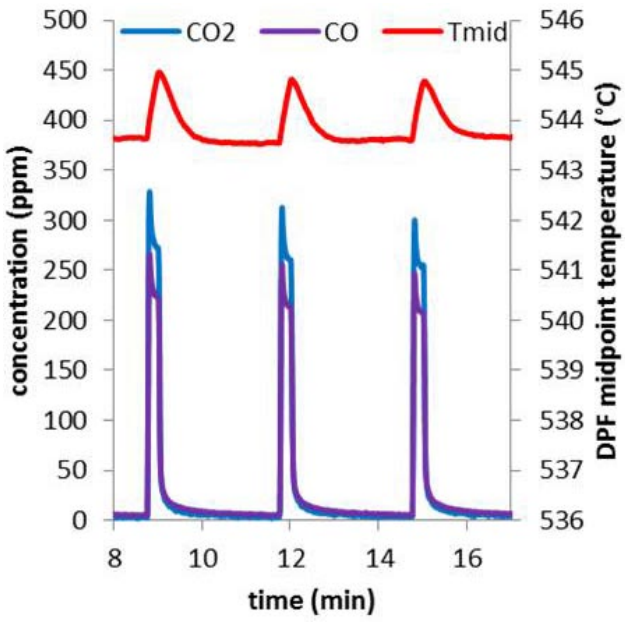

FIGURE 1. Gas concentrations and temperature for a pulsed oxidation experiment conducted on a miniature $AlTi_2O_5$ DPF. The DPF was loaded with 7 grams of soot per liter of filter in engine exhaust. The oxidation experiment was conducted in a flow reactor at 550°C and a gas hourly space velocity (GHSV) of 20,000 hr^{-1} under a constant flow of 5% H_2O in a balance of N_2. The 15 second oxygen pulses contained 10% O_2. Soot oxidation rates were calculated based on CO and CO_2 production during the O_2 pulses.

of α. However, it is apparent from the curvature of the data in Figure 2 that the reaction rate is not a simple exponential function of the amount of soot in the DPF. We postulated that soot active surface area, rather than total soot quantity, would have a simpler correlation to oxidation rate. Using the results from our O_2 chemisorption experiments, we looked for an equation that described the surface area evolution (Figure 3) during the course of the filter regeneration process. The simplest function that came somewhat close to capturing the surface area evolution was of the following form:

$$S_c = S_0(C/C_0)(s_m/s_{m,0}) = S_0(C/C_0)(\gamma(C/C_0)^2 + \delta(C/C_0) + \varepsilon)$$

After fitting the constants γ, δ, and ε to the O_2 chemisorption data, we modified our reaction rate expression to explicitly depend on surface area

$$r = Ae^{-Ea/RT}S_c^{\alpha}P_{O2}^{\beta}$$

and re-plotted the rate data in Figure 4. While still not perfect, using carbon surface area in the rate equation yields normalized rate data that comes closer to simple exponential behavior. Linear fits were also used to estimate the reaction order with respect to O_2 (not shown here) and the rate constant parameters A and E_a (Figure 5). The kinetic parameters extracted from

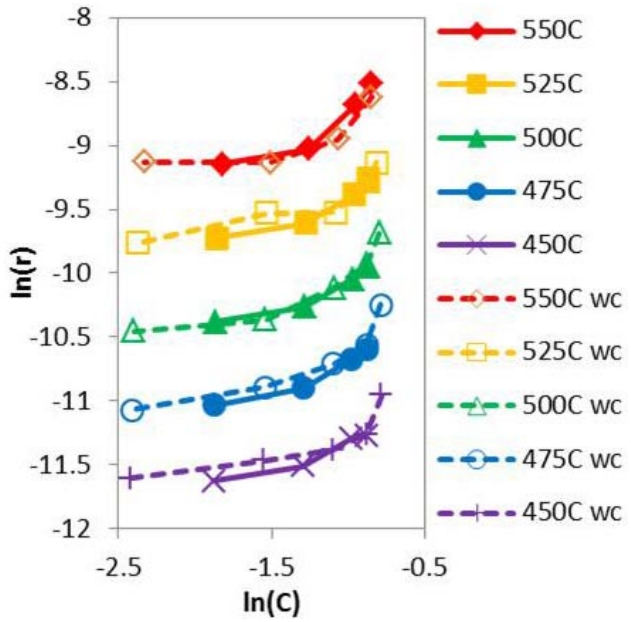

FIGURE 2. Soot oxidation rate as a function of carbon remaining and temperature in catalyzed ("wc") and uncatalyzed miniature $AlTi_2O_5$ DPFs initially loaded to 7 g/l in engine exhaust. Rates were measured from pulsed oxidation experiments with 15 sec pulses of 10% O_2 in the presence of 5% H_2O and balance N_2 at a GHSV of 20,000 hr^{-1}.

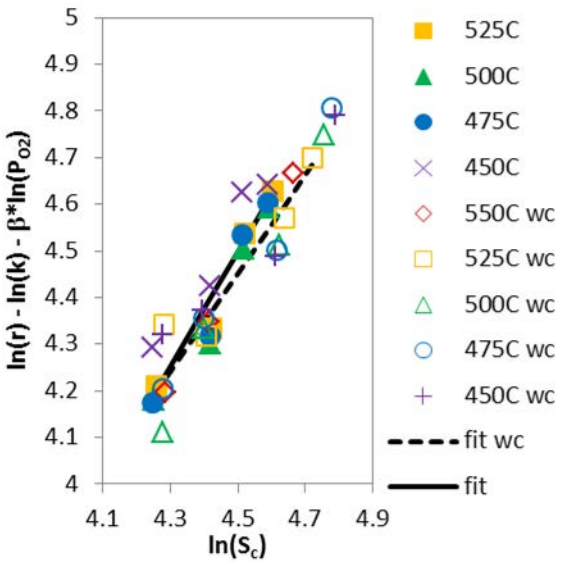

FIGURE 4. Normalized soot oxidation rate as a function of carbon surface area and temperature in catalyzed ("wc") and uncatalyzed miniature $AlTi_2O_5$ DPFs initially loaded to 7 g/l in engine exhaust. Rates were measured from pulsed oxidation experiments with 15 sec pulses of 10% O_2 in the presence of 5% H_2O and balance N_2 at a GHSV of 20,000 hr^{-1}. Lines represent best linear fits to each data set.

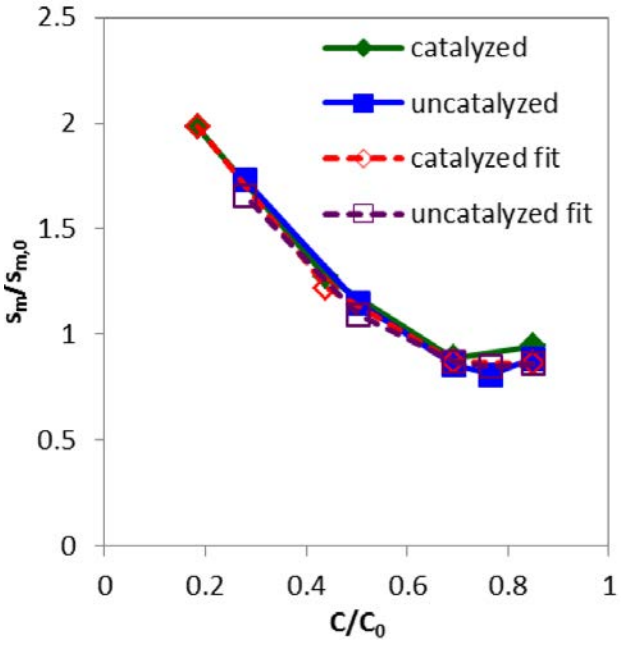

FIGURE 3. Normalized surface area as a function of fractional carbon remaining in catalyzed ("wc") and uncatalyzed miniature $AlTi_2O_5$ DPFs initially loaded to 7 g/l in engine exhaust. Surface area was measured by O_2 chemisorption. Fits represent best nonlinear estimates based on the surface area evolution equation described in the text.

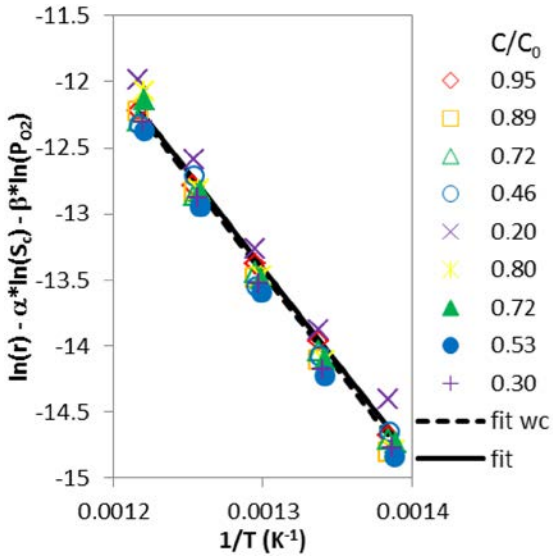

FIGURE 5. Normalized soot oxidation rate as a function of temperature and fractional carbon remaining (C/C0) in catalyzed ("wc") and uncatalyzed miniature $AlTi_2O_5$ DPFs initially loaded to 7 g/l in engine exhaust. Rates were measured from pulsed oxidation experiments with 15 sec pulses of 10% O_2 in the presence of 5% H_2O and balance N_2 at a GHSV of 20,000 hr^{-1}. Lines represent best linear fits to each data set.

the data for soot oxidation by O_2 in both catalyzed and uncatalyzed DPF samples are summarized in Table 1.

TABLE 1. Kinetic Parameters for Soot Oxidation Rate Expressions for Catalyzed and Uncatalyzed DPFs

Parameter	Uncatalyzed	Catalyzed	Units
A	581	255	mol sec^{-1} m^{-2} $bar^{-0.5}$
E_a	127	121	kJ/mol
α	1	1	---
β	0.5	0.5	---
γ	3.2	3.2	---
δ	-5.0	-5.0	---
ε	2.8	2.8	---

Conclusions

The goal of our recent work was to reduce the fuel penalty associated with DPF regeneration by developing more accurate simulation tools which could lead to better control strategies. During FY 2011, we developed an O_2 chemisorption method for measurement of soot active surface area in a miniature DPF on a flow reactor. We also conducted a series of isothermal pulsed oxidation experiments on the flow reactor to measure reaction rates as a function of gas composition, temperature, and soot burnout. We developed a rate law that describes the rate of soot oxidation by O_2 over a wide range of conditions and estimated parameters from the pulsed oxidation and O_2 chemisorption experiment data.

References

1. A. Strzelec, T.J. Toops, C.S. Daw, D. Foster, C. Rutland, "ULSD and Biodiesel Particulate Oxidation Model: Combined Effects of Volatiles and Fixed Carbon Combustion", SAE 2010-01-2127 (2010).

FY 2011 Publications/Presentations

1. J.A Pihl, B. West, T.J. Toops, B. Adelman, E.M. Derybowski, "CRADA Final Report for Advanced Engine/Aftertreatment System R&D," ORNL technical report 00-0605, 2011.

Nomenclature

r	rate of reaction (in this case soot oxidation)
A	Arrhenius equation pre-exponential constant
E_a	activation energy
R	universal gas constant
T	temperature
C	amount of carbon (soot) in the DPF
α	reaction order with respect to carbon or carbon surface area
P_{O2}	partial pressure of O_2
β	reaction order with respect to O_2
S_c	active surface area of carbon in the DPF
S_0	active surface area of carbon in the DPF at the beginning of regeneration
s_m	active surface area per mole of carbon in the DPF
$s_{m,0}$	active surface area per mole of carbon in the DPF at the beginning of regeneration
C	amount of carbon in the DPF
C_0	amount of carbon in the DPF at the beginning of regeneration
γ, δ, and ε	constants in the surface area evolution equation

II.B.6 Fundamental Sulfation/Desulfation Studies of Lean-NO_x Traps, DOE Pre-Competitive Catalyst Research

Todd J. Toops (Primary Contact) and
Josh A. Pihl
Oak Ridge National Laboratory
2360 Cherahala Blvd.
Knoxville, TN 37932

DOE Technology Development Manager:
Kenneth Howden

Objectives

- Improve the fundamental understanding of operation and deactivation mechanisms in lean-NOx traps (LNTs).
- Investigate methods for improving performance and/or durability of LNTs:
  - Measure and characterize impact of changing LNT formulations.
  - Determine the optimum operating conditions.

Fiscal Year (FY) 2011 Objectives

- Investigate synergy between ceria, baria, and alumina phases with respect to oxides of nitrogen (NOx) storage and release mechanisms and overall NOx reduction performance.
- Develop new reactor to aid investigations into the fundamental chemistry on monolithic automotive catalysts:
  - Specifically designed for simultaneous spatially resolved analysis of adsorbates and gas-phase species.
- Investigate additional concentrations of Ca+Ba in LNT catalysts, between 0 and 10% Ca, to find optimum one for NOx reduction performance and tolerance to sulfur.

Approach

- Conduct pre-competitive LNT research.
- Investigate materials changes that can improve oxides of nitrogen (NOx) reduction performance and/or desulfation behavior.
- Study deactivation and regeneration mechanisms fundamentally.
- Coordinate efforts with other projects to maximize knowledge discovery.

Accomplishments

- Synthesized and evaluated additional formulations of Ca+Ba LNT catalysts.
- Illustrated ceria addition to alumina in conjunction with Ba leads to a highly active oxides of nitrogen storage and reduction (NSR) catalyst.
- Designed and built diffuse reflectance infrared Fourier-transform spectroscopy (DRIFTS) reactor for spatially resolved analysis of adsorbates on monolithic catalysts, allowing for both gas and surface analysis.

Future Directions

- Combine with engine-based lean gasoline project:
  - Team with automotive manufacturers and catalyst suppliers.
- Project will set aggressive milestones to drive down fuel penalty and precious metal costs associated with meeting emissions standards in lean gasoline applications.

Introduction

Increasingly stringent emissions regulations have necessitated the introduction of new catalytic emissions control devices for vehicles with lean-burn engines. While lean-burn engines are typically more fuel efficient than their stoichiometrically operated counterparts, meeting these regulations requires the system to operate at non-optimal conditions. In designing the controls to operate the system, the manufacturer must make a decision between these extreme scenarios:

- Operate the engine efficiently to achieve low emissions of NOx and particulate and having minimal reliance on emissions control devices, or
- Operate the engine at peak efficiency and rely on the larger more robust emissions control systems to "clean-up" the exhaust.

Most of the vehicles on the road today operate somewhere between these two conditions and thus there efficiency gains that can be achieved through more robust emissions control. The implementation of the emissions control systems can also incur a "fuel penalty." For example, LNT catalysts require periodic operation under fuel-rich conditions, increasing vehicle

fuel consumption. The key to deployment of lean-burn engine technology lies in optimizing the emissions control system such that emissions regulations are met without substantially increasing fuel consumption.

This project focuses on establishing a fundamental understanding of the underlying LNT chemistry to improve the accuracy of computer simulations used to design, develop, and control LNT aftertreatment systems. This includes identifying the roles of the catalytic phases of LNTs, investigating the impact of changes in catalyst formulations, elucidating reaction pathways, and determining the fate of sulfur in the catalyst. This effort is closely tied to the Cross-Cut Lean Exhaust Emissions Reduction Simulations kinetics activities and serves as guidance for the research undertaken in that project.

Approach

Our approach to understanding LNT fundamentals utilizes the unique capabilities and expertise developed in previous years of this project, i.e. the differential microreactor and the barrel-ellipse DRIFTS reactor. The microreactor is operated to minimize heat and mass transfer effects, enabling analysis of the underlying LNT reactions. The microreactor is capable of running a suite of catalyst characterization experiments, including surface area measurements through physisorption and chemisorption, quantification of reaction kinetics, characterization of catalyst performance under realistic operating conditions, and measurement of surface species stability through temperature programmed reactions. It was designed for relatively quick and easy sample loading, so several catalysts can be studied in a short period of time. In addition to the measurement of the reaction kinetics, it is important to understand the catalyst surface chemistry. The DRIFTS reactor enables these measurements at elevated temperatures and using simulated engine exhaust, including H_2O and CO_2. The ability to make these measurements under realistic conditions offers enables identification of reaction intermediates under "real-world" conditions and, thus, confirmation of mechanistic models or proposed new reaction pathways.

Results

Efforts this year targeted three areas: comparison of ceria's role in NSR functionality, development of a novel DRIFTS reactor for spatially-resolved inspection of surface species, and the expanded investigation of Ca+Ba LNTs. All of these investigations were performed with a focus on developing a fundamental understanding of LNT chemistry and durability.

Three kinds of model ceria-containing LNT catalysts, corresponding to $Pt/Ba/CeO_2$ (PBC), $Pt/CeO_2/Al_2O_3$ (PCA) and $Pt/BaO/CeO_2/Al_2O_3$ (PBCA), were prepared for comparison with a standard LNT catalyst of the $Pt/BaO/Al_2O_3$ type (PBA). The catalysts details can be found in Table 1. In these catalysts, ceria functioned as a NOx storage component and/or a support material. The influence of ceria on NOx storage capacity, regeneration behavior and catalyst performance during lean/rich cycling was investigated. The PBC and PBCA catalysts exhibited higher NOx storage capacity at 200ºC and 300ºC relative to the PBA catalyst (Figure 1), although the latter displayed superior storage capacity at 400ºC. Furthermore, the use of ceria as a support was found to result in an improved dispersion of the Ba storage material as compared to an alumina support; findings based on crystallographic analysis of X-ray diffraction patterns. Catalyst regeneration behavior at low temperature was also improved by the presence of ceria, as reflected by temperature programmed reduction measurements. These factors contributed to the superior NOx storage-reduction performance exhibited by the PBC and PBCA catalysts under cycling conditions in the temperature range 200-300°C (Figure 2). Overall, PBCA (which displayed well-balanced NOx storage and regeneration behavior), showed the best performance, affording consistently high NOx conversion levels in the temperature range 200°C to 400°C under lean-rich cycling conditions.

TABLE 1. Composition of Prepared Ceria Containing Catalysts

Catalyst	Catalyst code	Loading on support (wt%)		
		Pt	Ce	Ba
$Pt/CeO_2/Al_2O_3$	PCA	1	25	-
$Pt/BaO/Al_2O_3$	PBA	1	-	10
$Pt/BaO/CeO_2$	PBC	1	-	10
$Pt/BaO/CeO_2/Al_2O_3$	PBCA	1	25	10

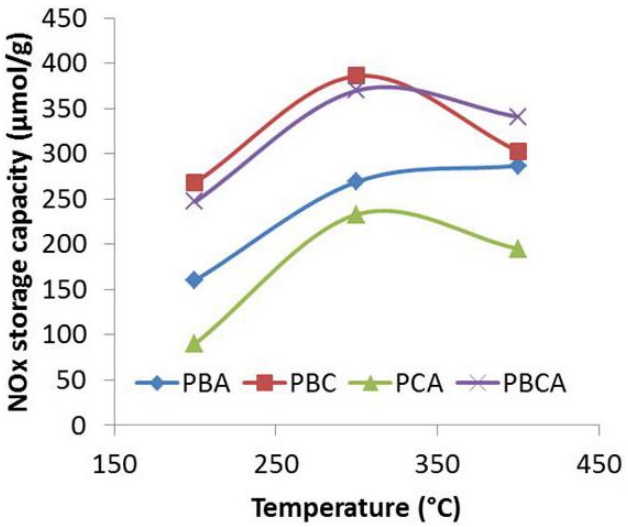

FIGURE 1. Comparison of NOx Storage under Lean Operation after 60 Minutes

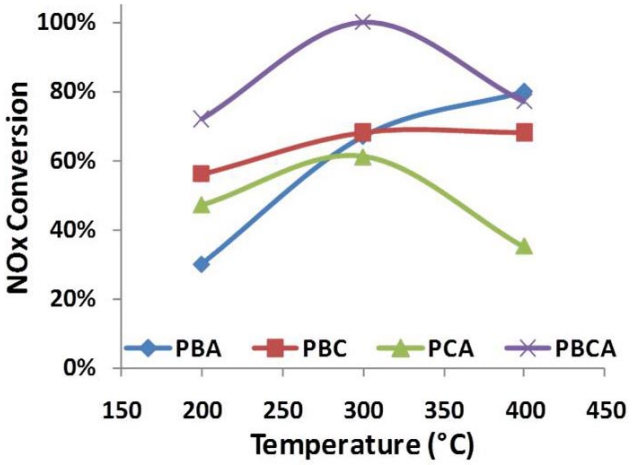

FIGURE 2. Comparison of NOx Conversion during NOx Storage/ Reduction Cycling

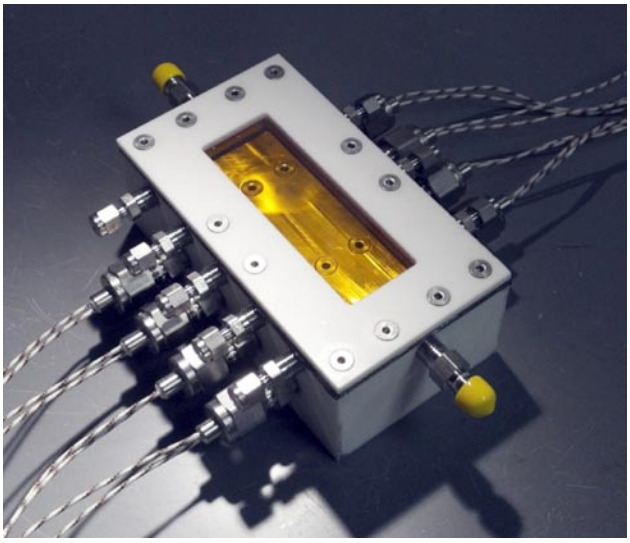

FIGURE 3. Newly Developed DRIFTS Reactor for the Simultaneous Measurement of Surface Adsorbates and Gas-Species

To improve on our ability to understand dynamics at the surface of the catalysts and how they relate to gas-phase measurements, we developed a reactor that could provide data on both fronts. Several commercially available reactors exist for the simultaneous measurements of surface and gas-phase species, but they are primarily associated with simple investigations of powder materials or pressed pellets. Additionally, the geometries in these commercially available reactors are not well defined, especially with respect to establishing kinetic parameters of adsorbed materials as they relate to gas-phase measurements. To measure the kinetic reactivity and the adsorbates on a material, there are only two known reactors available. Both of these reactors focus an infrared beam on the front face of a powder catalyst bed and allow the reactant gases to pass through the bed. Thus, it is possible to measure the adsorbates only on the very front of the catalyst bed while measuring the reactivity after the gas flows through the entire bed. Our new design improves on all of these shortcomings and enables evaluation of washcoated catalyst samples that are of interest to industry and commercial catalyst suppliers. The reactor utilizes a depression to hold either powder catalyst samples or washcoated materials. These materials are in close proximity to the heat source. The incoming gases flow over the top of the sample. There is a small gap between the sample and the infrared transparent window and there is access at the inlet, exit, or side of the reactor to insert a capillary that can sample small quantities of gases using capillary inlet techniques (mass spectrometry Fourier transform infrared, etc.) or provide distributed temperature measurements. This feature enables the measurements of gas-phase and surface adsorbates as a function of axial location along the reactor. Additionally, the gas-phase space is well defined to enable fast transients. This will enable modeling of the gas-flow dynamics in the reactor using established routines. An image of the developed reactor can be found in Figure 3.

To allow the unattended investigation of NOx reduction performance initially and during sulfation modifications were employed to the reactor system. This system was then employed to study the effect of varying the Ca dopant level in a Ca+Ba/Pt/Al_2O_3 series of LNTs. Earlier results have shown that doping at the 5% level was most beneficial compared to 10%, 20% and 100% Ca; also Ca was found to be better than doping with K or La [1]. These experiments were aimed at the range of additions between 3% and 9%. NOx conversion results for the newly synthesized LNT catalysts are shown in Figure 4a. These results indicate that blending Ba with 5% Ca results in unique properties that improve NOx reduction performance over all other compositions investigated. In addition to the NOx reduction performance, the catalysts were evaluated under sulfation conditions at 400°C, followed by the complete desulfation up to 1,000°C. The 5% Ca catalyst also maintains a higher NOx conversion during sulfation (Figure 4b). Desulfation behavior was not markedly different for these samples. Materials characterization of these catalysts to help explain this behavior is ongoing.

Conclusions

- The simultaneous addition of ceria with Ba on the alumina support results in improved Ba dispersion and showed the best performance, affording consistently high NOx conversion levels in the temperature range 200ºC to 400ºC under lean-rich cycling conditions.

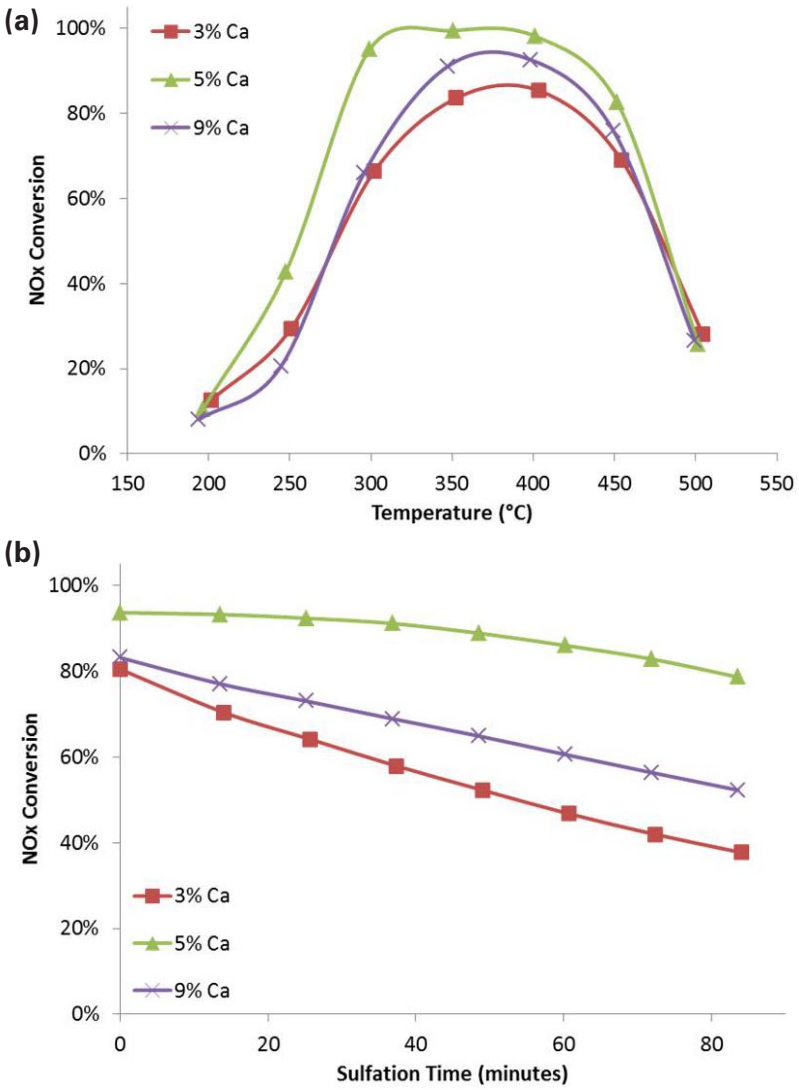

FIGURE 4. (a) Initial NOx Conversion of Ca+Ba LNTs and (b) NOx Conversion during Sulfation at 400°C

- A new reactor was developed to aid investigations into the fundamental chemistry on monolithic automotive catalysts; it is specifically designed for simultaneous spatially resolved analysis of adsorbates and gas-phase species.
- Additional concentrations of Ca+Ba LNT catalysts were synthesized and evaluated. Results suggest 5% Ca level continues to offer the best dopant balance for NOx reduction performance and tolerance to sulfur.

References

1. T.J. Toops, N.A. Ottinger, C. Liang, J.A. Pihl, A. Payzant, "Impact of lattice substitution in Ba-based NOx storage reduction catalysts on sulfation, desulfation and NOx reduction performance", Catalysis Today 160:1 (2011) 131.

FY 2011 Publications/ Presentations

1. C. Shi, Y. Ji, U. Graham, G. Jacobs, M. Crocker, Z. Zhang, Y. Wang, T.J. Toops, "NOx Storage and Reduction Properties of Model Ceria-based Lean NOx Trap Catalysts", submitted to Applied Catalysis B: Environmental.

2. N.A. Ottinger, T.J. Toops, J.A. Pihl, J.T. Roop, J.-S. Choi, W.P. Partridge, "Study of Nitrate and Sulfate Storage and Stability on Common Lean NOx Trap Components", submitted to Applied Catalysis B: Environmental.

3. (INVITED) T.J. Toops, N.A. Ottinger, C. Liang, J.A. Pihl, A. Payzant, "Impact of lattice substitution in Ba-based NOx storage reduction catalysts on sulfation, desulfation and NOx reduction performance", Catalysis Today 160:1 (2011) 131.

4. (INVITED) T.J. Toops, C. Liang, J.A. Pihl, N.A. Ottinger, "Impact of Dopants in Ba-Based NOx Storage Reduction (NSR) Catalysts on Sulfation, Desulfation, and Performance", 2011 Annual Meeting of the American Chemical Society, Denver, CO, August 28, 2011.

5. C. Shi, Y. Ji, T.J. Toops, M. Crocker, "NOx Storage and Reduction Properties of Ceria-based Lean NOx Trap Catalysts", 2011 Annual Meeting of the American Chemical Society, Denver, CO, August 28, 2011.

6. C. Shi, Y. Ji, T.J. Toops, M. Crocker, "NOx Storage and Reduction Properties of Ceria-based Lean NOx Trap Catalysts", 22nd North American Catalysis Society Meeting, Detroit, MI, June 5–10, 2011.

7. N.A. Ottinger, T.J. Toops, J.A. Pihl, J.-S. Choi, and W.P. Partridge, "Impact of the Support Material on the Stability of Nitrates and Sulfates in NOx Storage-Reduction Catalysts", 22nd North American Catalysis Society Meeting, Detroit, MI, June 5–10, 2011.

8. T.J. Toops, J.A. Pihl, J. Lewis, "Pre-Competitive Catalysis Research: Fundamental Studies of Lean NOx Traps", and J. Parks, S. Huff, V. Prikhodko, J.A. Pihl, "Emissions Control for Lean Gasoline Engines", 2011 DOE Annual Merit Review, Crystal City, VA, May 9–13, 2011.

Invention Disclosures

1. J.A. Pihl, W.P. Partridge, and T.J. Toops, "High-temperature reactor for Diffuse Reflectance Infrared Fourier-Transform Spectroscopy (DRIFTS)", ORNL invention disclosure.

II.B.7 Cummins-ORNL SmartCatalyst CRADA: NO_x Control and Measurement Technology for Heavy-Duty Diesel Engines

Bill Partridge[1] (Primary Contact), Neal Currier[2], Jae-Soon Choi[1], Maggie Connatser[1], Jim Parks[1], Xavier Auvray[3], Louise Olsson[3], Krishna Kamasamudram[2], Alex Yezerets[2]
[1]Oak Ridge National Laboratory (ORNL), [2]Cummins Inc., [3]Chalmers University of Technology
2360 Cherahala Blvd.
Knoxville, TN 37932

DOE Technology Development Manager:
Ken Howden

Overall Objectives

- Improve diesel engine-catalyst system efficiency through better combustion uniformity, engine calibrations and catalyst control.
- Work with industrial partner to develop full-scale engine-catalyst systems to meet efficiency and emissions goals.

Fiscal Year (FY) 2011 Objectives

- Develop capabilities for broadly characterizing selective catalytic reactor (SCR) catalyst performance parameters consistent with enabling self-diagnosing catalyst systems.
- Characterize Cu-Beta SCR catalyst under standard SCR conditions in degreened and hydrothermally aged states.
- Identify basic and practical performance characteristics consistent with enabling self-diagnosing catalyst systems.

Accomplishments

- Characterized distributed performance of model Cu-Beta catalyst under standard SCR conditions and at three temperatures (200, 325 and 400°C):
  - SCR reaction occurs in the catalyst front.
  - SCR reaction moves progressively to catalyst front with correspondingly greater reaction gradients with increasing temperature.
  - 1:1 NO:NH_3 conversion throughout catalyst for all temperatures indicating zero parasitic oxidation; despite significant oxides of nitrogen (NO_x)-free NH_3 oxidation at 325 and 400ºC.
- Characterized the impact of hydrothermal (HT) ageing on the distributed performance of the same Cu-Beta SCR catalyst:
  - A progressively greater portion of the catalyst is required with increasing HT ageing; the SCR reaction extends deeper into the catalyst.
  - Zero parasitic NH_3 oxidation is observed for all degreened and HT aged conditions.
  - SCR inhibition, presumably due to $[NH_3]_g$, is observed to progressively greater extents with increasing HT ageing.
- Enabled transient analysis determination of distributed catalyst NH_3 capacities via development of analysis methodologies accounting for transient instrument response.
- The full NH_3 catalyst capacity is used within the SCR zone for degreened and HT aged samples:
  - Unused NH_3 capacity exists only downstream of the SCR zone.
  - NH_3 capacity measurements are an indirect indicator of the catalyst portion used for SCR and can possibly be used for control.
- Worked in collaboration with the Cross-Cut Lean Exhaust Emissions Reduction Simulations (CLEERS) program and the Institute of Chemical Technology, Prague to identify N_2O formation pathways in lean-NO_x trap (LNT) catalysts.
- In collaboration with Professor Louise Olsson at Chalmers University of Technology, master student Soran Shwan modeled the spatially distributed intra-LNT performance measured previously in this Cooperative Research and Development Agreement (CRADA).

Future Directions

- Improve instrument response models for better transient analysis of:
  - NH_3 capacities, particularly unused capacity.
  - Instantaneous conversion.
  - Performance with NO_2 feed (e.g., fast SCR conditions).
  - Inhibition detection.
- Analyze distributed performance of commercial Cu-chabazite-zeolite SCR catalyst.
- Apply optical-fiber based NH_3 sensors for intra-catalyst detection, to demonstrate advanced control strategy methodologies.

Introduction

A combination of improved technologies for engine and aftertreatment control of NO_x and particulate emissions is required to efficiently meet increasingly stringent emission regulations. This CRADA section focuses on catalyst technologies, while a parallel section (Characterization and Reduction of Combustion Variations) focuses on combustion and engine technologies. Improved catalyst-system efficiency, durability and cost can be achieved through advanced control methodologies based on continuous catalyst-state monitoring; the overarching goal of this CRADA section is to enable self-diagnosing or smart catalyst systems. This approach is applicable to all catalyst types including LNT and SCR. In LNT applications, advanced control methods reduce the fuel penalty associated with catalyst maintenance (e.g., desulfation, regeneration) and extend the lifetime of the catalyst by triggering maintenance events only when and for as long as required as indicated by real-time catalyst-state monitoring, as opposed to being preprogrammed based on end-of-life performance. Continuous catalyst-state monitoring also provides a solution for 2013 regulations which require identification of the specific component function (e.g., oxidation) responsible in the event that a component's (e.g., NO_x catalyst) performance falls outside the regulatory window. Self-diagnosing catalyst technologies are enabled by basic and practical insights into the distributed nature of catalyst performance, improved catalyst models, insights suggesting control methodologies, and instrumentation to demonstrate and drive advanced control technologies. These catalysis advances require development and application of enhanced diagnostic tools to realize these technology improvements. While the CRADA has a strong diagnostic focus, it is involved, often through synergistic partnerships, in the other enabling research activities discussed previosly.

Approach

Developing and applying minimally invasive advanced diagnostic tools to resolve spatial and temporal variations within operating engines and catalysts has been central to the historical successes of this CRADA partnership, and continues to be a key element of the project approach. These include small capillary and optical-fiber based technologies which are able to resolve spatiotemporal variations without changing the measurement environment or requiring significant hardware modifications for applications. Integral to this work are coating technologies to create localized fiber and capillary transducers to detect variations; e.g., species, temperature, pH, etc. The approach relies heavily on optical and mass-spectrometry, but also includes other techniques such as electrical impedance spectroscopy. Diagnostics are developed and demonstrated on bench reactors and engine systems (as appropriate) at ORNL prior to field application at Cummins. In some cases discrete-sensor technology is a stepping stone and may be further developed and integrated in system components; e.g., to create self-diagnosing smart catalyst systems.

Diagnostics are applied at ORNL and Cummins to study the nature and origins of performance variations. In catalyst studies, this may be spatial and temporal variations unique to each catalyst function (e.g., SCR, NH_3 storage and parasitic oxidation, NO_x storage and reduction, oxygen storage capacity, water-gas shift) during operation and how these vary with thermal ageing or poisoning by exhaust constituents (hydrocarbons or sulfur, for example). This detailed information is applied to understand how catalysts function and degrade, develop device and system models, and develop advanced control strategies.

Results

The axially distributed intra-catalyst performance of a Cu-Beta-zeolite catalyst [1] under standard SCR conditions was studied using the Cummins 4-Step Protocol [2]; this provides for quantifying a wide range of performance parameters including NO oxidation, NO and NH_3 SCR conversion, parasitic and NO_x-free NH_3 oxidation, and various (dynamic, unused and total) NH_3 capacities. Figure 1 shows the NO and NH_3 conversion distributions at 325°C. The SCR zone is in the front ca. 1/4 of the catalyst length (1/4 L), and ca. half of the conversion is concentrated in a high-gradient region in the front 1/16 L. The equivalent NH_3 and NO conversions in Figure 1, within experimental limits, indicate that parasitic NH_3 oxidation is zero, as was also the case for the other (200 and 400°C)

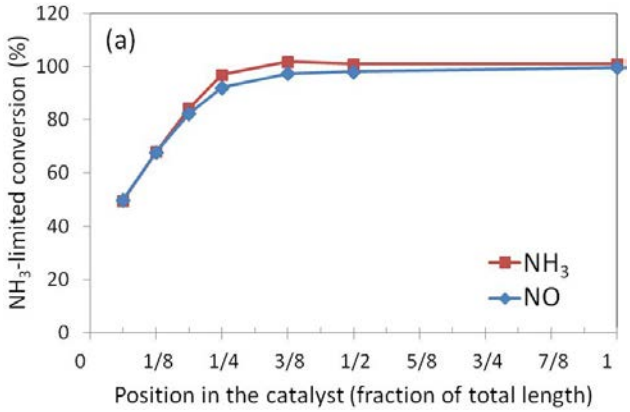

FIGURE 1. Steady-State Axial NH_3 and NO Conversion Distributions at 325°C

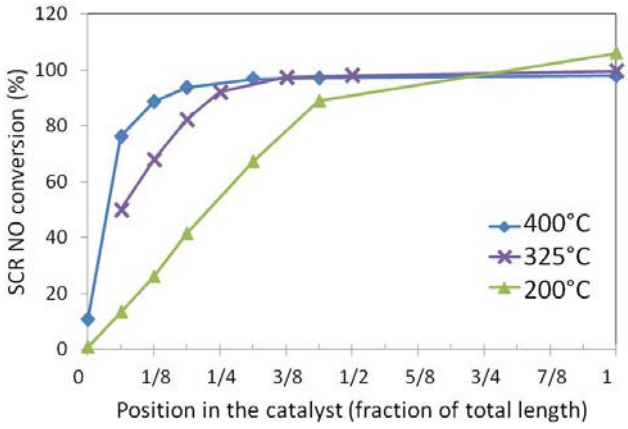

FIGURE 2. Progressive Shift in the Steady-State Axial SCR Distribution with Increasing Temperature

temperatures studied (not shown here). Specifically, although NO_x-free NH_3 oxidation is significant at 325 and 400°C, it does not occur to an appreciable extent under SCR conditions, suggesting that the SCR reactions are faster than NH_3 oxidation reactions. Figure 2 shows the distributed SCR NO conversion at the three temperatures, and how the SCR reaction progressively shifts to the catalyst front resulting in higher gradients with increasing temperature. Notably, there is no change in the complete conversion measured at the catalyst outlet despite the dramatic intra-catalyst changes associated with the various operation temperatures.

Catalyst NH_3 capacities were determined from transient analysis of the 4-Step Protocol as shown in Figure 3; dynamic capacity (DC), unused capacity (UC), and total capacity (TC), in Steps 2, 3 and 4, respectively. DC is the NH_3 capacity under SCR conditions, which may be UC less than the TC; i.e., there is a capacity balance such that DC+UC=TC. Capacities are determined from integrating between a step and the actual measured response of specific species transients. This is appropriate for species such as NO and N_2 which have approximately step instrument response. However, other species such as NH_3 and NO_2 have non-step-like instrument response; the effect is as though there is some number of storage sites for those species within the instrument. In this case it is appropriate to determine capacity components as the difference between the measured response and the instrument response rather than a step response. A fit of the NH_3 instrument response was determined from NH_3 span steps in various calibrations at multiple temperatures; this fit was scaled and used in the difference integral to determine the NH_3 portion of the DC and TC. Instrument responses in Step 3, where UC is determined, are more complicated because they start from different NH_3 levels (and thus different number of instrument sites filled) depending on the extent of SCR up to that location in the catalyst.

Analysis of the various capacity distributions can give insights into how that capacity is used in the SCR reactions, and possibly advanced control strategies for these complex catalysts. The dynamic and total capacities measured at 200°C and 325°C, and calculated using the methods described, are presented in Figure 4a and 4b, respectively. All NH_3 storage values at 400°C were very small, and are thus not shown. The TC distributions shown in Figure 4 are nominally linear at both temperatures although some zoned variations are apparent at 325°C; such a linear trend is expected for a catalyst with an axially uniform washcoat loading, and indeed nonuniform washcoat loading may contribute to the zoned variations observed at 325°C. The TC ranged from 0 to 63 µmol at 200°C, and from 0 to 19 µmol at 325°C. The coverage depends on the temperature, and NH_3 apparently becomes increasingly unstable at higher temperatures. The maximum storage at 400°C, observed at the exit, is only ca. 2 µmol (not shown), which is consistent with the fact that total storage capacity decreases with temperature. The DC reflects the competition between NH_3 storage, surface-NH_3 thermal stability and the SCR reaction. At higher temperatures the surface NH_3 is less stable (cf. TC trends) and the SCR reaction is faster (cf. Figure 2), both of which could result in a smaller DC. Figure 4 indicates that DC increases and follows the TC in the front of the catalyst and then levels off. Comparing these results to the conversion profiles in Figure 2, it is apparent that DC increases within the SCR zone only. Beyond the SCR zone, where gas-phase NH_3 is fully consumed, DC can no longer increase, and thus the

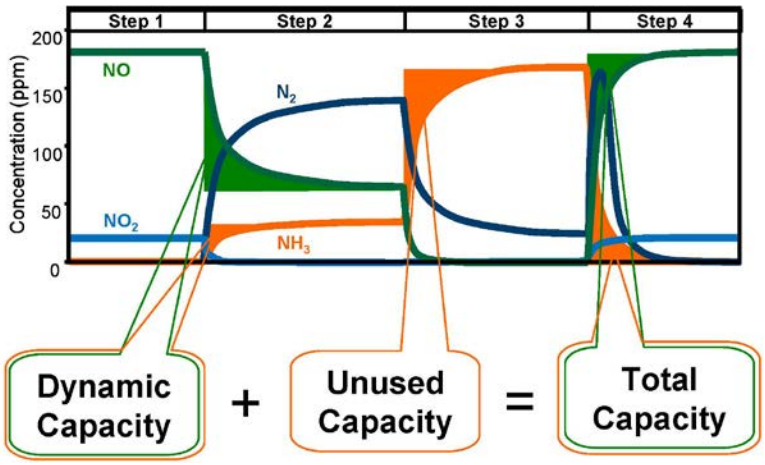

FIGURE 3. Methodology for Determining NH_3 Capacities from Transient Analysis of the 4-Step Protocol Data

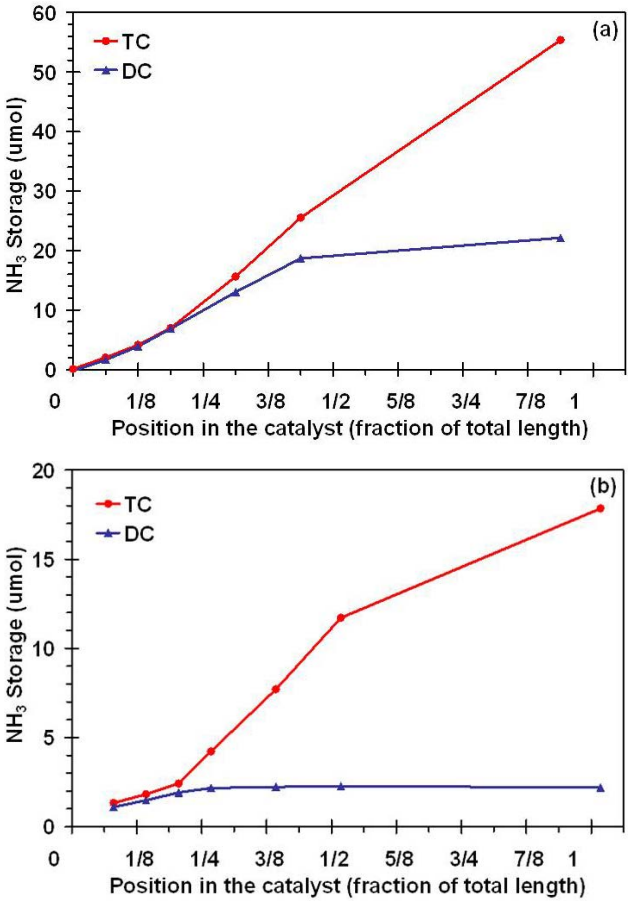

FIGURE 4. Total and Dynamic NH_3 Storage Capacity Distributions at a) 200°C b) 325°C

plateau after the SCR zone. The salient point though is that DC matches TC within the SCR zone. At 200°C, SCR occurs in the front half since the NH_3 conversion reaches 100% by 1/2 L; correspondingly at 200°C DC increases linearly and practically matches TC up to the 1/2 L location, and then plateaus. The same correlation is made at 325°C where SCR and dynamic storage both occur within the front quarter of the catalyst, and DC matches TC. Indeed, the same DC:TC correlation exists at 400°C in the front 1/16 L where ca. 80% of the SCR conversion occurs, despite the significantly lower capacity and higher SCR rate at this high temperature. The implication of this observation is that the full NH_3 capacity is used throughout the SCR zone for this catalyst over the full range of temperatures studied (i.e., 200, 325 and 400°C). This heretofore undemonstrated observation has been independently corroborated by the UC trends (not shown here).

Ammonia storage sites in the post-SCR region cannot be filled during SCR since NH_3 is fully reacted or stored within the SCR zone. However, the NH_3 sites in the post-SCR region are NH_3 free and able to store NH_3 in Step 3 (NH_3 saturation); this additional storage capacity is the UC. A corollary of the conclusion from the preceding paragraph is that UC is zero in the front SCR-region of the catalyst. Thus, UC is indicative of the catalyst portion not used for SCR, and provides a potential control parameter indirectly indicative of the catalyst portion used for SCR.

In addition to the degreened performance discussed above, the impact of hydrothermal (HT) ageing on intra-catalyst distributed performance was investigated. The catalyst was subsequently exposed to two HT ageing conditions with 10% O_2 + 5% H_2O environments. Mild HT ageing was effected by six temperature ramps to 600°C and a subsequent two-hour soak at 500°C. More traditional and extensive HT ageing was caused by a three-hour soak at 700°C. Following each HT ageing, distributed performance was evaluated under standard SCR conditions at 325°C. In general the SCR reaction slowed with HT ageing causing the SCR reaction to extend deeper into the catalyst; indeed the effluent conversion was complete for all catalyst ageing despite very different intra-catalyst reaction distributions. Furthermore, parasitic NH_3 oxidation was negligible for all conditions, as evident from the 1:1 NO:NH_3 conversion. And, as observed for the degreened samples, the full NH_3 capacity was used throughout the SCR zone for all HT aged samples. However, HT ageing did degrade the DC and TC throughout the catalyst; this is consistent with separate effluent measurement observations using the same catalyst [3]. Inhibition of the SCR reaction was observed at the catalyst front in the HT aged samples; and this inhibition becomes greater, and extends deeper into the catalyst with increasing HT ageing. This inhibition is presumably due to greater NH_3 concentrations existing deeper into the catalyst with increasing HT ageing. Specifically, lower DC degrades SCR conversion, spreading the SCR reaction deeper into the catalyst and causing $[NH_3]_g$ to exist correspondingly deeper into the catalyst. The inhibition spatial trend follows the $[NH_3]_g$ trend; indeed, inhibition was observed in the degreened 200°C sample where SCR conversion was slow, despite high DC. Inhibition in Cu-zeolite catalysts is not generally recognized to exist and is not typically observed because it is generally confined to the front zone inside the catalyst. Finally, we suggest that DC loss associated with HT ageing has a multiplied impact on SCR degradation; i.e., directly lower SCR from lower $[NH_3]_s$, and an indirect degradation via inhibition due to greater $[NH_3]_g$. Indeed, we expect that inhibition should be observed on this catalyst in the efficient (325 and 400°C) degreened conditions if one could sample very close to the catalyst front where $[NH_3]_g$ is high.

Conclusions

- A fraction of the Cu-beta zeolite catalyst is used for NH_3 SCR:
  - SCR zone confined to the catalyst front section.

- The SCR zone extends deeper into the catalyst at lower temperatures and with increasing HT ageing.
- Parasitic NH_3 oxidation was negligible for all degreened and HT aged conditions studied.
- The full NH_3 capacity is used throughout the SCR zone:
  - Unused capacity is an indirect indicator of catalyst portion used for SCR.
- HT ageing reduces SCR activity and NH_3 capacity.
- SCR inhibition is observed on the Cu-beta catalyst at axial locations where gas-phase NH_3 concentrations are high.

References

1. Wilken, N., Kamasamudram, K., Currier, N.W., Li, J., Yezerets, A. and Olsson, L., "Heat of adsorption for NH3, NO2 and NO on Cu-Beta zeolite using microcalorimeter for NH3 SCR applications," Catalysis Today 151 (2010) 237-243.

2. K. Kamasamudram, N.W. Currier, X. Chen, A. Yezerets, Overview of the practically important behaviors of zeolite-based urea-SCR catalysts, using compact experimental protocol, Catalysis Today, 151 (2010) 212-222.

3. K.W.N. Wilken, K. Kamasamudram, N.W. Currier, R. Vedaiyan, A. Yezerets, L. Olsson, Applied Catalysis B: Environmental, (2011).

FY 2011 Publications/Presentations

1. Alexandre Goguet, Cristina Stere, Jacinto Sá, Daniel Luis Abreu Fernandes, Farid Aiouache, Christopher Hardacre, David, Lundie, Wasif Naeem and William P. Partridge, "Spatial Resolution of Kinetic Oscillations Within a Catalytic Monolith," Oral Presentation, ICEC 2010: 6th International Conference on Environmental Catalysis, Beijing China, September 12, 2010.

2. Jae-Soon Choi, William P. Partridge, Josh A. Pihl, Kalyan Chakravarthy, and C. Stuart Daw (2010). "Factors affecting the NH3 selectivity of lean NOx traps – Insights from spatiotemporal distribution of reactions," **Keynote Lecture**, 2nd International Symposium On Air Pollution Abatement Catalysis (APAC 2010), CRACOW, Poland, September 8, 2010. **Invited**

3. W.P. Partridge, X. Auvray, N. Currier, L. Olsson, J.-S. Choi, A. Yezerets, K. Kamasamudram (2010). "Ammonia Storage & Reaction Distributions Within an Operating SCR Catalyst," 9th Annual Symposium of the Southeastern Catalysis Society, Asheville, SC, September 27, 2010.

4. Bill Partridge, Jae-Soon Choi, Josh Pihl, Todd Toops, Jim Parks, Nathan Ottinger, Alex Yezerets , Neal Currier (2010). "Advanced LNT DeSulfation Control via Understanding the Distributed Intra-Catalyst Impacts of Sulfation on Water Gas Shift, NOx Storage & Reduction Reactions," DEER 2010 Conference, Emissions Control Technologies, Detroit, MI, September 28, 2010.

5. Jae-Soon Choi, William P. Partridge, Josh A. Pihl, Michael J. Lance, Nathan A. Ottinger, C. Stuart Daw, Kalyan Chakravarthy and Todd J. Toops (2010). "Functionality of Commercial NOx Storage-Reduction Catalysts and the Development of a Representative Model," DEER 2010 Conference, Emissions Control Technologies, Detroit, MI, September 29, 2010.

6. Todd Toops, Nathan Ottinger, Justin Roop, Josh Pihl, Jae-Soon Choi, Bill Partridge (2010). "Sulfate Storage and Stability on Lean NOx Trap Components," DEER 2010 Conference, Emissions Control Technologies, Detroit, MI, September 29, 2010.

7. Bill Partridge, Xavier Auvray, Louise Olsson, Jae-Soon Choi, Krish Kamasamudarm, Alex Yezerets, Neal Currier, "Distributed Transient Performance of a Model Cu-Beta SCR Catalyst: for development of Self-Diagnosing Catalyst Systems," 2011 DOE Crosscut Workshop on Lean Emissions Reduction Simulation, University of Michigan, Dearborn, Michigan, April 19th, 2011.

8. Petr Koci, Milos Marek, William Partridge, Josh Pihl, Jae-Soon Choi, "N2O Formation During the Regeneration of Lean NOx Traps," 2011 DOE Crosscut Workshop on Lean Emissions Reduction Simulation, University of Michigan, Dearborn, Michigan, April 21st, 2011.

9. Jae-Soon Choi, Josh Pihl, Miyoung Kim, Bill Partridge, Stuart Daw, Petr Koci, "Correlation between LNT NH3 and N2O selectivities under fast cycling conditions," 2011 DOE Crosscut Workshop on Lean Emissions Reduction Simulation, University of Michigan, Dearborn, Michigan, April 21st, 2011.

10. Soran Shwan, Bill Partridge, Jae-Soon Choi, Louise Olsson, "Kinetic Modeling of NOx Storage and Reduction Using Spatially Resolved MS Measurements," Mobile/Stationary Emissions Control topical area, North American Catalysis Society, 22nd North American Meeting, Detroit, Michigan, June 6, 2011.

11. Jae-Soon Choi, Josh Pihl, Bill Partridge, Miyoung Kim, Stuart Daw, "Axial Redistribution of NOx Storage and Impact on LNT Performance under Fast Cycling Conditions," Mobile/Stationary Emissions Control topical area, North American Catalysis Society, 22nd North American Meeting, Detroit, Michigan, June 7, 2011.

12. Petr Koci, Milos Marek, Josh Pihl, Jae-Soon Choi, William Partridge, "N2O Formation During the Regeneration of Lean NOx Traps," Mobile/Stationary Emissions Control topical area, North American Catalysis Society, 22nd North American Meeting, Detroit, Michigan, June 7, 2011.

13. Bill Partridge, Xavier Auvray, Louise Olsson, Jae-Soon Choi, Krish Kamasamudarm, Alex Yezerets, Neal Currier, "Temperature & Hydrothermal Ageing Impacts on Intra-Catalyst SCR-Reaction Distribution," Mobile/Stationary Emissions Control topical area, North

American Catalysis Society, 22nd North American Meeting, Detroit, Michigan, June 8, 2011.

14. Soran Shwan, William Partridge, Jae-Soon Choi and Louise Olsson, "Kinetic Modeling of NOx Storage and Reduction Using Spatially Resolved MS Measurements," Oral Presentation, AVL Advanced Simulation Technologies (AST) International User Conference, Graz, Austria, June 28, 2011.

15. Bill Partridge, Xavier Auvray, Louise Olsson, Jae-Soon Choi, Josh Pihl, Krish Kamasamudram, Alex Yezerets, Neal Currier, "Temperature & Hydrothermal Ageing Impacts on Intra-Catalyst SCR-Reaction Distriubutions," **Keynote Lecture**, Environmental Catalysis Session, EuropaCat X, Glasgow, Scotland, United Kingdom, August 30, 2011. **Invited**

16. Jae-Soon Choi, Josh Pihl, Petr Koci, Bill Partridge, Miyoung Kim, Stuart Daw, "Axial Redistribution of NOx Storage and Impact on LNT Performance under Fast Cycling Conditions," Environmental Catalysis Session, EuropaCat X, Glasgow, Scotland, United Kingdom, August 30, 2011.

17. Petr Koci, Milos Marek, Josh Pihl, Jae-Soon Choi, William Partridge, "Modelling of N2O Formation During the Regeneration of NOx Storage Catalysts," Environmental Catalysis Session, EuropaCat X, Glasgow, Scotland, United Kingdom, August 30, 2011.

18. Alexandre Goguet, Cristina Stere, Jacinto Sá, Daniel Luis Abreu Fernandes, Farid Aiouache, Christopher Hardacre, David, Lundie, Wasif Naeem and William P. Partridge, "SPACIMS – spatial and temporal operando resolution of structured catalysts," Catalyst Characterization Session, EuropaCat X, Glasgow, Scotland, United Kingdom, September 2, 2011.

19. Petr Koci, Sarka Bartova, Milos Marek, Josh Pihl, Jae-Soon Choi, William Partridge, "Modelling of N2O Formation During the Regeneration of NOx Storage Catalysts," MODEGAT II (2nd International Symposium on Modeling of Exhaust-Gas After-Treatment), Bad Herrenalb/ Kalrsruhe, Germany, September 19, 2011.

20. Jae-Soon Choi, Bill Partridge, Josh Pihl, Petr Koci, Miyoung Kim, Stuart Daw, "Spatiotemporal Distribution of NOx Storage: a Factor Controlling NH3 and N2O Selectivities over a Commercial LNT Catalyst," Environmental Catalysis Session, 17th DEER Conference, Detroit, Michigan, October 5, 2011.

Special Recognitions & Awards/Patents Issued

Invited Keynote Lecture

Bill Partridge presented an invited Keynote Lecture at EuropaCat X conference in Glasgow, Scotland, based on the Cummins CRADA work in partnership with Chalmers University of Technology. The presentation details are listed under the Presentation section of this report.

II.B.8 Efficient Emissions Control for Multi-Mode Lean DI Engines

James Parks (Primary Contact), Josh Pihl, Sam Lewis, Vitaly Prikhodko
Oak Ridge National Laboratory (ORNL)
2360 Cherahala Boulevard
Knoxville, TN 37932

DOE Technology Development Manager:
Ken Howden

Objectives

- Assess the relative merits of meeting emission regulations via catalytic aftertreatment or advanced combustion for diesel engines capable of operating in multiple combustion modes ("multi-mode" engines).
- Determine the fuel efficiency of combinations of catalytic aftertreatment and advanced combustion modes.
- Characterize exhaust chemistry from advanced combustion and the resulting evolution of chemistry in catalysts for emissions control to improve the understanding of advanced engine and aftertreatment systems.

Accomplishments

- Demonstrated that oxidation catalysts effectively control particulate matter emissions from reactivity controlled compression ignition (RCCI) combustion for particulate sizes less than 23 nm (oxidation not effective above 23 nm size range).
- Characterized low temperature oxidation performance of Nanostellar diesel oxidation catalysts under premixed charge compression ignition (PCCI) operating conditions.
- Demonstrated the reversibility of hydrocarbon fouled Cu- and Fe-zeolite selective catalytic reactor (SCR) catalysts from both conventional and PCCI combustion, and identified the chemical nature of the hydrocarbon species causing the fouling to occur.

Future Directions

This project ended in Fiscal Year (FY) 2011. Similar research will continue in a separate ORNL project to continue study of the emissions control challenges from advanced fuel efficient combustion strategies.

Introduction

New combustion regimes are being investigated as a means to increase the efficiency of, and to reduce the emissions from, diesel engines. The reduction of emissions during combustion is beneficial to the fuel efficiency of the system as a whole (engine plus emissions control system or "aftertreatment"). For example, lower engine-out oxides of nitrogen (NOx) emissions can remove some burden from post-combustion emissions controls, and can thereby reduce the fuel penalty associated with NOx reduction. Although new combustion techniques have been developed that offer advantages for both engine fuel efficiency and emissions, often the techniques are not attainable over the entire range of load and speed required for market acceptance. Thus, engines designed to implement the new combustion techniques often operate in a "multi-mode" fashion where, at certain loads, the engine is operated with advanced combustion techniques and, at other loads, the engine is operated with more traditional diesel combustion. While modern control systems enable switching between the multiple modes of operation, the optimization of the system for fuel efficiency and emissions becomes more complex. One particular challenge is optimizing the size, cost, and complexity of the emissions control system. This project is aimed at understanding the complex issues of efficiency and emissions management for multimode engines with advanced emission control systems. Characterization of combustion exhaust chemistry and catalytic control are conducted to assist industry in the design of multi-mode engine and emission control systems.

Approach

This research was conducted on a modern General Motors 1.9-liter 4-cylinder diesel engine on an engine dynamometer at ORNL. The original equipment engine controller for the engine has been replaced with a full pass control system made by Drivven that enables complete control of all engine operating controls such as fuel injection timing, exhaust gas recirculation (EGR) levels, and intake manifold pressure. With this advanced control system, the engine is operated with unique advanced combustion strategies that achieve high efficiency and low emissions. The development of the advanced combustion strategies is conducted in other projects at ORNL and other collaborating entities; this project leverages those efforts by simply transferring

the "recipes" for control to duplicate the advanced combustion. Advanced combustion strategies utilized in this project include: low-temperature combustion (LTC), high efficiency clean combustion (HECC), and RCCI. All of these combustion strategies achieve extremely low NOx and particulate matter emissions while maintaining low brake specific fuel consumption; however, in some cases CO and hydrocarbon (HC) emissions increase. Formaldehyde emissions can increase as well; formaldehyde is classified as a mobile source air toxic by the Environmental Protection Agency. Thus, the burden of the emissions control system to control NOx and particulate matter emissions is significantly reduced with advanced combustion, but higher CO and HC emission control is needed. Experiments are conducted to understand the synergies between advanced combustion and advanced aftertreatment with the objective of achieving high efficiency combined with low emissions and low cost. Commercial and prototype catalysts for the studies are obtained from a variety of vendors and representatives of the Manufacturers of Emission Control Association. Catalysts technologies include: catalyzed diesel particulate filters, diesel oxidation catalysts (DOCs), lean-NOx traps, urea-SCR, and HC-SCR.

In FY 2011, experiments conducted during the project included studies of zeolite-based urea-SCR catalysts, DOC control of CO and HC emissions at low exhaust temperatures combustion, and particulate matter control via DOC technology for RCCI combustion. For this report, the technical results from the study of HC fouling of zeolite-based urea-SCR catalysts are presented; for other studies see detailed technical results in the references. To study HC fouling, SCR catalyst cores were exposed to engine exhaust at aggressive low temperature (150°C) conditions that would result in HC adsorption on the catalysts. Exposures were performed at 1,500 rpm and 2.6 bar for both conventional and PCCI combustion. HC levels varied based on combustion mode with a PCCI HC emission rate of 2.19 g/bhp-hr or about twice as much compared with the conventional HC emission rate of 1.35 g/bhp-hr. After exposure for equal amounts of time, the catalysts were analyzed in a bench flow reactor for NOx reduction performance. Furthermore, detailed analysis of the HC species adsorbed on the catalysts was conducted by extracting the HCs off of the catalyst samples and analyzing the chemistry with a gas chromatography technique.

Results

NOx reduction performance as a function of temperature for both Cu-SCR and Fe-SCR catalysts is shown in Figure 1 and Figure 2, respectively. NOx reduction results are shown during a temperature ramp for an unexposed sample ("Degreened"), after exposure to HCs from conventional exhaust ("After Conventional"), and after exposure to HCs from PCCI exhaust ("After PCCI"). In addition, after completing the temperature ramp of the exposed samples, the temperature ramp was repeated, and results are represented by the "Cleaned Conventional" and "Cleaned PCCI" data after exposure and thermal desorption of HCs from conventional and PCCI exhaust, respectively. The Cu-SCR results in Figure 1 show that HC fouling diminished low temperature NOx reduction for both conventional and PCCI exposed cases, but more performance loss occurred from the higher HC emission condition associated with PCCI combustion. However, in both cases, after thermal desorption of the HCs, full low temperature NOx reduction performance was restored. Results from the Fe-SCR catalyst in Figure 2 show more severe low temperature NOx reduction performance loss, but interestingly, less difference occurred between the conventional and PCCI cases. Again, we observed full recovery of the

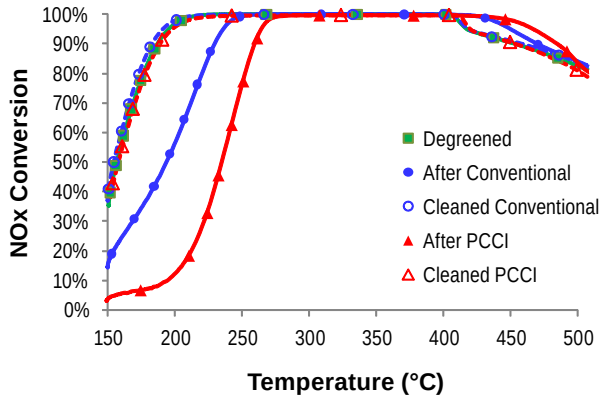

FIGURE 1. NOx reduction performance expressed as conversion as a function of temperature for the Cu-zeolite SCR catalyst at various stages of exposure.

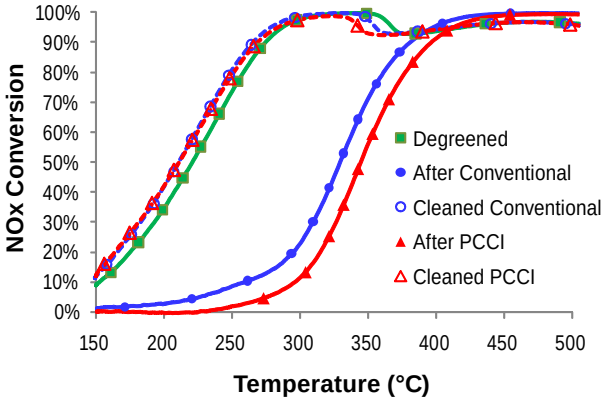

FIGURE 2. NOx reduction performance expressed as conversion as a function of temperature for the Fe-zeolite SCR catalyst at various stages of exposure.

NOx performance loss after thermal desorption of the HCs occurred.

The HC fouling process is affected by the HC species and interactions of the HC molecules with the zeolite structure of the SCR catalysts. Thus, measurements of the HCs adsorbed on the SCR samples were conducted to classify the HCs. Figure 3 shows the distribution of HCs adsorbed onto the SCR catalyst from conventional combustion; in comparison, Figure 4 shows the HC distribution from PCCI combustion. HCs from PCCI exhaust are of lower molecular weight and size in comparison to the conventional exhaust HCs. The difference is important as the Cu-zeolite SCR consists of a different structured zeolite than the Fe-zeolite SCR catalyst. The combination of zeolite material differences coupled with the HC molecular size difference have a large effect on the HC fouling affect on performance.

Further understanding of the reversibility of the HC fouling was studied via integration of the thermal desorption of HCs from the SCR catalysts.

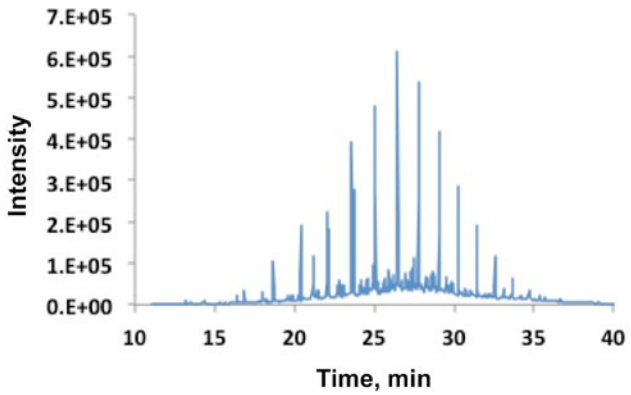

FIGURE 3. Gas chromatograph distribution of HCs adsorbed on the Cu-zeolite SCR during exposure to conventional combustion exhaust.

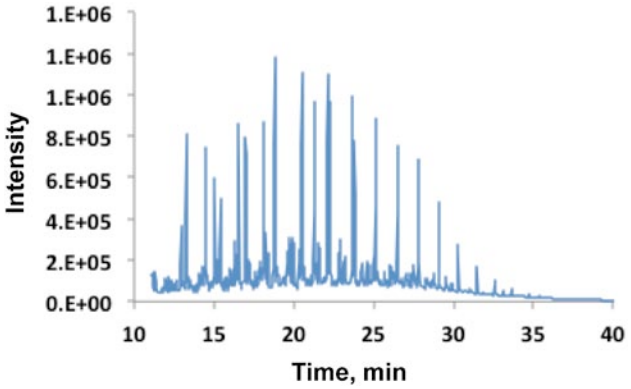

FIGURE 4. Gas chromatograph distribution of HCs adsorbed on the Cu-zeolite SCR during exposure to PCCI combustion exhaust.

Figure 5 shows a HC desorption curve as a function of temperature where the species observed downstream of the catalyst during a temperature ramp are separated between oxidized HCs ($CO+CO_2$) and un-oxidized HCs. While HCs began desorbing below 200ºC, most of the HCs desorbed at higher temperatures where they were oxidized or partially oxidized to CO or CO_2. Comparison of the NOx performance as a function of temperature shown in Figure 1 to the HC desorption as a function of temperature in Figure 5 is interesting as the HCs remaining on the catalyst above 250ºC had little effect on NOx reduction performance. Further analysis of the HC desorption data was performed by integrating the desorbed species released for all catalyst and combustion technique combinations (Figure 6). Less overall HCs were stored on the Cu-SCR catalyst, but there was a greater difference in HC storage on the Cu-SCR catalyst due to HC chemistry differences between conventional and PCCI combustion. Based

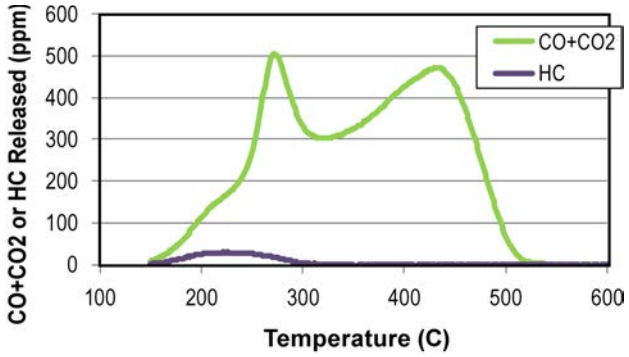

FIGURE 5. $CO+CO_2$ and HC emissions during desorption from the Cu-zeolite SCR catalyst via thermal processes as a function of temperature.

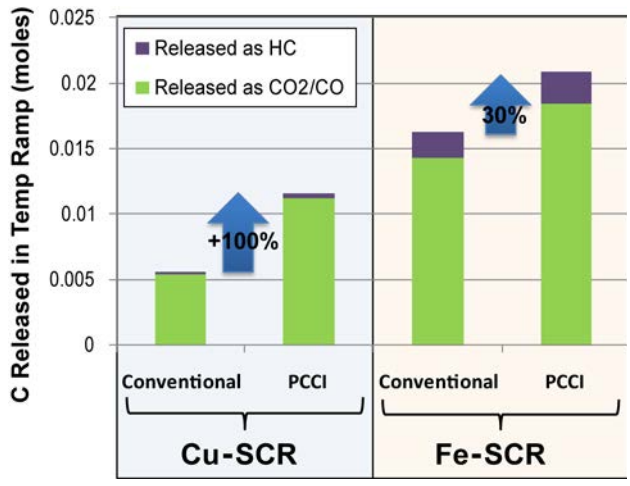

FIGURE 6. Summary of total C released in $CO+CO_2$ and HC forms from Cu-SCR and Fe-SCR catalysts after exposure to both conventional and PCCI exhaust.

on the combination of results on NOx reduction performance and HC adsorption/desorption, Cu-SCR catalysts show more resistance to HC fouling, but the sensitivity of Cu-SCR to HC speciation is greater. Thus, careful understanding and control of the relation between HC species and zeolite material design for SCR catalysts will be important for optimal performance.

Conclusions

Cu- and Fe-zeolite SCR catalysts were exposed to engine exhaust during both conventional and PCCI combustion to understand HC fouling of NOx reduction performance. Higher levels of HCs resulted from PCCI combustion, and importantly, the molecular size of HCs from PCCI differed significantly from conventional combustion HCs. HC fouling was observed to degrade low temperature performance, but the process was found to be reversible via thermal desorption processes. Careful understanding and control of the relation between HC species and zeolite material design for SCR catalysts will be important for optimal performance.

FY 2011 Publications/Presentations

1. Jim Parks, Vitaly Prikhodko, Sam Lewis, and Josh Pihl, "Hydrocarbon fouling of SCR during Premixed Charge Compression Ignition (PCCI) combustion", *2011 Directions in Engine-Efficiency and Emissions Research Conference (DEER)*, October 3–6, 2011 (2011).

2. Vitaly Y. Prikhodko, Scott J. Curran, Teresa L. Barone, Samuel A. Lewis, John M. Storey, Kukwon Cho, Robert M. Wagner, and James E. Parks II, "Diesel Oxidation Catalyst Control of Hydrocarbon Aerosols from Reactivity Controlled Compression Ignition Combustion", *Proceedings of the ASME 2011 International Mechanical Engineering Congress and Exposition*, November 11–17, 2011, Denver, CO, Paper IMECE2011-64147 (2011). [*paper accepted*]

3. Vitaly Y. Prikhodko, Josh A. Pihl, Samuel A. Lewis, and James E. Parks II, "Effect of Higher Hydrocarbon Emissions from PCCI-Type Combustion on the Performance of Selective Catalytic Reduction Catalysts", *Proceedings of the ASME 2011 Internal Combustion Engine Division Fall Technical Conference (ICEF2011)*, October 2–5, 2011, Morgantown, West Virginia, Paper ICEF2011-60129 (2011). [*paper accepted*]

4. Josh A. Pihl, Vitaly Y. Prikhodko, James E. Parks II, "Fouling of commercial urea SCR zeolite catalysts exposed to diesel engine exhaust", *2011 Meeting of the North American Catalysis Society*, June 6–9, 2011 (2011).

5. Vitaly Y. Prikhodko, Josh A. Pihl, Samuel A. Lewis, and James E. Parks, "Hydrocarbon fouling of Cu- and Fe-zeolite SCR catalysts in conventional and advanced diesel combustion modes", *14th DOE Crosscut Workshop on Lean Emissions Reduction Simulation*, April 19–21, 2011 (2011).

6. Teresa L. Barone, Anshuman A. Lall, John M.E. Storey, George W. Mulholland, Vitaly Y. Prikhodko, Jennifer H. Frankland, James E. Parks, Michael R. Zachariah, "Size-Resolved Density Measurements of Particulate Emissions from an Advanced Combustion Diesel Engine: Effect of Aggregate Morphology", *Energy and Fuels* **25**, pp. 1978-1988 (2011).

7. Teresa Barone, John Storey, Vitaly Prikhodko, Scott Curran, James Parks, Robert Wagner, "Particle Emissions Reduction by In-Cylinder Blending of Gasoline and Diesel Fuel", *21st CRC Real World Emission Workshop*, March 20–21, 2011, San Diego, CA (2011).

8. Kukwon Cho, Scott Curran, Vitaly Prikhodko, Scott Sluder, James Parks, and Robert Wagner, "Experimental Investigation of Fuel-Reactivity Controlled Compression Ignition (RCCI) Combustion Mode in a Multi-Cylinder, Light-Duty Diesel Engine", *7th U.S. National Combustion Meeting of the Combustion Institute*, March 21-23, 2011 (2011).

9. Scott J. Curran, Vitally L. Prikhodko, Robert M. Wagner, James E. Parks II, Kukwon Cho, C. Scott Sluder, Sage L. Kokjohn, Rolf D. Reitz, "In-Cylinder Fuel Blending of Gasoline/Diesel for Improved Efficiency and Lowest Possible Emissions on a Multi-Cylinder Light-Duty Diesel Engine", *SAE Technical Paper Series* 2010-01-2206 (2010).

10. Vitaly Y. Prikhodko, Scott J. Curran, Teresa L. Barone, Samuel A. Lewis, John M. Storey, Kukwon Cho, Robert M. Wagner, James E. Parks II, "Emission Characteristics of a Diesel Engine Operating with In-Cylinder Gasoline and Diesel Fuel Blending", *SAE Technical Paper Series* 2010-01-2266 (2010). [*selected for publication in SAE International scholarly journal*]

11. Alexander Sappok, Leslie Bromberg, James Parks II, Vitaly Prikhodko, "Loading and Regeneration Analysis of a Diesel Particulate Filter with a Radio Frequency-Based Sensor", *SAE Technical Paper Series* 2010-01-2126 (2010).

II.B.9 Cross-Cut Lean Exhaust Emission Reduction Simulation (CLEERS): Administrative Support

Stuart Daw
Oak Ridge National Laboratory (ORNL)
National Transportation Research Center
2360 Cherahala Boulevard
Knoxville, TN 37932-6472

DOE Technology Development Manager:
Ken Howden

Key ORNL personnel involved in this activity are Stuart Daw, Vitaly Prikhodko, and Charles Finney.

Objectives

Coordinate the CLEERS activity for the Diesel Cross-Cut Team to accomplish the following:

- Promote development of improved computational tools for simulating realistic full-system performance of lean-burn engines and associated emissions controls.
- Promote development of performance models for emissions control components such as exhaust manifolds, catalytic reactors, and sensors.
- Provide consistent framework for sharing information about emissions control technologies.
- Help identify emissions control research and development (R&D) needs and priorities.

Accomplishments

- Continued co-leading the CLEERS Planning Committee and facilitation of the CLEERS Focus telecoms with strong domestic and international participation.
- Continued to assist in refinement of the standard lean-NOx trap (LNT) and selective catalytic reactor (SCR) materials protocols.
- Conducted another survey of the Cross-Cut companies and collaborating suppliers to identify updated technical priorities for emissions controls and CLEERS activities.
- Continued to advise and adjust current DOE national lab projects associated with CLEERS to bring them into closer alignment with the updated CLEERS industry partner priority surveys.
- Provided regular update reports to DOE Advanced Combustion Engine Cross-Cut Team.
- Organized the 2011 CLEERS workshop at University of Michigan, Dearborn on April 19–21, 2011.
- Maintained the CLEERS website (www.cleers.org) including functionalities, security, and data to facilitate web meetings and serve focus group interactions.
- Increased utilization of models and kinetic parameters produced by CLEERS projects in full system simulations of alternative advanced powertrain options.

Future Directions

- Continue co-leading CLEERS planning committee.
- Continue co-leading the focus groups.
- Continue providing standard reference LNT, SCR, and oxidation catalysts, data, and kinetic modeling results for focus group evaluation.
- Organize and conduct the 2012 CLEERS workshop in the spring of 2012.
- Continue expanding basic data and model exchange between CLEERS and other Office of Vehicle Technologies projects.
- Continue maintenance and expansion of CLEERS website.
- Continue providing regular update reports to the DOE Advanced Combustion Engine Cross-Cut team.
- Implement recommendations of the CLEERS Planning Committee industry in response to the industry survey, subject to budget constraints and Cross-Cut Team approval.

Introduction

Improved catalytic emissions controls will be essential for utilizing high efficiency lean-burn engines without jeopardizing the attainment of much stricter U.S. Environmental Protection Agency emission standards that will take effect in 2012 and beyond. Simulation and modeling are recognized by the DOE Diesel Cross-Cut Team as essential capabilities needed to achieve this goal. In response to this need, the CLEERS activity was initiated to promote improved computational tools and data for simulating realistic full-system performance of lean-burn engines and the associated emissions control systems. Specific activities supported under CLEERS include:

- Public workshops on emissions control topics.
- Collaborative interactions among Cross-Cut Team members, emissions control suppliers, universities, and national labs under organized topical focus groups.
- Development of experimental data, analytical procedures, and computational tools for understanding performance and durability of catalytic materials.
- Establishment of consistent frameworks for sharing information about emissions control technologies.
- Recommendations to DOE and the DOE Cross-Cut Team regarding the most critical emissions control R&D needs and priorities.

ORNL is involved in two separate DOE-funded tasks supporting CLEERS:

- Overall administrative support; and
- Joint development of benchmark LNT kinetics with Sandia National Laboratories and Pacific Northwest National Laboratory.

Approach

In the administrative task, ORNL coordinates the CLEERS Planning Committee, the CLEERS focus groups, CLEERS public workshops, and the CLEERS website (http://www.cleers.org). The specific activities involved include:

- Coordination of the CLEERS Planning Committee and the LNT Focus Group.
- Organization of the annual CLEERS public workshops.
- Maintenance of the CLEERS website.
- Preparation and presentation of status reports to the Cross-Cut Team.
- Response to requests and inquiries about CLEERS from the public.
- Coordination of periodic Cross-Cut Team member surveys regarding R&D priorities for CLEERS.

Results

The updated CLEERS industry survey was completed in February. Detailed results from 24 responses have been summarized in a written report to the DOE Cross-Cut Team and posted on the CLEERS website [1]. Some highlights from the survey are:

- Specific priorities for aftertreatment technology vary widely over industry, creating special challenges, opportunities for cross-disciplinary interactions. The greatest concerns among the diesel community center on kinetics, sensing, and diagnostics for diesel particulate filters (DPFs) and kinetics and catalyst durability for urea-SCR. The gasoline sector is currently less concerned about particulate controls and more concerned about fundamental lean particulate characterization. The most pressing concern associated with LNT technology is reduction of precious metals in the catalyst (due to cost). Interest in oxidation catalyst aging and poisoning remains strong and has possibly increased. Interest is also strong among the diesel community regarding DPF interactions with LNT and SCR. Interest in hydrocarbon-based SCR continues to be very low.
- Regarding current CLEERS activities, there is broad support for the public workshop, coordination and facilitation of industry access to national labs, and distribution of fundamental, pre-competitive data. Monthly telecoms, standard catalyst characterization protocols, and sharing of commercially relevant catalyst data also ranked relatively high in priority. Overall results indicate CLEERS continues to be successful in meeting its original goals.
- There also appears to be growing interest in expanding the CLEERS role in certain areas. Specific areas of interest revealed by the survey include generation and distribution of open source aftertreatment component models, atomistic-scale catalyst modeling, and public distribution of large datasets of reference reactor and engine measurements and corresponding simulations. Interest is low in non-public/proprietary data and model sharing.

In addition to the detailed results, the survey report includes specific recommendations by the CLEERS Planning Committee. These include:

- Continued emphasis on R&D supporting the aftertreatment technology areas listed in the first bullet above.
- Continued support of the CLEERS public workshops, national laboratory R&D coordination, open sharing of pre-proprietary data, limited access technical telecoms, development of standard catalyst characterization protocols, and identification and sharing of reference catalysts.
- Establishment of a panel of experts from industry, national labs, and academia to consider ways in which CLEERS can help support development and distribution of pre-competitive aftertreatment models, experimental and aftertreatment modeling results, and opportunities for promoting utilization of atomistic-scale catalyst modeling.

CLEERS technical telecoms with presentations by various experts in emissions control experimentation, modeling, and simulation continued to be held

throughout the year. The presenters included Jason Lupescu (Ford), James McCarthy (Eaton), John Storey (ORNL), Chuck Folkerts (Argonne National Laboratory), Jim Parks (ORNL), Dick Blint (formerly from General Motors, now N2Kinetics), Alex Sappok (Massachusetts Institute of Technology), and Bill Schneider (University of Notre Dame). As has been the tradition for several years, these telecoms sometimes include unpublished or sensitive information and are restricted to Cross-Cut Team member institutions and their close collaborators. Typically, there are between 20 and 30 participants, several of whom may be from Europe and/or India.

The 2011 (14th) CLEERS workshop was held April 19-21, 2011 in the meeting facilities of the Institute of Advanced Vehicle Studies at the Dearborn campus of the University of Michigan (Figure 1). The program was structured around four invited speakers (In-Sik Nam [Pohang University], Bill Epling [University of Waterloo], Bernd Krutzsch [Daimler], and Dick Blint [N2Kinetics]) and an industry panel discussion on utilization of engine and vehicle emissions data for model parameterization and validation (Bernd Krutzsch [Daimler], Karthik Ramanathan [General Motors], Lars Henrichsen [Cummins], and Jeff Hepburn [Ford]). There were also 33 contributed talks on emissions control measurements, modeling, and simulation. An open discussion of the most recent CLEERS industry survey results was held at the no-host dinner on the second evening of the workshop. Details of the technical program and presentation downloads are available on the CLEERS website [2] under the 14th workshop heading.

FIGURE 1. The 2011 CLEERS Workshop included invited presentations by internationally recognized emissions control researchers from industry and academia, an industry panel discussion, and contributed talks on chemical kinetics measurements and computational modeling and simulation.

Under the CLEERS activity, ORNL has continued collaborating with Sandia National Laboratories on LNT modeling and the Pacific Northwest National Laboratory on SCR modeling. A journal article summarizing the most recent microkinetic LNT model has been submitted to Chemical Engineering Science. The SCR work has been focused on identifying and characterizing the kinetic and aging properties of conventional and chabazite copper-zeolite SCR catalysts, which have been recently utilized commercially by automotive and truck manufacturers. These catalysts have been recognized as a breakthrough for urea-SCR NOx control because of their good performance over a wide temperature range and low hydrocarbon sensitivity, but adequate information for modeling their dynamic performance under drive cycle conditions has not been available. Results from the experimental SCR catalyst measurements under the CLEERS kinetics activity are being incorporated into models suitable for vehicle systems simulations. Simulation studies of these and previous SCR models are being made available for public access via journal publications and public presentations [3].

This year the CLEERS team also began investigating passive adsorber devices to capture and subsequently release pollutants during engine start-up, when the main aftertreatment catalysts are too cool to function. The low activity of aftertreatment catalysts at cool temperatures is a growing area of concern, especially in regard to hybrid vehicles where engine operation can be very intermittent. Typically, passive adsorbers are inserted upstream of the main aftertreatment devices so that they can physically adsorb species such as hydrocarbons or NOx when the engine-out exhaust temperature is low. As the exhaust heats up, the adsorbed species are released by the adsorber device and then passed on to the main catalysts. The low cost and simplicity of passive adsorbers makes them very attractive for reducing emissions under transient low temperature conditions. Figure 2 illustrates example laboratory adsorption behavior for hydrocarbons on Ag-exchanged beta zeolite. Based on these and similar measurements in the literature, we have been able to implement simulations of the potential impact on hydrocarbon emissions for both conventional and hybrid passenger cars. Our preliminary results indicate that such devices could have a major impact on the integrated drive cycle emissions (e.g., >50% reduction).

Regular reports on all the above CLEERS activities were presented to the DOE Advanced Engine Cross-Cut Team at their bimonthly meetings at USCAR headquarters [4].

Conclusions

CLEERS continues to provide a unique mechanism for non-proprietary communication among emissions

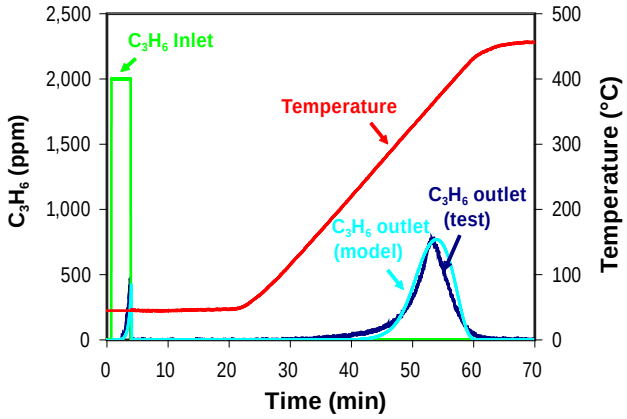

FIGURE 2. Experimental and predicted breakthrough profiles for propylene (C_3H_6) in an Ar carrier passing through a Ag-exchanged beta-zeolite adsorber. At low temperature, the propylene is completely captured. As temperature increases to about 300°C, the adsorbed propylene is released. Computer simulations indicate that passive adsorbers of this type could significantly reduce cold-start engine emissions of hydrocarbons.

control researchers from industry, national labs, universities, and emissions controls suppliers. This informal interaction helps keep industry abreast of the latest developments coming from fundamental research at the national labs and universities. CLEERS also helps keep national labs and universities more attuned to the leading technical challenges faced by industry in transforming the best available transportation technology into commercial reality. CLEERS continues to have heavy participation from industry, labs, and universities in the public workshops and the technical focus meetings and is providing explicit feedback and guidance to DOE and the DOE Diesel Cross-Cut Team in optimizing use of their shared R&D resources.

References

1. "2011 CLEERS Industry Priorities Survey Final Report: Analysis, Summary, and Recommendations," C.S. Daw, October, 2011.

2. 2011 (14th) CLEERS Workshop agenda and presentations at http://www.cleers.org.

3. Z. Gao, C.S. Daw, J.A. Pihl, and M. Devarakonda, "Evaluation of 2010 urea-SCR technology for hybrid vehicles using PSAT system simulations," 2011 DOE-DEER Conference, October 3–6, 2011.

4. "CLEERS Updates to the DOE Advanced Engine Crosscut Team," C.S. Daw, W. Li, and R. Blint, Nov. 4, 2010; Jan. 13, 2011; March 17, 2011; May 19, 2011; July 21, 2011; Sept. 8, 2011 (limited distribution).

FY 2011 Publications/Presentations

1. 2011 (14th) CLEERS Workshop agenda and presentations at http://www.cleers.org.

2. "CLEERS Coordination & Joint Development of Benchmark Kinetics for LNT & SCR," J.-S. Choi et al, 2011 DOE Hydrogen Program and Vehicle Technologies Annual Merit Review, Washington, D.C., May 9–13, 2011.

3. Z. Gao, C.S. Daw, J.A. Pihl, and M. Devarakonda, "Evaluation of 2010 urea-SCR technology for hybrid vehicles using PSAT system simulations," 2011 DOE-DEER Conference, October 3–6, 2011.

4. "CLEERS Updates to the DOE Advanced Engine Crosscut Team," C.S. Daw, W. Li, and R. Blint, Nov. 4, 2010; Jan. 13, 2011; March 17, 2011; May 19, 2011; July 21, 2011; Sept. 8, 2011 (limited distribution).

5. "2011 CLEERS Industry Priorities Survey Final Report: Analysis, Summary, and Recommendations," C.S. Daw, October, 2011.

6. "Microkinetic Modeling of Lean NOx Trap Storage and Regeneration," R.S. Larson, V.K. Chakravarthy; J.A. Pihl; C.S. Daw, submitted to Chemical Engineering Science.

II.B.10 Cross-Cut Lean Exhaust Emissions Reduction Simulations (CLEERS): Joint Development of Benchmark Kinetics

Stuart Daw (Primary Contact), Jae-Soon Choi, Josh Pihl, Bill Partridge, Kalyana Chakravarthy, Mi-Young Kim
Oak Ridge National Laboratory (ORNL)
2360 Cherahala Boulevard
Knoxville, TN 37932-1563

DOE Technology Development Manager:
Ken Howden

Objectives

Coordinate ORNL's collaboration with Pacific Northwest National Laboratory (PNNL) and Sandia National Laboratories (SNL) in the development of kinetics information needed for aftertreatment component simulation through the following:

- Provide benchmark laboratory measurements of oxides of nitrogen (NOx) reduction chemistry and reaction rates in lean-NOx traps (LNTs) and selective catalytic reduction (SCR) catalysts under realistic operating conditions.
- Correlate laboratory measurements of LNT and SCR catalysts with test-stand/vehicle studies.
- Develop and validate global chemistry and "low-order" models for LNT and SCR kinetics.

Fiscal Year (FY) 2011 Objectives

- Investigate impacts of reductant composition and spatial reaction distributions on LNT regeneration efficiency and product selectivity.
- Identify chemical reaction pathways that generate N_2O during LNT regeneration.
- Exercise CLEERS Transient SCR Protocol to generate benchmark model calibration data on a commercial copper zeolite SCR catalyst.
- Quantify impacts of hydrothermal aging on the catalytic properties of a commercial copper zeolite SCR catalyst.
- Provide mechanistic insights and experimental data sets for model development and calibration to modeling collaborators.

Accomplishments

- Continued systematic experimental measurements of LNT regeneration chemistry with an emphasis on resolving the effects of different reductants and the spatiotemporal distribution of key reactions.
- Combined experimental lab reactor measurements and modeling results to confirm that reduction of nitrates by intermediate NH_3 is a major source of N_2O in LNTs.
- Continued collaboration with SNL, the Institute of Chemical Technology, Prague, and Chalmers University of Technology in LNT modeling and with PNNL in SCR modeling.
- Revised the CLEERS laboratory transient SCR catalyst characterization protocol in collaboration with PNNL to improve its relevance to extraction of key kinetic parameters.
- Evaluated the impact of hydrothermal aging on a commercial copper zeolite SCR catalyst and identified two distinct types of NH_3 storage sites.

Future Directions

- Use the CLEERS LNT laboratory protocol to characterize commercial LNT catalyst samples from the BMW 120i spark ignition direct injection vehicle that has been extensively studied in chassis dynamometer experiments at ORNL.
- Develop and publish a set of kinetic and aging parameters for the commercial chabazite Cu-zeolite SCR catalyst under joint investigation by ORNL and PNNL.
- Continue identification of key surface species and associated catalyst sites in SCR zeolite catalysts through diffuse reflectance infrared Fourier-transform spectroscopy measurements.
- Utilize above results to improve models for simulating LNT and SCR NOx reduction performance under both laboratory and vehicle drive cycle conditions.

Introduction

Improved catalytic emissions controls will be essential for utilizing high-efficiency lean-burn engines without jeopardizing the attainment of increasingly strict emission standards. Simulation and modeling are recognized by the DOE Diesel Cross-Cut Team as essential capabilities needed to achieve this goal. In response to this need, the CLEERS activity was initiated to promote improved computational tools and data for

simulating realistic full-system performance of lean-burn engines and the associated emissions control systems [1].

ORNL is involved in two separate DOE-funded tasks supporting CLEERS:

- Overall administrative support; and
- Joint development of benchmark LNT kinetics with SNL and PNNL.

Approach

In the benchmark kinetics task (covered by this report), ORNL is collaborating with SNL and PNNL to produce kinetic information for LNT and urea-SCR aftertreatment devices, both as individual and system integrated components. The results of this work are discussed with the LNT, diesel particulate filter (DPF), and SCR Focus groups prior to publication to provide technical review and guidance to the labs. Specific activities involved include:

- Regular direct interactions among ORNL, PNNL, and SNL.
- Experimental measurements of LNT and SCR chemistry and reaction rates using laboratory reactors and prototype devices installed on engine test stands and vehicles.
- Analysis and reconciliation of experimental data from different sources with predictions from computer simulations.
- Publications in journals and presentations in public meetings and on the CLEERS Web site.

Results

ORNL assisted SNL in further updating a microkinetic chemical reaction mechanism for NOx storage and regeneration in LNT catalysts. Details of the mechanism are provided in the SNL annual report, but briefly, the proposed mechanism includes explicit elementary reaction rates for precious metal, barium oxide (NOx storage), and cerium oxide sites of the catalyst. The mechanism has been used in conjunction with a transient plug flow reactor code (including boundary layer mass transfer) to replicate observed trends in both long-time-scale storage/regeneration cycles with a CO/H_2 reductant and also steady-flow temperature sweep experiments at ORNL. Kinetic parameters for the entire mechanism have been inferred by finding the best overall fit to the complete set of ORNL experiments while enforcing rigorous thermodynamic consistency for all reaction pathways.

We continued bench reactor studies of the LNT regeneration chemistry to identify key chemical processes controlling NH_3 and N_2O selectivities under relevant conditions. First, the CLEERS reference LNT catalyst (Umicore GDI) was evaluated with various reductants (H_2, CO, C_3H_6, C_3H_8, and mixtures thereof) over a wide temperature window (150-550°C) to probe NH_3 and N_2O production during fast lean/rich cycling. We observed that significant NH_3 and N_2O can be emitted and that the peak in NH_3 and N_2O production for all of the reductants corresponds to the NOx conversion near "light-off" temperatures (see Figure 1).

To better understand the observed trends with respect to NH_3 and N_2O yields and the relationship between NH_3 and N_2O, we performed a series of transient response experiments at different temperatures on a bench flow reactor. Results indicated that various modes of NH_3 interaction with LNT surfaces – NH_3 adsorption, desorption, decomposition, oxidation – can affect global NOx conversion and yields of NH_3 and N_2O. In particular, we determined that the reduction of surface nitrates by NH_3 can lead to significant N_2O formation (see Figure 2), while the reduction of oxygen storage capacity by NH_3 generates negligible N_2O. These experimental findings were used to extend the global LNT model at the Institute of Chemical Technology in Prague (in collaboration with Dr. Petr Kočí). A good agreement between model predictions and experimental

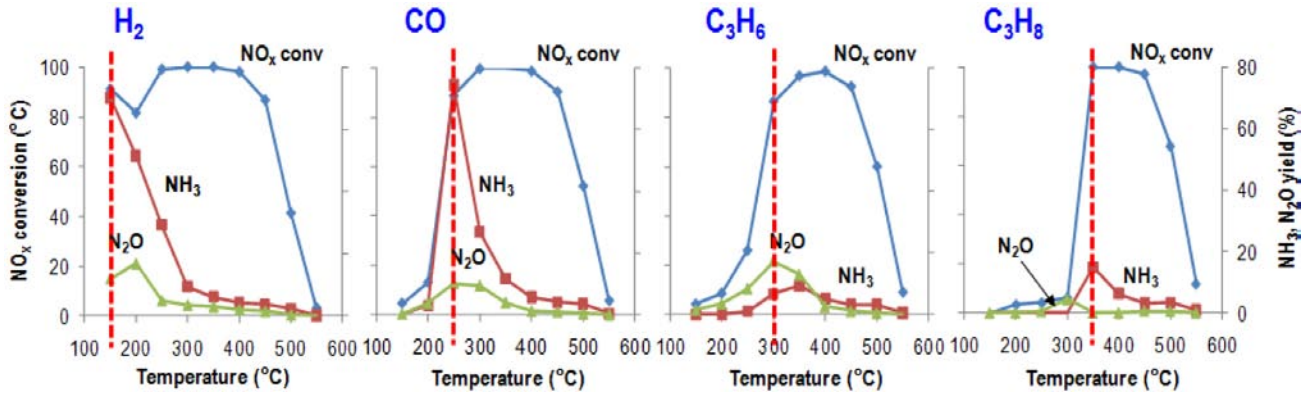

FIGURE 1. Fast cycle experiment results show cycle-average NOx conversion and N_2O and NH_3 yields as a function of temperature and reductant species.

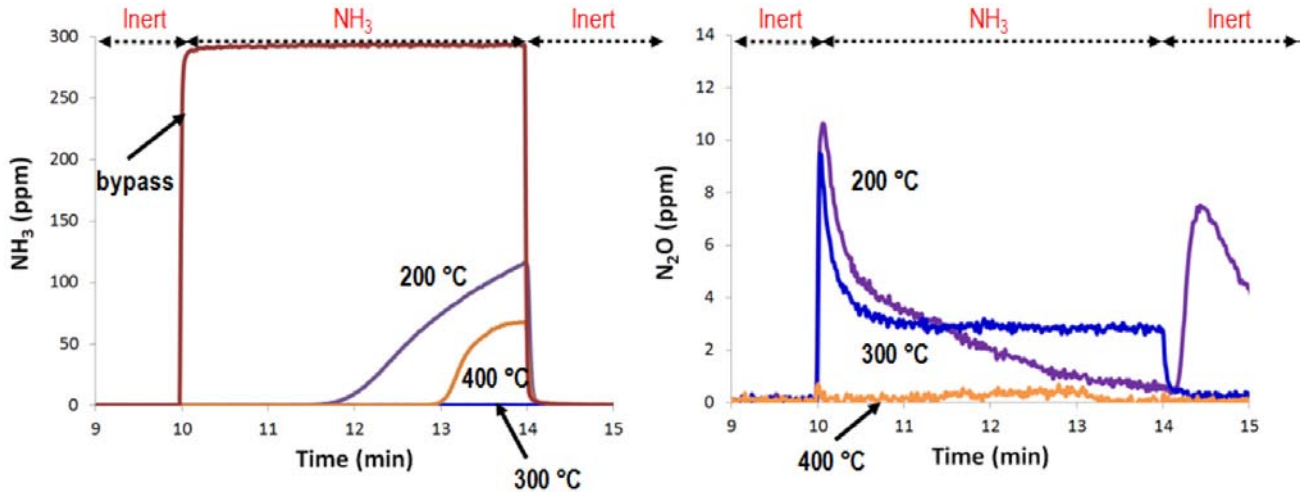

FIGURE 2. Transient response experiments (300 ppm NH_3 pulse input to a pre-nitrated LNT surface) reveal the NH_3 reduction of surface nitrates as a pathway to N_2O.

results was achieved, confirming that NH_3 reduction of nitrates is a major source of N_2O (see Figure 3). In addition, experiment-model comparisons helped to further explain how variations in the axial stored NOx distribution contribute to the temporal separation of different species at the reactor exit.

Our SCR work for FY 2011, conducted in close collaboration with PNNL, focused on understanding how hydrothermal aging impacts the performance, catalytic properties, and modeling parameters for a commercial copper chabazite NH_3 SCR catalyst. We hydrothermally aged core samples cut from a full-size brick in a laboratory furnace at three different conditions recommended by PNNL: 700°C for 4 hr, 800°C for 6 hr, and 800°C for 16 hr. We then used the CLEERS transient SCR protocol to experimentally evaluate the impact of hydrothermal aging on catalyst properties and performance in a flow reactor. The reactor data was transferred to PNNL for use in recalibrating their SCR model. The recalibration process will provide insights into which model parameters must be adjusted to account for performance degradation over the life of the catalyst.

Looking at steady state NOx conversion (Figure 4), we found that the hydrothermal aging conditions we used had very little impact on the low temperature catalyst performance. For NO SCR there was a small drop in NOx conversion with successive aging; for NO+NO_2 SCR there appeared to be no impact at all. Interestingly, hydrothermal aging had a larger effect on high temperature performance: NOx conversion decreased with aging for both NO and NO+NO_2 SCR conditions. The SCR NH_3 conversion remained high (close to 100% at high temperatures) with aging, so the drop in SCR performance appears to be due to a decrease in the rate of SCR reaction relative to NH_3 oxidation.

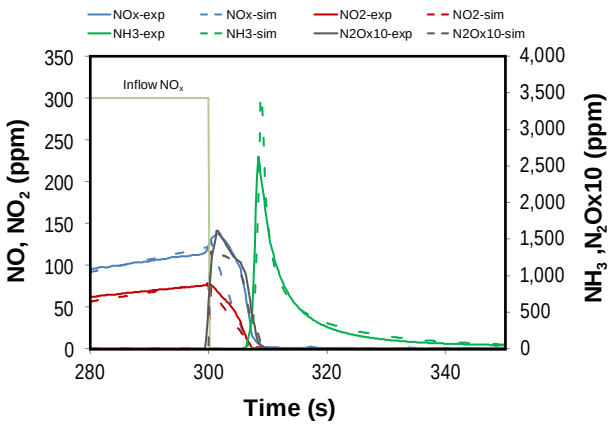

FIGURE 3. Outlet concentration profiles of N_2O, NH_3, NO, and NOx during 300/300-s lean/rich cycling at T=300°C (H_2 reductant); comparison between experiments and simulation.

Hydrothermal aging had a much more noticeable impact on NH_3 storage capacity, and particularly on the stability of the stored NH_3. Figure 5 summarizes the results from the NH_3 adsorption/isothermal desorption/temperature programmed desorption portions of the CLEERS transient SCR protocol. Increased aging resulted in a small reduction in total NH_3 uptake at 150°C, while the amount of loosely bound NH_3 that was isothermally desorbed did not change at all. However, the temperature programmed desorptions reveal significant changes with hydrothermal aging. The fresh sample showed two distinct high temperature desorption features, implying the presence of two different storage sites. Aging decreased the high temperature desorption feature and increased the low temperature feature, consistent with a conversion of more stable NH_3 storage sites into less stable ones. The loss of stable high

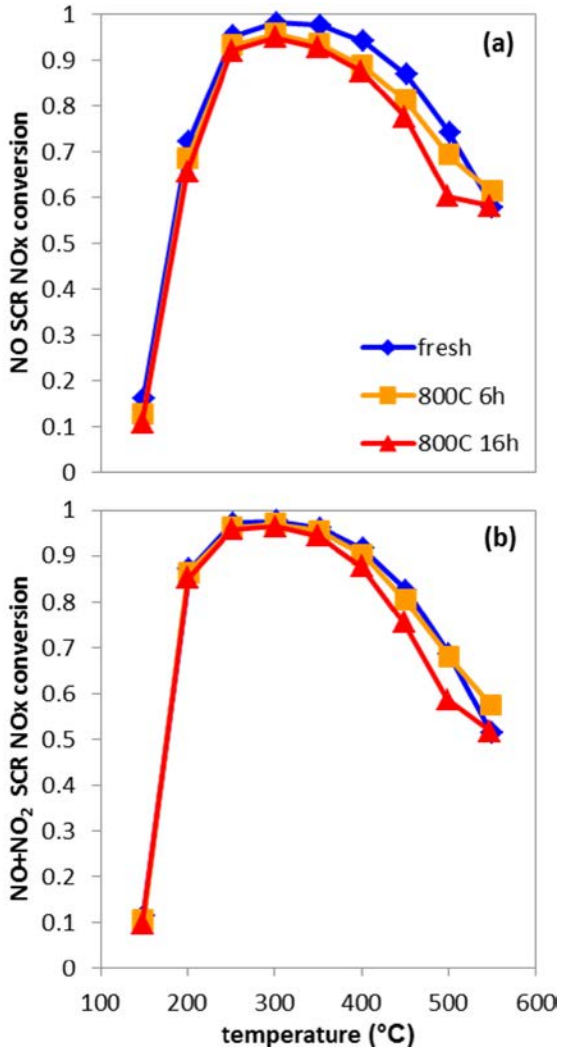

FIGURE 4. Steady-state NOx conversion as a function of temperature for (a) NO SCR and (b) equimolar NO + NO_2 ("fast") SCR over three core samples (5 cm long by 2 cm diameter) cut from a commercial copper chabazite NH_3 SCR catalyst and hydrothermally aged to varying degrees. Experiment conditions: 350 ppm NOx, 350 ppm NH_3, 10% O_2, 5% H_2O, 5% CO_2, balance N_2, gas hourly space velocity = 60,000 hr^{-1}.

temperature NH_3 storage sites may provide an indirect explanation for loss of high temperature NOx conversion with hydrothermal aging. We will pursue more detailed investigations into the nature of the NH_3 storage and other catalyst active sites and how they change with aging in the coming year.

Conclusions

Ongoing collaborations among ORNL, PNNL, and SNL continue to reveal new insights into the fundamental mechanisms controlling the performance of both LNT and urea-SCR catalysts for lean NOx control. The resulting kinetic parameters and device simulation models are providing critical information for guiding vehicle and system simulations studies as well as development of more fuel efficient, lower cost emissions control options for advanced combustion engines. Continuing input via the CLEERS Focus Groups, public workshop, industry surveys, and Cross-Cut Team updates is helping to ensure practical commercial relevance of the results.

References

1. "2011 CLEERS Industry Priorities Survey Final Report: Analysis, Summary, and Recommendations," C.S. Daw, October, 2011, http://www.cleers.org.

FY 2011 Publications/Presentations

1. J.-S. Choi, W.P. Partridge, J.A. Pihl, M.-Y. Kim, P. Kočí, C.S. Daw, "Spatiotemporal distribution of NOx storage and impact on NH_3 and N_2O selectivities during lean/rich cycling of a Ba-based lean NOx trap catalyst", submitted to Catalysis Today.

2. "Microkinetic Modeling of Lean NOx Trap Storage and Regeneration," R.S. Larson, V.K. Chakravarthy, J.A. Pihl, C.S. Daw, submitted to Chemical Engineering Science.

3. P. Kočí, Š. Bártová, M. Marek, J.A. Pihl, J.-S. Choi, W.P. Partridge, "Modeling of N_2O formation during the regeneration of NOx storage catalyst", oral presentation, 2nd International Symposium on Modeling of Exhaust-Gas After-Treatment (MODEGAT), Bad Herrenalb, Germany, September 19–20, 2011.

4. J.-S. Choi, J.A. Pihl, P. Kočí, W.P. Partridge, M.-Y. Kim, C.S. Daw, "Axial redistribution of NOx storage and impact on LNT performance under fast cycling conditions", oral presentation, 10th European Congress on Catalysis (EuropaCat), Glasgow, Scotland, August 28 – September 2, 2011.

5. P. Kočí, M. Marek, J.A. Pihl, J.-S. Choi, W.P. Partridge, "Modeling of N_2O formation during the regeneration of lean NOx trap", oral presentation, 10th European Congress on Catalysis (EuropaCat), Glasgow, Scotland, August 28 – September 2, 2011.

6. J.-S. Choi, "Lean NOx trap regeneration chemistry studies", invited seminar, GM Global R&D Center, Warren, MI, August 17, 2011.

7. J.-S. Choi, J.A. Pihl, W.P. Partridge, M.-Y. Kim, C.S. Daw, "Axial redistribution of NOx storage and impact on LNT performance under fast cycling conditions", oral presentation at the 22nd North American Catalysis Society Meeting (NAM), Detroit, MI, June 5–10, 2011.

8. P. Kočí, M. Marek, J.A. Pihl, J.-S. Choi, W.P. Partridge, "Modeling of N_2O formation during the regeneration of lean NOx trap", oral presentation at the 22nd North American Catalysis Society Meeting (NAM), Detroit, MI, June 5–10, 2011.

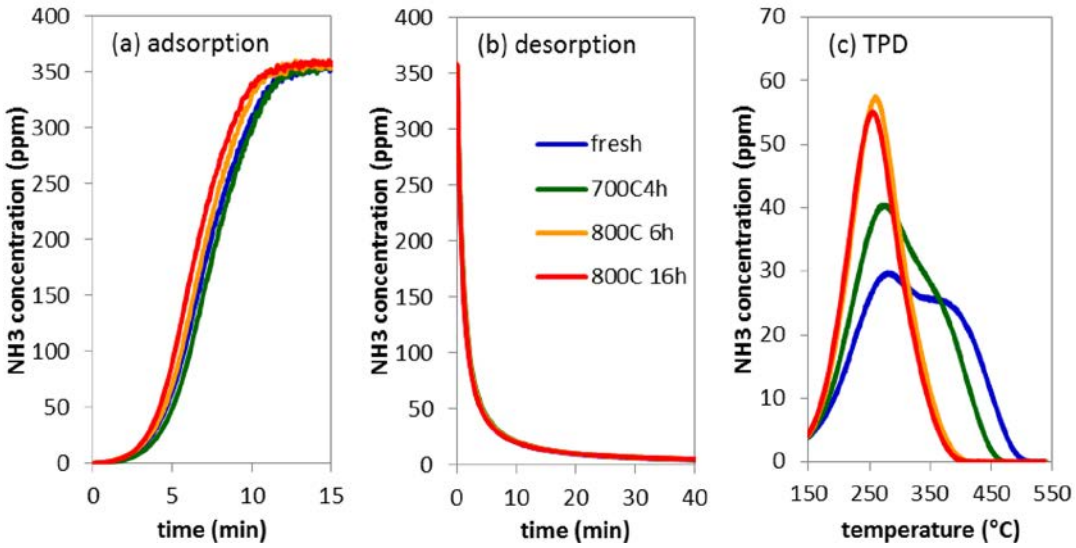

FIGURE 5. (a) Adsorption of 350 ppm NH_3 at 150°C; (b) isothermal desorption at 150°C after removal of NH_3 from feed gas; and (c) temperature programmed desorption from 150 to 550°C at 5°C/min conducted on four commercial Cu zeolite SCR samples aged to varying extents. Experiment conditions: 5% H_2O, 5% CO_2, N_2, gas hourly space velocity = 60,000 hr^{-1}.

9. S. Shwan, W.P. Partridge, J.-S. Choi, L. Olsson, "Kinetic modeling of NOx storage and reduction using spatially resolved MS measurements", oral presentation at the 22nd North American Catalysis Society Meeting (NAM), Detroit, MI, June 5–10, 2011.

10. N.A. Ottinger, T.J. Toops, J.A. Pihl, J.-S. Choi, W.P. Partridge, "Impact of the support material on the stability of nitrates and sulfates in NOx storage-reduction catalysts", poster at the 22nd North American Catalysis Society Meeting (NAM), Detroit, MI, June 5–10, 2011.

11. J.-S. Choi, C.S. Daw, J.A. Pihl, W.P. Partridge, M.-Y. Kim, V.K. Chakravarthy, V. Prikhodko, C.E.A. Finney, T.J. Toops, M.J. Lance, "CLEERS coordination and joint development of benchmark kinetics for LNT & SCR", presentation at the DOE Vehicle Technologies Program Annual Merit Review, Washington, DC, May 9–13, 2011.

12. M. Devarakonda, J.H. Lee, J.A. Pihl, C.S. Daw, "Development of Cu SCR model using CLEERS transient SCR reactor protocol", oral presentation at the 14th DOE Crosscut Workshop on Lean Emissions Reduction Simulation, Dearborn, MI, April 19–21, 2011.

13. J.-S. Choi, J.A. Pihl, M.-Y. Kim, W.P. Partridge, C.S. Daw, P. Kočí, "Correlation between LNT NH_3 and N_2O selectivities under fast cycling conditions", oral presentation at the 14th DOE Crosscut Workshop on Lean Emissions Reduction Simulation, Dearborn, MI, April 19–21, 2011.

14. P. Kočí, M. Marek, W.P. Partridge, J.A. Pihl, J.-S. Choi, "N_2O formation during regeneration of lean NOx traps", oral presentation at the 14th DOE Crosscut Workshop on Lean Emissions Reduction Simulation, Dearborn, MI, April 19–21, 2011.

Special Recognitions & Awards/Patents Issued

1. J.-S. Choi, "Lean NOx trap regeneration chemistry studies", invited seminar, GM Global R&D Center, Warren, MI, August 17, 2011.

II.B.11 Development of Advanced Diesel Particulate Filtration Systems

Kyeong Lee
Argonne National Laboratory
9700 S. Cass Ave.
Argonne, IL 60564

DOE Technology Development Manager:
Ken Howden

Overall Objectives

- Characterize pressure drops in particulate filter to improve fuel efficiency.
- Develop technologies to reduce pressure drops across the diesel particulate filter (DPF) membrane.
- Measure the thermo-physico-chemical properties of diesel particulate matter (PM) emissions for future numerical calculations.

Fiscal Year (FY) 2011 Objectives

- Analyze filter microstructures to find technologies for improving pressure drop.
- Perform soot oxidation experiments to acquire database used for evaluating heat release from DPF regeneration.
- Characterize soot morphology from various different combustion types for developing future DPF systems.

Accomplishments

- Measured pore size distributions and pressure drops for three different DPF membranes with different amount of catalytic coating.
- Evaluated kinetic parameters governing the oxidation of surrogate soot.
- Defined the effects of ambient experimental conditions and analytical methodology on kinetic parameters.
- Characterized the morphology of soot particles from low-temperature combustion (LTC) with biofuels.

Future Directions

- Evaluate PM filtration efficiency at different engine conditions.
- Conduct regeneration experiments to evaluate regeneration efficiency and obtain optical images.
- Perform thermogravimetric experiments of surrogate soot with various flue gases (NOx, CO, CO_2, and O_2) to evaluate kinetic parameters.

Introduction

With growing concern about energy saving in the diesel engine system, the optimal design of aftertreatment systems has been discussed with priority, in addition to its practical benefit for the conservation of a clean environment. As a result, lowering the pressure drop across the DPF and managing the excess thermal energy released in its regeneration have been primary tasks in improving DPF performance. This year, therefore, this research project was focused on revealing detailed microstructures of DPF filters and evaluating the pressure drop characteristics with different filter material properties. In addition, the research team accurately evaluated the kinetic parameters of soot governing its thermal oxidation, while the effects of ambient conditions were also found. This effort aims at, first, acquiring the database of kinetic parameters for various oxidation conditions, and ultimately providing the efficient thermal management scheme for DPF regeneration.

Approach

Analysis for Microstructures of DPFs

The research team preformed the detailed examinations of pore structures using an optical microscopy system that could visualize micro-pore structures in detail at appropriate resolutions. Examinations of pressure drops were followed at no soot-loading conditions, with different levels of catalyst coating on the filter materials.

Analysis of Kinetic Parameters with Different Ambient Conditions and Analytical Methodologies

Ambient experimental conditions and analytical methodologies for kinetic parameters are often chosen in soot oxidation inadvertently. In this work, therefore, the principle investigator examined the effects of inert gas and heating rate on soot oxidation and also compared three different analytic methodologies to finally propose an optimal analytic methodology suitable for evaluating accurate kinetic parameters.

Soot Morphology in LTC

Morphological properties were analyzed for soot particles from a LTC engine with different fuels, including ultra-low sulfur diesel (ULSD), soy bean 20% blend, and palm oil 20% blend, in terms of particle sizes and fractal dimension. For the analyses, a novel thermophoretic soot sampling system and a transmission electron microscope (TEM) were used.

Results

Microscopic images were displayed for three different cordierite DPF filters in Figures 1(a)-(c), coated with different amount of catalyst: (a) non-catalyzed filter, (b) lightly catalyzed filter, and (c) heavily catalyzed filter. The green background inset displays micro-pores at a local area of the filter (b) at a higher magnification. The filter surface color changes with the amount of catalyst coated, as shown in the figures. The pore diameter (D_p) was defined as a maximum diameter of a sphere that can pass through the pore on the surface.

Figures 2(a)-(c) show pore size distributions for (a) non-catalyzed filter, (b) lightly catalyzed filter, and (c) heavily catalyzed filter, respectively. A total of 100 pores were analyzed for each filter. As shown in the figures, a majority of pores are distributed in a diameter range of 20 to 40 microns, while the largest population is shifted to larger pore diameters with catalyst coating. The size distribution becomes more even with catalyst coating. Indeed, the number of smaller pores was reduced with catalyst coating, while the number of medium/large pores relatively increased. This result is caused mainly by the coating process, in which small micro-pores are readily blocked by initially liquid-phased catalyst materials. The average pore diameters were measured to be 28.4 μm, 34.2 μm, and 41.9 μm, respectively. A more population of larger pores involved in the measurement resulted in a larger average pore size for the #3 case.

Pressure drops were measured for the three DPF filters as a function of air flow rate, as shown in Figure 3. The pressure drop linearly increased with increasing air flow, regardless of catalyst coating. And the magnitude of pressure drop significantly increased with catalyst coating through the entire flow rate range, indicating a nearly two-fold increase with heavy catalyst coating (#3), compared to the bare filter. Reduction in the void space of pores per unit filter volume, i.e., porosity, seems to be mainly responsible for the increase in pressure drop with the #3 filter, although the average diameter (from the same number of pore samples) appeared to be largest with the #3 filter.

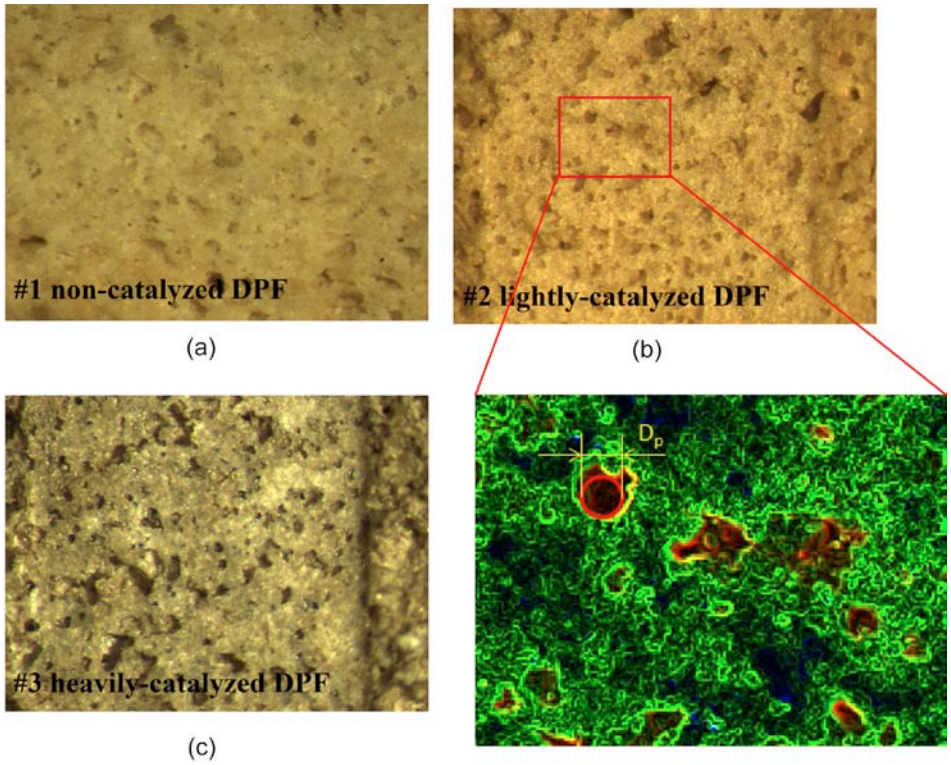

FIGURE 1. Microscopic images for three different cordierite filters coasted with different amount of catalysts: (a) non-catalyzed, (b) lightly catalyzed, and (c) heavily catalyzed.

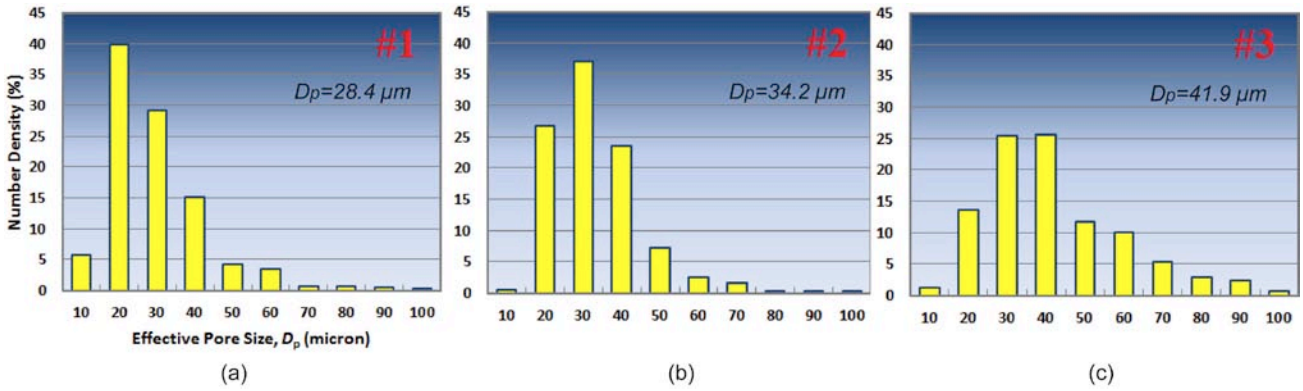

FIGURE 2. Pore size distributions of (a) non-catalyzed, (b) lightly catalyzed, (c) heavily catalyzed filter.

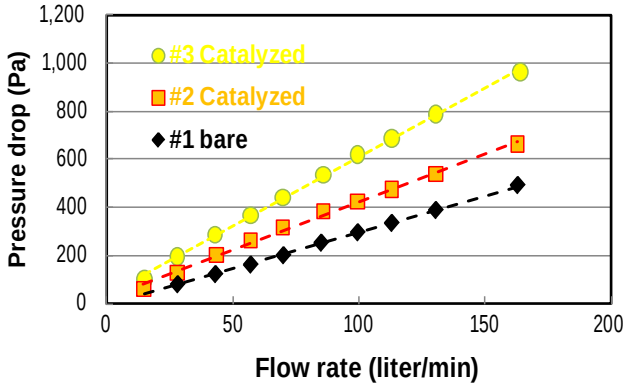

FIGURE 3. Pressure drops measured for three different cordierite filters as a function of air flow rate.

It has been overlooked particularly in engineering communities that the magnitude of kinetic parameters depends on inert gas, heating rate, and analytic methodology of thermogravimetric data. In this work, therefore, kinetic parameters were first evaluated for three different inert gases, N_2, Ar, and He. In addition, kinetic parameters were also evaluated by using three different analytic methodologies – isothermal method, non-isothermal integral method, and non-isothermal iso-conversional method. Also proposed was Argonne's analytic method, called the differential method, which offered a representative value of activation energy independent of inert gases. The theory of each methodology is described only with the final result below, due to the text limitation of this report.

Isothermal Kinetics

Rate of reaction:

$$d\alpha/dt = A \exp(-E_a/RT)\cdot f(\alpha),\ f(\alpha) = (1 - \alpha)^n$$

where α is the degree of soot conversion in mass.

Non-Isothermal Methods

Integral method

$$\log\frac{g(\alpha)}{T^2} = \log\left[\frac{AR}{\beta E_a}\left(1-\frac{2RT}{E_a}\right)\right] - \frac{E_a}{2.3RT}$$

where $\beta = (dT/dt)$ is the heating rate, $g(\alpha) = (AE_a/R\beta)\cdot p(x)$, and $p(x) = e^{-x}\frac{x-2}{x^3}$.

Iso-Conversional Method

$$g(\alpha) = (AE_a/R\beta)\cdot p(x),$$
$$p(x) = \exp(-x)/x'(x^2+10x+18)/(x^3+12x^2+36x+24)$$

where $x = E_a/RT$.

Differential Method (Proposed)

$$log(d\alpha/dt) - n\ log(1 - \alpha) = -E_a/RT + log\ A$$

Using thermogravimetric analysis data for mass and temperature under non-isothermal conditions, one can evaluate the kinetic parameters from the plots displaying data for the left-hand terms versus 1/T with variations of *n* value hypothesized.

Due to space limitation, the results are briefly described in text only. The activation energies evaluated with nitrogen, argon, and helium gases were all different from each other, when those first three analytic methodologies were used. Activation energy varied with the heating rate to a certain degree, regardless of the inert gas. Finally the differential method proposed by our working team revealed a single value of activation energy (155 kJ/mole) at the lowest heating rate employed in this work, 1°C/min, independent of the inert gases. In summary, Table 1 lists the activation energies evaluated for those three inert gases by the four different analytic methods.

Engine-out particulate emissions from an LTC engine were collected at a 2,000 rpm and 5.5 bar indicated mean effective pressure condition, by means of a novel thermophoretic sampling system, and examined

TABLE 1. Activation energies evaluated for three different inert gases by means of four different analytic methods.

Inert gas Methodology		N_2 (kJ/mole)	Ar (kJ/mole)	He (kJ/mole)
Isothermal		164.5	163.9	149.5
Non-isothermal	Integral	138 – 155	← (Approx. same)	138 – 148
	Iso-coversional	145.7	152.8	127
	Differential	155 – 170 (Avg. ≅ 160)	← (Approx. same)	120 – 155

by using a TEM in terms of sizes and fractal geometry. Figures 4(a)-(c) show the TEM images of representative aggregate particles collected from the combustion of three different fuels: soy bean 20% blend, palm oil 20% blend, and ULSD. In visual observation, biofuels produced more small particles than did ULSD. These LTC-derived particles looked more spherical in shape and amorphous in nano-structures than did those from conventional diesel combustion.

Figures 5(a) and (b) display the number distributions of primary particle diameter (D_p) and radius of gyration of aggregate particles (R_g) for all the three fuels, respectively. The number 22 in the inset stands for the fuel injection angle, 22° before top-dead center. Table 2 summarizes average primary particle diameters, radii of gyration, and fractal dimensions for the three biofuels. It appears that the primary particle size (D_p) of palm oil blend turned out to be smallest, while the aggregate size (R_g) was smallest for the soy bean blend. The

TABLE 2. Average primary particle diameters, radii of gyration, and fractal dimensions for three different biofuels.

Dimensions	Soy bean B20	Palm oil B20	ULSD
Avg. Dp (nm)	23.2	22.2	23.0
Avg. Rg (nm)	22.9	27.4	27.5
Df	1.73	1.54	1.57

fractal dimension appeared to be largest with the soy bean blend (D_f=1.73) among the three fuels. This large magnitude of fractal dimension with the soy bean blend is verified as the fractal geometry is compared each other in Figure 4, where the soy bean derived particles appear to be more spherical than others.

Conclusions

- The regeneration system has been completed to fabricate by adding the electric heating system.
- Catalytic coating on DPF membranes changed pore structures and increased back pressure up to a factor of two.
- Activation energy turned out to be sensitive to the inert gas and heating rate.
- The proposed differential method accurately evaluated an activation energy (155 kJ/mole), which is independent of the inert gas.
- The modified DPF membrane significantly reduced back pressure for the majority of filtration period.
- The use of biofuels for LTC significantly changed particulate morphology, in terms of nano-structures, size (particularly by soy bean fuel), and fractal geometry, compared to those from the conventional diesel combustion.

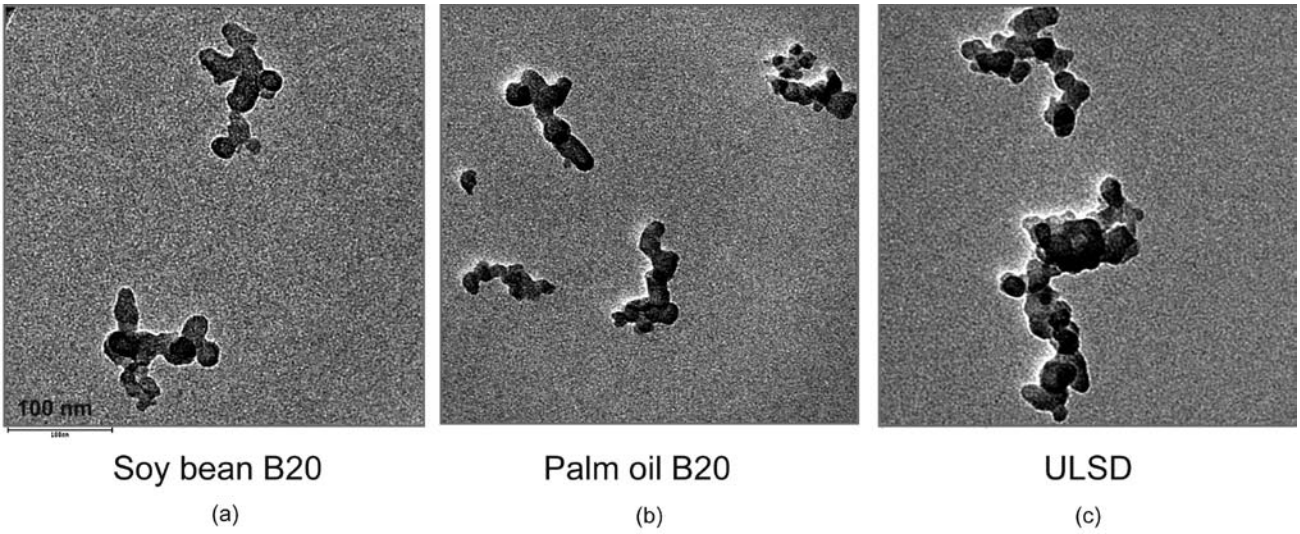

FIGURE 4. TEM images of representative aggregate particles from combustion of (a) soy bean 20% blend, (b) palm oil 20% blend, (c) ULSD.

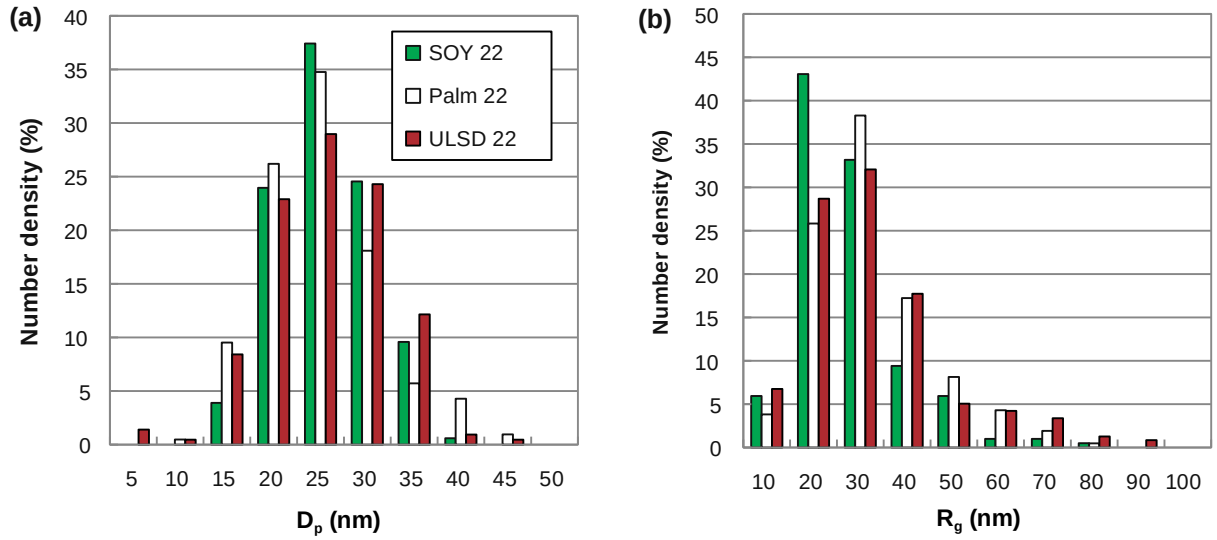

FIGURE 5. Number distributions of primary particle diameter (D_p) and radius of gyration (R_g) of aggregate particles.

FY 2011 Publications/Presentations

1. "Detailed Morphological Investigation of Diesel Nano-Particles for Their Efficient Control," 14th ETH Conference, Zurich, Switzerland, Aug. 1-4, 2010.

2. "Characterization of Oxidation Behaviors and Chemical-Kinetics Parameters of Diesel Particulates Relevant to DPF Regeneration," SAE 2010-01-2166, SAE Powertrain, Fuels and Lubricants Meeting, San Diego CA, Oct. 2010.

3. "Measurements of Heat Release of Diesel PM for Advanced Thermal Management Strategies for DPF Regeneration," Journal of Combustion Science and Technology, 183:1-4, 2011.

II.B.12 Combination and Integration of DPF-SCR After-Treatment

Kenneth G. Rappé (Primary Contact),
Jong H. Lee, Mark L. Stewart,
Maruthi N. Devarakonda, Gary D. Maupin
Pacific Northwest National Laboratory (PNNL)
Post Office Box 999
Richland, WA 99354

DOE Technology Development Manager:
Ken Howden

Overall Objectives

- Develop a fundamental understanding of the integration of selective catalytic reactor (SCR) and diesel particular filter (DPF) technologies for on-road heavy-duty diesel applications.
- Probe DPF-SCR interactions with a view to proper function and greater integration.
- Determine system limitations and define basic design requirements for efficient on-board packaging and integration with the engine to minimize impact on vehicle efficiency.

Fiscal Year (FY) 2011 Objectives

- Determine limitations and optimization strategies for the physical integration of SCR catalyst on ultra-high porosity cordierite DPFs, with the drivers being oxides of nitrogen (NO_X) reduction efficiency and pressure drop.
- Evaluate and optimize the effect of the presence of the SCR reduction reactions on the passive soot oxidation activity exhibited in the integrated SCR-DPF system.

Accomplishments

- Identified that the downstream portion of the filter within the wall microstructure is the optimum location for SCR catalyst loading for maximizing NO_X reduction efficiency while minimizing pressure drop (with loaded soot).
- Identified that on high-porosity cordierite, it is not advantageous to load additional SCR catalyst passed ~90 g/L.
- Identified an optimum SCR catalyst loading target for facilitating maximum passive soot oxidation in the integrated device while retaining maximum NO_X reduction efficiency.

Future Directions

- Evaluate the value of additional substrates for interrogation, including possibly silicon carbide. Consider quick screening studies for comparison to cordierite wash coating results.
- Continue to interrogate passive soot oxidation feasibility in the integrated device, including continued parametric investigations interrogating the effect of NO_2:NO_X ratio, SCR catalyst loading, NH_3:NO_X ratio.
- Quickly pursue facilitating on-engine testing, as well as on-truck testing.

Introduction

Exhaust after-treatment is considered an enabler for widespread adoption of more fuel efficient diesel engines. In the last decade extensive research has resulted in the development and advancement of many after-treatment technologies. However there are still many unanswered questions that relate to how these technologies can work together synergistically, especially when tightly integrated. It is anticipated that in the future there will be a need to minimize the volume and mass of after-treatment systems on ever increasingly more complex truck platforms. However, to date research focused on combining technologies into an integrated system has been relatively sparse. With the inevitable need to consider how SCR and DPF technologies will function in synergy to reduce both NO_X and particulate matter, as well as how CO and hydrocarbons need to be managed, an integrated investigation and approach is essential. The determination of important synergies will require study both under steady-state and through transient conditions.

Approach

PNNL and PACCAR will execute a project to understand the critical developmental gaps and subsequently close these for a single container DPF-SCR system. The primary thrust in the project is to study the synergies of DPF-SCR systems in order to develop a pathway to a singular catalytic brick that combines the function of both a DPF-SCR. It is not envisioned that a flow-through open monolith would have sufficient contact with particulate matter in order to reach future U.S. heavy-duty diesel engine particulate matter emission regulations. As such, wall flow filters will be

the focus of the study. Corning has provided proprietary ultra-high porosity cordierite as the current subject of study for the DPF. BASF has worked intimately with the project to coat the Corning DPF filters with Cu-zeolite SCR catalyst. These samples are the subject of the investigations presented in the work reported on here.

Results

DPF-SCR samples were loaded to catalyst densities of ~60 g/L, ~90 g/L, and ~150 g/L. The samples were directionally loaded by BASF with the intent to locate the catalyst predominantly on the downstream portion of the filter microstructure. Figure 1 shows scanning electron microscope imaging of the 60 g/L (left) and 150 g/L (right) samples provided by BASF. The 60 g/L sample shows the coating strategy is largely successful at placing the catalyst predominantly on the downstream portion of the filter wall microstructure. However, granted this is a two-dimensional image of the filter, it is apparent that there exist areas of significant catalyst deposition adjacent to areas largely void of catalyst. With the 150 g/L sample, there appears to be significant catalyst deposition across the full width of the filter wall, together with what appears to be significant catalyst deposition on the outlet channel wall surface. Additionally, the deposition of catalyst appears to be fairly uniform throughout the filter, but there is still evidence of significant catalyst deposition in areas adjacent to pores apparently largely void of catalyst. It is believed that the nature of distribution of catalyst within the filter wall microstructure is largely a function of the cordierite structure employed in the system.

Hg porosimetry was performed on the samples. Figure 2 shows the pore distribution and porosity characteristics of the integrated samples. With the incorporation of 60 g/L catalyst, the sample porosity drops from 68% (uncoated sample) to 60%, with little to no shift of the overall pore distribution curve. This confirms qualitatively what was observed in the scanning electron microscope imaging of areas of significant catalyst deposition adjacent to areas largely void of SCR catalyst. Then the porosity further drops to 53% with the incorporation of 90 g/L catalyst, with what does appear to be a very slight shift of the pore distribution curve asymmetrically to smaller pore sizes. Then the incorporation of 150 g/L catalyst exhibits little effect on the sample porosity versus the 90 g/L sample, with the catalyst only depositing into a small number of very large pores in the filter microstructure. The majority of SCR catalyst loaded above 90 g/L appears to largely deposit on the outlet channel wall surface, and not deposit in the filter wall microstructure.

Figure 3 compares the dynamic pressure drop soot loading characteristics of the 90 and 150 g/L SCR catalyst loaded samples, presented as pressure drop versus accumulated soot. Shown are samples configured both with the SCR catalyst loaded on the downstream portion of the filter (as described in Figure 1) as well as with the samples configured in the opposite direction, i.e. with the catalyst configured on the upstream portion of the filter. The most predominant effect demonstrated is on the depth filtration exhibited by the samples, with both the orientation and the SCR catalyst loading having significant effect. The cake filtration characteristics of the samples are all very similar, with the exception of the 150 g/L sample configured with the SCR catalyst in the upstream configuration: this sample exhibits approximately twice the pressure drop rise per mass of accumulated soot versus the other three curves. This can be attributed to the large amount of SCR catalyst present on the inlet channel wall in the configuration that this sample is tested. This demonstrates that both the amount as well as the location of the SCR catalyst has measureable impact on the dynamic permeability of the integrated samples.

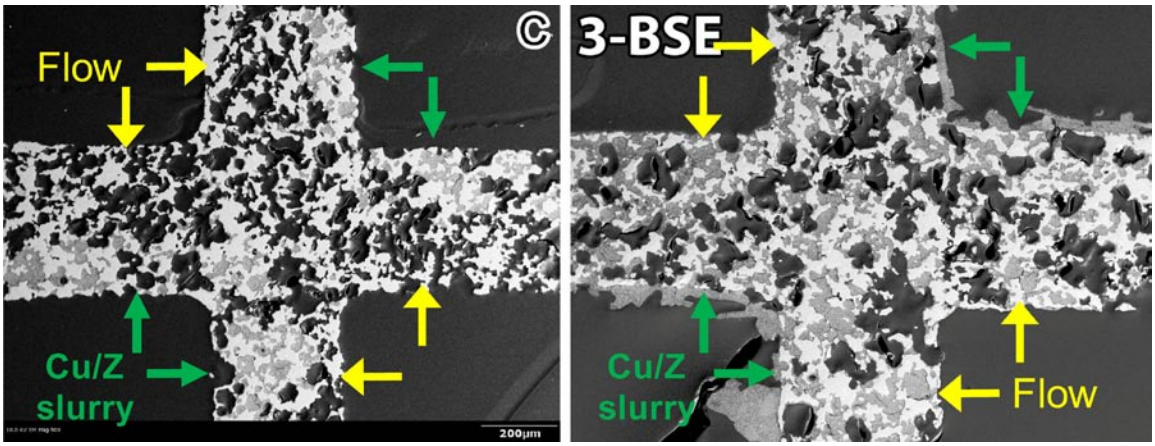

FIGURE 1. Scanning electron microscope imaging of high porosity diesel particulate filters coated with 60 g/L SCR catalyst (left) and 150 g/L SCR catalyst (right).

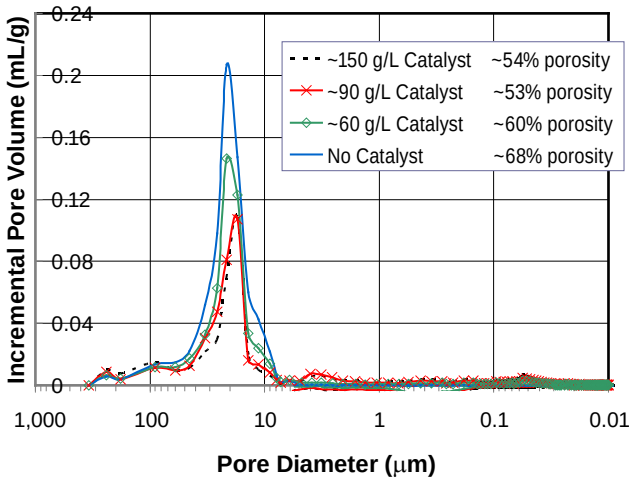

FIGURE 2. Hg porosimetry pore size distribution results for the integrated SCR-DPF samples, as well as the high porosity cordierite DPF void of SCR catalyst.

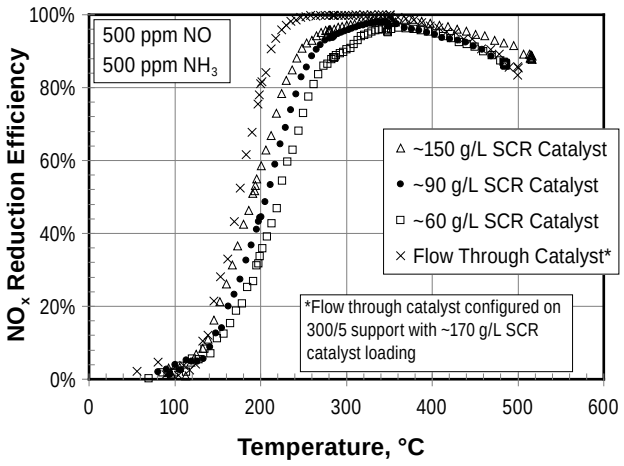

FIGURE 4. NO_x reduction efficiency versus temperature for standard SCR reaction on integrated SCR-DPF samples, compared to standard flow-through configured sample.

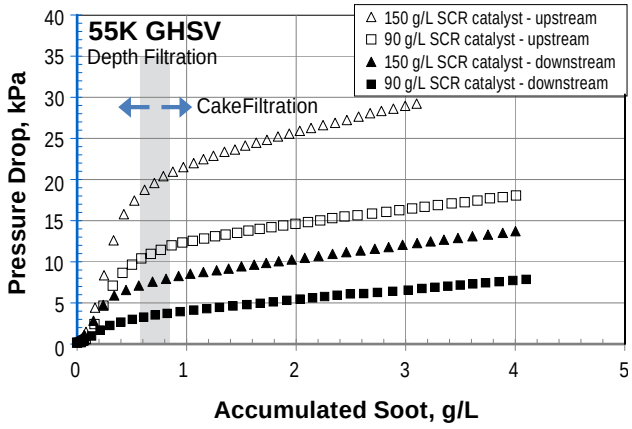

FIGURE 3. Dynamic pressure drop of high porosity cordierite DPF filters loaded with 90 g/L and 150 g/L SCR catalyst versus accumulated soot; data presented includes catalyst configured in both the upstream and downstream portions of the filter wall microstructure.

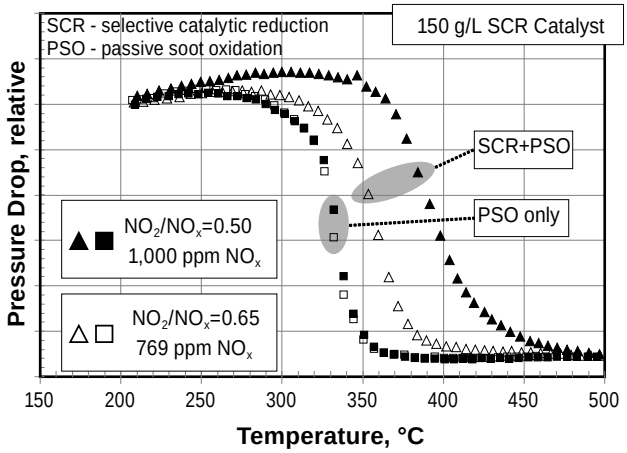

FIGURE 5. Temperature programmed oxidation studies on 150 g/L SCR catalyst loaded sample, presented as pressure drop versus temperature, in the presence (SCR+PSO) and absence (PSO only) of 500 ppm NH_3 reductant.

Figure 4 compares the standard SCR NO_x reduction efficiencies of the samples, along with the analogous results for a flow thru sample. The discrepancy between the 150 g/L wall flow sample and the flow thru sample demonstrates that there is a detrimental effect of the wall flow configuration versus the flow-through configuration on these cordierite samples. Additionally, the increased activity of the 90 g/L SCR sample versus 60 g/L (30 g/L in the filter wall microstructure) is comparable to the increase in activity of 150 g/L sample versus the 90 g/L sample (60 g/L catalyst on channel wall).

Figures 5 and 6 present temperature programmed oxidation studies performed on the 90 and 150 g/L samples, using the dynamic dP measured across the sample to provide a representation of the extent of passive soot oxidation exhibited in each system. The temperature programmed oxidation studies presented were conducted in the absence of SCR reaction exhibiting passive soot oxidation alone, and in the presence of the SCR reaction along with passive soot oxidation. The dP traces in these two figures demonstrate a quantifiable measure of the retarding effect of the SCR process on the passive soot oxidation exhibited in the systems.

Figure 5 compares NO_2/NO_x ratio of 0.5 (500 ppm NO_2, 1,000 ppm NO_x) to a ratio of 0.65 (500 ppm NO_2, 769 ppm NO_x). The latter test (NO_2/NO_x=0.65) exhibited significantly less retardation of the passive soot oxidation process in the presence of the SCR reaction versus the former (NO_2/NO_x=0.5). Figure 6

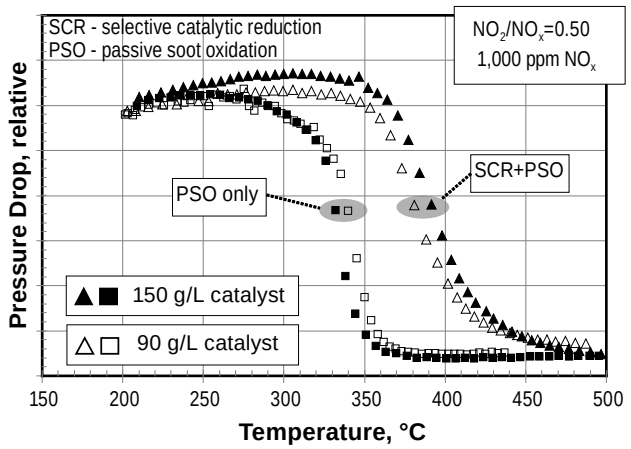

FIGURE 6. Temperature programmed oxidation studies on 90 and 150 g/L SCR catalyst loaded samples, presented as dP versus temperature, in the presence (SCR+PSO) and absence (PSO only) of 500 ppm NH_3 reductant.

compares a 90 g/L SCR loaded sample to a 150 g/L sample. The 90 g/L SCR loaded sample exhibited less retardation of the passive soot oxidation process in the presence of the SCR reaction versus the 150 g/L sample. These results confirm the results suggested from pulsed oxidation studies (data not presented here) that there in an optimum SCR catalyst loading target for facilitating maximum passive soot oxidation feasibility in the integrated system.

Conclusions

The results indicate the importance of both the amount and also the location of the SCR catalyst in the integrated system. It was shown that the location of the catalyst in the filter wall has significant impact on the wall permeability (i.e. dP) when loaded with soot, with the preferred location being on the downstream portion of the filter wall microstructure. It was demonstrated that above 90 g/L catalyst loading, little to no additional catalyst deposits into the filter wall microstructure of these cordierite samples. It was also shown that the SCR catalyst is better utilized for NO_X reduction efficiency embedded within the filter wall microstructure versus on the filter channel wall surface. Also finally, the adverse effects that the presence of this additional catalyst on the filter channel wall can have on the dynamic pressure drop characteristics of the system when loaded with soot were demonstrated.

The results also demonstrate that the presence of the SCR reactions have measureable detrimental effect on the magnitude of passive soot oxidation exhibited in the system. This is believed to be attributed to the competition for NO_2 that exists between the SCR and passive soot oxidation processes. There is a desire to optimize the system to facilitate maximum passive soot oxidation (i.e. minimize the detrimental effect of the SCR process on passive soot oxidation). The results above indicate that the NO_2/NO_X ratio, as well as the total SCR catalyst loading should and can be optimized for facilitating maximum passive soot oxidation feasibility in the integrated system.

FY 2011 Publications/Presentations

1. K. Rappe, D. Herling, "Combination and Integration of DPF – SCR Aftertreatment Technologies", 2011 DOE Hydrogen Program and Vehicle Technologies Program Annual Merit Review and Peer Evaluation Meeting (Washington D.C.; May 2011).

1. K. Rappe, J. Lee, M. Stewart, M. Devarakonda, G. Maupin, "Combination & Integration of DPF – SCR Aftertreatment", 2011 Directions in Engine Efficiency and Emission Research Conference (Detroit, MI; October 2011).

II.B.13 Deactivation Mechanisms of Base Metal/Zeolite Urea Selective Catalytic Reduction Materials, and Development of Zeolite-Based Hydrocarbon Adsorber Materials

Ja Hun Kwak, Jong H. Lee, Do Heui Kim, Shari Li, Diana N. Tran, Chuck Peden (Primary Contact)
Institute for Integrated Catalysis
Pacific Northwest National Laboratory (PNNL)
P.O. Box 999, MS K8-93
Richland, WA 99354

DOE Technology Development Manager:
Ken Howden

Cooperative Research and Development Agreement (CRADA) Partners:
Yisun Cheng, Jason Lupescu, Giovanni Cavataio, Christine Lambert, Robert McCabe (Ford Motor Company)

Objectives

- Develop an understanding of the deactivation mechanisms of the urea selective catalytic reduction (urea-SCR) catalyst used in diesel aftertreatment systems.
- Understand similarities and differences between actual field aging and aging under laboratory conditions, information essential in developing a rapid assessment tool for emission control technology development.
- Determine the role of the various aging factors impacting long-term performance of these catalyst systems, in order to provide information about what operating conditions should be avoided to minimize catalyst deactivation.
- Help fuel-efficient advanced combustion engines meet the current and future hydrocarbon (HC) emission standards with effective, inexpensive and reliable HC adsorber technologies.
- Improve the understanding of interaction between engine-out HCs and HC adsorber materials during the cold-start and the catalyst warm-up periods.

Fiscal Year (FY) 2011 Objectives

- Complete detailed studies of SCR catalyst poisoning by sulfur and phosphorus.
- Continue mechanistic studies of hydrothermal aging of SCR catalysts with particular reference to unusual high temperature performance observed after mild hydrothermal aging of some zeolite-based catalysts.
- Initiate new joint Ford/PNNL studies of zeolite-based hydrocarbon trap materials. In particular, initial FY 2011 studies will focus on effects of Si/Al ratio in, and pore size and structure of the zeolites, as well as the effects of added metals.

Accomplishments

- Completed studies of the differing effects of SO_2 to SO_3, including identification of the mechanism of poisoning by SO_3.
- Characterized the nature and distribution of phosphorus deposits observed on engine-aged urea-SCR catalysts.
- Performed studies aimed at an understanding of unusual hydrothermal aging of zeolite-based urea-SCR catalysts observed at Ford.
- Investigated the physicochemical properties of model zeolite materials with respect to hydrothermal aging.
- Evaluated the effects of physicochemical properties of model zeolite materials on the adsorption and desorption of ethanol.

Future Directions

- Complete mechanistic studies of phosphorus deactivating effects.
- Detailed studies of hydrothermal dealumination in Cu-SSZ-13 (CHA).
- Preparing additional CHA zeolite for joint Ford/PNNL studies of Cu loading effects (aimed at high temperature performance).
- Some new areas of focus for this fiscal year:
  - SCR degradation mechanisms due to upstream lean-NOx trap (LNT).
  - SCR deactivation due to use of biofuels.
- Examine the effects of physicochemical properties of zeolite materials with other fuel-component HC species.
- Investigate the role of metals on HC retention at higher temperatures.

Introduction

Because diesel engine-powered vehicles offer considerable fuel economy advantages over traditional gasoline-powered internal combustion engines, the U.S. Department of Energy considers a vehicle fleet that incorporates significantly more diesels to be highly desirable as at least a temporary solution to current "energy crisis", and to help reduce carbon dioxide emissions that are leading to global warming. Unfortunately, the high oxygen content of diesel exhaust makes onboard control of the emission of oxides of nitrogen (NOx) complicated and challenging. Reducing NOx emissions and particulate matter (PM) are primary concerns for diesel vehicles required to meet current LEV II and future LEV III emission standards which require 90+% NOx conversion. The technology with the most potential to achieve 90+% NOx conversion with minimal or no fuel economy penalty is SCR with an ammonia-based reductant such as aqueous urea. Currently, urea-SCR as the NOx reductant [1] and a catalyzed diesel particulate filter are being used for emission control system components by Ford Motor Company for 2010 and beyond diesel vehicles. To ensure successful NOx control, a urea-SCR catalyst with high activity and durability is critical for the emission control system. Because the use of this technology for vehicle applications is new, the relative lack of experience makes it especially challenging to satisfy the durability requirements. Of particular concern is being able to realistically simulate actual field aging of the catalyst systems under laboratory conditions. This is necessary both as a rapid assessment tool for verifying improved performance and certifiability of new catalyst formulations, and to develop a good understanding of deactivation mechanisms that can be used to develop improved catalyst materials.

In addition to NOx and PM, the HC emission standards are expected to become much more stringent during the next few years, because the California Air Resources Board plans to roll out LEV III standards and Environmental Protection Agency plans to follow with Tier 2 Bin 4 fleet averages. Meanwhile, the engine-out HC emissions are expected to increase and/or be more difficult to remove. For example, advanced combustion technologies (e.g., premixed charge compression ignition, homogeneous charge compression ignition) result in low exhaust temperatures, while the electrification of vehicles may increase the HC emissions due to repeated start-and-stop engine operations. The diversification of fuel sources, such as non-petroleum-based fuels, also result in increased HC emissions, because typically excess fuel injection is required for ethanol-containing fuel (e.g., E85) during the cold start for engine start and drivability. Since HCs can be removed only when the catalyst becomes warm enough for its oxidation, three-way catalyst and diesel oxidation catalyst formulations often contain proprietary zeolite materials to hold the HCs produced during the cold-start period until the catalyst reaches its operating temperature (e.g., >200°C). Unfortunately, much of trapped HCs tend to be released before the catalyst reaches the operating temperature. As a result, meeting the Super Ultra-Low Emission Vehicle standard (0.01 g/mi HC) with effective and affordable technologies is expected to become a major challenge. Among materials effective for trapping HCs during the catalyst warm-up period, siliceous zeolites are commonly used because of their high surface area and high stability under typical operating conditions. However, there has been little research on the physical properties of these materials related to the adsorption and release of various hydrocarbon species found in the engine exhaust. For these reasons, automakers and engine manufacturers have difficulty improving their catalytic converters for meeting the stringent HC emission standards.

In this collaborative project, scientists and engineers in the Institute for Integrated Catalysis at PNNL and at Ford Motor Company are investigating laboratory- and engine-aged SCR catalysts, containing mainly base metal zeolites. These studies are leading to a better understanding of various aging factors that impact the long-term performance of SCR catalysts and improve the correlation between laboratory and engine aging, saving experimental time and cost. We are investigating SCR catalysts with reduced ammonia slip, increased low temperature activity, and increased product selectivity to N_2. More recent recognition that high temperature performance, under regimes that sometimes cause deactivation, also needs to be improved is driving current work focused on catalyst materials modifications needed to achieve this enhanced performance. We are also studying materials effective for the temporary storage of HC species during the cold-start period. In particular, we examine the adsorption and desorption of various HC species produced during the combustion with different fuels (e.g., gasoline, E85, diesel) over potential HC adsorber materials, and measure the kinetic parameters to update Ford's HC adsorption model.

Approach

This project is focusing on the characterization of catalyst materials used in the urea-SCR and HC absorber technologies with special attention to changes in the materials properties under conditions of laboratory (e.g., oven and laboratory reactor) and realistic (e.g., engine dynamometer and vehicle) aging protocols. In particular, a primary area of emphasis of earlier studies on this project was establishing the relevance of rapid laboratory catalyst aging protocols with the specific aging phenomena observed in realistic engine operating conditions. This information has aided in the development of optimized rapid aging protocols at Ford.

Ford has been providing both fresh and aged catalyst materials used in the urea-SCR technology and making experimental measurements of changes in the catalytic performance of these materials before and after the aging. PNNL has been utilizing state-of-the-art analytical techniques to investigate the surface and bulk properties of these catalysts as well as the changes in these properties induced by the aging process. In particular, catalyst characterization techniques such as X-ray diffraction (XRD), X-ray photoelectron spectroscopy (XPS), transmission electron spectroscopy (TEM)/energy-dispersive spectroscopy, Brunauer-Emmett-Teller/pore size distribution, and ^{27}Al solid state nuclear magnetic resonance (NMR) are being utilized to probe the changes in physicochemical properties of SCR catalyst and HC absorber samples after various pretreatments. This work is being performed on a group of model and development catalysts. Specifically, we utilize a variety of zeolites, a class of microporous aluminosilicate materials that include a wide range of natural minerals. For SCR, Cu-exchanged beta and SSZ-13 zeolite catalysts have been exposed to deactivating conditions; e.g., hydrothermal aging at various temperatures. For HC absorbers, we are identifying catalytic materials that are effective for the temporary storage of HCs produced from different fuels during the cold-start period or advanced combustion processes. Various silicate and aluminosilicate materials, including novel zeolites, will be evaluated with respect to hydrophobicity, surface area, pore size and connectivity for the adsorption and desorption of hydrocarbon species found in the engine exhaust. Once the potential materials are characterized, fuel component and combustion product HC species are used to probe the adsorption and desorption characteristics of different HC adsorber materials. These characterization measurements are complimented by studies at Ford that include performance testing following a variety of laboratory and realistic engine aging protocols.

Results

Physicochemical Investigations of the Degradation Mechanisms for SCR Catalysts

In this section, we briefly describe some results in two areas: 1) our recently completed mechanistic studies of the variable effects of SO_2 to SO_3 on the performance of Cu-zeolite SCR catalysts; and 2) investigations of unusual performance behavior for recent generation Cu-zeolite SCR catalysts after a mild hydrothermal aging.

The Different Impacts of SO_2 and SO_3 on Cu/Zeolite SCR Catalysts: The different impacts of SO_2 and SO_3 on Cu/zeolite SCR catalysts were investigated by SCR performance tests and multiple characterization techniques including temperature programmed desorption, XPS and X-ray absorption fine structure [2]. The results indicate that a larger amount of highly dispersed $CuSO_4$ formed in the zeolite catalysts (Z-$CuSO_4$) upon SO_3 poisoning, explaining the much more significant deactivation of the Cu/zeolite catalysts that were exposed to SO_3 compared to poisoning by SO_2. In these studies, we provided the first demonstration that active sites of Cu/zeolite SCR catalysts involved in the storage and removal of sulfur can react with SO_2 and SO_3 in very different ways. In particular, the significant differences in the extent of sulfur uptake account for the considerably different impacts of SO_2 and SO_3 poisoning on the performance of Cu/zeolite SCR catalysts. The Cu/zeolite SCR catalyst used in this study was a fully-formulated cordierite monolith with Cu/zeolite washcoat from a catalyst supplier. For proprietary reasons, details of CatA cannot be given in this report except to note that it was designed for transient diesel engine applications.

The NOx activities for CatA samples before and after sulfur poisoning by SO_2 or SO_3 at 200°C, 300°C, and 400°C are shown in Figure 1. Also shown in this figure are results for a freshly degreened catalyst (T1). The NOx activity of SO_2-poisoned Cu/zeolite SCR catalysts decreased to a relatively small extent after being exposed to 40 ppm SO_2 for 1.5 hours regardless of the aging temperatures. The lower SO_2 aging temperature resulted in higher NOx activity decreases: the NOx activities performed at 178°C decreased by 33%; by 21% for the sample aged at 300°C, and only by 8% for the sample aged at 400°C. In contrast, the NOx activities of CatA Cu/zeolite catalysts after sulfur poisoning by SO_3 at 200, 300, and 400°C were significantly decreased for all samples after being exposed to 40 ppm SO_3 for 1.5 hours regardless of the exposure temperatures, with NOx activities of all samples being extremely low at T <250°C. The sample aged with SO_3 at lower temperature had better NOx activity between 250°C and

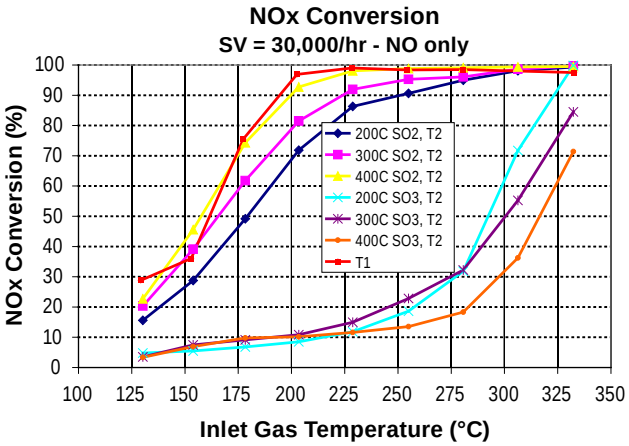

FIGURE 1. Steady-state NOx conversions for CatA Cu/zeolite SCR catalysts before and after SO_2 and SO_3 aging at 200°C, 300°C, and 400°C. Also shown are results for a freshly degreened catalyst (T1).

340°C. Notably at a 340°C test temperature, the NOx activity of the sample aged at 200°C was close to 100%, while the NOx activity of sample aged at 400°C showed only 70% conversion.

In order to obtain the information on the oxidation state and amount of sulfur species, we applied XPS for the CatA samples treated at 200ºC with SO_2 and SO_3. For the 27 mm (1 inch) long monolith samples, five points were analyzed separated by a distance of 6 mm, allowing us to determine the spatial distribution along the monolith z-axis. Spectra of both samples contain a single peak at 169 eV, indicating that only sulfates (SO_4^{2-}) are formed by the interaction with either SO_2 or SO_3. However, there was a drastic difference in the amount of sulfate species between the samples treated with SO_2 or SO_3. As shown in Figure 2, the sample treated with SO_3 clearly had larger amounts of sulfur, especially up to 13 mm from the inlet, followed by a significant decrease thereafter. We suggest that sulfate saturates the catalyst from the inlet, gradually moving toward the outlet. In contrast, the sample treated with SO_2 had considerably smaller amount of sulfur in the inlet and along the monolith. The summed amounts of sulfur along the monolith indicates that the sample treated with SO_3 contained at least five times larger concentrations than the one treated with SO_2, which points to the relative ease of sulfate formation by reaction with SO_3. XPS results on the samples after the desulfation (deSOx) showed essentially no sulfur remained on the surface of the catalyst (not shown). This result implies that all sulfates are desorbed as a result of thermal desorption during the deSOx, as evidenced also by the full recovery of the activity after deSOx (not shown).

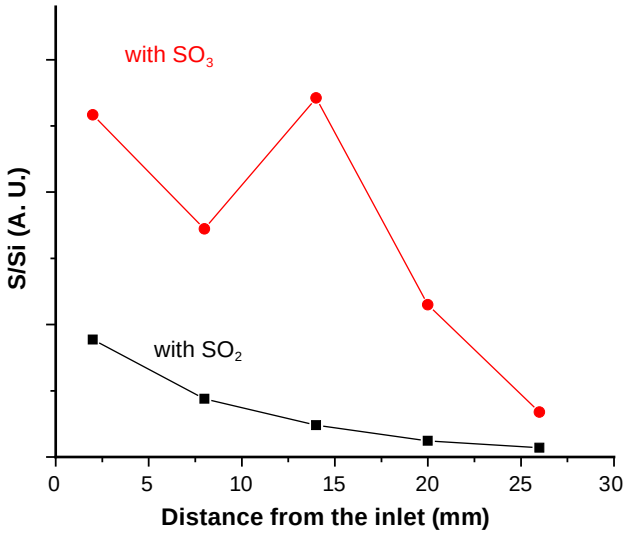

FIGURE 2. Distribution of sulfur, plotted as normalized S/Si ratios, as a function of distance from the inlet of the monolith-type CatA sample.

Unusual Performance Behavior for Cu-zeolite SCR catalysts After Mild Hydrothermal Aging: The hydrothermal stability of Cu/beta NH_3 SCR catalysts with respect to their interesting ability to maintain and even enhance high-temperature performance for the "standard" SCR reaction after modest (900°C, 2 hours) hydrothermal aging [3]. Characterization of the fresh and aged catalysts was performed with an aim to identify possible catalytic phases responsible for the enhanced high temperature performance. Two model catalysts, suggested by these characterization data as possible mimics of the catalytic phase formed during hydrothermal aging of Cu/beta, were prepared and tested for their performance in the "standard" SCR and NH_3 oxidation reactions. The similarity in their reactivity compared to the 2-hour hydrothermally-aged Cu/beta catalyst suggests possible routes for preparing multi-component catalysts that may have wider temperature windows for optimum performance than those provided by current Cu/zeolite catalysts. As perhaps the most promising zeolite-based SCR catalyst prior to the discovery of the newest generation of CHA zeolite-based materials, the catalyst chosen for this study was Cu ion-exhanged beta zeolite. The beta zeolite (CP-814C, $Si/Al_2 = 38$) was obtained from Zeolyst International Co., and Cu/beta catalysts were prepared by aqueous ion-exchange using a $Cu(NO_3)_2$ precursor. These Cu-exchanged/beta (Cu/beta) catalysts were calcined in an oven at 500°C for 2 hours prior to testing and characterization.

As part of studies carried out a couple of years ago at Ford on the comparative hydrothermal stability of several pre-commercial Cu-zeolite catalysts [4], some very interesting SCR performance behaviour was observed after hydrothermal aging at very high (900°C) temperatures. In particular, this study described Ford's first observations of an SCR Cu-zeolite formulation (referred to as a "best in class 2007 SCR formulation" in this SAE International paper) that is able to maintain stable NOx performance at 200°C after exposure to such severe hydrothermal aging conditions. Not discussed in this paper, however, was the maintenance of unusual high-temperature SCR performance for an older generation catalyst ("best in class 2006 formulation"), even though this latter catalyst's low-temperature activity was reduced significantly due to the high-temperature aging (see Figure 7 in [4]). Here, we briefly describe our collaborative studies aimed at understanding the properties of zeolite-based catalysts after hydrothermal aging, especially with respect to shedding light on the nature of the material giving rise to this interesting, and potentially useful high temperature SCR performance.

Figure 3 shows results for the temperature dependence of the "standard" SCR (Figure 3a) and NH_3 (Figure 3b) oxidation reactions over the Cu/beta catalyst after various hydrothermal treatments. These

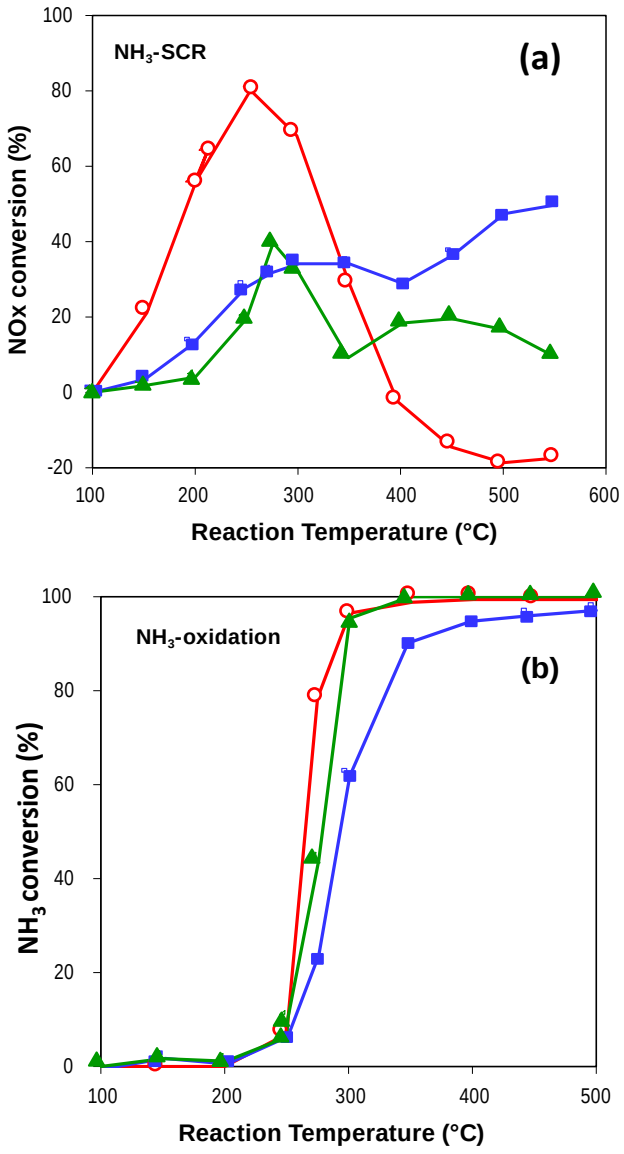

FIGURE 3. (a) NO conversion to N_2 during the "standard" SCR reaction, and (b) NH_3 conversions during the NH_3 oxidation reaction (no NOx present) over a Cu-beta zeolite catalyst as a function of temperature after various thermal aging treatments at 900°C: 1 hour in dry air (open red circles); 2 hours in air with 10% H_2O (solid blue squares); and 10 hours in air with 10% H_2O (solid dark green triangles). Gas composition for SCR reaction: 350 ppm NO, 350 ppm NH_3, 14% O_2, 2% H_2O in balance N_2. Gas composition for the NH_3 oxidation reaction: 350 ppm NH_3, 14% O_2, 2% H_2O in balance N_2.

treatments, separately performed on fresh catalyst samples, included calcination at 900°C for one hour in the absence of H_2O (red curves), 900°C hydrothermal (H_2O present) treatment for 2 hours (blue curves), and hydrothermal treatment at 900°C for 10 hours (green curves). Following a 900°C calcination without H_2O present, the Cu/beta catalyst still displays good performance for the "standard" SCR reaction at lower temperatures (Figure 2a, red curve), although its higher (>300°C) temperature activity is significantly degraded. In fact, negative NOx conversions observed at temperatures above 400°C indicate little, if any, SCR activity for this catalyst aged by calcination, while non-selective NH_3 oxidation by O_2 (light-off just below 300°C, red curve in Figure 3b) is responsible for the formation of NOx.

Significantly different "standard" SCR performance data were obtained following a 2-hour hydrothermal (H_2O present) aging treatment (Figure 3a, blue curve). In this case, while lower (< 350°C) temperature performance is significantly degraded, NOx conversions above 400°C are maintained and even perhaps enhanced. Also interesting to note is the fact that the light-off temperature for NH_3 oxidation by O_2 has increased (Figure 3b, blue curve). Further increasing the hydrothermal aging time to 10 hours results in a loss of SCR performance for the Cu/beta catalyst at all temperatures (Figure 3a, green curve). The distinct "standard" SCR and NH_3 oxidation activity of the hydrothermally-aged Cu/beta catalysts, particularly after a relatively short aging time of 2 hours, suggests that a new catalytic phase may have formed during the moderately severe treatment. In order to identify the nature of this potential new phase, we characterized the fresh and aged catalysts with XRD, TEM and ^{27}Al NMR spectroscopy.

Strong peaks in the ^{27}Al NMR spectra of alumino-silicate zeolites at ~50-60 ppm (using the signal due to aluminum in an aqueous solution of $Al(NO_3)_3$ as a 0 ppm reference) are due to tetrahedrally-coordinated Al atoms that substitutionally occupy Si lattice sites within the zeolite. For fresh Cu-beta zeolite, the peak associated with tetrahedral zeolite-lattice Al appears at ~55 ppm as illustrated in Figure 4 (black curve). Calcination at 900°C results in little, if any, change in the ^{27}Al NMR spectrum (Figure 4, red curve), consistent with both XRD and TEM data (not shown). In contrast, hydrothermal aging at 900°C for 2 hours results in a dramatic decrease in the size of the peak associated with tetrahedrally-coordinated Al (Figure 4, blue curve). This feature is essentially absent from the Cu/beta catalyst that was hydrothermally aged for 10 hours (Figure 4, green curve). Note, however, that no new features appear in the spectra for the hydrothermally-aged samples. A possible explanation for this loss of signal in the ^{27}Al NMR spectra for these aged catalysts is a strong interaction between paramagnetic Cu and the Al species that are newly formed as a result of hydrothermal dealumination. Such a strong interaction would render the ^{27}Al NMR signal 'invisible'.

The characterization results obtained in these studies were used to suggest possible model catalyst mimics of the catalytic phase formed upon hydrothermal aging that is responsible for its enhanced high temperature performance for the "standard" SCR

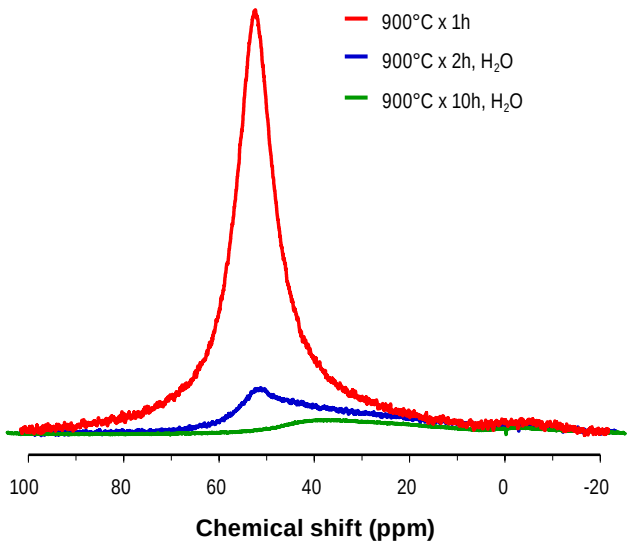

FIGURE 4. ^{27}Al solid state NMR spectra of the Cu/beta samples aged at 900°C in dry air for 1 hour (red curve), and in dry air that contained 2% H_2O separately added for 2 (blue curve) and 10 (green curve) hours.

reaction shown in Figure 3. In fact, the reactivity of the model catalysts (not shown here) were remarkably similar to those of the hydrothermally-aged Cu/beta catalyst suggesting the possibility that multi-component catalysts can be prepared with wider temperature windows than currently available with Cu/zeolite catalysts alone. A specific catalyst structure able to achieve both good high- and low-temperature NOx reduction performance is not proposed here since it will depend on the locations of other emission control components (i.e., diesel oxidation catalyst, diesel particulate filter, etc.). However, the results presented here suggest that an SCR catalyst system consisting of both Cu-zeolite and Cu-alumina materials will provide for a desirably wider temperature window for optimum SCR performance [3].

Physicochemical Investigations of HC Absorber Materials

During FY 2011, our HC adsorber investigation activities have focused on understanding the effects of various physicochemical properties of zeolite materials. In particular, three model zeolite materials were obtained to probe the effects of different pore size and connectivity: beta (large pore, three-dimensional pore connectivity); ZSM-4 (medium pore, three-dimensional pore connectivity); and ZSM-12 (large pore, one-dimensional pore structure). The effects of hydrothermal aging on their physicochemical properties were then examined using various analytical techniques, including XRD and NH_3- temperature programmed desorption. Following the hydrothermal treatment at 800°C for 60 hours, it was found that the surface area, number of acid sites and acidic strength were all reduced significantly, although the zeolite frameworks were found to remain largely intact. Interestingly, the loss of acid sites was more pronounced among samples of high Si/Al ratios.

Considering the challenges associated with renewable fuels (e.g., E85, E-diesel), the adsorption and desorption of ethanol was examined in detail. We found that ethanol could adsorb weakly via chemisorption, and strongly on acid sites via chemisorption. Weakly adsorbed ethanol was found to desorb at <200°C, whereas chemisorbed ethanol was dehydrated to ethylene which desorbed at higher temperatures (i.e., >200°C). Interestingly, the presence of water was found to affect the weakly adsorbed ethanol only. Following the hydrothermal treatment at 800°C for 60 hours, significant loss of ethanol adsorption was observed because of the reduced surface area and acidity.

Conclusions

PNNL and its Cooperative Research and Development Agreement partners from Ford are carrying out a project to study the properties and mechanisms of deactivation of SCR and HC-absorber materials arising from thermal aging. Because the catalytically active sites certainly include isolated and very small (even mono-atomic) ion-exchanged metals in the zeolite cages, we are currently pursuing a molecular-level understanding of the deactivation mechanisms related to the activity degradation by using a number of state-of-the-art catalyst characterization techniques. The effects of hydrothermal aging on physicochemical properties of model zeolite materials have been examined. In particular, the adsorption and desorption of ethanol on model zeolite materials were investigated with respect to physicochemical properties.

References

1. S. Brandenberger, O. Krocher, A. Tissler, R. Althoff, Catal. Rev.-Sci. Eng. 50 (2008) 492-531.

2. Y. Cheng, C.K. Lambert, D.H. Kim, J.H. Kwak, S.J. Cho, C.H.F. Peden, *Catalysis Today* 151 (2010) 266-270.

3. C.H.F. Peden, J.H. Kwak, S.D. Burton, R.G. Tonkyn, D.H. Kim, J.H. Lee, H.W. Jen, G. Cavataio, Y. Cheng, C.K. Lambert, *Catalysis Today* (2012) in press.

4. G. Cavataio, H.W. Jen, J.R. Warner, J.W. Girard, J.Y. Kim, C.K. Lambert, SAE 2008011025.

FY 2011 Publications/Presentations

1. C.H.F. Peden, J.H. Kwak, S.D. Burton, R.G. Tonkyn, D.H. Kim, J.H. Lee, H.W. Jen, G. Cavataio, Y. Cheng, and C.K. Lambert, "Possible Origin of Improved High

Temperature Performance of Hydrothermally-Aged Cu/Beta Zeolite Catalysts", *Catalysis Today* (2012) in press.

2. Y. Cheng, M. Jagner, H.W. Jen, C.K. Lambert, J.H. Kwak, D.H. Kim, and C.H.F. Peden, "Characterizations of Engine Aged Cu/CHA Urea SCR Catalysts", *SAE* (2012) submitted for publication.

3. Y. Cheng, C.K. Lambert, D.H. Kim, J.H. Kwak, S.J. Cho, C.H.F. Peden, "The Different Impacts of SO_2 and SO_3 on Cu/Zeolite SCR Catalysts." *Catalysis Today* **151** (2010) 266-270.

4. Y. Cheng, M. Jagner, H.W. Jen, C.K. Lambert, J.H. Kwak, D.H. Kim, and C.H.F. Peden, "Characterizations of Engine Aged Cu/CHA Urea SCR Catalysts", presentation at the 22nd National Meeting of the North American Catalysis Society, Detroit, MI, June 2011.

5. C.H.F. Peden, J.H. Kwak, R.G. Tonkyn, D.H. Kim, J. Szanyi, D.N. Tran, J.H. Lee, "Excellent Activity and Selectivity of Cu-SSZ-13 in the Selective Catalytic Reduction of NOx with NH_3," presentation at the 22nd North American Catalysis Society Meeting, Detroit, MI, June 2011.

6. J.H. Kwak, D.H. Kim, J.H. Lee, C.H.F. Peden, D.N. Tran, Y. Cheng, J. Lupescu, G. Cavataio, C. Lambert, R. McCabe, "Deactivation Mechanisms of Base Metal/Zeolite Urea Selective Catalytic Reduction Materials, and Development of Zeolite-Based Hydrocarbon Adsorber Materials", presentation at the DOE Combustion and Emission Control Review, Washington, DC, May, 2011.

7. Y. Cheng, H.W. Jen, M. Jagner, C.K. Lambert, J.H. Kwak, D.H. Kim and C.H.F. Peden, "Non-uniform Aging on Super Duty Diesel Truck Aged Urea Cu/Zeolite SCR Catalysts", presentation at the 2010 DEER Conference, Detroit, MI, September 2010.

II.B.14 Fuel-Neutral Studies of PM Transportation Emissions

Mark Stewart (Primary Contact), Alla Zelenyuk
Pacific Northwest National Laboratory (PNNL)
902 Battelle Boulevard
Richland, WA 99352

DOE Technology Development Manager:
Ken Howden

Subcontractors:
- University of Wisconsin Engine Research Center, Madison, WI
- Pennsylvania State University, University Park, PA

Overall Objectives

- Characterize exhaust particulates from advanced combustion engines such as spark ignition direct injection (SIDI) using readily available fuel blends.
- Use insight gained and prior experience with diesel aftertreatment to jump-start development of optimum aftertreatment technologies *in case they are needed.*

Fiscal Year (FY) 2011 Objectives

- Transmission electron spectroscopy (TEM) analysis of SIDI particulates:
  - Corroborate particulate features such as primary particle size estimated by SPLAT II[1] data.
  - Compare SIDI soot nano-structure (relevant to formation mechanisms and oxidation behavior) to those from a wide variety of other combustion sources.
- Publish results of first round cooperative experiments with prototype SIDI engine at the University of Wisconsin Engine Research Center (ERC).
- Plan second round cooperative experiments.
- Fundamental filtration studies with lab-generated particles:
  - Focus on number efficiency of clean filters.
  - Examine effect of coatings.

Accomplishments

- Soot from a developmental SIDI engine has been thoroughly characterized with respect to size distribution, particle morphology, and composition; addressing technical barrier F in the Vehicle Technologies Multi-Year Program Plan: Lack of actual emissions data on pre-commercial and future combustion engines.
- Suitability of current exhaust filter technologies for SIDI applications has been evaluated, as well as strategies for improvement, helping to address technical barrier B in the Vehicle Technologies Multi-Year Program Plan: Lack of cost-effective emission control.
- Modeling tools have been developed to assist in the development and evaluation of SIDI exhaust filter systems, helping to address technical barrier C in the Vehicle Technologies Multi-Year Program Plan: Lack of modeling capability for combustion and emission control.

Future Directions

- Complete second round cooperative experiments with a prototype SIDI engine at the ERC using SPLAT II and other advanced analytical tools:
  - Confirm significant trends in initial observations.
  - Expand test matrix in regions of particular interest for future system development.
  - Explore particulate generation with alternate fuel blends (such as E85).
  - Employ data from new aerosol particulate mass instrument to more definitively characterize the population of particle sizes and shapes.
- Publication of second round SIDI soot characterization results.
- Apply improved unit collector models to likely SIDI applications — e.g. filtration for high number efficiency across a realistic SIDI size spectrum in a nearly soot-free filter.

Introduction

Technologies such as SIDI offer the possibility of dramatically increasing the fuel efficiency of engines which run on gasoline and similar hydrocarbons. Development of this technology and application to a range of fuel blends will blur the lines that have traditionally existed between gasoline and diesel engines. Although some similarities are expected between diesel soot and particulates generated by lean-burn engines designed to use other fuels, significant differences

[1] Custom instrument that determines aerosol vacuum aerodynamic diameter and mass spectra of individual particles.

could require adaptation of existing aftertreatment technologies. Initial data indicates that SIDI particles are smaller than diesel particles, and particle production can vary widely between engine operating conditions. Regulation of engine particulate emissions in Europe is moving from mass-based standards toward number-based standards, and it is likely that North American regulators will move in the same direction. This will place more emphasis on the reliable removal of smaller particles, which make up the vast majority of the particulates generated on a number basis.

Reliable and efficient regeneration of particulate filters is a significant issue on diesel vehicles. Soot accumulated in filters must be removed by oxidation to maintain acceptable back-pressures, often necessitating complicated estimation and control schemes. Many strategies for removing the soot require the use of additional fuel to raise exhaust temperatures. Gasoline engines typically run significantly hotter than diesel engines, raising the possibility that soot may be continuously oxidized without burning additional fuel, especially if the filter can be close-coupled to the engine. Filtration efficiency could be a major issue if there is little accumulation of soot in the filter, since a soot cake performs much of the filtration over the operating cycle of a typical diesel particulate filter (DPF). This is particularly true for meeting number-based particulate emissions standards.

Approach

A fuel-neutral single-cylinder research engine (Figure 1) has been constructed at the ERC with support from General Motors. This test engine has been configured to generate particulate matter from a wide variety of fuels and engine operating conditions. Joint experiments conducted by the ERC and PNNL using a wide array of analytical techniques are generating an extensive set of data on particulate size, shape, and composition. Experiments will include alternative fuels, including ethanol blends. Analysis of these results is expected to yield more insight into variation of particulate populations with SIDI operating conditions.

Knowledge of SIDI particulates gained by these activities is also being used to anticipate filtration technologies and system design approaches which may be necessary for SIDI applications in the future. Filtration experiments were performed to estimate the number removal efficiency of close-coupled filters which are not likely to maintain a soot cake over the majority of their operating cycle. Options have been identified for re-engineering DPF technology for optimal performance on SIDI systems. In particular, the use of coatings to increase clean filtration efficiency has been explored. Micro-scale and reduced order models are also being developed to assist in the evaluation of candidate technologies.

FIGURE 1. Single-Cylinder Fuel-Neutral Test Engine Constructed at the ERC with Support from General Motors

Results

An initial round of cooperative experiments at the ERC generated a very large set of SIDI particulate data over a wide range of engine operating parameters with standard gasoline. Particle mobility size distributions were measured using TSI scanning mobility particle sizers. Vacuum aerodynamic diameter and composition data were collected using the SPLAT II instrument developed at PNNL, which obtains size and complete mass spectra for up to 100 individual particles per second. Aerodynamic and mobility diameter are two measures of particle size which would be the same for simple spherical particles having unit density. Combining these measurement techniques provides clues as to the complex structure of soot particles, which are fractal agglomerates made up of smaller primary particles. Specifically, correlation of the two diameters was used to estimate fractal dimensions ranging from 2.03 to 2.22 and primary particle sizes between 14 and 30 nm. Calculated primary particle size was observed to shift as a function of end of injection as shown in Figure 2.

Subsequent investigations using TEM provided direct observation of particle morphology and primary particle size, as well as the nano-structure of primary particles. Lower resolution images were used to examine aggregate morphology and survey primary particle size. Aggregates had a somewhat more open structure than is typically observed for diesel particles. Primary particle size distributions were observed to be somewhat broader than those in diesel soot. Figure 2 also shows that TEM measurements of primary particle size variation at various end of injections agree remarkably well with estimates previously made using aerosol analysis methods. High resolution TEM images (Figure 3) were used to examine the nanostructure of primary particles. Image processing algorithms [1] were used to quantify the extent of order observed in the graphene sheets which make up the solid particle matrix. A range of nanostructures was observed, even within some samples. Nanostructures were generally more amorphous (less graphitic) than is typical for diesel soot. Lack of order is thought to be indicative of integrated organic compounds that tend to interrupt growth of the graphene layers. Higher organic content as well as higher proportions of edge sites and curved lamella suggest that SIDI soot will be more reactive than diesel soot.

SPLAT II mass spectra indicate that the SIDI particulates contained significant organic content, up to 40% of the particulate mass. European particle number emissions standards include an elaborate sampling and dilution specification, including volatile particle removal (VPR) methods, which strip away volatile components from diesel aerosols before counting, typically altering the particle size distribution as well as particle composition. The first round of

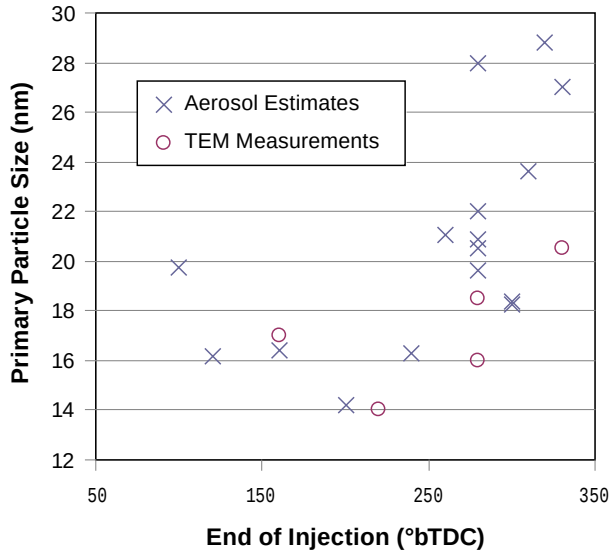

FIGURE 2. Primary Particle Size Calculated from Aerosol Behavior and Measured by TEM

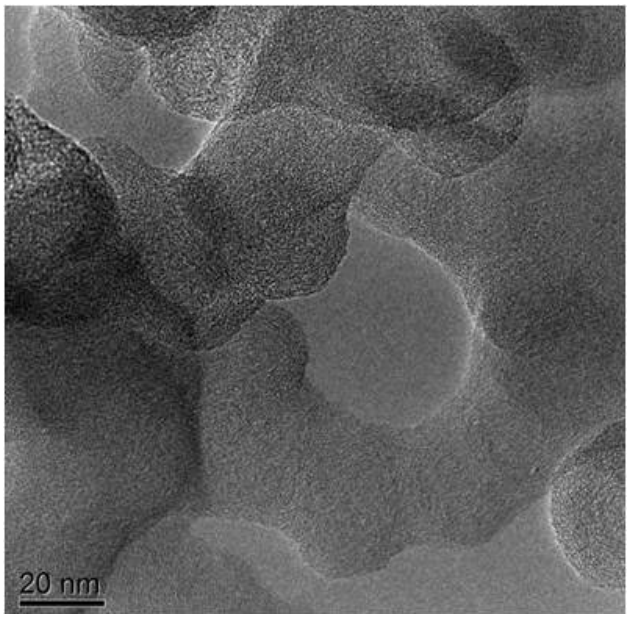

FIGURE 3. TEM Image of SIDI Soot

cooperative experiments at the ERC examined two VPR methods, a thermodenuder and an evaporative chamber. Under most of the conditions studied, neither of these treatments significantly altered the particle size distributions or compositions. The only exception was a set of conditions intended to mimic a cold start. In this case, the particle size distribution was narrowed and shifted to smaller particles (Figure 4) by both VPR methods, while SPLAT II mass spectra showed a significant reduction in polycyclic aromatic hydrocarbons and other organics. The evaporative chamber removed about twice the amount of organics as the thermodenuder. The fact that the significant organic content observed under other engine operating conditions was so difficult to remove suggests that organics were not present as separate droplets or as coatings on the surfaces of solid soot particles, as is often observed in raw diesel exhaust.

Attenuated total reflectance Fourier transform infrared spectroscopy and X-ray photoelectron spectroscopy were also used to investigate the bulk and surface chemical composition of soot particles, respectively. Significant organic content was observed by both techniques. The quantitative XPS measurements nevertheless showed a large proportion of inorganic carbon on the particle surfaces, adding more evidence that organic content is integrated into the solid matrix throughout the bulk of the primary particles. This is consistent both with the TEM observations of particle nanostructure and with the difficulty in removing by VPR organics observed in SPLAT II mass spectra.

Subsequent joint experiments will explore the effects of fuel composition on SIDI particulates. Figure 5

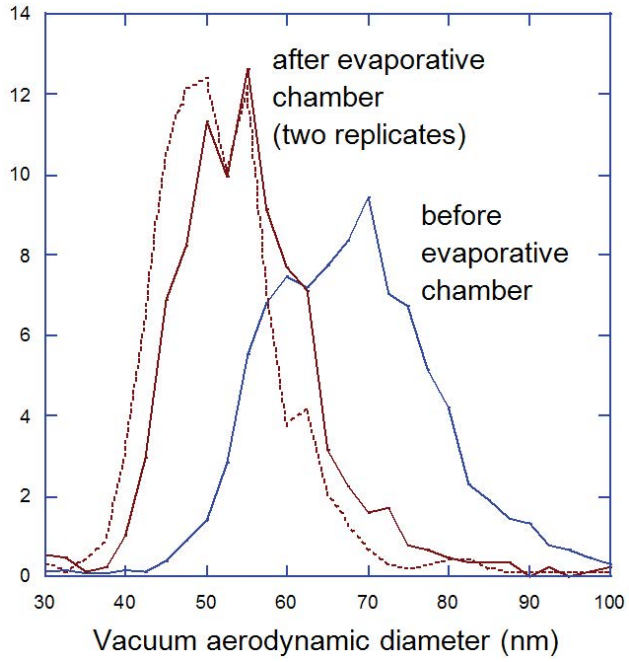

FIGURE 4. Distribution of Vacuum Aerodynamic Diameters Measured by SPLAT II Before and After Evaporative Chamber, Conditions Intended to Mimic Cold Start

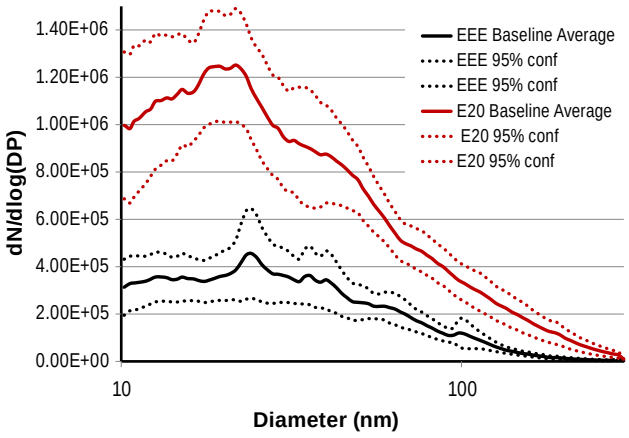

FIGURE 5. Preliminary Particulate Production Data for E20 Ethanol Blend Compared to Gasoline

shows preliminary scanning mobility particle sizer data from the ERC comparing particulate production from standard gasoline and an E20 ethanol blend. Fuel rates were set for equivalent fuel energies and air to fuel ratios were set to maintain the same equivalence ratio. Spark timing was adjusted to match combustion phasing.

Experiments were carried out to evaluate current production DPF substrates for SIDI applications. Aerosolized salt particles were used as a simple surrogate for soot, as in [2]. Narrow particle size ranges were selected using a TSI differential mobility analyzer,

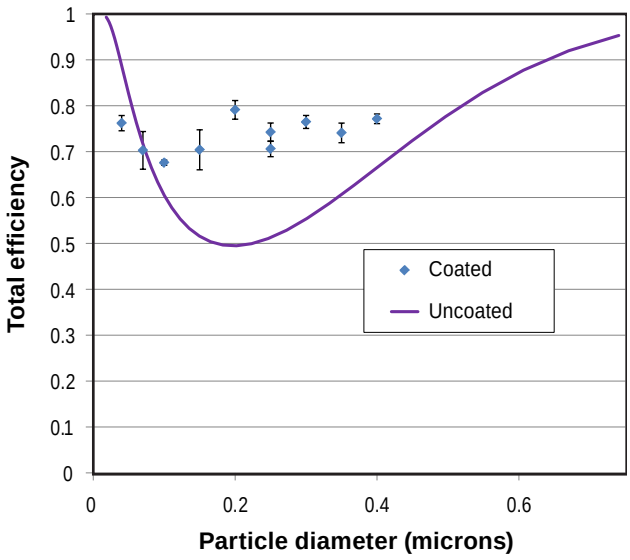

FIGURE 6. Coating on Standard DPF Substrate Improves Clean Filtration Efficiency at Intermediate Particle Sizes

and particle concentrations were measured before and after a small filter sample using TSI condensation particle counters similar to the method used in [3]. In this way, filtration efficiency could be measured as a function of particle size without building up a cake of particulates on the filter sample. As expected, filter efficiencies were lowest for intermediate sized particles. Capture efficiencies as low as 40% were observed under relevant conditions. Several techniques were explored to create coatings for enhanced filtration efficiency. A unit collector model [4] was used to fit the filter efficiency data for uncoated samples and compare to coated samples, since sample size and flow conditions were not identical. Coatings increased the filtration efficiency for intermediate particle sizes (Figure 6), at the expense of somewhat higher backpressures.

Conclusions

- The first round of cooperative experiments has yielded a number of important conclusions regarding the particulates from the SIDI test engine:
  - No nuclei mode particles were observed.
  - Particles contained elemental carbon, polycyclic aromatic hydrocarbons, and inorganics, all tightly bound together within the same fractal structures.
  - Neither thermodenuder nor evaporative chamber significantly altered particle size distributions or compositions for most conditions examined.
  - Conditions intended to mimic cold start did result in some additional organic content that could be stripped away by volatile particulate removal methods.

  - The fractal dimensions of all particles observed fell in the range 2.03-2.22.
  - Primary particle sizes changed with end of injection timing and generally fell within the range of 14-29 nm.
- TEM image analysis and advanced chemical analysis of particulates support conclusions drawn from aerosol methods:
  - Pattern of primary particle size variation with end of injection previously calculated by aggregate mobility and aerodynamic diameter seems to be borne out by direct observation.
  - A range of nano-structure was observed, but primary particles were generally less graphitic that diesel particulates.
  - Less ordered structure could imply incorporation of organic compounds during particle formation (also suggested by VPR experiments at the ERC).
  - Attenuated total reflectance Fourier transform infrared spectroscopy analysis indicates significant volume-averaged organic content.
  - X-ray photoelectron spectroscopy shows mostly elemental carbon at particle surfaces, with some surface-bound organics:
    - Taken with attenuated total reflectance Fourier transform infrared spectroscopy measurements, there is strong evidence for matrix-distributed organic content (also suggested by VPR experiments).
- Tested DPF substrates had number capture efficiencies of less than 50% for intermediate particle sizes in the absence of any particulate cake:
  - Coatings can improve clean capture efficiency at the expense of higher backpressure.

References

1. Vander Wal, R. and A. Tomasek, "Soot oxidation: dependence upon initial nanostructure". *Combustion and Flame*, 2003. 134(1-2): p. 1-9.

2. Yang, J., M. Stewart, G. Maupin, D. Herling, and A. Zelenyuk, "Single wall diesel particulate filter (DPF) filtration efficiency studies using laboratory generated particles". *Chemical Engineering Science*, 2009. 64(8): p. 1625-1634.

3. Miyairi, Y., T. Noguchi, T. Hiramatsu, S. Hirose, M. Ogawa, S. Miwa, and P. Busch, "Diesel Particulate Filter (DPF) Trapping Efficiency Improvement Under No-Soot-Layer Conditions Obtained Through Pore Size Distribution Optimization". *SAE*, 2006. 2006-01-1528.

4. Konstandopoulos, A. and J.H. Johnson, "Wall-Flow Diesel Particulate Filters - Their Pressure Drop and Collection Efficiency". *SAE*, 1989. 890405.

FY 2011 Publications/Presentations

1. Carolyn Farron, Matt Coyne, Mitch Hageman, Dave Foster, Mike Andrie, Roger Krieger, Alla Zelenyuk, Nick Matthias. "Fuel Neutral Particulate Measurements Project". Special Presentation - CLEERS teleconference. August 5, 2010.

2. Carolyn Farron, Nicholas Matthias, David Foster, Michael Andrie, Roger Krieger, Paul Najt, Kushal Narayanaswamy, Arun Solomon - General Motors, Alla Zelenyuk. "Particulate Characteristics for Varying Engine Operation in a Gasoline Spark Ignited, Direct Injection Engine". 2011 SAE World Congress and Exhibition. Detroit, MI. SAE 2011-01-1220.

3. Nicholas Matthias, Carolyn Farron, David Foster, Michael Andrie, Roger Krieger, Paul Najt, Kushal Narayanaswamy, Arun Solomon - General Motors, Alla Zelenyuk. "Particulate Matter Sampling and Volatile Organic Compound Removal for Characterization of Spark Ignited Direct Injection Engine Emissions". 2011 JSAE Powertrains, Fuels and Lubricants. Kyoto, Japan. JSAE 20119383, SAE 2011-01-2100.

4. A Strzelec, TJ Toops, CS Daw, R Vander Wal. "Trends in Particulate Nanostructure." Directions in Engine-Efficiency and Emissions Research Conference, Detroit, MI. October 2011.

Acknowledgements

General Motors Corporation: Kushal Naranayaswamy, Paul Najt, Arun Solomon, Michael Viola, Wei Li

University of Wisconsin Madison: David Foster, David Rothamer, Carrie Farron, Nicholas Matthias, Matthew Coyne, Michael Andrie, Mitchell Hageman, Roger Krieger, Axel Maier

Pennsylvania State University: Randy Vander Wal, Chethan Kumar Gaddam

PNNL: Andrea Strzelec, Josef Beranek, John Lee, Shelley Carlson, Gary Maupin, Maruthi Devarakonda, Sarah Suffield

A portion of the research was performed using Environmental Molecular Sciences Laboratory, a national scientific user facility sponsored by the Department of Energy's Office of Biological and Environmental Research and located at Pacific Northwest National Laboratory.

II.C.1 Health Effects from Advanced Combustion and Fuel Technologies

John Storey (Primary Contact), Teresa Barone, Jim Parks, Sam Lewis, Maggie Connatser
Oak Ridge National Laboratory (ORNL)
P.O. Box 2008, MS 6472
Oak Ridge, TN 37831-6472

DOE Technology Development Manager:
James Eberhardt

Overall Objectives

- Understand potential impact of developing fuel, combustion, and aftertreatment technologies on air quality and, thereby, human health.
- Ensure that byproducts of engine efficiency and alternative fuels do not result in unintended consequences limiting their future application.

Fiscal Year (FY) 2011 Objectives

- Quantify particulate matter (PM) and other air toxic emissions from direct-injection spark ignition (DISI) technologies.
- Morphological analysis of PM from advanced combustion technologies.

Accomplishments

- Completed analysis of PM emissions from both stoichiometric and lean-burn DISI vehicles operating on gasoline and ethanol blends (E0, E10 and E20):
  - Highest PM number emissions were associated with transient acceleration events; increased ethanol content reduced PM number emissions.
- Completed measurements of PM emissions from an advanced DISI engine operating on gasoline-ethanol blends:
  - The size distributions and number counts were affected by injection timing and ethanol content.
  - Transmission electron microscopy (TEM) of the particles shows solid structures as small as 10 nm.
- Completed PM emissions characterization for an engine operating in dual-fueled reactivity controlled compression ignition (RCCI):
  - RCCI PM was >95% organic carbon.
- Size distribution measurements show low particle numbers for the soot fraction, typically >20 nm.

Future Directions

Research will continue within the Advanced Combustion Technologies subprogram to assess potential emissions challenges to new combustion regimes.

Introduction

Scientists and engineers at national laboratories, universities, and industrial companies are developing new fuels and energy efficient technologies for transportation, and the U.S. DOE actively supports innovative research in these areas. However, care must be taken to ensure that any new fuel or technology developed for transportation must not adversely affect public health in a direct way or through the contamination of the environment. To address this need, DOE sponsors research studies on the potential health impacts of advanced technologies for transportation including advanced fuels, combustion techniques, and emissions controls. DOE-sponsored health impact research activities at ORNL are presented in this report.

ORNL conducts research on advanced fuel, combustion and emissions control technologies at the Fuels, Engines, and Emissions Research Center. As research is conducted to evaluate advanced engine and vehicle performance, the potential adverse health effects of the technologies are assessed by the ORNL team for DOE's Health Effects activity. Results from ongoing ORNL studies in FY 2011 are presented here. The first two tasks focused on the impact of ethanol blends on emerging gasoline vehicle technologies. PM and air toxic emissions were characterized for two light-duty DISI gasoline vehicles, as well as an ethanol-optimized DISI engine. The engine and vehicles were operated on gasoline and gasoline-ethanol blends. A second focus has been on the impact of advanced combustion regimes on the emissions of PM. PM emissions from an engine operating in the mode of dual-fuel RCCI were evaluated. For dual-fuel RCCI, the use of gasoline and diesel blends in-cylinder dampens fuel reactivity and allows control of combustion phasing. This enables the extension of advanced combustion regimes to high load operation with both low oxides of nitrogen (NOx) and low PM emissions.

Approach

PM Number Emissions from DISI Vehicles Fueled with Gasoline-Ethanol Blends

The U.S. DISI vehicle operated under stoichiometric conditions with a three-way catalyst and the European DISI vehicle operated primarily under lean-stratified conditions with a NOx trap catalyst. U.S. transient driving schedules (Federal Test Procedure [FTP] and US06), transient acceleration modes, and steady-state operation were used in the evaluation. PM mass and number concentration emissions were measured over the transient cycles; composition and size distributions were measured during steady-state operation. PM number emissions during transients were calculated based on instantaneous exhaust flows.

PM Size Distributions and Morphological Analysis for an Ethanol-Optimized DISI Engine

A 2.0-L turbocharged DISI engine equipped with port fuel injection as well as direct injection was used for this study. Engine operating parameters, including injection mode and timing, ignition timing, and variable valve timing, were tuned to investigate fuel efficiency, gaseous emissions, and particle number emissions for ethanol blend fuels. For the health effects portion of the study, we have designed an engine emissions sampling system which provides the greatest separation between gas and particle phase hydrocarbons while providing enough sample to maintain good instrument resolution. The system is a two-stage diluter with an intermediate high-temperature evaporator tube for hydrocarbon volatilization. Fuels included E0, E20, and E85, ethanol-gasoline blends of 0%, 20%, and 85%, respectively. For the morphological studies, TEM grids were collected with a specially design electrostatic collector [1], and analyzed at the ORNL High Temperature Materials Laboratory by TEM.

PM Characteristics for a Diesel Engine Operating in Advanced Combustion Mode

The first studies of dual-fuel RCCI combustion were carried out on single-cylinder research engines [2,3]. For the past two years, ORNL has extended the analysis to a 4-cylinder, General Motors production engine and broadened the operating load range to encompass the Federal Test Procedure. For the health effects portion of this study, the engine was operated at 2,300 rpm and 4.4 bar brake mean effective pressure; particle emissions were sampled using both a single-stage micro-tunnel dilution system, and the heated dual-stage system described previously. Particle number-size distributions, mass, organic carbon and elemental carbon and particle morphology were all measured for conventional diesel operation, a single direct injection of diesel fuel and split injection of diesel fuel. Split injection was hypothesized to lower emission by improving fuel-air mixing and homogeneity in the cylinder.

Results

PM Number Emissions from DISI Vehicles Fueled with Gasoline-Ethanol Blends

A comparison of particle number emissions over different engine cycles for the lean-DISI vehicle is shown in Figure 1 (a). The lean vehicle showed less variability with ethanol content than the stoichiometric vehicle [4], and the cold-start test (cold LA4[1]) shows the highest emissions which is consistent with previous studies. In Figure 1 (b), a comparison of the particle per mile emissions for the lean and stoichiometric vehicle is shown. The lean vehicle emits higher numbers of particle over all cycles which is consistent with the mass emissions results reported previously [5].

[1] Phase 1 and 2 of the FTP cycle

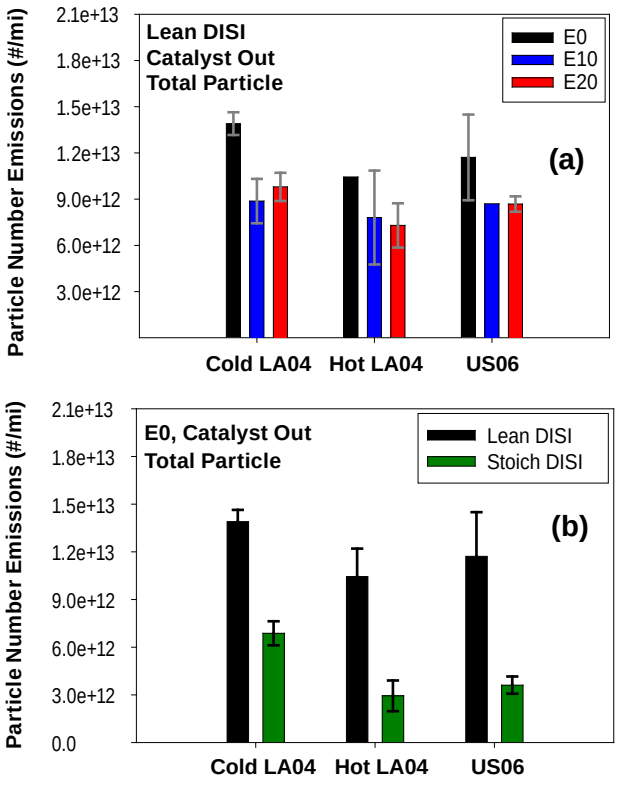

FIGURE 1. (a) PM number emissions expressed as number mile for the lean vehicle with gasoline blends (b) a comparison of the PM number emissions for the lean and stoichiometric vehicles operating on gasoline.

PM Characterization of an Advanced DISI Engine Operating on Ethanol Blends

The particle emissions produced by two fueling strategies were investigated, early injection (320 degrees before top dead center, DBTDC) and injection optimized for low particle number emissions (280 DBTDC). E20 was used for the study given the likelihood of increased ethanol content in widely available fuel. The number-size distributions of particles produced at 1,500 rpm and 8 bar were compared for early and optimized fuel injection as shown in Figure 2. Early injection resulted in about 10-20 times greater particle number concentration over all sizes (somewhat less for particles <100 nm and more for >100 nm). For reference, the size distribution from conventional light-duty diesel operation at 1,500 rpm/8 bar are given in Figure 2 as well. Comparing the three distributions, the un-optimized DISI distribution has the highest number of 100 to 500 nm particles, and thus the highest mass. In contrast, the optimized DISI injection reduces particle number below that of diesel. Because of the broad range of nanoparticles in DISI exhaust, we investigated the nature of the particles with TEM analysis.

Our TEM analysis results show single solid particles were produced at the optimum injection condition and an image of typical particles is given in Figure 3. The most abundant single solid particles were in the 10 to 15 nm range, and the second most abundant were 5 to 10 nm (Figure 2). These particles escape proposed emissions standards and have the potential to penetrate to the lower airways of the lung [6]. In addition, their high relative surface area makes them an effective vehicle for delivering biologically active compounds [7]. Using the TEM sampler collection efficiency calibration, the number-size distribution of 10 to 50 nm particles was calculated and compared with that of the scanning mobility particle sizer (Figure 4). The agreement between the TEM and scanning mobility particle sizer size distributions indicates that the majority of sub-23 nm particles, which escape the proposed emissions standards, are solid. Thus regarding nanoparticle exposures, DISI particle emissions may be more of a public health concern than diesel particle emissions. Improvements in engine design and in-cylinder fuel and air mixing can prevent nanoparticle emissions and avoid possible future barriers to technology deployment.

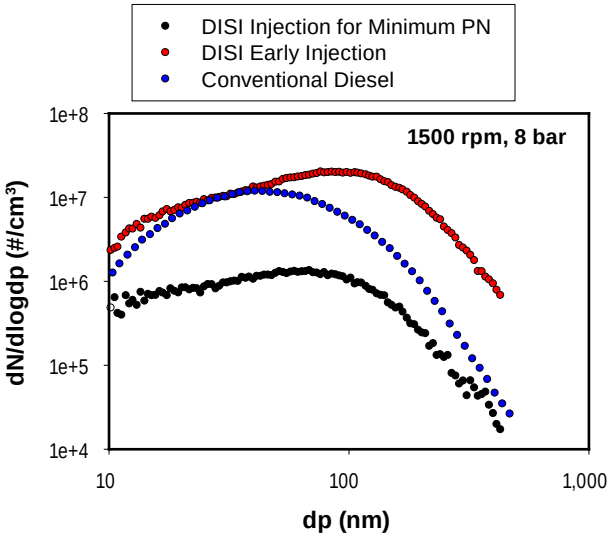

FIGURE 2. Particle number-size distributions for DISI engine emissions produced by early and optimized fuel injection at 1,500 rpm, 8 bar brake mean effective pressure. Conventional diesel particle number-size distribution for similar size engine (1.9-L), operating at the same load, is shown for comparison.

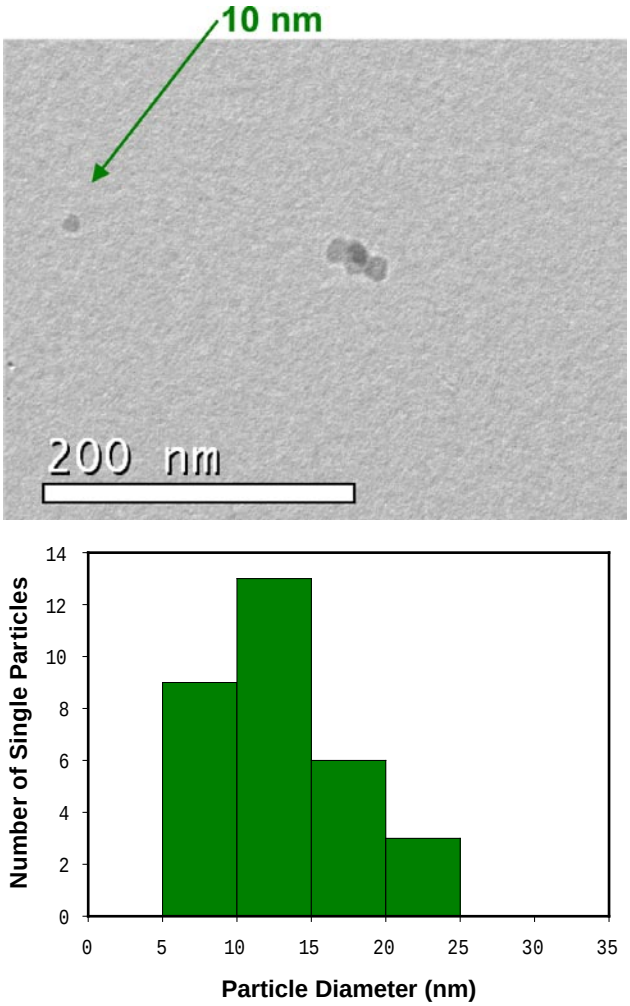

FIGURE 3. The number and size of single solid particles (non-aggregate soot) analyzed by TEM. The most abundant size was 10-15 nm. Fuel injection was optimized for low particle number emissions.

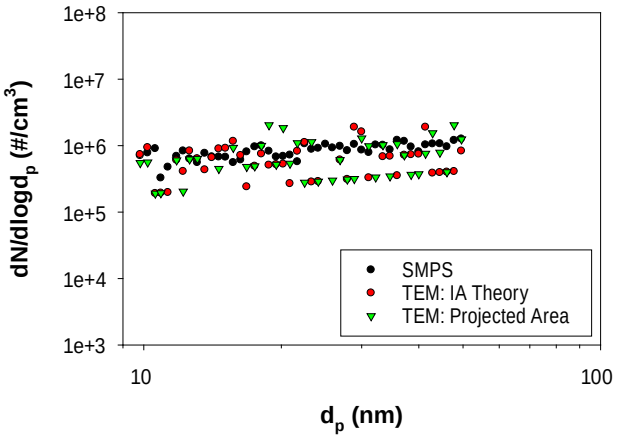

FIGURE 4. DISI number-size distributions for 10 to 50 nm particles based on scanning mobility particle sizer (SMPS) and TEM measurements for the condition in which fuel injection timing was modified for low particle number concentration emissions at 1,500 rpm and 8 bar. For aggregate mobility diameters calculated using TEM measurements, two different methods were used, idealized aggregate (IA) theory [8] and projected area equivalent diameter [9].

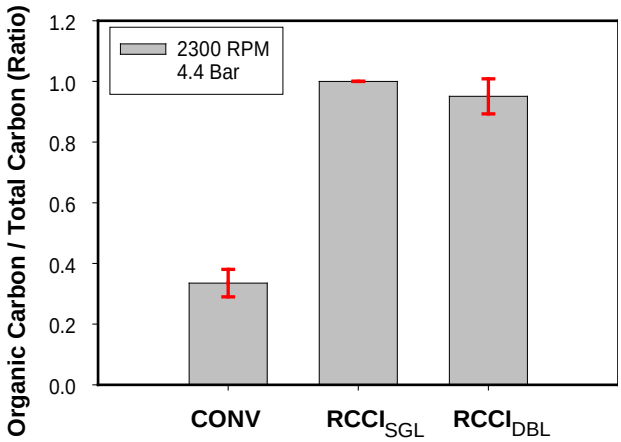

FIGURE 5. Ratio of organic to total carbon in particles collected from the emissions of a 1.9-L engine at 2,300 RPM and 4.4 bar brake mean effective pressure. Comparison for conventional diesel (CONV), RCCI with single diesel fuel injection ($RCCI_{SGL}$) and RCCI with split or double injection diesel fuel ($RCCI_{DBL}$). $RCCI_{SGL}$ particles were entirely organic carbon, while $RCCI_{DBL}$ particles had about 5% elemental carbon.

PM Characteristics for a Diesel Engine Operating in Advanced Combustion Modes

The results of this study reported last year [5] indicated that the particle mass emissions for dual-fuel combustion (0.027 ± 0.007 g/hp-hr) are much less than that for conventional diesel (0.115 ± 0.016 g/hp-hr) but are similar to pre-mixed charge compression ignition (0.028 ± 0.001 g/hp-hr). However, the smoke number is lower for the RCCI possibly indicating less elemental carbon is produced. Thus, in the current year, samples were collected for organic carbon and elemental carbon analysis, and the results shown in Figure 5 for conventional diesel, single injection RCCI, and split injection RCCI. In comparison to about 35% organic carbon in conventional diesel PM, Figure 5 shows that RCCI with single injection particles were entirely organic carbon and there was very low error associated with experiment repeatability (0.01%). Thus, a diesel oxidation catalyst may suffice for treatment of the exhaust PM from this type of operation. The results for split or double injection RCCI were similar, with the exception of about 5% elemental carbon (or soot). This difference is confirmed with size distribution measurements shown in Figure 6. Accumulation mode (>20 nm) particles were more abundant for split injection than for single injection. Diesel was input at 60 and 35 DBTDC for split injection and may have impinged on the piston crown during the second pulse. Thus, enhanced fuel and air mixing by dispersing the fuel in two pulses was most likely diminished by small pool fires that led to soot formation.

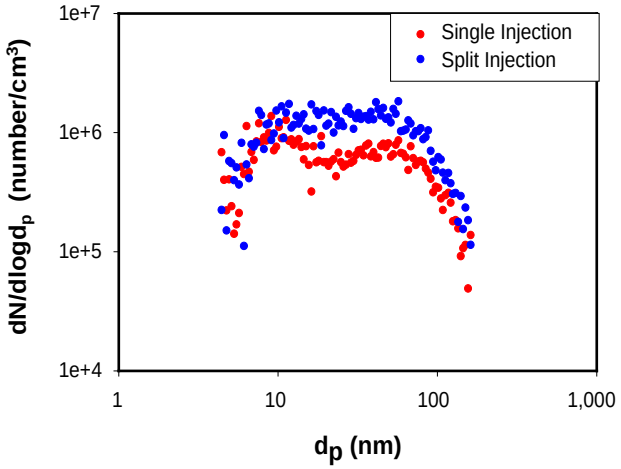

FIGURE 6. Comparison between particle number-size distributions RCCI with single diesel fuel injection and RCCI with split injection of diesel fuel. 1.9-L engine at 2,300 RPM and 4.4 bar brake mean effective pressure.

Conclusions

- DISI engines and vehicles can emit PM in significant mass and number concentrations:
  - Size distributions are broad and include solid particles <10 nm.
  - Control of PM emissions may be possible with injection timing.
- RCCI combustion results in low PM and NOx emissions:

– PM consists primarily of organic carbon making it amenable to simplified emissions control technologies.

References

1. Fierz, M., Kaegi, R., Burtscher, H., 2007. Theoretical and experimental evaluation of a portable electrostatic TEM sampler. Aerosol Science and Technology 41, 520-528.

2. Inagaki, K., Fuyuto, T., Nishikawa, K., Nakakita, K., Sakata, I., "Dual-Fuel PCI Combustion Controlled by In-Cylinder Stratification of Ignitablity," SAE Technical Paper 2006-01-0028, 2006.

3. Kokjohn, S.L., Hanson, R.M., Splitter, D.A., Reitz, R.D. "Experiments and Modeling of Dual-Fuel HCCI and PCCI Combustion Using In-Cylinder Fuel Blending," SAE Technical Paper 2009-01-2647, 2009.

4. Storey, J.M., Barone, T., Norman, K. and Lewis, S. Ethanol blend effects on direct injection spark- ignition gasoline vehicle particulate matter emissions. SAE International Journal of Fuels and Lubricants 3, 650-659.

5. Storey, J.M.E., Barone, T.L., Parks, J.E., Lewis, S.A., and Connatser, R.M. Health effects from advanced combustion and fuel technologies. *FY 2010 Advanced Combustion Technologies Annual Report,* Department of Energy, 2010b.

6. Heyder, J., 2004. Deposition of inhaled particles in the human respiratory tract and consequences for regional targeting in respiratory drug delivery. Proceedings of the American Thoracic Society 1, 315-320.

7. Nell, A., Xia, T., Mädler, L., Li, N., 2006. Toxic potential of materials at the nanolevel. Science 311, 622-627.

8. Lall, A.A., Friedlander, S.K., 2006. On-line measurement of ultrafine aggregate surface area and volume distributions by electrical mobility analysis. I. Theoretical analysis. Journal of Aerosol Science 37, 260-271.

9. Rogak, S.N., Flagan, R.C., Nguyen, H.V., 1993. The mobility and structure of aerosol agglomerates. Aerosol Science and Technology 18, 25-47.

FY 2011 Publications/Presentations

1. J.M.E. Storey, T.L. Barone, S.A Lewis, and K. Norman, "Ethanol blend effects on direct injection spark- ignition gasoline vehicle particulate matter emissions." *SAE International Journal of Fuels and Lubricants* **3,** 650-659. 2010.

2. J.E. Parks, V.Y. Prikhodko, J.M.E. Storey, T.L. Barone, S.A Lewis, M.D. Kass, S.P. Huff, "Emissions from Premixed Charge Compression Ignition (PCCI) Combustion and Affect on Emission Control Devices", *Catalysis Today*, **151**, pp. 278-284, 2010.

3. V.Y. Prikhodko, S.J. Curran, T.L. Barone, S.A. Lewis, J.M. Storey, K. Cho, R.M. Wagner, J.E. Parks, "Emission Characteristics of a Diesel Engine Operating With In-Cylinder Gasoline and Diesel Fuel Blending", Society of Automotive Engineers Technical Paper 2010-01-2266, 2010.

4. J.M. Storey, T.L. Barone, S.A Lewis, J.F. Thomas, S. Huff, K. Norman, "Measurement and Characterization of Unregulated Emissions from Advanced Technologies," *invited presentation* at Aerodyne Research, Billerica, MA. November, 2010.

5. J.M.E. Storey, T.L. Barone, S.A Lewis, J.F. Thomas, S. Huff, K. Norman, "Measurement and Characterization of Unregulated Emissions from Advanced Technologies: PM and MSATs from Direct-Injection, Spark Ignited Vehicles Operating on Ethanol Blends" *invited presentation* at The Health Effects Institute, Boston, MA. November, 2010.

6. T.L. Barone, J.M.E. Storey, V.Y. Prikhodko, S.J. Curran, J.E. Parks, R.M. Wagner, "Particle Emissions Reduction by In-Cylinder Blending of Gasoline and Diesel Fuel," CRC Real World Emissions Workshop, San Diego, CA, March 20-23, 2011.

7. T.L. Barone, J.M.E. Storey, A.D. Youngquist, J.P. Szybist, "An analysis of direct-injection spark-ignition (DISI) particle morphology." Atmospheric Environment, in press, 2011.

8. J.M.E. Storey, T.L. Barone, S.A. Lewis, J. N. Thomas, S.P. Huff, "Measurement and Characterization of Unregulated Emissions from Advanced Technologies." *presented* at the 2011 DOE Annual Merit Review, June, 2011.

9. J.M.E. Storey, Teresa L. Barone, J.N. Thomas, and Shean P. Huff, "Exhaust particle characterization for lean and stoichiometric DI vehicles operating on ethanol-gasoline blends," *under review for publication* by the Society of Automotive Engineers, September, 2011.

10. T.L. Barone, A.A. Lall, J.M.E. Storey, G.W. Mulholland, V.Y. Prikhodko, J.H. Frankland, J.E. Parks, M.R. Zachariah, "Size-Resolved Density Measurements of Particulate Emissions from an Advanced Combustion Diesel Engine: Effect of Aggregate Morphology," *Energy and Fuels*, **25,** 1978-1988. May, 2011.

II.C.2 Collaborative Lubricating Oil Study on Emissions (CLOSE) Project

Wendy Clark
National Renewable Energy Laboratory (NREL)
1617 Cole Boulevard
Golden, CO 80401

DOE Technology Development Manager:
Dr. James J. Eberhardt

Subcontractors:
- Desert Research Institute
  2215 Raggio Parkway
  Reno, NV 89512
- Elemental Analysis Inc.
  2101 Capstone Drive
  Lexington, KY 40511
- Southwest Research Institute®
  6220 Culebra Road
  San Antonio, TX 78228

Objective

The objective of this project is to quantify the relative contributions of fuels and engine lubricating oil on particulate matter (PM) and semi-volatile organic compound (SVOC) emissions from in-use motor vehicles fueled with gasoline, 10% ethanol in gasoline (E10), diesel fuel, biodiesel, and natural gas while operating with fresh and used crankcase lubricants.

Fiscal Year (FY) 2011 Objectives

Publish final results of complete emissions testing from light-, medium- and heavy-duty vehicles.

Accomplishments

All vehicle emission testing has been completed and final emissions testing results have been published.

Future Directions

This project is complete.

✧ ✧ ✧ ✧ ✧

Introduction

Air quality studies conducted in Denver, Phoenix, Washington D.C., Pittsburgh, Portland, and the Vehicle Technologies Program's Gasoline/Diesel PM Split Study in Los Angeles have shown that PM from gasoline engines is a more significant contributor to ambient air quality than PM from diesel engines [1]. For example, data collected in Washington, D.C., over a ten-year period suggest that PM from gasoline exhaust is 10 times more important to the emission inventory than diesel exhaust, as shown in Figure 1 [2,3].

The Vehicle Technologies Program's Comparative Toxicity Study demonstrated that the toxicity from gasoline exhaust on a per-unit-mass basis is at least as toxic as that from diesel exhaust, and that high emitters' toxicity is even greater than that from normal emitters [4].

Because PM and SVOC emissions from both gasoline and diesel exhaust are so important to human health and ambient air quality, it is important to understand their source – whether it derives from the fuel, the lubricant, or both, and to understand the engine operating conditions that are responsible for PM emissions.

Approach

A variety of light-, medium-, and heavy-duty vehicles have been tested over different driving test cycles at room (72°F) and cold (20°F) temperatures on

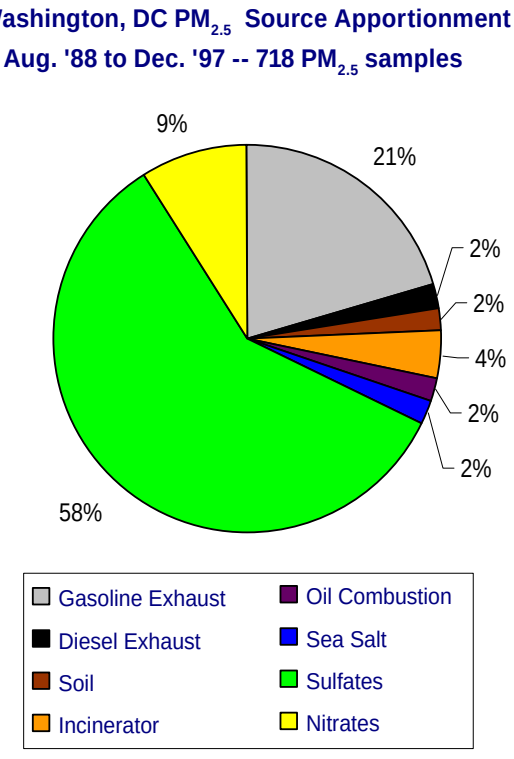

FIGURE 1. Source Apportionment of $PM_{2.5}$ in the Washington, D.C. Area, Ambient Air Quality Samples Collected between 1988 and 1997

chassis dynamometers. The test matrix depicting the vehicles and test conditions is shown in Table 1.

The engine lubricating oil used in the project was doped with deuterated hexatriacontane ($C_{36}D_{74}$). This tracer, along with other naturally occurring compounds found in lubricating oil such as hopanes and steranes, and metals used as lubricant additives, are being used to quantify the relative contributions of PM and SVOC formed from the fuels and the lubricants in the vehicles in the CLOSE Project. In addition, detailed hydrocarbon speciation of compounds found in fuels and lubricants, are used to identify the portions of exhaust produced by fuels and lubricants, which are the "parent materials" of species found in vehicle pollution.

TABLE 1. CLOSE Project Test Matrix

Test Temperature	72°F (nominal)				20°F			
Test Lubricant	Fresh		Aged		Fresh		Aged	
Vehicle/Sample Number	1	2	1	2	1	2	1	2
LD gasoline ("normal" PM emitter)	√	√	√	√	√	√	√	√
LD gasoline (high PM emitter)	√	√	√	√	√	√	√	√
LD E10 ("normal" PM emitter)	√	√	√	√	√	√	√	√
LD E10 (high PM emitter)	√	√	√	√	√	√	√	√
MD diesel ("normal" PM emitter)	√	√	√	√	√	√	√	√
MD diesel (high PM emitter)	√	√	√	√	√	√	√	√
MD biodiesel ("normal" PM emitter)	√	√	√	√	√	√	√	√
MD biodiesel (high PM emitter)	√	√	√	√	√	√	√	√
HD CNG ("normal" PM emitter)	√	√	√	√				
HD CNG (high PM emitter)	√	√	√	√				
HD diesel ("normal" PM emitter)	√	√	√	√				
HD diesel (high PM emitter)	√	√	√	√				

LD – light-duty; MD – medium-duty; HD – heavy-duty

"Normal" and high-emitting vehicles representing gasoline, diesel, and compressed natural gas (CNG)-powered vehicles have been tested. Lubricants used in each technology are representative of those currently on the market, with both new and aged lubricants being tested. The fuels used in the vehicles were gasoline containing no ethanol, E10, Texas-mandated low-emission diesel fuel, biodiesel, and CNG. Room temperature and cold temperature testing was conducted on all of the light- and medium-duty vehicles. Cold temperature testing was not conducted on the heavy-duty vehicles due to funding limitations.

The data collected throughout the study were chemically analyzed with detailed speciation to quantify the relative importance of the fuel and lubricant to PM and SVOC emissions from these vehicles under the variety of testing conditions specified in the study design.

Results

All CLOSE Project vehicle testing has been completed for all "normal" and high-emitting vehicles. Figure 2 shows the "high-emitting" natural gas heavy-duty bus that was procured by the South Coast Air Quality Management District (one of the project sponsors) and tested in the CLOSE Project, while Figure 3 shows the sampling ports and equipment used in the dilution exhaust sampling tunnel.

Polynuclear aromatic hydrocarbon (PAH) compounds were used as markers for fuel combustion

FIGURE 2. Heavy-Duty High-Emitting CNG-Powered Heavy-Duty Bus Tested in the CLOSE Project

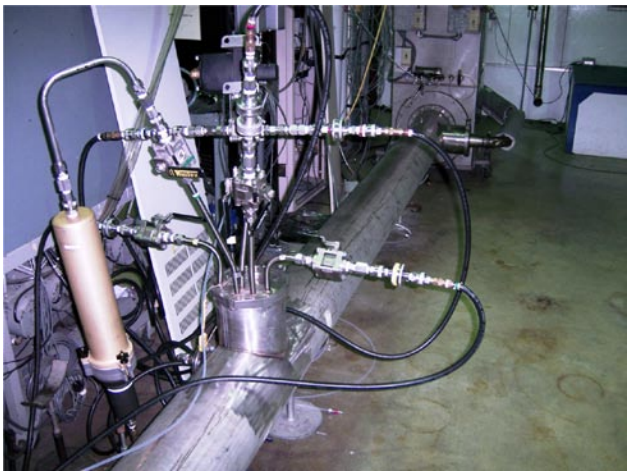

FIGURE 3. Sampling Probes used to Collect Exhaust Emissions Samples from the Dilution Tunnel

products; however, for vehicles with normally functioning exhaust catalysts, the PAH levels were too low for the measurement technique, and thus uncertain data were obtained. Normal emitters also have much higher ratios of fuel consumed to lubricant consumed compared to high emitters. The reduced certainty of the derived PM allocations from normal emitters may also be due to confounding of fuel and lubricant derived markers. In general, as indicators, PAHs accounted for less than one percent of organic carbon (OC) emitted.

Results of measurements showed that unburned crankcase lubricant made up 60 to 90 percent of measured OC emissions from this small sample of on-road vehicles. These results were consistent across the four vehicle types and all fuels. This organic carbon represented 20 to 50 percent of all emitted PM, except for the normal emitting light-duty gasoline passenger car (OC was <10 percent of PM) and the heavy-duty natural gas-fueled transit bus (OC was >90 percent of PM).

The OC fraction of PM for the four compression ignition diesel vehicles was less than for the two spark ignition natural gas buses and the high emitter spark ignition gasoline light-duty passenger car. However, overall OC mass emissions rates for the four diesel vehicles were up to an order of magnitude higher than from the normal emitter spark ignition light-duty gasoline-fueled passenger car. The high PM emitter spark ignition vehicle had OC emissions rates comparable to the four diesel-powered vehicles.

Normally functioning three-way catalysts are effective at reducing most of the OC. With high PM emitters or vehicles with deteriorated aftertreatment, high molecular weight fuel components and unburned lubricant were emitted at higher rates (one to two orders of magnitude) than in vehicles in proper engine repair and functioning emissions systems. In most cases, over 75 percent of lubricating oil components were combusted or converted across exhaust catalysts.

For the normally operating light-duty gasoline and medium-duty diesel vehicles and for both heavy-duty natural gas vehicles, fresh oil produced more particles than aged oil. The opposite trend occurred with the light- and medium-duty high PM emitters. This effect was not readily apparent with the heavy-duty diesel vehicles. One explanation could be that, since the lubricant represented a much smaller fraction of the total PM (around 20 percent) in the HD diesel vehicles, the effect was lost in the precision of the testing methodology.

In many cases, emitted PM was incompletely accounted for with chemical analyses. It is possible that some fraction of unburned and/or partially combusted fuel and oil, or some polar fraction of PM, was not measured with the analytical techniques used in this project.

Conclusions

- Normally functioning emission control systems for gasoline light-duty vehicles are very effective at controlling OC emissions.
- Diesel vehicles without aftertreatment emission control systems have OC emissions approximately one order of magnitude higher than gasoline vehicles with normally functioning emission control systems.
- Exhaust catalysts combust or convert over 75 percent of lubricating oil components in the exhaust gases.
- High emitter gasoline vehicles can have OC emissions similar to diesel vehicles without exhaust aftertreatment emission control.

Future Directions

Follow-up studies should assess the methods of PM allocations used in this study on vehicles representing the diverse spectrum between normal emitters and high emitters, and should estimate the precision of the allocations obtained by running multiple analyses. Vehicles should be tested with fuels without hopanes and steranes in order to help clarify the potential confounding (or lack thereof) when markers are parented by both fuel and lubricant. Studies should be conducted to understand the relative frequency of various types and intensities of 'high emitters' to facilitate modeling of the on-road vehicle fleet.

Future work could consider testing emissions from diesel vehicles equipped with normally functioning particle filters to determine if this type of aftertreatment system produces similar results. Also, it would be informative to utilize the latest engine and emissions system hardware for all the vehicles to determine if the considerable efforts by regulators and vehicle and engine manufacturers have impacted PM levels. Noting that aged lubricants sometimes produce less PM than fresh oil, it would be interesting to investigate the effects of base oil volatility and type (i.e., mineral-based versus synthetic) on PM and SVOC formation.

References

1. Fujita, E.M., D.E. Campbell, W.P. Arnott, B. Zielinska, J.C. Chow. Evaluations of Source Apportionment Methods for Determining Contributions of Gasoline and Diesel Exhaust to Ambient Carbonaceous Aerosols, *J. Air & Waste Manage. Assoc.*, Vol. 57, pp. 721-740 (2007).

2. Kim, E. and P. K. Hopke. Source Apportionment of Fine Particles in Washington, DC, Utilizing Temperature-Resolved Carbon Fractions, *J. Air & Waste Manage. Assoc.*, Vol. 54, pp. 773-785 (2004).

3. Lough, G.C. and J.J. Schauer. Sensitivity of Source Apportionment of Urban Particulate Matter to Uncertainty in Motor Vehicle Emissions Profiles, G.C. Lough and J.J. Schauer, *J. Air & Waste Manage. Assoc.*, Vol. 57, pp. 1200-1213 (2007).

4. McDonald, J.D., I. Eide, J.C. Seagrave, B. Zielinska, K. Whitney, D.R. Lawson, J.L. Mauderly. Relationship between Composition and Toxicity of Motor Vehicle Emission Samples, *Environ. Health Persp.,* Vol. 112, pp. 1527-1538 (2004).

FY 2011 Publications/Presentations

1. "The Collaborative Lubricating Oil Study on Emissions (CLOSE) Project," progress reports presented at CRC AVFL program review meetings February, May and October 2010.

2. "The Collaborative Lubricating Oil Study on Emissions (CLOSE) Project," presented at DOE Annual Merit Review Meeting, Washington, D.C.; May 2011.

"COLLABORATIVE LUBRICATING OIL STUDY ON EMISSIONS (CLOSE) FINAL REPORT," James N. Carroll, Imad A. Khalek, and Lawrence R. Smith, Department of Emissions R&D, Southwest Research Institute, and Eric Fujita, Barbara Zielinska, Desert Research Institute, August 2011.

II.C.3 The Advanced Collaborative Emissions Study (ACES)

Dan Greenbaum (Primary Contact),
Rashid Shaikh, Maria Costantini,
Annemoon van Erp
Health Effects Institute (HEI)
101 Federal Street, Suite 500
Boston, MA 02110

DOE Technology Development Manager:
James Eberhardt

NETL Project Manager: Carl Maronde

Subcontractors:
- Coordinating Research Council (CRC), Alpharetta, GA
- Lovelace Respiratory Research Institute (LRRI), Albuquerque, NM

Overall Objectives

- **Phase 1**: Extensive emissions characterization at Southwest Research Institute® (SwRI®) of four production-intent heavy duty diesel engine and control systems designed to meet 2007 standards for particulate matter (PM) and nitrogen oxides (NOx). One engine/aftertreatment system will be selected for health testing.
- **Phase 2**: Extensive emissions characterization of a group of production-intent engine and control systems meeting the 2010 standards (including more advanced NOx controls to meet the more stringent 2010 NOx standards).
- **Phase 3**: One selected 2007-compliant engine will be installed and tested in a specially-designed emissions generation and animal exposure facility at the LRRI (Phase 3A) and used in chronic and shorter-term health effects studies to form the basis of the ACES safety assessment (Phases 3B and 3C). This will include periodic emissions characterization during both a core 24-month chronic bioassay of cancer endpoints in rats and biological screening assays in both rats and mice (Phase 3B) as well as emissions characterization during a set of shorter animal exposures and biological screening using accepted toxicological tests after the end of the chronic bioassay (Phase 3C). (NOTE: Only the emissions characterization and biological screening activities during Phase 3 are components of the DOE ACES contract).

Fiscal Year (FY) 2011 Objectives

- **Phase 2**: Plan emissions characterization at SwRI®of production-intent engine and control systems meeting the 2010 standards. Negotiate with and finalize engine manufacturers to participate in Phase 2.
- **Phase 3**: Complete Phase 3A Emissions Characterization report and short-term exposures in mice and rats. Conduct expert peer review of the final reports describing those short-term results. Continue the long-term exposures in rats and conduct and intensive exposure characterization campaign during the first months of animal exposures.

Accomplishments

Key Accomplishments

- Received a revised final report with results of Phase 3A, which will be published in early 2012. Completed shorter-term bioscreening studies in mice and rats (Phase 3B) and received five draft final reports with those results that entered a rigorous peer review process.
- Agreed on protocols, company participation, and costs for Phase 2 Emissions Characterization of 2010-compliant engines.

General Oversight

- Conducted the first Phase 3B investigator and stakeholder workshop in Chicago, IL (November 2010).
- Held a second Phase 3B investigator and stakeholder workshop to discuss the results from short-term biological screening in rats and mice, including results from the first two intensive emissions characterizations (April 2011).
- Presented Phase 3B short-term biological screening results at the HEI Annual Conference (May 2011).
- Presented progress in ACES at the DOE Annual Merit Review (May 2011).

Phase 2

- Continued detailed planning of the Phase 2 comprehensive emissions characterization for Class 8 engines (October 2010-September 2011).
- Agreed on a statement of work and solicited a proposal from SwRI®, the previously selected contractor for Phases 1 and 2 (December 2010).
- Received a proposal for Phase 2 SwRI® (January 2011).

- Reviewed the proposal for Phase 2 with CRC and its technical panel (February 2011).
- Communicated the final scope of work and list of compounds to be measured to the investigators at SwRI® (April 2011).
- Three engine manufacturers were confirmed to participate (April 2011).
- Received a revised statement of work and budget from SwRI® and sent the materials to the CRC technical panel for their review (May 2011).
- Received a revised cost estimate from SwRI® with options for substantial cost savings measures and shared it with the CRC technical panel (June 2011).
- Approved the cost estimate with a decision to exercise all cost savings, i.e. eliminating Federal Test Procedure testing without crankcase blowby, California Air Resources Board cycle testing, and unnecessary tunnel blanks. Continued to look for additional funding to include California Air Resources Board cycle testing, if possible (June 2011).
- Began to finalize plans and budget for Phase 2 (July 2011).
- Received a final budget estimate from SwRI® for Phase 2 and initiated a contract to start Phase 2 in the fall of 2011 (August 2011).

Phase 3A

- Requested a further revised report with results from Phase 3A (characterization of engine emissions and exposure atmospheres in the inhalation chambers at LRRI) (November 2010).
- Received a final revised report with results from Phase 3A (September 2011).

Phase 3B

- Completed the second of four detailed chemical characterizations of exposure atmospheres at LRRI and completed the *short-term* engine technology bioscreening exposures for the chronic inhalation study at LRRI (January 2011).
- Continued engine technology bioscreening exposures of rats for the *chronic* inhalation study at LRRI and completed the first 12 months of the long-term exposure study (May 2011).
- Shared results of two intensive exposure characterizations with members of the HEI ACES Oversight Committee for their feedback (May 2011).
- Communicated feedback on the intensive exposure characterizations to the LRRI team (June 2011).
- Received the first draft final report with Phase 3B short-term biological screening results on genotoxicity (by Dr. Bemis at Litron Laboratories) (June 2011).
- Terminated one of the five Phase 3B ancillary studies of genotoxicity due to technical problems and retirement of the principle investigator (Dr. Veranth at the University of Utah) (June 2011).
- Received a second draft final report with Phase 3B short-term results on core pathology and lung inflammation (by Dr. McDonald at LRRI) and sent both the draft reports by Drs. Bemis and McDonald to the Special Review Panel for rigorous peer review (July 2011).
- Received three additional draft final reports with Phase 3B short-term results on vascular effects (by Dr. Conklin at the University of Louisville and Dr. Sun at Ohio State University) and genotoxicity (by Dr. Hallberg at the University of Texas) and sent the draft reports to the Special Review Panel for rigorous peer review (August 2011).
- Distributed samples from the 12-month exposures to investigators for toxicological analyses (August 2011).
- Held a Special Review Panel meeting to review the five draft final reports with Phase 3B short-term biological screening results (September 2011).

Future Directions

Phase 2

- Conduct and complete Phase 2 characterization of 2010-compliant engines; the expectation is that testing will start in January 2012.

Phase 3

- Expose rats for 24 or 30 months at three selected diesel exhaust exposure concentrations (high, medium, and low) or clean air (2011 and part of 2012).
- Publish the final report with results from Phase 3A as an HEI Publication (Winter 2012).
- Receive revised final reports from biological screening in rats and mice from all Phase 3B investigators and publish them as HEI Publications in the Spring of 2012).
- Conduct combined investigator and stakeholder workshops to discuss progress in Phase 3B.

Introduction

The ACES is a cooperative, multi-party effort to characterize the emissions and assess the safety of advanced heavy-heavy duty diesel engine and aftertreatment systems and fuels designed to meet the 2007 and 2010 emissions standards for PM and

NOx. The ACES program is being carried out by HEI and the CRC. It is utilizing established emissions characterization and toxicological test methods to assess the overall safety of production-intent engine and control technology combinations that will be introduced into the market during the 2007-2010 time period. This is in direct response to calls in the U.S. Environmental Protection Agency (EPA) Health Assessment Document for Diesel Engine Exhaust [1] for assessment and reconsideration of diesel emissions and health risk with the advent of new cleaner technologies.

The characterization of emissions from representative, production-intent advanced compression ignition engine systems will include comprehensive analyses of the gaseous and PM, especially those species that have been identified as having potential health significance. The core toxicological study will include detailed emissions characterization at its inception, and periodically throughout a two-year chronic inhalation bioassay similar to the standard National Toxicology Program bioassay utilizing two rodent species. Other specific shorter-term biological screening studies also will be undertaken, informed by the emissions characterization information, to evaluate these engine systems with respect to carefully selected respiratory, immunologic, and other effects for which there are accepted toxicologic tests. It is anticipated that these emissions characterization and studies will assess the safety of these advanced compression ignition engine systems, will identify and assess any unforeseen changes in the emissions as a result of the technology changes, and will contribute to the development of a data base to inform future assessments of these advanced engine and control systems.

Approach

Experimental work under ACES is being conducted in three phases, as outlined in the Objectives. Detailed emissions characterization (Phases 1 and 2) is performed by an existing engine laboratory (SwRI®) that meets the U.S. Environmental Protection Agency specifications for 2007 and 2010 engine testing. In Phase 1, emissions from four 2007-compliant engine/control systems have been characterized. One engine has been selected for health testing in Phase 3. In Phase 2, emissions from four 2010-compliant engine/control systems will be characterized. In Phase 3, the selected 2007-compliant engine/control system has been installed in a specially designed emission generation facility connected to a health testing facility at LRRI to conduct a chronic inhalation bioassay and shorter term biological screening in rats and mice. During the two-year bioassay, emissions will be characterized at regular intervals throughout the testing.

The emissions characterization work is overseen by CRC and CRC's ACES Panel. The health effects assessment is overseen by HEI and its ACES Oversight Committee (a subset of the HEI Research Committee augmented by independent experts from several disciplines), with advice from an Advisory Committee of ACES stakeholder experts. The overall effort is guided by an ACES Steering Committee consisting of representatives of U.S. Department of Energy, engine manufacturers, EPA, the petroleum industry, the California Air Resources Board, emission control manufacturers, and the Natural Resources Defense Council. Set-up of the emission generation facility at LRRI (for Phase 3) and establishment of periodic emissions characterization throughout Phase 3 has been done with input from the team of investigators who conducted Phase 1 and the CRC ACES Panel.

Results

The results obtained during this reporting period pertain to the ongoing Phase 3B animal exposures. Daily analysis of exposure atmospheres shows that the 2007-compliant engine system has been operating reliably and has consistently provided the targeted exposure concentrations (at 4.2, 0.8, and 0.1 ppm of NO_2; see Table 1). However, in the summer of 2011 it became apparent that the specially-designed 16-hour test cycle is taking a toll on the engine and dynamometer. As a result, the back-up engine and back-up dynamometer have been installed and the original engine and dynamometer have been sent out for repair.

TABLE 1. Summary of Mean Concentrations of Major Constituents (-CO_2 /H_2O) of Exposure Atmospheres for Rats (Daily Measurements)

	Rat Exposure (Average)		
	High Mean	**Mid Mean**	**Low Mean**
Gases:			
NO_2 (ppm)	3.6	0.95	0.11
NO (ppm)	5.1	1.47	0.15
NO_x (ppm)	8.6	2.41	0.26
CO (ppm)	11	n/a	n/a
THC (ppm)	0.3	n/a	n/a
PM ($\mu g/m^3$):			
DPM: Chamber Inlet (filter)	13	4	2
PM: Chamber (filter)	32	30	27

THC – total hydrocarbons; DPM – diesel particulate matter

Two intensive exposure characterizations have provided additional detailed information on the exposure atmospheres. Particle concentrations in the exposure chambers are very low, and only noticeable during trap regeneration, which takes place on average once and sometimes twice per day. Figure 1 illustrates

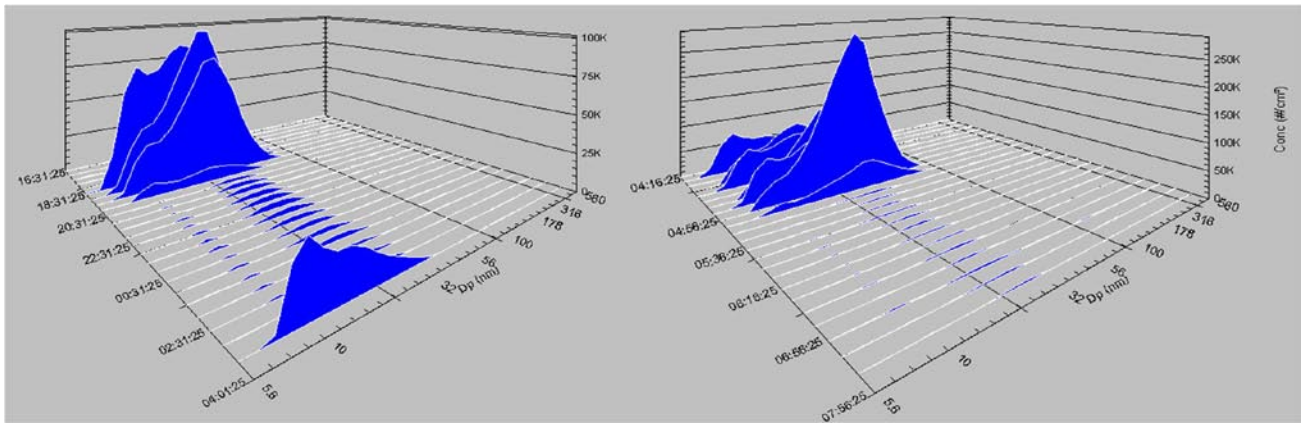

FIGURE 1. Particle Size Distribution at the High Exposure Level Chamber, April 12 2010

particle distributions in the high diesel concentration exposure chamber, with two trap generations that day.

These results are included in the LRRI Phase 3B report on short-term exposures in rats and mice.

There were no exposure-related differences in mortality or clinically-evident morbidity in mice or rats after one or three months of exposure. Among the more than 100 biological response variables evaluated, the great majority showed no significant difference from control as a result of exposure to diesel exhaust. There was an observation of early (mild) lung remodeling in the rats (Table 2), accompanied by some changes in inflammatory markers and subtle changes in respiratory function. In general, statistically significant effects were observed only at the highest exposure level, however. The mice had fewer responses than the rats.

TABLE 2. Incidence of Selected Lung Findings in Male and Female Wistar Han Rats after 13 Weeks of Diesel Exhaust Exposure

Male Lung	Control	Low	Mid	High
Hyperplasia Epithelium Periacinar	0/10	0/10	0/10	10/10
Accumulation Macrophage	0/10	0/10	0/10	3/10
Fibrosis Interstitial	0/10	0/10	0/10	4/10
Female Lung	**Control**	**Low**	**Mid**	**High**
Hyperplasia Epithelium Periacinar	0/10	0/10	0/10	9/10
Accumulation Macrophage	0/10	0/10	0/10	3/10
Fibrosis Interstitial	0/10	0/10	0/10	2/10

The primary importance of these early interim results is their demonstration that: 1) the great majority of health tests showed no effect of exposure; 2) several plausibly coherent responses may indicate early, exposure-related, subclinical impacts on lung inflammation, structure, and function of rats; 2) statistically significant effects were observed primarily at the highest exposure level (the lowest level has produced no observable effects to date); and 3) mice are less responsive than rats to three months of exposure.

Conclusions

Short-term exposure of mice and rats to emissions from a 2007-compliant engine were completed successfully and biological assays were completed during the winter of 2011. Preliminary results indicate few effects although there are some mild exposure-related changes in biological endpoints after one and three months of exposure, potentially due to the NO_2 exposure. These effects were seen mostly in rats and only at the highest concentration of diesel exhaust. Continued exposure will show whether these mild effects persist after 12 months of exposure. All this work has been conducted with input from the ACES stakeholders.

References

1. U.S. Environmental Protection Agency. 2002. Health Assessment Document for Diesel Engine Exhaust. EPA/600/8-90/057F. U.S. Environmental Protection Agency, National Center for Environmental Assessment, Office of Research Development, Washington, D.C.

FY 2011 Publications/Presentations

1. Platform and poster presentations at the HEI Annual Conference in Boston MA, May 2011:

- "Micronucleated Reticulocytes as an Indicator of Genotoxicity Following Exposure to Diesel Exhaust" (PI Bemis - poster).
- "Effects of Diesel Emissions on Vascular Inflammation" (PI Conklin - poster).

- "Assessment of the Genotoxicity of Diesel Exhaust/ Diesel Exhaust Particulates from Improved Diesel Engines" (PI Hallberg - poster).
- "Phase 3B Update: Summary of 1 and 3 Month Exposures" (PI McDonald - platform).
- "ACES Phase 3: 4 and 13 Week Results from Rats and Mice Exposed to 2007 Compliant Diesel Emissions" (PI McDonald – poster).
- "Diesel Exhaust Exposure and Cardiovascular Dysfunction: Part of ACES Phase 3" (PI Sun - poster).
- "Lung Cell Gene Transcription Responses to Diesel Particulate" (PI Veranth - poster).

2. Platform presentation at the annual DOE Vehicle Technologies Program Annual Merit Review, Washington DC, June 2011: "Advanced Collaborative Emissions Study (ACES)."

3. Platform presentations at the Directions in Engine-Efficiency and Emissions Research (DEER) conference in Dearborn MI, September 2010: "ACES Phase 3: 4 and 13 Week Results from Rats and Mice Exposed to 2007 Compliant Diesel Emissions, " and "Status of Phase 2 of the Advanced Collaborative Emissions Study (ACES)."

4. Published an article in the Zentralblatt für Arbeitsmedizin, Arbeitsschutz, und Ergonomie (German journal for occupational medicine), December 2010, "Current Status of the Toxicology of Diesel Engine Exhaust – and the ACES Project."

5. Published results from Phase 1 (emissions testing of the 2007-compliant engines at SwRI) in the Journal of the Air & Waste Management Association, March 2011.

III. SOLID STATE ENERGY CONVERSION

III.1 High Efficiency Thermoelectric Waste Energy Recovery System for Passenger Vehicle Applications

John LaGrandeur[1] (Primary Contact), Douglas Crane[1], Vladimir Jovovic[1], Clay Maranville[2], Boris Mazar[3], Klaus Heller[3], Ed Kinnaird[4]

[1] Amerigon, INC
5462 Irwindale Avenue
Irwindale, CA 91706

[2] Ford Motor Company
Research & Innovation Center
Room 2417, MD 3182
2101 Village Road
Dearborn, MI 48124

[3] BMW AG
80788 Munich
Germany

[4] Faurecia
1050 Wilshire,
Suite 200
Troy, MI 48084

DOE Technology Development Manager:
John Fairbanks

NETL Project Manager: Carl Maronde

Subcontractors:
- BMW of North America, LLC
- Ford Motor Company, Dearborn, MI
- Faurecia, Troy, MI and Columbus, IN

Fiscal Year (FY) 2011 Objectives

The primary objectives of 2011 were to complete the build and test of a high temperature cylindrical thermoelectric generator (TEG) subsystem, followed by integration and test in BMW and Ford vehicles. The design of the TEG subsystem included integration into the underfloor exhaust system of the target vehicles using a bypass valve built into the in-out section of the exhaust. Objectives for 2011 also include:

- Improving on the 1st cylindrical TEG manufacturing process and tooling to improve the TEG performance.
- Selecting TE materials for commercialization.
- Defining key characteristics of the thermoelectric (TE) engines required for manufacturing readiness.

Accomplishments

Two fully functional high temperature cylindrical TEGs were built using improved tooling with minor design modifications over the 2010 prototype and tested at Amerigon. The TEG produced over 700 watts of electric power in bench tests with exhaust gas temperatures in the range of nominal operation as defined by the project partners (~620°C). Hot side temperatures in the TE engines reached approximately 450°C.

Following extensive test and characterization on the bench at Amerigon, the TEGs were fitted into BMW and Ford vehicle exhaust systems and operated over extended periods of time including over 3,000 miles of road testing by BMW. Power produced in driving conditions reached over 600 watts in road testing, which could provide a significant improvement in fuel efficiency during a highway operational profile.

The TEG-equipped exhaust systems performed as predicted by the simulation tools developed for the project (a key result) and demonstrated a level of robustness, evidenced by day-over-day repeatable performance that exceeded the expectations of the project partners.

Future Directions

The project formally concluded on 30 September, 2011. In the fourth quarter, 2011 Amerigon and its partners Ford, BMW, Faurecia and Caltech began a subsequent DOE-funded project to make ready for commercialization TE materials and engines leading to an initial commercialization at an annual run rate starting at 100,000 vehicles annually.

Approach

The prototype TEG design is shown in Figure 1.

Exhaust gas enters from the left, passes through the TEG system, and exits to the right. In normal operation, the valve on the outlet side (right) is closed so that gas is prevented from passing through the central (bypass) region of the heat exchanger subassembly. At high flow rates passing all the exhaust gas through the heat exchanger would raise backpressure above the limit for optimal engine operation and expose the thermoelectric materials to potentially harmful temperatures. The valve allows excess exhaust gas flow to bypass the heat exchanger reducing backpressure to within allowable limits. The valve, designed and implemented by project partner, Faurecia, has proportional control so that the maximum available thermal power in the exhaust stream can be utilized. Similarly, the valve position is adjusted to prevent the TE system from exposure to the

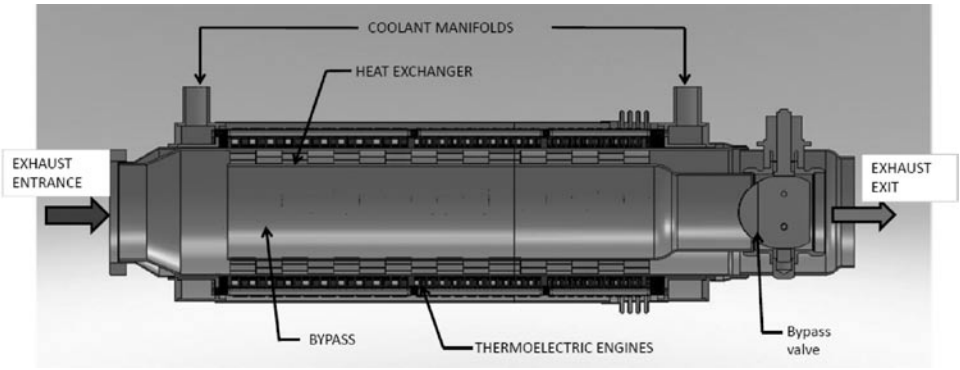

FIGURE 1. Cross Sectional View of Waste Heat Recovery Thermoelectric Generator

excess temperatures experienced during extreme driving conditions. The thermal power collected by the heat exchanger fins is conducted through the cylinder wall to hot side shunts. The shunts are electrically isolated from the cylinder. Thermal power flows from the hot side shunts through the TE elements to the cold side shunts. Sleeve assemblies transfer waste thermal power to the coolant through tubes which are electrically isolated from the cold side shunts. The coolant enters a manifold at the right side, passes through an array of tubes and is collected at the left before exiting the system. In the test vehicles equipped with TEG systems, the coolant was an ethylene glycol mixture with water and is part of the powertrain coolant circuit.

Two TEGs were built comprising Half Heusler (HH) and bismuth telluride (BiTe) TE materials. In the higher temperature sections of the TEG, TE engines included segmented HH/BiTe elements. In the cooler portion of the TEG, BiTe was used singularly in the TE engines.

Results

Bench testing was performed at Amerigon's Irwindale Laboratories for approximately six weeks. TEG performance was characterized over a wide range of temperatures using a hot air test system.

Peak power produced on the Amerigon test bench exceeded 700 watts. Many tests were performed simulating a wide range of fixed and transient operating conditions. Following bench testing at Amerigon, the TEGs were delivered to Ford and BMW for installation into Lincoln MKT and X6 exhaust systems for vehicle evaluation. In BMW's X6, the exhaust bypass valve was controlled using closed-loop control, and TEG data displayed on the vehicles with a built-in display. In Ford's testing, the exhaust bypass was controlled using open-loop control and the power was shunted to a load resistor to obtain precise power production data.

The TEG installation into BMW's X6 exhaust system is shown in Figure 2, with exhaust lines thermally insulated upstream from the TEG.

BMW's vehicle installation of the TEG included full integration with the vehicle exhaust and cooling systems, a closed-loop automated control strategy for the exhaust valve and water pump and TEG visualization concept integrated into the vehicle display. Power produced in the BMW X6 test vehicle vs. driving speed is shown in Figure 3.

Ford's vehicle installation of the TEG on the Lincoln MKT was done behind the after treatment system in the center tunnel, just beneath the drive shaft. The installation also incorporated an auxiliary electric water pump. The installation is shown in Figure 4.

FIGURE 2. BMW X6 TEG Installation, Courtesy of the BMW Group

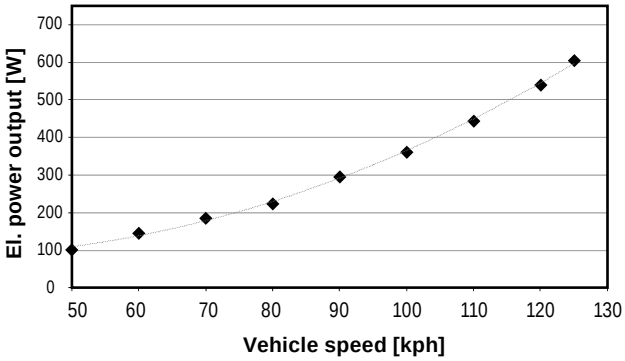

FIGURE 3. TEG Electric Power Produced vs. Driving Speed in the BMW X6

FIGURE 4. TEG Installation in the Ford Lincoln MKT

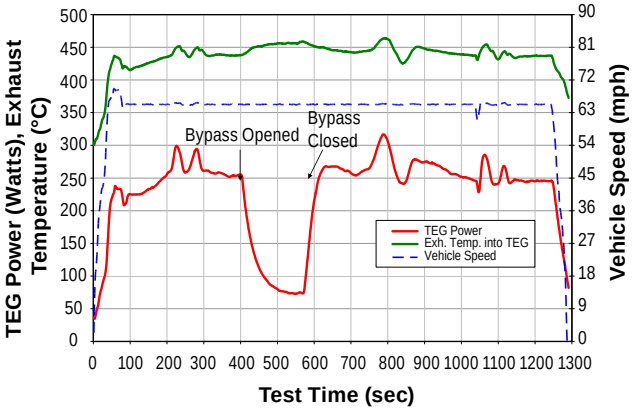

FIGURE 5. 65 MPH Freeway Cruise Data, Courtesy of Ford Motor Company

Test results from Ford's testing are shown in Figures 5 and 6 for highway and city driving conditions.

Conclusions

Amerigon and its partners BMW, Ford and Faurecia successfully concluded the DOE-funded TEG project with vehicle level evaluations of TE exhaust gas heat to power in one each BMW and Ford vehicles.

A cylindrical TEG was modeled, designed, built and tested by Amerigon incorporating proprietary stack design TE engines. The hot side temperature of the engines reached ~450°C, and the TEGs continue to provide stable performance after six months of testing and vehicle operation including over 3,000 miles of road testing by BMW. These results validate the stack design TE engines and cylindrical form factor pioneered by Amerigon.

Static and dynamic TEG computer performance models using MATLAB®/Simulink® were validated in the effort providing vehicle system designers an

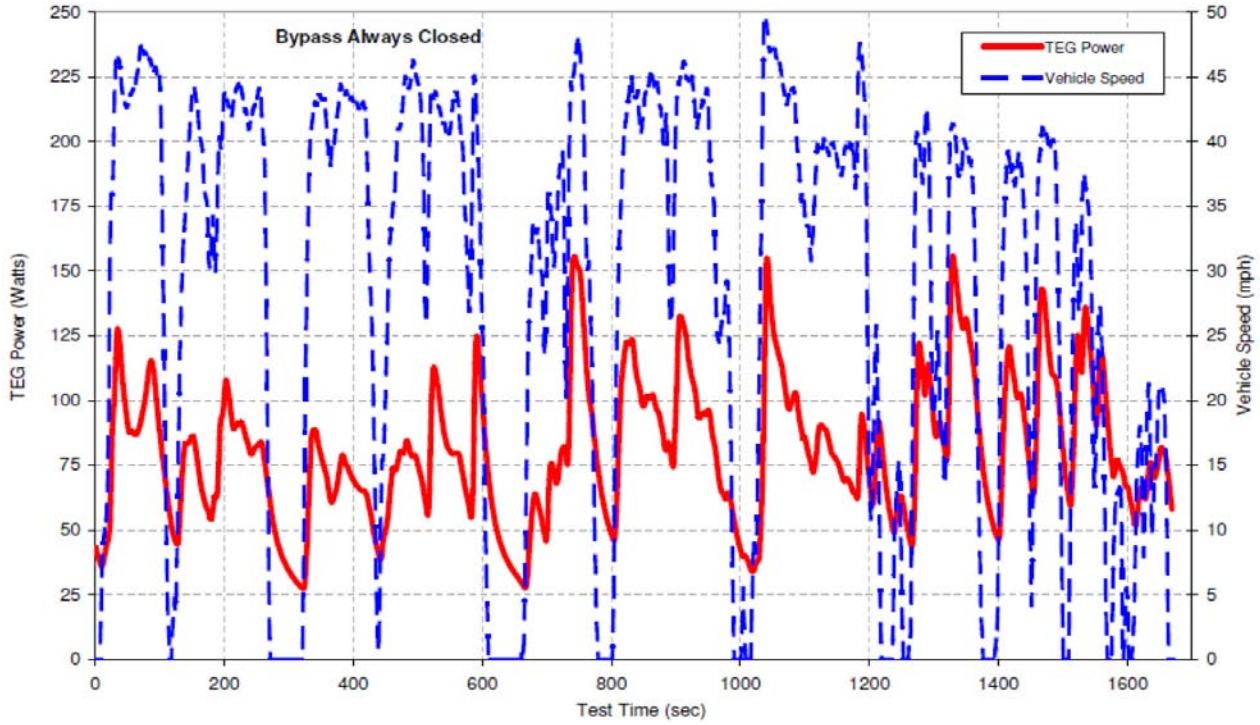

FIGURE 6. City Driving Performance, Courtesy of Ford Motor Company

important tool in the design and optimization of future systems utilizing TEG technology.

While the cylindrical TEG performance was stable and met modeling predictions, several issues were identified that need to be addressed in subsequent work. These issues include:

1. A reduction in the number of parts is needed to simplify and lower the cost of manufacturing.
2. TE materials need to be protected from atmospheric corrosion and in a related area, the volume required for hermetic enclosure needs to be reduced to insure long life and stable performance.
3. The voltage output of the TEG needs to be increased to provide a more effective integration with the vehicle's power buss.
4. Lower cost TE materials with appropriate technologic maturity and intrinsic low cost potential need to be identified and developed. Skutterudite TE materials have emerged as a promising candidate material as they possess a maturity level in terms of performance, contact metallization and low cost elements compared to tellurium-based chemistries and the currently used half-Heusler materials.

FY 2011 Publications/Presentations

1. Crane, D.T., LaGrandeur, J., Bell, L.E., "Status of Segmented Element Thermoelectric Generator for Vehicle Waste Heat Recovery", Thermoelectric Applications Workshop, San Diego, CA, 1/3/11.

2. Crane, D.T., *An Introduction to System-Level, Steady-State and Transient Modeling and Optimization of High-Power-Density Thermoelectric Generator Devices Made of Segmented Thermoelectric Elements*, Journal of Electronic Materials, Vol. 40, No. 5, May 2011, p 561 – 569.

3. Crane, D.T., Koripella, C.R. , Jovovic, V., "Validating Steady-State and Transient Modeling Tools for High Power Density Thermoelectric Generators", International Conference on Thermoelectrics, Traverse City, MI, July 2011.

4. Jovovic, V., Heian, E., Harris, F., Crane, D.T., Koripella, C.R., Kossakovski, D., "High perfoming PbTe based thermoelectric materials", International Conference on Thermoelectrics, Traverse City, MI, July 2011.

III.2 NSF/DOE Thermoelectrics Partnership Project SEEBECK: Saving Energy Effectively by Engaging in Collaborative Research and Sharing Knowledge

Joseph P. Heremans
The Ohio State University
Department of Mechanical and Aerospace Engineering
Columbus, OH 43210

NSF Manager: Sumanta Acharya

DOE Technology Development Manager: John Fairbanks

NETL Project Manager: Carl Morande

Subcontractor:
ZT:Plus, Azusa, CA

Overall Objectives

- Develop high-efficiency (high figure of merit [zT]) thermoelectric materials that contain no rare or precious elements, and are non-toxic. Those materials are (1) PbSe in year 1, to transition to (2) Mg_2Sn later.
- Develop contact technologies to them.
- Evaluate electrical contact resistances.
- Develop and evaluate new thermal designs.
- Develop metrology to evaluate device performance.

Fiscal Year (FY) 2011 Objectives

- Report experimental galvanomagnetic and thermomagnetic properties of synthesized samples of n-type PbSe doped with indium at varying concentrations within the solid solution solubility range.
- Find resulting dimensionless figure of merit values zT.
- Find any experimental evidence of resonant impurity levels in this system.
- Learn preparation techniques and published properties of Mg_2Sn.
- Acquire equipment and setup experiments at ZT:Plus.

Accomplishments

- Attained a new high zT value for n-type PbSe reaching zT=1.2.
- Used indium as a dopant, but determined indium is not a resonant impurity level.
- Experimental data for galvanomagnetic and thermomagnetic properties gathered/analyzed.
- Initial literature study of Mg_2Sn reveals several previously unnoticed properties that we theoretically predict may lead to a new approach to obtaining high efficiencies in this material.

Future Directions

- Refine PbSe experimental procedure for optimizing zT varying indium content from 1/8% to 1/4%.
- Confirm previous data with this set of samples and determine optimum doping level for high temperature applications.
- Prepare Mg_2Sn.
- Measure properties of intrinsic material, confirm experimentally the presence of a high anharmonicity.
- Find resonant acceptor impurity for Mg_2Sn.
- Develop contact technologies with Virginia Tech and ZT:Plus.

Introduction

Thermoelectric devices directly convert heat to electricity and vice-versa. The best thermoelectric material for automotive waste heat recovery to date is PbTe, both as n and p-type material, but because Te is not abundant in the earth's crust it is perceived that it could become expensive. There is also a scientifically unjustified popular aversion to PbTe because lead is one of its constituents, in spite of the fact that the toxicity of a compound is not related to that of the constituent atoms (think of H_2, N_2, and C, versus hydrogen cyanide on the one hand, and the continued use of PbO, the exact analog of PbTe, in food-safe crystal glasses on the other). While there are high-zT n-type high-temperature skutterudite thermoelectric materials ($CoSb_3$-based with rare-earth additives), the rare-earths and cobalt are also strategic materials, and there are no high-zT equivalent p-type materials.

Our project first embarks on developing PbSe equivalents to PbTe, collaboratively both at Northwestern University and at Ohio State University. Transport properties of lead selenide are measured and recorded after a small amount of indium has been introduced to the system. With the help of these properties, a more complete picture of how lead

selenide behaves as a thermoelectric material can be seen. Lead selenide was used for a focus in this project because p-type [1,2] and n-type [3] PbSe have recently exhibited good thermoelectric properties without using the relatively pricey element tellurium. In addition, the introduction of indium in lead selenide might have been expected to create a "resonant level" leading an efficiency increase for this type of thermoelectric device. Therefore our goal is to experimentally record certain transport properties of this material at different concentrations of indium and to quantify how these different concentrations effect thermoelectric efficiency.

The research on PbSe is intended as a safe first step; in the longer term, the properties of Mg_2Sn will be investigated. The study of the latter material was catalyzed by the observation that $Mg_2Si_{1-x}Sn_x$ alloys can reach zT values near 1; however, despite heroic recent efforts, the zT values in that system have stagnated. Fresh ideas based on a possible anharmonicity of the bonds in Mg_2Sn have been developed by us this year, and will be tested experimentally in collaboration with Northwestern University.

Approach

Galvanomagnetic and thermomagnetic properties of synthesized bulk samples of lead selenide doped with indium will experimentally be measured by a conventional flow liquid nitrogen cryostat technique. Uniformity of the samples is confirmed using X-ray diffraction (XRD) data while thermal conductivity data is derived using data from a flash diffusivity measurement. Based on the experimental data, the thermoelectric figure of merit and resonant level effects will be considered.

Results

PbSe

Samples were synthesized with various atomic percents of indium from 1/8% to 2%. Measured properties from cryostat data include Seebeck coefficient, Nernst coefficient, resistivity, carrier density, mobility, and power factor. In the interest of brevity, the measured transport properties will not be shown here. The measured X-ray diffraction data (Figure 1) matches well with literature data for pure lead selenide so it was concluded that samples are of the expected cubic structure and of the right composition. Therefore, the particular heat treatment process was concluded to be an acceptable method of sample formation.

Resonant effects are evident by an increase in the Seebeck magnitude for a given carrier density. Based on the Seebeck magnitude and the carrier density from the

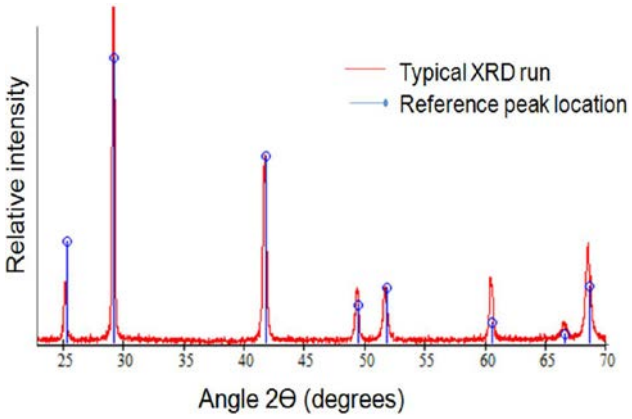

FIGURE 1. X-ray Diffraction Data on PbSe with Reference Peaks Marked

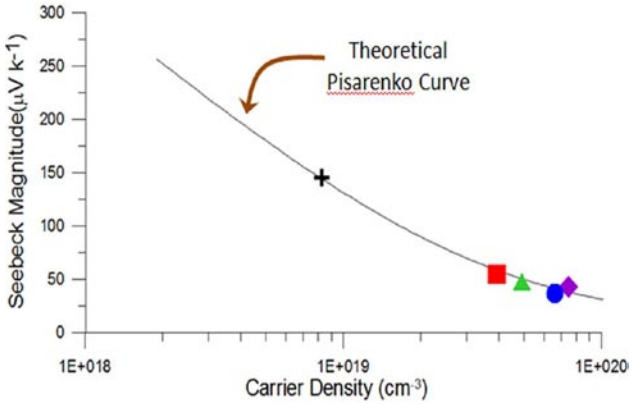

FIGURE 2. Pisarenko (Seebeck coefficient versus hole concentration) Curve with for Different Indium Concentrations: Indium is not a Resonant Level

above measurements, there is no evidence of a resonant effect since all concentrations lie on the theoretical Pisarenko curve (Figure 2).

Specific heat values used were derived from the Dulong-Petit formula. Specific heat, density and thermal diffusivity from a flash measurement are combined to give thermal conductivity (Figure 3). Thus, the dimensionless zT (Figure 4) which describes the efficiency of the thermoelectric device can be obtained via the temperature, power factor, and thermal conductivity. Results indicate the figure of merit for the 1/8% sample is well above 1 which is considerably higher than parallel studies [3] at our collaborator's laboratory at Northwestern. The reason for this is that the samples prepared here have a better mobility, as a consequence of the particular heat treatment developed here. Should this material become of industrial importance (for ZT:Plus to determine), the details of the optimal heat treatment will be of course shared with all parties involved in this group project.

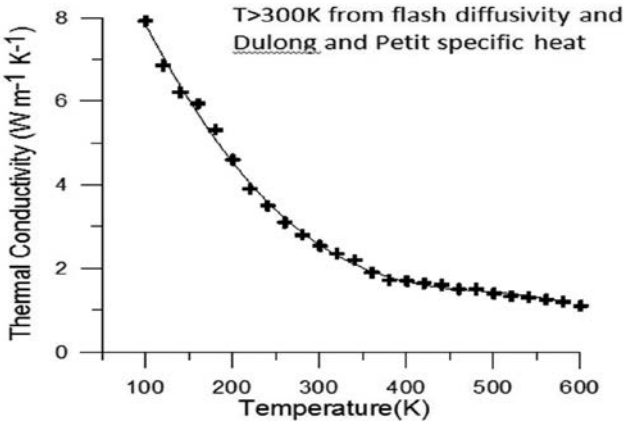

FIGURE 3. Thermal Conductivity of PbSe vs. Temperature

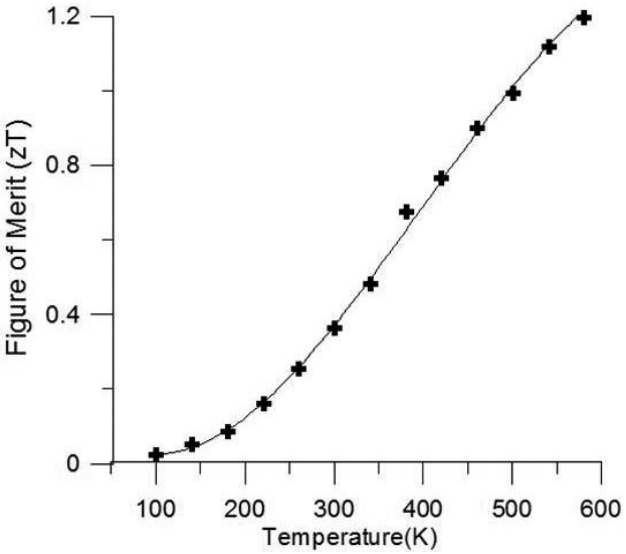

FIGURE 4. Figure of Merit of In-Doped PbSe vs. Temperature

Mg_2Sn

Regarding Mg_2Sn, progress has been made on two fronts.

Firstly, a literature study has identified derivative properties that are indicative of a very high anharmonicity of the chemical bonds in the binary Mg_2Sn compound. If confirmed experimentally, this could lead to the binary compound having an intrinsically low high-temperature lattice thermal conductivity (it is 6 W/mK at 300 K, about three times higher than PbTe). One conclusion would then be that alloying with Si, as has been historically done to reduce thermal conductivity, is unnecessary. This is important to know, as Mg_2Si has a higher melting temperature than Mg_2Sn. At the melting temperature of Mg_2Si, the vapor pressure of Mg is very high and Mg losses from the samples create synthesis difficulties, which are much attenuated in Mg_2Sn. Samples of the latter can therefore be prepared with better control of the defect chemistry; its thermal conductivity is also smaller (it is 8 W/mK for Mg_2Si at 300 K). Understanding, exploiting, and hopefully increasing, the anharmonicity of the bonds in Mg_2Sn would result in an attractive way to reduce thermal conductivity.

Secondly, a preliminary theoretical study (unpublished) has identified a number of potential candidate resonant impurities for the valence bands of Mg_2Sn. We are in the process of learning to synthesize Mg_2Sn, and once we develop control over its defect chemistry, we will add selected impurities during the second year of the project.

Conclusions

- Based on the Pisarenko curve, there is no evidence of resonant effects at the measured quantities of indium.
- The *zT* value of well above 1 exceeds previous values [3[for this material. PbSe is definitely a most promising thermoelectric material for waste heat recovery applications that avoids the high cost of tellurium, and, as a salt, it is not toxic in spite of popular perception.
- Mg_2Sn looks theoretically promising as a binary thermoelectric semiconductor, both because potentially the lattice thermal conductivity could be limited by high anharmonicities, and because the power factor of *p*-type material shows the promise to be increased by doping it with resonant impurity levels.

References

1. D.J. Parker et al, Phys. Rev. B 82, 035204 (2010).
2. H. Wang et al, Adv. Mater. 23 1366-1370 (2011).
3. J. Androulakis et al, Phys. Rev. B 83, 195209 (2011).

FY 2011 Publications/Presentations

1. "Resonant Impurity Level of PbSeIn", International Conference on Thermoelectrics, Traverse City, MI August 2011, Poster.

III.3 NSF/DOE Thermoelectrics Partnership: Purdue – GM Partnership on Thermoelectrics for Automotive Waste Heat Recovery

Xianfan Xu (Primary Contact),
Timothy S. Fisher, Stephen D. Heister,
Timothy D. Sands, and Yue Wu
Purdue University
585 Purdue Mall
West Lafayette, IN 47907

NSF Manager: Sumanta Acharya

DOE Technology Development Manager:
John Fairbanks

NETL Project Manager: Carl Morande

Overall Objectives

This research project is in collaboration with the General Motors Global R&D (GM) to enable ultimately the broad adoption of thermoelectric (TE) waste heat recovery systems, or TE generators (TEG), at a scale commensurate with the global vehicle manufacturing enterprise. We exploit the complementary missions of research/development at Purdue and deployment/commercialization at GM to develop the fundamental understanding and technology improvements needed to make viable the efficient conversion of waste heat in automotive exhaust systems to electricity. We address the key elements for the development and deployment of commercial automotive TEGs. The specific research activities are:

1. Advancing the performance of skutterudites that are currently used as the TE material at GM through thermal conductivity reduction and phonon engineering.
2. Development of nanowire TE materials.
3. Development of metal-semiconductor laminate TE materials.
4. Development of efficient heat exchanger and system level thermal modeling.
5. Development of thermal interface materials.

Fiscal Year (FY) 2011 Objectives

- Justify the filling of multiple elements in skutterudites for scattering phonons and reducing thermal conductivity of TE materials.
- Quantify the feasibility of using nanostructured TE materials for large-scale energy harvesting, optimize the synthesis and fabrication of nanostructured TE materials, and demonstrate high-performance TE materials with performance superior to bulk materials.
- Characterize the electronic properties of ScN (semiconductor) with Mn and Al alloying.
- Design baseline heat exchanger topology and evaluate overall TEG performance.
- Create thermal interface materials capable of handling low-temperature operation and optimize the interface material to achieve minimum interface resistance and maximum TE conversion efficiency.

Accomplishments

- Proved that filling in skutterudites can provide new channels for phonon scattering which can significantly reduce thermal conductivity of skutterudites. Different weights of the filled elements scatter phonons of different frequencies, therefore multiple filling is an effective way to reduce thermal conductivity.
- Understood the materials abundance, cost, and toxicity of various nanostructured TE materials and identified the complex metal oxides as potential candidates for high-temperature TE energy harvesting, developed new synthetic method to mass produce TE nanowires, and demonstrated 13% enhancement in TE figure of merit in spark plasma sintered n-type Bi_2Te_3 nanowire samples compared to bulk crystals and 64% reduction in thermal conductivity in $SrTiO_3$ nanowire samples compared to bulk crystals.
- Developed a strategy for manipulating the electronic properties of ScN semiconductor layers (via Al and Mn alloying) in order to effectively tune the barrier height of metal-semiconductor superlattices for optimized TE performance.
- Designed heat exchanger and TEG to achieve high power output.
- Successfully synthesized carbon nanotubes (CNTs) on copper foil, alumina, and graphitic material and increased TE power generation by 40% with the use of a double-sided CNT array on copper foil, as compared to the absence of an interface material, and 20% in comparison to standard interface materials.

Future Directions

- Understand the interaction between the filling metal atoms and the parent skutterudite material.

- Evaluate the impacts of nanostructure size, surface roughness, and composition modulation on TE figure of merit, analyze other material systems such as PbTe, Sb_2Te_3, $Ca_3Co_4O_9$, etc, and conduct research in the scalable synthesis of nanowire heterostructures to further decouple electron and phonon transport.
- Evaluate the effect of the altered electronic properties of Mn-Al alloyed ScN semiconductor layers on the transport properties of nitride metal-semiconductor superlattices (e.g. ZrN/(Al,Mn,Sc) N superlattices), and conduct copper-copper lamination experiments to fabricate bulk-like metal-semiconductor superlattice TE legs for electronic transport characterization.
- Refine the heat exchanger design with the use of multiple types of TE materials.
- Explore the possibility of developing other nanostructures for TE application, explore the possibility of applying a B-C-N chemical treatment to the interface materials to improve stability at high temperatures, and study the thermal stability of the interface materials by performing thermal cycling tests at high temperatures.

Introduction

The development of a TEG requires research and development in multiple areas, from TE materials to thermal management. The current project consists of five different tasks as indicated in the "Overall Objectives" section. The progress on these five tasks are reported in the following.

1. Advance the Performance of Skutterudites that are currently used as the TE Material at GM through Thermal Conductivity Reduction and Phonon Engineering

Skutterudites filled with heavier elements are found to have significantly reduced thermal conductivity, which can be candidates for efficient TE materials. Study of the role of the filling atoms can help to optimize the design of TE materials and thus to make better use of the waste heat.

Approach

Raman spectroscopy measurement is conducted to identify the intrinsic oscillation modes in skutterudites that scatter phonons. Femtosecond time-resolved reflectance measurement is performed to obtain the temporal oscillation signal and Fourier transform is used to extract the phonon frequency information. The results by the two measurements are compared to analyze the role of filling atoms in phonon scattering and thermal conductivity reduction.

Results

- In the Raman spectra in Figure 1, we observe the low-energy A_g mode of the Sb_4 rings (which is at about 150 cm^{-1}), which agrees with the results in [1].
- From the Fourier transform of the results obtained by the optical measurements, shown in Figure 2, we observe the vibration modes associated with the filling metal atoms which are not Raman active

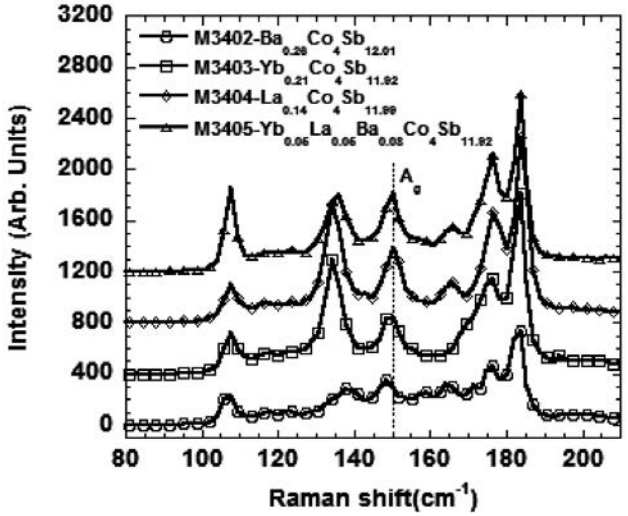

FIGURE 1. Raman spectra for the four partially filled skutterudites. The dashed line marks the low-energy Ag mode of the Sb_4 rings.

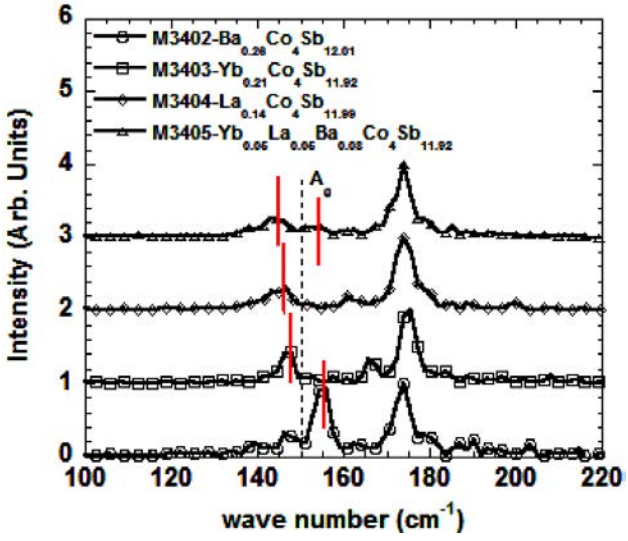

FIGURE 2. Fourier transform of the results from the optical measurements. The dashed line marks the low-energy Ag mode of the Sb_4 rings. The red lines mark the created modes by rattling of the filling metal atoms.

[2]. In single-element filled samples, one such mode is observed while in the triple-element filled sample, two distinct such modes are observed, which indicates that different filling atoms can create different vibration modes and can thus scatter phonons with different frequencies.

2. Development of Nanowire TE Materials

Significant scientific progress has been achieved using nanostructured materials for TE energy harvesting and solid-state cooling through the conversion of waste heat into electricity and vice verse. However, the connection between the small-scale proof-of-concept results achieved in research labs and real industrial-scale manufacture is still missing. Herein we perform an analysis to determine the appropriate TE nanomaterials for the large-scale manufacture and deployment in the near future. We cover key parameters such as ZT value, cost, abundance, and toxicity. Maximum ZT values are considered at three temperature ranges. Material cost and abundance are visually demonstrated to improve ease of interpretation. Toxicity is also evaluated to minimize the environmental impact during manufacture and recycle. Lastly, a parameter termed "efficiency ratio" is calculated to give a better qualitative understanding into the feasibility and sustainability of these nanomaterials. The identified materials are investigated to further improve their performance using nanoscale engineering.

Approach

We identified complex metal oxides, for example $SrTiO_3$ and $Ca_3Co_4O_9$ as potential candidates for high temperature application. Through nanoscale engineering, we have successfully converted them into nanowires using a self-templated growth method that can mass produce ultrathin nanowires. Similar approaches have been used to convert other traditional TE materials, such as Bi_2Te_3 and PbTe into quantum-confined nanowires with high performance.

Results

- The large thermal conductivity of bulk complex metal oxides such as $SrTiO_3$, $NaCo_2O_4$, and $Ca_3Co_4O_9$ has set a barrier for the improvement of TE figure of merit and the applications of these materials in high temperature (≥1,000 K) TE energy harvesting and solid-state cooling. Here, we present a self-templated synthesis approach to grow ultrathin $SrTiO_3$ nanowires with an average diameter of 6 nm in large quantity. The thermal conductivity of the bulk pellet made by compressing nanowire powder using spark plasma sintering shows a 64% reduction in thermal conductivity at 1,000 K, which agrees well with theoretical modelling.
- A rational yet scalable solution phase method has been established, for the first time, to obtain n-type Bi_2Te_3 ultrathin nanowires with an average diameter of 8 nm in high yield (up to 93%). TE properties of bulk pellets fabricated by compressing the nanowire powder through spark plasma sintering have been investigated. Compared to the current commercial n-type Bi_2Te_3-based bulk materials, our nanowire devices exhibit an enhanced ZT of 0.96 peaked at 380 K due to a significant reduction of thermal conductivity derived from phonon scattering at the nanoscale interfaces in the bulk pellets, which corresponds to a 13% enhancement compared to that of the best n-type commercial $Bi_2Te_{2.7}Se_{0.3}$ single crystals (~0.85) and comparable to the best reported result of n-type $Bi_2Te_{2.7}Se_{0.3}$ sample (ZT=1.04) fabricated by hot pressing of ball-milled powder. The uniformity and high yield of the nanowires provide a promising route to make significant contribution to the manufacture of nanotechnology-based TE power generation and solid-state cooling devices with superior performance in reliable and reproducible way.

3. Development of Metal-Semiconductor Laminate TE Materials

Approach

Our approach is to use nitride metal-semiconductor superlattices to improve TE efficiency for high temperature applications. ScN was chosen as the semiconductor due to its high melting point and the ability to integrate ScN in pseudomorphic heterostructures that will allow phonon glass-electron crystal approaches to nanostructured TEs.

Results

(Mn,Sc)N and (Al,Sc)N thin films were deposited with varying concentrations of Mn and Al via direct current reactive magnetron sputtering. The crystal structure of ScN and MnN is rocksalt while AlN is wurtzite. Fortunately, the rocksalt phase of AlN can be stabilized in ScN up to 40% AlN. Solid solution (Mn,Al,Sc)N alloys can therefore be deposited across the entire spectrum for (Mn,Sc)N and up to 40% for (Al,Sc)N. The effect of Mn and Al alloying on the electronic properties of (Mn,Al,Sc)N was evaluated by 4-point probe and Hall effect.

Figure 3 shows the resistivity of (Mn,Sc)N thin films as a function of Mn concentration. Pure ScN is an n-type semiconductor. The carrier concentration in the pure ScN films is relatively high (e.g. ~10^{20} cm^{-3}) due to oxygen incorporation during growth, with oxygen acting as a donor. The incorporation of Mn (acceptor) in ScN compensates the oxygen donors, thereby decreasing

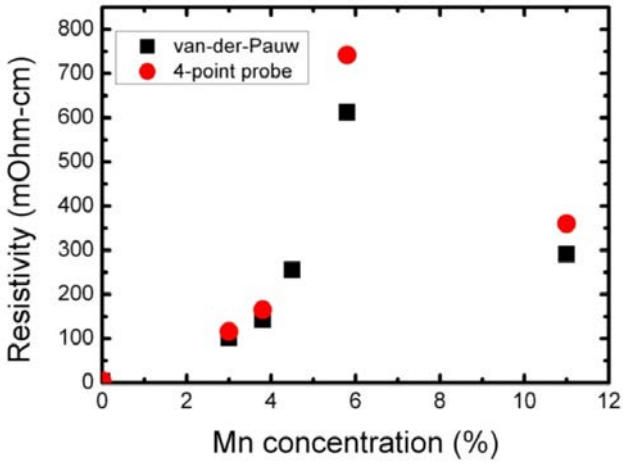

FIGURE 3. Resistivity of (Mn,Sc)N thin films as a function of Mn concentration. ScN is intrinsically n-type. Mn acts as an acceptor, compensating the donors before transitioning to p-type. The transition from n-type to p-type occurs in the 6%-11% Mn range.

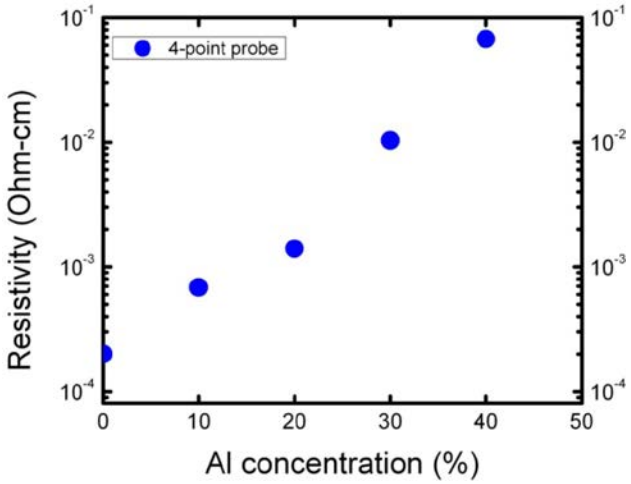

FIGURE 4. Resistivity of (Al,Sc)N thin films as a function of Al concentration. The resistivity of the (Al,Sc)N can be varied over three orders of magnitude, which provides additional flexibility in controlling the electronic properties of the semiconductor layer. AlN retains the rocksalt crystal structure (ScN is also rocksalt) up to 40% Al, before transitioning to stable wurtzite AlN.

the carrier concentration and increasing the resistivity. At a Mn concentration above 6% the oxygen donors are fully compensated and further Mn incorporation leads to p-type (Mn,Sc)N. These results demonstrate that Mn provides the ability to manipulate the carrier concentration and type of ScN, which is useful towards optimizing the electronic properties of nitride metal-semiconductor superlattices.

Figure 4 shows the resistivity of (Al,Sc)N thin films as a function of Al concentration. The resistivity varies by three orders of magnitude with Al additions up to 40%. This large resistivity variation provides an additional parameter for tuning the electronic properties of ScN.

4. Development of Efficient Heat Exchanger and System Level Thermal Modeling

Approach

In the present work, the electrical power output of the TEG is maximized by optimizing TEG geometry for a given volume by performing numerical simulations. Temperature and heat fluxes are computed numerically by discretizing TEG domain into finite volumes. Basic heat transfer equations linked with temperature dependent fluid and material properties are solved sequentially for each control volume using a C++ code.

In the current study, a box-type topology of the TEG is analyzed with TE modules (TEMs) being placed on the top and bottom surface of the TEG box as shown in Figures 5 and 6 with the engine coolant on the other side. The side walls are assumed to be adiabatic and the inlet conditions are kept constant for all

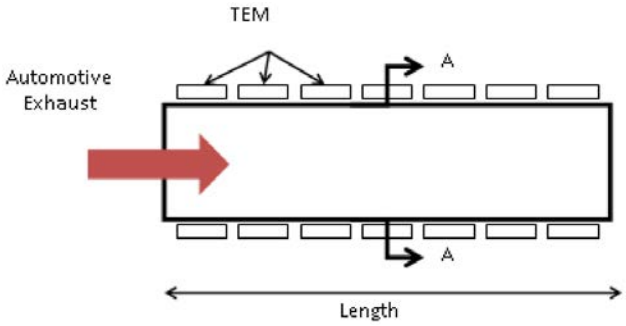

FIGURE 5. Schematic of TEG for One-Dimensional Analysis

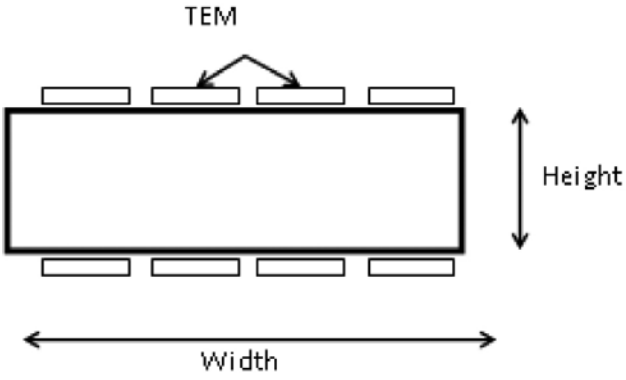

FIGURE 6. A-A Cross-Sectional View of TEG from Figure 5

configurations. Dimensions (width, height and length) of the TEG box for constant volume are varied within allowed bounds for a sub-urban vehicle. The fraction of heat transfer through TEMs is enhanced by placing a plate-fin type heat exchanger in the exhaust air flow region. TE properties of multiple filled skutterudites ($Ce_{0.1}In_{0.1}Yb_{0.2}Co_4Sb_{12}$) [3] exhibiting very good ZT values are modeled as TE materials. The numerical code also computes the optimal number of fins and fin spacing for each configuration to maximize power output. The pressure drops due to viscous drag on heat exchanger fins are also calculated. The configuration with pressure drops exceeding the allowable limit are not considered for optimization study. Radiations heat transfer is also considered since the hot side surface is >300˚C.

Results

The numerical code is run for box-type topography for a given volume of 0.00358 m^3. The TEG inlet is subjected to hot air exhaust at 550˚C having an average mass flow rate of 35 g/s. The coolant temperature is assumed to be constant at 100˚C. The geometry configurations with pressure drops less than the allowed limit are displayed in Figures 5 and 6 having the optimum heat exchanger configuration. The effect of number of the TEMs on maximum power output is also analyzed. Figure 7 represents a three-dimensional contour of power output for various geometry configurations (Case 1). Figure 8 exhibits the similar analysis with the number of TEMs restricted to 50 (Case 2). For each configuration, optimal number of fins and fins spacing were computed. Figures 9 and 10 show the variation of parameters along the flow direction for the optimal configuration for Case 1. Figure 9 represents the variation of temperature of hot surface along the flow direction. Figure 9 shows the variation of energy fluxes on the combined top and bottom surfaces of the TEG along the flow direction. This shows a huge chunk

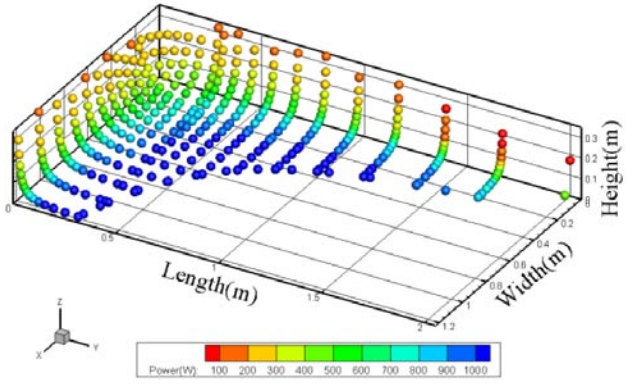

FIGURE 7. Contour plot showing optimal exhaust heat exchanger topology to maximize power output.

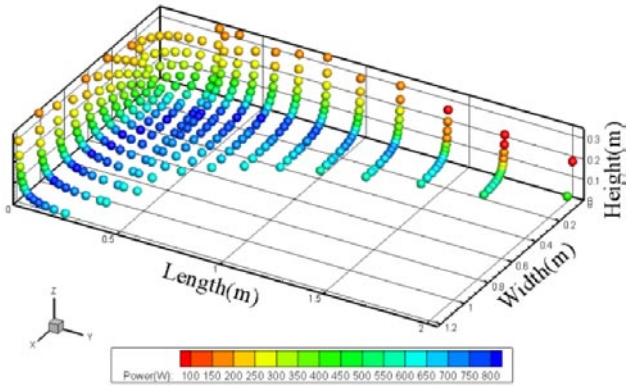

FIGURE 8. Contour plot showing optimal exhaust heat exchanger topology to maximize power output with number of TEMs restricted to 50.

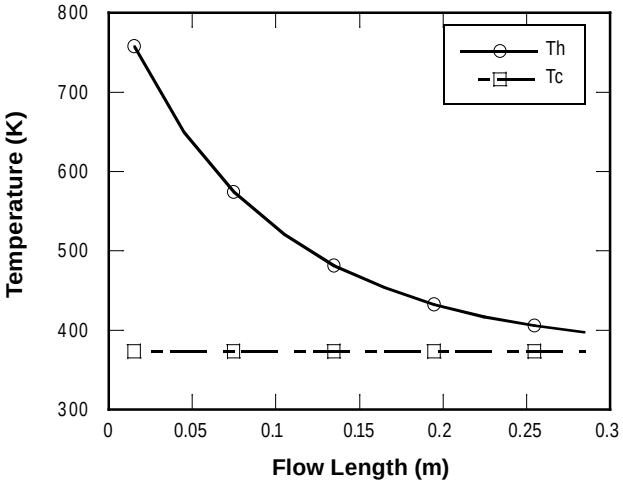

FIGURE 9. Variation of hot surface temperature along the flow direction.

of incoming energy carried by hot gas (Qg) transferred to coolant (Qc). Pout is the electrical power generated per area along the flow direction.

5. Thermal Interface Materials Development

Since their discovery in 2001, it has become apparent that CNTs have the potential to advance technology in a wide variety of fields. In the present work, the fundamental science of nanotechnology is applied to the overarching goal of creating more fuel efficient vehicles. An integral part to providing a large temperature gradient is to decrease the thermal resistance at the interface where the TE contacts both the heat source (exhaust) and the heat sink (cooling fluid). Because of their excellent thermal characteristics, CNT arrays can be implemented at these two interfaces, leading more efficient harvesting of waste heat. The work accomplished to date includes synthesizing CNTs

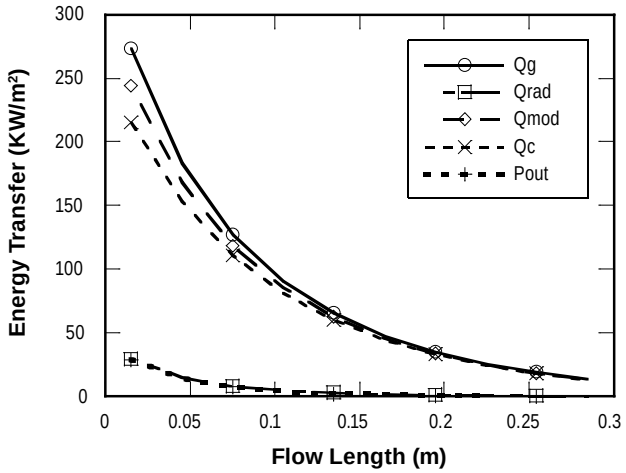

FIGURE 10. Variation of energy fluxes hot surface temperature along the flow direction.

on various substrates in various conditions and testing their effect on TE output efficiency.

Approach

The investigators are focused on experimentally determining the ideal configuration of CNTs that will lead to a minimal thermal interface resistance using a microwave plasma chemical vapor deposition process. The microwave plasma chemical vapor deposition equipment is shown in Figure 11. The substrate materials of interest are copper foil, alumina, and graphitic material. In the synthesis process, parameters can be varied such as growth time, power supplied to the microwave generator, substrate temperature, and flowrate of feed gases. Subsequently, the performance of the array is determined by measuring the actual thermal interface resistance by means of a one-dimensional reference bar technique. This is a measurement where a temperature gradient is applied across the interface material, and the thermal interface resistance is directly calculated from data gathered by a thermal imaging camera. Another method of determining the performance of an array is to measure and compare the TE power output efficiency in different arrays (performed by General Motors).

Results

CNTs have successfully been synthesized on all three materials of interest–copper foil, alumina, and graphitic material of the TE. The alumina material is significant as it represents the possibility of synthesizing CNTs directly on the TE module, meaning that only one interface would be present on each side of the TE. Also, double-sided samples have been created on copper foil and graphitic material. It was observed that a key

FIGURE 11. Microwave Plasma Chemical Vapor Deposition Equipment

condition for CNTs synthesis on the graphitic material is the presence of nitrogen gas in the plasma chamber.

Testing has been performed by General Motors to determine the effect of using the interface materials on the energy conversion efficiency. A standard bismuth-telluride TE module was used and the conversion efficiency was measured (electrical power produced/ thermal power supplied). For a bare substrate, the conversion efficiency was measured to be 0.6%. A single-sided copper foil with CNTs produced an efficiency of 0.9%, and a double-sided copper foil with CNTs increased the efficiency to 1.05-1.10%. A comparison of these interface materials is shown in Figure 12. This translates to an increase in TE power generation of 40% over a bare interface, and 20% as compared to foil alone. These results are very promising and indicated strong potential for significant increases in TE efficiency using CNT interface materials. Images of this sample (CNT array on copper foil) generated using a scanning electron microscope are shown in Figures 13 and 14.

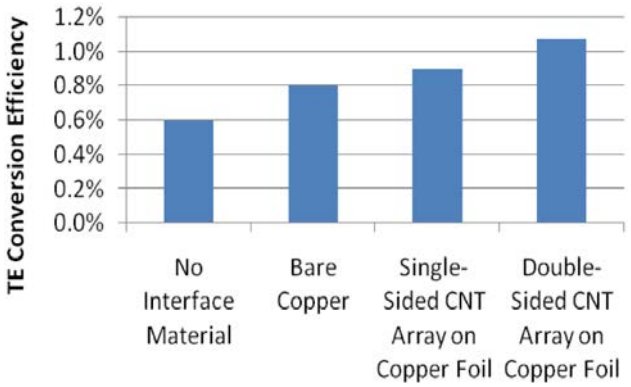

FIGURE 12. Effect of Interface Material on TE on Conversion Efficiency

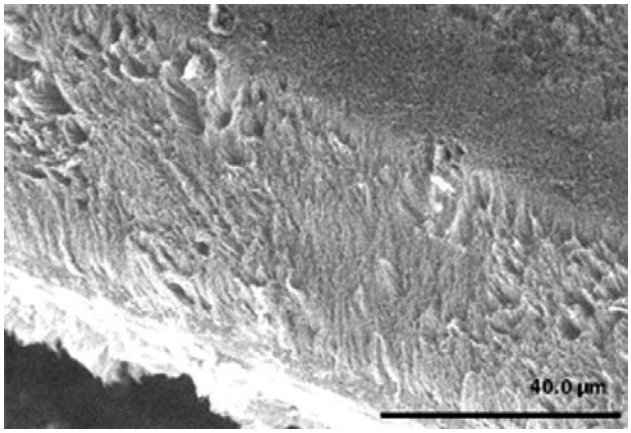

FIGURE 13. Scanning Electron Microscope Image of CNT on Copper

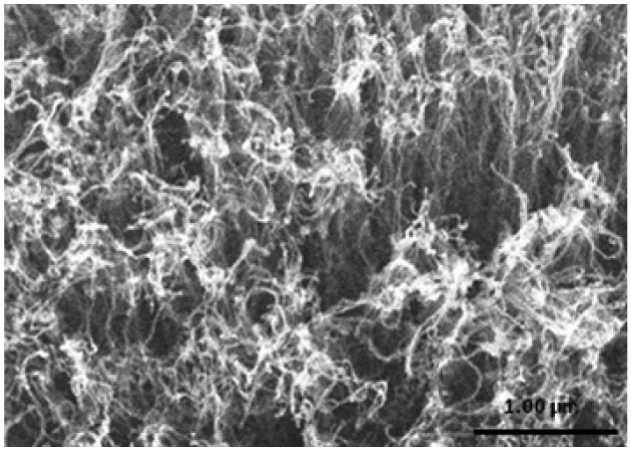

FIGURE 14. Scanning Electron Microscope Image of CNT on Copper

Conclusions

Task 1

- Filling metal atoms in skutterudites can provide new channels for phonon scattering, which can significantly reduce thermal conductivity of skutterudites.
- Filling metal atoms with different weights scatter phonons with different frequencies, so multiple filling is an efficient way to reduce thermal conductivity.

Task 2

By converting traditional TE materials into ultrathin nanowires, significant improvement in TE figure of merit can be achieved to improve the feasibility of large-scale deployment.

Task 3

Rocksalt (Mn,Al,Sc)N solid solution alloys provide a large range of electronic properties suitable for optimizing the electronic properties of the semiconductor layers in nitride metal-semiconductor superlattices for thermionic energy conversion.

Task 4

For the first case, the power can be maximized by minimizing the height and maximizing the box width. However, for a limited number of TEMs this does not hold true. For the configuration to be optimum, its top and bottom cumulative surface area should be equal to the total surface area of allowed number of TEMs. Hence the location of optimum configuration depends on the number of TEMs.

The present calculations will be refined by adding thermal resistances between contact surfaces of TEMs. To enhance TE power generation, the TE materials like Bi_2Te_3 will be used in TEMs for lower temperature regions.

Task 5

- CNTs can successfully be synthesized both single-sided and double-sided on copper foil, alumina, and graphitic materials.
- A key component of synthesizing CNTs on graphitic material is the presence of nitrogen.
- A double-sided copper foil is able to increase TE power generation by at least 20%.

References

1. L.X. Li et al., Chem. Phys. Lett. 347, 373 (2001).

2. J.L. Feldman et al., Phys. Rev. B 68, 094301 (2003).

3. J. Graff, S. Zhu, T. Holgate, J. Peng, J. He, T.M. Tritt, High-Temperature Thermoelectric Properties of Co_4Sb_{12}-Based Skutterudites with Multiple Filler Atoms: $Ce_{0.1}In_XYb_YCo_4Sb_{x12}$, J. Electronic Materials, Vol. 40, No 5, 2011.

FY 2011 Publications/Presentations

1. Wang, Y., Xu, X, and Venkatasubramanian, R., Phonon Scattering in Bi2Te3/Sb2Te3 Superlattice, Proceedings of the ASME/JSME 2011 8th Thermal Engineering Joint Conference, Paper No. aJTEC2011-44012, Honolulu, HW, March, 2011.

2. X. Xu, Invited talk "Energy transfer in energy conversion materials" Shanghai Jiaotong University, Shanghai, China, June 2011.

3. X. Xu, Invited talk "Energy transfer in nanoscale energy conversion materials" Vanderbilt University September 2011.

4. Gautam, Yadav G.; Susoreny, Joseph A.; Zhang, Genqiang; Yang, Haoran; Wu, Yue* Nanostructure-based thermoelectric conversion: an insight into the feasibility and sustainability for large-scale deployment. Selected as feature article, *Nanoscale*, (2011), 3, 3555.

5. Gautam, Yadav G.; Zhang, Genqiang; Qiu, Bo; Susoreny, Joseph A.; Ruan, Xiulin; Wu, Yue* Self-templated synthesis and thermal conductivity investigation for ultrathin perovskite oxide nanowires. *Nanoscale*, 2011, 3, 4078-4081.

6. Qiu, Bo; Bao, Hua; Zhang, Gengqiang; Wu, Yue; Ruan, Xiulin. Molecular dynamics simulations of lattice thermal conductivity and spectral phonon mean free path of PbTe: Bulk and nanostructures. *Computational Materials Science*, 2012, 53, 278-285.

7. Zhang, Genqiang; Kirk, Benjamin; Jauregui, Luis A.; Yang, Haoran; Xu, Xianfan; Chen, Yong P.; Wu, Yue* Rational Synthesis of Ultrathin n-type Bi2Te3 Nanowires with Enhanced Thermoelectric Properties. *Nano Letters*, 2011, accepted, **DOI:** 10.1021/nl202935k

8. Wu, Yue (Invited talk) "Advanced Nanostructures for Thermoelectric Energy Harvesting", National Center for Nanoscience and Technology of Chinese Academy of Sciences, December 2010.

9. Wu, Yue (Invited talk) "Metal Oxide-based Solid-State Cooling and Energy Harvesting", 2011 EPRI Workshop, June, 2011.

10. Wu, Yue (Invited talk) "Advanced Nanostructures for Thermoelectric Energy Harvesting", Wright-Patterson Air Force Research Lab, August, 2011.

11. Wu, Yue (Invited talk) "Advanced Nanostructures for Thermoelectric Energy Harvesting", DuPont, September, 2011.

12. Wu, Yue (Invited talk) "Advanced Nanostructures for Thermoelectric Energy Harvesting", 2011 AIChE Meeting, October, 2011.

13. Wu, Yue (Contribution talk) "Hybrid Nanowire/Polymer Composite for Thermoelectric Energy Harvest", 2011 AIChE Meeting, October, 2011.

14. Wu, Yue (Contribution talk) "Thermoelectric Energy Harvesting from Molecular Scale Nanowires", 2011 MRS Meeting, December, 2011.

15. Wu, Yue (Contribution talk) "Advanced Nanostructures for Thermoelectric Energy Harvesting", 2011 MRS Meeting, December, 2011.

Special Recognitions & Awards/Patents Issued

1. X., Xu, Invited talk "Energy transfer in energy conversion materials" Shanghai Jiaotong University, Shanghai, China, June 2011.

2. X. Xu, Invited talk "Energy transfer in nanoscale energy conversion materials" Vanderbilt University September 2011.

3. Wu, Yue (Invited talk) "Advanced Nanostructures for Thermoelectric Energy Harvesting", National Center for Nanoscience and Technology of Chinese Academy of Sciences, December 2010.

4. Wu, Yue (Invited talk) "Metal Oxide-based Solid-State Cooling and Energy Harvesting", 2011 EPRI Workshop, June, 2011.

5. Wu, Yue (Invited talk) "Advanced Nanostructures for Thermoelectric Energy Harvesting", Wright-Patterson Air Force Research Lab, August, 2011.

6. Wu, Yue (Invited talk) "Advanced Nanostructures for Thermoelectric Energy Harvesting", DuPont, September, 2011.

7. Wu, Yue (Invited talk) "Advanced Nanostructures for Thermoelectric Energy Harvesting", 2011 AIChE Meeting, October, 2011.

III.4 Automotive Thermoelectric Modules with Scalable Thermo- and Electro-Mechanical Interfaces

K.E. Goodson[1] (Primary Contact), George Nolas[2] and Boris Kozinsky[3]
[1]Mechanical Engineering Department
Stanford University
Stanford, CA 94305-3030
[2]Department of Physics, University of South Florida,
[3]Energy Modeling, Control, and Computation,
Robert Bosch LLC

NSF Manager: Sumanta Acharya

DOE Technology Development Manager: John Fairbanks

NETL Project Manager: Carl Morande

Overall Objectives

- Evaluate novel nanostructured interface options that can accommodate large fluctuations in thermo-mechanical strain while maintaining thermal and electrical contact.
- Create and measure efficient and stable high-temperature p and n type thermoelectric (TE) materials, which can be reliably attached to heat sinks and electrodes.
- Develop practical metrology and metrics relevant for system development, which also can be used to assess durability during thermal cycling of TE generators (TEGs).

Fiscal Year (FY) 2011 Objectives

- Develop carbon nanotube (CNT)-based thermal interface material (TIM) tape technology for TEG application.
- Develop in situ measurement techniques, tools and rigs for characterization and reliability testing of TEG devices at elevated temperatures.
- Develop new TE high-temperature materials and computational tools to optimize the process and reduce the iterations.

Accomplishments

- CNT-based TIM tape technology for TEG application.
- In situ measurement techniques and tools for characterization and reliability testing of TEG devices using high resolution infrared thermometry.
- Measured thermal transport properties of TE pellets and interfaces.
- Designed and completed a prototype rig for in situ characterization of TE pellets and TIMs up to 800 K.
- Completed extensive mechanical and thermal characterization of stand-alone CNT films using nano/picosecond thermoreflectance and atomic force microscopy nanoindentation techniques.
- Improved theoretical ab initio computational methodology for predicting transport properties of TE materials (e.g., skutterudites).
- Developed new TE high-temperature materials such as skutterudites and half-Heusler alloys.

Future Directions

- Develop new processes for fabrication, assembly and integration of CNT-based TIM tape technology to TE pellets/modules.
- Conduct in situ characterization and reliability tests for TE pellets and Interfaces as well as TE modules.
- Complete and implement the high-temperature (800 K) rig for in situ thermal and mechanical characterization.
- Continuation of the ab initio computational effort to engineer TE materials (e.g., skutterudites).
- Developing new TE high-temperature materials such as skutterudites and half-Heusler alloys.

Introduction

This project addresses three critical challenges improving TE device performance for combustion systems: 1) the need for scalable TIMs that are stable under high temperatures and thermal cycles, which is addressed by utilizing nanostructured materials; 2) the need to develop TE materials with a high figure of merit (zT) under high temperature operating conditions; and 3) the need for device characterization accounting for interface reliability and thermal cycling degradation at high temperatures, which is addressed by our proposed infrared-imaging TE characterization rig. We are supporting these activities through systems-level modeling and full device-scale characterization, with the

ultimate goal of constructing a complete architecture for optimizing a TEG system for recovering waste heat from automobile combustion.

Approach

We use an array of thermal (nano- and picosecond time-domain thermo-reflectance systems) and mechanical characterization tools to investigate the performance of CNT TIMs. For the out-of-plane modulus measurement, we use a resonator technique which involves measurement of the resonant frequency of each microfabricated cantilever before and after CNT film growth. The elastic modulus is extracted by modeling the Si-CNT cantilevers as two-layer composite beams. We also extract the out-of-plane mechanical modulus of CNT films using a nanoindentation technique [1].

For TE materials, we propose fundamental research by means of experimental science and first principle calculations to enhance and fine tune transport properties of filled Skutterudites and half-Heusler intermetallic alloys. The Materials Computation group at Robert Bosch, led by Dr. Kozinsky, conducted state-of-the-art ab initio simulations for TE materials design. We are in the process of constructing a dedicated high-temperature facility to perform measurements on high-temperature performance of TEs, which will be complemented by standard high-temperature TE property measurements at the National Institute of Standards and Technology.

Results

Nanostructured Thermal Interface Materials

CNT films grown on silicon substrates are transferred to TE material using a metallic bonding layer. To preserve high temperature stability, a tin-plated aluminum/nickel superlattice foil is used to weld a metalized CNT film to an opposing metalized substrate, as shown in Figure 1(a). The growth silicon is then removed, completing the transfer of the CNT film to the new substrate. Figure 1(b) shows metal nanowire films that are grown via electrodeposition in ion-track polycarbonate membranes. These films preserve the high thermal and electrical conductivity of bulk metals while gaining the mechanical compliance of a low volume-fraction nanostructured material. This method of template growth allows for variation in geometry and composition necessary to optimize the transport properties of the film. We use these templates to produce nanowires from traditionally conductive metals, such as copper, and from noble metals which do not readily oxidize.

CNT Engagement and Thermal Properties for TIMS

Here we report data for both the through-plane thermal resistance and the in-plane elastic modulus of vertically aligned single-wall carbon nanotube (SWCNT) films grown under identical conditions over a range of film thicknesses. Preliminary results using nanosecond thermoreflectance show that the effusivity of the CNT films range from 370-380 W $s^{0.5}$ m^{-2} K^{-1}. This technique only results in sensitivity to effusivity and not explicitly thermal conductivity k_{eff} or heat capacity $C_{v,eff}$ separately. The boundary resistance between the CNT film and metal transducer layer $R"_{CNT\text{-}Metal}$ is between 0.1-1.8 m^2 K MW^{-1} and the boundary resistance between the CNT film and substrate $R"_{CNT\text{-}Sub}$ is between 2.6-11.2 m^2 K MW^{-1}. We are currently testing a new frequency domain thermoreflectance system that will allow us to pinpoint the values of thermal conductivity and heat capacity [2].

Mechanical Property Measurements and Modeling of CNT Films

Figure 2 shows the measured effective in-plane modulus using the microresonator technique. The results, which assume a homogeneous film, show a clear trend of decreasing modulus with CNT height. We believe that this is due to the presence of a thin,

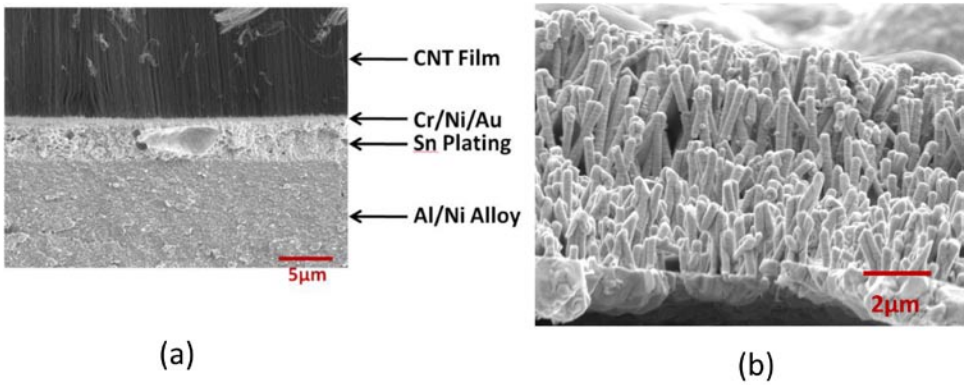

FIGURE 1. (a) Scanning electron micrograph image depicting the bond between a metalized CNT film and a metallic Sn-plated Al/Ni bonding layer. (b) Scanning electron micrograph of the freestanding metal nanowire film.

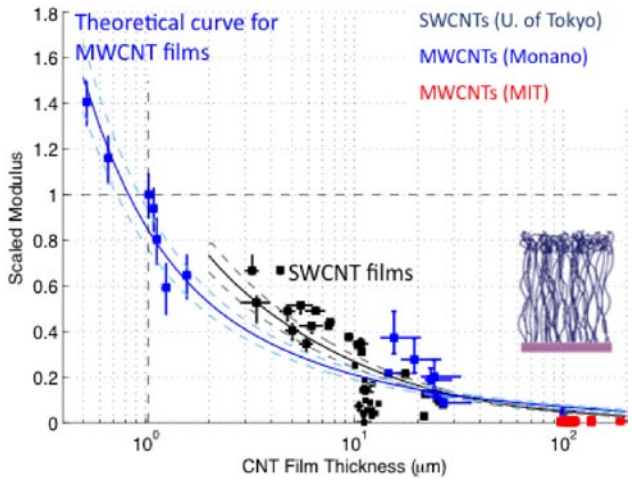

FIGURE 2. Normalized modulus of SWCNT (Black), multi-walled CNT (Blue), and thick multi-walled CNT (red) films. These films range from 0.5-220 μm in thickness and the effective modulus ranges from 1 to 370 MPa. Solid lines show the theoretical curves that include separate values for the crust and middle layer, with the crust ~600 MPa and the middle ~10 MPa. Dashed lines indicate the effect of ±10% variation of the theoretical modulus on the effective modulus. The inset shows a diagram of the VACNT structure with a crust layer at the top surface.

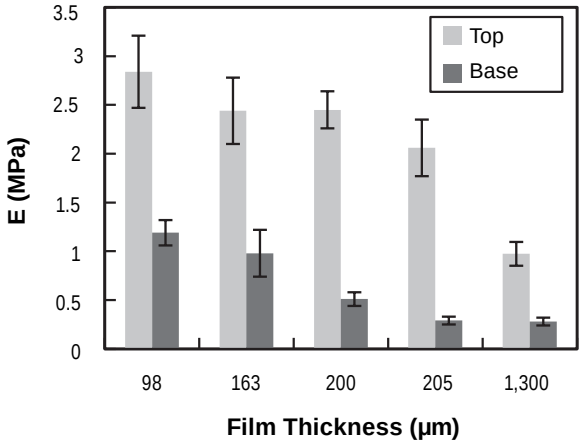

FIGURE 3. Elastic modulus measured from the top and bottom surface respectively of VACNT samples of varying thicknesses. The error bars correspond to the standard deviation of the data points.

entangled crust layer with higher modulus. The data is then analyzed using a three-layer beam analysis where the top layer is the crust, the middle layer is the aligned CNT section, and the bottom layer is the substrate. The extracted modulus decreases with CNT film height due to the stiff crust layer. As the CNT film grows taller, the middle layer modulus becomes more dominant, and consequently the overall modulus of the film decreases.

The out-of-plane Young's modulus is measured using an atomic force microscopy nanoindentation technique that allows resolution of nanoscale forces on the soft vertically aligned CNT (VACNT) films. The large contact area of the spherical indenter allows sampling of bulk film properties rather than individual tubes. The measurements are performed on the base side of the film as well as the top surface. The modulus at bottom surface is measured by releasing the film from the substrate and indenting from the backside. Comparing the modulus between the two surfaces is of interest because the base of the film may have a different morphology than the top due to effects of the growth process [3,4]. This is supported by image analysis performed on scanning electron micrographs of the sample structure. The results in Figure 3 show that the elastic modulus varies significantly between the top and bottom surface as expected based on image analysis. The results indicate the VACNT films have the desired compliance of thermal interface materials and that there is a depth dependent modulus of the film dictated by the alignment and density of the tubes.

We have also developed two models of the mechanical behavior of the CNT film. The first is a simple cellular model of the CNT film which assumes the film is comprised of tube sections of length l oriented at an angle θ to the plane of the film. The in-plane and out-of-plane modulus can be predicted by considering the behavior of a single tube in a unit cell [5]. We have also developed a new method of modeling vertically aligned nanotube films by adapting an atomic scale molecular dynamics algorithm to simulate the mesoscopic behavior of nanotube films. This work, which we call the coarse-grain model, investigates intertube interactions including self-organization and zipping behaviors of nanotubes and how these occur in films of different alignment and nanotube densities. Image analysis performed on scanning electron micrographs of the sample structures provides inputs into the models. This allows us to detect different morphologies within a film to predict the modulus variation.

High Temperature Measurement Rigs

We have fabricated a rig that can achieve a hot side temperature of 180°C with a range of applied forces limited by the load cell integrated into the actuator. The hot side is heated via a TE heater, which sets the current upper bound on temperature. The cold side heat exchanger is maintained at the ambient temperature using a chilled water loop and/or a TE heat pump. The integrated load cell enables us to study the effect of pressure on the TE materials and nanostructured interfaces. The rig has three orthogonal linear stages that enable perfect alignment and even pressure distribution between the hot side and the cold side.

A high temperature rig is needed to measure the mechanical characteristics of TE materials up to 700 K.

Furthermore, the sample needs to be in a vacuum environment in order to prevent oxidation. A separate rig was therefore designed to produce this high temperature and to allow optical access to the sample. This rig utilizes a high power electrical resistance cartridge to heat and maintain the temperature of the hot side. The cold side is cooled using a fin array heat exchanger with a chilled water loop. The sample is compressed between the hot side and the cold side via a clamping system that minimizes misalignments. Temperatures up to 400°C have been achieved on the hot side in open air. This entire clamping mechanism is adjacent to a chilled water loop heat exchanger, and this temperature difference serves to drive the heat flux through the sample. Figure 4 shows the entire heating assembly and clamping mechanism are contained within a vacuum chamber. The vacuum environment prevents oxidation of the sample and the measurement components. Alternatively, the chamber can be pressurized with an inert gas, such as nitrogen or argon. A sapphire window, which is transparent to thermal infrared radiation, is positioned above the cross-section of the sample stack to provide optical access during the measurement.

Skutterudite Synthesis

Binary skutterudites (compounds with composition MX_3 where M = Co, Rh or Ir and X = P, As or Sb) and have attracted attention as intermediate temperature TE materials because of their excellent electrical properties [6-8]. The crystal structure of these compositions allow for two large "voids", or icosahedrons formed by 12 Sb atoms, per cubic unit cell that can accommodate "guest" species such as alkali metals, alkali earths or rare earths. Filling of the voids in the structure with these undersized "guest" atoms, relative to the voids, yields a marked reduction in thermal conductivity, κ. These void-filling atoms "rattle" in their voids (dynamic disorder) substantially affecting the phonon propagation through the lattice. N-type skutterudties have been relatively well investigated [7,8] however the TE properties of p-type compositions remain much lower than that of n-type compositions. Our efforts focus on investigating the fundamental properties in understanding and optimizing the transport of p-type $CoSb_3$-based skutterudites.

Our recent efforts have centered on the preparation and characterization of filled ternary skutterudites that are isoelectronic to the binary skutterudites. Ternary skutterudites can be obtained either by substitution at the anion site, X, by a pair of elements from groups 14 and 16 (e.g. $CoGe_{1.5}S_{1.5}$) [9], or by isoelectronic substitution at the cation site, M, by a pair of elements from groups 8 and 10 (e.g. $Fe_{0.5}Ni_{0.5}Sb_3$) [10]. The filler atoms can be a rare earth metal like Ce and Yb. Although a number of ternary skutterudites have been reported [9,14], there has been little work to date on the structural and physical properties of these materials. While ternary skutterudites formed by cation substitution appear to be isostructural to the binary skutterudites, structural studies carried out on materials prepared by anion substitution, such as $CoSn_{1.5}S_{1.5}$ and $CoGe_{1.5}Te_{1.5}$ [11,12], suggest that these compounds crystallize in a modification (Rhombohedral, R-3) of the skutterudite structure (Cubic, Im-3). We have recently synthesized filled-$Co_4X_6Y_6$ compositions where X is Ge or Sn and Y is Se or Te (Figure 5). We are in the process of investigating the transport properties of these novel skutterudite composition.

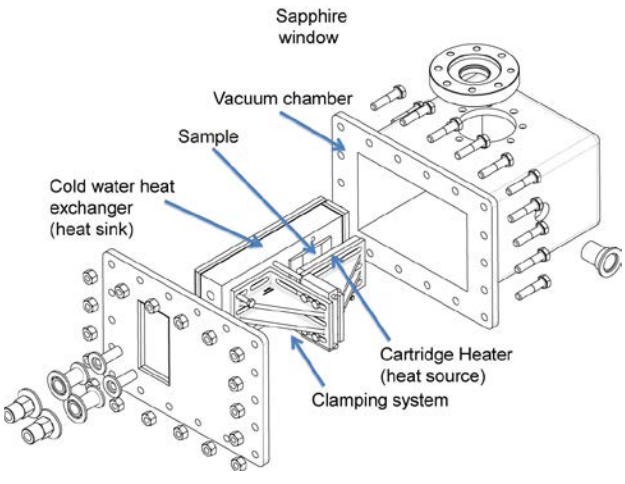

FIGURE 4. Exploded computer-aided design view of clamping system, vacuum chamber, and infrared-transparent sapphire viewport.

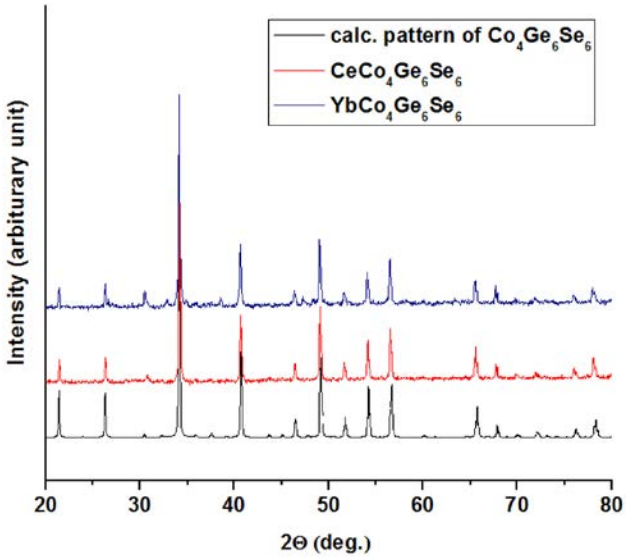

FIGURE 5. X-ray diffraction spectra of $CeCo_4Ge_6Se_6$ and $YbCo_4Ge_6Se_6$ in comparison to that of calculated spectra for $Co_4Ge_6Se_6$.

Conclusions

The following achievements have been completed in FY 2011 under this project:

- We developed CNT-based TIM tape technology that improves the reliability and performance of TEGs.
- We developed in situ measurement techniques and tools for characterization and reliability testing of TEG devices using high resolution infrared thermometry.
- We have measured the thermal transport properties of TE pellets and interfaces.
- We have designed and are manufacturing a rig for in situ characterization of TE pellets and TIMs up to 800 K.
- We have done extensive mechanical and thermal characterization of stand-alone CNT films using nano/picosecond thermoreflectance and atomic force microscopy nanoindentation techniques. Experimental data for the in-plane and out-of-plane modulus of CNT films are reported.
- University of South Florida team has developed TE high-temperature materials including skutterudites and half-Heusler alloys.

References

1. Y. Won, Y. Gao, M.A. Panzer, S. Dogbe, L. Pan, T.W. Kenny, and K.E. Goodson, "Mechanical Characterization of Aligned Multi-Wall Carbon Nanotube Films," Carbon, vol. 50, pp. 347-355, 2012.

2. Schmidt, A. J., Cheaito, R., and Chiesa, M., 2009, "A Frequency-Domain Thermoreflectance Method for the Characterization of Thermal Properties," Review of Scientific Instruments 80(9), pp. 094901-6.

3. A.A. Zbib, et al., *Nanotechnology,* vol. 19, p. 175704, 2008.

4. M. Bedewy, *et al.*, *The Journal of Physical Chemistry C,* vol. 113, pp. 20576-20582, 2009.

5. Markaki, A.E., & Clyne, T.W. (2003). Mechanics of thin ultra-light stainless steel sandwich sheet material. Acta Materialia, 51(5), 1341–1350.

6. G.S. Nolas, J.W. Sharp, H.J. Goldsmid, *Thermoelectrics: Basics Principles and New Materials Developments*. Springer-Verlag, 2001.

7. G.S. Nolas, D.T. Morelli, T.M. Tritt, "Skutterudites: A phonon-glass-electron crystal approach to advanced thermoelectric energy conversion applications." *Annu. Rev. Mat. Res*., vol. 29, p. 89, 1999, and references therein.

8. C. Uher in *Semiconductors and Semimetals*, Vol. 69, edited by T.M. Tritt, (Academic Press,

San Diego, 2000) p. 139, and references therein.

9. R. Korestein, S. Soled, A. Wold, G. Collin, *Inorg. Chem*. 16 (1977) 2344.

10. A. Kjeshus, D.G. Nicholson, T. Rakke, Acta Chem. Scand. 27 (1973) 1315.

11. J. Navrátil, T. Plecháček, L. Beneš, Č. Drašar, F. Laufek, *J. Elec. Mater*. 39 (2010) 1880.

12. P. Vaqueiro, G.G. Sobany, A.V. Powell, *Dalton Trans*. 39 (2010) 1020.

13. F. Laufek, J. Navrátil, J. Plášil, T. Plecháček, Č. Drašar, *J. Alloys Compd*. 479 (2009) 102.

14. G.S. Nolas, J. Yang, R.W. Ertenberg, *Phys. Rev. B*68 (2003) 193206.

FY 2011 Major Publications/Presentations

1. Marconnet, A.M., Yamamoto, N., Panzer, M.A., Wardle, B.K., and Goodson, K.E., 2011, "Thermal Conduction in Aligned Carbon Nanotube-Polymer Nanocomposites with High Packing Density," ACS Nano, Vol. 5, pp. 4818-4825.

2. Won, Y., Gao, Y., Panzer, M.A., Dogbe, S., Pan, L., Kenny, T.W., and Goodson, K.E. "Mechanical Characterization of Aligned Multi-Wall Carbon Nanotube Films," *Carbon*, vol. 50, pp. 347-355, 2012.

3. Lee, J., Marconnet, A., Asheghi, M., Kim S., Wong, H.S., in 't Zandt, M.A.A., Goodson, K.E. "Thermoelectric Power Generation using an SOI-Based Device," *Journal of MicroElectroMechanical Systems*, in press.

4. A. Marconnet, "Multi-functional Carbon Nanotube Films and Composites," in *Nanotechnology for Defense Symposium, 2011 (invited talk)*.

5. *K. Goodson, "Nanostructured Interfaces for Thermoelectric Energy Conversion," Keynote Address, ASME IMECE, Denver, Colorado, November, 2011.*

III.5 Integrated Design and Manufacturing of Cost-Effective and Industrial-Scalable TEGs for Vehicle Applications

Lei Zuo[1] (Primary Contact), Jon Longtin[1], Sanjay Sampath[1], Qiang Li[2]
[1]Stony Brook University
Stony Brook, NY 11777
[2]Brookhaven National Laboratory
Upton, NY 11973

NSF Manager: Sumanta Acharya

DOE Technology Development Manager: John Fairbanks

NETL Project Manager: Carl Morande

Overall Objectives

- Development of a scalable high-throughput, non-equilibrium synthesis process for high-figure of merit (ZT) thermoelectric (TE) materials from abundant low-cost feedstock by using rapid quenching.
- Development of an integrated manufacturing process to fabricate TE structures directly onto exhaust pipe components with enhanced performance, durability, and heat transfer using thermal spray and laser micromachining.

Fiscal Year (FY) 2011 Objectives

- Non-equilibrium synthesis of silicide-based TE materials.
- Benchmark study of thermal sprayed TE materials ($FeSi_2$).
- Thermal spray of high-ZT TE materials (Mg_2Si, etc.).
- ZT measurement and performance characterization of fabricated materials.
- Initial development of manufacturing/laser machining processes.

Accomplishments

- Introduced melt-spinning method and demonstrated non-equilibrium synthesis of single-phased $MnSi_{1.75}$ (higher manganese silicide, HMS), achieving a reduction of 15% in thermal conductivity and 15% in electrical resistance, with the Seebeck coefficient unchanged.
- Conducted thermal spray study of FeSi using masks, and successfully demonstrated the spraying of 2 mm-thick FeSi materials.
- Investigated plasma spray and high velocity oxygen fuel (HVOF) spray of Mg_2Si, and obtained reasonable thermal and electric conductivity, and identified the key challenges to improve the Seeback coefficient.
- Performed detailed survey of exhaust heat sources of several vehicles under different operation conductions, and optimized the geometric parameters of the thermoelectric generator (TEG) elements for these heat loads.
- Conducted laser micromachining of several candidate TE materials and conductor layers, and optimized laser cutting parameters.

Future Directions

- Reduce the oxide in the thermal spray by using vacuum spray and higher particle velocity, and examine the electron carried density to increase Seeback.
- Analyze the micro- and nanostructures of thermal sprayed silicide materials, study the interface of the microstructures, and seek approaches to improve the ZT.
- Demonstrate the three-dimensional (3D) fabrication of a TEG structures on both a flat coupon and cylindrical exhaust pipe component using thermal spray and laser micromachining. Verify operation.
- Evaluate the rapid quench effect of melting spinning and thermal spray, fine tune the chemical and structural parameters to optimize their thermoelectric and mechanical properties, and explore $MnSi_{1.75}$ as a leading TE candidate material.

Introduction

In contrast to traditional state-of-the-art vehicle TEG technologies based on material synthesis, module assembly, subsystem and vehicle integration, this project aims at an innovative, integrated approach towards cost effective and industrially-scalable TEGs. It builds on recent advances in TE materials at Brookhaven National Laboratory and thermal spray material processing at Stony Brook University with novel design and fabrication strategies to directly fabricate TE structures in a layered fashion onto exhaust components for robust and durable performance. The fabrication involves a novel extension to the thermal spray process, namely direct-write thermal spray

coupled with laser micromachining to create two-dimensional and 3D mesoscale TE structures. The non-equilibrium conditions produced during the thermal spray process is expected to provide increased ZT in the resulting deposited thermoelectric material. Further, the manufacturing process itself is readily scalable for industrial volumes required for practical implementation of vehicle TEGs.

Using a system-driven approach, in year 1 we have successfully obtained single-phase HMS using melt-spinning and successfully demonstrated thermal spray of silicide materials. We obtained reasonable thermal and electrical property of sprayed Mg_2Si, and identified that the key challenges are to reduce oxides in the deposited material and improve the Seebeck coefficient. We are also developing 3D TEG fabrication techniques using thermal spray and laser cutting. The planned goals of year 1 were successfully achieved. The year 2 goals are to achieve high-ZT TE materials using thermal spray and to demonstrate the fabrication of working 3D TE structures.

Approach

The team worked on three tasks simultaneously: melt spinning of HMS, thermal spray of silicides, and engineering design and fabrication.

- The phase diagram of Mn-Si indicates it is rather difficult to synthesize through conventional solid state reaction methods due to the high melting point and MnSi and Si secondary phases. We introduced non-equilibrium synthesis method (melt spin) and successfully obtained a single-phased HMS by using the induction coil to fully melt the raw material on the melt spinner, followed by an extremely high quench rate, which minimized phase separation during cooling.
- For the thermal spray activities, we conducted a series experimental studies on FeSi and Mg_2Si using plasma spray and HVOF both with and without a shroud gas (to minimize oxidation), at different spray speeds ranging from 90 to 210 m/s. We then characterized the samples using X-ray diffraction (XRD), scanning electron microscopy, and energy dispersive spectrometer, and measured the thermal conductivity, electrical conductivity, and Seebeck coefficient for the samples.
- In terms of design and fabrication, we performed an extensive survey of vehicle heat sources including the temperature, mass flow rate, and waste heat power of different vehicles [2]; we optimized the geometric parameters (shape, thickness, gap) of the TE elements used in our devices, explored laser cutting of sprayed TE materials and conductor layers.

Results

Figure 1 presents the overall system concept. TEG devices are fabricated directly onto exhaust pipe components using thermal spray deposition and laser micromachining. The TEG devices are fabricated layer-by-layer to provide the required device functionality.

Figure 2 shows characterization results for both single-step melt spinning traditional solid state reaction methods for $MnSi_x$: (a) XRD, (b) thermal conductivity, (c) electrical resistivity. Specifically:

- Single-phased $MnSi_{1.75}$ was obtained using single-step melt spinning.
- The thermal conductivity and electrical resistivity are both reduced by more than 15%.
- The Seebeck coefficient remains unchanged (not shown).

Figure 3 shows the results of thermal spray of Mg_2Si, including (a) XRD, (b) thermal conductivity, (c) electrical conductivity, (d) Seebeck coefficient. It should be noted that for the year 1 the benchmark study of thermal spray, we use less expensive Mg_2Si powders with higher impurity. Once the thermal spray parameters are optimized we will use high-purity powder.

- The Mg_2Si feedstock powder has purity 95%, with 3.4% MgO and 1.4% Mg impurities.
- Compare with HVOF spray, arc plasma spray suppressed oxide, but the MgO content in the sprayed sample was still as high as 16%. An inert gas shroud slightly reduced the oxide. A smaller

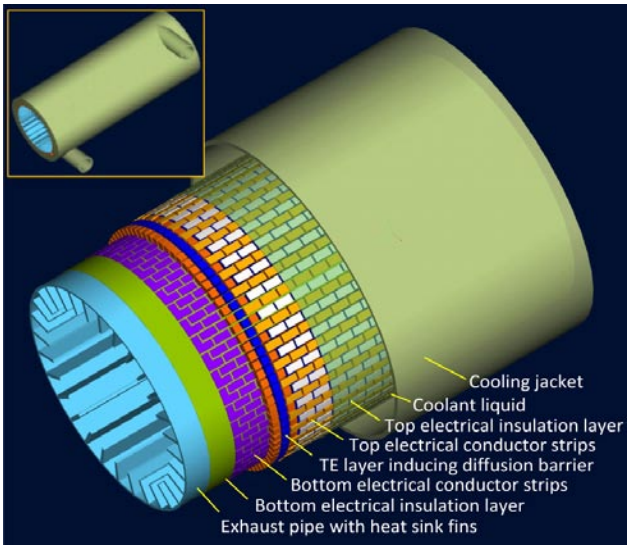

FIGURE 1. System driven approach to the vehicle TEG: funcational materials are directly deposited onto automotive exhaust component, and integrated heat sink removes exhaust heat and redirects to multilayer conformal thermoelectric device layer.

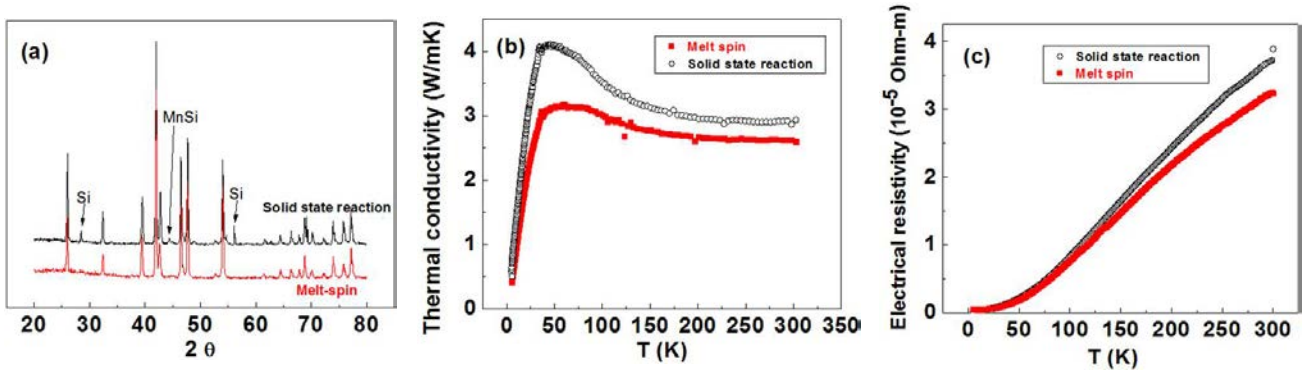

FIGURE 2. Comparison between one-step melt spinning method and traditional solid state reaction method of MnSi using (a) XRD, (b) thermal conductivity and (c) electrical resistivity.

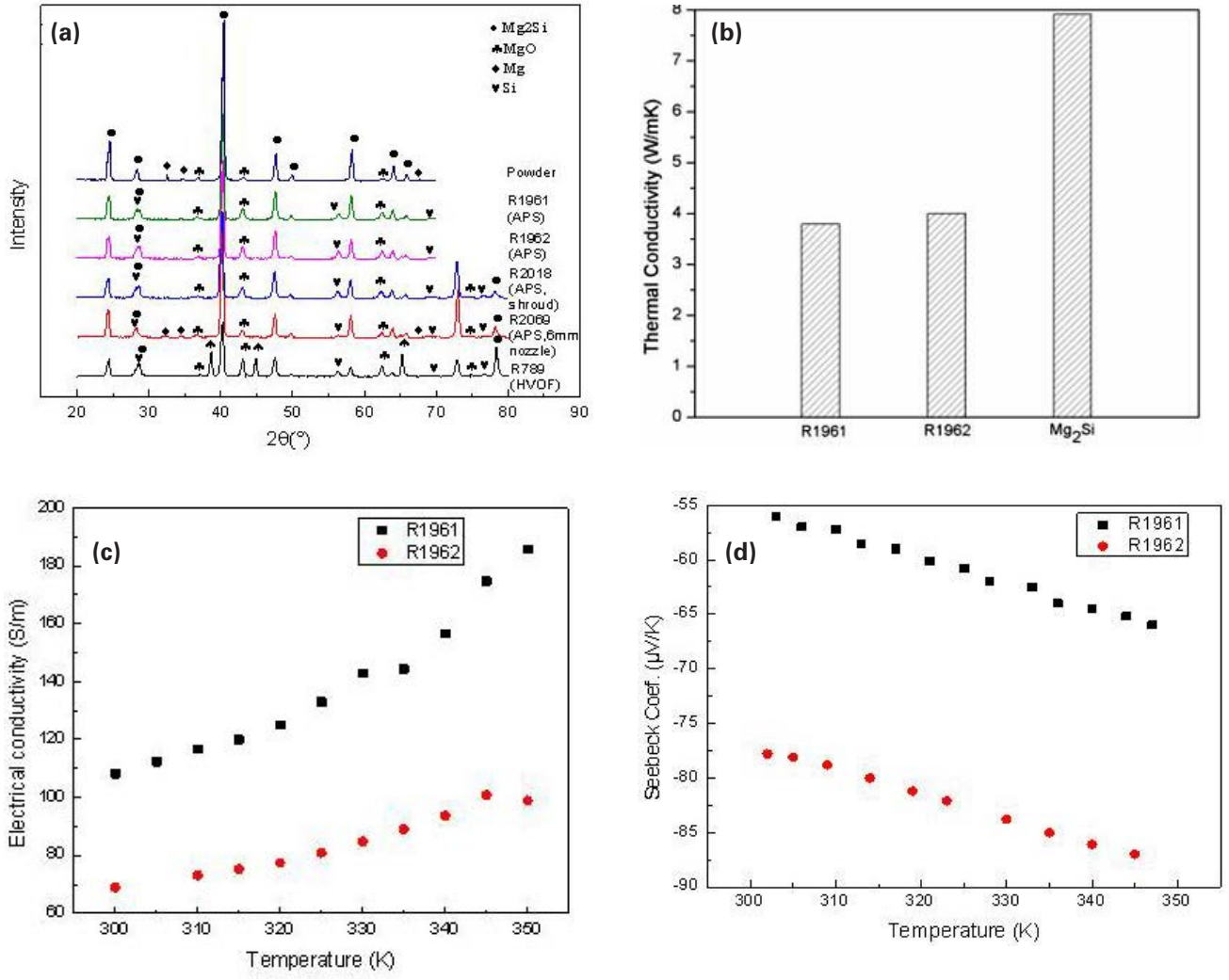

FIGURE 3. Properties of Mg_2Si fabricated with thermal sprayed: (a) XRD of feedstock powder and sprayed samples, (b) thermal conductivity in comparison with bulked Mg_2Si, (c) electrical conductivity, and (d) Seebeck coefficient. The Seeback coefficient is significantly worse than the values obtained using traditional methods in literature. The spray parameters for samples R1961, R1962 and R2069 are temperature 1,781, 1,834, and 1,787 K, and velocities 155, 183, and 211 m/s, respectively.

nozzle and higher particle speed yielded modestly better results, but the MgO is as high as 10%.

- Compared with data for Mg_2Si prepared using a hot press in the literature, the electrical conductivity and thermal conductivity decreases slightly, but the Seeback coefficient is significantly worse.
- More research is required to reduce the oxide in thermal spray. The team is investigating vacuum spray for Mg_2Si materials to reduce the oxide. We are also looking into the micro and nano structures and electron carried density to better understand their relationship on the measured thermoelectric properties.

Figure 4 shows the demonstration of a thick film deposition for device fabrication. In this example, several pillars of FeSi silicide with dimensions of 6 mm wide by 10 mm long were sprayed with a thickness of 2 mm. The deposition was done using thermal spray through a mask, i.e., a thin metal sheet with windows placed adjacent to the substrate and through which sprayed material passes to form features. The pillars are uniform in shape and exhibit excellent adhesion.

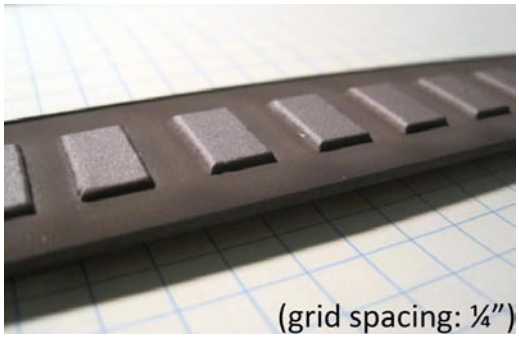

FIGURE 4. Thick (2 mm) metal silicide film fabricated with thermal spray by the team. When using TEG materials, these pillars would form the p- and n-type device legs.

Figure 5 shows the successful laser cutting of several thermal-sprayed TEG materials, including Mg_2Si, MnCoNi, CoO, and TiO_x. Cutting was performed using nanosecond pulsed lasers with wavelengths of 1060 nm and 527 nm. The Mg_2Si sample was 1.5 mm thick sprayed onto an alumina substrate, while the CoO and MnCoNi were 50 um thick and the TiOx sample was 2 mm thick. Several trials were required to establish that the optimum laser beam parameters including laser power, cutting speed, number of passes and focal spot size. For Mg_2Si, CoO, and TiO_x, cutting in ambient air resulted in oxidation. Cutting using nitrogen, carbon dioxide, argon and helium shield gases yielded considerable improvement in cut quality, with reduced oxidation.

Conclusions

We have met the planned goals of year 1 of achieving high performance silicide-based TE using melt spinning non-equilibrium synthesis and conducting benchmark studies of thermal spray for metal silicides.

- The HMS obtained through non-equilibrium synthesis with fast quenching has improved thermoelectric properties over bulk materials.
- Thick films of Mg_2Si were formed using thermal spray.
- Oxidation is a problem for magnesium silicide when thermal spraying; as a result, the Seebeck coefficient is significant lower than that obtained using traditional method.
- Arc plasma spray is better than HVOF, but there is still too much oxide present. Faster particle speeds and smaller nozzles should further suppress oxide.

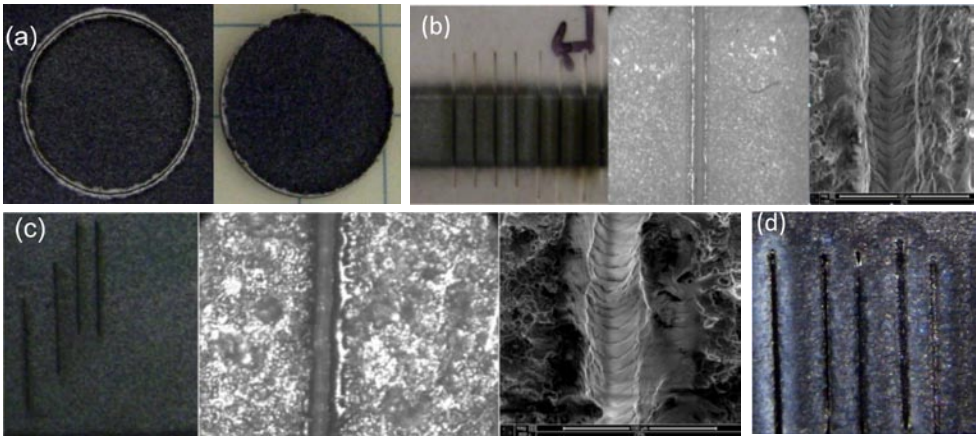

FIGURE 5. Laser cuts of several candidate TEG materials. Clockwise from upper left: (a) MgSi cut through substrate to form self-standing pellet, (b) MnCoNi, (c) CoO, (d) TiO_x. Cuts are clean in all cases, even through 1-2 mm thick coatings, with good feature quality overall.

Vacuum spray is also being explored to reduce oxide formation.

- Laser micromachining with optimized cutting parameter works well for the cutting of sprayed metal conductor and metal-silicide. Parameters need to be further optimized to reduce the thermal stress and improve adhesion.

Our goals in year 2 are:

- Improve the thermal properties of Mg_2Si when thermal spraying, especially the Seebeck coefficient. The approaches include (1) reducing oxide by using vacuum spray and (2) tuning the spray temperature and velocity to reduce the electron carrier density and analyzing the microstructure of the sprayed sample.
- Fine tune the chemical and structural parameters to optimize their thermoelectric and mechanical properties in melt spinning, and scale up the non-equilibrium synthesis from melt spinning of HMS to thermal spray by taking advantage the similarity between the melt spin and the thermal spray techniques.
- Demonstrate the fabrication of 3D interconnected TE structure on both flat plate, and then cylindrical pipe substrates using thermal spray and laser micro machining.

FY 2011 Publications/Presentations

1. "Integrated Design and Manufacturing of Cost-Effective and Industrial-Scalable TEG for Vehicle Applications", Lei Zuo, Jon Longtin, Sanjay Sampath, Qiang Li and Baosheng Li, *DOE 2nd " Thermoelectric Applications Workshop*, San Deigo, CA, 01/04-01/05/2011.

2. "Review of exhaust heat energy of automobiles", Gaosheng Fu, Lei Zuo, Bo Zhang, and Jon Longtin, submitted to *ASME 2012 Summer Heat Transfer Conference*.

3. "Thermal and electrical properties of Mg_2Si layeres prepared with plasma spraying methods," Yikai Chen, Bo Zhang, Gaosheng Fu, Lei Zuo, Jon Longtin, and Sanjay Sampath, submitted to *International Thermal Spray 2012 Conference and Exposition* (ITSC 2012).

4. "Thermoelectric Properties of Mg_2Si Prepared by Thermal Spraying," Bo Zhang, Yikai Chen, Gaosheng Fu, Lei Zuo, Jon Longtin, and Sanjay Sampath, submitted to the *ASME 2012 Summer Heat Transfer Conference*.

5. "Fabrication of Thermoelectric Devices for Vehicle Exhaust Applications Using Thermal Spray," Jon Longtin, Lei Zuo, David Hwang, and Sanjay Sampath, submitted to the *ASME 2012 Summer Heat Transfer Conference*.

6. Portions of this research have also been presented at several technical presentations at *6th Annual Energy Harvesting Workshop* in Roanoke VA, *Northeastern University*, Boston, MA, the *Long Island ASM Chapter*, NY, and *Accelerate Long Island Showcase*, NY.

Special Recognitions & Awards/Patents Issued

New Technology Disclosure, "Cost-Effective and Industrial-Scalable Thermoelectric Material and Device Fabrication for Automotive Applications using Thermal Spray," Stony Brook University, filed 2/3/2011.

III.6 Inorganic-Organic Hybrid Thermoelectrics

Sreeram Vaddiraju
Department of Chemical Engineering
237 Jack E. Brown Bldg., 3122 TAMU
Texas A&M University
College Station, TX 77843

NSF Manager: Sumanta Acharya

DOE Technology Development Manger: John Fairbanks

NETL Program Manager: Carl Morande

Overall Objectives

- Synthesis of inorganic nanowires and quantum wires of both $CoSb_3$ and InSb, and organic conducting polymer thin films, and assembling them into inorganic-organic hybrid thermoelectrics cells with sizes ranging from a few mm^2 to a few cm^2, using conjugated linker molecules to tether the nanowires to each other or to conducting polymer thin films.
- Systematically studying the effect of inorganic nanowire size and organic conducting polymer thin film chemistry and thickness on their individual thermoelectric performance, and also on their performance when used in unison as 'molecular wired' inorganic-organic hybrids, in the temperature range of 300-1,100 K.
- Determine the type of the metal required for assembling individual thermoelectric devices into thermoelectric modules without lowering their performance, i.e., finding metals that have very low contact resistance with individual thermoelectric cells.

Fiscal Year (FY) 2011 Objectives

- Synthesis of $CoSb_3$ and InSb nanowires in a contaminant-free manner using self-catalysis schemes and producing gram-quantities of these nanowires.
- Determine the performance of individual $CoSb_3$ and InSb nanowires in the 300-1,100 K temperature regime.
- Deposition of conducting polymer thin films by chemical vapor deposition (CVD) and understanding the effect of thickness on the thermoelectric performance of conducting polymers.

Accomplishments

- Accomplished the synthesis of pristine InSb nanowires, devoid of any oxide, for thermoelectric performance measurement.
- Accomplished the synthesis of phase-pure $CoSb_3$ skutterudite nanowires, without any CoSb and $CoSb_2$ phase contaminants.
- Determined the effect of nanowire morphology on the thermoelectric performance of an additional material, namely Zn_3P_2. This task included the synthesis of Zn_3P_2 nanowire powder, pressing the nanowire powder into 7 mm-diameter, 2 mm-thick pellets, and measuring the thermoelectric performance of Zn_3P_2 nanowire pellets. The knowledge gained form this materials is expected to be helpful in the bulk production of InSb and $CoSb_3$ nanowire powders and pellets.

Future Directions

- Evaluate the thermoelectric performance of $CoSb_3$ and InSb nanowire pellets in the 300-1,100 K temperature range. This task includes bulk synthesis of $CoSb_3$ nanowire powders (scale up of the current microgram production capability), in situ functionalization of the nanowires and pressing nanowire powder into pellets. Experiments performed for the bulk production of Zn_3P_2 nanowires is expected to greatly aid in the large-scale synthesis of $CoSb_3$ and InSb nanowire powders. The thermoelectric performance measured will be verified in-house at the Jet Propulsion Laboratory in collaboration with Dr. J.P. Fleurial's group.
- Compare the performance of $CoSb_3$ and InSb nanowire pellets and their hybrids (composed of nanowires bound together with organic conjugated linker molecules) with that of single nanowires.
- Compare the performance of $CoSb_3$ and InSb nanowire pellets and nanowire-conducting polymer hybrids, with that of individual nanowires.

Introduction

The operational anatomy of a typical automobile engine shows that approximately 40% of the heat generated by gasoline combustion is lost through the exhaust gases [1]. Solid-state thermoelectric modules could convert this heat into electricity in a clean manner, without the generation of any additional greenhouse gases.

The performance of thermoelectrics depends on a dimensionless number called the figure of merit (zT). This figure of merit (zT) is related to the Seebeck coefficient (s), electrical conductivity (σ), the thermal conductivity (κ) and the absolute temperature (T) according to the following relationship: $zT = s^2\sigma T/\kappa$ [2,3]. The contribution to thermal conductivity comes from both the lattice ($\kappa_{lattice}$) and the carriers (κ_e) in semiconductors, i.e. $\kappa = \kappa_{lattice} + \kappa_e$ [2,3]. The fabrication of thermoelectrics requires a material that is a good electrical conductor, but a poor thermal conductor. According to the Wiedemann-Franz relationship, κ_e cannot be reduced without significantly reducing the electrical conductivity. But, $\kappa_{lattice}$ could be reduced (through enhanced phonon scattering) without significantly affecting the electrical conductivity [2,3]. Nanostructuring of materials serves as an ideal route for selectively reducing the $\kappa_{lattice}$ of materials [4]. In this context, the primary objective of this project is the development of simple strategies for the bulk synthesis, assembly and thermoelectric performance evaluation of sub-5-nm thick nanowires of two materials systems, $CoSb_3$ and InSb. Large-scale assembly of the nanowires is proposed to be performed by binding them together using conjugated organic linker molecules. Thermal and electrical transport across the nanowires interfaces will be tuned by varying the chemistry of the linker molecules. $CoSb_3$ and InSb are chosen as the two materials systems because of the unique, but distinctive, advantages they offer. $CoSb_3$ has a skutterudite structure with empty cages in the lattice [5]. Phonon scattering can be enhanced and hence the lattice thermal conductivity could be reduced in skutterudites by either employing quantum wires with diameters less than the mean free path of the phonons or by filling the cages with foreign atoms. InSb has a zincblende crystal structure with very large Bohr exciton radius of 54 nm [6] and high mobility of 7.8×10^4 $cm^2V^{-1}S^{-1}$ [7]. The large Bohr exciton radius of InSb makes it an ideal candidate for understanding its thermoelectric behavior under quantum confined conditions.

Approach

All the nanowire synthesis experiments were performed using a typical hot-walled CVD chamber. This chamber comprised of a quartz tube, housed inside an oven, connected to a vacuum pump at one end and precursor supply at the other. This CVD chamber was also equipped with all the accessories necessary for temperature and pressure measurement and control. For the synthesis of InSb nanowires, vapor transport of antimony (using either $SbCl_3$ or polycrystalline InSb powders as sources) onto indium-coated substrates was employed. Vapor transport of both cobalt and antimony onto substrates was employed for the synthesis of $CoSb_3$ nanowires. $CoCl_2$ and $SbCl_3$ served as the sources for cobalt and antimony, respectively. Finally, the synthesis of Zn_3P_2 nanowires was accomplished using vapor transport of phosphorus onto heated zinc foils. Additional, experimental details are provided in the Results section below.

Seebeck coefficient of the pellets was measured using the analogue subtraction method, [8] while the electrical and thermal conductivities were measured, respectively, using the 4-point probe method the comparative method [9]. For these measurements, Zn_3P_2 nanowire powders were pressed into 7 mm-diameter, 2 mm-thick pellets. The pelletization of nanowire powders was accomplished by pressing them at a pressure of 1 GPa for 1 hour, followed by sintering them at 825 K for 6 hours.

Results

Indium Antimonide Nanowire Synthesis

The indium-antimony binary phase diagram [10] indicates that reaction of indium with antimony, under excess indium conditions, leads to the precipitation of indium antimonide from the eutectic indium droplets. Consequently, the supersaturation of indium droplets with antimony is expected to lead to the nucleation and basal growth of InSb nanowires from indium [11]. Experiments for the synthesis of InSb nanowires were performed by supplying antimony from a mixture of InSb polycrystalline powder and $SbCl_3$ onto indium coated substrates. The antimony source temperature in these experiments was 873 K and the temperature of the substrate was 773 K. A key improvement made was the synthesis of InSb nanowires, in a pristine manner devoid of any indium oxide. Typically formation of InSb is accompanied with the formation of indium oxide. The oxygen required for the oxidation of indium comes either from the native indium oxide layer on top of the indium source or from the moisture associated with $SbCl_3$. Remedies, such as the removal of the native indium oxide layer on the indium source by etching it with acid, reduce the amount of indium oxide formed, [12] but do not completely eliminate its formation. To completely prevent indium oxide formation, salt substrates (obtained by pressing KBr powders into pellets) were employed instead of the amorphous quartz substrates. InSb nanowires (Figure 1a) synthesized on pressed KBr pellet substrates were observed to be free of any oxide (Figure 1b). This might be due to the reduction of any indium oxide present by KBr into indium, similar to the way salt is used in metallurgy to remove aluminum oxide from aluminum [13].

Cobalt Antimonide Nanowire Synthesis

The binary phase diagram of cobalt and antimony [14] indicates that reaction of antimony and cobalt, under excess antimony conditions, should lead to

the precipitation of $CoSb_3$ from antimony. If the experimental conditions are tuned, reaction of antimony and cobalt should lead to the self-catalytic growth of $CoSb_3$ nanowires via liquid phase epitaxy through antimony droplets at the tips [15]. The formation of the desired skutterudite phase ($CoSb_3$) requires the reaction of 87% antimony with 13% cobalt by weight on substrates. The large difference in the vapor pressures of the two metals also adds another complexity to the $CoSb_3$ nanowire synthesis experiments.

CVD experiments performed using $CoCl_2$ and $SbCl_3$ as the sources for cobalt and antimony, respectively, at a temperature of 1,050 K, resulted in the formation of CoSb nanowires. At the same temperature, increasing the flux of antimony resulted in the formation of $CoSb_2$ nanowires. It is useful to note that the $CoSb_2$ nanowires shown are growing out of a thin film of $CoSb_3$. Further increase in the flux of antimony led to the formation of pure-phase $CoSb_3$ nanowires (Figure 2a), growing out from an underlying antimony thin film. The phase purity of the nanowires was verified using XRD (Figure 2b). Currently, thermoelectric measurements are being performed on single $CoSb_3$ nanowires, and the bulk nanowire production scale-up to make macro-devices from $CoSb_3$ nanowires is underway.

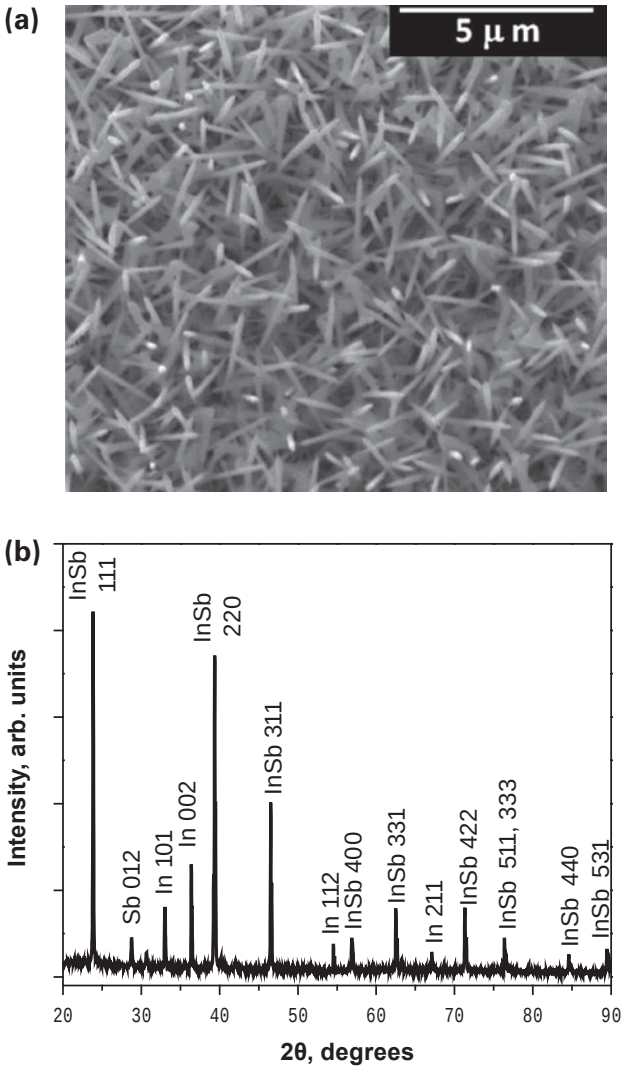

FIGURE 1. (a) Scanning electron micrograph and (b) X-ray diffraction (XRD) pattern of InSb nanowires synthesized on pressed KBr pellet substrates. The XRD pattern clearly indicated that no oxide is formed during the synthesis of InSb nanowires. XRD analysis also showed the presence of excess indium and antimony on the substrate (indicated using In for indium and Sb for antimony).

Zinc Phosphide Nanowire Synthesis

To understand the challenges involved in scaling up the production of nanowires by self-catalysis schemes, Zn_3P_2 nanowire synthesis was accomplished and the process was scaled-up for the bulk production of nanowire powders. These experiments were performed concurrently with the $CoSb_3$ and InSb

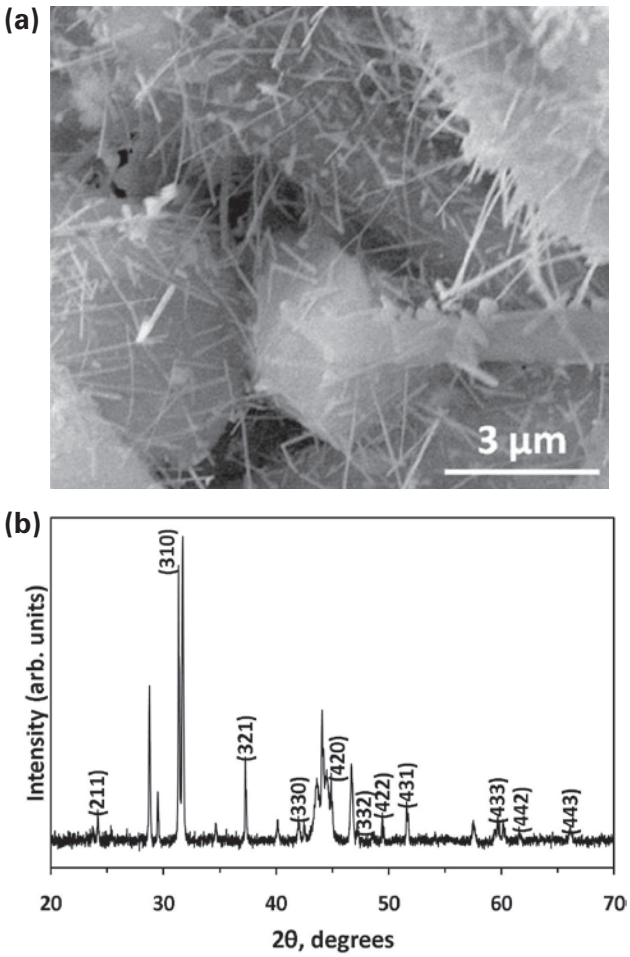

FIGURE 2. (a) Scanning electron micrograph of phase-pure $CoSb_3$ nanowires synthesized by using vapor transport of both cobalt and antimony onto substrates. (b) XRD pattern of the nanowires synthesized indicating the presence of only $CoSb_3$.

nanowire synthesis experiments. Zn_3P_2 nanowires were synthesized by reactive vapor transport of zinc and phosphorus onto substrates. Polycrystalline zinc phosphide powder served as the source for this purpose. For the synthesis of nanowires, the source was maintained at a temperature of 1,375 K and the substrates at 875 K. This reactive vapor transport procedure typically produced high quality single crystalline nanowires with diameters of 25 nm.

The synthesis process was scaled up by using phosphorus as a source and transporting it via the vapor phase onto heated zinc substrates. These experiments were carried out at a phosphorus source temperature of 775 K and a zinc substrate temperature of 700 K. Using this method, gram quantities of Zn_3P_2 nanowire powder were produced. Micrographs of zinc foil before and after reactive vapor transport of phosphorus are depicted in Figure 3(a). Another micrograph of a 100 cm^2 area zinc foil covered with Zn_3P_2 nanowires is shown in Figure 3(b). The supersaturation of zinc droplets formed on top of the foil with phosphorus led to the bulk nucleation and basal growth of nanowires. Following the reactive vapor transport experimentation, the Zn_3P_2 nanowires covering the zinc foils were simply brushed off (Figure 3(c)). A scanning electron micrograph and a transmission electron micrograph of Zn_3P_2 nanowires obtained are shown in Figure 3(d) and 3(e), respectively. Transmission electron micrograph analysis indicated that the growth direction of the nanowires is [131].

In Situ Functionalization of Zn_3P_2 Nanowires

A simple route for the large-scale assembly of inorganic nanowires is pelletization of nanowire powders. Control over the thermal and electrical properties of the interfaces between the nanowires in the pellets can be accomplished by decorating these interfaces with conjugated linker molecules. The conjugated linker molecules also offer the additional advantage of covalently binding nanowires in the pellets making them robust. In the case of Zn_3P_2, surface functionalization also offers a third advantage of stabilizing their surfaces. Although functionalization of nanowires can be performed ex situ, this process exposes the nanowires to ambient atmosphere. Exposure to ambient atmosphere leads to the oxidation of Zn_3P_2 nanowire surfaces into $Zn_3(PO_4)_2$. In order to avoid such oxidation, in situ functionalization was performed. In situ functionalization, the process of functionalizing nanowires by exposing them to a vapor of the functional molecules immediately after their synthesis, is observed to impart high stabilities to the nanowire surfaces. Preliminary in situ functionalization experiments were performed using Zn_3P_2 nanowires–4-aminothiophenol linker molecule system. Functionalization of Zn_3P_2

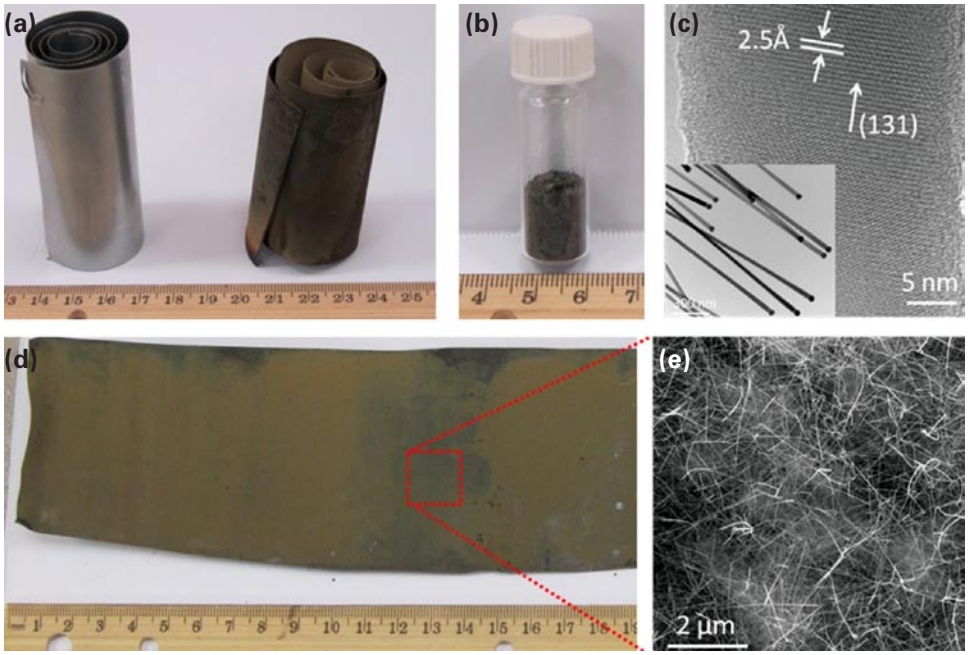

FIGURE 3. (a) Optical micrograph of a coil of zinc foil before and after the vapor transport of phosphorus. After the vapor transport of phosphorus onto heated zinc foil substrate, the substrate was observed to be completely covered with Zn_3P_2 nanowires. (b) Optical micrograph of a 100 cm^2 zinc foil covered with Zn_3P_2 nanowires. (c) Zn_3P_2 nanowire powder obtained by simply brushing the nanowire covered foil substrates. (d) Scanning electron micrograph of the synthesized Zn_3P_2 nanowires, and (e) a transmission electron micrograph of Zn_3P_2 nanowires showing that the growth direction is [131].

nanowires with 4-aminothiophenol, led to the formation of thiolate bonds between thiol groups and the zinc atoms on the nanowires surfaces. Fourier transform infrared spectroscopy (FTIR) and X-ray photoelectron spectroscopy (XPS) of the functionalized nanowires verified the formation of these thiolate bonds (Figures 4a and 4b). FTIR spectrum of functionalized nanowires showed the presence of no free thiol groups, unlike that of pure 4-amniothiophenol molecules. XPS spectrum of the functionalized nanowires clearly showed the formation of thiolate bonds between the nanowires and the 4-aminothiophenol molecules. Characteristic sulfur 2s and 2p peak binding energies of 226.9 eV [16] and 163.4 eV, [17] respectively, indicative of thiolate bonds are clearly observed in the XPS spectrum (Figure 4b). The unfunctionalized nanowires were shown to oxidize into phosphates even after a brief time out of the reactor, while this degradation was not seen in the in situ functionalized samples.

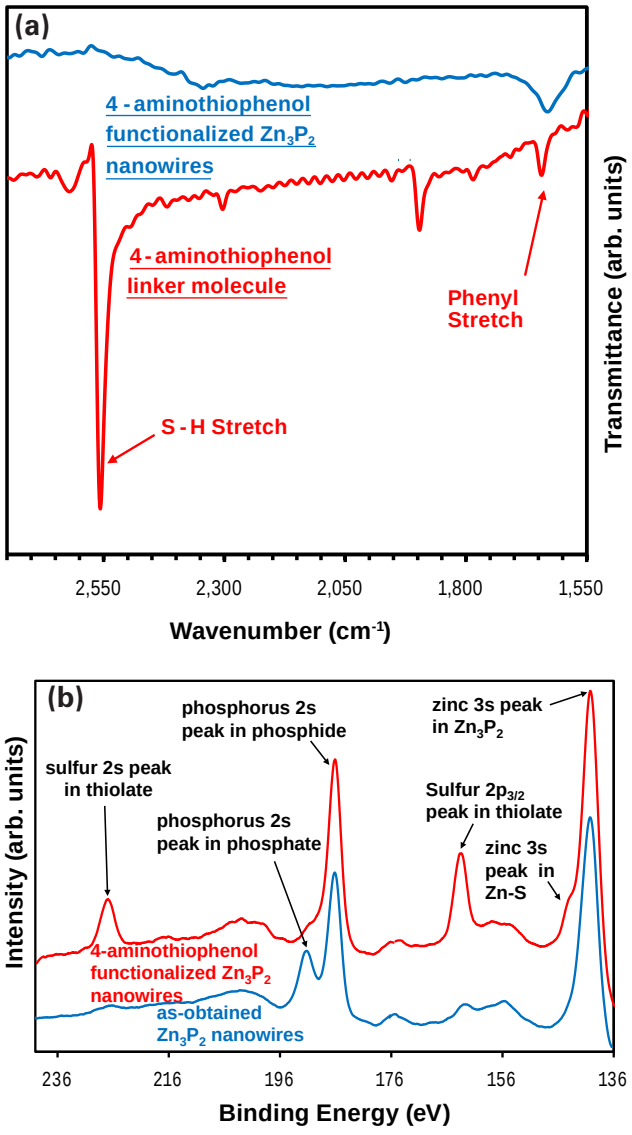

FIGURE 4. (a) FTIR spectrograph of the 4-aminothiophenol linker molecule and the functionalized nanowires showing the disappearance of the thiol stretch after the nanowires were functionalized. (b) XPS of functionalized Zn_3P_2 nanowires showing the thiolate bond formation between the 4-aminothiophenol and the nanowire surfaces. Unlike the in situ functionalized nanowires, the surfaces of the unfunctionalized nanowires oxidized into $Zn_3(PO_4)_2$.

Thermoelectric Performance of Zn_3P_2 Nanowire Pellets

As mentioned above, Zn_3P_2 nanowires powders were pressed into pellets for the measurement of their thermoelectric performance. A high Seebeck coefficient of 1.1 mV/K was observed at a temperature of 450 K. In the measured temperature range, the Seebeck coefficient was observed to increase with temperature, up to a temperature of 450 K, before decreasing gradually at temperatures higher than 450 K (Figure 5a). Electrical conductivity was also found to increase with temperature, and conductivities as high as high as 10 $(\Omega m)^{-1}$ were observed (Figure 5b). The thermal conductivity of the Zn_3P_2 nanowire pellet ranged from 0.25 to 2.2 $Wm^{-1}K^{-1}$ over the temperature range measured (Figure 5c). The obtained thermal conductivities are smaller than those previously reported [18]. Further, the activation energy of electrical conductivity was shown to be 0.34 eV, significantly less than the 1.1 eV reported previously [18]. Our experimentation also indicated that inorganic-organic hybrid pellets comprised of 4-aminothiophenol functionalized Zn_3P_2 nanowires have thermal conductivities 4.1 times lower than that of pellets comprised of only unfunctionalized nanowires.

FY 2011 Publications and Presentations

1. Brockway, L., Pendyala, C., Jasinski, J., Sunkara, M.K., & Vaddiraju, S. (2011). A Postsynthesis Decomposition Strategy for Group III-Nitride Quantum Wires. *Crystal Growth & Design, 11*(10), 4559-4564.

2. Vaddiraju, S. "NSF/DOE thermoelectrics partnership: Inorganic-organic hybrid thermoelectrics," poster presentation at the DOE Hydrogen Program and Vehicle Technologies Program Annual Merit Review and Peer Evaluation Meeting, Washington, D.C., May 9–13, 2011.

References

1. Yang, J.H.; Stabler, F.R., Automotive Applications of Thermoelectric Materials. *J. Electron. Mater.* **2009,** *38*, 1245-1251.

2. Snyder, G.J.; Toberer, E.S., Complex thermoelectric materials. *Nat. Mater.* **2008,** *7*, 105-114.

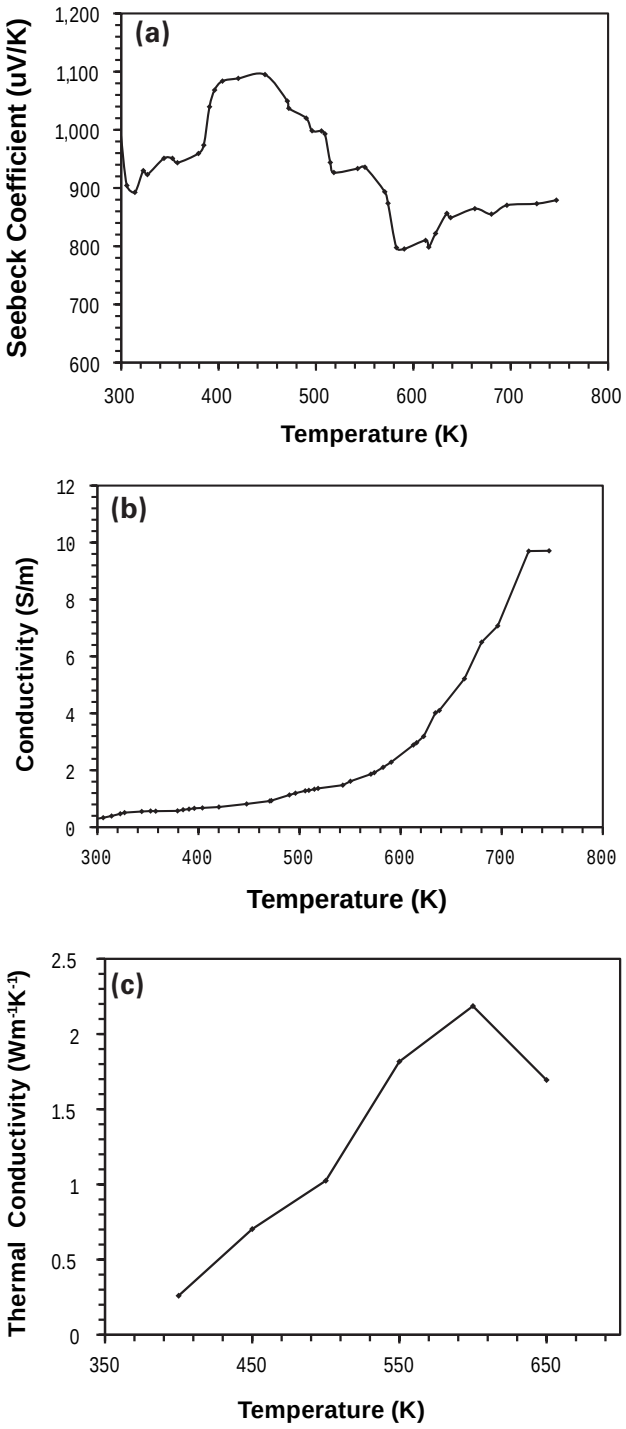

FIGURE 5. Plots indicating the variation of the (a) Seebeck coefficient, (b) electrical conductivity, and (c) thermal conductivity of a pressed Zn_3P_2 nanowire pellet with temperature.

3. Chen, G.; Shakouri, A., Heat transfer in nanostructures for solid-state energy conversion. *Journal of Heat Transfer-Transactions of the Asme* **2002,** *124*, 242-252.

4. Chen, G.; Dames, C., Thermal Conductivity of Nanostructured Thermoelectric Materials. In *Thermoelectrics Handbook*, CRC Press: 2005.

5. Caillat, T.; Borshchevsky, A.; Fleurial, J.P., Properties of single crystalline semiconducting $CoSb_3$. *Journal of Applied Physics* **1996,** *80*, 4442-4449.

6. Wise, F.W., Lead salt quantum dots: The limit of strong quantum confinement. *Accounts of Chemical Research* **2000,** *33*, 773-780.

7. Ashley, T.; Dean, A.B.; Elliott, C.T.; Pryce, G.J.; Johnson, A.D.; Willis, H., Uncooled high-speed InSb field-effect transistors *Applied Physics Letters* **1995,** *66*, 481-483.

8. Sumanasekera, G.U.; Grigorian, L.; Eklund, P.C., Low-temperature thermoelectrical power measurements using analogue subtraction. *Meas Sci Technol* **2000,** *11*, 273-277.

9. Mirkovic, V.V., Comparative method and choice of standards for thermal conductivity determinations. *Journal of the American Ceramic Society* **1965,** *48*, 387-&.

10. Reddy, S.R.; Hajra, J.P., Thermodynamics and phase equilibria in the In-Sb system. *Calphad-Comput. Coupling Ph. Diagrams Thermochem.* **1994,** *18*, 39-45.

11. Vaddiraju, S.; Sunkara, M.K.; Chin, A.H.; Ning, C.Z.; Dholakia, G.R., Synthesis of group III antimonide nanowires. *Journal of Physical Chemistry C* **2007,** *111*, 7339-7347.

12. Vaddiraju, S.; Mohite, A.; Chin, A.; Meyyappan, M.; Sumanasekera, G.; Alphenaar, B.W.; Sunkara, M.K., Mechanisms of 1D crystal growth in reactive vapor transport: Indium nitride nanowires. *Nano Lett.* **2005,** *5*, 1625-1631.

13. Tenorio, J.A.S.; Espinosa, D.C.R., Effect of salt/oxide interaction on the process of aluminum recycling. *Journal of Light Metals* **2002,** *2*, 89-93.

14. Okamoto, H., Co-Sb phase diagram. In *ASM Alloy Phase Diagrams Center, P. Villars, editor-in-chief; H. Okamoto and K. Cenzual, section editors; available online at http://www.asminternational.org.lib-ezproxy.tamu.edu:2048/AsmEnterprise/APD*, ASM International, Materials Park, OH: 2006.

15. Pendyala, C.; Vaddiraju, S.; Kim, J.H.; Jacinski, J.; Chen, Z.Q.; Sunkara, M.K., Self-nucleation and growth of group III-antimonide nanowires. *Semiconductor Science and Technology* **2010,** *25*, 024014.

16. Koestner, R.J.; Salmeron, M.; Kollin, E.B.; Gland, J.L., Adsorption and surface reactions of H_2S on clean and S-covered Pt(111). *Surf. Sci.* **1986,** *172*, 668-690.

17. Bandyopadhyay, K.; Vijayamohanan, K.; Venkataramanan, M.; Pradeep, T., Self-assembled monolayers of small aromatic disulfide and diselenide molecules on polycrystalline gold films: A comparative study of the geometrical constraint using temperature-dependent surface-enhanced raman spectroscopy, X-ray photoelectron spectroscopy, and electrochemistry. *Langmuir* **1999,** *15*, 5314-5322.

18. Nagamoto, Y.; Hino, K.; Yoshitake, H.; Koyanagi, T. In ***Thermoelectric properties of*** α***-Zn$_3$P$_2$,*** Proceedings of the XVII International Conference onThermoelectrics, 24-28 May 1998, pp 354-357.

III.7 Integration of Advanced Materials, Interfaces, and Heat Transfer Augmentation Methods for Affordable and Durable Thermoelectric Devices

Y. Sungtaek Ju (Primary Contact) and Bruce Dunn
Univeristy of California, Los Angeles
420 Westwood Plaza
Los Angeles, CA 90095-1597

NSF Manager: Sumanta Acharya

DOE Technology Development Manager: John Fairbanks

NETL Project Manager: Carl Morande

Overall Objectives

Develop novel materials and interfaces for improved thermomechanical reliability of thermoelectric (TE) vehicle exhaust waste heat harvesting devices.

Fiscal Year (FY) 2011 Objectives

- Synthesize Ag-based metal-matrix nanocomposites incorporating nano-fillers with isotropic negative coefficients of thermal expansion (CTE) materials.
- Demonstrate tunable CTEs by varying volume fraction of the nano-fillers.

Accomplishments

- Successfully synthesized ZrW_2O_8 powders with isotropic negative thermal expansion (NTE) coefficients.
- Demonstrated successful production of Ag-based nanocomposites with variable CTEs from approximately 7 to 15 ppm/°C.
- Characterized the thermal and electrical transport properties of the composites and achieved values comparable to those of aluminum.

Future Directions

- Explore metal-matrix nanocomposites using less expensive metals (such as Cu, Al, or Ni) using similar production methods and having tunable CTEs.
- Reduce the size of and improve upon the homogeneous dispersion of the oxide inclusions in the metal matrix in order to reduce the scattering of the experimental results and provide even more reliable and reproducible composites.
- Characterize the CTE of metal-ceramic nanocomposites up to higher temperature limit of 500°C, for practical use in TE devices.
- Investigate the feasibility of liquid-based flexible thermal interfaces for high-temperature applications.

Introduction

As different material systems are investigated for practical use in TE devices, many properties are considered, including the thermoelectric figure of merit (*ZT*), production costs and complexity, mechanical properties, supply limit of materials, and/or potentials for environmental hazards. Two silicide materials, magnesium silicide (Mg_2Si) and iron disilicide ($FeSi_2$), show some potential to achieve high *ZT* over the mid-temperature range of about 230 to 730°C [1]. These are abundant and low cost material systems with good mechanical properties and low toxicity. The low density of Mg_2Si makes it particularly ideal for weight-sensitive applications. However, an important issue to also consider is the reliability of interfaces which are formed between the TE materials and the structure with which they are integrated. Large mismatches in CTEs at such interfaces result in large thermomechanical stresses [2] which often lead to device failure. Furthermore, poor thermal and/or electrical contacts across the interfaces can significantly degrade the efficiency of TE devices [3]. The reported CTEs of Mg_2Si and $FeSi_2$ are relatively low, varying from only 6 to 10 ppm/°C [4-7].

We have developed metal-matrix nanocomposite materials with a CTE value tuned to match a specific value. This aids in circumventing the CTE mismatch issue by producing a material useful for either TE electrodes or interfacial layers. The NTE material, ZrW_2O_8, has been successfully incorporated into Ag matrix composites enabling us to adjust the CTE between approximately 7 to 15 ppm/°C. ZrW_2O_8 has an isotropic NTE over a wide temperature range (-272 to 777°C), making it ideal for use in TE systems [8-14]. During fabrication, a continuous Ag matrix forms around the NTE filler thus providing high thermal conductivity (k) and electrical conductivity (σ) for use in TE devices. A facile sol-gel-based synthesis for ZrW_2O_8 and simple hot press sintering of composite powders make the production of the Ag/ZrW_2O_8 composites an appealing alternative to more complex infiltration, metal extrusion, or stir casting processes used for materials such as AlSiC [15-16].

Approach

Our approach to fabricating metal-matrix nanocomposite materials is to use nanosized metal powders (commercial and lab-synthesized) and lab-synthesized ZrW_2O_8 powder. The NTE ZrW_2O_8 powder was synthesized using benchtop sol-gel chemistry and characterized for its crystalline phase and CTE. The metal and ceramic powders were mixed thoroughly and then sintered by hot pressing (~3 hrs at 500°C and 80 MPa). Dilatometry measurements for CTE of the sintered metal-matrix nanocomposites were performed between 50 and 150°C. The metal-ceramic nanocomposite materials were also characterized for electrical and thermal conductivity and porosity.

Results

We successfully prepared the desired cubic α-phase of ZrW_2O_8 and verified its crystalline phase. Dilatometry experiments showed that this material had an overall average CTE of -13.6 ppm/°C. The expected CTE for α-ZrW_2O_8 is about -9 ppm/°C, however, more negative experimental values (about -12 ppm/°C) have been reported from 50 to 150°C [14]. The onset of decomposition of ZrW_2O_8 within the metal-matrix nanocomposite occurs after 1-hour heating at about 650°C. This behavior suggests that the nanocomposites may be suitable for use in devices built for waste heat harvesting from heavy duty vehicle systems which operate at temperatures as low as 500°C [17]. Sintered metal-matrix nanocomposites were produced having open porosity ≤1% for samples ranging from 82 to 54 and ZrW_2O_8 in composites will be further notated using a v/v Ag/ZrW_2O_8 format.

Figure 1 compares the change in length as a function of temperature for pure nano Ag, pure α-phase ZrW_2O_8 and a 54v/46v Ag/ZrW_2O_8 composite. The slopes of these lines are the CTE, α. The data in Figure 1 demonstrate directly that the combination of positive and negative CTE materials can be used to obtain an intermediate value of CTE. We prepared nanocomposites of three different compositions, 54v/46v, 66v/34v, and 82v/18v Ag/ZrW_2O_8 and characterized their CTE values (Figure 2). The linear rule of mixtures (ROM) was used to predict the CTE as a function of composition [18] and is consistent with the average measured CTE values listed in Table 1. CTEs as low as 6.5 ppm/°C were achieved with several individual 54v/46v Ag/ZrW_2O_8 samples, although the average CTE for that composition was ~7.2 ppm/°C. The measured CTE values for these three compositions cover the expected range of CTEs for $FeSi_2$ and Mg_2Si, making our metal-matrix nanocomposite an ideal material for use in a TE device with improved interfacial thermomechanical relability. Furthermore this directly accomplishes two of our 2011 objectives; first, to synthesize Ag-based metal-matrix nanocomposites

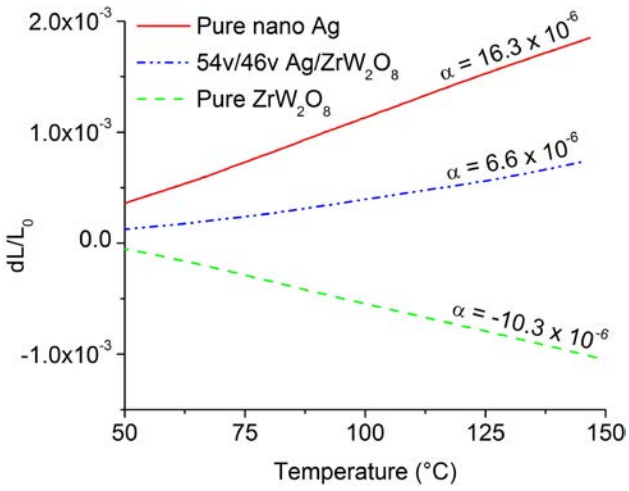

FIGURE 1. Measured Dilatometry Data comparing Pure Nano Ag and α-Phase ZrW_2O_8 with a 54v/46v Ag/ZrW_2O_8 Composite

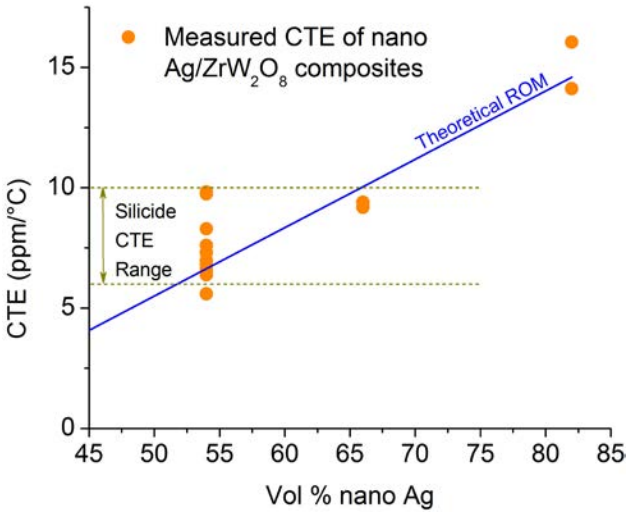

FIGURE 2. Experimentally determined CTEs of Ag/ZrW_2O_8 composites with compositions ranging from 54-82 vol% Ag compared to the theoretical prediction. The expected CTE range of silicide-based TE materials is also shown.

incorporating nano-fillers with isotropic NTE materials and second, to demonstrate tunable CTEs by varying volume fraction of the nano-fillers.

The measured thermal (k) and electrical (σ) conductivities are reported in Table 1. For samples processed under the same hot pressing conditions, the composite containing 54 vol% Ag shows approximately 50% of the k obtained from a pure Ag sample. The poor thermal conductivity of the ZrW_2O_8 phase and increased electron and phonon scattering at the interfaces are responsible for this observed reduction. However, the continuous Ag matrix of the composites still provides k values comparable to that of pure Al. The electrical

conductivities of the metal-matrix nanocomposites are on the same order of magnitude as that of bulk Ag, but again some decrease in σ is expected due to the presence of the insulating oxide phase and additional scattering of electrons at the phase interfaces. These measured conductivity values for our metal-matrix nanocomposites are promising for practical use in TE devices.

TABLE 1. Measured Thermal Expansion, Thermal Conductivity, and Electrical Conductivity Data for Sintered Ag/ZrW_2O_8 Composites

Vol% Ag/ZrW_2O_8	Theoretical ROM CTE (ppm/°C)	Average CTE (ppm/°C)	Average Thermal Conductivity (W/m·°C)*	Electrical Conductivity (S/cm)*
54/46	6.6	7.2	117	2.0×10^5
66/34	10.0	9.3		3.3×10^5
82/18	14.6	15.1	142	
100/0	19.7	18.7	219	

*For pure bulk Ag, standard *k* is 428 W/m·°C and standard σ is 6.8×10^5 S/cm

Conclusions

- Fully dense metal-matrix nanocomposites successfully combine positive and negative thermal expansion materials to have predictable and tunable CTEs.
- The average CTE values for 54v/46v and 66v/34v Ag/ZrW_2O_8 nanocomposites (7.2 and 9.3 ppm/°C, respectively) fall within the expected range of CTEs for the silicide-based TE materials $FeSi_2$ and Mg_2Si.
- The metal-matrix nanocomposites have thermal conductivity >100 W/m·°C and electrical conductivity $>2.0 \times 10^5$ S/cm, which are promising for practical use in TE devices.
- Our Ag-based metal-matrix nanocomposites can be easily processed using inexpensive hot pressing techniques at modest temperatures and pressures.

References

1. H. Lange, *Phys. Status Solidi B* 201, 3 (1997).

2. V. Ravi, S. Firdosy, T. Caillat, E. Brandon, K.V.D. Walde, L. Maricic, A. Sayir, *J. Electron. Mater.* 38, 1433 (2009).

3. Y.S. Ju, U. Ghoshal, *J. Appl. Phys.* 88, 4135 (2000).

4. K. Herz, M. Powalla, A. Eicke, *Phys. Status Solidi A* 145, 415 (1994).

5. E. Muller, C. Drasar, J. Schliz, W.A. Kaysser, *Mat. Sci. Eng. A-Struct.* 362, 17 (2003).

6. S.K. Thakur, B.K. Dhindaw, N. Hort, K.U. Kainer, *Metall. Mater. Trans. A* 35A, 1167 (2004).

7. Y. Oguni, T. Iida, A. Matsumoto, T. Nemoto, J. Onosaka, H. Takaniwa, T. Sagamoto, D. Mori, M. Akasaka, J. Sato, T. Nakajima, K. Nishio, Y. Takanashi, *Mat. Res. S. C.*, 413 (2008).

8. G.D. Barrera, J.A.O. Bruno, T.H.K. Barron, N.L. Allan, *J. Phys.-Condens. Mat.* 17, R217 (2005).

9. J.S.O. Evans, T.A. Mary, T. Vogt, M.A. Subramanian, A.W. Sleight, *Chem. Mater.* 8, 2809 (1996).

10. T.A. Mary, J.S.O. Evans, T. Vogt, A.W. Sleight, *Science* 272, 90 (1996).

11. A.W. Sleight, *Annu. Rev. Mater. Sci.* 28, 29 (1998).

12. D.K. Balch, D.C. Dunand, *Metall. Mater. Trans. A* 35A, 1159 (2004).

13. A.K. Arora, V.S. Sastry, P.C. Sahu, T.A. Mary, *J. Phys.-Condens. Mat.* 16, 1025 (2004).

14. P. Lommens, C.D. Meyer, E. Bruneel, K.D. Buyseer, I.V. Driessche, S. Hoste, *J. Eur. Ceram. Soc.* 25, 3605 (2005).

15. R. Asthana, *Adv. Perform. Mater.* 5, 213 (1998).

16. V. Jayaseelan, K. Kalaichelvan, M. Kannan, S.V. Ananth, *Int. J. Appl. Eng. Res.* 1, 194 (2010).

17. T.J. Hendricks, J.A. Lustbader, *Int. Conf. Thermoelectr.*, Long Beach, CA, 2002.

18. H.A. Bruck, B.H. Rabin, *J. Am. Ceram. Soc.* 82, 2927 (1999).

FY 2011 Publications/Presentations

1. J.E. Trujillo, J.W. Kim, E.H. Lan, S. Sharrat, Y.S. Ju, B. Dunn, "Metal-matrix nanocomposites with tailored coefficients of thermal expansion (CTE) for improved thermomechanical reliability of thermoelectric devices," oral presentation at the 30th International Conference on Thermoelectrics, July 17-21, 2011, Traverse City, Michigan.

2. J.E. Trujillo, J.W. Kim, E.H. Lan, S. Sharrat, Y.S. Ju, B. Dunn, "Metal-matrix nanocomposites with tailored coefficients of thermal expansion for improved thermomechanical reliability," J. Electron. Mater. (Accepted for publication)

III.8 High Performance Thermoelectric System Based on Zintl Phase Materials with Embedded Nanoparticles

Ali Shakouri (Primary Contact), Zhixi Bian
University of California, Santa Cruz
Electrical Engineering Department
1156 High Street
Santa Cruz, CA 95064

Susan M. Kauzlarich
University of California, Davis
Chemistry Department
One Shields Ave.
Davis, CA 95616

NSF Manager: Sumanta Acharya

DOE Technology Development Manager: John Fairbanks

NETL Project Manager: Carl Morande

Overall Objectives

- Develop novel thermoelectric materials based on abundant and non-toxic Zintl phase magnesium silicide alloys.
- Demonstrate that with the use of embedded nanoparticles of appropriate concentration (0.01-5%) and diameter (2-15 nm), thermal conductivity will be reduced by scattering of mid to long wavelength phonons.
- Optimize the thermoelectric power factor and figure of merit by band engineering and electron filtering using Mg_2Si nanoparticles embedded in $Mg_2Si_xSn_{1-x}$ alloys.

Fiscal Year (FY) 2011 Objectives

- Synthesis of both n- and p-type Mg_2Si and $Mg_2Si_xSn_{1-x}$ with embedded Si and Mg_2Si nanoparticles.
- Structural and thermoelectric characterizations.
- Thermoelectric transport modeling using Boltzmann equation.
- Optimization of both thermal conductivity and TE power factor by modifying the alloy composition, nanoparticle sizes and concentrations.

Accomplishments

- Low temperature synthesis and spark plasma sintering (SPS) of n-type Mg_2Si with embedded Si nanoparticles.
- Characterization and transport modeling.

Future Directions

- Low temperature synthesis and SPS of n-type $Mg_2Si_{1-x}Sn_x$ with embedded Si and Mg_2Si nanoparticles.
- Low temperature synthesis and SPS of n-type $Mg_{2-x-}Yb_xSi$ with embedded YbSi nanoparticles.
- Low temperature synthesis and SPS of p-type Mg_2Si with embedded nanoparticles.
- Characterization and transport modeling.

Introduction

We will develop novel thermoelectric materials based on abundant and non-toxic Zintl phase magnesium silicide alloys. We propose a synthetic method that naturally provides embedded nanoparticles within a magnesium silicide alloy matrix, providing uniform mixing with minimal aggregation. With the use of embedded nanoparticles of appropriate concentration (0.01-5%) and diameter (2-15 nm), thermal conductivity will be reduced by scattering of mid to long wavelength phonons. Controlling the heterostructure band offset and the potential barrier of nanoparticles with respect to matrix, power factor will be increased by selective scattering of hot carriers. Preliminary transport calculations show that ZT>1.8 at 800 K could be achieved.

Approach

Mg_2Si can be synthesized at relatively low temperature with MgH_2 and Si powders as starting materials. By changing the ratio of the starting materials, a proper amount of Si nanocomposites can be easily cooperated with the matrix. N-type or p-type dopants are intentionally mixed with starting materials homogeneously in a ball mill to tune the carrier concentration. Flow furnace and SPS are employed to achieve the Mg_2Si product as well as dense pellets for transport properties characterizations. A robust and accurate high temperature thermoelectric system is built to characterize the Seebeck coefficient and the electrical conductivity of Si/Mg_2Si nanocomposites simultaneously in a large temperature range. We also develop a multiband Boltzmann transport model to explain the Seebeck and electrical conductivity measurement results and provide a guideline for material optimization of Mg_2Si:$Mg_2Si_{1-x}Sn_x$ system.

Results

Silicon (Si) nanoparticle embedded Mg_2Si composite (Mg_2Si/xSi) has been successfully synthesized at 623 K from MgH_2 and Bi containing Si nanoparticle powders. This synthetic route avoids the production of oxides through the generation of hydrogen and allows for easy alloy formation. In addition, it provides a route to homogeneously mixed Si nanoparticles within a doped Mg_2Si matrix along with the opportunity to control particle size. The composition of the samples was characterized by powder X-ray diffraction (XRD) shown in Figure 1. The crystallite size of Mg_2Si obtained from the XRD patterns is about 50 nm for all the samples. The microstructure of the Bi-doped Mg_2Si/xSi nanocomposites from scanning transmission electron microscopy (STEM) indicated that the Bi dopant has a much higher concentration at grain boundaries and that Bi preferentially substitutes Mg instead of Si as a substitutional dopant at the grain boundaries, shown in Figure 2. The Mg_2Si/xSi nanocomposites suppress the phonons, and yielded a significant reduction of lattice thermal conductivity, shown in Figure 3. The 2.5 vol% sample has ~20 mW/cm K at 775 K, which is about 30% reduction comparing to ~30 mW/cm K for the reference. As a result, a ZT ~0.7 was obtained at 775 K for the sample with 2.5 vol% Si nanoparticles, shown in Figure 4.

We also developed a model based on the Boltzmann transport equation which included multiple conduction valleys as well as dominant electron-phonon and impurity scattering mechanisms. Various parameters were identified by comparing with experimental electron mobility, electrical conductivity and the

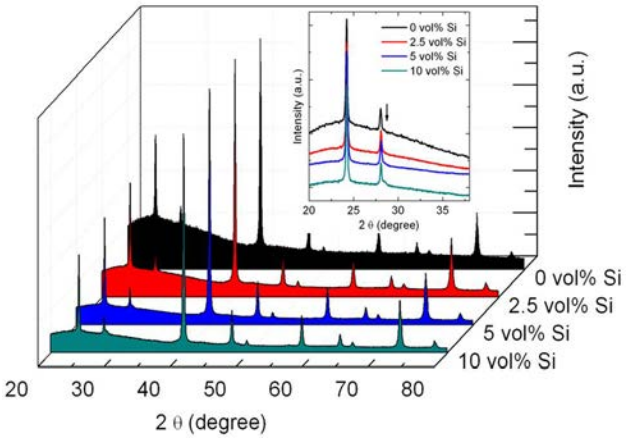

FIGURE 1. XRD of $Mg_2Si/xSi_{1\%Bi}$ (x = 0, 2.5, 5, 10 vol%), the inset is an enlarged view showing the (111) peak of Si which is the shoulder of the (200) peak of Mg_2Si around 2θ of 28° marked by an arrow.

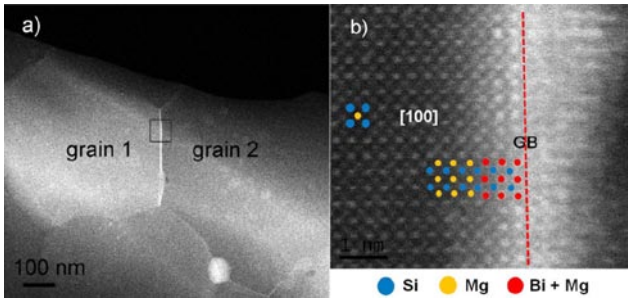

FIGURE 2. STEM-high angle annular dark field images of a) Mg_2Si grains, b) enlarged view of the rectangle area indicated at the grain boundary in a). The modeling of where Bi resides at the grain boundary is indicated.

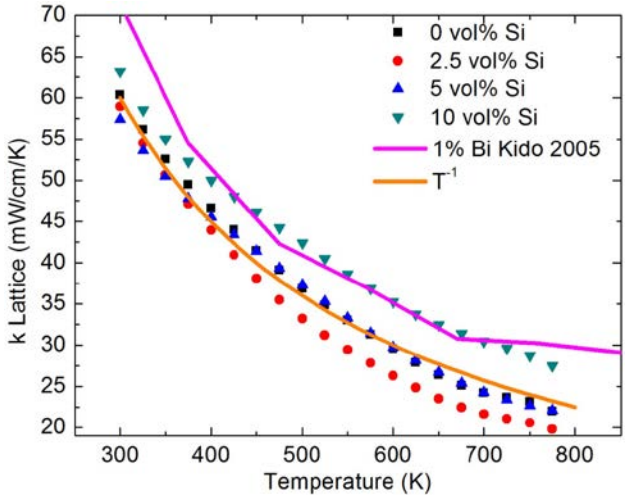

FIGURE 3. Lattice thermal conductivity of Mg_2Si/xSi (x = 0, 2.5, 5, 10 vol%) samples and the 1 mol% Bi doped reference compared with $\kappa_L \sim T^{-1}$.

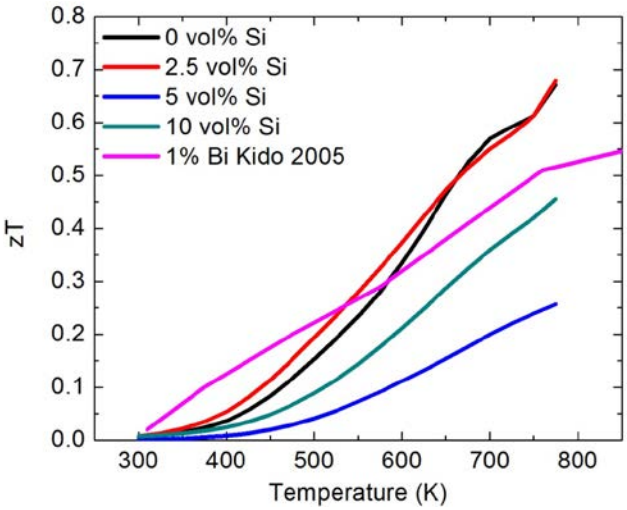

FIGURE 4. The figure of merit ZT of Mg_2Si/xSi (x = 0, 2.5, 5, 10 vol%) samples and the 1 mol% Bi-doped reference.

Seebeck coefficient. The most significant feature of the band structure of Mg_2Si-based materials is that there are two conduction bands at the X-point. The band offset between these two conduction bands depends on the alloy composition, and is also a function of temperature. Figure 5 shows the experiment data of electrical conductivity and Seebeck coefficient of our measurements and from literatures [1,2] and the calculation curves produced from our model with fine tuning of fitting parameters. The calculations match the experimental data very well. We further performed thermoelectric transport calculations for

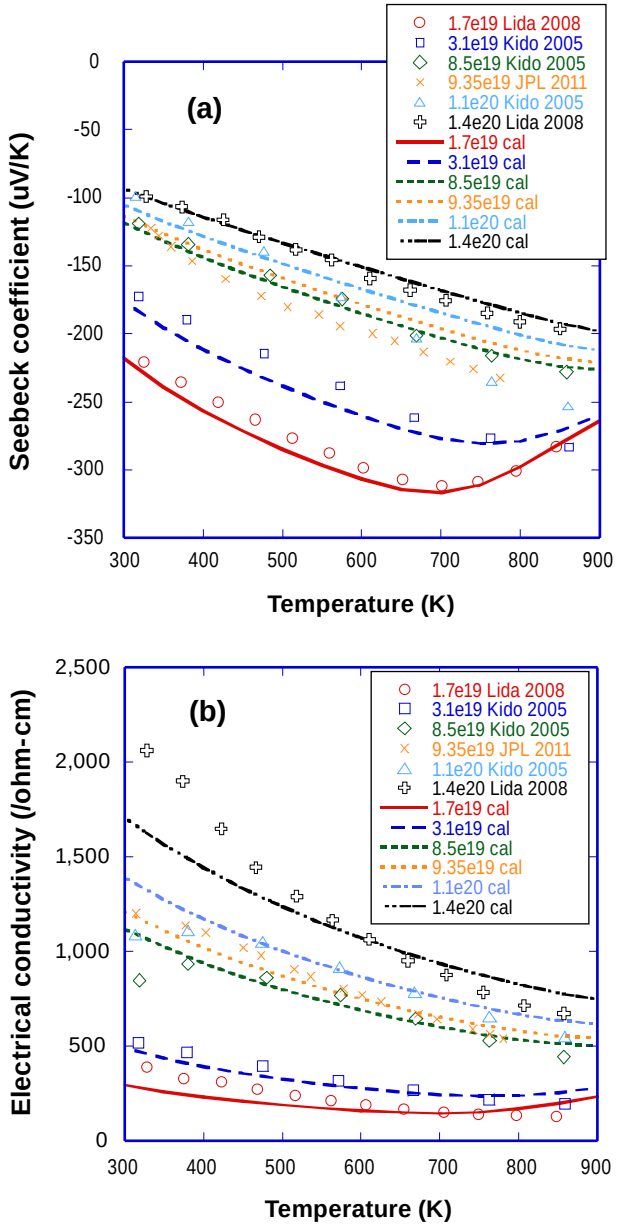

FIGURE 5. Calculated Seebeck coefficient (a) and electrical conductivity (b) in comparison with the measurement data from several sources.

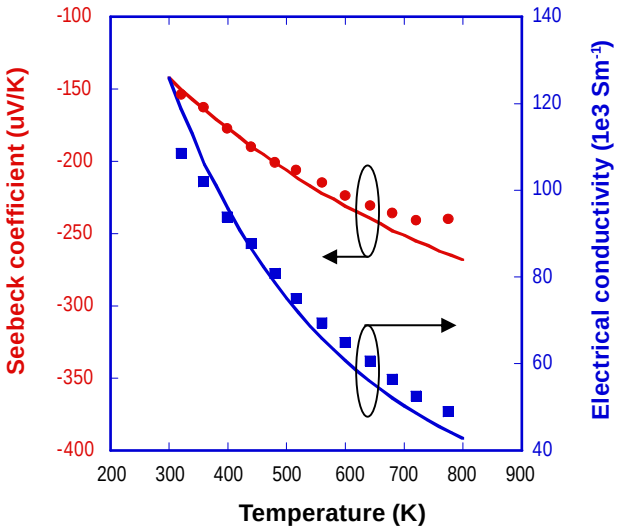

FIGURE 6. Calculated (solid line) Seebeck coefficient and electrical conductivity in comparison with the measurement data (dots) from several sources.

$Mg_2Si_{1-x}Sn_x$, which also fits with the published results [3], as seen in Figure 6. A ZT ~1.1 has been achieved for $Mg_2Si_{0.4}Sn_{0.6}$ from the published results. With optimization of the alloy composition of the matrix and embedded nanoparticles, further enhancement of the thermoelectric figure of merit may be achieved.

Conclusions

Mg_2Si with Si nanocomposites, $Mg_2Si/xSi_{1\%Bi}$, were obtained by reacting MgH_2 and Si nanoparticles. The distribution of Si nanocomposites and Bi in Mg_2Si pellets were characterized by electron microprobe. The aggregation of Si nanoparticles become significant when the concentration of Si exceeds 5 vol%. Bi is favorable to cooperate with Mg_2Si rather than Si, and the microstructure from STEM indicates higher Bi concentration at grain boundaries. In addition, Bi prefers to substitute for Mg at boundaries. The measurements of transport properties confirm that a proper amount of Si nanocomposites in Mg_2Si causes a significant reduction of lattice thermal conductivity. As a consequence, the figure of merit ZT is improved, and a ZT ~0.8 at 775 K is achieved for the sample with 2.5 vol% Si inclusions. A detailed model for multiband thermoelectric transport is developed and validated by the experimental data. Further optimization of matrix composition and embedded nanoparticles are underway for maximizing the thermoelectric figure of merit.

References

1. Masataka Fukano, Tsutomu Lida, Kenichiro Makino, Masayasu Akasaka, Yohei Oguni, and Yoshifumi Takanashi,

Crystal growth of Mg_2Si by the vertical Bridgman method and the doping effect of Bi and Al on thermoelectric characteristics, Mater. Res. Soc. Symp. Proc. Vol. 1044, 2008.

2. Jun-ichi Tani, Hiroyasu Kido, Thermoelectric properties of Bi-doped Mg_2Si semiconductors, Physica B 364 (2005) 218-224.

3. Q. Zhang, J. He, T.J. Zhu, S.N. Zhang, X.B. Zhao, and T.M. Tritt, High figures of merit and natural nanostructures in $Mg_2Si_{0.4}Sn_{0.6}$ based thermoelectric materials, Applied Physics Letters 93, 102109 (2008).

FY 2011 Publications/Presentations

1. Tanghong Yi, Shaoping Chen, Sabah Bux, Jean-Pierre Fleurial, Zhixi Bian, Natalio Mingo, Ali Shakouri, Susan Kauzlarich, Enhancement of Thermoelectric Efficiency of Mg_2Si with Si Nanocomposites, The 30th International Conference on Thermoelectrics, Traverse City, MI, 2011 July.

2. Oliver Janka, Tanghong Yi, Susan M. Kauzlarich, $Mg_{2-x}Yb_xSi$: Ytterbium doped Mg_2Si as a thermoelectric material, Presented at the 26th Rare Earth Research Conference, Santa Fe, NM, June 19–23, 2011.

3. Oliver Janka, Andrew Hwang, Tanghong Yi, Susan M. Kauzlarich, Modifying Mg_2Si for enhanced thermoelectric properties, Presented at the ACS Fall Meeting 2011, Denver, CO, August 28 – September 1, 2011.

4. Zhixi Bian, Tela Favaloro, Ali Shakouri, Tanghong Yi, Susan Kauzlarich, Sabah Bux, Jean-Pierre Fleurial, Thermoelectric Transport Modeling of Mg_2Si with Embedded Nanoparticles, The 30th International Conference on Thermoelectrics, Traverse City, MI, 2011 July.

III.9 High-Performance Thermoelectric Devices Based on Abundant Silicide Materials for Vehicle Waste Heat Recovery

Li Shi (Primary Contact), Matthews J. Hall, Jianshi Zhou, John Goodenough, Chad Baker, Xi Chen, Libin Zhang
The University of Texas at Austin
Department of Mechanical Engineering
Austin, TX 78712

NSF Manager: Sumanta Acharya

DOE Technology Development Manager: John Fairbanks

NETL Project Manager: Carl Morande

Overall Objectives

- Increase the figure of merit (ZT) of abundant silicide materials to a level competitive with the state of the art found in materials containing much more scarce and expensive elements.
- Enhance the thermal management system performance for silicide thermoelectric (TE) devices installed in a diesel engine.

Fiscal Year (FY) 2011 Objectives

- Synthesize and dope p-type nanostructured bulk higher manganese silicide (HMS) to enhance the TE properties.
- Synthesize Mg_2Si-based n-type TE materials.
- Establish a combined heat exchanger and TE device model for optimizing the system design.
- Build heat exchanger test rig to validate the heat transfer model.

Accomplishments

- Demonstrated the synthesis of HMS via solid state reaction, cold press, and annealing.
- Attained bulk-size (20 mm diameter and 5-8 mm thickness) HMS pellets via solid state reaction and spark plasma sintering (SPS).
- Achieved thermal conductivity reduction by up to a factor of three in the polycrystalline HMS samples compared to single-crystal HMS.
- Succeeded in Ru substitution to increase the Seebeck coefficient of HMS by 30% at room temperature and below.
- Established a combined heat exchanger and TE device model for optimizing system design.
- Designed, fabricated, and measured a heat exchanger for verifying the heat transfer computation model.

Future Directions

- Investigate complex doping of HMS to increase the power factor.
- Conduct SPS synthesis of n-type Mg_2Si-based pellets.
- Establish a position-dependent doping method to match the peak ZT with the local operating temperature of the TE leg.
- Develop a method for spatial mapping of the TE properties.
- Investigate silicide interface materials.
- Design, fabricate, and model alternative heat exchanger geometries to enhance the heat transfer efficiency.

Introduction

The objective of this project is to achieve high-performance TE devices based on low-cost silcicide materials that are abundant on earth, and yet hold promise for achieving a ZT value comparable to or higher than the state of the art over the temperature range between 300 K and 800 K relevant for vehicle waste heat recovery. Based on this research team's prior fundamental research results, one hypothesis behind the proposed research is that the lattice thermal conductivity of p-type HMS ($MnSi_{1.75}$) and also possibly n-type $Mg_2Si_{1-x}Sn_x$ can be suppressed from the already low single-crystal bulk values by a factor of 2-3 to approach the amorphous limit in bulk materials with nano-grains or nano-precipitations, without considerable reduction in the power factor. Consequently, the already useful peak ZT of 0.7–1.1 in HMS and $Mg_2Si_{1-x}Sn_x$ can be enhanced by a factor >1.5 via nanostructuring. The project consists of four tasks on TE materials, thermal management, interfaces, and metrology.

Approach

One key approach in our TE materials research is to employ nano-grained materials and nano-phase separation to reduce the lattice thermal conductivity of

bulk silicides. In addition, a new approach of position-dependent doping is investigated to achieve a single-body TE leg where the peak ZT occurs near the local operating temperature along the leg. Besides materials synthesis, system- and device level- computation tool is developed in conjunction with experiments in order to maximize the hot side temperature and enhance heat transfer to the TE devices, to match the temperature distribution with the position- and temperature-dependent ZT of the silicide legs, and to control the exhaust aftertreatment catalyst temperature under transient exhaust flow conditions. Several interface materials are studied to achieve low electrical and/or thermal interface resistances between the metal interconnects and the TE materials or heat sinks/sources, as well as to endure vibration, high temperature and the associated thermal expansion mismatch. High-fidelity metrology methods are developed for accurate characterizations of temperature- and position-dependent transport properties of the TE and interface materials, temperature distribution in the devices, and system-level performance.

Results

A. Synthesis of TE Materials

A.1 P-Type Materials

Synthesis of Nanostructured Bulk HMS

HMS is investigated in our work as the p-type leg of the thermoelectric module (TEM). With the use of a solid-state reaction method, we have synthesized single-phase polycrystalline HMS powders with a grain size of about 2 μm. The HMS powder was cold-pressed up to 1 GPa pressure at room temperature to decrease the grain size to about 200 nm and increase the density. We annealed the pressed samples at different temperatures to increase the electrical conductivity (σ), and have investigated the effect of annealing on the thermal conductivity (κ). As shown in Figure 1, the thermal conductivity values of the as-synthesized materials can be lower than the literature values of single-crystal HMS by up to a factor of three.

In addition, we have employed ball milling and SPS to synthesize HMS pellets as large as 20 mm in diameter and 5-8 mm in thickness (Figure 1(b)), which is adequate for device fabrication. Although the ball milling method is very efficient to reduce the grain size to 50 nm, we found the presence of a small fraction of MnSi phase after 8-hr ball milling of single-phase HMS powers. Because the MnSi phase is metallic with low Seebeck coefficient (*S*), inclusion of continuous MnSi phase in the HMS sample can lower the $ZT \equiv S^2\sigma T/\kappa$. We addressed this issue by adding a small amount of extra Si powders during synthesis of the HMS powder in the solid state reaction step prior to ball milling.

Chemical Doping of HMS by Ruthenium Substitution

We have taken the first step to identify doping elements that can be used to increase the ZT in the medium–low temperature range, with the initial focus on Ru substitution. We have found that the solid-solution limit of Ru substitution in $Mn_{1-x}Ru_xSi_{1.78}$ is at least $x = 0.1$. In addition, we found that Ru substitution can lead to enhanced Seebeck coefficient by about 30% at room temperature and below compared to HMS made with the same method without Ru doping, as shown in Figure 2.

A.2 N-Type Materials

Doped Mg_2Si-based materials are investigated for use as the n-type legs of our TE devices. Chemical stability of Mg_2Si at high temperatures is a major challenge. Another challenge is the prevention of the formation of MgO during the synthesis. In order to address these issues, we have investigated different synthesis routes, including the flux method, sealing pellets of starting powders in a quartz tube, and ball milling synthesis. We found that a reproducible method for synthesizing high-purity Mg_2Si samples is to sinter cold-pressed pellets in the H_2/Ar atmosphere. During the sintering, however, Mg powder is evaporated slightly so as to leave small amount of silicon phase in the final product. We have overcome this problem by adding 8% extra Mg powder in the starting materials. We analyzed the products by powder X-ray diffraction (XRD) to determine the Mg concentration in the final product as a function of the sintering time. We found that single-phase Mg_2Si can be obtained by carefully controlling the sintering time. We have further confirmed the crystalline quality of the sample by the Rietveld analysis of the XRD profile, as shown in in Figure 3. Moreover, the method has been employed to synthesize a series of $Mg_2Si_{1-x}Sn_x$ solid solution samples. Figure 3 shows the measured lattice parameters versus x, in comparison with literature data. We have also measured the Seebeck at low temperatures, which indicates that all Sn substituted samples are close to intrinsic semiconductors.

B. Modeling and Experiments of System-Level Performance of TE Devices Installed in 6.7 liter Cummins Diesel Engine

To optimize the device and system design, over the past year we developed a computational model consisting of two integrated sub-models, a heat exchanger model and a TE device model. A numerical model of the TE device was written to optimize the geometry of the devices for the silicide TE elements given the boundary temperature and flow conditions. The effects on heat transfer rates of placing fins in the

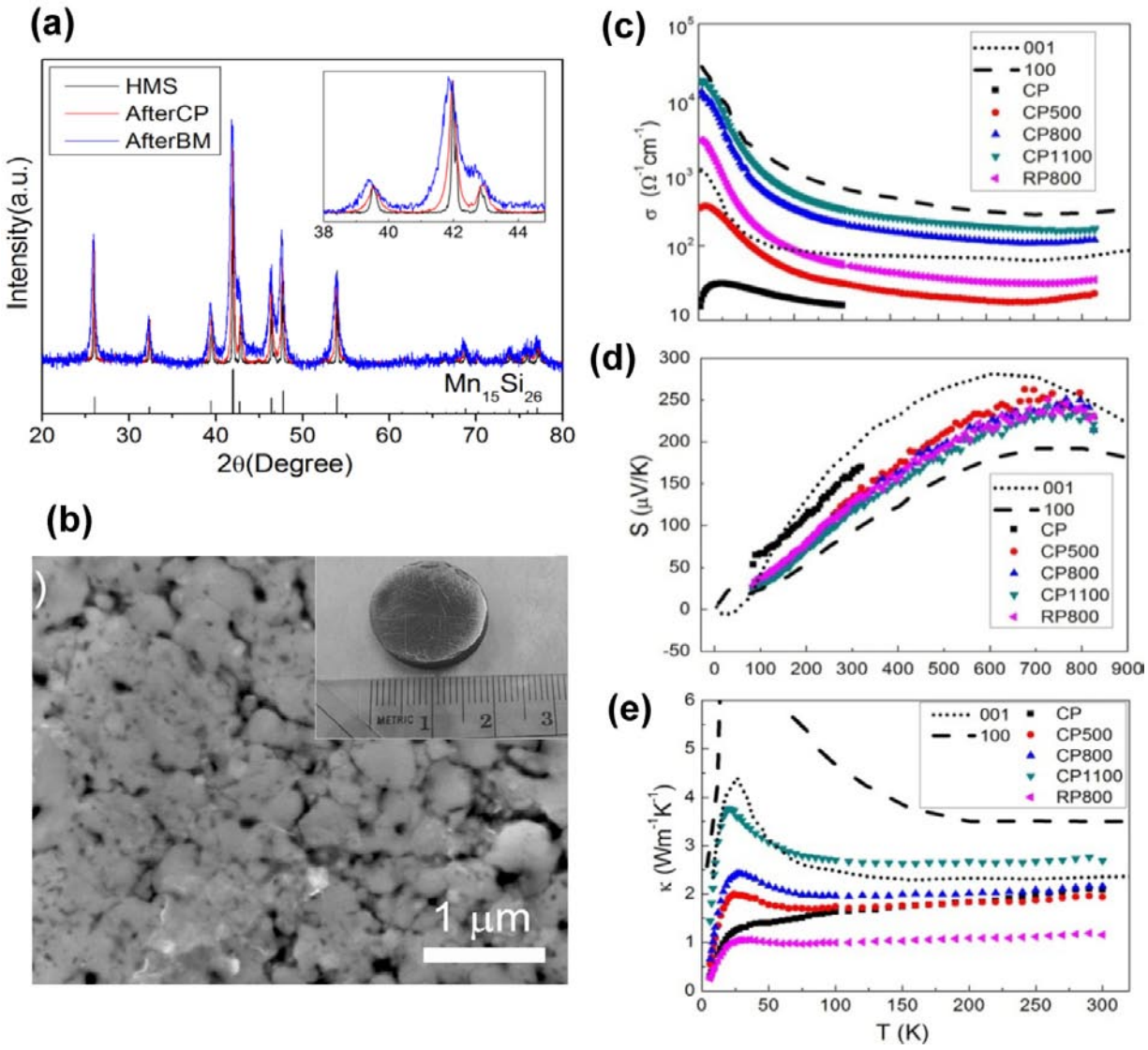

FIGURE 1. (a) XRD of the HMS samples after solid state synthesis, cold pressing (CP), and ball milling (BM), labeled in the legend as HMS, CP, and BM, respectively. The inset shows the detail XRD profile near the main peak. (b) scanning electron microscope images of the HMS after SPS. Inset is a photograph of a HMS pellet after SPS. (c-e) Temperature dependence of the transport properties of the cold-pressed HMS and the HMS prepared by the regular pressing (RP), (c) electrical conductivity, (d) Seebeck coefficient, (e) thermal conductivity. The number following CP or RP in the legend is the post-press annealing temperature. Dashed line and dotted line represent results of HMS single crystal reported in the literature along [100] and [001], respectively.

hot-side channel were investigated as were multiple parallel ducts. The model was used to optimize the following design parameters: (i) TE leg height, (ii) n-type and p-type leg area ratio, (iii) leg and void area ratio, (iv) electric current density or load resistance, (v) exhaust duct height, (vi) coolant duct height, (vii) fin spacing in the exhaust duct, and (viii) number of heat exchanger modules arranged in parallel. The outputs from the model include: (i) exhaust gas and liquid coolant pressure drops as a function of fin geometry and flow area; (ii) TE electrical power output and total heat extracted, and (iii) the overall system efficiency as a function of engine speed and load at steady state.

For validating the computational model, we designed, fabricated, and tested a heat exchanger that was scaled down in size from what would be needed for an actual vehicle application. As shown in Figure 4, the flat plate aluminum heat exchanger was fabricated from welded quarter-inch thick aluminum plate. The heat exchanger consisted of a core hot-section through which a portion of the engine exhaust flowed, sandwiched between the two water-cooled cold-sides. Alumina paper with 1 mm thickness was chosen as a surrogate for the TE devices, having an estimated equivalent thermal resistance as the TE devices under development.

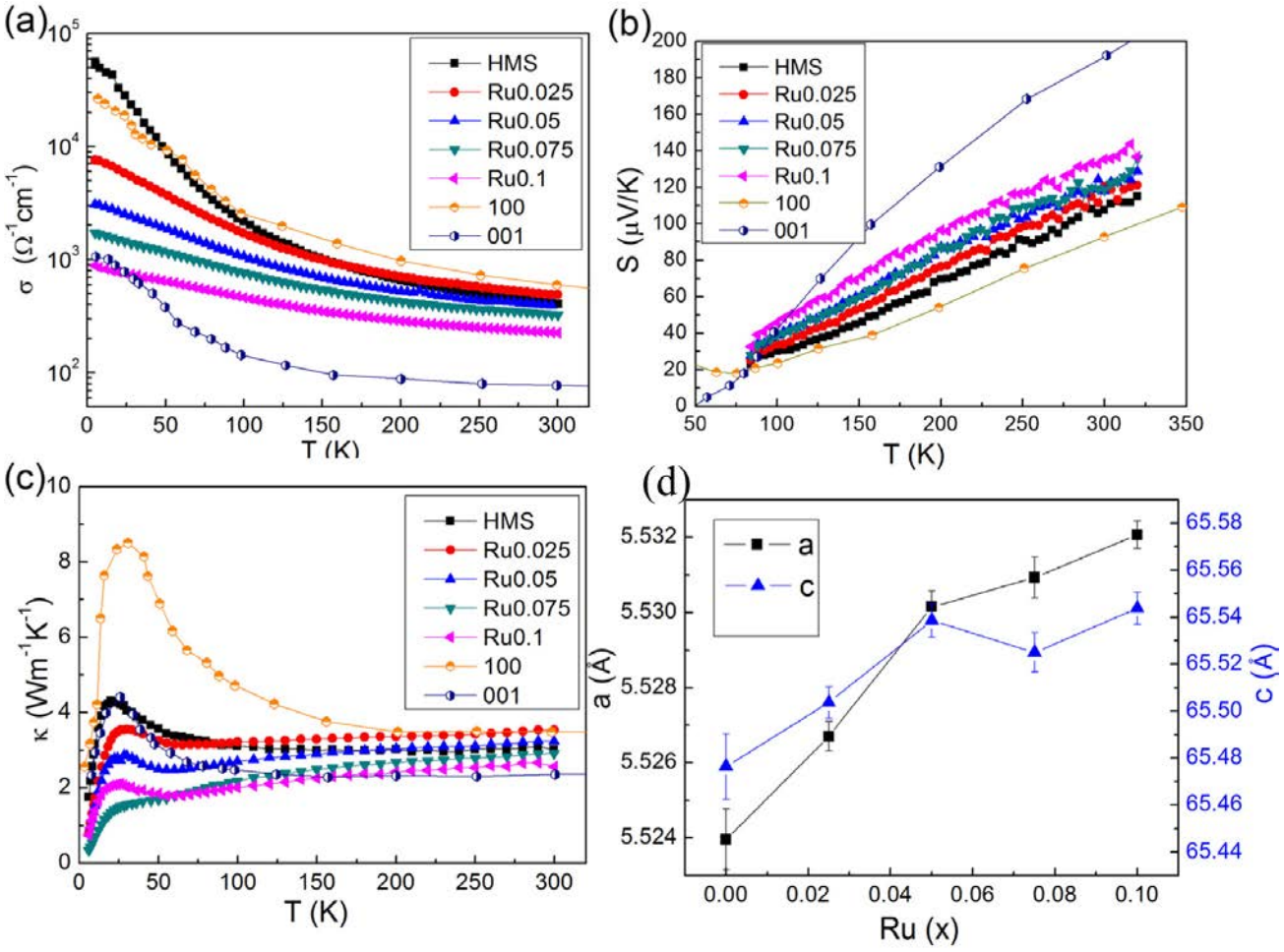

FIGURE 2. Temperature dependence of the transport properties of $Mn_{1-x}Ru_xSi_{1.78}$: (a) electrical conductivity, (b) Seebeck coefficient (c) thermal conductivity. Yellow and blue half-filled dots represent literature results of HMS single crystal along [100] and [001], respectively. (d) Measured lattice constants of $Mn_{1-x}Ru_xSi_{1.78}$.

The heat exchanger was installed in the exhaust system approximately 30 cm downstream of the turbocharger turbine and in parallel with the main exhaust pipe which served as a bypass pipe. Experiments were conducted to measure the heat transfer rate from the hot engine exhaust gases to the coolant flow over a range of inlet temperatures considered typical for on-road engine operation, and to determine the effectiveness of the heat exchanger for a range of scaled exhaust flow rates. The heat transfer rate versus flow rate from the experiment is compared with the results of the model in Figure 5. While the simulations predicted the approximate magnitudes of the heat transfer rates quite well, at lower flow rates the model under-predicted the experimental heat transfer, and at higher flow rates, the model over-predicted the experimental heat transfer. The discrepancy may be attributed to the un-insulated triangular manifold at the entrance to the rectangular cross-section exhaust channel, as well as the ignorance of the contact resistance between the hot-side and cold-side in the model.

Conclusions

- The thermal conductivity of nanostructured HMS can be reduced by as much as a factor of three compared to HMS single crystals.
- Ru substitution can be used to increase the Seebeck coefficient of HMS by 30% at room temperature and below.
- The heat transfer model is in general agreement with the measurement results.

FY 2011 Publications/Presentations

1. X. Chen, A. Weathers, D. Salta, A.L. Moore, J.S. Zhou, L. Shi, "Thermoelectric Properties of Cold-Pressed Higher Manganese Silicides for Waste Heat Recovery," Presented

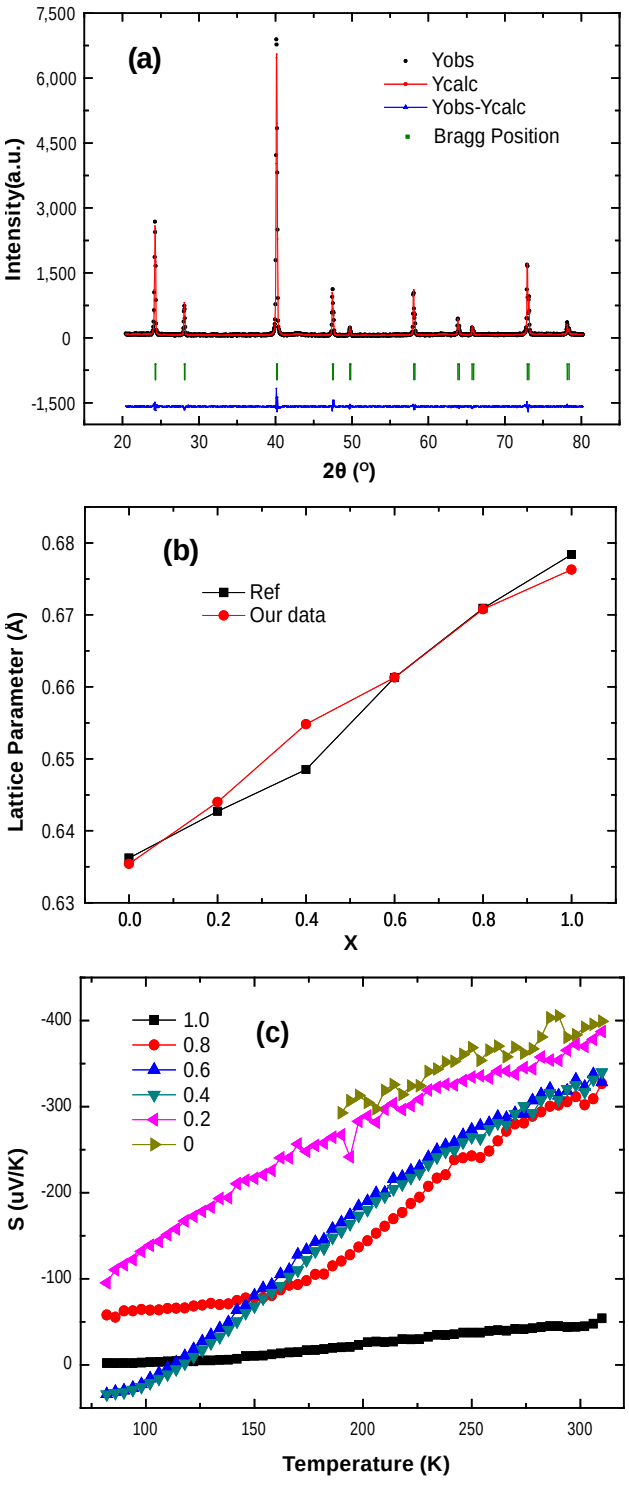

FIGURE 3. (a) XRD of Mg_2Si and results of the Rietveld analysis, (b) the lattice parameter versus x in $Mg_2Si_{1-x}Sn_x$, (c) temperature dependence of TE power for $Mg_2Si_{1-x}Sn_x$ of different x values shown in the legend.

at the 2011 Conference of the International Thermoelectric Society, Traverse City, MI, July 17–21, 2011, and in review for publication in Journal of Electronic Materials.

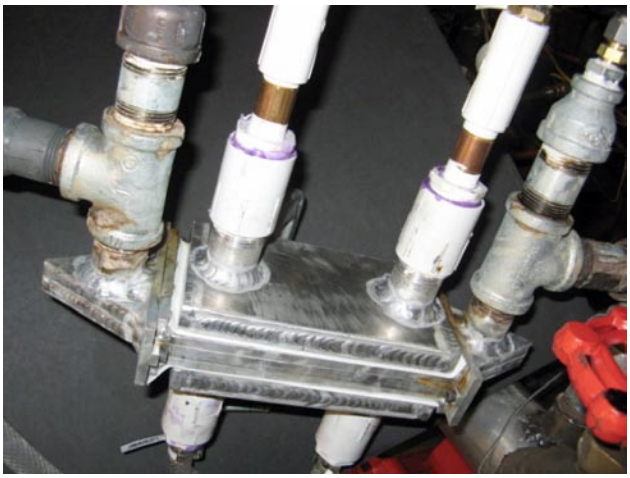

FIGURE 4. Photograph of the Heat Exchanger

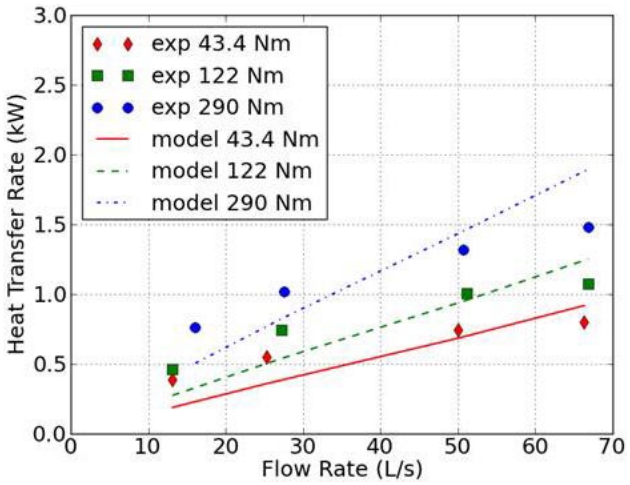

FIGURE 5. Comparison of the measured and calculated heat transfer from exhaust gas of the heat exchanger as a function of the flow rate for varied engine torque shown in the legend.

2. C. Baker, P. Vuppuluri, L. Shi, and M.J. Hall "Model of Heat Exchanger for Waste Heat Recovery from Diesel Engine Exhaust for Thermoelectric Power Generation," Presented at the 2011 Conference of the International Thermoelectric Society, Traverse City, MI, July 17–21, 2011, and in review for publication in Journal of Electronic Materials.

3. A. Pokhrel, J. Higgins, S. Jin, X. Chen, A. Weathers, A.L. Moore, J.S. Zhou, L. Shi *"Synthesis of Bulk Nanostructured Higher Manganese Silicides for Thermoelectric Applications",* Presented at the 2011 Conference of the International Thermoelectric Society, Traverse City, MI, July 17–21, 2011.

4. J.G. Cheng, F. Zhou, J.S. Zhou, J.B. Goodenough, and Y. Sui, "Enhanced thermoelectric power near the quantum phase transition in the itinerant-electron ferromagnet MnSi," Physical Review B, vol. 82, p. 214402 (2010).

5. J.G. Cheng, J.S. Zhou, J.B. Goodenough, Y.T. Su, Y. Sui, "Evidence of three-dimensional Ising ferromagnetism in the A-site-ordered perovskite CaCu3Ge4O12", Physical Review B, vol. 83, p. 212403 (2011).

III.10 An Integrated Approach towards Efficient, Scalable, and Low Cost Thermoelectric Waste Heat Recovery Devices for Vehicles

Scott Huxtable (Primary Contact),
Srinath Ekkad, and Shashank Priya
Virginia Tech
111 Randolph Hall
Department of Mechanical Engineering
Blacksburg, VA 24061

NSF Manager: Sumanta Acharya

DOE Technology Development Manager:
John Fairbanks

NETL Project Manager: Carl Morande

Subcontractor:
Romny Scientific (Dr. Andrew Miner), San Bruno, CA

Overall Objectives

- Fabricate and characterize new thermoelectric (TE) materials growth with techniques capable of producing large quantities of efficient, yet non-toxic and inexpensive elements capable of long-term operation at high temperatures over thousands of thermal cycles.
- Design, fabricate, and characterize novel heat sinks that include mini-channels and swirl impingement in order to enhance heat transfer with minimal rise in back pressure and without increases in cost or complexity.
- Characterize thermo-electrical transport properties, species diffusion, and adhesion for interfaces to reveal the effects of material composition, microstructure, processing and assembly techniques, on thermoelectric generator (TEG) performance and lifetime.
- Assemble a laboratory-scale test bed comprising of recirculating hot air flow through an automotive exhaust system that is fitted with a complete TEG system to evaluate system level models and to quantify individual component and overall system performance.

Fiscal Year (FY) 2011 Objectives

- Develop and refine scalable isostatic pressing processes capable of creating high quality TE materials at optimum sizes and various shapes.
- Fabricate and characterize Mg silicide-based TE materials.
- Develop quantitative models to drive the design and subsequent fabrication of efficient, low-cost, heat exchangers.
- Examine the feasibility of using nanoscale powders with ceramic oxide materials to reduce thermal conductivity, yet maintain large power factor.
- Fabricate ZnO TE elements with nanoscale Al_2O_3 powders and examine the structure-property relationship of the resulting materials.

Accomplishments

- Demonstration of feasible isostatic pressing processes capable of making TE elements of various shapes and sizes with minimal wasted material.
- Successful fabrication of N-type Mg silicide TE materials with ZT >0.3 from 150-300°C, with performance per raw material cost twice that of state-of-the-art Pb-Te materials.
- Demonstrated that heat exchangers based on swirl jet impingement can reduce cold side TE element temperatures by 6-8°C, leading to efficiency gains of ~0.25%.
- Synthesized nanostructured ZnO materials, characterized the TE properties, and developed structure-property relationships for Al-modified ZnO.

Future Directions

- Develop low cost P-type thermoelectric materials to complement the N-type Mg silicide produced this year.
- Create diffusion barriers for the new TE materials and examine those interfaces in series with brazes and thin dielectric layers required for assembly of TE systems (quantify the interfaces in terms of species diffusion, thermal conductance, and electrical resistance).
- Quantify the effects that long-term exposure to high temperatures and thermal cycling has on the TE materials and interfaces.
- Finish assembly of the laboratory-scale exhaust system and TEG test.
- Fabricate and evaluate modified TE oxides and binary alloys with eutectic decomposition.

Introduction

Vehicles waste an enormous amount of energy in the form of high temperature exhaust gases. Recovery of just a fraction of this wasted energy would translate into tremendous savings in fossil fuel usage as well as a reduction in vehicle emissions. TE devices that can directly convert the otherwise wasted thermal energy in the hot exhaust gases into useful electrical energy offer a possible method for partial recovery of this wasted energy. However, TE materials and devices suffer from several drawbacks including poor efficiency, high cost, manufacturability at the large volumes needed for automobiles, and durability to withstand rugged use on vehicles.

In this work we aim to address several of the limitations with TE materials and devices. Specifically, we are exploring new fabrication techniques, including aerosol deposition and isostatic pressing, for creating high-quality elements from abundant, low-cost, materials at optimum sizes and shapes. We are also designing and testing inexpensive heat sinks that use swirl jet impingement and other strategies to improve heat transfer and device efficiency. Along the same lines, we are examining thermal management from the micro (interface) to macro (system) level through models and experiments. Finally, at the device interfaces we are performing extensive characterization of thermo-electrical transport properties, diffusion, and interface adhesion for various materials and assembly technologies to improve device lifetime.

Approach

Our overall approach is to focus on making practical, industry relevant, advances in several key areas – materials, heat sinks, thermal management, interfaces, and durability – that are critical for the realization of widespread deployment of thermoelectric devices in vehicles. We have examined several approaches for creating micro/nano structured bulk TE materials, where we aim to take advantage of nanoscale effects, yet rapidly fabricate materials at a bulk scale. These approaches include isostatic pressing of TE powders, sintering TE powders with quantum dots, and using reactive-templated grain growth to create textured materials. Our approach for the heat sinks is to employ swirl jet impingement to enhance heat transfer while limiting back pressure and maintaining relatively simple, low-cost, and manufacturable designs. For thermal management, we are taking an integrated approach where appropriately scaled heat sinks, TE elements, and packaging are examined collectively for device performance and durability in models and laboratory-scale experiments. Interfaces are characterized thermally with optical techniques, and mechanically for adhesion and lifetime following thermal cycling, and diffusion barriers are evaluated chemically (e.g. transmission electron microscopy, X-ray spectroscopy, etc.) to evaluate effectiveness.

Results

We have made significant progress this year towards the goal of developing high performance, low-cost, lead-free thermoelectric materials and devices. We began with N-type alloys within the family of magnesium–tin–silicon that have the potential of meeting the project goals. We examined a variety of synthesis methods including mechanical alloying and solid-liquid reactions in oxygen-free environments and optimized TE properties by varying doping, hot press temperature, and time. The materials synthesis process developed is summarized in Figure 1. In Figure 1(a), a crucible is shown that

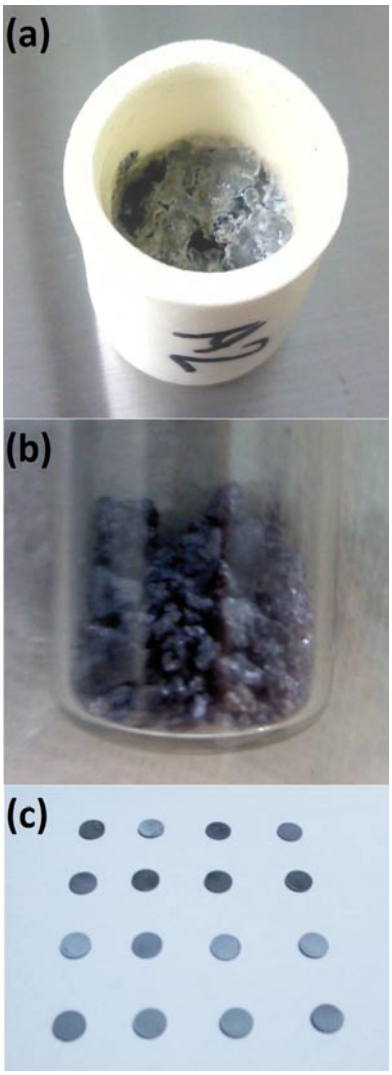

FIGURE 1. Mg-Silicide Thermoelectric Materials (a) crucible containing doped Mg-silicide elemental materials, (b) granules of the Mg-silicide materials, (c) hot-pressed pucks of N-type Mg-silicide TE elements.

had been loaded with elemental materials, including dopants. These raw materials are already processed at high temperature, allowing the desired phase to form and dopants to be incorporated into the lattice. Figure 1(b) shows granules of these materials, which are then powderized and hot pressed into test pucks, as shown in Figure 1(c). The hot press systems are capable of reaching pressures up to 60 kpsi and temperatures of 1,000°C, and are operated inside of a glove box in an environment that is less than 1 ppm oxygen. Our most recent results give dimensionless figure of merit (ZT) values of ZT=0.37 at 150°C, and 0.33 at 300°C. While these ZT values still lag those of state-of-the-art lead telluride materials, the performance per raw material cost is already twice (2x) that of Pb-Te, with the potential for that metric to increase to a factor of 3x.

In addition to the Mg silicides, ZnO is a promising TE material candidate due to its large power factor, thermal stability, oxidation resistance, nontoxicity, low cost, and scalability and variety of available growth techniques. In order to improve ZT in ZnO-based materials, we examined several approaches for reducing thermal conductivity including embedding quantum dots in the matrix, and creating nanoscale textured ceramics.

For the quantum dot materials, we synthesized samples of composition $(Zn_{1-x}Al_x)O$ (x=0, 0.01, 0.02, 0.03, 0.04) by solid-state reaction methods. These samples utilized nano to micro size Al_2O_3 powders and were sintered at 1,100-1,400°C for ~5 hours in air. X-ray diffraction and energy dispersive spectroscopy analyses indicated that the main phase was ZnO with homogeneous distribution of a second phase of $ZnAl_2O_4$ for all samples, and scanning electron microscope images revealed that we could control the grain size through the Al doping (Figure 2). The thermal conductivity of ZnO was found to decrease significantly with the addition of the nanoscale Al secondary phase Figure 3(a). Further analysis of samples with varying grain sizes from 1-15 μm indicated that the reduction in thermal conductivity was primarily the result of scattering at the nanoscale secondary phase rather than at the grain boundaries. This further analysis also revealed the dependence of mobility and electrical conductivity on grain size and growth temperature. The electrical resistivity varied from insulator (10^8 Ω-cm) when sintered at 1,100°C to semiconductor (1 Ω-cm) when sintered at 1,400°C (Figure 3(b)). Thus we see an opportunity to selectively tune the electrical and thermal properties through variations in powder size, metal dopant and concentration, and sintering temperature. The optimization of these relationships is currently being explored further.

Our efforts on the thermal side have thus far focused on system level thermal management strategies, and the design and evaluation of swirl jet impingement heat sinks as shown in Figure 4. Figure 4(a) shows a model of a jet impinging on a surface and inducing a

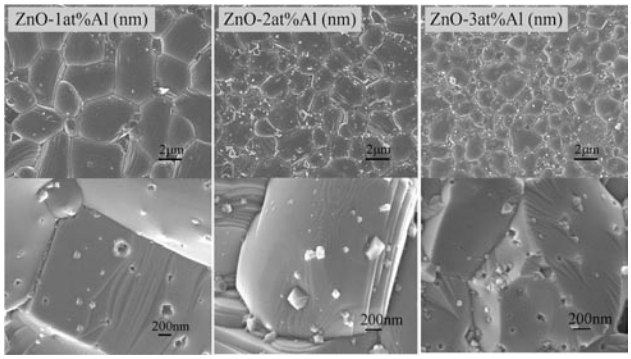

FIGURE 2. Scanning electron microscope images of $(Zn_{1-x}Al_x)O$ quantum dot TE materials where x=0.00-0.03. These materials were synthesized using solid-state reaction methods with nanoscale powders of Al_2O_3.

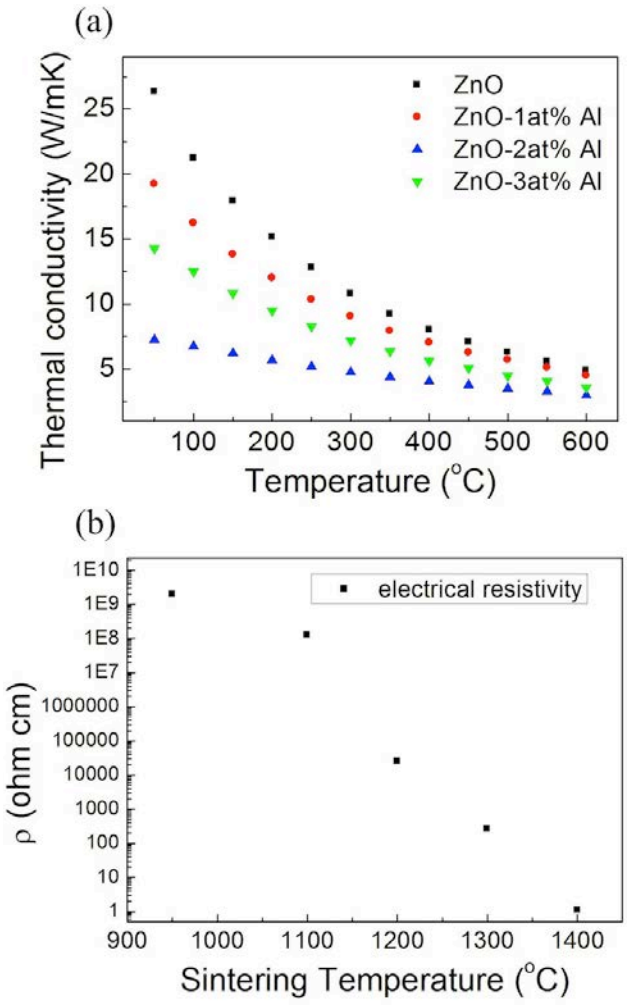

FIGURE 3. Thermal conductivity and electrical resistivity of $(Zn_{1-x}Al_x)O$ quantum dot TE materials. (a) Thermal conductivity of $(Zn_{1-x}Al_x)O$ synthesized from nanoscale Al_2O_3, showing a strong reduction in thermal transport for 2 at% of Al. (b) Room temperature electrical resistivity ZnO-2% Al as a function of sintering temperature.

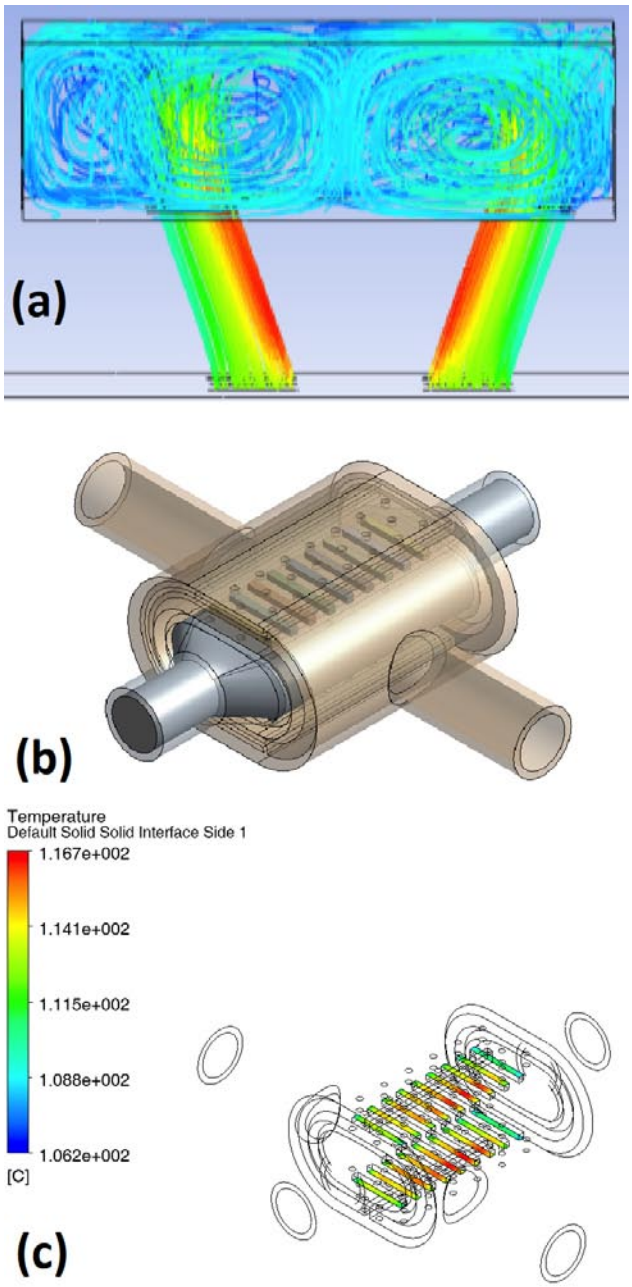

FIGURE 4. Heat Exchangers Employing Swirl Impingement Flow (a) Computational fluid dynamics model of a coolant jet impinging on a surface and inducing a turbulent swirling flow, (b) model of a TEG, exhaust system, and heat exchanger assembly created in ANSYS, (c) representative contour plot of temperatures, in °C, within the heat sink and TEG assembly.

swirling flow to enhance heat transfer, while Figure 4(b) is an image from an ANSYS model of a heat sink and TEG assembly on the exhaust system of a vehicle. Figure 4(c) shows a representative contour plot of temperatures within the heat sink and TEG assembly. We have found that through appropriate scaling of the jet diameter, spacing, and impingement angle we can enhance heat transfer with minimal rise in back pressure. Our models indicate that heat sinks with swirl impingement can reduce the cold side temperature of the TE elements by 6-8°C in comparison with standard cross-flow heat exchangers for a typical TEG assembly, which translates to an efficiency gain of ~0.25%.

Conclusions

- Isostatic pressing presents a scalable method for creating large quantities of optimized TE materials of a wide range of shapes and sizes.
- Mg silicide materials are promising candidates for large volume TE applications where cost is a premium.
- The introduction of nanoscale powders in ceramic TE materials presents a promising opportunity for creating high quality TE elements with tailorable TE properties.
- Heat exchangers employing swirl impingement flow offer a possible route for enhancements in heat transfer with minimal penalty in terms of pressure drop or fabrication/assembly complexity and cost.

FY 2011 Publications/Presentations

1. Paper accepted at the 50th AIAA Aerospace Sciences Meeting "Heat Exchanger Design for Waste Heat Recovery from Automobile Exhaust Using Thermoelectric Generators," J. Pandit, M. Dove, S. Huxtable, and S. Ekkad, Nashville, TN, January 2012.

2. Y. Zhao, Y. Yan, S. Priya, "Electrical conductivity enhancement of Al in ZnO (in preparation), to be submitted to the Journal of Materials Chemistry, December 2011.

3. Y. Zhao, Y. Yan, S. Priya, "Role of grain size and nano secondary phase composition towards thermoelectric properties of ZnO," to be submitted to ACS Nano, January 2012.

III.11 High-Performance Thermoelectric Devices Based on Abundant Silicide Materials for Vehicle Waste Heat Recovery

Song Jin
University of Wisconsin-Madison
1101 University Ave.
Madison, WI 53706

NSF Manager: Sumanta Acharya

DOE Technology Development Manager: John Fairbanks

NETL Project Manager: Carl Morande

Overall Objectives

Synthesize nanostructured abundant higher manganese silicides (HMS) in bulk with enhanced thermoelectric performance for thermoelectric applications.

Fiscal Year (FY) 2011 Objectives

Use Mn and $MnCl_2$ vapor to fully convert silicon (Si) nanostructures to HMS nanostructures as an alternative route to prepare nanostructured HMS in bulk.

Accomplishments

- Attained optimal conditions for the conversion of Si nanoparticles (NPs) to HMS using Mn and $MnCl_2$ vapor.
- Extended the HMS conversion approach using Si NPs to using electrochemically etched Si nanowires (NWs).
- Minimized the formation of impurity silicide phases by optimizing conditions and using Si NWs.

Future Directions

- Acquire phase-pure nanostructured HMS in larger quantity via conversion reactions.
- Prepare nanostructured HMS composites with silicon using phase segregation and precipitation approach.
- Work with the team members at University of Texas at Austin to evaluate the physical properties of the nanostructured HMS.

Introduction

Higher manganese silicides are interesting semiconducting thermoelectric (TE) materials with reported figures of merit (*ZT*) up to 0.7-0.8 in bulk crystals. The abundance, low cost, and robustness of silicides make them particularly promising for large scale thermoelectric applications, such as in automobile waste heat recovery. We have previously shown that the free-standing one-dimensional NWs and nanoribbons (NRs) of HMS can be successfully synthesized using chemical vapor deposition (CVD) of a single source precursor [1] and that the thermal conductivity of these nanostructures are suppressed from the already low bulk HMS value of 2-4 W/m-K to a value approaching 1 W/m-K and the amorphous limit. However, the demand for large amount of TE materials limits the use of NWs and NRs in devices. In our current project, we are developing nanostructured HMS in bulk with improved TE properties for practical applications in automobile waste heat recovery. We use both solid state and solution-based synthesis approaches to prepare nanostructured HMS in bulk. Such bulk nanomaterials, after a densification step, would have improved electrical conductivity, which, in combination with reduced thermal conductivity, would lead to improved TE performance.

Approach

We have so far been using vapor phase conversion reactions [2] to selectively synthesize HMS nanostructures starting from Si nanostructures. We have used two different conversion approaches. In the first approach, we are using manganese (Mn) vapor to react with Si nanostructures in a sealed stainless steel reactor, which was designed to provide a closed environment for the diffusion of Mn into Si. In the second approach, we evaporate manganese chloride ($MnCl_2$) precursor in a CVD setup to react with Si nanostructures to synthesize HMS nanostructures [3]. So far, we have used silicon NPs that were purchased from commercial sources and silicon NWs that we synthesized via electrochemical etching as the starting silicon nanostructures. The challenges in such conversion reactions include: 1) controllably forming the HMS phase among the various Mn silicide phases; 2) ensure there is sufficient kinetics to allow the reaction to proceed within reasonable a time frame while not making the nanoscale domain size to grow.

Results

1A) In the first approach, we are using manganese (Mn) vapor to react with Si nanostructures in a sealed stainless steel reactor, which was designed to provide a closed environment for the diffusion of Mn into Si. We initially reacted Mn vapor with Si NPs at a temperature range of 600-1,050ºC. By performing the reactions at several temperatures and for different reaction times, we have been able to control the delivery of Mn flux to Si and successfully synthesize different phases of Mn silicides. Based on the powder X-ray diffraction (PXRD) patterns and extensive energy-dispersive spectroscopy analysis, we have concluded that MnSi, Mn_5Si_3 and HMS can be formed. These results indicate that at these temperatures there is sufficient vapor pressure of Mn to allow facile reactions to form different silicide phases. We also learned that MnSi is the first phase formed when Mn vapor is in excess between the temperature ranges of 600-900ºC and that continuous supply of Mn vapor after the formation of MnSi in the sealed environment results in the formation of undesirable Mn-rich silicides, specifically Mn_5Si_3, as shown in Figure 1.

1B) In order to clearly understand the formation mechanism of different silicides and selectively form HMS, we have further prepared alternate Si nanostructures and have carried out the Mn vapor conversion reactions with those starting materials. We have electrochemically etched Si wafer to obtain vertically aligned Si NWs that are attached to the Si substrate. In addition to the facile preparation with relatively high yield, these NWs provide the additional benefit of excess Si source, which we believe encourage the formation of HMS.

Using our optimized conditions for the Si NP conversion reactions (based on the fraction of HMS formed), we have successfully obtained HMS starting from these Si NWs as the only Mn-silicide phase, when the reaction is carried out at 1050ºC for 2 h. However, due to the high temperature and relatively longer reaction time, the morphology of the original NW morphology is lost under this condition. By slightly modifying the reaction setup to provide faster transfer of Mn vapor to Si NWs and working at lower reaction temperature range of 850-950ºC, we have successfully preserved the morphology of the starting NWs while forming HMS as the dominant silicide phase. We have also found that the fraction of HMS formation increases with increasing temperature within this temperature range, where the fraction of HMS is highest when the reaction is performed at 950ºC for 45 min as shown in Figure 2.

2A) In the second approach, we evaporate manganese chloride ($MnCl_2$) precursor in a CVD setup to react with Si nanostructures to synthesize HMS nanostructures. We performed this reaction with Si NPs at temperature ranging from 875 to 950ºC for time ranging from 30 min to 12 h. We found that under appropriate conditions, we can successfully form MnSi and HMS, as shown in the PXRD in Figure 3, indicating that the vapor pressure of Mn species in this setup is sufficient in forming the silicides.

2B) We have also carried out reactions using the electrochemically etched Si NWs as the starting Si nanostructures. Using the optimized condition we have established for Si NPs, we have successfully obtained HMS as the major silicide with minor MnSi impurity

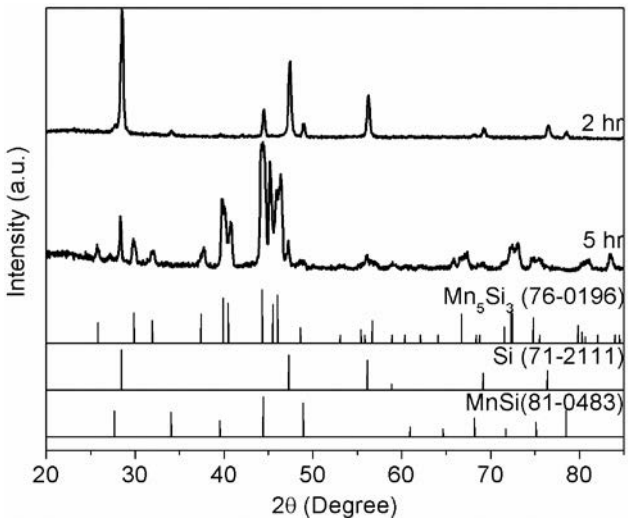

FIGURE 1. PXRD pattern showing the presence of MnSi and Si in a sample converted from Si NPs in a stainless steel reactor at 800°C for 2 h and the subsequent formation of Mn_5Si_3 when reacted for 5 h with continuous Mn flux.

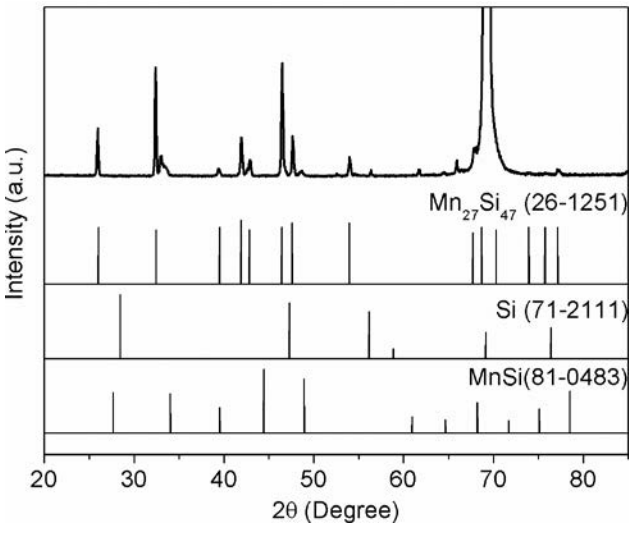

FIGURE 2. PXRD pattern showing the presence of HMS and Si as major peaks and MnSi as the minor peak in a sample converted from Si NWs in a stainless steel reactor with restricted Mn flux at 950ºC for 45 min.

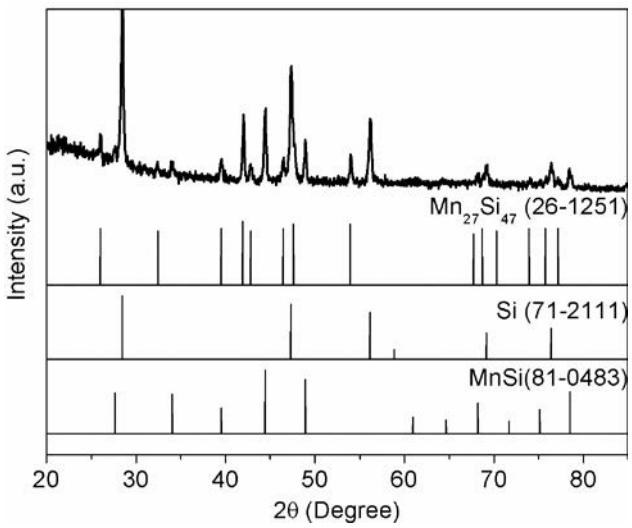

FIGURE 3. PXRD pattern showing the presence of HMS, MnSi and Si in sample prepared by reacting $MnCl_2$ vapor with Si NPs at 940°C for 10 h.

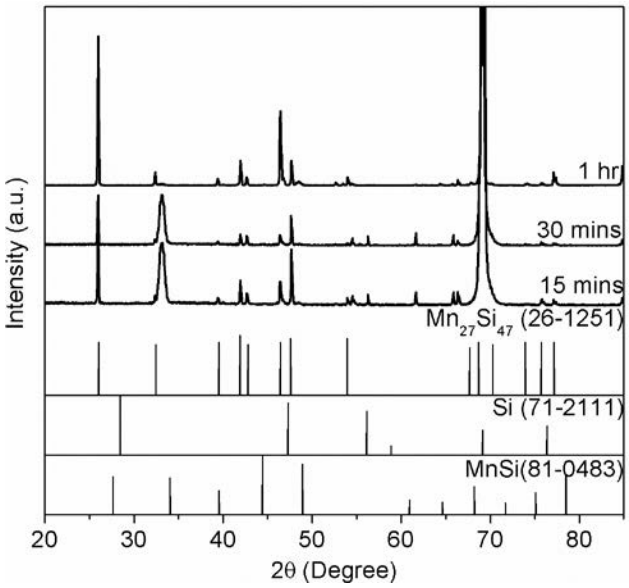

FIGURE 4. PXRD pattern showing the presence of HMS and Si as major peaks and MnSi as the minor peak in a sample prepared in sample prepared by reacting $MnCl_2$ vapor with Si NWs at 950°C for 15 min, 30 min and 1 h.

when the reaction is carried out with Si NWs at 950°C for time ranging from 15 min to 1 h (Figure 4). While we can selectively form HMS, the morphology of the NWs is lost with this reaction setup. We are currently working at lower temperature ranges to better preserve the nanomorphology.

Conclusions

- HMS nanostructures can be successfully synthesized using Mn and $MnCl_2$ vapor to convert Si NPs and Si NWs.
- In terms of the fraction of HMS formation, higher temperature is favorable for HMS formation for both conversion reactions.
- Formation of MnSi phase can be minimized for conversions using vertically aligned Si NWs on Si, which can be attributed to the continuous supply of Si to the nanostructures during the conversion reaction.

References

1. Higgins, J.M.; Schmitt, A.L.; Guzei, I.A.; Jin, S. "Higher Manganese Silicide Nanowires of Nowotny Chimney Ladder Phase", *J. Am. Chem. Soc.* **2008**, *130*, 16086-16094.

2. Szczech, J.R.; Jin, S. "Mg_2Si Nanocomposite Converted from Diatomaceous Earth as a Potential Thermoelectric Material" *J. Solid State Chem.* **2008**, *181*, 1565-1570.

3. Higgins, J. M.; Ding, R.; Jin, S.; "Synthesis and Characterization of Manganese-Rich Silicide (α-Mn_5Si_3, β-Mn_5Si_3 and β-Mn_3Si) Nanowires" *Chem. Mater.* **2011**, *23, 3848-3853.*

FY 2011 Publications/Presentations

Publications

1. Higgins, J.M.; Ding, R.; Jin, S.; "Synthesis and Characterization of Manganese-Rich Silicide (α-Mn5Si3, β-Mn5Si3 and β-Mn3Si) Nanowires" *Chem. Mater.* **2011**, 23, 3848-3853.

2. Yan, C.-Y.; Higgins, J.M.; Faber, M.S.; Lee, P.-S.; Jin, S.; "Spontaneous Growth and Phase Transformation of Highly Conductive Nickel Germanide Nanowires" *ACS Nano* **2011,** *5,* 5006-5014.

3. Higgins, J.M.; Carmichael, P.; Schmitt, A.L.; Lee, S.; DeGrave, J.P.; Jin, S.; "Mechanistic Investigation of the Growth of $Fe_{1-x}Co_xSi$ ($0 \le x \le 1$) and $Fe_5(Si_{1-y}Ge_y)_3$ ($0 \le y \le 0.33$) Ternary Alloy Nanowires" *ACS Nano* **2011,** *5,* 3268-3277.

4. Szezech, J.R.; Higgins, J.M.; Jin, S.; "Enhancement of the Thermoelectric Properties in Nanoscale and Nanostructured Materials" *J. Mater. Chem.* **2011,** *21,* 4037-4055.

Presentations

1. 30th International Conference on Thermoelectrics "*Synthesis of Bulk Nanostructured Higher Manganese Silicides for Thermoelectric Applications*", Pokhrel et. al.; Traverse City, MI, July 2011(poster).

2. 30th International Conference on Thermoelectrics "*Synthesis and thermoelectric properties of nanowires and bulk nanostructured manganese silicide ($MnSi_{1.75}$)*", Higgins et. al.; Traverse City, MI, July 2011(oral).

III.12 Enhancement of TE Performance of Mg_2Si with Embedded Si Nanoparticles

Co-PI: Susan M. Kauzlarich
University of California, Davis
Chemistry Department
One Shields Ave.
Davis, CA 95616

Senior Participant: Nigel Browning
Pacific Northwest National Laboratory

PI: Al Shakouri; Senior Participant: Zhixi Bian
University of California, Santa Cruz

NSF Manager: Sumanta Acharya

DOE Technology Development Manager: John Fairbanks

NETL Project Manager: Carl Morande

Overall Objectives

- Develop novel thermoelectric (TE) materials based on abundant and non-toxic Zintl phase magnesium silicide alloys.
- Demonstrate that with the use of embedded nanoparticles of appropriate concentration (0.01-5%) and diameter (2-15 nm), thermal conductivity will be reduced by scattering of mid to long wavelength phonons.

Fiscal Year (FY) 2011 Objectives

- Synthesis of both n- and p-type Mg_2Si and $Mg_2Si_xSn_{1-x}$ with embedded Si and Mg_2Si nanoparticles.
- Structural and TE characterizations.
- Thermoelectric transport modeling.
- Optimization of both thermal conductivity and TE power factor by modifying the alloy composition, nanoparticle sizes and concentrations.

Accomplishments

- Low temperature synthesis and spark plasma sintering (SPS) of n-type Mg_2Si with embedded Si nanoparticles.
- Characterization and transport modeling.

Future Directions

- Low temperature synthesis and SPS of n-type $Mg_2Si_{1-x}Sn_x$ with embedded Si and Mg_2Si nanoparticles.
- Low temperature synthesis and SPS of n-type $Mg_{2-x-}Yb_xSi$ with embedded YbSi nanoparticles.
- Low temperature synthesis and SPS of p-type Mg_2Si with embedded nanoparticles.
- Characterization and transport modeling.

Introduction

We will develop novel TE materials based on abundant and non-toxic Zintl phase magnesium silicide alloys. We propose a synthetic method that naturally provides embedded nanoparticles within a magnesium silicide alloy matrix, providing uniform mixing with minimal aggregation. With the use of embedded nanoparticles of appropriate concentration (0.01-5%) and diameter (2-15 nm), thermal conductivity will be reduced by scattering of mid to long wavelength phonons. Controlling the heterostructure band offset and the potential barrier of nanoparticles with respect to matrix, power factor will be increased by selective scattering of hot carriers. Preliminary transport calculations show that ZT>1.8 at 800 K could be achieved.

Approach

Mg_2Si can be synthesized at relatively low temperature with MgH_2 and Si powders as starting materials. By changing the ratio of the starting materials, a proper amount of Si nanocomposites can be easily cooperated with the matrix. N-type or p-type dopants are intentionally mixed with starting materials homogeneously in a ball mill to tune the carrier concentration. Flow furnace and SPS are employed to achieve the Mg2Si product as well as dense pellets for transport properties characterizations.

Results

Silicon nanoparticle embedded Mg_2Si composite (Mg_2Si/xSi) has been successfully synthesized at 623 K from MgH_2 and Bi containing Si nanoparticle powders. This synthetic route avoids the production of oxides through the generation of hydrogen and allows for

easy alloy formation. In addition, it provides a route to homogeneously mixed Si nanoparticles within a doped Mg_2Si matrix along with the opportunity to control particle size. The composition of the samples was characterized by powder X-ray diffraction shown in Figure 1. The crystallite size of Mg_2Si obtained from the X-ray diffraction patterns is about 50 nm for all the samples. The microstructure of the Bi doped Mg_2Si/xSi nanocomposites from scanning transmission electron microscopy (STEM) indicated that the Bi dopant has a much higher concentration at grain boundaries and that Bi preferentially substitutes Mg instead of Si as a substitutional dopant at the grain boundaries, shown in Figure 2. The Mg_2Si/xSi nanocomposites suppress the phonons, and yielded a significant reduction of lattice thermal conductivity, shown in Figure 3. The 2.5 vol% sample has ~20 mW/cm K at 775 K, which is about 30% reduction comparing to ~30 mW/cm K for the reference. As a results, a dimensionless figure of merit zT ~ 0.7 was obtained at 775 K for the sample with 2.5 vol% Si nanoparticles, shown in Figure 4. With optimization of the electronic states of the matrix and

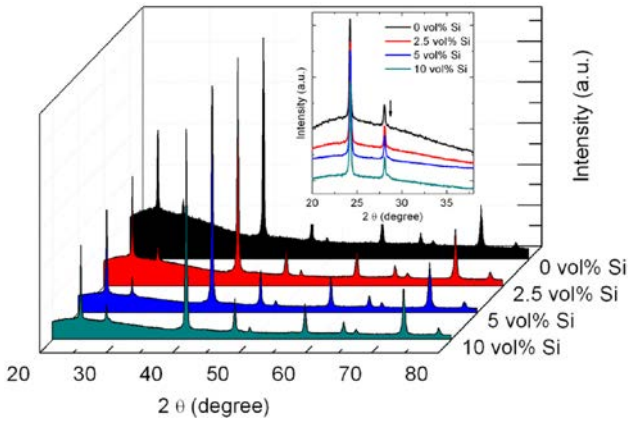

FIGURE 1. X-ray diffraction of $Mg_2Si/xSi_{1\%Bi}$ (x = 0, 2.5, 5, 10 vol%), the inset is an enlarged view showing the (111) peak of Si which is the shoulder of the (200) peak of Mg_2Si around 2θ of 28° marked by an arrow.

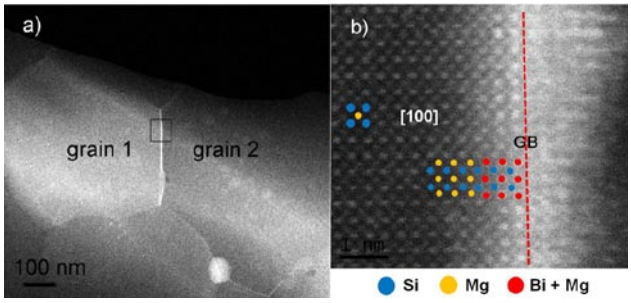

FIGURE 2. STEM high angle annular dark field images of a) Mg_2Si grains, b) enlarged view of the rectangle area indicated at the grain boundary in a). The modeling of where Bi resides at the grain boundary is indicated.

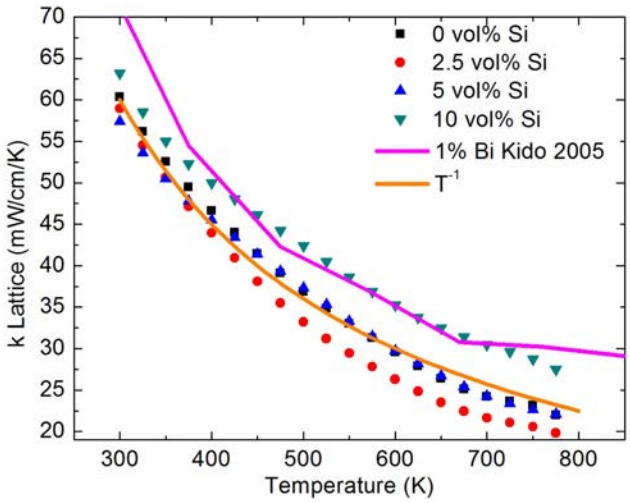

FIGURE 3. Lattice thermal conductivity of Mg_2Si/xSi (x = 0, 2.5, 5, 10 vol%) samples and the 1 mol% Bi doped reference compared with $\kappa_L \sim T^{-1}$.

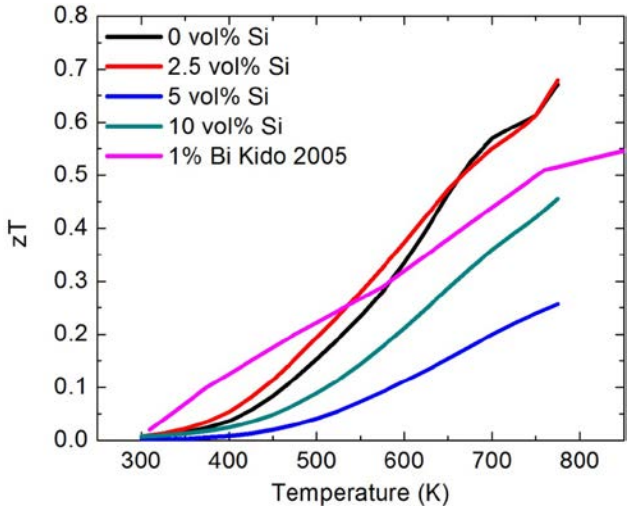

FIGURE 4. The figure of merit zT of Mg_2Si/xSi (x = 0, 2.5, 5, 10 vol%) samples and the 1 mol% Bi doped reference.

nanoparticle, further enhancement of the figure of merit may be achieved.

Conclusions

Mg_2Si with Si nanocomposites, $Mg_2Si/xSi_{1\%Bi}$, were obtained by reacting MgH_2 and Si nanoparticles. The distribution of Si nanocomposites and Bi in Mg_2Si pellets were characterized by electron microprobe. The aggregation of Si nanoparticles become significant when the concentration of Si exceeds 5 vol%. Bi is favorable to cooperate with Mg_2Si rather than Si, and the microstructure from STEM indicates higher Bi concentration at grain boundaries. In addition,

Bi prefers to substitute for Mg at boundaries. The measurements of transport properties confirm that a proper amount of Si nanocomposites in Mg_2Si causes a significant reduction of lattice thermal conductivity. As a consequence, the figure of merit zT is improved, and a zT ~ 0.8 at 775 K is achieved for the sample with 2.5 vol% Si inclusions.

FY 2011 Publications/Presentations

1. Tanghong Yi, Shaoping Chen, Sabah Bux, Jean-Pierre Fleurial, Zhixi Bian, Natalio Mingo, Ali Shakouri, Susan Kauzlarich, Enhancement of Thermoelectric Efficiency of Mg_2Si with Si Nanocomposites, The 30th International Conference on Thermoelectrics, Traverse City, MI, 2011 July.

2. Oliver Janka, Tanghong Yi, Susan M. Kauzlarich, $Mg_{2-x}Yb_xSi$: Ytterbium doped Mg_2Si as a thermoelectric material, Presented at the 26th Rare Earth Research Conference, Santa Fe, NM, June 19–23, 2011.

3. Oliver Janka, Andrew Hwang, Tanghong Yi, Susan M. Kauzlarich, Modifying Mg_2Si for enhanced thermoelectric properties, Presented at the ACS Fall Meeting 2011, Denver, CO, August 28 – September 1, 2011

III.13 NSF/DOE Thermoelectrics Partnership Project SEEBECK: Saving Energy Effectively by Engaging in Collaborative Research and Sharing Knowledge

Dr. Guo-Quan Lu, Professor
Virginia Polytechnic Institute and State University
Department of Materials Science and Engineering
Blacksburg, VA 24061

NSF Manager: Sumanta Acharya

DOE Technology Development Manager: John Fairbanks

NETL Project Manager: Carl Morande

Overall Objectives

- Develop an interface bonding metallurgy between thermoelectric (TE) elements and heat exchangers with an electrical contact resistance smaller than 10^{-5} Ω cm^2 and a thermal contact resistance smaller than 10^{-3} K W^{-1} cm^2.
- Integrate and package TE devices with an overall performance that is not degraded by more than 20% over the theoretical performance of the material, with a 10-year lifetime, and the capability to withstand 10^6 thermal cycles from 773 K to 300 K.

Fiscal Year (FY) 2011 Objectives

- Study the interface issues relevant to the metallization of the TE materials to identify a suitable diffusion barrier material to silver diffusion.
- Demonstrate the sintering of nanoscale silver paste as attachment technique and evaluate the bonding quality of sintered silver.

Accomplishments

- Characterized the surface roughness of deposited Ag/Ti coating on silicon substrate.
- Attained the diffusivity of Ag in Ti at 500°C to be $2\times10^{-15}cm^2/s$.
- Obtained uniform bonding layer of sintered nanosilver paste without large-scale voids and cracks using a low-temperature, low-pressure processing profile.
- Developed a nanosilver sintering process for bonding on bare copper in nitrogen atmosphere.

Future Directions

- Other barrier materials, such as titanium-tungsten alloy will be studied to evaluate effectiveness for slowing silver diffusion.
- The die-attach process by low-temperature sintering of nanosilver paste will be further improved.
- The thermal and electrical contact resistance, as well as the thermomechanical reliability of nanosilver sintered bonding layer will be characterized.

Introduction

The sintered silver joint has been shown to be (1) highly reliable in thermal and power-cycling tests attributed to its porous microstructure and absence of intermetallic phases; (2) capable of supporting chips running at high junction temperature because silver melts at 1,234 K; and (3) highly conductive of heat and electrons as the joint is made of pure silver [1-3]. As Ag is reduced from its oxide near about 200°C, Ag nanoparticles are densified at such low temperatures, provide a metal-metal bond that is then stable to well above the maximum operating temperature (500°C) needed in this project. The resulting sintered bond is porous. As the modulus of the compound is proportional to the square of the porosity, a 70% dense Ag sinter is flexible enough to shield TE materials from thermal shocks, while still providing over 50% of the heat and electrical conduction of the parent metal (the highest of all metals). This approach is most promising for mounting TE materials. However, several problems need to be researched. Silver diffuses fast, and is notoriously mobile as an ion in the presence of chalcogens. In addition, pressure is usually needed during silver sintering [4], which is a barrier for industrial process. So, in year 1, we focused on identifying a suitable diffusion barrier material to silver diffusion and furthering the nanosilver die-attach process for bonding TE components.

Approach

Titanium and silver with thickness of 100 nm were deposited on glass and silicon substrates by physical vapor deposition. The silicon or glass served as surrogate substrates in place of actual TE materials/substrates. The Ti layer enables the succeeding layer

to bond to the substrate, which in turn is bondable to the attachment material. The coated substrates were annealed at 500°C for 1 hour and the roughness and concentration profile were characterized by atomic force microscopy (AFM) and X-ray photoelectron spectroscopy, respectively. The diffusivity of Ag in Ti was calculated by Sauer–Freise–den Broeder inverse solution.

Low-temperature, low-pressure sintering of nanosilver paste was used to attach mechanical chips on silver-coated and bare copper substrates. A focused effort was placed on simplifying the hot-pressing requirement for bonding large-area (greater than 3 mm x 3 mm) chips and exploring the use of nitrogen atmosphere for sintering chips on bare copper substrate. Quality of the sintered interfaces was characterized by X-ray imaging and scanning electron microscopy.

Results

Evaluation of Titanium as Barrier to Silver Diffusion

Glass and silicon substrates were coated with Ti and Ag layers. The thicknesses of Ti and Ag were both 100 nm. The Ti/Ag diffusion couples were annealed at 500°C for 1 hour.

Surface roughness was evaluated before and after annealing by AFM, as shown in Figure 1. Roughness of the Ti/Ag coating surfaces before annealing was about ±10 nm, and that after annealing was ±80 nm. The AFM images also indicated that Ti/Ag particle coarsening occurred during the annealing process.

Interdiffusion between Ag and Ti was characterized by means of X-ray photoelectron spectroscopy. Concentration profiles of silver and titanium before and after annealing were plotted in Figure 2 and Figure 3, respectively. Figure 3 indicated that silver diffused through titanium layer after 1 hour annealing at 500°C. Diffusivity of silver in titanium has also been calculated by Sauer–Freise–den Broeder inverse solution. As shown in Figure 4, the diffusivity is about $2\times10^{-15}cm^2/s$.

Nanosilver Die-Attach Process

The processing steps for attaching mechanical silicon chips on silver-coated substrates using a nanosilver paste are: (1) applying an initial layer of the nanoscale silver paste on a substrate to a thickness of 50 µm; (2) drying the print at 180°C for 5 minutes by heating from room temperature at a rate of 5°C/min; (3) applying a second layer of the paste on the dried print to a thickness of 10 µm; (4) mounting a silicon chip

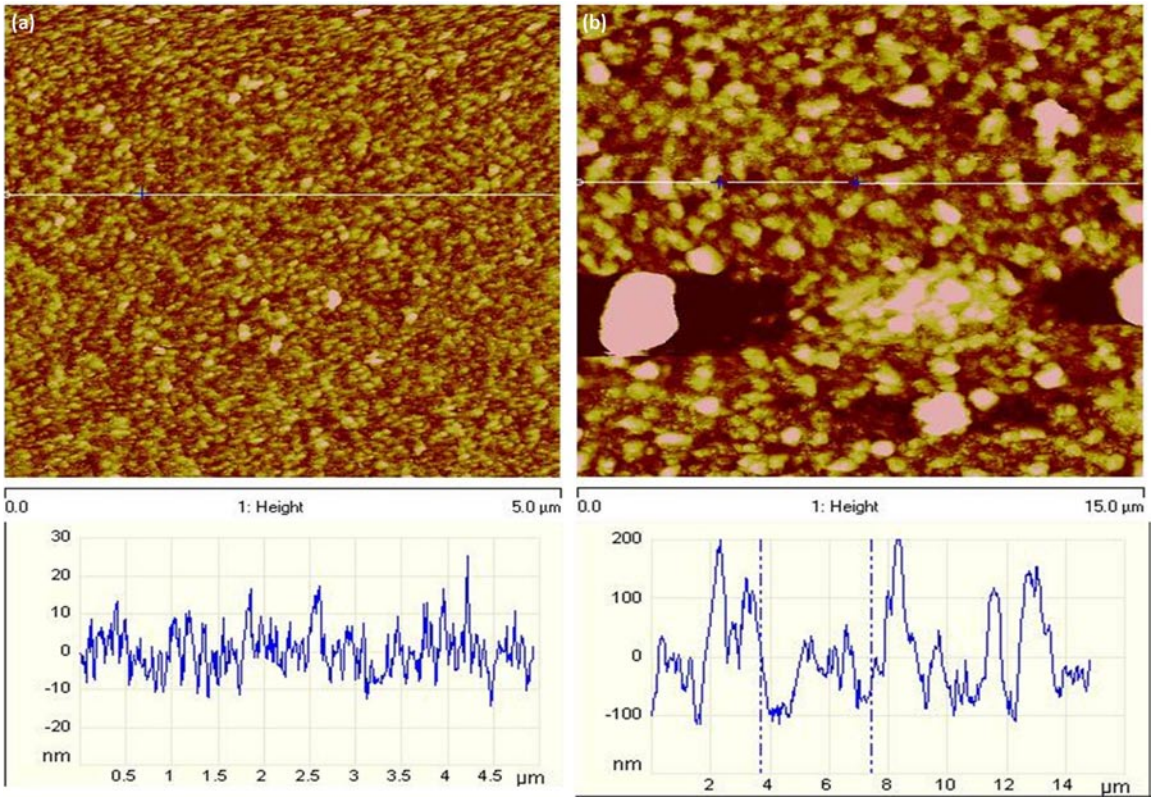

FIGURE 1. AFM images of Ti/Ag-coated surfaces, which showed the roughness (a) before annealing was about ±10 nm, and that (b) after annealing was ±80 nm.

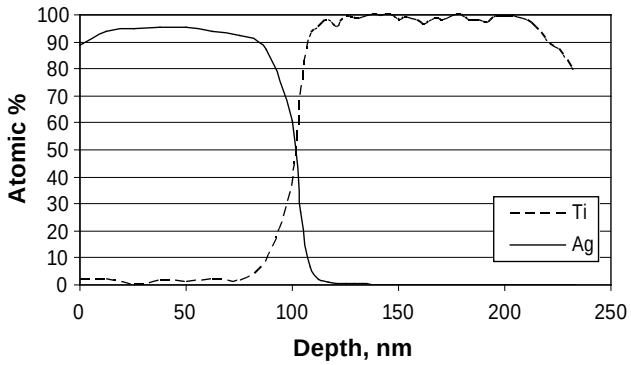

FIGURE 2. Silver and Titanium Concentration Profiles at Room Temperature for 120 Hours

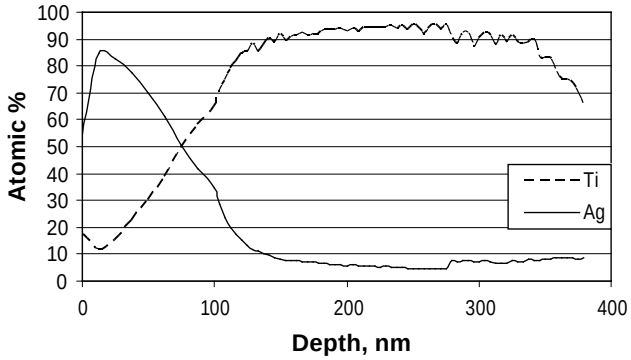

FIGURE 3. Silver and Titanium Concentration Profiles after Annealing at 500°C for 1 Hour

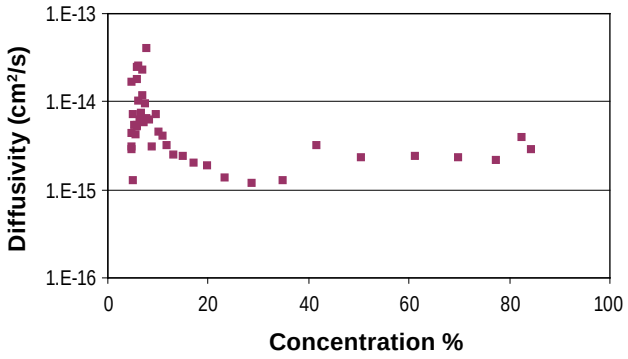

FIGURE 4. Diffusivity of Silver in Titanium vs. Concentration at 500°C

(or a TE component in the future) on the fresh print; (5) heating to 180°C at a rate of 30°C/min for 5 minutes under a constant pressure of 3 MPa; and then (6) rapidly heating the assembly to 275°C for 30 minutes to sinter the silver joint. The last step was carried out with 3 MPa pressure or without any pressure.

The processing steps for attaching chips on bare copper substrates is similar to the above, except that

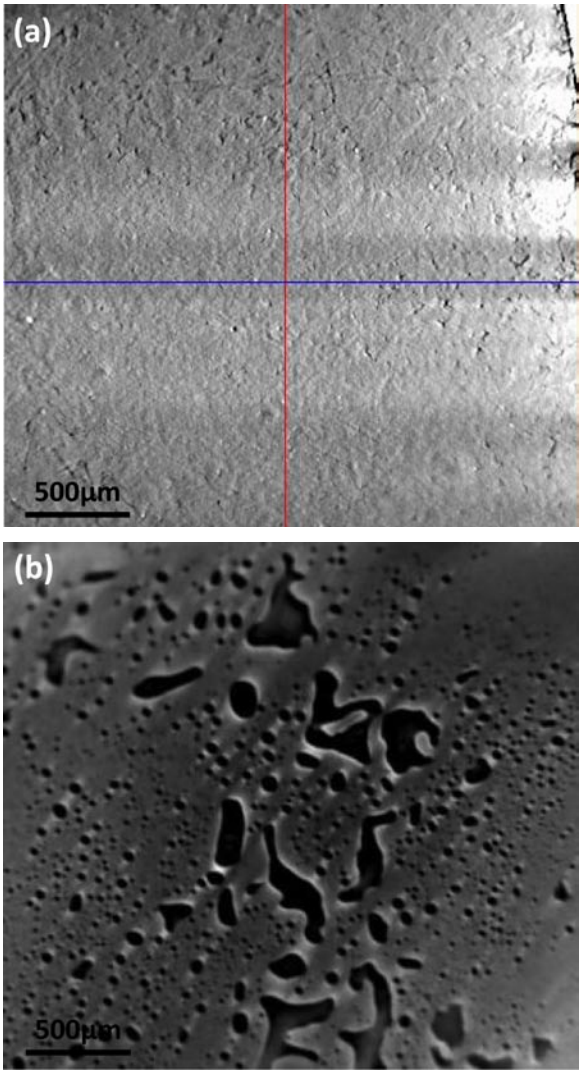

FIGURE 5. X-ray reconstructed image of (a) sintered nanoscale silver paste layer showing a relatively uniform microstructure and (b) reflowed SN100C solder attachment layer showing the presence of large voids.

an inert gas, such as nitrogen was used during drying and sintering to prevent copper from oxidation. The bonding strength was estimated to be over 20 MPa by die-shear tests.

Quality of the various bonding interfaces was evaluated by X-ray imaging and scanning electron microscopy. Figure 5 shows the X-ray images of the samples bonded by the lead-free solder paste (SN100C) and nanosilver paste, respectively. The sintered nanosilver paste layer did not show large-scale pores and cracks that are present in solder layer. A scanning electron microscope image of the cross-section of the sintered nanosilver is shown in Figure 6. Adhesion is excellent, with no obvious cracks or delamination at the interfaces.

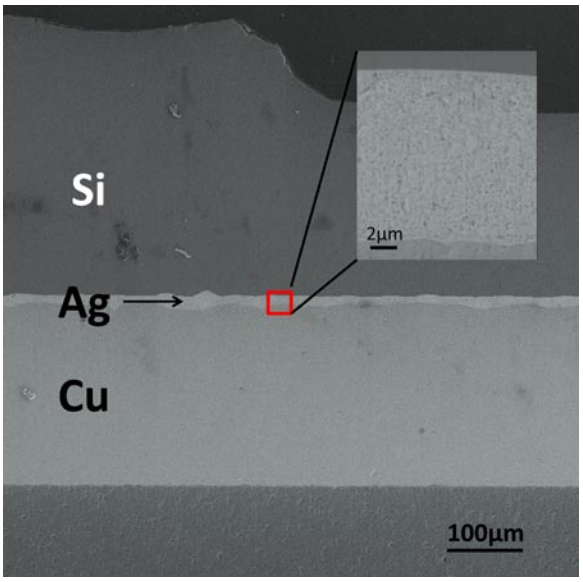

FIGURE 6. Scanning electron microscope image showing the cross-section area of sintered nanosilver die-attach layer, revealing a microstructure free of large voids and cracks.

Conclusions

- Titanium and silver as the metallization were developed on silicon and glass surfaces by means of physical vapor deposition. Interdiffusion between titanium and silver were characterized. Titanium does not appear to be effective in preventing silver from diffusion at high temperatures (>500°C).
- Low-temperature, low-pressure sintering process for attaching chips on silver-coated and bare copper substrates were experimented. Uniform bonding layers of sintered nanosilver paste without large-scale voids and cracks were obtained.

References

1. U. Scheuermann and P. Wiedl, "Low Temperature Joining Technology - A High Reliability Alternative to Solder Contacts", Workshop on Metal Ceramic Composites for Functional Application, Vienna, Austria, p.181 (1997).

2. U. Scheuermann and U. Hecht "Power Cycling Lifetime of Advanced Power Modules for Different Temperature Swings", International Exhibition & Conference for Power Electronics Intelligent Motion Power Quality (PCIM), Nuremberg, Germany, p.59 (2002).

3. H. Schwarzbauer and R. Kuhnert, "Novel large-area joining technique for improved power device performance", IEEE Trans. Ind. Appl., **27** p.93 (1991).

4. C. Göbl, P. Beckedahl and H. Braml, "Low Temperature Sinter Technology Die Attachment for Automotive Power Electronic Applications", Automotive Power Electronics (APE), Paris, France, (2006).

FY 2011 Publications/Presentations

1. H. Zheng, L. Xu, and G-Q Lu, "Effect of Oxygen Partial Pressure on Sintering Nanoscale Silver Die-Attachment on Copper Substrate", International Conference on Electronics Packaging (ICEP), Nara, Japan, (April 13-15, 2011).

2. K. Xiao, J. Calata, K. Ngo, D. Ibitayo and G-Q Lu, "Large-Area Chip Attachment by Sintering Nanosilver Paste: Nondestructive Characterization by X-ray Imaging and Curvature Measurements", International Conference on Electronics Packaging (ICEP), Nara, Japan, (April 13-15, 2011).

III.14 NSF/DOE Thermoelectrics Partnership Project SEEBECK: Saving Energy Effectively by Engaging in Collaborative Research and Sharing Knowledge

Mercouri Kanatzidis
Department of Chemistry
2145 Sheridan Road
Northwestern University (NU)
Evanston, IL 60208-3113

NSF Manager: Sumanta Acharya

DOE Technology Development Manager: John Fairbanks

NETL Project Manager: Carl Morande

Overall Objectives

- Materials research (led by Ohio State University and NU) to develop advanced thermoelectric materials made from earth-abundant, geographically dispersed elements and compounds.
- Thermal management system design (led by BSST) to minimize losses by minimizing number of interfaces, minimizing amount of thermoelectric material used and maximize the durability of the product.
- Research interfaces, (led Virginia Polytechnic Institute and State University, Stanford University and ZTPlus), that focuses on the metallization of the thermoelectric materials and device interconnection. Flexible bonding of metallized elements to the heat spreaders to increase durability and reduce device level performance losses.

Fiscal Year (FY) 2011 Objectives

- Identify the most attractive materials system that meets the selection criteria of lost cost, comprising elements of high earth abundance. The first material thus chosen is PbS.
- Apply nanostructuring concepts to create nanocomposites with very low thermal conductivity. Then select nanocomposite with lowest lattice thermal conductivity and optimize doping to achieve highest power factor and figure of merit ZT.
- Demonstrate that nanostructuring approach is effective in raising figure of merit ZT of lost cost material comprising elements of high earth abundance.

Accomplishments

- We reduced the lattice thermal conductivity of PbS greatly by adding selected metal sulfide phases. The thermal conductivity at 723 K was reduced by ~50%, 52%, 30% and 42% through introduction up to 5.0 mol% Bi_2S_3, Sb_2S_3, SrS and CaS, respectively.
- Achieved lattice thermal conductivity of 0.6 W/m-K at 900 K for a sample of n-type PbS containing Bi_2S_3 nanostructures.
- The second phases (Bi_2S_3, Sb_2S_3, SrS and CaS) added to PbS form as nanoscale precipitates in the PbS matrix, as confirmed by transmission electron microscopy and the experimental results show that they cause huge phonon scattering.
- As a consequence of this nanostructuring, ZT values as high as 0.8 and 0.78 at 723 K can be obtained for nominal bulk PbS material.
- When processed with spark plasma sintering, PbS samples containing 1.0 mol% Bi_2S_3 and doped with 1.0 mol% $PbCl_2$ show even lower levels of lattice thermal conductivity. This further enhanced ZT to 1.1 at 923 K. This is a great move forward to meeting DOE targets.

Future Directions

- Continue to optimize nanostructured n-type PbS. Goal: achieve ZT~1.3 at 900 K.
- Initiate research on nanostructured p-type PbS.
- Achieve lattice thermal conductivity or 0.6 W/m-K at 900 K on nanostructured p-type PbS. Goal: achieve ZT~1.1 at 900 K.
- Initiate research on nanostructured n-type Mg_2Sn and Mg_2Si. Achieve ZT~1.1 at 900 K.

Introduction

PbS is the least expensive thermoelectric material that can be conceived. Its constiuents are highly earth abundant and are found anywhere on earth. PbS has many attractive features. For example, it shares the same highly symmetric NaCl-type cubic structure as its heavier congeners, it has a very high melting point (1391 K) and energy band gap of 0.41 eV. Success with PbS will allow DOE to meet its objectives raising vehicle efficiency by 10% and being available to every vehicle on earth. Previous work in the literature performed

decades ago indicated that PbS was not an attractive thermoelectric materials with a maximum ZT~0.4 at 800 K and it was subsequently neglected in favor of PbTe [1]. Our current work however shows that this is not the case. PbS-based materials may in fact be very promising for high temperature application with continued improvements.

Approach

We are applying a general nanostructuring technique invented in our group called liquid encapsulation. To achieve nanoscale matrix encapsulation of a minor phase Y inside a major phase B (e.g. PbS), we choose the minor phase to have very low or no solubility in the solid state, but complete solubility in the liquid state. If the major phase PbS has an equal or higher melting point than the minor phase (guest or inclusion) on rapid cooling, it will be first to solidify, thereby precipitating and simultaneously encapsulating nanocrystals of phase Y. The minor phase is a suitable nonreactive material capable of altering the phonon scattering processes of the medium. This technique allows the rapid preparation of bulk nanostructured materials and results in significant reductions in thermal conductivity and increases in ZT. With PbS as the encapsulating matrix, we introduce nanocrystals of semiconductor particles of Y (e.g. CaS, SrS, Bi_2S_3, Sb_2S_3).

Results

In the PbS system we targeted the reduction of thermal conductivity using the nanostructuring technique. The technique used for the formation of precipitates is elaborated in Figure 1. The estimated

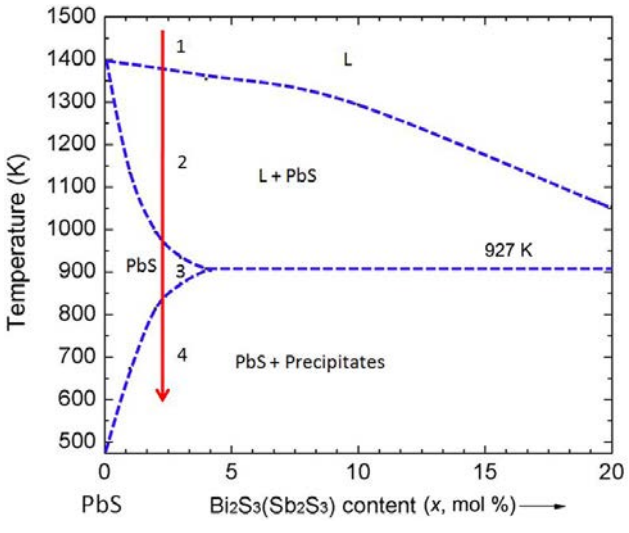

FIGURE 1. Binary phase diagram of PbS-Bi_2S_3(Sb_2S_3), indicating a strongly temperature dependent solubility of Bi_2S_3 (Sb_2S_3) in PbS.

section of the pseudo-binary phase diagram for PbS–Bi_2S_3 (Sb_2S_3) system is adapted from reference, and it suggests a strongly temperature dependent solubility of Bi_2S_3 (Sb_2S_3) in PbS. The mixture of PbS and Bi_2S_3 (Sb_2S_3) gives a homogeneous melt above 1391 K (step 1), which then is cooled down in step 2, and after that the sample is quenched and annealed within the single phase region (at this stage the Bi_2S_3 or Sb_2S_3 dissolve in the PbS matrix). In step 3, phase separation and precipitation of the second phases is achieved by cooling down after reaching the solid state solubility limit curve in step 4. For these samples we chose $PbCl_2$ as the electron donor dopant to tune the carrier concentration through substituting S^{2-} by Cl^{1-} in order to optimize the power factor. The nanoscale phases of Bi_2S_3 and Sb_2S_3 greatly reduce the thermal conductivity of PbS to levels similar to those achieved in nanostructured PbTe. As a result, we have obtained the ZT value of 1.1 at 923 K for n-type PbS samples nanostructured with 1.0 mol% Bi_2S_3 and doped with 1.0 mol% $PbCl_2$, which is the highest ever reported for this system, Figure 2.

We first started with pristine PbS doped with x mol% $PbCl_2$ (no second phases). $PbCl_2$ is used as the n-type dopant. The solid state solution limit of the electron donor dopant $PbCl_2$ in PbS is not reached even as the doping content climbs to 0.1 mol%. Therefore, to determine the solubility limit of $PbCl_2$ in PbS we increased the $PbCl_2$ doping content up to 5.0 mol%. As shown in Figure 2 (a), all the powder X-ray diffraction (PXRD) patterns can be indexed to the NaCl structure as a nearly single PbS phase. However, a small impurity phase of $PbCl_2$ can be indexed as the doping content exceeds 1.0 mol%, as shown in the expanded PXRD pattern range from 20° to 60° (2θ) in the inset of Figure 2 (a) – (I), suggesting that somewhere between 1.0-2.0 mol% doping reaches the solubility limit. This conclusion is supported by the variation of the lattice parameters and carrier concentration as a function of $PbCl_2$, as shown in Figure 2 (b). The lattice parameter decreases significantly up to 1.0 mol% $PbCl_2$ doping content and beyond that decreases slowly stabilizing as the content reaches 5.0 mol%. The lattice contraction is consistent with the radius of Cl^- ions (~1.81 Å) being smaller than that of S^{2-} ions (~1.84 Å) and suggests that Cl^- was successfully incorporated into the PbS lattice. Also, the carrier concentrations (n_H) at room temperature increase rapidly from $0.44 \times 10^{19} cm^{-3}$ for pristine PbS to $6.85 \times 10^{19} cm^{-3}$ for the sample with 1.0 mol% $PbCl_2$ doping, and then increase more slowly with increasing doping content reaching a maximum value of $11.6 \times 10^{19} cm^{-3}$ for the sample with 5.0 mol% $PbCl_2$, see Figure 2 (b). Collectively, the lattice parameter variation and carrier concentration indicate that the solubility limit of $PbCl_2$ in PbS ranges between 1.0 and 2.0 mol%.

By adding the nanoscale phases of Bi_2S_3 and Sb_2S_3 we find that they greatly reduce the thermal

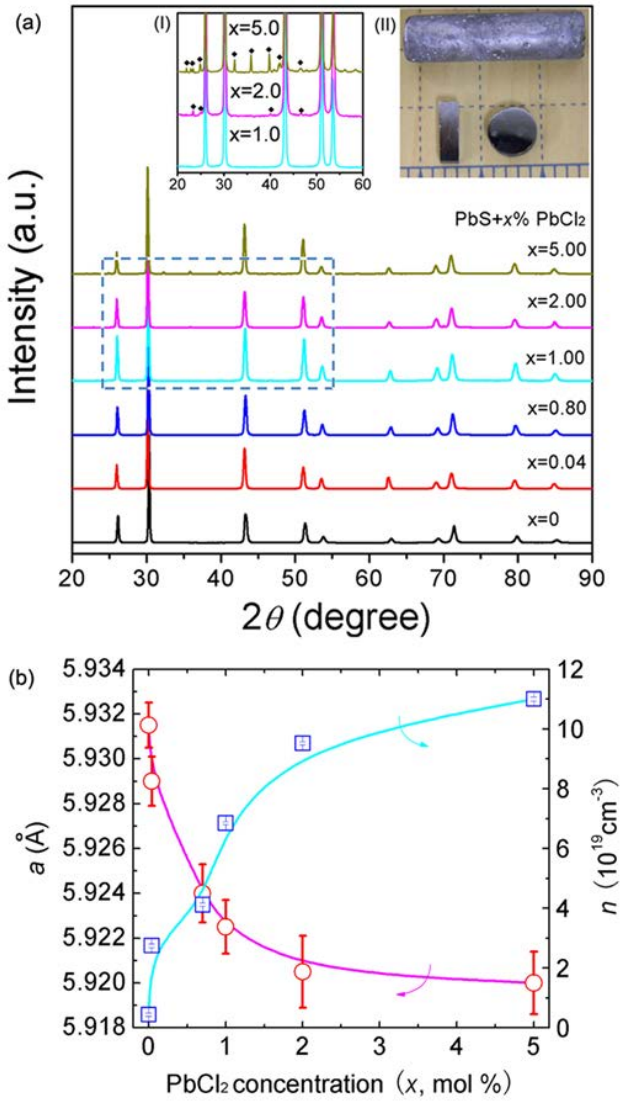

FIGURE 2. (a) Powder X-ray diffraction patterns for PbS with x mol% $PbCl_2$ doping, and (b) the lattice parameters and carrier density as a function of $PbCl_2$ concentration. The inset of (a) – (I) shows the enlarged powder X-ray diffraction pattern ranges from 20° to 60° (2θ degree), (a) – (II) typical melting reaction ingot and samples used in this study.

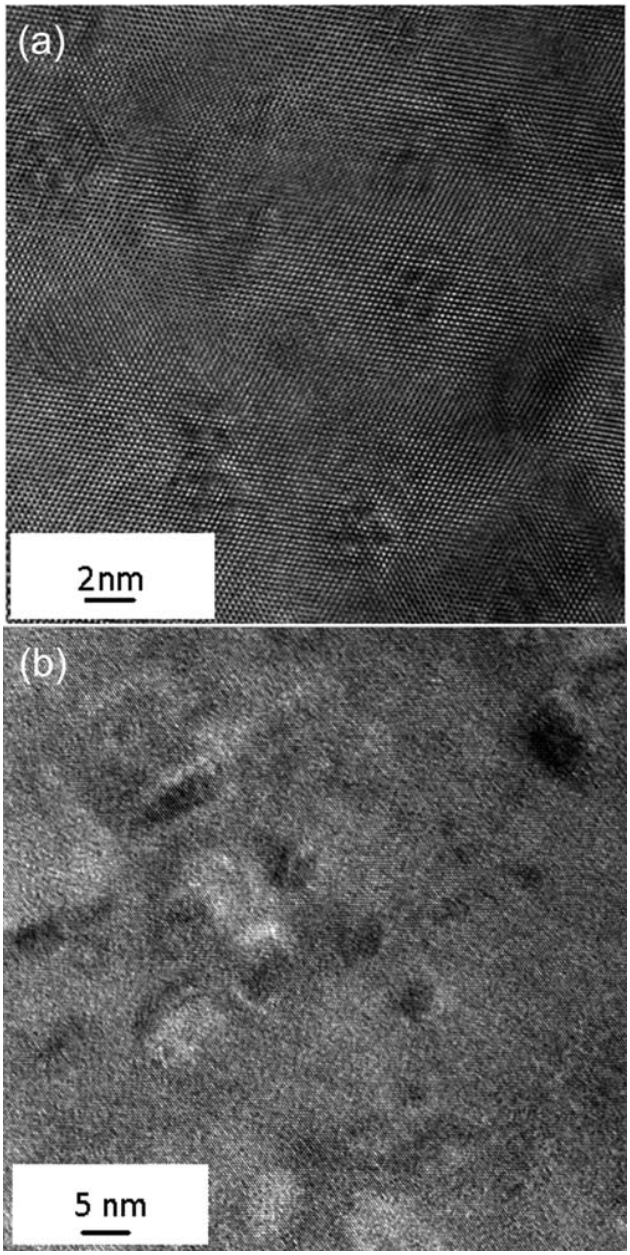

FIGURE 3. High resolution transmission electron microscopy images of (a) PbS with 1.0 mol% Bi_2S_3 and doped with 1.0 mol% $PbCl_2$, with modulation due to different stacking directions between matrix and precipitates and (b) PbS with 1.0 mol% Sb_2S_3 and doped with 1.0 mol% $PbCl_2$. Both of them exhibit comparable spherical/oval-like shape and the common size range from 2 to 10 nm.

conductivity of PbS to levels similar to those achieved in nanostructured PbTe. The nanostructured nature of our PbS is shown in Figure 3. All the relevant thermoelectric properties as a function of temperature of the best materials PbS with 1.0 mol% Sb_2S_3 and 1.0 mol% $PbCl_2$ doping is shown in Figure 4. As a result, we have obtained the ZT value of 1.1 at 923 K for n-type PbS samples nanostructured with 1.0 mol% Bi_2S_3 and doped with 1.0 mol% $PbCl_2$, which is the highest ever reported for this system, Figure 4. We plan to supply our co-principle investigator Guo-Quan Lu at Virginia Polytechnic Institute and State University with samples of these materials for metallization studies. Further we also plan to ship material to ZTPlus for independent validation and further evaluation.

Conclusions

- The lattice thermal conductivity of PbS was reduced to 0.6 W/m-K at 900 K by nanostructuring with Bi_2S_3 as the second phase.

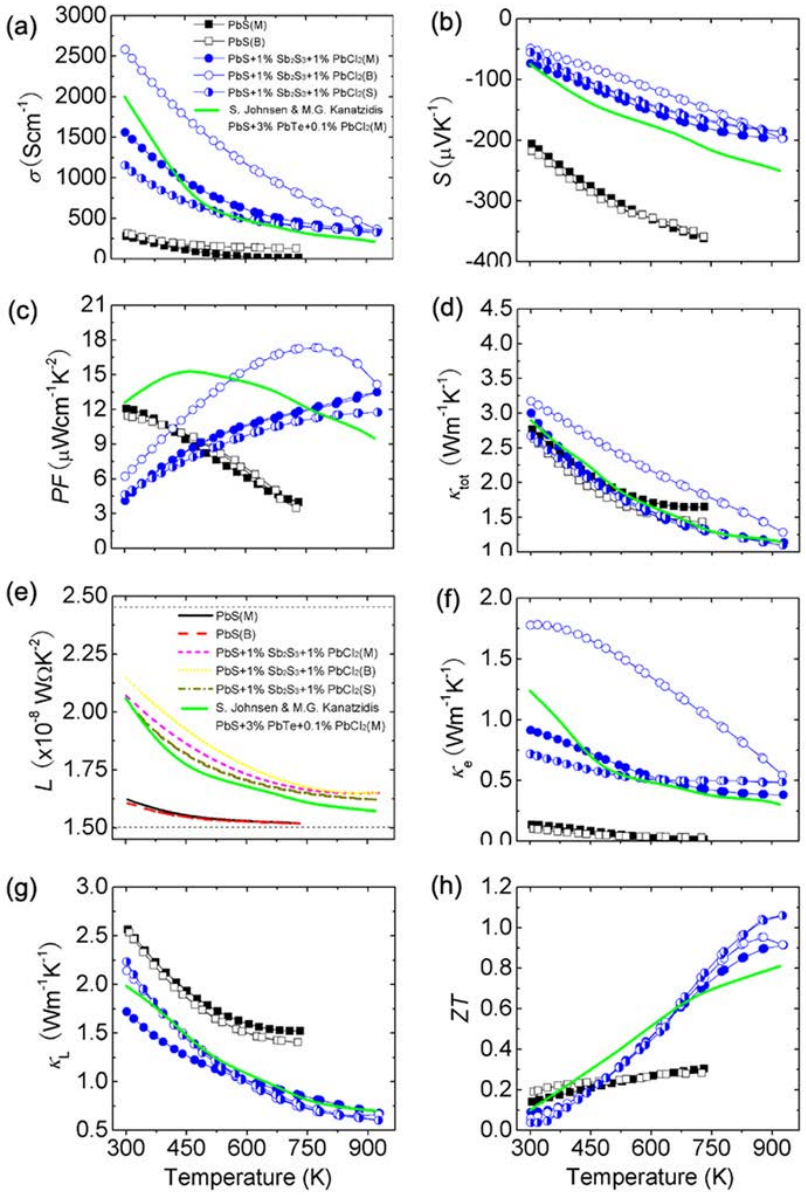

FIGURE 4. Thermoelectric properties as a function of temperature of PbS with 1.0 mol% Sb_2S_3 and 1.0 mol% $PbCl_2$ doping: (a) electrical conductivity; (b) Seebeck coefficient; (c) power factor; (d) total thermal conductivity; (e) Lorenz number; (f) electronic thermal conductivity; (g) lattice thermal conductivity; (h) ZT. "M" presents the sample prepared by the melting reaction, "B" the Bridgman method, "S" the spark plasma sintering powder processing method.

- Samples of n-type PbS with 1.0 mol% Bi_2S_3 and doped with 1.0 mol% $PbCl_2$ processed with the spark plasma sintering technique exhibit record high ZT~1.1 at 900 K.

References

1. Wood, C. *Rep. Prog. Phys.* 51, 459(1988).

FY 2011 Publications/Presentations

1. "High performance thermoelectrics from earth-abundant materials: Enhanced figure of merit in PbS by second phase nanostructures" Li-Dong Zhao, Shih-Han Lo, Jiaqing He, Hao Li, Kanishka Biswas, John Androulakis, Chun-I Wu, Tim Hogan, Duck-Young Chung, Vinayak P. Dravid, and Mercouri G. Kanatzidis, *J. Am. Chem. Soc.* 2011, accepted.

III.15 Improving Energy Efficiency by Developing Components for Distributed Cooling and Heating Based on Thermal Comfort Modeling

Edward Gundlach (Primary Contact), Jeffrey Bozeman (General Motors Global Vehicle Engineering), Kuo-Huey Chen, Shailendra Kaushik, Taeyoung Han, Bahram Khalighi, Gregory Meisner, James Salvador

General Motors Global Research & Development (GM)
MC 480-106-244
30500 Mound Road
Warren, MI 48090

DOE Technology Development Manager:
John W. Fairbanks

NETL Project Manager: Carl Maronde

California Energy Commission Project Manager:
Reynaldo Gonzales

Subcontractors:
- Delphi Thermal Systems, Lockport, NY
- Marlow Industries, Dallas, TX
- Oak Ridge National Laboratory (ORNL), Oak Ridge, TN
- University of California, Berkeley (UCB), Berkeley, CA
- University of Nevada, Las Vegas (UNLV), Las Vegas, NV

Overall Objectives

- Identify distributed cooling and heating strategies that can efficiently augment or replace a vehicle's central heating, ventilation and air conditioning (HVAC) system by delivering localized cooling/heating of key human body segments that strongly influence an occupant's perceived thermal comfort.
- Evaluate the effectiveness of distributed cooling and heating strategies for providing thermal comfort to vehicle occupants, and update the UCB Thermal Comfort model to accurately predict their effect on passenger thermal sensation and thermal comfort.
- Prioritize the development of individual local cooling/heating HVAC components and optimal combinations of these strategies based on their energy-efficient impact to human comfort and on practical considerations about their implementation within a vehicle.
- Develop prototype local cooling/heating components that utilize thermoelectric (TE) technology to implement these distributed cooling and heating strategies and demonstrate energy savings from an integrated HVAC system installed in a five-passenger vehicle.
- Develop computer-aided engineering (CAE) tools that support the inclusion of local cooling/heating HVAC components in future energy-efficient vehicle designs.
- Explore further applications of TE technology with the potential to improve the energy efficiency of electric vehicles such as the Chevrolet Volt, thereby increasing their effective electric-only range.
- Investigate new TE material systems for improved waste heat recovery performance.

Fiscal Year (FY) 2011 Objectives

- Update the UCB Thermal Comfort model based on thermal mannequin and human subject feedback from the testing of localized cooling and heating in a mule vehicle.
- Identify the final set of locations for distributed cooling and heating that will be further developed into prototype local cooling/heating HVAC components.
- Release a personal computer (PC)-based version of the updated model in a CAE tool that supports the rapid evaluation of potential distributed HVAC systems in various vehicle platforms.
- Develop a design concept for an energy-efficient TE device to replace the passenger compartment resistive heater of the Chevrolet Volt extended-range electric vehicle.

Accomplishments

- Updated the UCB Thermal Comfort model for the localized cooling and heating of vehicle occupants and correlated the model's predictions with the test responses of a thermal mannequin and human subjects.
- Compiled climatic wind tunnel test results and modeling analyses to identify the final set of distributed cooling and heating locations for further development into prototype local cooling/heating components.
- Released and validated a PC-based CAE tool that uses the updated thermal comfort model and computational fluid dynamics (CFD) models of vehicle interiors to forecast the performance of future HVAC system configurations that feature energy-saving local cooling/heating components.

- Completed an initial design concept for a TE device with the potential to heat the passenger compartment of the Chevrolet Volt using less electricity, which would increase the Volt's effective electric-only range during cold weather conditions.

Future Directions

- Complete the development and evaluation of initial prototype local HVAC components that feature thermoelectric technology to deliver energy savings.
- Develop final prototype local HVAC components and evaluate the energy savings of the integrated HVAC system in the demonstration vehicle.
- Continue to develop and enhance CAE tools that support the inclusion of local cooling/heating HVAC components in future energy-efficient vehicle designs.
- Evaluate and improve the initial design concept for an energy-efficient TE device to replace the passenger compartment resistive heater of the Chevrolet Volt extended-range electric vehicle.
- Continue to investigate new and improved TE material systems for improved automotive waste heat recovery performance.

Introduction

The primary goal of the project is to achieve a 30% reduction in the fuel used to provide passenger thermal comfort. This will be accomplished by reducing the energy used by the central HVAC system and supplementing it with energy-efficient distributed cooling and heating components that feature TE technology. These prototype components will deliver localized cooling/heating to key human body segments that strongly influence an occupant's perceived thermal comfort. The project team will update the existing UCB Thermal Comfort model to comprehend the effect of locally cooling and heating specific body segments. The updated Thermal Comfort model will be incorporated into CAE tools that will support the inclusion of local cooling/heating HVAC components into future energy-efficient vehicle designs. The project will also explore other methods of using TE technology to improve the energy efficiency of electric vehicles, including the development of a TE device concept to replace the resistive heater in the Chevrolet Volt. Another secondary project goal is to improve the efficiency of TE-based generators that directly convert engine waste heat into electricity by developing new and improved TE material systems.

Approach

The main goal of this project is to develop distributed cooling and heating strategies and components that efficiently supplement the central HVAC system and then to integrate and test the distributed HVAC system in a demonstration vehicle. The project team used experimental test data and CFD analyses to assess the human response to the localized cooling/heating of various body segments. The team updated the UCB Thermal Comfort model by using regression analyses of the overall whole body sensation, the local body sensations, and the comfort votes from the human subject tests to arrive at the overall sensation and comfort models (see Figure 1). The project's 18-month first phase culminated in the identification of optimal locations for distributed cooling/heating. During the remainder of the project, the team will develop and execute strategies for implementing the most effective locations as prototype local cooling/heating components that form an integrated HVAC system on two demonstration vehicles. The first prototype HVAC system application is a Buick LaCrosse with eAssist ("light electrification") fuel-saving technology. The second prototype HVAC system application is a Chevrolet Volt, and this development activity will include a TE device concept for efficiently heating the passenger compartment during cold weather operation. The team will also develop CAE tools that support the configuration of HVAC systems with local cooling/heating components for future energy-efficient vehicle designs.

The secondary project objective focused on waste heat recovery. The basic physics and chemistry of new and breakthrough TE materials are being studied at GM. This fundamental research of new materials is assisted by theoretical work performed at UNLV and by characterization analyses performed at ORNL. In addition, GM is working with Marlow to develop and improve the processes needed to implement advanced TE materials into functional modules that are needed for constructing TE-based generators.

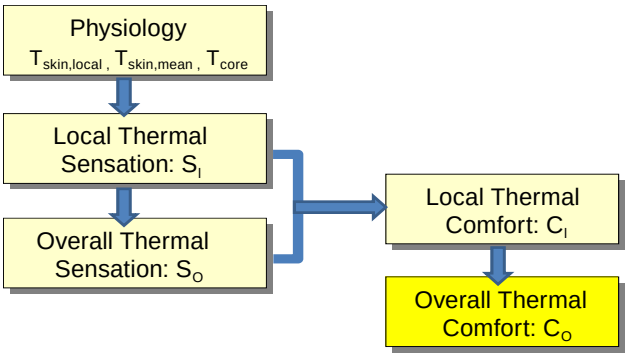

FIGURE 1. Flow Chart showing how the UCB Thermal Comfort Model is Developed

Results

During this second year of the project, the project team made significant progress towards successfully achieving the overall project objectives. Based on knowledge about how the temperature sensations of various body parts influence a person's perception of thermal comfort, the team identified several distributed cooling and heating strategies with high potential for supplementing the vehicle's central HVAC system in an energy-saving manner. CFD analysis was used to comprehend and optimize the airflow around the vehicle passengers for various combinations of local cooling/heating components. Figure 2 shows the airflow traces from the four main HVAC outlet registers in the baseline case where all local cooling/heating components were disabled. The project team extensively used CFD analyses to model the potential efficacy of different levels of airflow from various HVAC nozzle locations targeting specific body parts.

The team created simulated implementations of these strategies in a mule vehicle for testing by a thermal mannequin and human subjects in the Delphi climatic wind tunnel (see Figure 3). The team developed a tunnel test protocol and executed the associated procedures for warm weather testing of local cooling components in the fall of 2010 and for cold weather testing of local heating components in the spring of 2011. The wind tunnel testing provided critical data for the evaluation of distributed cooling/heating locations. The hot and cold weather test data was analyzed and integrated in order to update the UCB Comfort Model for the accurate prediction of the expected human sensation and comfort from the localized cooling and heating of body segments. The updated model was refined and validated by correlating the model's predictions with the test responses of the thermal mannequin and

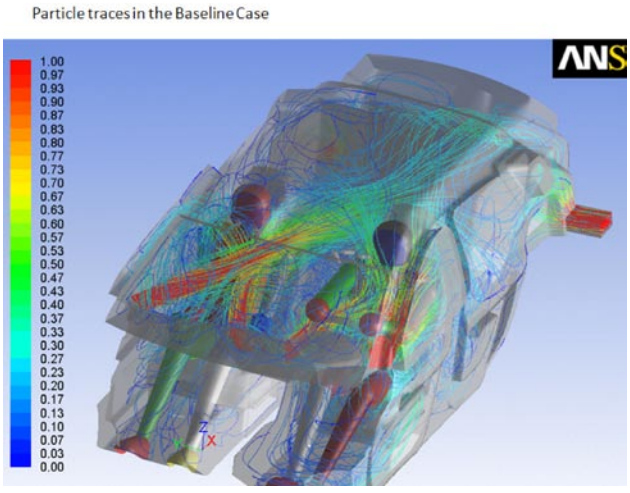

FIGURE 2. Particle Trace for the Baseline Case where the Color Indicates the Flow Velocity in m/s

FIGURE 3. Mule Vehicle with Simulation and Monitoring Equipment in the Climatic Wind Tunnel

human subjects. Based on these analyses and guided by practical considerations for implementing these strategies within a vehicle, the team identified the final set of locations for further development of local cooling/heating HVAC components.

A PC-based CAE tool was also developed to support rapid evaluations of HVAC system configurations for future vehicles. To perform its analysis, this tool combines the updated Thermal Comfort model with a surface mesh model of the vehicle interior and a CFD airflow database that represents the various HVAC system operating modes. The first three vehicles implemented in the PC-based CAE tool are shown in Figure 4. The tool is being validated for both thermal sensation and comfort by comparing its predictions to the tunnel test data. As shown by the baseline assessment of thermal comfort in Figure 5, the initial validation shows good correlation considering the asymmetric thermal environment; the tool will undergo further refinement.

The project team is developing a TE device for the Chevrolet Volt to provide improved heating efficiency beyond the current electrical resistive method. To accomplish this objective, Marlow proposed an enhanced plate and frame heat exchanger concept that is designed specifically for use in conjunction with TE technology (see Figure 6). The goal of the design concept was to achieve a thermal system that integrated multiple TE modules and exchanger plates into a compact package while improving heat transfer across the active surfaces. The final thermal system is expected to operate within GM's specifications for electrical input power, performance, volumetric flow rates, pressure drops, available pump power, and other various

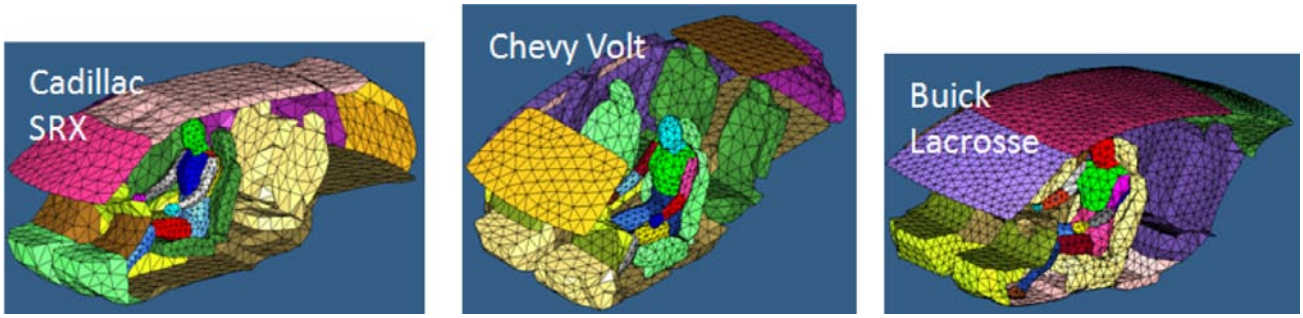

FIGURE 4. Three Vehicles Implemented into the PC-Based CAE Tool

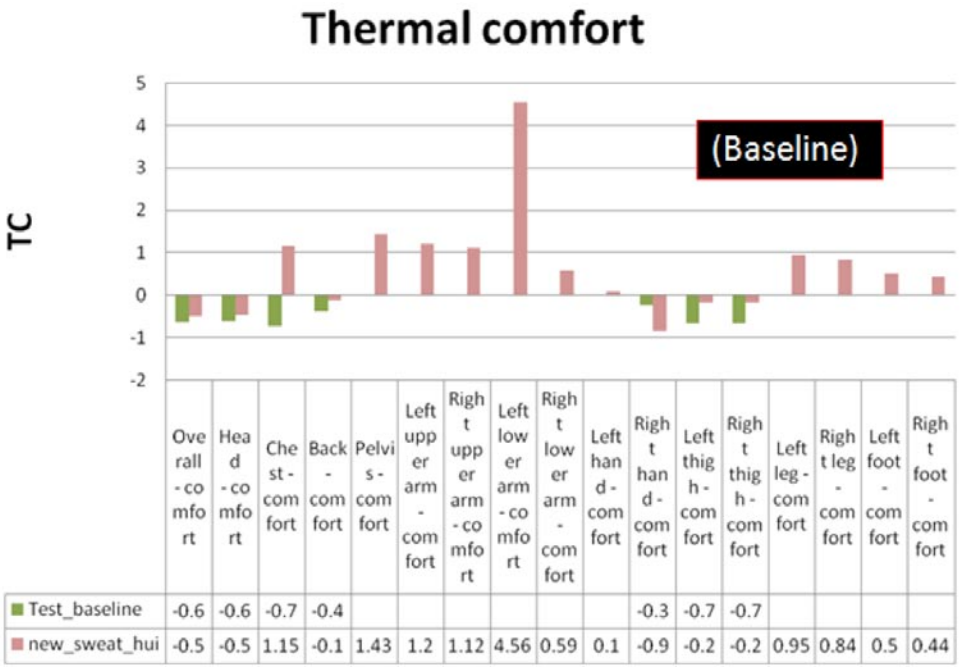

	Overall - comfort	Head - comfort	Chest - comfort	Back - comfort	Pelvis - comfort	Left upper arm - comfort	Right upper arm - comfort	Left lower arm - comfort	Right lower arm - comfort	Left hand - comfort	Right hand - comfort	Left thigh - comfort	Right thigh - comfort	Left leg - comfort	Right leg - comfort	Left foot - comfort	Right foot - comfort
Test_baseline	-0.6	-0.6	-0.7	-0.4							-0.3	-0.7	-0.7				
new_sweat_hui	-0.5	-0.5	1.15	-0.1	1.43	1.2	1.12	4.56	0.59	0.1	-0.9	-0.2	-0.2	0.95	0.84	0.5	0.44

FIGURE 5. Comparison of Thermal Comfort between the CAE Tool Prediction and the Actual Tunnel Test Data for the Baseline Case

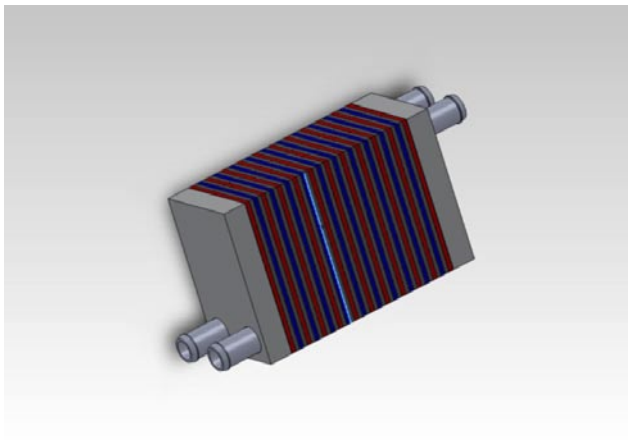

FIGURE 6. TE Design Concept for Chevrolet Volt Heater - Plate and Frame Exchanger System

attributes. Testing and evaluation of the initial prototype has resulted in a refined concept for a second prototype.

The project continues to explore new TE materials and to optimize existing materials at General Motors. This work includes collaboration with UNLV on fundamental theoretical research involving new computational approaches for determining lattice thermal conductivity, phonon densities of states, nano-cluster doping, and electronic band structure of doped Skutterudites. Our aim is to investigate and understand the very low thermal conductivities and the power factor enhancements seen experimentally for some TE materials.

Conclusions

- When the general cabin temperature is outside a range that is normally considered comfortable, our

test data shows that the application of localized cooling/heating to key body segments can create the perception of thermal comfort for vehicle occupants.

- Our preliminary analysis indicates that the project's energy-saving target can be achieved while maintaining the baseline level of thermal comfort by reducing the output of the central HVAC system and supplementing it with local cooling/heating components.
- The revised UCB Thermal Comfort model with updates for localized cooling and heating demonstrates good correlation with data gathered from a thermal mannequin and human subjects during mule vehicle testing.

FY 2011 Publications/Presentations

1. Shailendra Kaushik, Kuo-Huey Chen, Taeyoung Han, and Bahram Khalighi, "Micro-Cooling/Heating Strategy for Energy Efficient HVAC System", SAE paper #2011-01-0644, 2011.

2. Shailendra Kaushik, Kuo-Huey Chen, Taeyoung Han, and Bahram Khalighi, "Micro-Cooling/Heating Strategy for Energy Efficient HVAC System", SAE-2011-01-0644, presented at 2011 SAE World Congress, Detroit, MI, April 12, 2011.

3. Jeffrey Bozeman, Kuo-Huey Chen, and Shailendra Kaushik, "Distributed Climate System Impact on Human Comfort and MAC Efficiency", 11AAR-0029, presented at SAE Alternative Refrigerant and System Efficiency Symposium, Scottsdale, AZ, Sep. 29, 2011.

4. GM R&D internal report #VDR-282, Shailendra Kaushik, Kuo-Huey Chen, Taeyoung Han, and Bahram Khalighi, "Micro-Cooling/Heating Strategy for Energy Efficient HVAC System", May 17, 2011.

5. GM R&D internal report #VDR-289, Shailendra Kaushik, Taeyoung Han, and Kuo-Huey Chen, "Development of A Virtual Thermal Manikin to Predict Thermal Comfort in Automobiles", Sep. 20, 2011.

IV. UNIVERSITY RESEARCH

IV.1 University Consortium on Efficient and Clean High-Pressure Lean-Burn (HPLB) Engines

Margaret Wooldridge
University of Michigan (UM)
Mechanical Engineering
2156 GGB
Ann Arbor, MI 48109-2125

DOE Technology Development Manager:
Gurpreet Singh

NETL Project Manager: Ralph Nine

Subcontractors:
- Massachusetts Institute of Technology (MIT), Cambridge, MA
- University of California, Berkeley (UCB), Berkeley, CA

Overall Objectives

- Explore new HPLB combustion strategies that can enable future gasoline engines with 20-40% improved fuel economy.
- Determine the fuel economy benefits of engines and engine cycles designed to utilize advanced combustion modes.

Fiscal Year (FY) 2011 Objectives

- Refine analysis of optimum combustion strategy in connection with turbochargers. Determine the fuel economy benefits of engines and engine cycles designed to utilize advanced combustion modes.
- Determine effects of dilution and equivalence ratio in a rapid compression machine (RCM). Apply to stratification studies.
- Explore variations in partition of flame vs. autoignition heat release in spark-assisted compression ignition (SACI) in a fully flexible valve actuation (FFVA) engine.
- Determine effects of fuel properties such as octane number on homogeneous charge compression ignition (HCCI) combustion. Explore ethanol/gasoline fuel blends.

Accomplishments

- The thermodynamic cycle analysis for engines was extended to include effects of turbochargers. The results were coupled to a vehicle drive cycle framework to provide vehicle fuel economy estimates for the various combustion modes.
- Autoignition times for gasoline-air mixtures were determined in an RCM for varying equivalence ratio and nitrogen dilution (exhaust gas recirculation [EGR] surrogate). The results help to interpret data from a diesel engine fueled with gasoline in a stratified charge mode.
- The computational singular perturbation analysis to identify ignition regimes for stratified mixtures has been extended to investigate autoignition of n-heptane/air mixtures in the presence of temperature and composition inhomogeneities. The automated computational diagnostic tool allows in situ identification of important dynamic processes associated with chemistry and transport for a mixture exhibiting two-stage ignition behavior.
- In studies of mixing using the Reynolds averaged Navier Stokes approach it was found that the transport equation for the mixture fraction variable must incorporate the differential diffusion terms that have been commonly neglected for the sake of simplicity. In a separate study, for large eddy simulation applications, the effects of the subgrid filter size have been investigated. It was revealed that turbulence is completely uncorrelated with scalar mixing. Based on this observation, a new model for cross scalar dissipation rate was proposed and excellent correlations were found.
- The interaction of flame generated vs. autoignition heat release was investigated in SACI experiments. The two combustion modes behaved in a manner consistent with estimated flame speed and autoignition properties in the high preheat high dilution regime. The flame appears to influence autoignition primarily through increased heat release and unburned temperature.
- The laminar flame speed correlation previously developed for air dilution under high preheat-high dilution conditions has been extended to EGR dilution. After compensating for temperature differences, lower observed flame speeds for EGR dilution appear to be due to lower O_2 concentrations.
- New image analysis tools have been developed for rapid and automated processing of optical engine imaging data into quantitative metrics on ignition and flame propagation in HCCI and spark-assisted HCCI systems. The tools have been applied to recent studies of indolene spark-assisted HCCI.
- Experimental testing of a microwave-assisted spark plug at UCB has demonstrated stability improvements in HCCI combustion in a Cooperative Fuels Research engine under lean

conditions with potential application to SACI. Tests in a combustion bomb show that the benefit of a microwave-assisted spark plug is greatest at low pressures and diminishes as pressure is increased.

- Rapid Compression Facility (RCF) speciation studies of intermediates formed during ignition of methyl-3-hexenoate/air mixtures have provided quantitative insight into the important reaction pathways. We are working with Dr. Charles Westbrook of Lawrence Livermore National Laboratory to finalize a reaction mechanism which can accurately represent the combustion chemistry of this compound important to biodiesel fuels.
- Fuels with lower octane numbers were tested in the FFVA engine. Results showed an increase in maximum load with lower octane, possibly due to the tendency of lower octane fuels to demonstrate negative temperature coefficient (NTC) behavior, but may also be related to lower levels of internal EGR required for ignition, and the subsequent reduction in thermal stratification.

Future Directions

- Expand thermodynamic and system analyses of mixed combustion modes in a representative turbocharged engine system to include realistic combustion constraints, different compression ratios, and if time, hybridization. Assess the potential benefit of lean/dilute burn, high pressure engine operation under optimal engine-vehicle drivetrain scenarios.
- Apply RCM work on fuel ignition properties to engine experiments with different injection strategies. Combine RCM results and engine findings to understand and identify potential benefits of advanced combustion modes.
- Bring together experimental work on SACI with recently completed models to provide new insight. Perform additional experiments as necessary.
- Continue SACI imaging studies in RCF over wider range of pressures and mixture ratios.
- Assess the validity of the flamelet-based combustion sub-models in mixed-mode combustion under HPLB conditions. Conduct parametric studies to identify sensitivities of key control variables.
- Reconfigure optical engine for direct injection studies. Investigate effects of varying turbulent intensities, transient phenomena, and expanded operating range.
- Complete analysis of the optical engine SA HCCI data of ethanol/indolene blends including engine performance and imaging results.
- Explore opportunities for improved engine efficiency through chemistry and properties of novel fuels. Carry out engine experiments with fuels characterized in RCM and RCF studies.

Introduction

Low-temperature combustion is a desirable thermodynamic regime that can provide improved fuel efficiency in gasoline engines with low emissions, because the properties of the working fluid are best at lower temperature and because oxides of nitrogen (NOx) emissions are reduced. Unfortunately, practical and reliable combustion under these dilute conditions has traditionally been unattainable due to ignition limits. HCCI is one method to achieve good combustion in this regime and has been the subject of much recent research. Because of the limited loads possible with HCCI, advanced combustion modes such as SACI, stratified or dual fuel mixtures are being considered as a way to increase achievable engine loads. At the same time turbocharging is another means of improving fuel economy, by capturing some wasted exhaust energy, but more importantly and in combination with engine downsizing, by permitting an increase of engine load without excessive temperatures while also reducing the relative importance of friction.

As seen in the results section, thermodynamic analysis indicates that advanced combustion modes at high pressures can provide vehicle fuel economy gains of up to 55%, exceeding the DOE Vehicle Technologies Program target of 20-40% improvement. Accordingly, the goal of the consortium is to explore how this improvement can be achieved; in particular to look at means of enabling the required advanced combustion under the highly dilute, boosted high-pressure conditions necessary for optimal engine-vehicle fuel economy.

Approach

Our research project, now at the end of its second year, combines experiments and modeling at three university research centers in order to acquire the knowledge and technology to explore the HPLB advanced combustion regime, which is key to achieving optimal fuel economy. To accomplish this, both single-cylinder and multi-cylinder engine experiments are being used to investigate direct fuel injection strategies, fuel and thermal stratification, turbo/supercharging, advanced ignition and combustion modes as well as the ignition characteristics of alternate fuels and blends with gasoline.

At the same time an array of modeling tools are being developed and refined, and brought to bear on the specific limit problems of importance. These models cover a range of detail from system models for engines

and vehicles, through fully coupled computational fluid dynamics (CFD)/kinetic models, to detailed chemical mechanisms. Our intent is to take advantage of the broad range of capabilities of the university partners and the collaborative relationships among them.

The overall technical approach is focused on light-duty automotive engine application using primarily gasoline and gasoline blends with alcohols as the fuel. The research agenda addresses the following areas:

- Thermodynamics of engines and engine cycles operating in advanced combustion modes.
- Fuel and thermal stratification and its interaction with fuel properties and heat transfer.
- Advanced multi-mode ignition and combustion.
- Novel fuel opportunities for improved efficiency.

Results

Thermodynamic Conditions for Optimum Engine Efficiency

GT-POWER was used to perform a parametric study exploring the thermodynamic conditions necessary for best engine efficiency. The idea was to identify these conditions taking into account heat transfer, friction and pumping losses, dilution (air or EGR), and boosting. In this way the best brake efficiency could be linked to the desired in-cylinder conditions. A constant fixed burn rate was assumed, leaving to a future study the question of whether viable combustion can be achieved at these conditions. On an indicated basis, leaner or more dilute conditions were always best. However when friction losses were taken into account an optimum condition was observed as a result of the fact that friction losses make up a smaller proportion of the power when the engine is operating at higher brake mean effective pressure. Results for air and EGR dilution were similar when compared using a "total dilution" equivalence ratio defined as $\varphi' = \varphi\ (1 - EGR)$. An ideal turbocharger was assumed with fixed overall efficiency.

Results are shown in Figure 1 for the case of 50% turbocharger efficiency, compression ratio of 12, and at 2,000 rpm. The dashed lines in the figure show brake efficiency plotted against brake load for different intake pressures ranging from 1 to 3 bar. The right end of each curve corresponds to stoichiometric mixture with progressively more dilute conditions toward the left. The best fuel efficiency conditions are traced by the upper envelope of all the pressure lines. This engine strategy is labeled "ADV-TC" for advanced combustion with turbocharging. Across the top of this curve are the three combustion regimes along the curve: HCCI ($\varphi' \leq 0.45$), advanced ($0.45 \leq \varphi' \leq 0.65$), and spark ignited (SI) ($0.65 \leq \varphi'$). Other engine operating strategies have lower engine efficiencies as indicated by the curves labeled "SI-thottled (φ=1)" corresponding to most current SI engines, "SI-TC (φ=1)" for SI turbocharged, and "ADV-NA" for advanced combustion, naturally aspirated. The figure clearly shows that the best efficiency can be obtained by a combination of HCCI and advanced combustion modes in a turbocharged engine. Combustion under these conditions is the subject of much of the work of the consortium.

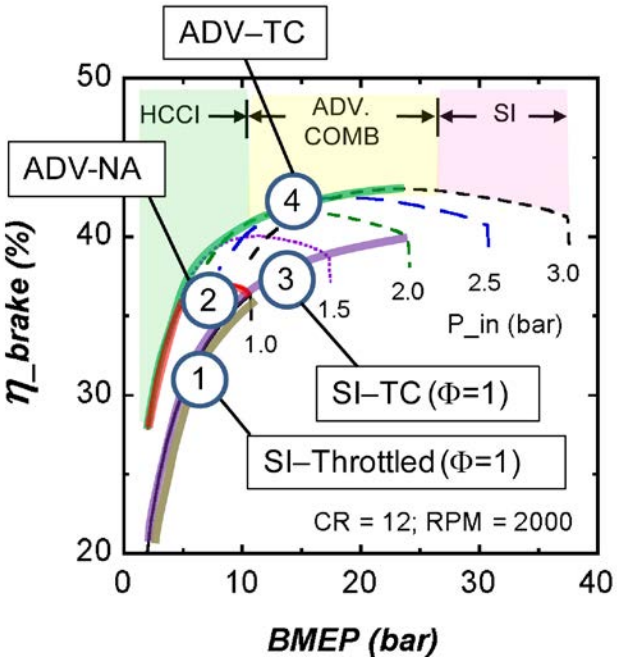

FIGURE 1. Brake Efficiency Projections for Various Combustion and Boosting Strategies

Fuel Economy Assessment Tool

A model-based framework has been developed for evaluating fuel economy improvements of new engine technologies and control strategies. The framework couples GT-POWER-generated engine maps to a MATLAB®/Simulink® representation of a vehicle/transmission to provide vehicle fuel economy estimates. In this case the four strategies of Figure 1 were considered: strategies 1 and 2, were set up in a naturally aspirated 3.3-L engine, while the two boosted strategies (3 and 4) were modeled in a downsized 2.2-L engine. The same vehicle of 1,500 kg, and transmission were used for all strategies.

Projected relative fuel economy (FE) results for combined city/highway are shown in Figure 2. Advanced combustion in a naturally aspirated engine, or turbocharging/downsizing with conventional spark ignition are both projected to provide 20-25% gain. Turbocharging/downsizing together with advanced combustion has the potential to provide ~55% improvement.

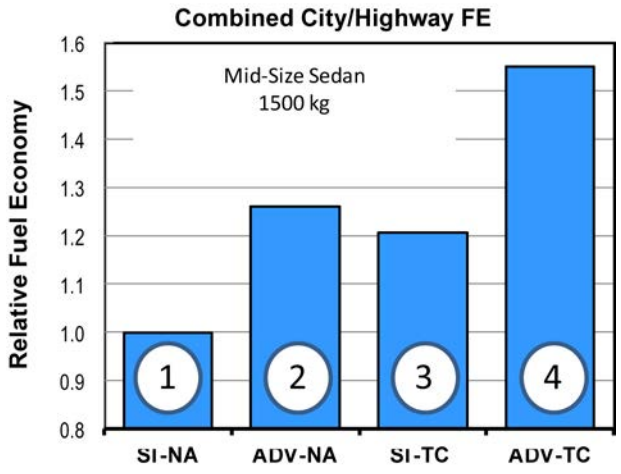

FIGURE 2. Relative fuel economy projections of four combustion engine strategies: 1) conventional SI – naturally aspirated; 2) advanced combustion - naturally aspirated; 3) SI turbocharged/downsized; 4) advanced combustion turbocharged/downsized.

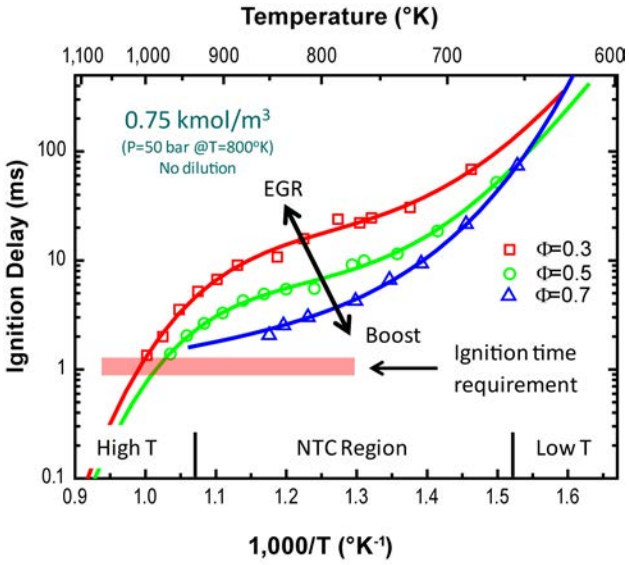

FIGURE 3. RCM Ignition Delay Measurements Showing Φ Dependence and Effects of EGR and Boost on Φ and T Sensitivity

Charge Stratification Studies

The objectives of this task are first to experimentally study stratification strategies for HPLB engines and the interaction between fuel properties, heat transfer and stratification, and second to develop advanced simulation tools to predictively describe the combustion characteristics in the presence of temperature and composition inhomogeneities arising from stratified charge, exhaust/residual gas recirculation, and wall heat loss.

The RCM was used to assess the sensitivity of the ignition delay to fuel equivalence ratio and to dilution. The data shown in Figure 3 indicate that the effectiveness of stratification as a means of controlling the heat release rate depends on the ignition regime. If ignition occurs in the high temperature or in the low temperature regimes, the ignition delay is not sensitive to the equivalence ratio and thus fuel stratification does not play a strong role in the heat release schedule, which will primarily be influenced by temperature stratification. However, if ignition occurs in the NTC regime, the delay is sensitive to the equivalence ratio (Φ) and less sensitive to temperature. Hence in this regime, the heat release is affected by Φ stratification. For an engine operating with ignition in the high temperature regime, since boosting moves the ignition delay curves (as a function of temperature) downwards, for the same ignition delay requirement, ignition will tend to shift to the NTC regime. Thus boosting would enable Φ stratification for sequential ignition. The opposite effect would occur with EGR: increasing EGR would shift the operating point to a higher temperature region.

Based on a series of a priori tests to investigate the mixing model in the Reynolds averaged Navier Stokes context it was found that the transport equation for the mixture fraction variable must incorporate the differential diffusion terms that have been commonly neglected for the sake of simplicity. Therefore, the general conservation equation for the mixture fraction variable has been derived and various strategies have been developed to close the additional source terms arising from the differential diffusion effects. Further validation and demonstration of the improvement in the model prediction is underway.

For large eddy simulation applications, the effects of the subgrid filter size have been investigated. It was revealed that turbulence is completely uncorrelated with scalar mixing, such that the mean scalar dissipation rate can be easily modeled as a direct function of the scalar variance, with the same proportionality constant for both the mixture fraction and the total enthalpy variables. Based on this observation, a new model for cross scalar dissipation rate was proposed and excellent correlations were found.

Experiments in Multi-Regime Ignition Strategies

As previously reported, SACI in the UM FFVA engine was employed to extend the high load limit of HCCI to near 7.5 bar net mean effective pressure. A more detailed study has now been carried out to better understand the factors affecting the relative proportions of flame and autoignition generated heat release. Figure 4 shows an example of the data obtained. In this experiment temperature was modified by changing the internal EGR through negative valve overlap changes; external EGR was adjusted to keep the overall composition constant. The effect of lowering

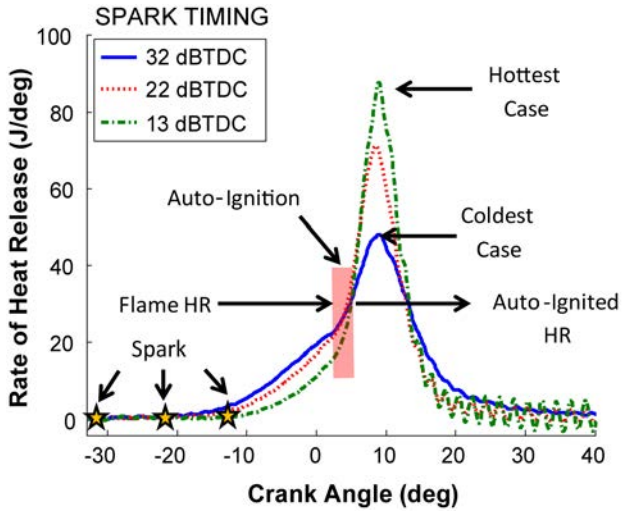

dBTDC - degrees before top-dead center

FIGURE 4. Heat release curves from the UM FFVA engine. Spark assist compensates for lower intake temperature while reducing peak heat release rate.

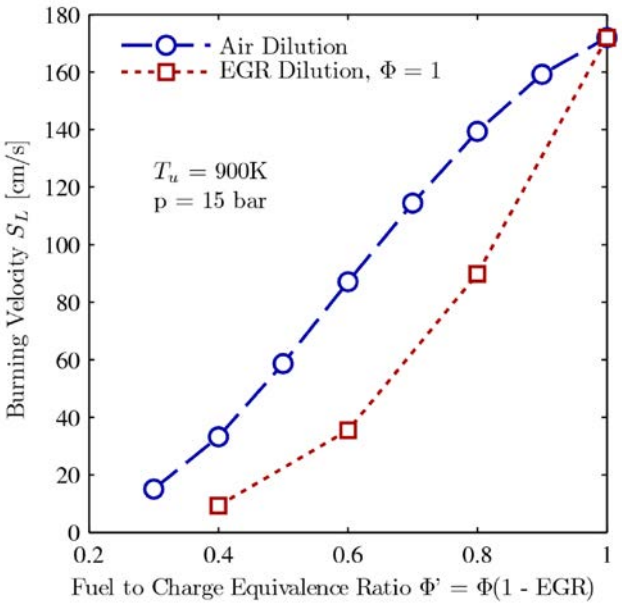

FIGURE 5. New Correlations of EGR Diluted Flames at High Preheat and High Dilution

temperature was to retard combustion phasing. By advancing the spark, the phasing could be brought back to the original position. The result was to increase the fraction of mass consumed by flame before autoignition from 14% to 32%; at the same time the peak heat release decreased from 90 to 50 J/deg. Estimates of temperatures at the time of spark were used to calculate laminar flame speeds during early flame development; these correlated inversely with the time required to burn 10% of the charge consistent with the flame generated heat release. Also the estimated unburned temperature at the time of autoignition was approximately constant at 1,100 ±10 K. This suggests that the flame is responsible for maintaining the unburned gas temperature at the value required for proper autoignition.

Laminar Flame Speed Correlation for EGR Dilution

In order to develop the CFD model of SACI completed and reported on last year, laminar flame speed data was required under high preheat and high dilution conditions. A large number of simulations were carried out with the transient Hydrodynamics, Chemistry, Thermodynamics (HCT) code for diluted flames, and the results for air dilution were correlated for use in the computational fluid dynamics model. That work has now been extended to include EGR dilution. Based on additional flame simulations with HCT, the original correlation has been updated to include explicit terms for oxygen concentration which captures the effect of EGR.

Figure 5 shows HCT results (symbols) and the correlation (lines) comparing air and EGR dilution. Laminar flame speeds at high preheat conditions of 900 K are plotted vs. fuel to charge equivalence ratio $\varphi' = \varphi\ (1 - \mathrm{EGR})$. The figure is qualitatively similar to literature data at lower temperatures and dilution. The figure shows that for equal φ' (with almost equal adiabatic flame temperatures) the EGR diluted flames are significantly slower than those diluted with air. Analysis of the results suggests that this is due to the scarcity of oxygen in the EGR diluted cases. The implication is that SACI with EGR dilution is likely to be effective over a smaller operating range than with air dilution.

Microwave-Assisted Spark Plug

Microwave spark ignition tests with wet-ethanol fuel in the Cooperative Fuels Research engine show that the microwave-assisted spark plug extends the "flame limit" for spark-ignited engines. The microwave spark plug allows stable operation with a minimum top-dead-center burned gas temperature that is approximately 100 K lower than is possible with spark-only ignition. The microwave enhancement of flame limit occurred over calculated top-dead-center unburned gas temperatures ranging from 620 K to 890 K.

Fundamental explorations of microwave-assisted spark plug performance have been conducted in a constant volume combustion chamber. Experiments with methane and air mixtures at various initial pressures and dilution levels have identified important characteristics of microwave flame enhancement: at one atmosphere initial pressure microwaves strongly enhance flame development as compared to spark-only ignition,

but microwave effects diminish as pressure increases. Flame development enhancement by microwaves is strongest in slow-developing, highly diluted flames.

RCF Studies of Flammability Limits

We continue our studies of lean flammability limits and flame propagation using the UM rapid compression facility. This study focuses on supplementing the limited experimental data on flame propagation into premixed gases at high-pressure and moderate temperature conditions. For this work the RCF has been equipped with a spark electrode. Flames are initiated after pre-prepared mixtures of iso-octane and air have been compression heated to approximately 925-950 K and approximately 10 atm. The competing effects of flame propagation and autoignition are recorded via high speed imaging and pressure measurements. Fast image processing algorithms were coupled with pressure measurements to determine key quantitative metrics of reaction fronts initiated by the spark discharge, and propagated into premixed iso-octane and air. Initial reaction front results for P ~ 8 atm and T ~ 950 K indicate that the lean flammability limit is $\varphi = 0.4$. Flame speeds/reaction front propagation rates were measured in the range of 1.3-1.6 m/s. The presence of reaction fronts reduced the ignition delay time compared to conditions when no reaction fronts are initiated.

Fuel Chemistry for Improved Engine Efficiencies

As noted earlier, extending HCCI to higher loads offers potentially higher engine efficiency. To determine if fuel ignition characteristics can influence the maximum load, experiments were carried out in the UM FFVA engine with three fuels with different octane numbers: iso-octane (Research Octane Number, RON=100), RD387 gasoline (RON=90.5), and a 40/60 blend of RD387 and n-heptane, designated NH40 (RON=~53). For each fuel, operating maps were constructed by varying fueling rate and combustion phasing. In this way the limits were determined for early phasing (knock) and late phasing (net mean effective pressure coefficient of variance >3%) for each fueling rate. The maximum load was established where the knock and stability limits converged. The maps for the three fuels shown in Figure 6 indicate that the low octane fuel provides the highest load at the latest phasing. Analysis of the heat release curves shows that the low octane fuel also has the shortest combustion duration. A possible explanation is that the increased NTC behavior of the low octane fuel reduces the temperature sensitivity and as a result, reduces the effect of natural thermal stratification in the chamber, but may also be related to lower levels of internal EGR required for ignition, and the subsequent reduction in thermal stratification.

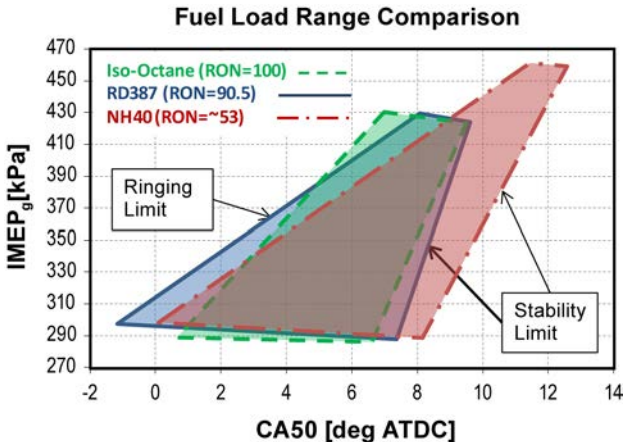

ATDC - after top-dead center

FIGURE 6. Effect of Octane Number on HCCI Gasoline Maximum Load and Combustion Phasing

The single-cylinder optical engine studies of ethanol/indolene blends have been completed. The data confirm that ethanol can be used to extend the lean HCCI limit when you compensate for evaporative cooling effects. The data also demonstrate that ethanol does not adversely impact engine exhaust emissions (e.g. NOx, CO, etc.).

RCF speciation studies of intermediates formed during ignition of methyl-3-hexenoate/air mixtures have provided quantitative insight into the reaction pathways important during ester combustion. We are working with Dr. Charles Westbrook of Lawrence Livermore National Laboatory to finalize a reaction mechanism which can accurately represent the combustion chemistry of methyl-3-hexenoate. This work advances our understanding of key unsaturated reference fuel compounds important to biodiesel fuels.

Conclusions

The work of the consortium has made considerable progress towards bringing together the knowledge and tools needed to achieve the fuel economy goals of the Vehicle Technologies Program for gasoline engines.

- The HPLB combustion regime has been identified as the most suitable for achieving optimal engine fuel economy for a typical engine/turbocharger configuration. The regime includes lean mixtures $0.45 < \varphi < 0.65$ for air or equivalent EGR dilution of stoichiometric mixtures, a region inaccessible to normal homogeneous SI engines.
- Engine-vehicle simulations have shown that fuel economy gains up to 55% can be achieved with advanced combustion, boosted/downsized engine strategies.

- The effect of dilution on ignition delay times has been investigated in an RCM under conditions relevant to engines; the results show that dilution significantly slows ignition. In related modeling studies, EGR dilution was shown to reduce laminar flame speeds more than the equivalent amount of dilution with air, under high preheat conditions.
- Engine experiments have demonstrated that SACI is a viable means of accessing the advanced combustion mode between upper limit HCCI and lower limit SI combustion. The observed characteristics of SACI are consistent with two relatively independent processes: flame and auto-ignition, the latter being advanced by the flame generated heat release.
- A low octane fuel (40/60) blend of n-heptane in gasoline was shown to exhibit a higher load limit than pure gasoline, possibly due to increased NTC behavior. In other experiments ethanol was found to extend the lean HCCI limit when compensation is made for evaporative cooling effects.

FY 2011 Publications/Presentations

1. Assanis, D., (2010) "A University Consortium on High Pressure, Lean Combustion for Efficient and Clean IC Engines," presentation at the 16th Directions in Engine-Efficiency and Emissions Research (DEER) Conference, Detroit, Michigan, September 27–30, 2010.

2. Assanis, Dim., Wagnon, S., Wooldridge, M.S., (2011) "An Experimental Study of Flame Propagation into High Temperature High Pressure Premixed Fuel Lean Iso-Octane/Air Mixtures," 7th U.S. National Combustion Meeting, Atlanta, Georgia, March 2011.

3. Bedoya, I.D., Saxena, S., Cadavid, F.J., Dibble, R.W., Wissink, M., Experimental evaluation of strategies to increase the operation range of a biogas HCCI engine for power generation, accepted for International Conference on Applied Energy, in review for Applied Energy Journal.

4. Bedoya, I.D., Saxena, S., Cadavid, F.J., Dibble, R.W., Wissink, M., Experimental study of biogas combustion characteristics and emissions in a HCCI engine for power generation, in preparation for Energy Conversion and Management Journal.

5. Cedrone, K., Cheng, W.K., Chahine, S., Williams, J., and VanDerWege, B. (2011) Fuel Effects on HCCI Operation in a Spark Assisted Direct Injection Gasoline Engine. SAE Paper No. 2011-01-1763.

6. DeFilippo A., Chen J.Y., (2011) " Chemical Kinetic Modeling of Plasma-Assisted Methane Ignition", 7th US National Technical Meeting of the Combustion Institute, March 20–13, 2011, Atlanta, GA.

7. DeFilippo A., Wolk B.M., Dibble R.W., Chen J.Y., Moon, A., Nishiyama, A., and Ikeda, Y., (2011) "A Multi-Parameter Study of the Extension of the Stable Operating Range of a Wet-Ethanol-Fueled Engine Using a Microwave-Assisted Spark Plug," Fall 2011 Meeting of the Western States Section of the Combustion Institute, October 16–18, 2011, Riverside, CA.

8. DeFilippo, A., Saxena, S., Rapp, V.H., Ikeda, Y., Chen, J-Y, Dibble, R.W., (2011) Extending the lean flammability limit of gasoline using a microwave assisted sparkplug, SAE Paper no. 2011-01-0663.

9. Fatouraie, M., Keros, P.E., and Wooldridge, M.S., (2011) "A comparative study of the ignition and combustion properties of ethanol-indolene blends during HCCI operation of a single cylinder engine," 7th U.S. National Combustion Meeting, Atlanta, Georgia, March 2011.

10. Gupta S., Keum S.H., Im H.G., (2011) Modeling of Scalar Dissipation Rates in Flamelet Models for HCCI Engine Simulation, *7th U.S. National Combustion Meeting*, Atlanta, Georgia, March 2011.

11. Gupta, S., Im, H.G., Valorani, M., (2011), "Classification of Ignition Regimes in HCCI Combustion using Computational Singular Perturbation," Proceedings of the Combustion Institute, v. 33, pp. 2991-2999.

12. Gupta, S., Im, H.G., Valorani, M., 2011, "Classification of Ignition Regimes in Thermally Stratified n-Heptane-Air Mixtures Using Computational Singular Perturbation," *Workshop on Verification & Validation in Computational Science*, University of Notre Dame, Notre Dame, Indiana, October 17–19, 2011.

13. Han, D., Ickes, A., Bohac, S.V., Zhen, H., Assanis, D.N., 2011, "Premixed Low-Temperature Combustion of Blends of Diesel and Gasoline in a High Speed Compression Ignition Engine," (Initially presented at 33rd International Symposium on Combustion, PROCI-D-10-00751, 2010) Proceedings of the Combustion Institute, 33: 2, 3039-3046.

14. Karwat, D.M.A., Wagnon, S., Teini, P.D., Wooldridge, M.S., (2011) "N-butanol ignition and speciation studies," 7th U.S. National Combustion Meeting, Atlanta, Georgia, March 2011.

15. Karwat, D.M.A., Wagnon, S., Teini, P.D., Wooldridge, M.S., (2011) "On the chemical kinetics of n-butanol: ignition and speciation studies," *Journal of Physical Chemistry*, v. 115, pp. 1796-1804, 2011. *Journal of Physical Chemistry A*, January 2011.

16. Keum, S.H., Im, H.G., and Assanis, D.N., (2011) "A Spray-Interactive Flamelet Model for Direct Injection Engine Combustion," *Combustion Science and Technology*, accepted.

17. Keum, S., Park, H., Babajimopoulos, A., Assanis, D.N. and Jung, D. (2011) Modeling of Heat Transfer in Internal Combustion Engines with Variable Density Effect. *International Journal of Engine Research*, vol. 12, no. 6, pp. 513-526.

18. Lavoie, G.A., Assanis, D., and Ortiz-Soto, E. (2011) Thermodynamic Sweet Spot under Highly Dilute and Boosted Gasoline Engine Conditions, Presented at the SAE 2011 High Efficiency IC engines Symposium, Detroit, Michigan, April 10–11, 2011.

19. Manofsky, L., Vavra, J., Assanis, D. and Babajimopoulos, A. (2011) Bridging the gap between HCCI and SI: Spark-assisted compression ignition. SAE Paper 2011-01-1179.

20. Martz, J.B., Kwak, H., Im, H.G., Lavoie, G.A., Assanis, D.N., (2011), Combustion Regime of a Reacting Front Propagating into an Auto-Igniting Mixture, Proceedings of the Combustion Institute, v. 33, pp. 3001-3006.

21. Martz, J.B., Lavoie, G.A., Im, H.G., Middleton, R.J., Babajimopoulos, A., and Assanis, D.N. (2011) The Propagation of a Laminar Reaction Front During End-Gas Auto-Ignition. Combustion and Flame (in press).

22. Martz, J.B., Middleton, R.J., Lavoie, G.A., Babajimopoulos, A., Assanis, D.N., (2011), A Computational Study and Correlation of Premixed Isooctane Air Laminar Flame Properties under Spark Ignited and Spark Assisted Compression Ignition Engine Conditions, Combustion and Flame, Vol. 158, No. 6, 1089-1096.

23. Middleton, R.J., Martz, J.B., Lavoie, G.A., Babajimopoulos, A., and Assanis, D. N. (2011) A Computational Study and Correlation of Premixed Isooctane Air Laminar Reaction Fronts Diluted with EGR. Combustion and Flame (submitted).

24. Ortiz-Soto, E., Assanis, D.N. and Babajimopoulos, A. (2011) A Comprehensive Engine to Drive-Cycle Modeling Framework for the Evaluation of Future Engine and Combustion Technologies. International Journal of Engine Research. In press.

25. Ortiz-Soto, E., Vavra, J. and Babajimopoulos, A. (2011) Assessment of residual mass estimation methods for cylinder pressure heat release analysis of HCCI engines with negative valve overlap. ASME Paper ICEF2011-60167. Proceedings of the ASME Internal Combustion Engine Division 2011 Fall Technical Conference, October 2–5, 2011, Morgantown, WV.

26. Rapp, V.H., DeFilippo, A., Saxena, S., Chen J.Y., Dibble, R.W. Nishiyama, A., Moon, A., Ikeda, Y. (2011) Extending lean operating limit of engines burning methane using a microwave-assisted spark plug, Submitted to Biomass & Bioenergy.

27. Saxena S., Schneider S., Krieck M., Maas U., and Dibble R., (2011) "Investigation of Wet Ethanol Combustion in a HCCI Engine Using an Exhaust Gas Heat Exchanger," Fall 2011 Meeting of the Western States Section of the Combustion Institute, October 16–18, 2011, Riverside, CA.

28. Saxena, S., Chen, J.-Y., and R.W. Dibble, (2010) "Increasing the signal-to-noise ratio of sparkplug ion sensors through the addition of a potassium acetate fuel additive," 33rd International Symposium on Combustion, Beijing, 2010. p. 3081-3088, doi: 10.1016/j.proci.2010.07.046.

29. Saxena, S., Chen, J-Y, Dibble, R.W., (2011) Characterization of HCCI ringing behavior using ion sensors, submitted for 2011 SAE Powertrains, Fuels and Lubricants meeting, Kyoto, Japan – JSAE 20119085.

30. Saxena, S., Corvers, M., Chen, J-Y, and Dibble, R.W., (2011) Detecting ringing in an HCCI engine using ion sensors, 2011 US National meeting of the Combustion Institute, Georgia Tech, Atlanta, GA, Mar. 2011.

31. Vavra, J., Bohac, S.V., Manofsky, L., Lavoie, G., Assanis, D., (2011), Knock in Various Combustion Modes in a Gasoline Fueled Automotive Engine, Proceedings of the ASME 2011 Internal Combustion Engine Division Fall Technical Conference, ICEF2011-60124.

32. Wagnon, S., Karwat, D.M.A., Wooldridge, M.S., (2011) "Chemical Kinetics of an Unsaturated Ester: Methyl Trans-3-hexenoate," 7th U.S. National Combustion Meeting, Atlanta, Georgia, March 2011.

33. Walton, S.M., Karwat, D.M., Teini, P.D., Gorny, A., and Wooldridge, M. S., (2011) "Speciation Studies of Methyl Butanoate Ignition," Fuel, vol 90, pp. 1796-1804 (2011).

34. Wolk B.M., DeFilippo A., Dibble R.W., and Chen J.Y., (2011) "Basic Explorations of Limits of Microwave-Assisted Spark Plug in Constant Volume Combustion Chamber," Fall 2011 Meeting of the Western States Section of the Combustion Institute, October 16–18, 2011, Riverside, CA.

35. Zigler, B.T., Keros, P.E., Helleberg, K.B., Fatouraie, M., Assanis, Dimitri, and Wooldridge, M. S., (2011) "An Experimental Investigation of the Sensitivity of the Ignition and Combustion Properties of a Single-Cylinder Research Engine to Spark-Assisted HCCI," International Journal of Engine Research, vol. 12, pp. 353-375, 2011.

IV.2 Optimization of Advanced Diesel Engine Combustion Strategies

Profs. Rolf Reitz (Primary Contact), David Foster, Jaal Ghandhi, Dave Rothamer, Christopher Rutland, Mario Trujillo, Scott Sanders
Engine Research Center
University of Wisconsin-Madison
1500 Engineering Drive
Madison, WI 53706

DOE Technology Development Manager: Gurpreet Singh

NETL Project Manager: Ralph Nine

Objectives

- Development of high efficiency internal combustion engines with goals of improved fuel economy by 20-40% in light-duty (LD) and 55% brake thermal efficiency (BTE) in heavy-duty (HD) engines.
- Develop methods to further optimize and control in-cylinder combustion processes, with emphasis on compression ignition engines.

Fiscal Year (FY) 2011 Objectives

- Further improve thermal efficiency by exploring the effect of piston design, fuel type and compression ratio on combustion in LD and HD diesel engines.
- Characterize advanced combustion regimes using in-cylinder optical diagnostics.
- Develop and apply advanced combustion models to help optimize engine performance.

Accomplishments

- Optimum spray and combustion chamber design recommendations made for improved efficiency of HD and LD diesel engines.
- Improved thermal efficiency over the stock LD engine achieved without the need for oxides of nitrogen (NOx) and particulate matter (PM) after-treatment using dual-fuel reactivity-controlled compression ignition (RCCI) combustion.
- Validated combustion and realistic fuel vaporization submodels developed for biofuels and gasoline/diesel surrogates for engine optimization and concept evaluation.
- Methodology formulated for efficient engine system transient control strategies appropriate for engine speed/load mode transitions.

Future Directions

- Methods to further increase fuel efficiency while maintaining low emissions will continue to be explored. The origins of CO and unburned hydrocarbons (UHCs) in HD and LD low-temperature combustion engines will be analyzed.
- Continue to explore optimized fuel injection strategies, matched with piston geometry and fuel types.
- Demonstrated and test transient control strategies for mixed-mode combustion.

Introduction

This work addresses the DOE's program goals of a 20-40% improvement in fuel efficiency in a LD vehicle and the attainment of 55% BTE in HD engine systems. To achieve these goals optimized combustion phasing and minimized in-cylinder heat transfer losses are required. There is also a need to minimize the fuel used for diesel particulate filter (DPF) regeneration, and thus it is necessary to minimize soot emissions. Significant challenges must be solved to achieve viable high thermal efficiency engine combustion. Conventional diffusion controlled combustion might be still be needed to reach full load, possibly with low-sooting lifted flames. Low-temperature combustion (LTC) (e.g., homogeneous charge compression ignition and early premixed charge compression ignition, HCCI/PCCI/RCCI) offers increased thermal efficiency with low NOx and reduced requirements for DPF regeneration for light-load operation. However, the inability to adequately control combustion phasing and to avoid liquid fuel impingement on combustion chamber surfaces with the use of high cetane number, low volatility fuels such as diesel, limits the practical load range and thermal efficiency benefits of LTC. In addition, reduction of combustion noise due to high rates of pressure rise, reduction of high levels of exhaust CO and UHC (which negatively impact fuel efficiency), and the need for optimizing mixture preparation is required to extend the light-load operating range. These issues are addressed in the present research by using novel fuel injection and fueling strategies.

Approach

The projects focus on advanced combustion research in LTC and lean-burn strategies, and in advanced modeling and control of vehicle emissions reduction (after-treatment) devices. The work is divided

into four main tasks with 12 sub-projects, featuring experimental and modeling components:

A. Combustion Strategies for Increased Thermal Efficiency
B. Fuels as an Enabler for Fuel Efficiency Improvement
C. Multi-Scale Predictive Tools for Understanding Combustion and Emissions
D. System-Level Engine Optimization (Air, Fuel, Emissions, After-Treatment)

A main focus of Tasks A, B and C is to improve fundamental understanding to overcome the technology barriers that control fuel efficiency. The impact of advanced combustion technologies on engine performance linked with the after-treatment system is also considered in Tasks C and D. Fully instrumented LD (General Motors [GM] 1.9 L) and HD (Caterpillar 3401) research diesel engines are used to reveal combustion fundamentals and to explore methods of controlling and optimizing fuel efficient combustion under steady-state and transient operation. Information from the engine experiments is incorporated into comprehensive multidimensional computational fluid dynamics (CFD) codes (KIVA with large eddy simulation [LES] turbulence models and detailed chemistry using CHEMKIN) and system models (GT-POWER and WAVE codes and their associated control algorithms). The developed models and experimental methods are used to explore methods to optimize diesel engine fuel efficiency while maintaining low emissions.

Results

Task A: Combustion Strategies for Increased Thermal Efficiency

RCCI is a dual-fuel partially premixed combustion concept that is also being studied in this subtask. The fueling strategy consists of in-cylinder fuel blending using port fuel injection of gasoline, or low reactivity fuel, and early-cycle, direct-injection of diesel, or high reactivity fuel. RCCI has demonstrated low NOx and soot with high thermal efficiency in a HD engine at loads up to 16 bar gross indicated mean effective pressure (IMEP). Extension to higher loads has been explored this year by using a reduced compression ratio (CR) piston (CR = 11.7). The KIVA code was used to compare the predicted energy budgets between the low compression ratio and stock pistons (CR=16.1) shown in Figure 1a. As can be seen in Figure 1b, the major differences are the heat transfer and thermal exhaust losses. The low compression ratio piston has lower in-cylinder temperatures and reduced surface area, and thus lower heat transfer losses. The modeling results indicate that full-load operation is possible with the low compression ratio piston, while simultaneously meeting emissions mandates [1].

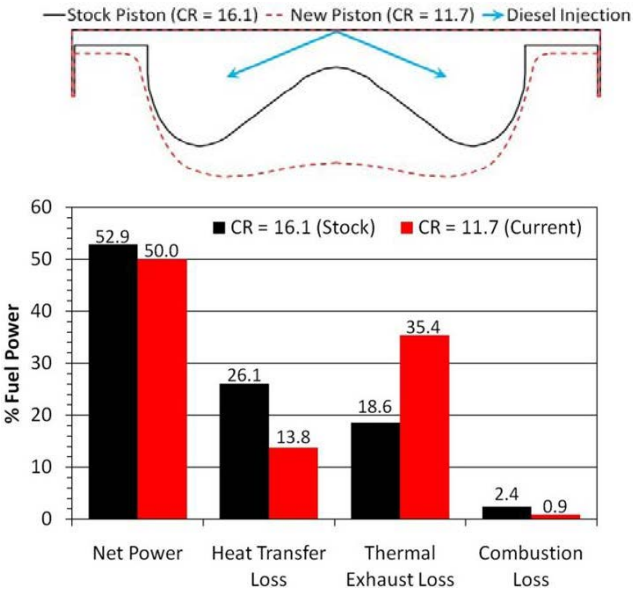

FIGURE 1. Stock (CR=16.1) and Low Compression Ratio RCCI pistons (CR=11.7), and Predicted Energy Budgets at 9 bar IMEP

LD RCCI engine experiments were performed in collaboration with the Oak Ridge National Laboratory on a multi-cylinder diesel engine at operating conditions representative of the Environmental Protection Agency LD FTP-75 emissions certification tests [2]. The stock engine configuration was compared to operation with both the original equipment configuration and custom machined pistons designed for RCCI operation using the KIVA code used with genetic algorithms. The results show that BTE was increased from 37%, with the stock EURO IV configuration, to 40% with RCCI at a 2,600 rev/min, 6.9 bar brake mean effective pressure (BMEP) condition. NOx and PM emissions targets were met without the need for exhaust after-treatment. In addition, the maximum pressure rise rate was 7.2 bar/degree (i.e., below target of 10 bar/degree). The increase in BTE was due to lower heat transfer losses from the LTC of RCCI and the lower friction losses from the high pressure fuel injection pump.

Interactions between engine operating parameters with different fuels under LTC conditions, and their effects on emissions, efficiency, and noise are also being evaluated in the LD GM 1.9 L engine. Successful operation of gasoline direct injection compression ignition was demonstrated up to 16 bar IMEP using multiple injections [3]. Intermediate and light-load operation has been studied this year at 4.5 bar BMEP (5.5 bar IMEP) at 2,000 and 1,500 rev/min and 0% exhaust gas recirculation (EGR). The engine operating ranges and associated crank angle (CA)50 and indicated specific fuel consumption are shown in Figures 2a and 2b. At 2,000 rev/min NOx emissions for a 80:20 double injection split were less than 5 ppm (0.15 g/kg-fuel injected), while NOx emissions for the 60:40 split were

~20 ppm (1 g/kg-fuel injected), and PM <0.01 g/kg-fuel injected. Pressure rise rates (PRR) for the 90:10 split were 7.5-8.5 bar/deg, while for the 80:20 split they were 6.5-7.5 bar/deg. Figure 2 shows that the size of the operating region is reduced when operating at 1,500 rev/min. But, unlike diesel LTC operation, gasoline direct injection compression ignition yields very low NOx emissions (below 0.25 g/kg-fuel injected), acceptable pressure rise rates, and little to no smoke. Interestingly, the second injection timing has little effect on ignition timing.

A combustion mode switch study has also been carried out under this subtask using full engine cycle analysis (including intake and exhaust) with three cycles of split injection, traditional diesel followed by a fourth LTC cycle. The mode switch is initiated by changing the in-cylinder fuel injection events in combination with changing the intake and exhaust valve timings. The study uses full engine CFD computations and the Engine Research Center's LES model integrated with the KIVA code. LES models resolve the interactions between cool flame, high temperature reaction zones and turbulent flow structures, and are being used to recommend mode-switch criteria.

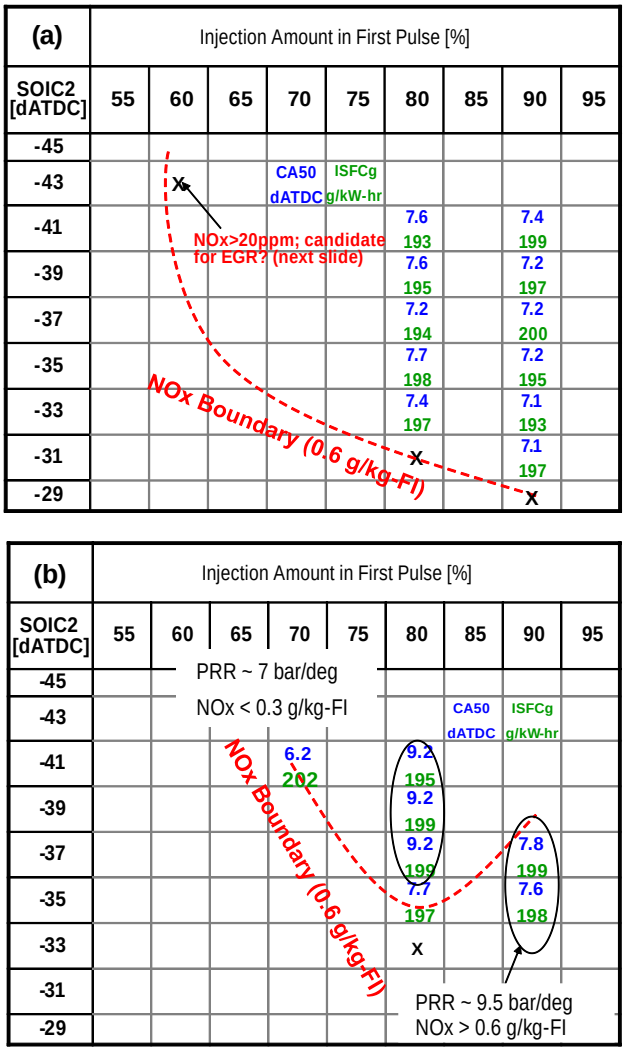

FIGURE 2. LD Gasoline Compression Ignition Operating Maps for 5.5 Bar IMEP a.) 2,000 rev/min; b.) 1,500 rev/min

Task B: Fuels as an Enabler for Fuel Efficiency Improvement

Optical investigations of RCCI have been using a Bowditch-style optical engine with a sapphire window in the piston crown. High-speed movies of combustion are acquired at 10,000 frames per second using an image intensifier with spectral response in the ultraviolet and visible ranges. Figure 3 shows comparisons between RCCI and HCCI combustion. The data were acquired at 1,200 rev/min, intake pressure of 1.6 bar and intake temperature of 100°C. The RCCI data were acquired using isooctane as the low-reactivity fuel and No. 2 diesel fuel directly injected. Two different RCCI fuel energy fractions were delivered through the port fuel injector, i.e., homogeneously mixed. The HCCI data were acquired with a 90 primary reference fuel mixture of n-heptane and isooctane.

The movies were used to create ignition maps that show the time when a pixel exceeds a set threshold level, i.e., when it ignites. The injection timings were adjusted for the RCCI cases and the intake temperature was changed for the HCCI case to have a constant CA50. The heat release rates show that the spatial reactivity gradient in RCCI extends the heat release duration and reduces the peak value compared to HCCI, and the effect of the reactivity gradient is clearly seen in the images. In HCCI the reactivity is nearly constant across the field of view, and the ignition is occurs during a very short heat release duration. In RCCI there is a pronounced spatial progression of the ignition process, and ignition preferentially occurs at the periphery and works its way toward the center of the images where there is a higher isooctane concentration which ignites later. These results confirm the role of the reactivity gradient in controlling the combustion progress.

In-cylinder laser/optical diagnostics are also being used to investigate extended-lift-off diesel combustion. The diagnostics include planar laser-induced fluorescence measurements of the fuel distribution, planar laser-induced incandescence measurements of the soot distribution, and OH chemiluminescence and/or OH planar laser induced fluorescence measurements, and high-speed natural luminosity and chemiluminescence imaging. Injector tips with two, four, and six orifices (with 0.11 mm orifice diameters) are available, and a series of tests have been run with the 2-hole tip. Maximum pressure rise rates of 7-9 bar/CA degrees were seen with an 8-hole, 0.133mm orifice diameter), while the new 2-hole tip had 1.5-2 bar/CA degrees. Start of injection sweeps have been run with

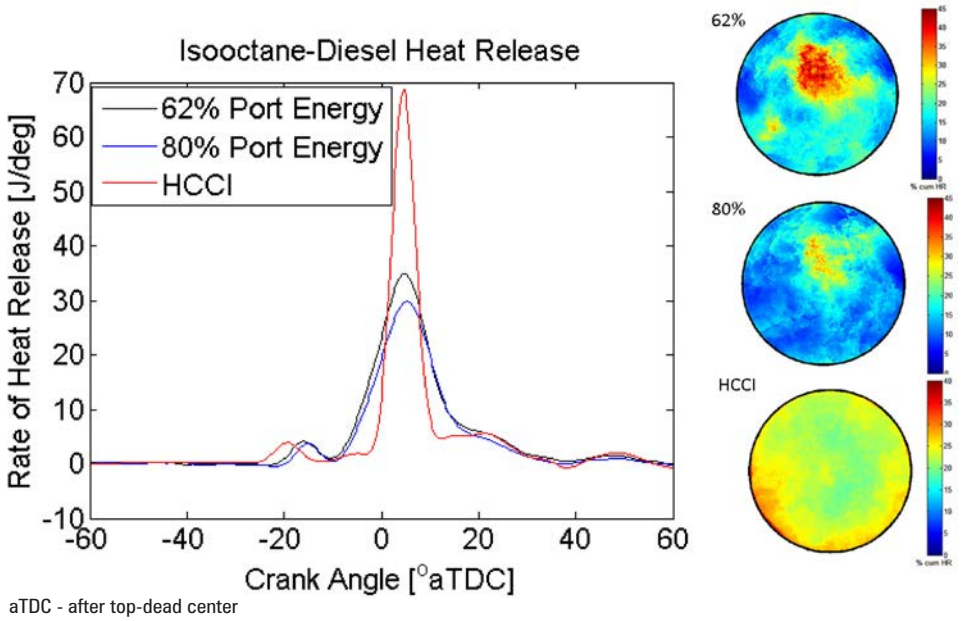

aTDC - after top-dead center

FIGURE 3. Heat Release And Combustion Phasing Images as a Function of the Amount of Port Injected Fuel

different engine swirl ratios (1.5, 2.6, and 5.5) using No. 2 diesel fuel, at 1,200 rev/min, and a rail injection pressure of 1,200 bar with an injection command duration of 2,000 µs. An example screenshot showing lifted flame operation is given in Figure 4.

Task C: Multi-Scale Predictive Tools for Understanding Combustion and Emissions

The goal of this sub-task is to develop and apply predictive, detailed-chemistry-based models to improve understanding of the combustion and emission formation processes for efficient engines. A combustion model is being developed that can model auto-ignition, flame propagation, and premixed and non-premixed combustion, and mixed-mode regimes that can conceivably all occur in the same engine cycle in advanced combustion concepts. A reduced reaction kinetics mechanism suitable for CFD models that employs a physical-surrogate, group-chemistry representation model for multi-component fuels has been developed to predict ignition delay times of realistic fuel blends. Generic reaction pathways to model reactions from the fuel components to basis components of chemical classes have been found to deplete the active radicals that are necessary to drive the overall oxidation processes, especially for blend fuels of low- and high-reactivity components. This problem has been resolved by including radical-generating reactions so as to balance the consumption and generation of active radicals during the process. The modified reactions include the effects of H-abstraction, radical generation and decomposition reactions that are critical reaction pathways of low-temperature oxidation. The performance of the reaction mechanism is shown in Figure 5 for three aromatic components blended with a three-component base fuel. The modified reaction mechanisms capture the expected trends of ignition delay times of the blended fuels, as well as those of the pure components.

Advanced spray and fuel film models for selective catalytic reduction after-treatment are also being developed in this subtask. Calculations have been performed of urea-water-solution (UWS) sprays and their subsequent vaporization, solidification and urea decomposition. The code has been extended to handle species transport and gas-liquid and liquid-solid migration. The validation process has been extended to include vaporization or gasification comparisons against C_7H_{16}, water, and UWS droplet experimental data. Since UWS sprays are injected in either cross flow or co-flow, a parallel investigation has been the study of the dynamics of sprays in cross flow to study the penetration and mixing characteristics in weak and strong cross-flows.

Measurements and control of turbulence mixing in engine flows is also being explored, and the results are being utilized for LES turbulent combustion model development and validation. Turbulent mixing is a controlling feature in LTC where the goal is to premix, to as large an extent as possible, the fuel and air prior to ignition. The goal of the project is to optically obtain full resolution of all relevant turbulent scales. Data have been acquired in a pent-roof chamber engine using a low momentum injected gas jet with different fluorescent tracers as method to characterize flow turbulence. Fluorobenzene, has been found to give adequate signal levels and signal-to-noise ratios and dissipation spectra

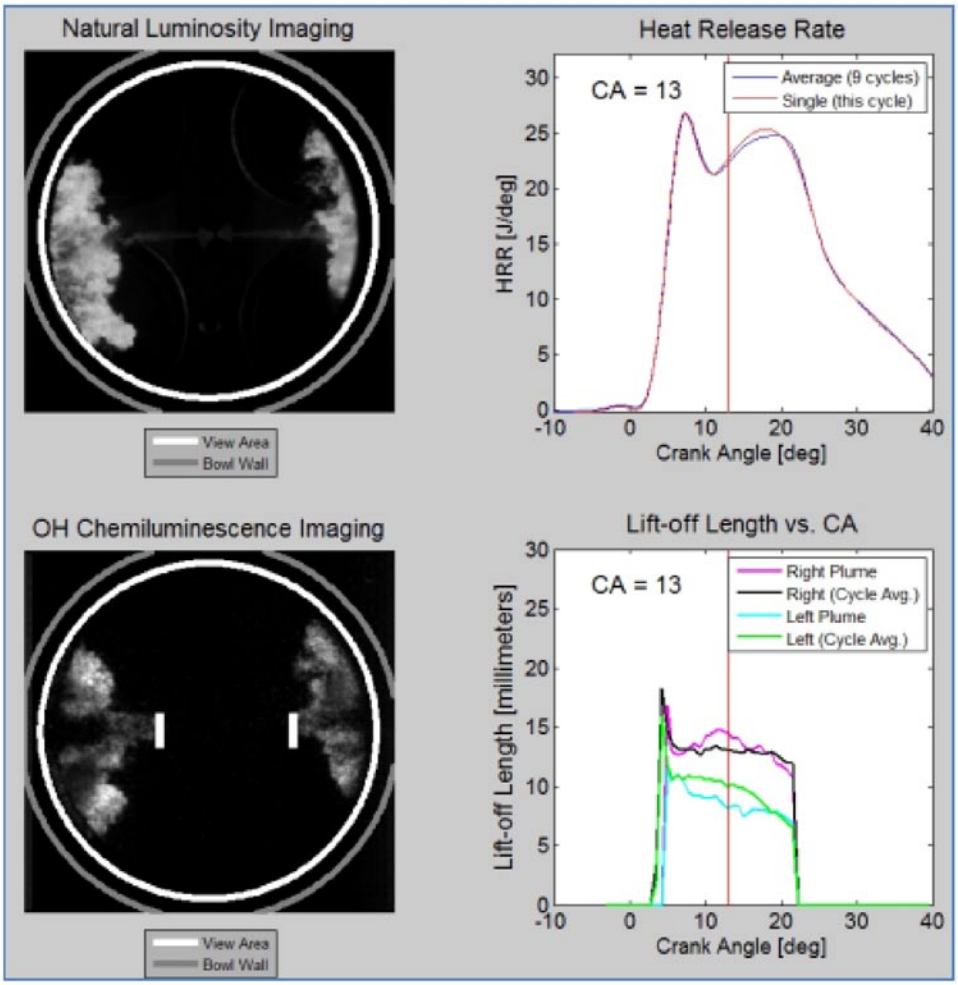

FIGURE 4. Combustion Images with 2-Hole Nozzle Showing Lifted Flame Operation

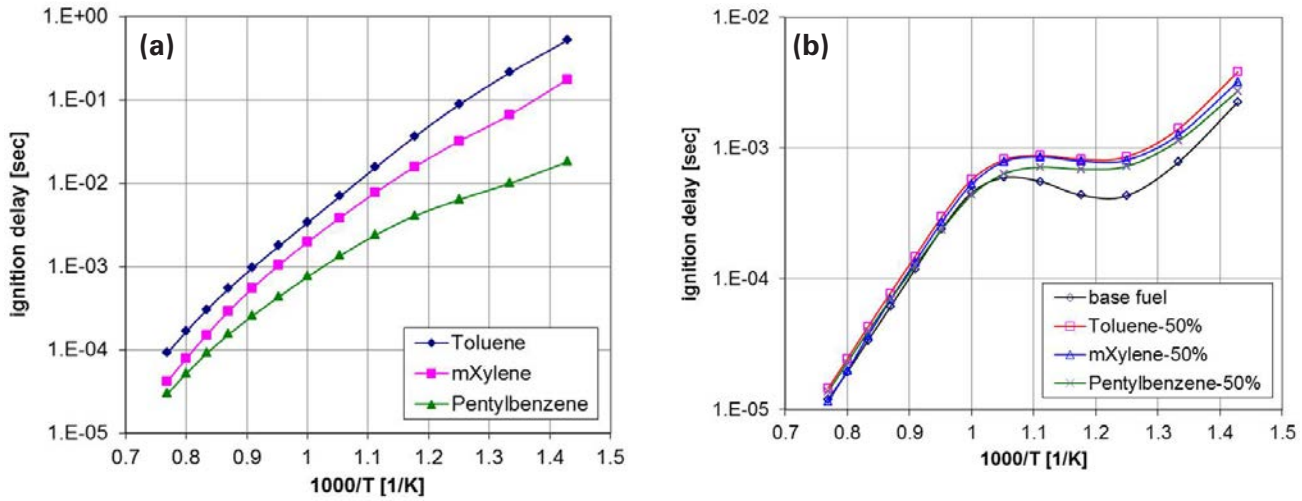

FIGURE 5. Predicted ignition delay times at constant volume conditions for various aromatic fuels. (a) ignition delay times of pure components, (b) ignition delay times of blended fuels. The base 3-component fuel consists of 29.7% n-heptane, 62.6% n-tetradecane, and 7.7% cyclohexane (mass). Stoichiometric mixtures at 40 bar initial pressure.

have been acquired at 40 degrees before top-dead center and top-dead center in the engine at 600 rev/min. The data achieve a good match with Pope's theoretical spectrum, indicating that there is sufficient data integrity to ascertain the Batchelor scales (important to characterize mixing).

Crank-angle-resolved species and temperature measurement diagnostics are also being developed for improved understanding of chemistry and mixing in LTC regimes. Previous work in this subtask developed an emission Fourier transform infrared technique that has been applied to in-cylinder RCCI measurements. A high-speed ultra-violet absorption spectrometer has been set up using ~80-fs-duration frequency-tripled titanium-sapphire laser with ~10 mW of transform-limited (modest spectral bandwidth) quasi-continuous wave output. The center wavelength of this output is adjustable throughout the 226 nm (NO) to 308 nm (OH) spectral range. It is planned to direct the beam through the engine and detect it with a 1.25-m grating spectrometer and kinetics-mode camera. The entire arrangement will allow high-speed (~30 kHz), high-spectral-resolution (~0.2 cm^{-1}) absorption spectroscopy in combustion environments. The first tests are being performed in a calibration flame (Hencken burner operating on CH_4-air), which is already operational in the lab.

Task D: System-Level Engine Optimization (Air, Fuel, Emissions, Aftertreatment)

Interactions between high- and low-pressure EGR systems with mixed-mode operation under load and speed transients are being evaluated for LTC phasing control. A low-pressure EGR loop has been incorporated to expand the load range. New hybrid-EGR systems exhibit cooler EGR temperatures, higher EGR flow rates at low loads, higher turbo speeds and boost pressures, and improved EGR response. The capability of meeting Tier II Bin 5 NOx emissions has been demonstrated on the multi-cylinder GM 1.9 L engine with comparable brake specific fuel consumption to the EURO4 calibration, but with lower emissions.

Work has focused on de-convolving the dependence of transient operation into the response of the relevant sub-systems and reproducing the transient measurements with a sequence of steady-state conditions. The steady-state conditions are set with the in-cylinder gas composition and manifold conditions that occurred during the transient. For example, a transient is run, and the speed/fueling points from specific cycles are matched to "reconstruct" the transient. Three different comparisons were used: the "steady state" where the engine control unit and engine are allowed to reach steady state at the specified speed/fuel rate; the "manifold air flow/pressure, or MAF-MAP" which starts from a steady-state condition and the boost and EGR rate are adjusted to match the air mass flow and intake manifold pressure that occurred during the transient. This technique implies that if those variables are matched, the results should be similar to the transient, however our work has indicated that excess oxygen in the EGR is also critical, especially for high EGR strategies. Therefore, we have developed a third "quasi-transient" estimation which uses intake O_2 instead of MAF and also considers the delays in intake temperature and rail pressure that actually occur during the transient. Injection timing and variable swirl vane position were matched to the transient in all cases since there was no delay in actuation for these controls. As shown in Figure 6, under low load early injection LTC transition conditions, the quasi-transient emissions results match very well to the transient emissions. The MAF-MAP approximation on the other hand is hardly different than the steady-state approximation. Results at other engine conditions have also been explored, which show that NO and soot trends are captured much better with the quasi-transient approximation than in either the steady state or MAF-MAP cases.

Engine and after-treatment optimization modeling is also being used to guide the transient engine experiments and to study engine-after-treatment options for low fuel consumption. System-level models capable of simulating multiple cycles and operating transients have been formulated based on GT-POWER, coupled with purpose-written emissions submodels. The standalone oxidation catalyst model was built by utilizing the existing three-way catalyst (TWC) from GT-POWER. The surface reaction mechanism for TWC [4] includes oxidation reactions for carbon dioxide, hydrocarbons (C_3H_6 and C_3H_8) and hydrogen, NOx reduction reactions, water-gas and steam reforming reactions and oxygen storage reactions. A sensitivity analysis of the model is being conducted to understand the effects of catalyst loading and device geometry on TWC performance. Steady-state experimental data at lean and rich engine operating conditions are used to validate the model.

Conclusions

- Novel diagnostics, fuel-types, injection concepts, optimized piston geometries continue to be explored successfully with advanced CFD models and coordinated engine experiments to explore efficient LTC concepts.
- The study has identified advanced combustion regimes with optimized control of fuel/air/diluent mixture preparation and control of fuel reactivity distributions that can offer substantial improvements in engine efficiency (>50% thermal efficiency over wide engine operating range) while meeting emissions mandates without the need for after-treatment.

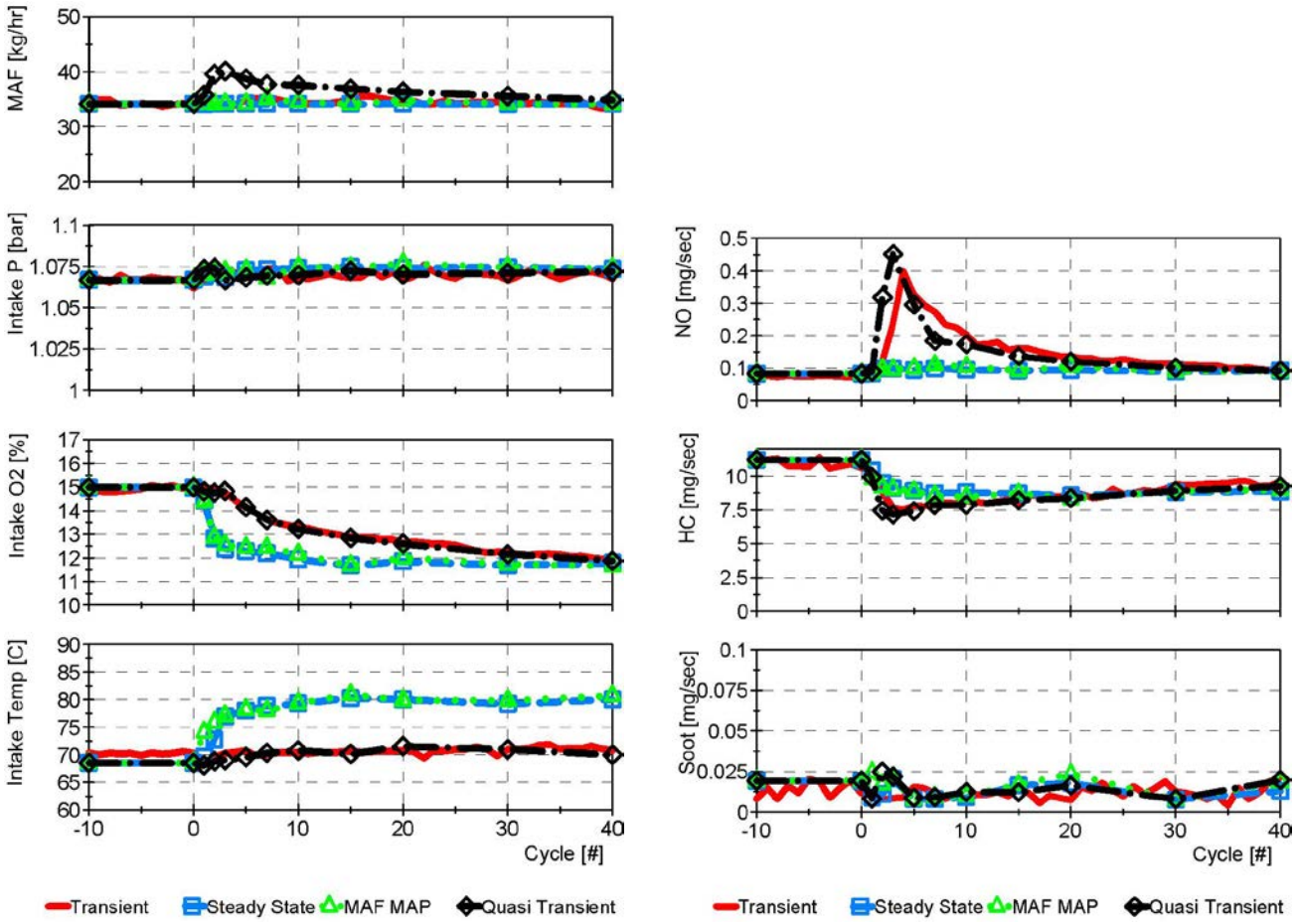

FIGURE 6. Comparison of the Steady State, MAF-MAP and Quasi-Transient Approaches for Reproducing the Actual Transient for Early Injection LTC, 1,500 rev/min, 0.5-2.0 Bar BMEP

- The study shows that significant opportunities exist to further improve engine operation in the LTC regime by tailoring fuel characteristics.

References

1. Dempsey, A.B., and Reitz, R.D., "Computational Optimization of Reactivity Controlled Compression Ignition in a Heavy-Duty Engine with Ultra Low Compression Ratio," SAE Paper 11ICE-0206, 2011-24-0015, 2011.

2. Hanson, R., Curran, S., Reitz, R.D., Kokjohn, S.L., and Briggs, T., "Piston Bowl Optimization for RCCI Combustion in a Light-Duty Multi-Cylinder Engine," SAE paper submitted for 2012 Congress, 12PFL-0950, 2011.

3. Youngchul Ra, Paul Loeper, Michael Andrie, Roger Krieger, David Foster, University of Wisconsin-Madison; Russ Durrett, GM R&D Center; Rolf Reitz, University of Wisconsin-Madison, "Gasoline DICI engine operation in the LTC regime using triple-pulse injection, SAE paper submitted for 2012 Congress, 12PFL-1009, 2011.

4. Ramanathan K. and Sharma C.S., "Kinetic Parameters Estimation for Three Way Catalyst Modeling", Industrial & Engineering Chemistry Research, 50 (17), p. 9960:9979, 2011.

FY 2011 Publications/Presentations

1. Dempsey, A.B., and Reitz, R.D., "Computational Optimization of a Heavy-Duty Compression Ignition Engine Fueled with Conventional Gasoline," SAE Paper 2011-01-0356, 2011.

2. Ra, Y., Loeper, P., Reitz, R.D., Krieger, R.B., Foster, D.E., Durrett, R.P., Gopalakrishnan, V., Plazas, A., Peterson, R., and Szymkowicz, P., "Study of high speed gasoline DICI engine operation in the LTC regime," SAE Paper 2011-01-1182, 2011.

3. Brakora, J.L., Ra, Y., and Reitz, R.D., "Combustion Model for Biodiesel-Fueled Engine Simulations using Realistic Chemistry and Physical Properties," SAE Paper 2011-01-0831, 2011.

4. Kokjohn, S.L., Hanson, R.M., Splitter, D.A., Kaddatz, J., and Reitz, R.D., "Fuel Reactivity Controlled Compression Ignition (RCCI) Combustion in Light- and Heavy-duty Engines," SAE Paper 2011-01-0357, SAE International Journal of Engines, 2011.

4. Hanson, R.M., Kokjohn, S.L., Splitter, D.A., and Reitz, R.D., "Fuel Effects on Reactivity Controlled Compression Ignition (RCCI) Combustion at Low Load," SAE Paper 2011-01-0361, 2011.

5. Splitter, D.A., Hanson, R.M., Kokjohn, S.L., and Reitz, R.D., "Reactivity Controlled Compression Ignition (RCCI) Heavy-Duty Engine Operation at Mid-and High-Loads with Conventional and Alternative Fuels," SAE Paper 2011-01-0363, 2011.

6. Dempsey, A.B., and Reitz, R.D., "Computational Optimization of Reactivity Controlled Compression Ignition in a Heavy-Duty Engine with Ultra Low Compression Ratio," SAE Paper 11ICE-0206, 2011-24-0015, 2011.

7. Splitter, D.A., Hanson, R.M., Kokjohn, S.L., Wissink, M., and Reitz, R.D., "Injection Effects in Low Load RCCI Dual-Fuel Combustion," SAE Paper 11ICE-0154, 2011-24-0047, 2011.

8. Kokjohn, S.L., Hanson, R.M., Splitter, D.A., and Reitz, R.D., "Fuel Reactivity Controlled Compression Ignition (RCCI): A Pathway to Controlled High-Efficiency Clean Combustion," International Journal of Engine Research, Special Issue on Fuel Efficiency, Vol. 12, pp. 209-226, doi:10.1177/1468087411401548, 2011.

9. Blessinger, M.K. and Ghandhi, J.B., "Initial Optical Investigation of Reactivity Controlled Combustion in an HSDI Engine," presented at the 7th US National Technical Meeting of the Combustion Institute, Georgia Institute of Technology, Atlanta, GA, March 20–23, 2011.

10. Deshpande, S.S., Gao, J., and Trujillo, M.F. (2011) Characteristics of Hollow Cone Sprays in Crossflow, 23rd Annual Conference on Liquid Atomization and Sprays Systems, Ventura, CA.

11. Brakora, J.L., and Reitz, R.D., "Improvements to a Biodiesel-fueled Engine Model using Realistic Chemistry and Physical Properties," ILASS Americas, 23rd Annual Conference on Liquid Atomization and Spray Systems, Ventura, CA, May 2011.

12. Kokjohn, S.L., Reitz, R.D., and Musculus, M.P.B, "Chemiluminescence and Fuel PLIF Imaging of Reactivity Controlled Compression Ignition (RCCI) Combustion," ILASS Americas, 23rd Annual Conference on Liquid Atomization and Spray Systems, Ventura, CA, May 2011.

13. Zhang, Y., and Rutland, C. J., "LES Scalar Dissipation Rate and Combustion Modeling for Diesel Engine", in 7th US National Technical Meeting of the Combustion Institute, 2011, Atlanta, Georgia.

14. Banerjee, S., Rutland, C. J., "Numerical Study of Diesel Combustion Regimes", SAE 2011-01-0823, 2011.

15. Puduppakkam, K.V., Liang, L., Naik, C.V., Meeks, E., Kokjohn, S.L., and Reitz, R.D., "Use of Detailed Kinetics and Advanced Chemistry-Solution Techniques in CFD to Investigate Dual-Fuel Engine Concepts," SAE paper 2011-01-0895, 2011.

16. Gao, J., Deshpande, S., and Trujillo, M.F. "Numerical Simulation of Hollow-Cone Sprays Interacting with Uniform Crossflow for Gasoline Direct Injection Engines" 10th International Conference on Engines & Vehicles ICE2011, Sept.11-15, Naples, Italy.

17. Perini, F., Reitz, R.D., and Cantore, G., "An analysis on time scale separation for engine simulations with detailed chemistry," SAE Paper 11ICE-0205, 2011-24-0028, 2011.

18. Glewen, W., Meyer, C. Krieger, R, Andrie, M. and Foster, D, "Experimental Investigation of Transient NO and UHC Emissions Sources for Low Temperature Diesel Combustion", SAE 2011 World Congress, 2011.

19. Dempsey, A.B., Adhikary, B. Das, Viswanathan, S., and Reitz, R.D., "Reactivity Controlled Compression Ignition (RCCI) using Premixed Hydrated Ethanol and Direct Injection Diesel," ASME Internal Combustion Engine Division Fall Technical Conference, 2011.

20. Dempsey, A.B., Reitz, R. D., Miles, P.C., Sahoo, D., Petersen, B., "Comparison of Quantitative In-Cylinder Equivalence Ratio Measurements with CFD Predictions for a Light Duty Low Temperature Combustion Diesel Engine", SAE World Congress 2012 (12PFL-1094)

21. Banerjee S., Rutland C.J., "On LES grid criteria for spray induced turbulence", to be published in SAE 2012 world congress.

22. Banerjee S., Rutland C.J., "Numerical Investigation of High Powered Diesel Mode Transition Using Large Eddy Simulations", to be published in SAE 2012.

23. S.S. Deshpande, J. Gao, and M.F. Trujillo "Characteristics of Hollow Cone Sprays in Crossflow" accepted for publication in Atomization & Sprays, 2011.

24. Perini, F., Brakora, J.L., Reitz, R.D., and Cantore, G., "Development of reduced and optimized reaction mechanisms based on genetic algorithms and element flux analysis," Combustion and Flame, doi:10.1016/j.combustflame.2011.06.012, (In press) 2011.

25. Zhang, Y. and Rutland, C.J. "A Mixing Controlled Direct Chemistry (MCDC) Model for Diesel Engine Combustion Modeling Using Large Eddy Simulation", submitted to Combustion Theory and Modeling.

Special Recognitions & Awards/Patents Issued/Pending

1. Reitz, R.D., Hanson, R., Splitter, D. and Kokjohn, S.L., "Engine Combustion Control at Low Loads via Fuel Reactivity Stratification," WARF Patent application P11092US01, March 2011.

IV.3 Flex Fuel Optimized SI and HCCI Engine

Guoming (George) Zhu (Primary Contact) and Harold Schock
Michigan State University (MSU)
Mechanical Engineering
E148 Engineering Research Complex South
East Lansing, MI 48824

DOE Technology Development Manager: Gurpreet Singh

NETL Project Manager: Ralph Nine

Subcontractor:
Chrysler, LLC, Auburn Hills, MI

Overall Objectives

- Demonstrate a spark ignition (SI) and homogeneous charge compression ignition (HCCI) dual combustion mode engine for any blend of gasoline and E85 (blend of 85% ethanol and 15% gasoline) for the best fuel economy.
- Develop a cost effective and reliable SI and HCCI dual combustion mode engine.
- Develop a control oriented (real-time) SI, HCCI and SI-HCCI combustion model and implement it into a hardware-in-the-loop (HIL) simulation environment.
- Develop model-based combustion mode transition control strategies for smooth mode transition between SI and HCCI combustions.
- Utilize closed-loop combustion control to minimize efficiency degradation with satisfactory engine out exhaust emissions under any blend of gasoline and E85.

Fiscal Year (FY) 2011 Objectives

- Develop a cost effective and reliable SI and HCCI dual combustion mode engine.
- Develop a control oriented (real-time) SI, HCCI and SI-HCCI combustion model.
- Develop combustion mode transition control strategies for smooth mode transition.

Accomplishments

- Completed target fuel injector droplet size study for different blends of fuels from gasoline to E85. The test results show that the target injector is suitable for our target engine since the droplet size remains almost unchanged under different blends of fuel.
- SI combustion optical test was completed and the test results will be used to compare to HCCI and SI-HCCI combustions in the future.
- The target engine head was redesigned to fit two-step valve and electrical cam phasing systems and the modification of the target head assembly is completed.
- HIL simulation results confirm that smooth mode transition between SI and HCCI can be achieved for an engine equipped with a two-step valve and electrical cam phasing systems.
- New mode transition control strategies (iterative learning individual cylinder fueling and linear quadratic [LQ] manifold air pressure [MAP] tracking control) were developed to further improve transition performance.
- The prototype engine controller development is completed. The engine controller consists of an Opal-RT prototype controller and a customer engine controller in-out box.

Future Directions

For FY 2012, our plan is to complete the project and to demonstrate the smooth combustion mode transition between SI and HCCI operations through both optical single-cylinder engine and multi-cylinder metal engine tests:

- Complete the target optical engine integration and tests in HCCI combustion mode.
- Complete HCCI closed-loop combustion control dynamometer tests, along with the determination of the HCCI operational range.
- Develop the final test plan and complete the final performance and emission tests.
- Complete the test data analysis and final project report.

Introduction

To obtain the benefit of high efficiency of compression ignition engines and low emissions of spark ignition engines, there has been a rekindled interest in HCCI engines in recent years. The major advantage of HCCI engines is realized by eliminating the formation of flames and results in a much lower combustion temperature [1-5]. As a consequence of the low temperature, the formation of oxides of nitrogen (NOx) is greatly reduced. The lean burn nature of the HCCI engine also enables un-throttled operation to improve

vehicle fuel economy. The main challenge of HCCI engines is the accurate control of the start of combustion and combustion duration. The practical application of the HCCI principle to gasoline engines is envisioned in a dual-mode combustion engine concept. At partial load conditions, the engine would operate under an un-throttled HCCI combustion mode, and at low or high load conditions, the engine operation needs to transition to the conventional SI combustion mode to avoid engine misfire or knocking. The objective of this project is to demonstrate an SI and HCCI dual-mode combustion engine for gasoline and E85. The operating efficiencies shall be obtained through closed-loop control, which will result in minimal efficiency degradation when E85 fuel or any blend of gasoline and E85 are used.

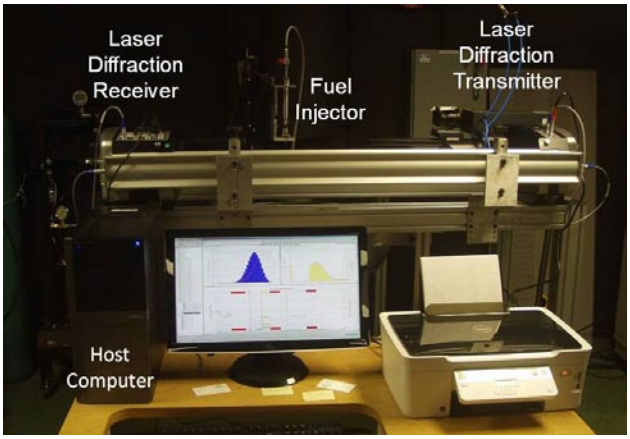

FIGURE 1. Spraytec/Malvern Laser Diffraction Drop Sizing Measurement Setup

Approach

This research activity adopts a model-based control approach to develop control strategies for smooth mode transition between SI and HCCI combustion with the support from our industrial partner, Chrysler LLC. The following methodology is and has been used in this research activity:

- Understand and optimize the HCCI and SI-HCCI hybrid combustion processes through optical engine study.
- Develop a control oriented SI, HCCI, SI-HCCI combustion model as well as the entire engine model, and calibrate it based upon GT-Power simulation results and optical/metal engine experiments.
- Utilize the developed control oriented engine model to study SI and HCCI combustion modes as well as SI-HCCI hybrid (spark assistant) combustion mode during combustion mode transition.
- Develop the closed-loop combustion control strategy for hybrid combustion and SI to HCCI combustion mode transition under a blend of gasoline and ethanol and validate it through HIL simulations.
- Validate the developed control strategy on the multi-cylinder metal engine for smooth mode transition between SI and HCCI combustions.

Results

- To study the spray characteristics of the Chrysler target injector under different blends of gasoline and E85, injector drop size tests were conducted using a Malvern Spraytec system (see Figure 1) for the Chrysler target and Bosch production injectors. The test results show that a) the drop size decreases as the fuel injection pressure increased; b) the Chrysler target injector demonstrates better robustness of the fuel drop size to fuel blend variations, compared with the Bosch production injector, which is very important to our flex fuel optimized engine; and c) at low fuel pressure (5 MPa) the fuel drop size of the Chrysler target injector is smaller than that of the Bosch injector for both gasoline and E85; however at 10 MPa, the drop sizes of both injectors are close for gasoline but the drop size of the Chrysler target injector is smaller than that of the Bosch injector for E85.
- Optical engine tests for SI combustion were conducted and the collected test images and combustion information such as in-cylinder pressure and mass fraction burned will be used to compare in the future with test data of HCCI and SI-HCCI combustion.
- MSU worked with Chrysler and Delphi engineers to integrate the two-step valve system to the target engine head. The integration design of both the two-step valve and electrical cam phaser and modification of the target engine head are completed, see Figure 2.
- The prototype engine controller development is completed. The engine controller consists of an Opal-RT prototype controller and a customer engine controller in-out box (see Figure 3) developed by MSU. The design of engine prototype controller is specially designed for controlling combustion mode transition between SI and HCCI operations.
- MSU continued studying the application of the SI-HCCI combustion to the mode transition between SI and HCCI combustions based on the developed control oriented engine model in the HIL simulation environment, where the iterative learning control was used to regulate the individual cylinder fueling during the mode transition cycles and the LQ optimal tracking control was used to optimize the engine throttle operation during the mode transition cycles (see Figure 4 for control system

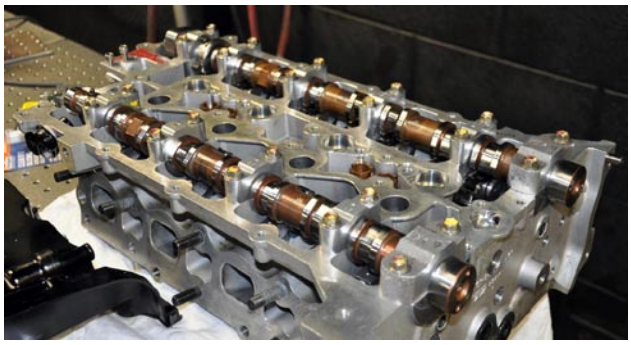

FIGURE 2. Modified Engine Head With Two-Step Valve and Electrical Cam Phasing Systems

FIGURE 3. Prototype Engine Controller In-Out Box

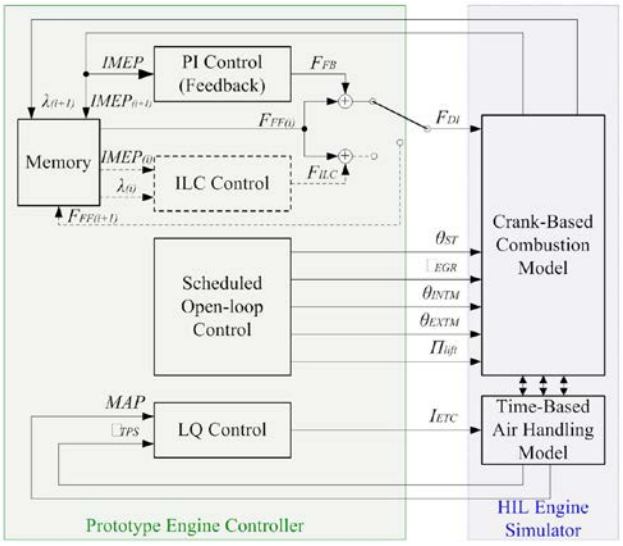

FIGURE 4. SI to HCCI Combustion Mode Transition Control Block Diagram

architecture). With the help of the two newly developed control strategies (iterative learning fueling and LQ MAP tracking control) [6-7], smooth mode transition can be achieved for an HCCI-capable SI engine equipped with two-step valve and electrical cam phasing systems (see Figure 5 and Figure 6 for the simulation results).

Conclusions

The research conducted in FY 2011 has shown progress toward the development, implementation, and demonstration of the proposed technology. Specific accomplishments are listed below:

- It is validated that a control oriented engine model sophisticated enough for combustion mode transition control development can be developed

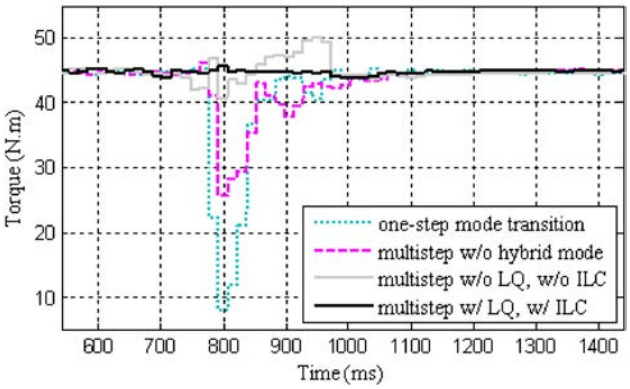

FIGURE 5. Engine Torque Performance of Different Control Strategies

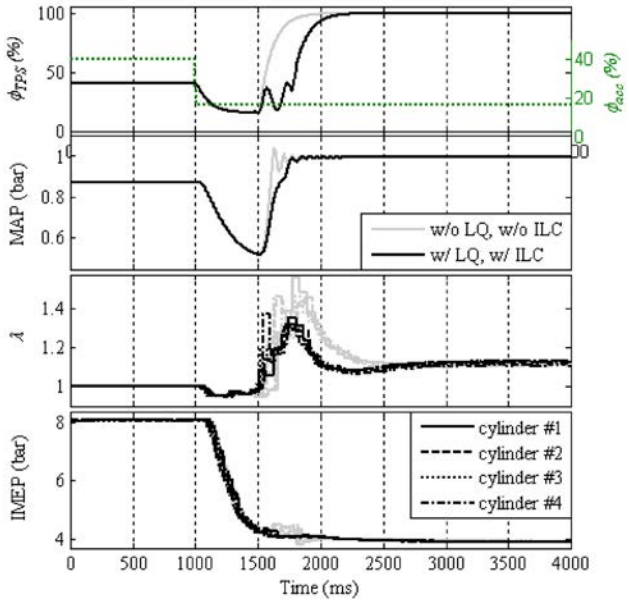

FIGURE 6. Engine Response During Tip-Out Operation

and is feasible to be implemented into a HIL simulation environment for real-time simulations. The simulation results were validated by GT-Power simulations.

- HIL simulation results confirm that smooth combustion mode transition between SI and HCCI combustions can be achieved for an engine equipped with two-step valve and electrical cam phasing systems.
- New combustion mode transition control strategies (iterative learning fueling and LQ MAP tracking control) [6-7] were developed and validated in the HIL simulation environment to further improve mode transition performance.
- With normal progress on the project, we are confident that we will be able to complete the project in FY 2012.

References

1. G. Shibata, K. Oyama, T. Urushihara, and T. Nakano, (2004) "The Effect of Fuel Properties on Low and High Temperature Heat Release and Resulting Performance of an HCCI Engine," SAE 2004-01-0553.

2. G. Haraldsson, J. Hyvonen, P. Tunestal, and B. Johansson, (2004) "HCCI Closed-Loop Combustion Control Using Fast Thermal Management," SAE 2004-01-0943.

3. H. Persson, M. Agrell, J.-O. Olsson, and B. Johansson, (2004) "The Effect of Intake Temperature on HCCI Operation Using Negative Valve Overlap," SAE 2004-01-0944.

4. G.M. Shaver, et al, (2005) "Dynamic Modeling of Residual-Affected Homogeneous Charge Compression Ignition Engines with Variable Valve Actuation," ASME Journal of Dynamics, Measurement, and Control, Vol. 127, pp. 374-381.

5. G.M. Shaver, (2005) "Physics Based Modeling and Control of Residual-Affected HCCI Engines using Variable Valve Actuation," PhD thesis, Stanford University.

6. X. Yang and G. Zhu, "SI and HCCI Combustion Mode Transition Control of a Multi-Cylinder HCCI Capable SI Engine," *IEEE Transaction on Control System Technology* (*Submitted in June, 2011, under review*).

7. X. Yang and G. Zhu, "Air-to-Fuel Ratio Regulation during SI to HCCI Combustion Mode Transition Using the LQ Tracking Control," *submitted to American Control Conference, June, 2012.*

FY 2011 Publications/Presentations

1. G. Zhu, and H. Schock, "SI and HCCI Combustion Mode Transition Control Using Hybrid Combustion Mode," *ACE Working Group Meeting, Livermore, CA, February, 2011.*

2. G. Zhu and H. Schock, "Flex Fuel Optimized SI and HCCI Engine," *DOE Vehicle Technology Program Annual Merit Review, Arlington, VA, May, 2011.*

3. X. Yang and G. Zhu, "A Two-Zone Control Oriented SI-HCCI Hybrid Combustion Model for the HIL Simulation," *Proceedings of 2011 American Control Conference, San Francisco, CA, June, 2011.*

4. Z. Ren and G. Zhu, "Modeling and Control of an Electrical Variable Valve Timing System for Si and HCCI Combustion Mode Transition," *Proceedings of 2011 American Control Conference, San Francisco, CA, June, 2011.*

5. G. Zhu, and H. Schock, "SI and HCCI combustion mode transition control using iterative learning and optimal tracking," *ACE Working Group Meeting, Southfield, MI, August, 2011.*

6. X. Yang and G. Zhu, "Air-to-Fuel Ratio Regulation during SI to HCCI Combustion Mode Transition Using the LQ Tracking Control," *submitted to American Control Conference, June, 2012.*

IV.4 Development of Optimal Catalyst Designs and Operating Strategies for Lean NOx Reduction in Coupled LNT-SCR Systems

Michael P. Harold (Primary Contact, University of Houston), Mark Crocker (University of Kentucky), Robert W. McCabe (Ford)
University of Houston
Dept. of Chemical & Biomolecular Engineering
S325 Engineering Building 1
Houston, TX 77204

DOE Technology Development Manager: Ken Howden

NETL Project Manager: Ralph Nine

Objectives

The overarching goal of this project is to identify the oxides of nitrogen (NOx) reduction mechanisms operative in lean-NOx traps (LNTs) and in situ selective catalytic reduction (SCR) catalysts, and to use this knowledge to design optimized LNT-SCR systems in terms of catalyst architecture and operating strategies. The project is split into three phases. Activities to date have concentrated on Phase 1, 2, and 3 objectives, which are as follows.

Phase 1

- Elucidate the mechanism of the non-NH_3 pathway for NOx reduction by means of bench-scale reactor, in situ diffuse reflectance infrared Fourier-transform spectroscopy (DRIFTS) reactor, and temporal analysis of products (TAP) reactor studies.
- Map LNT selectivity to NH_3 as a function of catalyst composition (ceria content and type) and relevant process parameters (NOx loading, purge duration, purge lambda and space velocity).
- Develop a microkinetic LNT model that takes into account the catalyst composition (storage component such as ceria and barium loading as well as precious metal such as Pt loading/dispersion) and H_2, CO, and C_3H_6 reductants.
- Develop low-dimensional models for the LNT and the coupled LNT-SCR unit for different catalyst architectures incorporating microkinetics.

Phase 2

- Determine optimum ceria type and content in model LNT catalysts to achieve best net NOx conversion in serial LNT-SCR catalysts.
- Determine the level of precious group metal (PGM) reduction possible in the serial LNT-SCR catalyst system while providing equivalent performance to the corresponding LNT-only system.
- Establish the optimal operating strategy of serial and double layer catalyst systems with respect to NOx conversion level and fuel penalty.
- Develop microkinetic SCR model that includes non-NH_3 mechanism.
- Carry out experimental optimization study of segmented LNT-SCR catalyst configurations.
- Perform simulations of the LNT and coupled LNT-SCR unit using the low-dimensional models to examine the performance features and to identify optimal periodic operation and how it depends on the axial and transverse distribution of the catalytic components.

Phase 3

- Study the surface chemistry and dynamics associated with NH_3 storage and consumption during LNT-SCR lean-rich cycling.
- Quantify the NOx storage-reduction behavior of aged LNT-SCR systems so as to pin-point the effects of aging on the different catalyst functions.
- Complete microkinetic model for the LNT-SCR system.
- Carry out modeling study of the LNT-SCR systems for real-time simulation and optimization.
- Experimentally verify model predictions of different segmented LNT-SCR reactor configurations.
- Use low-dimensional models to identify the optimal catalyst architectures and operating strategies of the overall LNT-SCR unit.

Accomplishments

The project is on track versus its objectives. During the second year of the project most of the Phase 1 and 2 objectives are complete with some progress on Phase 3 objectives. Highlights of accomplishments are as follows:

NOx Storage and Reduction: Ammonia Generation

- Through a combined mass spectrometry (MS)-DRIFTS technique, the formation and reactivity of isocyanate in LNT catalysts has been studied.
- Spatially resolved capillary inlet mass spectrometer (SpaciMS) studies have continued to provide

insights into the factors affecting rich phase NOx release and NH_3 formation in LNT catalysts.
- Systematic study of the effects of CO_2 and H_2O, Rh, and CeO_2 on the performance of a family of Pt/Rh/$BaO/CeO_2/Al_2O_3$ monolith catalysts completed.
- Comprehensive study of the reaction system comprising CO, H_2O, and NO carried out elucidates the main pathway to NH_3 generation.
- Crystallite-scale LNT reactor model of NOx storage and reduction has been developed that predicts the effect of Pt crystallite dispersion on the overall conversion and NH_3 selectivity.

Selective Catalytic Reduction: Kinetics, Mechanisms, and Catalyst Comparisons

- Mechanistic-based kinetics study and rate expression developed for standard SCR reaction on Fe/ZSM-5 completed.
- Mechanistic-based kinetics study of NO oxidation on Fe/ZSM-5, Cu/ZSM-5, and Cu/chabazite catalysts completed.
- Experimental study of the extent of washcoat diffusion limitations during several of the key reactions during NH_3-based SCR of NO and NO_2 was completed.
- Conception and development of a new dual-layer monolith catalyst containing Fe- and Cu-zeolite materials conducted shows a large expansion in the temperature window for which high NOx conversion is obtained.

Coupled LNT/SCR

- Sequential LNT/SCR reactor experiments conducted provide insight into coupling between the two catalyst functions.
- Adsorption experiments have shown that significant co-adsorption of NH_3 and propene can occur in the SCR catalyst of LNT-SCR systems. Under lean-rich cycling conditions the contributions of NH_3 and C_3H_6 to NOx conversion in the SCR catalyst are found to be additive.
- Double-layer LNT/SCR catalysts have been synthesized and evaluated.
- A one-dimensional two-phase LNT/SCR model with global rate expressions for various reactions was developed and used to study the performance of combined LNT-SCR catalyst systems. Influence of the architecture of LNT-SCR bricks, non-uniform precious metal loading and the cycle time were investigated.

Future Directions

The project team will converge on critical tasks related to experimental and modeling studies of the LNT/SCR technology. The main focus of the third year will be to conduct focused experiments involving the LNT/SCR sequential and double-layer configurations. As we learn more about the catalytic chemistry and kinetics we can incorporate those findings into models. As individual studies converge to conclusions, manuscripts will be prepared and presentations given at conferences. More specific plans are as follows.

LNT Studies

- **Ongoing Modeling and Simulation Studies.** Modeling will continue in parallel with experimentation. The crystallite-scale model will be further upgraded to include the use of mixtures of H_2 and CO/H_2O in order to move towards more realistic feeds. Kinetic models will be finalized for the LNT catalysts using a combination of bench-scale reactor, DRIFTS reactor, and TAP reactor experiments. The intent is to use the modeling to identify conditions for improved LNT performance, to understand trends in the data, and to recommend new experiments.
- **Coupled Modeling and Experiments.** SpaciMS data in combination with the crystallite-scale LNT model with the goal of finalizing the model for quantitative prediction of NH_3 generation on Pt/BaO LNT catalysts using H_2 as the reductant.

Selective Catalytic Reduction Studies

- **Ongoing Kinetics Study of Transient NOx Reduction with NH_3 on SCR Catalysts.** We will carry out designed transient experiments to probe the transient features of Cu-chabazite and Fe-ZSM-5 catalysts. Kinetic models developed from steady-state studies will be evaluated versus the transient data. Upgrades to the kinetic model will be made as needed and provided to the modeling effort.
- **Development of Predictive SCR Model.** This model will be incorporated into both LNT/SCR models. It will also be used to evaluate the combined Fe/Cu dual-layer and sequential brick catalyst configurations.

LNT/SCR Studies

- **Examination of the Effect of PGM/Ceria Loading on LNT-SCR Performance.** This task is key to determining the effect of reducing Pt loading to reduce overall LNT/SCR cost. A major question to

be answered involves the operating scheme needed to achieve a requisite NOx conversion using a minimal amount of PGM. The ceria may be critical for catalyst durability so it is important to quantify its effect.

- **Ongoing Spatiotemporal Study of LNT-SCR System Performance.** SpaciMS studies include studies on both segmented LNT-SCR systems and the University of Houston double layer LNT-SCR catalyst. This work will seek to identify the optimum system architecture and provide an understanding of the benefits and drawbacks of each approach.
- **Ongoing Synthesis and Study of Dual-Layer LNT-SCR Catalysts.** Dual-layer catalysts made of Pt/BaO/CeO_2/alumina (bottom layer) and Cu-ZSM5 (top layer) will be synthesized and evaluated under cyclic conditions.
- **Identification of Optimal Segmented LNT-SCR Configuration.** Bench-scale testing of the segmented LNT-SCR system will identify the best configuration in terms of overall NOx reduction.
- **Comparison Study of NOx Reduction Selectivity for Segmented LNT-SCR Configurations.** As part of the overall project to determine optimal catalyst configurations, experimental comparisons will be made directly to the segmented configurations to determine which of the configurations provides the highest NOx and NH_3 conversions with minimal PGM loading.
- **Optimization and Real-Time Simulations of LNT-SCR Catalyst with Reactor Model.** Numerical simulations with various catalyst architectures (e.g. segmented, layered) will be performed in order to identify the optimal catalyst distributions and operating strategies (in terms of maximizing NOx conversion with minimal fuel penalty, precious metal loading, operating pressure drop, etc.). Selected bench-scale experiments will be carried out to verify the predictions.

Introduction

The effective removal of NOx from lean exhaust represents a continuing challenge to the automotive industry. The LNT is a promising technology, particularly for light-duty diesel and gasoline lean-burn applications. Literature studies have shown that the performance of the LNT can be significantly improved by adding an in situ SCR catalyst in series downstream. SCR catalysts promote the selective reduction of NOx with ammonia (NH_3) in the presence of excess oxygen. An in situ SCR catalyst refers to a system where the NH_3 is generated in the upstream LNT and subsequently stored on the SCR catalyst where it reacts with NOx that breaks through the LNT. The overarching goal of this project is to advance our understanding of the LNT/SCR technology and to identify the best reactor designs and operating strategies for reducing NOx with NH_3 generated from engine-out NOx.

Approach

The project activities encompass catalyst synthesis and characterization, kinetics and reactor modeling, vehicle exhaust testing, and systems integration (Figure 1). In Phase 1 of the project, the studies focus on two main goals: first, elucidating the mechanism of the non-NH_3 pathway for NOx conversion in LNT-SCR systems and second, developing mechanistic-based kinetic models that describe the dependence of LNT selectivity to NH_3 and of NOx reduction with NH_3 as a function of relevant process parameters and catalyst composition. In Phase 2, efforts are directed towards improving the individual LNT and SCR catalyst functions in terms of NH_3 generation and NOx to N_2 conversion, respectively, and in elucidating the synergies between the LNT and SCR functions during periodic operation of the LNT/SCR. This is accomplished through targeted kinetics, catalyst synthesis, bench-scale reactor, TAP and DRIFTS measurements, and modeling studies, all with the goal of establishing the optimal catalyst architecture (Figure 2) and operating strategy of LNT-SCR catalyst systems that maximizes NOx conversion to N_2. A low dimensional LNT-SCR model is developed that incorporates the main NH_3 reduction pathway is used to quantify NOx conversion for different architectures, including an assessment of potential PGM reduction in LNT-SCR catalyst.

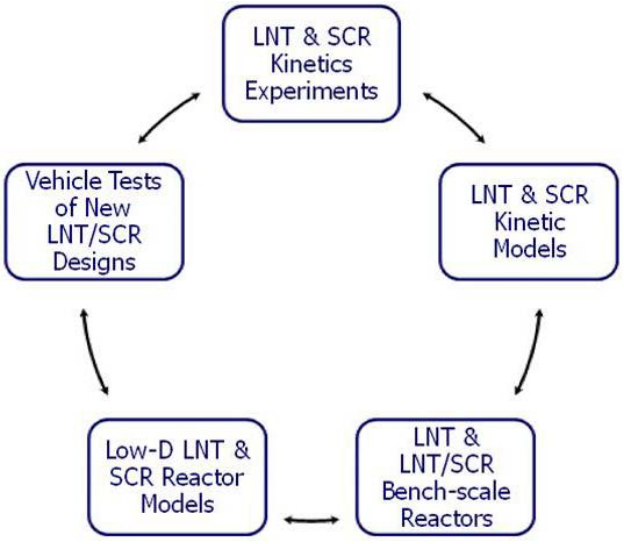

FIGURE 1. Organization of Activities Carried Out by the Project Team

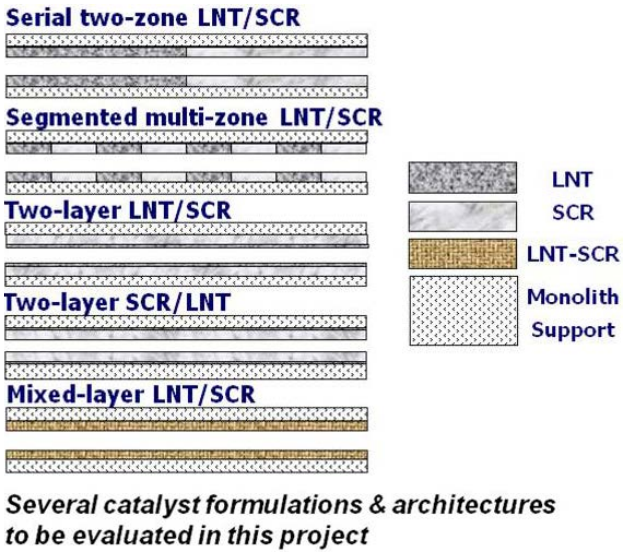

FIGURE 2. Several Catalyst Formulations and Architectures to be Evaluated in this Project

Additional activities include the synthesis of dual-layer SCR and LNT/SCR catalysts. In Phase 3 of the project, a LNT/SCR reactor model based on refined LNT and SCR models is used to evaluate different catalyst architectures spanning segmented zone and dual-layer catalysts. Complementary bench-scale reactor studies are conducted, for model verification and testing of promising designs predicted by the model. Bench-scale and vehicle tests will be conducted to include aged LNT-SCR systems, with the aim of assessing system durability.

Results

Selected results are reported to illustrate activities that have been completed or are in progress.

LNT Studies – NH_3 Generation

DRIFTS studies were performed with the aim of improving our understanding of NOx reduction on LNT catalysts, focusing on the role of isocyanate (representing a pathway for N_2/NH_3 formation when CO is the main reductant). The formation and reactivity of isocyanate was investigated on a model $Pt/BaO/Al_2O_3$ LNT under different atmospheres, including Ar, O_2, H_2O and NO. By means of a combined MS-DRIFTS technique, the evolution of both surface and gaseous species was simultaneously detected during reaction. To minimize reaction of isocyanate with Ba nitrate/nitrite, the approach was to generate NCO species by reaction of $^{15}N^{18}O$ with ^{13}CO at 350 °C (with minor formation of Ba nitrate/nitrite). After saturation of the surface with isocyanate species, the feed gas was switched to the reactant gas of interest. DRIFTS results indicated that isocyanate species are slowly removed under Ar purging, whereas a rapid decrease of –NCO band intensity was observed immediately after switching to H_2O. MS data showed that N_2 formation occurred during both thermal decomposition under Ar and reaction with O_2, NO, NO/O_2 and H_2O. A fast N_2 formation took place in the case of O_2 and NO/O_2, and an extended period of N_2 formation was found during NCO reaction with NO and in Ar. A slight delay of N_2 formation in the case of H_2O can be related to the fact that N_2 is a secondary product from the reaction of NH_3 with residual Ba nitrate (NH_3 being first generated from reaction of NCO with H_2O). Overall the results show that isocyanate species are readily generated on LNT catalysts and are highly reactive with respect to N_2 formation.

SpaciMS was employed to understand the factors influencing the NH_3 selectivity of two fully formulated LNT catalysts, both degreened and aged. Both catalysts contained Pt, Rh, BaO and Al_2O_3, while one of them also contained La-stabilized CeO_2. The amount of reductant required to fully regenerate each catalyst was first determined based on the oxygen storage capacity (OSC) of the catalyst and the NOx storage capacity (NSC). In this way a correction was made for the change in catalyst OSC and NSC after aging, thereby eliminating these as factors which could affect catalyst selectivity to NH_3. For both catalysts, aging resulted in an elongation of the NOx storage-reduction (NSR) zone due to a decrease in the concentration of NOx storage sites per unit catalyst length. In addition to decreased lean phase NOx storage efficiency, stretching of the NSR zone affected catalyst regeneration. Three main effects were identified, the first being an increase of the NOx "puff" that appeared during the onset of the rich front as it traversed the catalyst. Spatially, NOx release tracked the NSR zone, with the result that the NOx concentration peaked closer to the rear of the aged catalysts. Hence the probability that NOx could re-adsorb downstream of the reduction front and subsequently undergo reduction by NH_3 (formed in the reduction front) was diminished, resulting in higher rich-phase NOx slip. Second, the stretching of the NSR zone resulted in increased selectivity to NH_3 due to the fact that less catalyst (corresponding to the OSC-only zone downstream of the NSR zone) was available to consume NH_3 by either the NH_3-NOx SCR reaction or the NH_3-O_2 reaction. Third, the loss of OSC and NOx storage sites lead to an increase in the rate of propagation of the reductant front after aging. This, combined with the decreased rate of diffusion of NOx from the Ba storage sites to the PGM sites (as a result of Pt-Ba phase segregation), resulted in increased H_2:NOx ratios at the Pt/Rh sites and contributed to an increase in catalyst selectivity to NH_3.

The storage and reduction features of a family of $Pt/Rh/BaO/CeO_2/Al_2O_3$ washcoated monolith catalysts were compared in terms of NOx conversion and product selectivity using H_2 as the reductant. Several experimental parameters were varied including the

presence/absence of H_2O and CO_2 in the feed in order to identify trends and to elucidate effects. Pt/BaO is shown to be the most effective catalyst for converting NOx to NH_3. The addition of both CeO_2 and Rh to Pt/BaO increases the cycle-averaged NOx conversion and selectivity to N_2. CeO_2 is shown to be an inferior NOx storage component, but as a supplement to BaO, CeO_2 provides the role of promoting the oxidation of NH_3 to N_2. Fixed NOx storage experiments show the existence of at least two rate controlling regimes, one that is reductant feed rate limited, another that is limited by NOx storage phase diffusion, and a third that has a chemical or textural origin. On Pt/BaO the first two regimes are clearly distinguishable whereas a more complex picture emerges for Pt/CeO_2, with which a fraction of the stored NOx is kinetically inaccessible to reduction. Water inhibits the oxidation of NO on each catalyst but the cycle-averaged NOx conversion is largely unaffected. In contrast, CO_2 has only a minor effect on the conversion during steady-state NO oxidation but significantly inhibits the NOx conversion during cyclic storage and reduction. This effect is attributed to the known higher stability of $BaCO_3$ compared to $BaO/Ba(OH)_2$. The conversion of H_2 to the less effective reductant CO via reverse water-gas shift chemistry is a contributing factor based on steady-state activity tests. Building on the existing literature, most of the observed trends are interpreted in terms of the likely reaction pathways and transport processes.

The steady-state anaerobic reduction of NO was investigated with CO, H_2, $CO+H_2O$ and $CO+H_2$ on $Pt\text{-}BaO/Al_2O_3$ monolith catalyst in the intermediate temperature range (200-300°C). Ammonia is the major product of the $NO + CO + H_2O$ system under conditions of CO inhibition. In the absence of water the strong adsorption of CO leads to sharp transitions between a high rate, mass transport controlled regime and a low rate, kinetically controlled regime. When water is added with the CO feed the regime transitions are more gradual and mitigated by the enhancement afforded by H_2 formed in the water-gas shift (WGS) reaction. Collectively the steady-state findings are consistent with the major NH_3 formation pathway involving reaction of surface H (from WGS) and OH (from water) with adsorbed NO and N with the isocyanate hydrolysis route being only of secondary importance.

A recently developed crystallite-scale regeneration model developed at the University of Houston [1] is extended and additional data is obtained to explain the trends observed during NSR. The storage model is based on the concept of NOx spillover from Pt to BaO and diffusion of stored NOx in the barium phase, and spans a wide range of length scales (Figure 3). The model predicts the main features of NOx storage, such as the increase in NOx breakthrough time for increasing Pt dispersion at fixed Pt loading. The increase in NOx storage with Pt dispersion is a result of (i) an increase in exposed Pt area which increases the intrinsic NO oxidation activity, and (ii) an increase in the interfacial perimeter between Pt and BaO, which promotes the rate of spillover. A sensitivity analysis of the stored NOx diffusivity reveals the importance of this process.

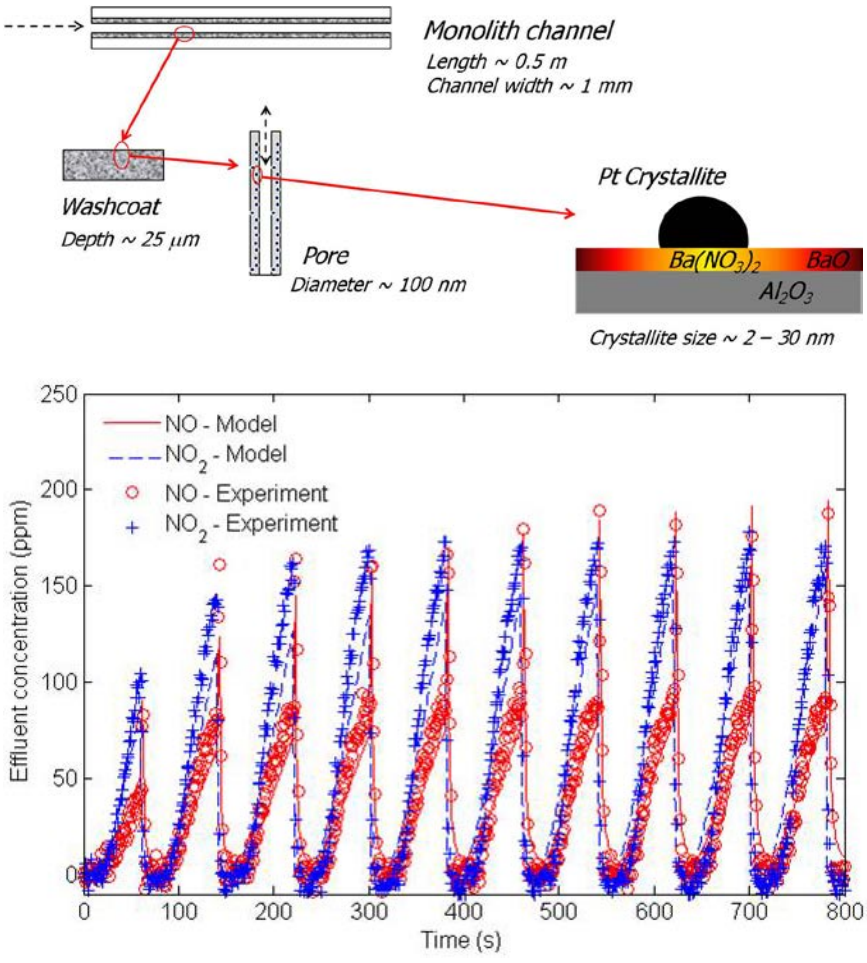

FIGURE 3. The crystallite-scale LNT model spans several length scales. Predictions capture subtle trends in the data such as t he uptake of NO/NO_2 on a pre-reduced Pt/BaO catalyst.

The combined NOx storage and regeneration model is used to simulate the complete lean-rich cycles to elucidate the effects of Pt dispersion on various cycle-averaged variables such as NOx/H_2 conversion and N_2/NH_3 selectivity. The simulation studies show that higher diffusivity of stored NOx during the regeneration is needed to satisfactorily predict the experimentally observed conversion and selectivity trends. This finding clearly suggests the involvement of enhanced diffusion during the regeneration. The model effectively captures the dependence of cycle-averaged selectivity and conversion on Pt dispersion and rich time. The model shows that the lower dispersion catalyst is not able to utilize all of the available barium sites because NOx diffusion is too slow to access barium sites far from the Pt crystallites. Finally, the model is used to study various storage and regeneration timing protocol which shows that shorter storage time is required for lower dispersion catalysts to achieve higher cycle-averaged NOx conversion. The model finding explains the experimentally observed trend that aging of NSR catalysts leads to enhanced ammonia production.

SCR – Non-NH_3 and NH_3-Based Pathways

In initial work in this project, it was shown that in addition to the NH_3 pathway for NOx conversion, a second pathway can operate in the SCR catalyst of LNT-SCR systems which is associated with the presence of hydrocarbons. LNT-SCR lean-rich cycling experiments revealed that when a CO+H_2+C_3H_6 mixture or C_3H_6 by itself was used as the reductant, more NOx was converted over the SCR catalyst than could be accounted for by NH_3 emitted from the LNT catalyst. This finding is attributed to the reaction of propene, which slipped through the LNT catalyst, with NOx slip from the LNT. Separate experiments, conducted under continuous flow and lean-rich cycling conditions, have confirmed the ability of propene and ethene to function as NOx reductants over the SCR catalyst. More recent cycling experiments have shown that the SCR catalyst is able to store propene (see Figure 4), such that NOx reduction by stored propene can continue into the lean phase (after the switch from rich conditions). According to the results of adsorption experiments, significant co-adsorption of NH_3 and propene can occur in the SCR catalyst, while under lean-rich cycling conditions the contributions of NH_3 and C_3H_6 to NOx conversion are found to be essentially additive. This finding suggests that under actual driving conditions, NOx reduction by non-NH_3 reductants (olefins and other hydrocarbons) in the SCR catalyst can contribute to the mitigation of NOx emitted by the LNT catalyst during rich phase regeneration, in addition to NOx that slips from the LNT catalyst during the initial part of the lean phase.

A comprehensive study of standard and fast SCR on Fe-zeolite catalysts was conducted. The reaction

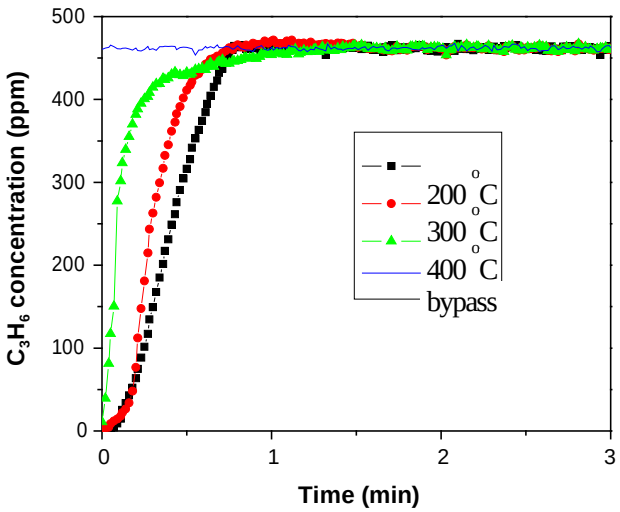

FIGURE 4. Adsorption of C_3H_6 on Cu-zeolite SCR catalyst at different temperatures. Feed: 460 ppm C_3H_6, 5% CO_2, 5% H_2O, N_2 as balance.

system was studied in a bench-flow reactor spanning a range of temperature, space velocity and washcoat thickness, affording an assessment of activity and selectivity, reaction pathways, temperature window, mass transport and pore diffusion effects. Experiments included NH_3 uptake and temperature-programmed desorption, steady-state and transient NO and NH_3 oxidation and standard SCR (NO+NH_3+O_2) reaction studies. In the temperature range of 200–300°C the standard SCR reaction was found to be nearly first-order and half-order with respect to NO and O_2, respectively, but moderately negative-order (-0.3) with respect to NH_3. Agreement in the kinetics for both reaction systems suggests that the oxidation of NO is the rate determining step, in line with recent literature studies. Rate inhibition by ammonia appears to be the result of blockage of NO oxidation reaction sites; a necessary step for the standard SCR reaction. Water is shown to inhibit the oxidation of NO significantly and of NH_3 to a moderate extent, while having only a negligible effect on the standard SCR reaction. A mechanistic-based Langmuir-Hinshelwood kinetic model is proposed in which NH_3 reacts with surface bound NO_2 and nitrous acid via a NH_4NO_2 intermediate. A redox mechanism in which gaseous NO reacts with adsorbed oxygen (Eley Rideal like reaction) cannot be ruled out. In the absence of NH_3 these species serve to inhibit the adsorption of NO and/or O_2 during NO oxidation. Both external mass transfer limitations and washcoat diffusion limitations were ruled out for moderate temperature conditions (≤300°C). However, experiments on monoliths with different washcoat thicknesses conclusively show the appearance of washcoat diffusion limitations at higher temperatures (≥350°C).

Another study involved an examination of the role of mass transport during SCR on Fe- and Cu-zeolite catalysts. An experimental study of steady-state SCR of NOx with NH_3 on both Fe-ZSM-5 and Cu-ZSM-5 monolithic catalysts was carried out to investigate the extent of mass transfer limitations in various SCR reactions. Catalysts with different washcoat loadings, washcoat thicknesses and lengths were synthesized for this purpose. SCR system reactions examined included NO oxidation, NH_3 oxidation, standard SCR, fast SCR, and NO_2 SCR. Comparisons of conversions obtained on catalysts with the same washcoat volumes but different washcoat thicknesses indicated the presence of washcoat diffusion limitations. NH_3 oxidation, an important side reaction in SCR system, showed the presence of washcoat diffusion limitations starting at 350°C on Fe-zeolite and 300°C on Cu-zeolite catalysts. Washcoat diffusion limitations were observed for the standard SCR reaction ($NH_3 + NO + O_2$) on both Fe-zeolite (≥350°C) and Cu-zeolite (≥250°C). For the fast ($NH_3 + NO + NO_2$) and NO_2 SCR ($NH_3 + NO_2$) reactions, diffusion limitations were observed throughout the temperature range explored (200-550°C). Even though the observed differences in conversions clearly indicate the presence of washcoat diffusion limitations, the contribution of external mass transfer was also found to be important under certain conditions. The transition temperatures for shifts in controlling regimes from kinetic to washcoat diffusion to external mass transfer are determined using simplified kinetics. The findings indicate the need to include of mass transfer limitations in SCR modeling, design and optimization.

The finding that NO oxidation is the rate limiting step for the standard SCR reaction prompted the study of NO oxidation on Fe-ZSM-5, Cu-ZSM-5 and the recently commercialized small pore Cu-chabazite catalysts. Steady-state integral measurements of NO oxidation showed Fe-zeolite to be a more active NO oxidation catalyst than Cu-zeolite. Both NO_2 temperature programmed desorption and decomposition experiments show that the NO_2 is more strongly bound on the Cu-chabazite compared to the Fe-ZSM-5. Increasing amounts of NO_2 in the NOx feed decreased the NO oxidation activity on both the catalysts. Differential kinetic studies carried out in the temperature range of 200-290°C show a positive order rate dependence of NO oxidation reaction with respect to both NO (~1) and O_2 (~0.5) while showing a negative order dependence with respect to NO_2 (-0.5 to -1), which confirms that NO_2 inhibits the NO oxidation reaction. NO_2 inhibition on NO oxidation was found to be more severe on Cu-chabazite (~ -1 order) compared to Fe-ZSM-5 (~ -0.5 order). The presence of feed water strongly inhibited the NO oxidation reaction. Transient NOx uptake experiments reveal nitrate formation on both catalysts. A global kinetic model is developed which accurately predicts the experimentally observed reaction orders, NO conversions and NO_2 and water inhibition effects for a wide temperature range and different feed conditions (Figure 5). The kinetic model confirms the experimentally observed instability of nitrates in the presence of feed NO and shows that the steady state NO oxidation data can be predicted with a kinetic model in which reaction between adsorbed O atoms and gaseous NO as the rate determining step.

The findings of the Fe- and Cu-zeolite catalysts led us to address the question whether the two catalysts can be combined to give a superior SCR catalyst. The effectiveness of a catalytic system comprising Fe- and Cu-based zeolites was examined for the standard ($NO + O_2 + NH_3$) and fast ($NO + NO_2 + NH_3$) SCR reactions. Experiments carried out with in-house and commercial Fe- and Cu-zeolite monoliths of varying lengths quantified their relative SCR activities. Three configurations of combined Fe and Cu-zeolite catalysts were compared: (1) "sequential brick" catalyst comprising Fe-zeolite and Cu-zeolite monolith; (2) "mixed washcoat" catalyst comprising a washcoat layer having equal mass fractions of Fe- and Cu-zeolites; (3) "dual layer" catalyst comprising monolith coated with individual layers of Fe- and Cu-zeolites of different thicknesses and mass fractions. The sequential brick design with Fe-zeolite brick followed by a Cu-zeolite brick gave a higher conversion than the Cu/Fe sequence of equal loadings with the Fe(33%)/Cu(67%) achieving the highest NOx conversion over a wide range of temperatures. The mixed washcoat catalyst achieved NOx conversion that was nearly an average of the individual Fe-only and Cu-only catalysts. The dual layer catalyst with a thin Fe-zeolite (33% of the total washcoat loading) layer on top of a thicker Cu-zeolite layer (67%) resulted in very high NOx removal efficiencies over a wide temperature range for both the standard and fast SCR reactions (Figure 6). The performance

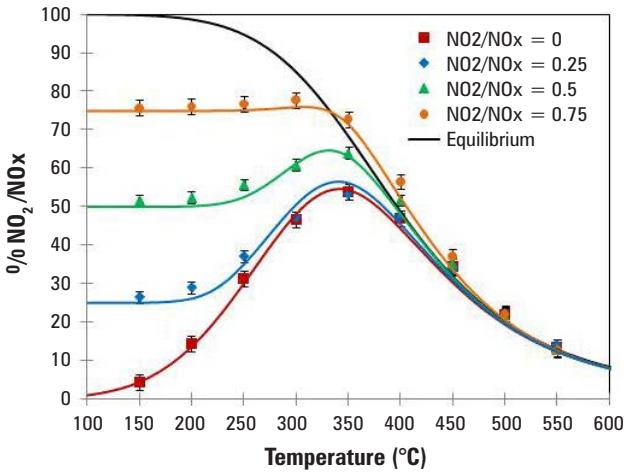

FIGURE 5. Comparison of experimental data and model prediction of NO conversion during NO oxidation on Fe-ZSM5 SCR catalyst.

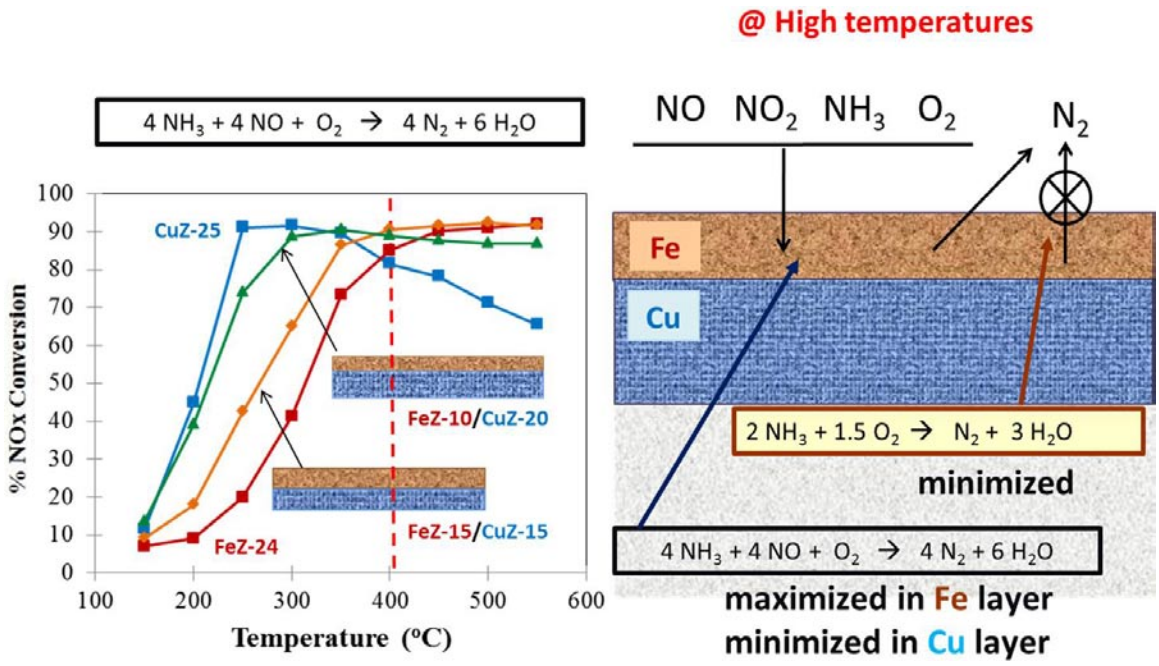

FIGURE 6. The dual-layer Fe/Cu monolith catalyst out-performs single layer Fe- and Cu-zeolite catalysts.

of this dual-layer system was comparable to the series arrangement of Fe and Cu-bricks. The Cu-zeolite on Fe-zeolite dual layer catalyst was not nearly as effective for the same loadings. Similar results were obtained for the fast SCR reaction. An assessment of the extent of washcoat diffusion limitations shows that the dual layer configuration is superior to the sequential brick configuration.

LNT/SCR Studies – Understanding Synergies of NH_3 Generation and NOx Reduction

A one-dimensional two-phase model with global rate expressions for various reactions is used to study the performance of combined LNT-SCR catalyst systems. Influence of the architecture of LNT-SCR bricks, non-uniform precious metal loading and the cycle time are investigated at three different temperatures in the range of 200°C–350°C. It is desirable to enhance the NO decomposition efficiency of combined LNT-SCR catalyst systems by maintaining the minimal amount of precious metal loading. NOx storage and reduction simulations are conducted on $Pt/BaO/Al_2O_3$ catalyst with two different BaO storage sites, designated as fast and slow sites. Similarly, Cu-ZSM5 catalyst is chosen for studying the SCR of NOx using NH_3. The model predicts the spatio-temporal concentration profiles of reactants and products inside the channel, which gives insight into the performance of each LNT and SCR catalyst during operation. It is found that series arrangement of alternate LNT and SCR catalysts, by dividing them into equal halves, improves NOx conversion. For fixed total catalyst length as the number of divisions increase, NOx conversion increases and reaches a limit which is theoretically equivalent to that of mixed catalyst. Spatio-temporal profiles indicate complete storage of NH_3 on SCR catalyst which can be efficiently used to reduce NOx slipping out of LNT. Further, non-uniform precious metal loading in LNT bricks contributes to the improvement in the NO decomposition performance of the combined system, especially at lower temperatures. Finally cycle time is found to have a significant impact on the NOx conversion. We investigated the impact of dividing each catalyst into equal fractions and arranging in alternative fashion. The total length of the combined LNT-SCR catalyst is fixed at 4 cm. A second study involves fixed total length of the combined catalyst with a varying ratio of the LNT to SCR lengths ('λ'). Here again the total length of the combined system is fixed at 4 cm. A schematic of the catalyst architecture studied is as shown in Figure 7. Here 'n' denotes number of LNT-SCR pair of bricks. Simulations are conducted at three different temperatures (237°C, 275°C, 335°C) and the results (at 335°C) are shown in Figure 7. In the figure cycle averaged NOx conversion is plotted against '1/n'. Further studies have been conducted on the combined LNT-SCR systems with two pairs of LNT and SCR bricks (n=2), by reducing the cycle time. The simulations shown in Figure 7 correspond to the temperature of 335°C. As the cycle time is reduced rapid regeneration occurs and less NOx slips out of the LNT brick. Hence the performance of combined LNT-SCR system increases as the cycle time is reduced. The impact of cycle time seems to be the dominant one

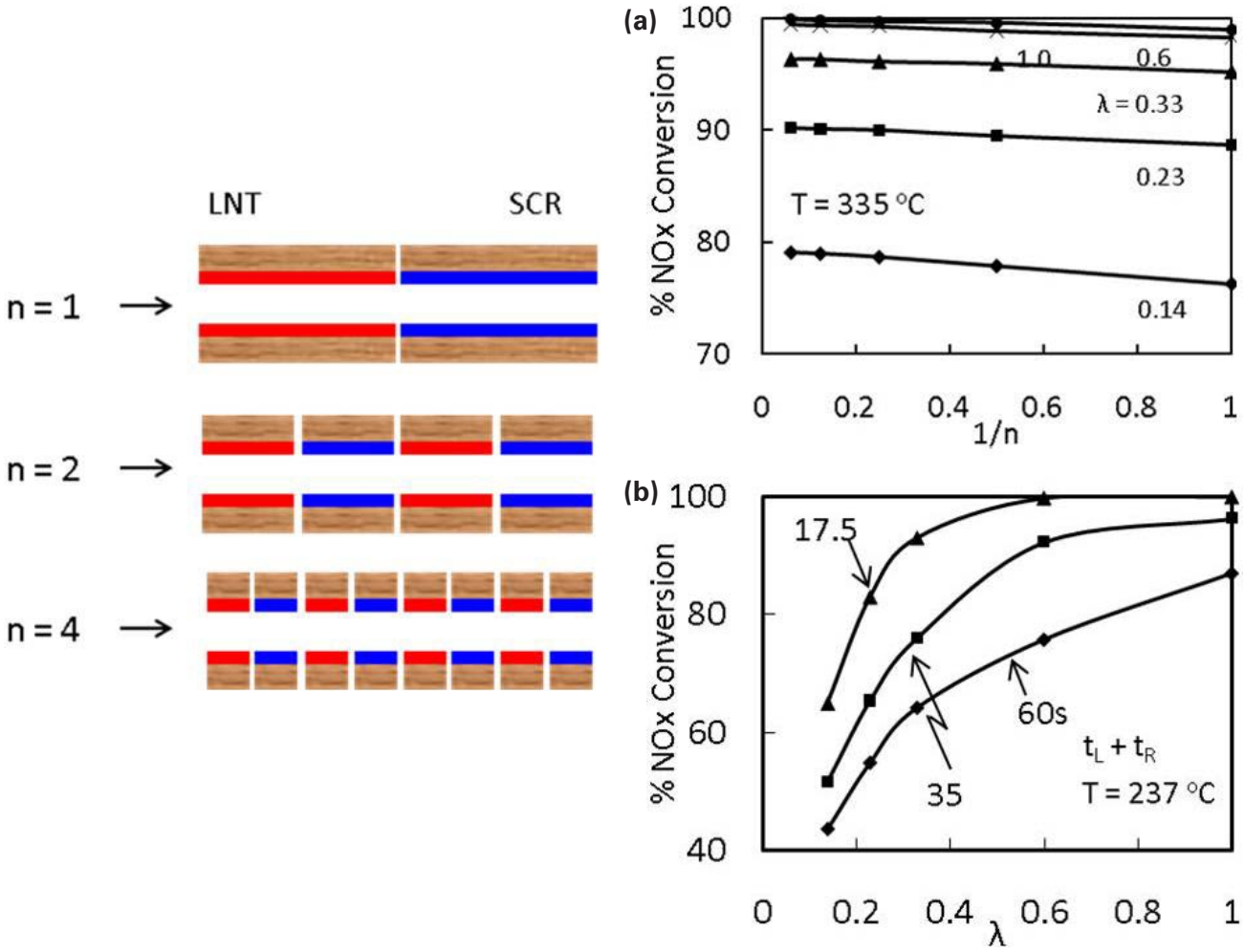

FIGURE 7. LNT/SCR model predictions on the effect of segmenting the LNT and SCR bricks. (Left) Architecture of n pairs of LNT-SCR bricks with fixed total length. (Right) (a) Dependence of cycle averaged NOx conversion on 'n' and 'λ' which is the length ratio of LNT to SCR. (b) Influence of total cycle time ($t_L + t_R$; $t_L = 6t_R$) on NOx conversion with two pairs (n=2) of LNT and SCR bricks.

among the parameters studied with approximately 15% improvement in NOx conversion for λ=0.33. Detailed results will appear in a forthcoming publication.

Synthesis and evaluation of dual-layer LNT/SCR monolithic catalysts were conducted. Both Fe- and Cu-containing zeolite layer was coated onto a Pt/BaO based LNT catalyst. Cycling studies showed the synergy of the two layers; NH_3 generated by the underlying LNT layer was trapped by the top layer of zeolite where it reacted with NO to form N_2. The addition of the SCR layer was shown to significantly enhance the N_2 selectivity. However, some undesired trapping of NO in the SCR layer led to an unexpected decrease in the overall NOx conversion. These preliminary findings are encouraging and have prompted a comprehensive study of a number of parameters such as the thicknesses of the two layers.

Summary

This project combines kinetics measurements, bench-scale reactor studies, and analytical methods including spatially-resolved mass spectrometry to advance the understanding of LNT, SCR, and LNT/SCR systems. Kinetic models are being developed based on measurements for the LNT and SCR chemistries, to be incorporated into reactor models for design and optimization. A LNT/SCR reactor model based on literature kinetics provides insight into potential improvements through zoning of LNT and SCR sections. Synthesis of double-layer SCR and LNT/SCR catalysts show the potential for novel catalyst compositions and architectures for improved performance. A double-layer Fe/Cu-based SCR catalyst exhibits significant expansion in the temperature window for which high NOx conversion is obtained. Initial findings with

double-layer LNT/SCR catalysts reveal potential for further improvements in terms of NOx conversion, N_2 selectivity, and precious metal utilization.

References

1. D. Bhatia, M.P. Harold and V. Balakotaiah, Catalysis Today 151 (2010) 314.

Fiscal Year 2011 Publications/Presentations

Publications

1. Joshi, S., Y. Ren, M.P. Harold, and V. Balakotaiah, "Determination of Kinetics and Controlling Regimes for H_2 Oxidation on Pt/Al_2O_3 Monolithic Catalyst Using High Space Velocity Experiments," *Applied Catalysis B: Environmental*, **102**, 484–495 (2011).

2. Metkar, P., N. Salazar, R. Muncrief, V. Balakotaiah, and M.P. Harold, "Selective Catalytic Reduction of NO with NH_3 on Iron Zeolite Monolithic Catalysts: Steady-State and Transient Kinetics ," *Applied Catalysis B: Environmental*, **104**, 110–126 (2011).

3. Kumar, A., X. Zheng, M.P. Harold, and V. Balakotaiah, "Microkinetic Modeling of the NO + H_2 System on Pt/Al_2O_3 Catalyst Using Temporal Analysis of Products ," *J. Catalysis*, **279**, 12–26 (2011).

4. Xu, J., M. Harold, and V. Balakotaiah, "Microkinetic Modeling of NOx Storage on $Pt/BaO/Al_2O_3$ Catalysts: Pt Loading Effects," *Applied Catalysis B: Environmental*, **104**, 305-315 (2011).

5. Wang, J., Y. Ji, U. Graham, C. Spindola Cesar de Oliveira, M. Crocker, "Fully Formulated Lean NOx Trap Catalysts Subjected to Simulated Road Aging: Insights from Steady-State Experiments", *Chin. J. Catal.*, **32** (2011) 736.

6. Wang, J., Y. Ji, V. Easterling, M. Crocker, M. Dearth, R.W. McCabe, "The effect of regeneration conditions on the selectivity of NO_x reduction in a fully formulated lean NOx trap catalyst", *Catal. Today*, 175 (2011) 83.

7. Ji, Y., V. Easterling, U. Graham, C. Fisk, M. Crocker, J,-S. Choi, "Effect of aging on the NO_x storage and reduction characteristics of fully formulated lean NO_x trap catalysts", *Appl. Catal. B* 103 (2011) 413.

8. Liu, Y., M.P. Harold, and D. Luss, "Spatiotemporal Features of $Pt/CeO_2/Al_2O_3$ Catalysts During Lean/Rich Cycling," *Applied Catalysis A, General*, **397**, 35-45 (2011).

9. Ren, Y., and M.P. Harold, "NOx Storage and Reduction with H_2 on $Pt/Rh/BaO/CeO_2$: Effects of Rh and CeO_2 in the Absence and Presence of CO_2 and H_2O," *ACS Catalysis*, 1, 969-988 (2011).

10. Metkar, P., V. Balakotaiah, and M.P. Harold, "Experimental Study of Mass Transfer Limitations in Fe- and Cu-Zeolite Based NH_3-SCR Monolithic Catalysts," *Chem. Eng. Sci.*, **66**, 5192–5203 (2011).

11. Wang, J., Y. Ji, Z. He, M. Crocker, M. Dearth, R.W. McCabe, "A Non-NH_3 Pathway for NOx Conversion in Coupled LNT-SCR Systems", Appl. Catal. B, in press; available at: 10.1016/j.apcatb.2011.11.008.

12. Metkar, P., V. Balakotaiah, and M.P. Harold, "Experimental Study of Selective Catalytic Reduction of NO_x on a Combined System of Fe and Cu-based Zeolite Monolithic Catalysts," *Appl. Catal. B. Environmental*, in press (October, 2011).

13. Joshi, S., Y. Ren, M.P. Harold, and V. Balakotaiah, "Determination of Kinetics and Controlling Regimes for Propylene and Methane Oxidation on Pt/Al_2O_3 Monolithic Catalyst Using High Space Velocity Experiments," *Ind. Eng. Chem. Res.*, in press (October, 2011).

14. Kota, A., D. Luss and V. Balakotaiah, "Modeling and Optimization Studies of Combined LNT-SCR Catalyst Systems", Ind. Engng. Chem. Res., under review (October, 2011).

15. Metkar, P., N. Salazar, R. Muncrief, V. Balakotaiah, and M.P. Harold, "Experimental and Kinetic Modeling Study of NO Oxidation: Comparison between Fe and Cu-zeolite Catalysts," Catalysis Today, revisions pending (October, 2011).

16. Shakya, B., M.P. Harold, and V. Balakotaiah, "Modeling the Effects of Pt Dispersion During NO_x Storage and Reduction on $Pt/BaO/Al_2O_3$," Catalysis Today, revisions pending (October, 2011).

17. Dasari, P., R. Muncrief, and M.P. Harold, "Elucidating NH_3 Formation During NO_χ Reduction by CO on Pt-BaO/Al_2O_3 in Excess Water," Catalysis Today, revisions pending (October, 2011).

Presentations

1. "Kinetic and Mechanistic Studies of Selective Catalytic Reduction of NO_x on Fe-Zeolite Monolithic Catalysts," presented at the AIChE National Meeting, Salt Lake City, 11/10 (with P. Metkar, presenter, R. Muncrief, V. Balakotaiah).

2. "Steady-state Reactions of NO, CO and H_2O on Pt-Ba/Al_2O_3 Monolith," presented at the AIChE National Meeting, Salt Lake City, 11/10 (with P. Dasari, presenter, R. Muncrief).

3. "TAP Studies of NOx Reduction Using H_2 and NH_3," presented at the AIChE National Meeting, Salt Lake City, 11/10 (with A. Kumar, V. Balakotaiah).

4. "Effect of Pt Dispersion On Observed Kinetics During Oxidation of H_2 On Pt/Al_2O_3 Monolithic Catalyst," presented at the AIChE National Meeting, Salt Lake City, 11/10 (with S. Joshi, V. Balakotaiah).

5. "Effect of Pt Dispersion On Observed Kinetics: Oxidations of Methane and Propylene On Pt/Al_2O_3 Monolithic Catalyst," presented at the AIChE National Meeting, Salt Lake City, 11/10 (with V. Balakotaiah, presenter, S. Joshi).

6. "Determination of Controlling Regimes in Catalytic Monoliths," presented at the AIChE National Meeting, Salt Lake City, 11/10 (poster; with V. Balakotaiah, presenter, S. Joshi).

7. "TAP Studies of NOx Reduction," presented at the Spring National Meeting of ACS, Anaheim, 3/10 (with X. Zheng, A. Kumar, V. Balakotaiah).

8. V. Easterling, M. Crocker, M. Dearth, R.W. McCabe, M.P. Harold, "A Spatio-temporal Study of Lean NOx Trap Regeneration", oral presentation (OB09) at the 22nd North American Catalysis Society Meeting, June 5–10, 2011, Detroit, MI.

9. M. Dearth, G. Cavataio, L. Xu, H. Jen, R.W. McCabe, J. Wang, Y. Ji, L. He, M. Crocker, "A Non-NH_3 Pathway for NOx Conversion in Coupled LNT-SCR Systems", oral presentation (OC19) at the 22nd North American Catalysis Society Meeting, June 5–10, 2011, Detroit, MI.

10. C. Shi, Y. Ji, T.J. Toops, M. Crocker, "NO_x Storage and Reduction Properties of Ceria-based Lean NO_x Trap Catalysts", poster presentation (P-Mo-119) at the 22nd North American Catalysis Society Meeting, June 5–10, 2011, Detroit, MI.

11. M. Harold, Catalysis Club of Philadelphia, *Multi-Functional Catalysts and Reactors for Lean NOx Reduction*, Newark, DE, 5/11.

12. M. Harold, North American Catalysis Society, North American Meeting, Keynote Lecture: *Probing and Exploiting Interactions between Storage, Reaction and Transport Processes During Lean NOx Reduction*, Detroit, MI, 6/11.

13. "Kinetic and Mechanistic Studies of Selective Catalytic Reduction of NO_x on Cu- and Fe-Zeolite Monolithic Catalysts," presented at the North American Catalysis Society Meeting, Detroit, 6/11 (with P. Metkar, presenter, V. Balakotaiah).

14. "Steady-state Reactions of NO, CO and H_2O on Pt-Ba/Al_2O_3 Monolith," presented at the North American Catalysis Society Meeting, Detroit, 6/11 (with P. Dasari, presenter, R. Muncrief).

15. C. Shi, Y. Ji, U. Graham, G. Jacobs, T.J. Toops, M. Crocker, "NOx storage and reduction properties of ceria-promoted lean NOx trap catalysts", oral presentation at the 242nd ACS National Meeting, Denver, CO, August 28-September 1, 2011, FUEL-2; Preprints of Symposia - American Chemical Society, Division of Fuel Chemistry, 2011, 56(2), 3-4.

16. M.P. Harold, M. Crocker, M. Dearth, R. McCabe, V. Balakotaiah, D. Luss, J.S. Choi, "Development of Optimal Catalyst Designs and Operating Strategies for Lean NO_x Reduction in Coupled LNT-SCR Systems", poster presented at the 2010 Directions in Engine-Efficiency and Emissions Research (DEER) Conference, Detroit, MI, September 27–30, 2010.

Patents

1. Harold, M.P., and P. Metkar, US Provisional Patent Application, "Multi-Component and Layered Formulations for Enhanced Selective Catalytic Reduction Activity," June 6, 2011.

IV.5 Three-Dimensional Composite Nanostructures for Lean NO_x Emission Control

P.-X. Gao[1] (Primary Contact), S.P. Alpay[1], R. Ramprasad[1], C. Brooks[2]

[1] University of Connecticut
97 North Eagleville Road
Storrs, CT 06269-3136

[2] Honda Research Institute
1381 Kinnear Road, Suite 116
Columbus, OH 43212

DOE Technology Development Manager: Kenneth Howden

NETL Project Manager: Ralph Nine

Fiscal Year (FY) 2011 Objectives

- Synthesize three-dimensional (3D) metal oxide nanowire arrays on both planar and monolith substrates.
- Fabricate 3D mesoporous metal oxide/perovskite composite structured nanowire arrays on both planar and monolith substrates.
- Characterize the chemical, morphology and structure of the grown metal oxide and metal oxide/perovskite composite nanostructures using a wide array of electron microscopy and spectroscopy techniques.
- Investigate the thermal and mechanical stability, CO and NO catalytic oxidation performance of fabricated planar and monolithic nanowire catalysts.
- Investigate the oxygen interactions with perovskite surfaces using first principle thermodynamics (FPT) and kinetic Monte Carlo (KMC) simulations.

Accomplishments

- Successful synthesized and characterized 3D metal oxide nanowire/rod arrays (such as ZnO and TiO_2, etc.) on both planar and monolith substrates.
- Successfully fabricated and characterized the Pt-deposited 3D composite nanowire/rod array (such as ZnO/(La,Sr)CoO_3(LSCO) and TiO_2/(La,Sr)MnO_3(LSMO), etc.) on both planar and monolith substrates.
- Investigated the thermal and mechanical stability, CO and NO oxidation performance of the above-mentioned 3D nanostructures.
- Investigated the oxygen interactions with perovskite (such as [La,Sr]MnO_3[LSMO], etc.) surfaces by the FTP and KMC simulations.

Future Directions

- Further optimize and quantitatively characterize the 3D composite nanowires/nanorods array based on metal oxides (e.g., ZnO, and TiO_2) and perovskite (e.g., LSMO, LSCO).
- Load precious metal nanoparticles (Pt, Au, Pd) before and after barium oxide and perovskite nanofilm loading on metal oxide 3D composite nanowires/nanorods array.
- Further evaluate the catalytic performance of 3D composite nanowires/nanorods arrays on the thermal stability, S-resistance and NO_x storage and reduction performance.
- Calculate the O_2, NO and NO_2 catalytic interactions with various surfaces of LSMO and LSCO, involving dopants like Sr.

Introduction

Nowadays, lean-burn engines are attracting more and more attention than conventional gasoline engines due to their higher fuel efficiency and lower CO_2 emissions [1-6]. However, under lean-burn conditions, the nitrogen oxides (NO_x) exhaust emissions cannot be efficiently reduced over the classical three-way catalysts in the presence of excessive O_2 [1,4,7]. The NO_x emissions have multi-fold hazards on the atmosphere, environment and human health, due to the formation of fine particles, ozone smog, acid rain and eutrophication [8]. NO_x storage/reduction technology is regarded as one of the most promising exhaust after-treatment technologies for lean-burn gasoline and diesel vehicles. Our overall project objective is to synthesize, characterize and model a new class of oxide-based 3D composite nano-catalysts for the NO_x storage, and NO_x reduction, HC and CO oxidation, and particular matter filtering under lean-burn conditions.

Approach

In the theory part, we use the FPT and KMC simulation approaches to construct surface phase diagrams of (001) AO- and BO_2-terminated ABO_3 perovskite surfaces and choose gaseous O_2 as the principal source of surface oxygen. In the experimental part, we use wet chemical methods to synthesize metal oxide nanowires arrays on planar and 3D honeycomb substrates. Sputtering and sol-gel methods were used to combine with wet chemical methods to fabricate

Pt/metal oxide/perovskite 3D composite nanostructure arrays. Annealing was used to improve the crystallity and stoichiometry of 3D composite nanostructures.

Results

During the past year, we have successfully synthesized metal oxides (such as ZnO and TiO_2, etc.) nanowire arrays and metal oxide/perovskites (such as LSMO, LSCO, etc.) composite nanowire arrays on 3D monolithic substrates such as ceramic cordierite and stainless steel.

Figures 1a, 1c and 1e show top view scanning electron microscope (SEM) images of ZnO nanorod arrays with different diameters rooted on 3D monolithic ceramic honeycomb (CH) substrate. From the cross-sectional view SEM images in Figures 1b, 1d and 1f, the average length of nanorods increases from 749 nm to 866 nm from sample A to sample C. However, the increasing trend does not apply to average diameter. Statistical results show that sample B has the smallest average diameter (84 nm), while both sample A and sample C have larger diameter about 153 nm and 121 nm, respectively. Therefore, sample B has the largest length/diameter aspect ratio (~10.2). Figure 2a shows a typical CH substrate with TiO_2 nanorods array grown on it. The CH substrate with 1 mm×1 mm square channels and 100 μm wall thickness is about 1 inch in diameter and 1 inch in height. As-synthesized TiO_2 nanorods arrays are highly uniform, aligned and densely packed on the side wall of CH channels. The TiO_2 nanorods are ~50 nm-130 nm in diameter and ~500 nm-1 μm long. Figure 2e indicates individual TiO_2 nanorod is of single crystalline. The high-resolution transmission electron microscope (TEM) image in Figure 2f demonstrates the completely crystallized nanorod with clear lattice fringes parallel to the wall. An inter-planar spacing of 0.34 nm is clearly imaged corresponding to the (11-1) plane perpendicular to the nanorod axis. The TEM images imply that the nanorod grows along the (11-1) crystal plane with a preferred [301] direction. The selected area electron diffraction pattern (inset of Figure 2e) confirms the single-crystalline brookite-TiO_2 nanorods.

Based on the metal oxide nanowire arrays, 3D metal oxide/perovskite composite nanowire arrays

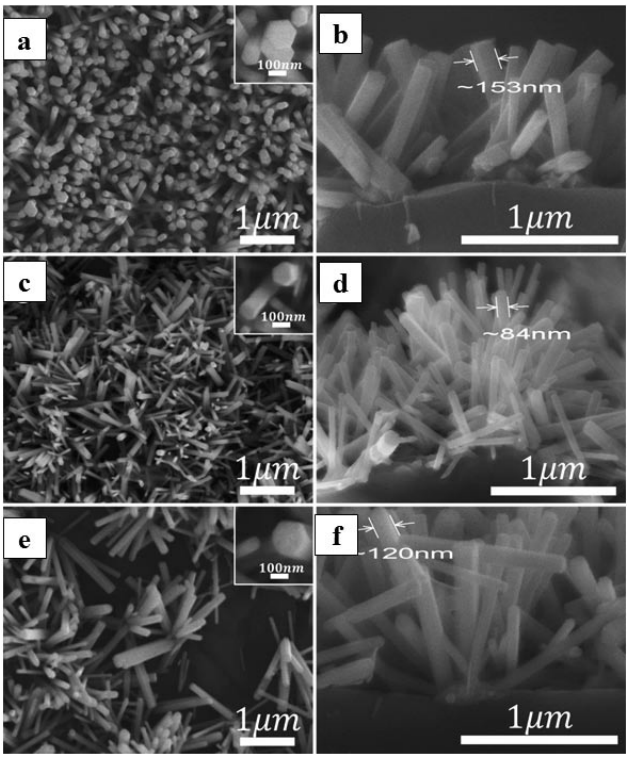

FIGURE 1. SEM micrographs of ZnO nanowire arrays on ceramic honeycomb (CH) substrates synthesized at different temperatures: 70°C (a and b); 80°C (c and d); 90°C (e and f). Other parameters were kept fixed. Plane view: a, c and f; cross-section view: b, d and f.

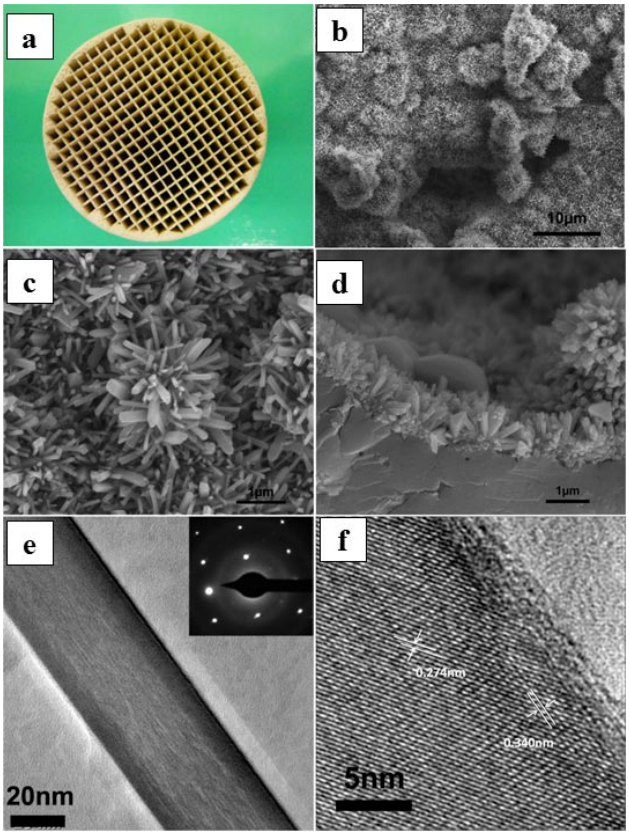

FIGURE 2. a) Photograph of typical CH substrate with TiO_2 nanorods array on it; b) a low-magnification SEM image of large-area TiO_2 nanorods arrays on the inside wall of CH substrate; c) a top-view high-magnification SEM image TiO_2 nanorods arrays; d) a cross-sectional view SEM image of the TiO_2 nanorods arrays on CH substrate; e) a TEM image of a typical TiO_2 nanorod and the corresponding selected area electron diffraction pattern (inset); f) a high-resolutin TEM image of TiO_2 nanorod.

were fabricated on CH substrate, with an example on ZnO/LSCO displayed in Figures 3a and 3b. The synthesized ZnO/ LSCO/Pt nanorods are ~30 nm-120 nm in diameter and ~1-5 μm long. The rough surface of ZnO/LSCO/Pt nanowires is due to the mesoporous LSCO nanofilm grown on the ZnO nanorod surface. Figure 3c shows the TEM image of two typical ZnO/LSCO/Pt composite nanorods. From Figures 3d and 3e, we can clearly see the fine nanoparticles on the rough nanorod surface. From energy-dispersive X-ray spectroscopy results (Figue 3f), we can see element information of Zn, La, Sr, Co and Pt, in ZnO/LSCO/Pt nanorods. In addition, Figures 4a and b show the large area TiO_2/LSMO nanorod arrays on Si planar substrate. The inset in Figure 4a depicts TiO_2/LSMO composite nanorod arrays and TiO_2 nanorod arrays on Si substrate. After 800°C ambient annealing, the X-ray diffraction pattern of TiO_2/LSMO composite nanorod array displays an obvious peak at 32.9° as indicated by an arrow in Figure 4d, matching to the (110) atomic planes of cubic perovskite $La_{0.8}Sr_{0.2}MnO_3$.

Various 3D metal oxide nanowire arrays on monolith substrates have been studied on their thermal and mechanical stabilities, including ZnO/LSCO and TiO_2/LSMO systems. Under high temperature reductive and oxidative atmospheres, they have been demonstrated to be of very good thermal (up to 800°C) and mechanical stability [9]. Here instead of highlighting the stability, we highlight the catalytic performance results over CO and NO oxidation, as described in the following.

To evaluate the catalytic performance of TiO_2/LSMO composite nanorod array, CO oxidation was monitored over the 800°C annealed TiO_2/LSMO composite nanorod array and TiO_2 nanorod array on Si substrate separately. Figure 4e shows temperature programmed CO oxidation conversion curves of the TiO_2/LSMO composite nanorod array and TiO_2 nanorod array, respectively. The onset oxidation temperature of TiO_2/LSMO composite nanorod array is ~330°C,

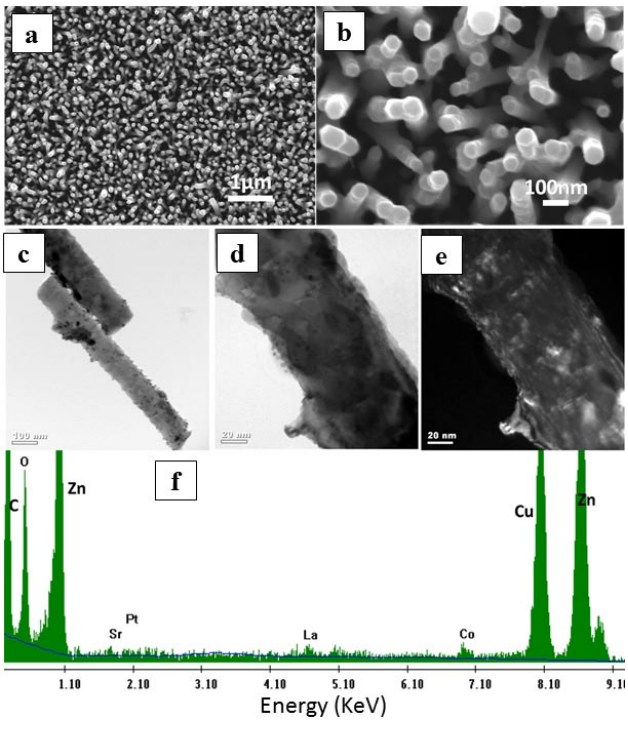

FIGURE 3. Top view SEM images of the prepared samples: a) ZnO/LSCO/Pt nanorods at a low magnification; b) ZnO/LSCO/Pt nanofilm-nanorod arrays at a high magnification. A set of TEM images corresponding to typical ZnO/LSCO/Pt nanorod array: c) two typical composite nanorods; d) bright-field image of nanorod; e) dark-field image of nanorod; f) energy-dispersive X-ray spectroscopy spectrum of ZnO/LSCO/Pt composite nanorods.

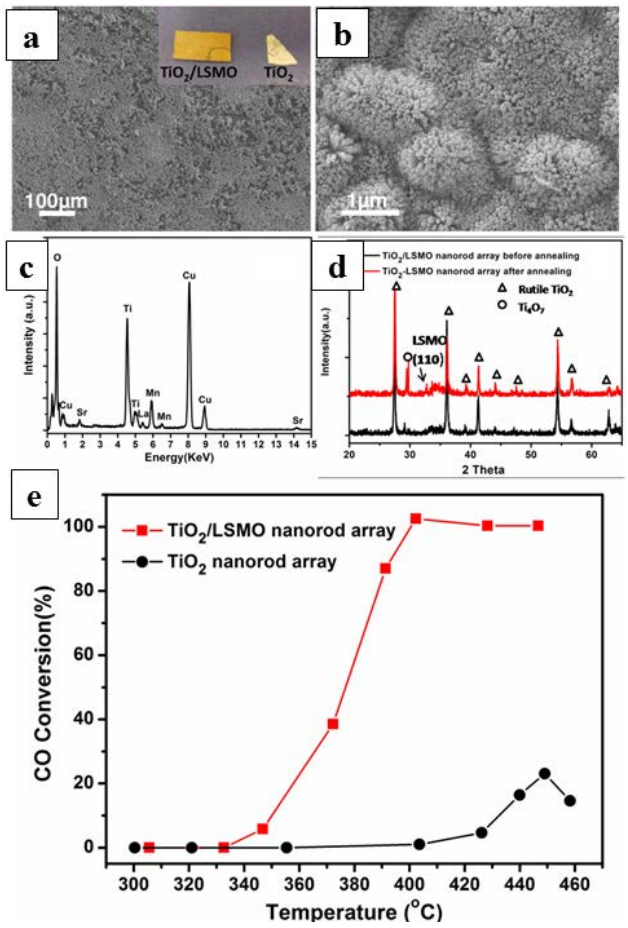

FIGURE 4. (a) a low-magnification SEM top view of large area TiO_2/LSMO nanorod arrays; inset: a photograph of Si substrates grown with TiO_2/LSMO nanorod array and TiO_2nanorod array, respectively; (b) a medium-magnification top view of TiO_2/LSMO nanorod array; (c) A typical energy-dispersive X-ray spectrum collected on TiO_2/LSMO composite nanorod array; (d) Typical X-ray diffraction patterns collected from as-synthesized composite nanorod array and 800°C annealed TiO_2/LSMO composite nanorod array; (e) CO oxidation conversion efficiency as a function of reaction temperature over the 800°C annealed TiO_2/LSMO composite nanorod array and TiO_2nanorod array.

about 90°C lower than TiO_2 nanorod array onset temperature of 420°C. The half conversion temperature and oxidation plateau temperature of 375°C and 400°C for the TiO_2/LSMO composite nanorod array are also 50-60°C lower than that of the TiO_2 nanorod array (ca. 435°C and 450°C). Moreover, compared to the low maximum CO conversion efficiency of TiO_2 nanorod arrays (ca. 20%), the TiO_2/LSMO composite nanorod array achieved 100% CO conversion efficiency at 400°C. The complete conversion temperature of TiO_2/LSMO composite nanorod array is also lower than reported perovskite ($La_{0.5}Sr_{0.5}MnO_3$) powder. The introduction of LSMO in the composite nanowire system clearly has promoted the CO oxidation.

On the basis of our 3D Pt/TiO_2 nanowire catalysts on CH substrates, we evaluated their CO oxidation catalytic performance. Temperature programmed CO oxidation conversion curves are shown in Figures 5a and 5b, corresponding to the Pt/TiO_2 nanorod and Pt, respectively. Under 1% CO oxidation tests, Pt-coated monoliths had an onset temperature of ca. 300°C. Complete conversion was not achieved using a Pt-coated monolith. While for Pt/TiO_2 nanorod catalysts, the CO oxidation results are significantly better than Pt. The onset temperature of Pt/TiO_2 nanorod catalysts is ca. 190°C, with complete conversion observed above 200°C.

Figures 5c and d display the NO oxidation performance of two typical 3D composite nanowire catalysts: Pt/LSCO/ZnO and Pt/LSMO/TiO_2 on CH substrates. As seen from 5c, the obvious onset oxidation temperature of NO for Pt/ZnO/CH, LSCO/ZnO/CH and Pt/LSCO/ZnO/CH is ca. 250°C; the temperature at maximum conversion for three catalysts are ca. 380°C; the temperature at a half of maximum conversion for three catalyst are ca. 290°C, 317°C and 300°C, respectively; the maximum conversion for three catalysts are ca. 36%, 27% and 22%, respectively. As shown in Figure 5d, the maximum conversion for Pt/TiO_2/CH and Pt/LSMO/TiO_2/ZnO/CH are ca. 24% and 22%, respectively, while LSMO/TiO_2/CH has little catalytic activity for NO oxidation. For both series of composite catalysts demonstrated relatively low catalytic activity toward NO oxidation, which is associated with the high space velocity testing condition and the roughly-controlled distribution of Pt and LSCO or LSMO nanoparticles. A detailed space velocity dependence study of NO conversion over nanowire catalysts is being conducted, while the deposition method of Pt and LSCO or LSMO is also being optimized toward quantitative control of weight and thickness loading.

Meanwhile, we also investigated oxygen interactions with perovskite surfaces by the FPT and KMC simulations. We address how the chemical environment interacting with surfaces plays a decisive role in the stabilization of a particular surface atomic structure and composition. We note that under realistic conditions, thermodynamic equilibrium cannot be always reached. By quantifying environmental conditions in terms of pressure, temperature and chemical potential of a given surface species (in our case oxygen), we present our results in terms of a (p,T) surface phase diagram. The resulting (p,T) surface phase diagrams generated from the KMC and FPT approaches are presented in Figure 6. The surface phase diagram depicted in the Figure 6a corresponds to the case where we start off from a fresh clean surface (LMO, (100) surface) at each temperature and pressure, while Figures 6b and 6c present results of the KMC simulation where the temperature was gradually ramped-down and ramped-up after starting up with a clean surface at a high (1,200 K) and low (100 K) temperature. The results of a first principles thermodynamics-based approach showing the equilibrium situation are also included in the Figure 6d for comparison.

Conclusions

In FY 2011, we have successfully advanced the project based on the projected timeline and milestones. Main accomplishments are listed as follows:

- Successful synthesis and characterization of various metal oxide (such as ZnO and TiO_2, etc.) nanowire/nanorod arrays on various substrate such as silicon, glass, and ceramic and stainless steel honeycomb substrates.
- Successful fabrication and characterization of 3D composite nanostructures (such as ZnO/LSMO, ZnO/LSCO, and TiO_2/LSMO, etc.) by pulsed laser deposition, sputtering process and wet chemical methods.
- Investigation of the thermal and mechanical stability, and CO and NO oxidation performance of the 3D composite nanowires based on metal oxide and perovskites.
- Identification of the oxygen interactions with perovskite surfaces by the FPT and KMC simulations.

References

1. R.M. Heck, R.J. Farrauto, Catalytic Air Pollution Control, Van Nostrand-Reinhold, New York, 1995.

2. L. Li, J. Chen, S. Zhang, F. Zhang, N. Guan, T. Wang, S. Liu, Environ. Sci. Technol. 39 (2005) 2841.

3. R.D. Clayton, M.P. Harold, V. Balakotaiah, Appl. Catal. B 84 (2008) 616.

4. F. Basile, G. Fornasari, A. Grimandi, M. Livi, A. Vaccari. Appl. Catal. B 69 (2006) 58.

5. Q. Wang, J.H. Sohn, J.S. Chung, Appl. Catal. B 89 (2009) 97.

6. J.E. Parks II, Science 327 (2010) 1584.

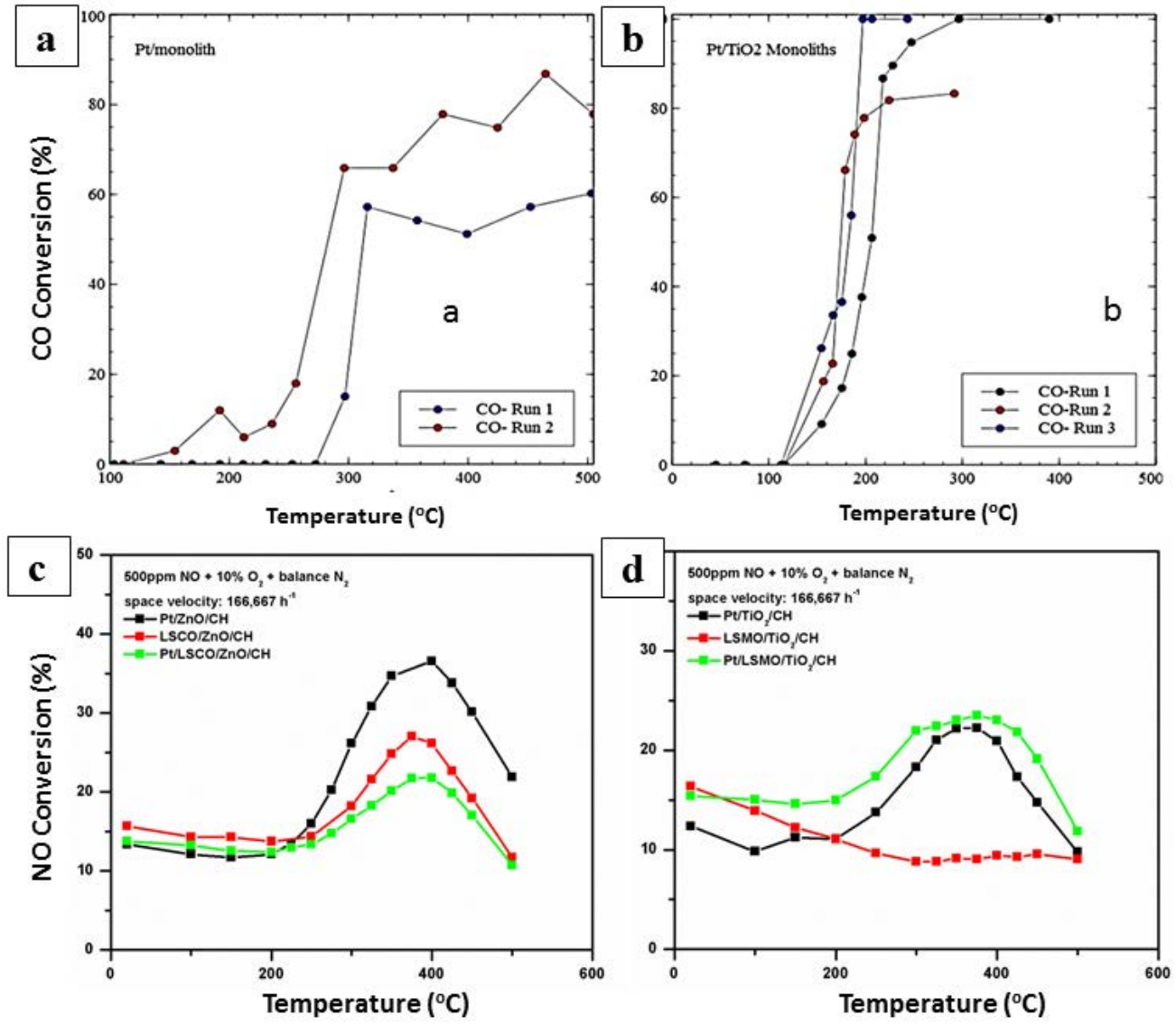

FIGURE 5. CO oxidation conversion curves: (a) Pt/TiO_2 nanorods/monolith (CH) and (b) Pt/monolith (CH); NO oxidation conversion curves of the composite catalysts based on ZnO nanorod arrays c) and TiO_2 nanorod arrays d) on CH substrates.

7. W.S. Epling, L.E. Campbell, A. Yezerets, N.W. Currier, J.E. Parks II, Catal. Rev. 46 (2004) 163.

8. P.S. Monks et al. Atmospheric Environment 43 (2009) 5268.

9. P.-X. Gao, DEER 2011 conference, Detroit, Oct. 5th, 2011.

FY 2011 Publications/Presentations

1. Y.B. Guo, Z.H. Zhang, H.Y. Gao, Z. Ren, and P.-X. Gao, "Synthesis and Characterization of TiO_2/(La,Sr)MnO_3 Composite Nanostructures as CO oxidation catalysts," *Catalysis Today*, **2011**, DOI:10.1016/j.cattod.2011.10.027.

2. K.-T. Liao, P. Shimpi, and P.-X. Gao, "Thermal oxidation of Cu nanofilm on three dimensional ZnO nanorod arrays," *J. Mater. Chem.*, **2011**, 21 (26), 9564-9569.

3. P. Shimpi, S. Yadav, R. Ramprasad, and P.-X. Gao, "Conversion of [0001] Textured ZnO Nanofilm into [01-10] Directed Nanowires Driven by CO Adsorption: In-Situ Carbothermal Synthesis and Complementary First Principles Thermodynamics Simulations," *J. Phys. Chem. C*, **2011**, 115, 7372.

4. G. Liu, and P.-X. Gao, "A review of NOx storage/reduction catalysts: Mechanism, materials and degradation studies," *Catal. Sci. Technol.*, **2011**, 1(4), 552–568.

5. H.Y. Gao, M. Staruch, M. Jain, P.-X. Gao, P. Shimpi, Y.B. Guo, W.J. Cai, and H.-J. Lin, "Structure and magnetic properties of three-dimensional (La,Sr)MnO_3 nanofilms on ZnO nanorod arrays," *Appl. Phys. Letts*, **2011**, 98, 123105.

6. L. Dong, S.P. Alpay, Theoretical analysis of the crystal structure, band-gap energy, polarization, and piezoelectric

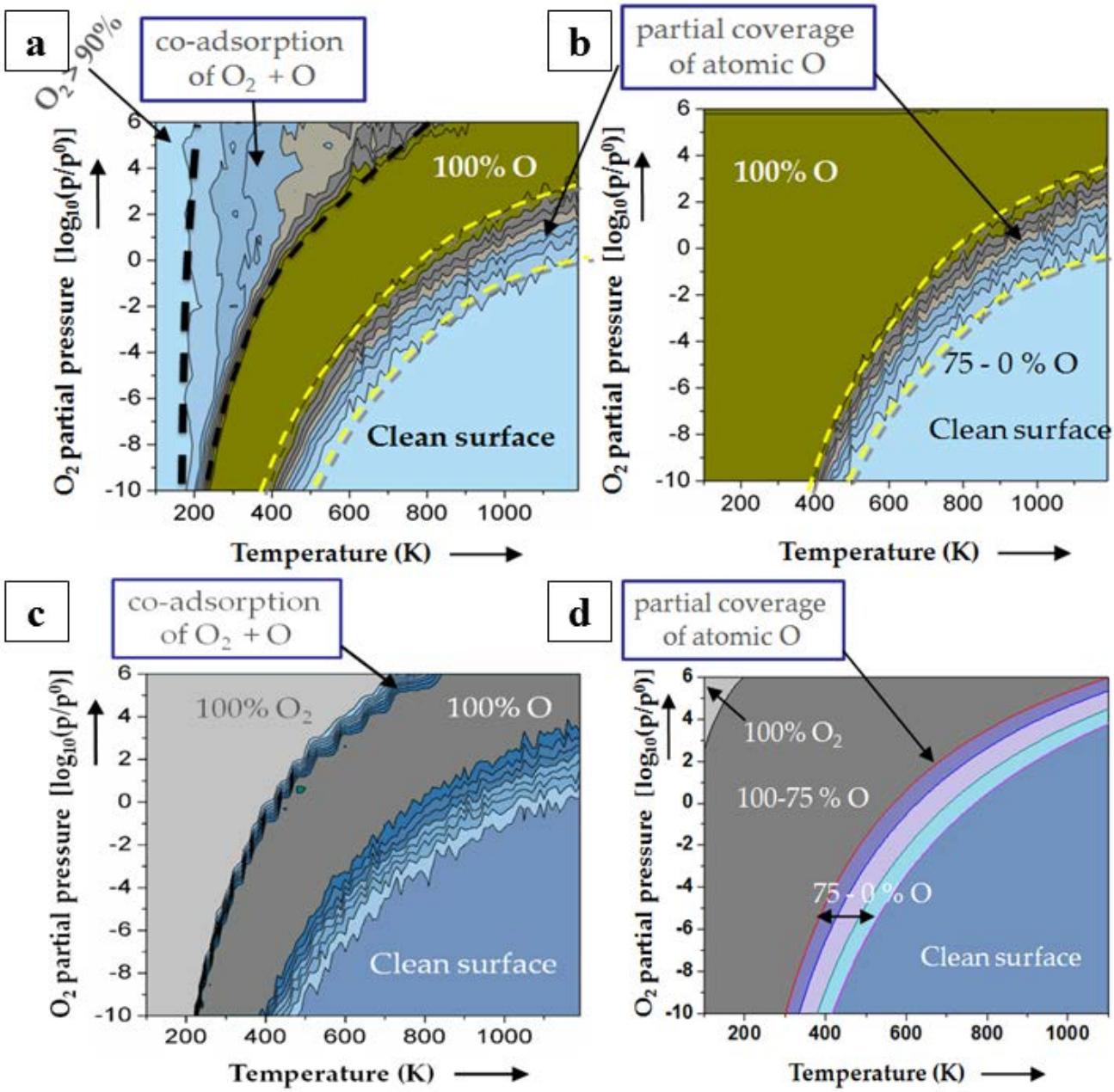

FIGURE 6. The (p,T) surface phase diagrams for MnO_2-terminated $LaMnO_3$ (001) surface in contact with oxidative environment. The surface phase diagrams in panel (a), (b) and (c) are generated using KMC approach and differ from each other in terms of the surface sample preparation (or sample "history"): (a) clean surface is the starting point for each (p,T) condition; (b) temperature ramp down; and (c) temperature ramp up (see text for further details). The surface phase diagram in panel (d) is obtained through a first principle thermodynamics based approach and represents a surface in thermodynamic equilibrium with the oxidative environment.

properties of ZnO-BeO solid solutions, *Phys. Rev. B*, **2011**, 84, 035315.

7. G. Wrobel, M. Piech, S. Dardona, P.-X. Gao, "Synthesis and Fire Retardant Property of Zinc Hydroxystannate coated microfibers," *Sci. Adv. Mater.*, **2011**, accepted. (invited)

8. P. Shimpi, K.-T. Liao, H.J. Lin, P.-X. Gao, "Conversion of functional nanofilm into nanowires using combination of in-situ carbothermal and stress induced recrystallization," *Sci. Adv. Mater.*, **2011**, accepted. (invited)

9. S. Dardona, A. Peles, G. Wrobel, M. Piech, P.-X. Gao, "Gas adsorption and high-emission current induced degradation of field emission characteristics in solution-processed ZnO nanoneedles," *J. Appl. Phys.*, **2010**, 108, 124318.

10. P.-X. Gao, P. Shimpi, W.J. Cai, H.Y. Gao, D.L. Jian, G. Wrobel, Hierarchical Composite Nanowires for Energy,

Environmental and Sensing Applications, *Proceedings of SPIE* Vol. 7940, pp. 79401A1-11, **2011**. (invited)

11. P.-X. Gao, P. Shimpi, H.Y. Gao, W.J. Cai, and G. Wrobel, Multifunctional Composite Nanostructures for Energy and Environmental Applications, The 4th International Symposium for Advancement of Chemical Science: Challenges in Renewable Energy, MIT, Boston, July 5–8, **2011**.

12. Y.B. Guo, H.Y. Gao, Z. Ren, and P.-X. Gao, Anisotropic surface control of catalytic and sensing properties in metal oxide-based composite nanowires, North American Catalysis meeting in Detroit, June 5–10, **2011**.

13. Y.B. Guo, H.Y. Gao, Z. Ren, and P.-X. Gao, Synthesis and multifunctional environmental catalysis properties of TiO_2/(La,Sr)MnO_3 composite nanostructures, North American Catalysis meeting in Detroit, June 5-10, **2011**.

14. W.J. Cai, and P.-X. Gao, Reversible catalytic multi-gas sensing based on single crystalline metal oxide-hybrid nanowires, North American Catalysis meeting in Detroit, June 5-10, **2011**.

15. W.J. Cai, and P.-X. Gao, Synthesis and characterization of SnO_2-based nanowires for energy and environmental applications, North American Catalysis meeting in Detroit, June 5-10, **2011**.

16. P.-X. Gao, Multi-functional Composite Nanowires for Energy, Environmental and Biomedical Applications, Institute of Materials Science Associates Program Annual Meeting, University of Connecticut, Storrs, CT, May 18, **2011**.

17. P.-X. Gao, Three-dimensional Composite Nanostructures for Lean NO_x Emission Control, DOE Vehicle Technology Program Annual Merits Review Meeting, Washington, D.C., May 12, **2011**.

18. P. Shimpi, Y. Ding, and P.-X. Gao, Synthesis, characterization and annealing induced photoluminescence property evolution of ZnMgO nanowire arrays for optoelectronic applications, CMOC meeting, New Haven, CT, March, **2011**.

19. L. Dong and S. P. Alpay, "Band Gap Tuning and Structural Transformation in GaN through Equi-biaxial In-plane Strains and Alloying with InN," Annual American Physical Society March Meeting, Symposium on Electricity-to-Light Conversion: Solid State Lighting, Dallas, TX, March **2011**.

20. P.-X. Gao, Hierarchical Oxide-based Nanoarchitectures for Energy, Environmental and Sensing Applications, SPIE Photonics West: Oxide based Materials and Devices, San Francisco, CA, January 25, **2011**.

21. Y.B. Guo, H.Y. Gao, G. Liu, Z. Ren, P. Shimpi, and P.-X. Gao, "Vertically Aligned ZnO/CeO_2 Composite Nanorod Arrays for Energy and Environmental Applications," Mateirals Research Society 2010 fall meeting, Boston, MA, Dec. 2, **2010**.

22. G. Pilania, R. Ramprasad, "Thermodynamics of oxygen chemistry on PbTiO3 and $LaMnO_3$ (001) surfaces," MRS Fall Meeting, Boston, MA, December **2010**.

23. G. Pilania, R. Ramprasad, "First principles thermodynamics and KMC simulations of oxygen interactions with perovskite surfaces," Fritz-Haber-Institut of Max Planck Society, Berlin, Germany, October **2010**.

Special Recognitions & Awards/Patents Issued

1. P.-X. Gao, Y.B. Guo, Z.H. Zhang, "Metal oxide nanorod arrays on monolithic substrates", US provisional patent filed, **2011**.

IV.6 Experimental Studies for DPF, and SCR Model, Control System, and OBD Development for Engines Using Diesel and Biodiesel Fuels

John Johnson (Primary Contact),
Gordon Parker, Jeffrey Naber, Jason Keith,
Song-Lin Yang
Michigan Technological University (MTU)
1400 Townsend Drive
Houghton, MI 49931

DOE Technology Development Manager:
Ken Howden

DOE Project Manager: Ralph Nine

Subcontractors:
- Oak Ridge National Laboratory (ORNL), Oak Ridge, TN
- Pacific Northwest National Laboratory, Richland, WA

Overall Objectives

- Experimentally validated reduced order models and state estimation algorithms.
- Quantify particulate matter (PM) maldistribution, loading and NO_2/PM ratio effects on passive regeneration, bio-fuel blends, and aging for catalyzed particulate filters (CPFs).
- Increased knowledge of ammonia (NH_3) storage behavior, optimal NH_3 loading, hydrocarbon (HC) poisoning, and aging for selective catalytic reduction (SCR) catalysts.
- Understanding effect of sensor type/configuration on state estimation quality.
- Optimal reductant strategies for SCR operation and CPF regeneration.

Fiscal Year (FY) 2011 Objectives

- Calibrate reduced order models with experimental data and quantify the effect of model reduction compared to high-fidelity models.
- Develop state estimation strategies and understand effects of sensor combination/types.
- Conduct studies in CPF PM oxidation kinetics and SCR oxides of nitrogen (NO_x) reduction kinetics.

Accomplishments

The most significant accomplishments of this project to date are listed in the following:

- A reduced order SCR model developed for Fe-zeolite SCR and calibrated against Fe-zeolite reactor data from ORNL. The model was successfully calibrated with Cu-zeolite SCR test data from MTU engine and ORNL bench reactor tests.
- State estimation strategies applied for diesel oxidation catalyst (DOC) and SCR systems.
- Passive oxidation tests completed using ultra low sulfur diesel (ULSD), 10 percent biodiesel blended fuel (B10) and 20 percent biodiesel blended fuel (B20).
- Activation energy for ULSD, B10, and B20 determined with the corresponding pre-exponential factors that correlate with the experimental PM active regeneration data.
- Multiple sensor technologies studied on the MTU engine/aftertreatment systems to characterize NO_x, NH_3, PM concentration and PM mass retained sensors.
- A high-fidelity one-dimensional (1-D) CPF model enhanced for reduced order model/state estimation.

Future Directions

- Hydrocarbon impact on SCR performance will be tested on an ORNL bench reactor. HC effect model will be built and calibrated from this.
- Similar estimation strategies to those for the SCR and DOC will be implemented for CPFs along with evaluation of sensor combinations for on-board diagnostics (OBD).
- Passive oxidation testing and the mass retained and concentration sensors study will be performed on MTU engines.
- Active regeneration test matrix will be completed and additional test points added to further understand the PM oxidation differences between B10, B20, and ULSD.
- Perform engine tests to characterize PM loading maldistribution in the CPF and its dependency on regeneration parameters.
- High-fidelity CPF model will be used to study optimization of PM kinetics using active regeneration and passive oxidation data.
- Transient testing with a Cummins 2010 6.7-L ISB engine SCR system to determine model response as compared to experimental data including NO_x and NH_3 sensor data.

Introduction

The project focus is to develop experimentally validated DOC, CPF and SCR models with real-time internal state estimation strategies that support future OBD, advanced control system, and system optimization objectives for aftertreatment systems that minimize the energy penalty of meeting emission regulations. Studying the effects of sensor type and combinations on state estimate quality is an inherent aspect of the process. Two additional phases of this work focus on developing SCR and CPF models in specific, high-impact areas. The CPF research includes PM maldistribution, loading and passive regeneration over large NO_x/PM ranges for engines using both diesel and biodiesel fuel blends, and optimal active regeneration. The SCR research will examine NH_3 distribution, optimal NH_3 loading, and HC poisoning as a function of engine and fuel type.

Approach

To achieve the goal of DOC, diesel particulate filter (DPF), and SCR state estimation strategies, a mix of simulation and experimental studies with a combination of off-the-shelf and prototype sensor technologies is used. Engine test cell and reactor data along with high-fidelity models are used for reduced order model forms, suitable for state estimation strategy development.

Results

SCR Model Calibration: The high fidelity SCR model previously developed and calibrated for a Fe-zeolite SCR with reactor data from ORNL was calibrated to a Cu-zeolite SCR with both reactor and engine data. It predicts SCR outlet concentrations including NO, NO_2, N_2O, and NH_3. The parameter identification includes activation energy and pre-exponential constants for 11 reactions, storage capacity of two sites, and five inhibition factors. A comparison of measured and model simulated SCR outlet concentrations for a representative condition is shown in Figure 1.

State Estimation: A reduced order model based on the high fidelity 1-D SCR model was developed for state estimation. The approach to the SCR reduced order model uses bulk gas concentrations instead of both bulk and surface concentrations. Two nonlinear state estimation strategies were applied to the SCR reduced order model, an Extended Kalman Filter and an Unscented Kalman Filter. The Extended Kalman Filter state estimation strategy was also applied to the DOC reduced order model. Figure 2 shows a schematic of the sensors and inputs used in DOC and SCR state estimators. The estimated states follow the simulated states within 1% for both estimators. The Unscented Kalman Filter approach provided slightly more accurate estimation of the states, but required significantly more

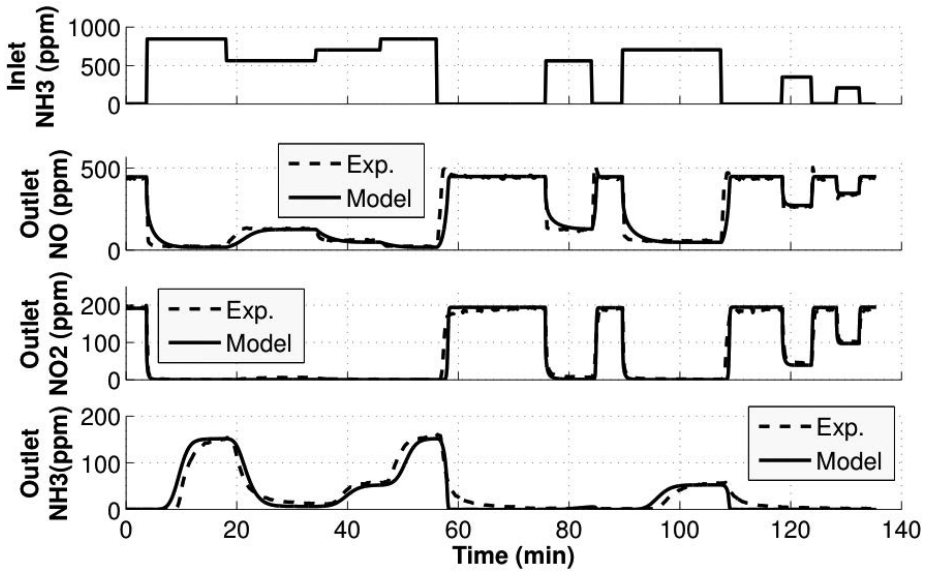

FIGURE 1. Comparison of Measured and Model Simulated SCR Outlet Concentrations for SCR Inlet Conditions with a Variable NH_3 Concentration, 430 ppm NO, 210 ppm NO_2, Temperature of 400°C and Space Velocity of 60k 1/hr

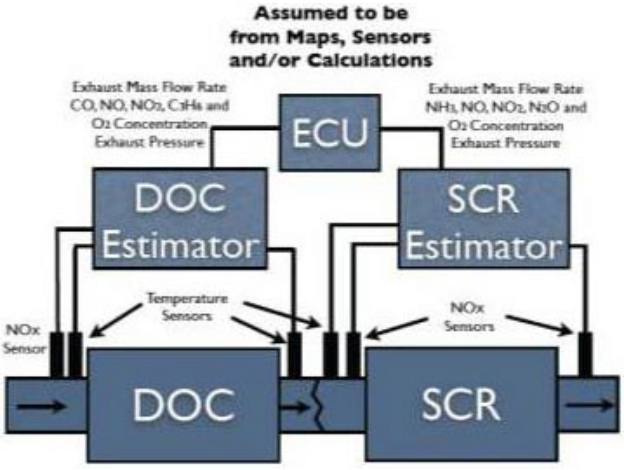

ECU - engine control unit

FIGURE 2. Schematic of the Inputs to the SCR State Estimator

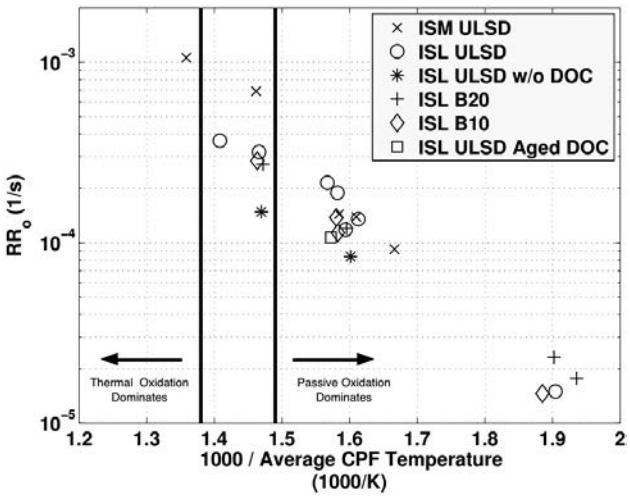

FIGURE 3. Arrhenius Plot of Calculated Reaction Rates during PM Passive Oxidation Testing as a Function of Temperature

computational resources. It was concluded that the Extended Kalman Filter state estimator was sufficient for these systems.

CPF Passive Oxidation: Fourteen passive oxidation tests have been completed on a Cummins 2007 8.9-L ISL engine using ULSD and biodiesel fuel blends. B10 and B20 fuels were tested to determine their effect on the passive oxidation within the CPF. Figure 3 shows the reaction rates for each of the passive oxidation tests as a function of temperature. This data will be used in the 1-D CPF model to determine the NO_2 oxidation kinetic parameters. Two SAE International papers are under review based upon the passive oxidation research.

CPF Active Regeneration: Progress to date includes the completion of 16 active regeneration tests using ULSD along with B10 and B20 biodiesel blends on the ISL. By using optimization methods, it was determined that activation energy for the three fuels can be considered to be constant (1.11E+05 kJ/mol). The reaction rates normalized by the molar fraction of O_2 are shown in Figure 4. The reaction rate increases with increasing CPF inlet temperature. Reaction rates also increased with increasing percentage of biodiesel as did the regeneration efficiency.

CPF Model Development: The 1-D CPF high-fidelity model is being improved based on results obtained in active and passive oxidation tests. The high-fidelity model is being used as the framework for the reduced order model. Specific improvements were made in the catalyst sub-model, wall PM oxidation sub-model (virtual wall layer concept), effective diffusivity calculations subroutine, pressure field calculations subroutine, convergence checks and criteria and PM flow rate axial distribution. An SAE paper was published in 2011 based on the results obtained from active regeneration simulations using the high-fidelity model. The changes significantly improved comparison

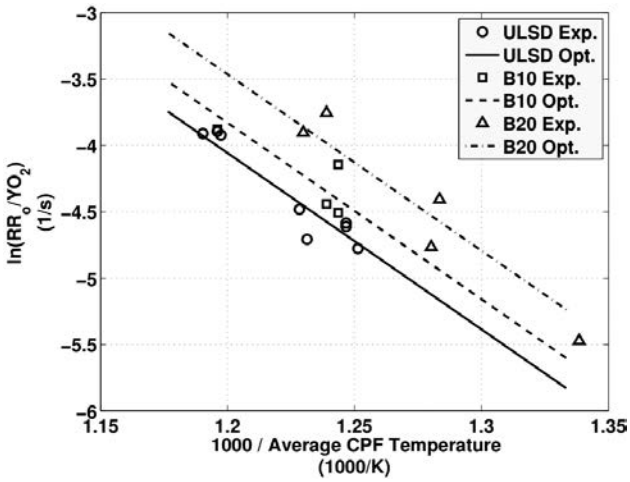

FIGURE 4. Normalized Active Regeneration PM Reaction Rate - Experimental Data and Optimized Model to Fit the Data

to data. The model is being used to determine the thermal and NO_2-assisted PM oxidation kinetics. The results will be published in a peer-reviewed publication in 2012 along with a DOE report.

PM Maldistribution: A review was completed to evaluate methods for determining PM maldistribution within a CPF. Additionally, Cummins has provided valuable input on their experience with a variety of imaging methods. Cummins is currently evaluating the Advantest imaging system [1] which uses terahertz waves to image the CPF. This system will be used for Phase 1 PM maldistribution testing.

Sensor Implementation and Characterization: Several sensors have been installed in the aftertreatment systems on the ISB and ISL as shown in Figure 5. Both prototype and production sensors are being evaluated for

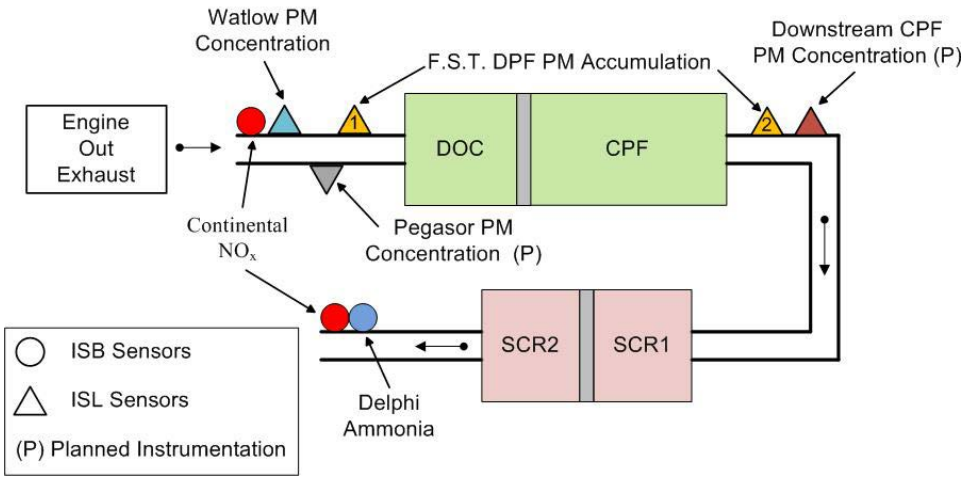

FIGURE 5. Sensor Utilization on the Cummins 2010 6.7-L ISB and 2007 8.9-L ISL (ISB Aftertreatment Components: DOC, CPF, SCR; ISL Aftertreatment Components: DOC and CPF)

use in state estimation. Evaluation and characterization of additional sensors will continue including a PM concentration sensor for upstream of the DOC and a second type for downstream the CPF.

Conclusions

This project has progressed the development of experimentally validated DOC, DPF, and SCR models with real-time internal state estimation strategies that support future OBD, advanced control system, and system optimization objectives for DOC-DPF-SCR aftertreatment systems that minimize the energy penalty of meeting emission regulations.

Specific conclusions are as follows:

- The new procedure to determine CPF's passive oxidation rate as a function of NO_2 concentration, temperature and PM loading, and NO_2/PM ratio is an advancement in determining passive oxidation rates. Two SAE papers have been submitted.
- The SCR and DOC models can be successfully calibrated to engine data and are suitable for model reduction and state estimation strategies. An American Controls Conference paper has been prepared on the DOC reduced order model.
- A reduced order SCR model was developed from the high fidelity model.
- The high fidelity simulation model of the CPF has been further developed and provides the basis for the reduced order model.
- The Extended Kalman Filter is an appropriate method for estimating the internal states for both the DOC and the SCR where reduced order models are used for each.
- The active regeneration data for ULSD, B10, and B20 has been correlated to a PM oxidation model that accurately describes the experimental data.

References

1. "Novel Nondestructive Imaging Analysis for Catalyst Washcoat Loading and DPF Soot Distribution Using Terahertz Wave Computed Tomography", S., Nishina, K., Takeuchi, M., Shinohara, M., Imamura, M., Shibata, Y., Hashimoto, F., Watanabe, SAE technical paper 2011-01-2064.

FY 2011 Publications/Presentations

1. "Development and Parameter Identification Of An Iron-Zeolite SCR Catalyst Model Using Reactor Data", Seth B. Deland, Master's Thesis, Michigan Technological University, 2010.

2. "A Kalman Filter Estimator for a Diesel Oxidation Catalyst During Active Regeneration of a CPF", H., Surenahalli, G., Parker, J., Johnson, and M., Devarakonda, *American Control Conference* 2012 (Review).

3. "Engine Test and Analysis Report for the Effects of Biodiesel Blends on Particulate Matter Oxidation in a Catalyzed Particulate Filter during Active Regeneration," James Pidgeon, Professor John H Johnson, Professor Jeffrey Naber," *Technical Report to DOE* (Oct 12, 2011).

4. "Modeling Study of Active Regeneration of a Catalyzed Particulate Filter Using One-Dimensional DOC and CPF Models", Harsha Shankar Surenahalli, Kiran Premchand, John Johnson, and Gordon Parker, SAE Technical Paper No. 2011-01-1242, 2011.

5. Oral Presentation: G. Parker, "Experimental Studies for DPF, and SCR Model, Control System, and OBD

Development for Engines Using Diesel and Biodiesel Fuels," 2011 DOE Vehicle Technologies Annual Merit Review, Washington, D.C.

6. "Investigation of NO_2 Oxidation Kinetics and Burning Mode for Medium Duty Diesel Particulate: Contrasting O_2 and NO_2 Oxidation", A., Strzelec, *DEER Conference*, 2011.

7. "Trends in Particulate Nanostructure: Impact of Engine Size and Biofuels" - A. Strzelec et al., DEER 2011 Poster Presentation 0 2001 Annual Meeting.

8. "A Parameterized Iron-Zeolite SCR Model Calibrated to Reactor Data" AICHE Abstract Submission #222827 - 2011 Annual Meeting. October 16–19, 2011.

9. "An Experimental Investigation into the Passive Oxidation of Particulate Matter in a Catalyzed Particulate Filter", Christopher Hutton, Master Thesis, Michigan Technological University, 2010.

10. "Engine Test and Analysis Report for Catalyzed Particulate Filter Particulate Matter Loading and Passive Oxidation with Ultra Low Sulfur Diesel and Biodiesel Fuels," Kenneth Shiel, Harsha Surenahalli, Christopher Hutton, Professor John H Johnson, Professor Jeffrey Naber, *Technical Report to DOE* (July 28, 2011).

11. "Baseline Estimator Study Form", H., Surenahalli, G., Parker, and M., Devarakonda, *Technical Report to DOE* (June 30th 2011).

12. "Engine Test and Analysis Report for Catalyzed Particulate Filter Particulate Matter Loading and Passive Oxidation with Ultra Low Sulfur Diesel", Christopher Hutton, Harsha Surenahalli , Kenneth Shiel, Professor John H Johnson, Professor Jeffrey Naber, *Technical Report to DOE* (Jan 31, 2011).

V. NEW PROJECTS

V. NEW PROJECTS

V.1 Amerigon Thermoelectric Waste Heat Recovery Program for Passenger Vehicles

Amerigon Inc.

PI: John LaGrandeur

Current light-duty passenger vehicles use approximately one-third of their fuel performing useful work, with the rest rejected as waste heat. The goal of Amerigon's project is to increase fuel efficiency and reduce emissions through the recovery and conversion of exhaust gas waste heat to electric power using thermoelectric (TE) technology. This solid state technology can help automakers meet increasingly stringent fuel economy and emissions requirements while providing a much needed source of additional electric power. Amerigon and its partners pioneered the integration of advanced TE material systems with gas and liquid heat exchangers to provide novel heat to power engines in a cylindrical form factor. This thermoelectric generator (TEG), which operated with a hot side temperature near 500°C, made over 700 watts electric power in Amerigon bench testing, was subsequently fitted into the underfloor exhaust systems of Ford and BMW test vehicles and successfully operated over 3,000 miles of road testing. In this project, BMW and Ford developed comprehensive bumper-to-bumper computer performance models to predict fuel efficiency improvements and to optimize the vehicle architectures. The models showed fuel economy improvements between 1 and 5% based on driving conditions. This prior work provides a proof of concept technology platform ready for a transition of the technology from research and development (R&D) to commercialization.

Key elements of this project include: 1) scale up of proven Skutterudite materials based on decades of experience. The scale up of processes and manufacture will be performed by Amerigon at Amerigon's TE material facility, ZT Plus, in Azusa, CA. ZT Plus has successfully transitioned materials from academic labs and will employ similar processes to transfer proven skutterudite technology to the commercial sector; 2) scale up of proof of concept TE engines using Skutterudite materials manufactured by ZT Plus. The engines will be based upon Amerigon's proprietary stack design and will be integrated with gas and liquid heat exchangers in the cylindrical form factor pioneered in a prior DOE-funded R&D project. Improvements will include element-level encapsulation to prevent atmospheric corrosion; 3) integration of the cylindrical TEG into the underfloor exhaust systems of Ford and BMW target vehicles including a Faurecia coaxial bypass valve. The exhaust system integration will be performed by Faurecia at Columbus, IN and Troy, MI facilities; 4) environmental withstanding testing of engines and TEG subsystems by Amerigon Irwindale, CA facilities; and 5) confirmatory testing of TEG efficiency and TEG system performance at the vehicle level by the National Renewable Energy Laboratory in Golden, CO.

V.2 Nanostructured High-Temperature Bulk Thermoelectric Energy Conversion for Efficient Automotive Waste Heat Recovery

GMZ Energy Inc.

PI: Chris Caylor

GMZ Energy Inc., along with team members Robert Bosch LLC (Bosch), Boston College (BC), and Oak Ridge National Laboratory will meet the DOE program goals of 5% fuel economy improvement by direct conversion of engine waste heat to useful electric power for light-duty vehicle application using significantly improved nanostructured bulk thermoelectric materials that our team members have developed and an innovative two-stage cascade design.

High-temperature compatible nanostructured half-heusler materials will give both high-thermoelectric power generation performance as well as robust, thermally stable and cyclable devices. These devices will form the top layer of a cascade approach using nanostructured bismuth telluride-based materials for the lower temperature stage to create a ~1 kW thermoelectric generator (TEG) system, to enable a 5% fuel efficiency improvement in a light-duty vehicle, a Chevrolet HHR modified by Bosch. The thermoelectric devices will interact with the exhaust gases through postcatalytic converter heat exchangers designed and fabricated to give minimal pressure drop while maximizing the heat removal from the gas and delivery to the thermoelectric devices. A key step in the optimization of the performance of the system will be the thermal and electrical interfaces both at the device level and at the system level. For the high-temperature compatible half-heusler devices, the team will capitalize on recently developed high ZT half-heusler materials and continue the current device development to enable high thermal stability and temperature cycling. The team will build on this device understanding along with the existing bismuth telluride technology to design devices for high heat-flux densities and large power densities to enable low-cost systems that use minimal thermoelectric materials. At the system level, the devices must interface with the heat exchangers at both the hot-side and cold-side with low thermal loss and low mechanical stress, especially under thermal cycling, while providing the necessary high thermal fluxes via thermal buses, spacers and insulations. The thermoelectric power conversion system will be integrated with a light-duty vehicle platform for testing the power output and fuel efficiency gains. The team will work to develop a vehicle model to predict and elucidate the thermoelectric system performance and the effects on fuel efficiency. The model will be verified by both steady-state engine-integrated dynamometer testing as well as vehicle-integrated dynamic drive cycle dynamometer testing. Finally, the team will provide a clear path to commercialization based on market assumptions and cost models for the system and past experience in large volume automotive products.

V.3 Development of Cost-Competitive Advanced Thermoelectric Generators for Direct Conversion of Vehicle Waste Heat into Useful Electrical Power

General Motors

PI: Gregory Meisner

General Motors (GM) will develop a cost-effective thermoelectric generator (TEG) that is fully integrated into a GM production light-duty vehicle. This will reduce automotive energy consumption and CO_2 emissions by generating usable electricity from exhaust gas waste heat. Our objectives are to overcome the major obstacles to TEG commercialization and demonstrate 5% fuel economy improvement over the US06 drive cycle. We will use electrical and thermal management strategies to reduce electrical accessory load on the alternator using thermoelectric (TE) generated power. To utilize this additional power, we will raise the electrical accessory load consumption by shifting some engine driven accessories to electrical drive, and we will attempt to use the excess electrical power for something other than the vehicle electrical load e.g., propulsion (optimal for hybrids). We will develop a TEG system and all vehicle controls and electrical systems for full vehicle integration. The TEG system will be modeled and analyzed for performance and cost and the heat exchangers and thermal interfaces between heat exchangers and TE modules will be optimized for TE performance. Other objectives of this project are to (1) further optimize compositions and processing parameters for TE materials, (2) develop suitable diffusion barriers, interfaces electrical interconnections, and thermal contacts within TE modules, (3) implement adequate protection of TE materials and modules from degradation during operation, and (4) develop manufacturing and assembly processes for large-scale production of TE materials and components that include scale up plans for the production of 100,000 TEG units per year. The project tasks are divided into three parallel phases with project management activities covered under the first phase. The second phase will develop the TEG and address vehicle integration issues, and the third phase will develop advanced TE materials and modules.

VI. Acronyms, Abbreviations and Definitions

η_g	Gross indicated thermal efficiency
γ	Ratio of specific heats (c_p/c_v)
κ	Thermal conductivity
λ	Stoichiometric ratio; air/fuel equivalence ratio
ϕ	Fuel/air equivalence ratio
σ	Electrical conductivity
µs	Micro-second
°C	Degrees Celsius
°CA	Degrees crank angle, 0° = TDC
°F	Degrees Fahrenheit
ΔP	Pressure change
ΔT	Delta (change in) temperature
0-D	Zero-dimensional
1-D, 1D	One-dimensional
2-D, 2D	Two-dimensional
3-D, 3D	Three-dimensional
T_{90}	90% volume recovered temperature
ABDC	After bottom-dead center
AC	Alternating current
ACES	Advanced Collaborative Emissions Study
A/F	Air to fuel ratio
AFM	Atomic force microscopy
Ag	Silver
AHRR	Apparent heat release rate
a.k.a.	Also known as
Al	Aluminum
Al_2O_3	Aluminum oxide
ANL	Argonne National Laboratory
API	American Petroleum Institute
ASI	After start of injection
ASME	American Society of Mechanical Engineers
atdc, ATDC, aTDC	After top-dead center
atm	Atmosphere
a.u.	Arbitrary units
Au	Gold
Avg.	Average
B	Boron
Ba	Barium
$BaAl_2O_4$	Barium aluminate
$Ba(NO_3)_2$	Barium nitrate
BaO	Barium oxide
bar	unit of pressure (14.5 psi or 100 kPa)
BBDC	Before bottom-dead center
BDC	Bottom-dead center
BES	Basic Energy Sciences
BET	Named after Brunauer, Emmett and Teller, this method for determining the surface area of a solid involves monitoring the adsorption of nitrogen gas onto the solid at low temperature and, from the isotherm generated, deriving the volume of gas required to form one monolayer adsorbed on the surface. This volume, which corresponds to a known number of moles of gas, is converted into a surface area though knowledge of area occupied by each molecule of adsorbate.
bhp-hr	Brake horsepower hour
BiTe	Bismuth telluride
BMEP	Brake mean effective pressure
BPT	Boiling point temperature
Bsfc, BSFC	Brake specific fuel consumption
bsNOx, BSNOx	Brake specific NOx emissions
BTDC, btdc	Before top-dead center
BTE	Brake thermal efficiency
BWR	Benedict-Webb-Rubin
ca.	About, approximately
CA	Crank angle
CA50	Crank angle at which 50% of the combustion heat release has occurred
CAD	Crank angle degrees, computer-aided design
CAE	Computer-aided engineering
CAFE	Corporate Average Fuel Economy
CARB	California Air Resources Board
CBS	Characteristic-based split
cc	Cubic centimeter
CCD	Charge coupled device
CDC	Conventional diesel combustion
CDI	Compression direct injection
Ce	Cerium
CeO_2	Cerium oxide
CFD	Computational fluid dynamics
CH_4	Methane
CHA	Cu-SSZ-13
CI	Compression ignition
CIDI	Compression ignition direct injection
CLC	Chemical looping combustion

CLEERS	Cross-Cut Lean Exhaust Emissions Reduction Simulations
CLOSE	Collaborative Lubricating Oil Study on Emissions
cm	Centimeter
cm^3	Cubic centimeters
CMOS	Complementary metal oxide semiconductor
CN	Cetane number
CNG	Compressed natural gas
CO	Carbon monoxide
CO_2	Carbon dioxide
COV	Coefficient of variation (variance)
cP	Centipoise
CPF	Catalyzed particulate filter
cpsi	Cells per square inch
CPU	Central processing unit
Cr	Chromium
CR	Compression ratio
CRADA	Cooperative Research and Development Agreement
CRC	Coordinating Research Council
CRF	Combustion Research Facility
CTC	Cummins Technical Center
CTE	Coefficient of thermal expansion
Cu	Copper
CVD	Chemical vapor deposition
DBTDC	Degrees before top-dead center
DC, dc	Direct current
deg	Degrees
°CA	Degrees crank angle, 0° = TDC
ΔT	Delta (change in) temperature
DFT	Density function theory
DI	Direct injection, direct-injected
DMP	Diesel micro pilot
DOC	Diesel oxidation catalyst
DOE	U.S. Department of Energy
DOHC	Double overhead camshaft
dP	Differential pressure
DPF	Diesel particulate filter
DRIFTS	Diffuse reflectance infrared Fourier-transform spectroscopy
E10	10% ethanol, 90% gasoline fuel blend
E15	15% ethanol, 85% gasoline fuel blend
E20	20% ethanol, 80% gasoline fuel blend
E85	85% ethanol, 15% gasoline fuel blend
ECM	Electronic (engine) control module
ECN	Engine Combustion Network
ECU	Electronic (engine) control unit
EDS	Energy-dispersive spectroscopy
EDX	Energy dispersive X-ray
EELS	Electron energy loss spectroscopy
EEVO	Early exhaust valve opening
EGR	Exhaust gas recirculation
EKF	Extended Kalman Filter
EOI	End of injection
EPA	U.S. Environmental Protection Agency
ERC	Engine Research Center
EVC	Exhaust valve closing
EVO	Exhaust valve opening
EWHR	Exhaust waste heat recovery
EXAFS	Extended X-ray absorption fine structure
FAME	Fatty acid methyl ester
Fe	Iron
FEA	Finite-element analysis
FEM	Finite-element method
FFVA	Fully flexible valve actuation
FID	Flame ionization detector
FiO	Fuel-in-Oil
FMEA	Failure mode and effects analysis
FMEP, fmep	Friction mean effective pressure
FPEG	Free-piston electric generator
FPT	First principle thermodynamics
FSN	Filter smoke number
FTIR	Fourier transform infrared
ft-lb	Foot-pound
FTP	Federal Test Procedure
FY	Fiscal year
g, G	Gram
g/bhp-hr	Grams per brake horsepower-hour
GC	Gas chromatography
GC-FID	Gas chromatograph combined with a flame ionization detector
GC-MS	Gas chromatography – mass spectrometry
GDC	Gadolinium-doped cerium oxide
GDCI	Gasoline direct injection compression ignition
GDI	Gasoline direct injection
Ge	Germanium
g/hphr	Grams per horsepower-hour
GHSV	Gas hourly space velocity
gIMEP	Gross indicated mean effective pressure
GM	General Motors
g/mi	Grams per mile
GPU	Graphical processing unit

GTDI	Gasoline turbocharged direct injection
GTI	Gas Technology Institute
H_2	Diatomic (molecular) hydrogen
H_2CO	Formaldehyde
H_2O	Water
H_2O_2	Hydrogen peroxide
HAADF STEM	High angle annular dark field scanning transmission electron microscopy
HC	Hydrocarbons
HCCI	Homogeneous charge compression ignition
HC-SCR	Hydrocarbon selective catalytic reduction
HCT	Hydrodynamics, Chemistry, Thermodynamics Code
HD	Heavy-duty
He	Helium
HECC	High-efficiency clean combustion
HEI	Health Effects Institute
HEV	Hybrid electric vehicle
HH	Half-Heusler
HHV	Higher heating value
HIL	Hardware-in-the-loop
HMN	Heptamethylnonane
HMS	Higher manganese silicide
hp	Horsepower
HPL	High pressure loop
hr	Hour
HR	Heat release
HRR	Heat release rate
HSDI	High-speed direct-injection
HT	Hydrothermal
HTHS	High-temperature, high-shear
HVA	Hydraulic valve actuation
HVAC	Heating, ventilation and air conditioning
HVOF	High velocity oxygen fuel
HWFET	Highway Fuel Economy Test
HWG	Hollow waveguide
IC	Internal combustion
I/C	Intercooler
ICCD	Intensified charged-coupled device
ICE	Internal combustion engine
ID	Internal diameter
IMEP	Indicated mean-effective pressure
$IMEP_g$	Indicated mean effective pressure, gross
$IMEP_{net}$	Indicated mean effective pressure, net
IR	Infrared
ISFC	Indicated specific fuel consumption
ISX	Cummins Inc. 15-liter displacement, inline, 6-cylinder heavy duty diesel engine
ITHR	Intermediate temperature heat release
IV	Intake valve
IVC	Intake valve closing
IVO	Intake valve opening
J	Joule
k	thousand
K	Kelvin
K	Potassium
kg	Kilogram
kHz	Kilohertz
KIVA	Combustion analysis software developed by Los Alamos National Laboratory
KIVA-CMFZ	KIVA Coherent Flamelet Multi-Zone
kJ	Kilojoules
kJ/L	Kilojoules per liter
kJ/m^3	Kilojoules per cubic meter
KMC	Kinetic Monte Carlo
kPa	Kilopascal
kW	Kilowatt
L	Liter
La	Lanthanum
LA4	Phase 1 and 2 of the FTP driving cycle
LANL	Los Alamos National Laboratory
LAST	Lead, antimony, silver, and tellurium, an n-type TE material
LAST/T	LAST/tin, a p-type TE material
LB	Lattice-Boltzmann
lb ft	Pound foot
lb/min	Pounds per minute
lbs	Pounds
lbs/sec	Pounds per second
L/D	Length-to-diameter ratio
LD	Light-duty
LDT	Light-duty truck
LED	Light-emitting diode
LES	Large eddy simulation
LHV	Lower heating value
LIF	Laser-induced fluorescence
LII	Laser-induced incandescence
LLNL	Lawrence Livermore National Laboratory
LNT	Lean-NOx trap
LP	Low pressure
LP-EGR	Low-pressure exhaust gas recirculation
LPL	Low pressure loop

LQ	Linear quadratic
LRRI	Lovelace Respiratory Research Institute
LSCO	$(La,Sr)CoO_3$
LSMO	$(La,Sr)MnO_3$
LTC	Low-temperature combustion
m^2	Square meters
m^2/gm	Square meters per gram
m^3	Cubic meters
mA	Milliamps
MAF	Manifold air flow
MAP	Manifold air pressure
MB	Mercedes-Benz
mbar	Millibar
MBT	Minimum (spark advance) for best torque; Maximum brake torque
MCE	Multi-cylinder experiments
MD	Medium-duty
MER	Molar expansion ratio
Mg	Magnesium
mg/cm^2	Milligrams per square centimeter
mg/mi	Milligram per mile
mg/mm^2	Micrograms per square millimeter
mg/scf	Milligrams per standard cubic foot
mi	Mile
µs	Micro-second
min	Minute
MIR	Mid-infra-red
MIT	Massachusetts Institute of Technology
µm	Micrometer
mm	Millimeter
mmols	Micro-moles
Mn	Manganese
Mo	Molybdenum
mol	Mole
mol/s	Moles per second
MPa	Megapascals
mpg	Miles per gallon
mph	Miles per hour
ms	Millisecond
MS	Mass spectrometry
MSAT	Mobile source air toxic
MSU	Michigan State University
MTU	Michigan Technological University
N_2	Diatomic nitrogen
N_2O	Nitrous oxide
N_2O_3	Nitrogen trioxide
Na	Sodium
NETL	National Energy Technology Laboratory
NH_3	Ammonia
NIR	Near-infra-red
nm	Nanometer
Nm	Newton meter
NMEP	Net mean effective pressure
NMHC	Non-methane hydrocarbon
NMOG	Non-methane organic gases
NMR	Nuclear magnetic resonance
NO	Nitric oxide
NO_2	Nitrogen dioxide
NOx, NO_X	Oxides of nitrogen
NP	Nanoparticle
NR	Nanoribbon
ns	Nanosecond
NSC	NOx storage capacity
NSE	NOx storage efficiency
NSR	NOx storage and reduction
NTC	Negative temperature coefficient
NTE	Negative thermal expansion
NVH	Noise, vibration, and harshness
NVO	Negative valve overlap
NW	Nanowire
O_2	Diatomic (molecular) oxygen
O_3	Ozone
OBD	On-board diagnostics
OC	Organic carbon
OEM	Original equipment manufacturer
OH	Hydroxyl
OH*	Hydroxyl radical that emits ultraviolet photons
OHC	Oxygenated hydrocarbons
OH PLIF	Planar laser-induced fluorescence of OH
ORC	Organic Rankine Cycle
ORNL	Oak Ridge National Laboratory
OSC	Oxygen storage capacity
OTR	Over-the-road
P	Pressure
PAH	Polycyclic aromatic hydrocarbon
PBA	$Pt/Ba/Al_2O_3$
PBC	$Pt/Ba/CeO_2$
PBCA	$Pt/BaO/CeO_2/Al_2O_3$
PBCZ	$Pt/Ba/CeO_2$-ZrO_2
PbTe	Lead telluride thermoelectric material
PCA	$Pt/CeO_2/Al_2O_3$
PCCI	Premixed charge compression ignition
PCS	Predictor-corrector split
PCZ	Pt/CeO_2-ZrO_2
PDF	Probability density function

PDI	Port direction injection
PFI	Port fuel injected, port fuel injection
PFS	Partial fuel stratification
P-G	Petrov-Galerkin
PGM	Platinum-grade metal, platinum group metal
PLII	Planar laser-induced incandescence
PLIF	Planar laser-induced fluorescence
PM	Particulate matter
PNA	Passive NOx adsorber
PNNL	Pacific Northwest National Laboratory
ppb	Parts per billion
PPC	Partially premixed combustion
PPCI	Partially premixed compression ignition
ppi	Pores per square inch
ppm	Parts per million
PRF	Primary reference fuel
PRF80	PRF mixture with an octane number of 80 (i.e., 80% iso-octane and 20% n-heptane)
PRR	Pressure rise rate
PSAT	Powertrain Systems Analysis Toolkit
psi	Pounds per square inch
psig	Pounds per square inch gauge
Pt	Platinum
PTO	$PbTiO_3$
PV	Pressure-volume
PVT	Pressure-volume-temperature
PXRD	Powder X-ray diffraction
Q	Heat
Q1, Q2, Q3, Q4	First, second, third and fourth quarters
QW	Quantum well
R&D	Research and development
RAPTOR	SNL massively-parallel LES solver
RAPTR	Regenerative Air Preheating with Thermochemical Recuperation
RCCI	Reactivity-controlled compression ignition
RCCIDBL	Split injection for RCCI
RCCISGL	Single direct-injection for RCCI
RCF	Rapid compression facility
RCM	Rapid compression machine
Re	Reynolds number
Redox	Reduction-oxidation
Rf	Radio frequency
RGF	Residual gas fraction
Rh	Rhodium
RME	Rapeseed methyl ester
RNG	Re-normalization Group
ROM	Rule of mixtures
RON	Research octane number
RPM, rpm	Revolutions per minute
RT	Room temperature
S	Seebeck coefficient
S	Sulfur
SA	Spark assist(ed)
SACI	Spark-assisted compression ignition
SCAQMD	South Coast Air Quality Management District
sccm	Standard cubic centimeters
SCF/min	Standard cubic feet per minute
SCORE	Sandia Compression-ignition Optical Research Engine
SCR	Selective catalytic reduction
sec	Second
SEM	Scanning electron microscopy
Si	Silicon
SI	Spark ignition, spark-ignited
SiC	Silicon carbide
SIDI	Spark ignition direct injection
SFC	Specific fuel consumption
SFTP	Supplemental Federal Test Procedure
SLPM	Standard liters per minute
SME	Soy methyl ester
SNL	Sandia National Laboratories
SO_2	Sulfur dioxide
SOC	Start of combustion; soluble organic compound
SOI	Start of injection
SOF	Soluble organic fraction
SO_x	Oxides of sulfur
SpaciMS	Spatially resolved capillary inlet mass spectrometer
SPLAT II	Custom instrument that determines aerosol vacuum aerodynamic diameter and mass spectra of individual particles
SPS	Spark plasma sintering
Sr	Strontium
Stdev	Standard deviation
STEM	Scanning transmission electron microscopy
SU	Stanford University
SULEV	Super Ultra-Low Emissions Vehicle
SUV	Sports utility vehicle
SVOC	Semi-volatile organic compound
SWCNT	Single-wall carbon nanotube

SwRI®	Southwest Research Institute®
T	Temperature
T_{90}	90% volume recovered temperature
TAP	Temporal analysis of products
TC	Turbocompound; total capacity
TCR	Thermo-chemical recuperation
TDC	Top-dead center
TDL	Tunable diode laser
TE	Thermoelectric
TEG	Thermoelectric generator
TEM	Transmission electron spectroscopy; thermoelectric module
TGM	Thermoelectric generator module
THC	Total hydrocarbon
TIM	Thermal interface material
TPD	Temperature-programmed desorption
TPO	Temperature-programmed oxidation
TPR	Temperature-programmed reduction or reaction
TPRX	Temperature-programmed reaction
TS	Thermal stratification
TUCO	Turbocompounding
TWC	Three-way catalyst
UC	Unused capacity
U/C	Turbine speed ratio
UCB	University of California, Berkeley
UDDS	Urban Dynamometer Driving Schedule
UHCs	Unburned hydrocarbons
UKF	Unscented Kalman Filter
ULSD	Ultra-low sulfur diesel
UM	University of Michigan
US06	Supplemental Federal Test Procedure (SFTP) drive cycle
UV	Ultraviolet
UW	University of Wisconsin
UW-ERC	University of Wisconsin Engine Research Center
UWS	Urea-water solution
V	Volt
VAC	Volts, alternating current
VACNT	Vertically aligned carbon nanotube
VCR	Variable compression ratio
VDC	Volts – direct current
VGT	Variable geometry turbocharger
VNT	Variable nozzle turbine
VOCs	Volatile organic compounds
VPR	Volatile particle removal
VVA	Variable valve actuation
VVT	Variable valve timing
W	Watt
WGS	Water-gas shift
WGSR	Water-gas shift reaction
WHR	Waste heat recovery
WOT	Wide-open throttle
wt%	Weight percent
WTT	Well-to-tank
XAFS	X-ray aborption fine structure
XANES	X-ray absorption near-edge spectroscopy
XPS	X-ray photoelectron spectroscopy
XRD	X-ray diffraction
Y	Yttrium
yr	Year
YSZ	Ytrria-stabilized zirconia
YTZP	Yttrium oxide (Y_2O_3) partially stabilized zirconia (Zr)
Zn	Zinc
Zr	Zirconium
zT	Dimensionless thermoelectric figure of merit; equal to: (electrical conductivity) (Seebeck coefficient)^2(temperature)/ (thermal conductivity)
ZTO	Zn_2SnO_4

VII. Index of Primary Contacts

U.S. DEPARTMENT OF ENERGY | Energy Efficiency & Renewable Energy

For more information
eere.energy.gov

DOE-ACE-2011AR December 2011
Printed with a renewable-source ink on paper containing
at least 50% wastepaper, including 10% post consumer waste.